Middle Atmosphere Program

HANDBOOK FOR MAP VOLUME 14

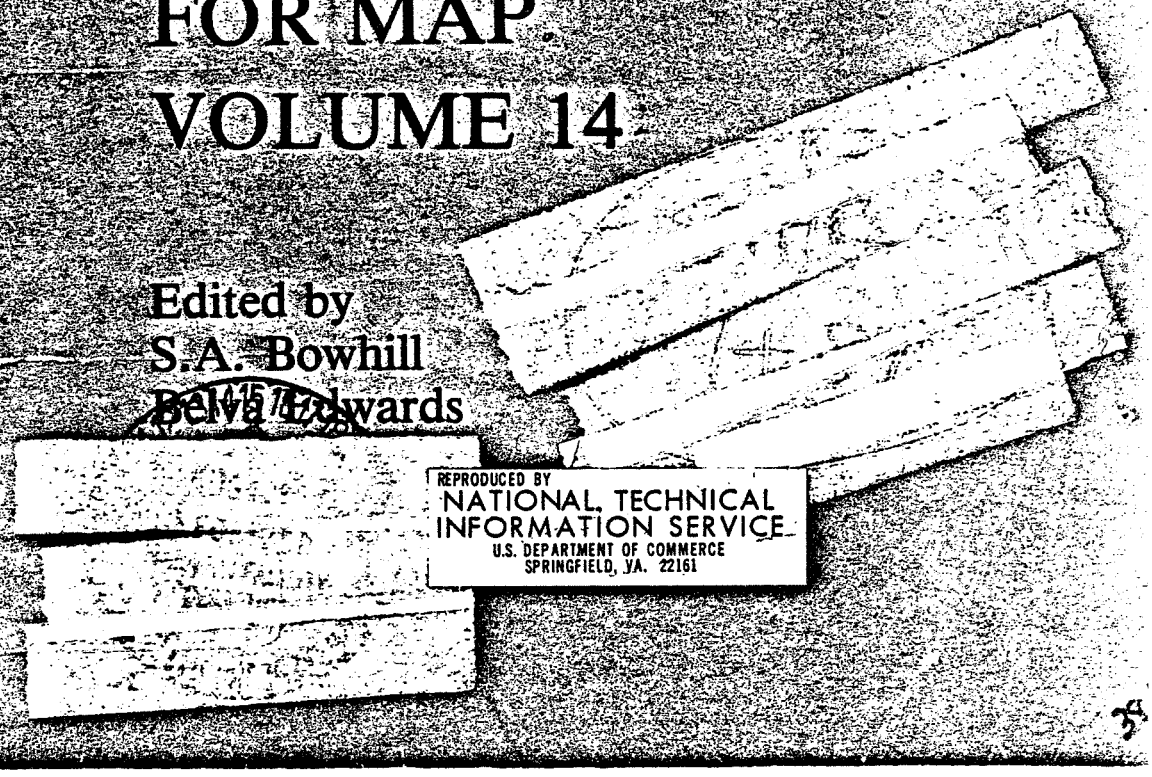

Edited by
S.A. Bowhill
Belva Edwards

ICSU

International Council of Scientific Unions

SCOSTEP

Scientific Committee on Solar-Terrestrial Physics
K. D. Cole, President
J. G. Roederer, Vice President
C. H. Liu, Scientific Secretary

MAP ORGANIZATION

MIDDLE ATMOSPHERE PROGRAM STEERING COMMITTEE

S. A. Bowhill, SCOSTEP, Chairman
K. Labitzke, COSPAR, Vice Chairman
C. H. Liu, SCOSTEP, Secretary

R. D. Bojkov, WMO
A. D. Danilov, COSPAR
J. C. Gille, COSPAR
A. H. Manson, SCOSTEP
I. Hirota, IUGG/IAMAP
J. W. King, URSI
L. R. Megill, IUGG/IAGA
T. Nagata, SCAR
R. G. Roper, IAMAP
P. C. Simon, IAU
J. Taubenheim, IUGG/IAGA
T. E. VanZandt, URSI
M. Wada, IUPAP

MAP STANDING COMMITTEES

Data-Management -- G. Hartmann and I. Hirota, Co-Chairmen
Dynamics Calendar -- T. E. VanZandt, Chairman
Publications -- C. F. Sechrist, Jr., Chairman

MAP STUDY GROUPS

MSG-5 Ions and Aerosols, F. Arnold and M. P. McCormick, Co-Chairmen
MSG-6 Scientific Aspects of an International Equatorial Observatory, S. Kato, Chairman
MSG-7 Penetration of Solar Radiation into the Atmosphere, J. E. Frederick, Chairman
MSG-8 Atmospheric Chemistry, G. Witt, Chairman
MSG-9 Measurement of Middle Atmosphere Parameters by Long Duration Balloon Flights, J. E. Blamont, Chairman

APPROVED MAP PROJECTS

	Coordinator		Coordinator
AMA:	T. Hirasawa	GOSSA:	M. P. McCormick
ATMAP:	J. M. Forbes	GRATMAP:	M. A. Geller
CAMP:	G. Witt	MAE:	N. C. Maynard
CLIMAT:	J. M. Russell	MSTRAC:	P. K. Rastogi
DYNAMICS:	K. Labitzke	OZMAP:	D. F. Heath
GLOBMET:	R. G. Roper	SSIM:	P. C. Simon
GLOBUS:	D. Offermann	WINE:	U. von Zahn

MAP REGIONAL CONSULTATIVE GROUP

Europe M. L. Chanin, Chairman

URSI/SCOSTEP Workshop on Technical Aspects of MST Radar

May 22-25, 1984

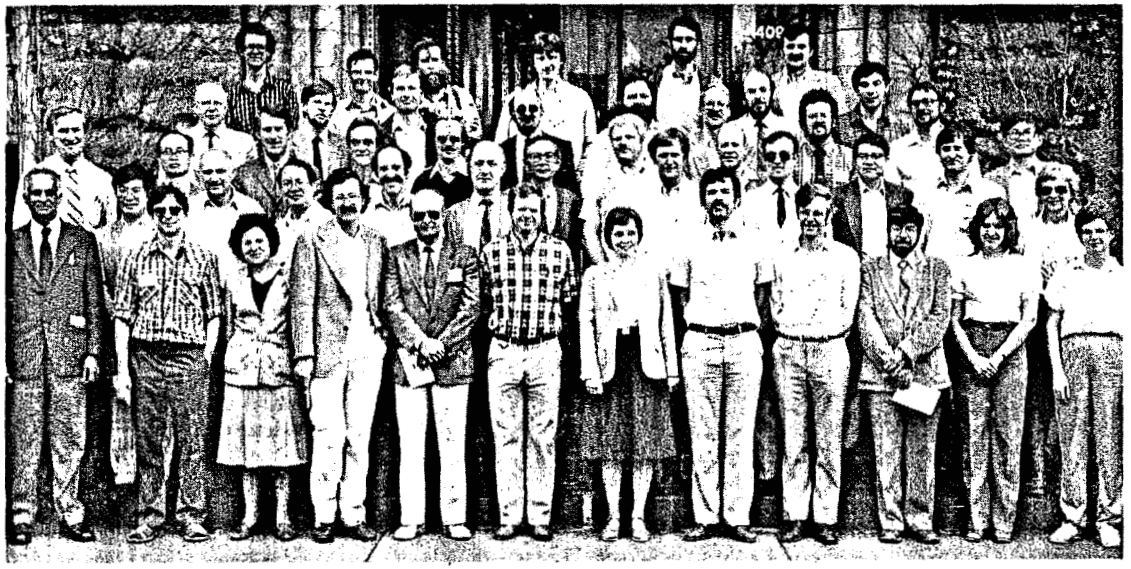

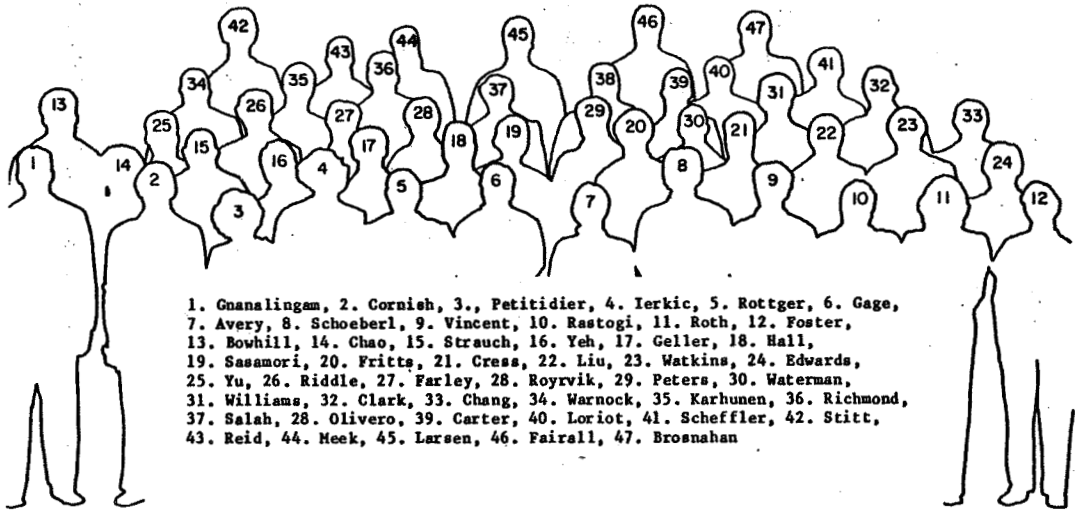

1. Gnanalingam, 2. Cornish, 3., Petitidier, 4. Ierkic, 5. Rottger, 6. Gage,
7. Avery, 8. Schoeberl, 9. Vincent, 10. Rastogi, 11. Roth, 12. Foster,
13. Bowhill, 14. Chao, 15. Strauch, 16. Yeh, 17. Geller, 18. Hall,
19. Sasamori, 20. Fritts, 21. Cress, 22. Liu, 23. Watkins, 24. Edwards,
25. Yu, 26. Riddle, 27. Farley, 28. Royrvik, 29. Peters, 30. Waterman,
31. Williams, 32. Clark, 33. Chang, 34. Warnock, 35. Karhunen, 36. Richmond,
37. Salah, 28. Olivero, 39. Carter, 40. Loriot, 41. Scheffler, 42. Stitt,
43. Reid, 44. Meek, 45. Larsen, 46. Fairall, 47. Brosnahan

M I D D L E

A T M O S P H E R E

P R O G R A M

HANDBOOK FOR MAP

Volume 14

Papers presented at the
URSI/SCOSTEP Workshop on
Technical Aspects of MST Radar
May 22-25, 1984

Edited by

S. A. Bowhill
Belva Edwards

December 1984

Published for the ICSU Scientific Committee on Solar-Terrestrial Physics (SCOSTEP) with financial assistance from the National Aeronautics and Space Administration Contract NASW 3805 and Unesco Subvention 1983-1984

Copies available from SCOSTEP Secretariat, University of Illinois, 1406 W. Green Street, Urbana, Illinois 61801

FOREWORD

The Second Workshop on Technical Aspects of MST Radar was held May 22-25, 1984 and this volume contains the papers presented at that meeting.

This Workshop was a successor to the first Workshop, held on May 23-27, 1983, papers from which were published in HANDBOOK FOR MAP, VOL. 9. As before, the topics were divided into nine major topics, with a Keynote Speaker for each. These keynote addresses were modified in the light of discussions presented at the meeting.

The continued growth in use of the technique is reflected by descriptions of seven new MST radars in Section 9, beyond those which were described in the previous Workshop just one year before.

The availability of new results from MST radars during the Middle Atmosphere Program has given a major impetus to studies of the dynamics of the stratosphere and mesosphere, as witnessed by a greatly increased volume of publications of theoretical and experimental results, leading to a greatly expanded understanding of the physics of the middle atmospehre.

My Co-Organizer, Dr. C. H. Liu, and I again would like to thank the sponsoring organizations (The International Union of Radio Science, URSI, and the Scientific Committee on Solar-Terrestrial Physics, SCOSTEP), and the conveners and discussion leaders for their unstinted contributions to the success of the meeting. The staff and students of the Aeronomy Laboratory, under the leadership of Mrs. Belva Edwards, again ensured that the arrangements ran smoothly, and we are very grateful to them also.

S. A. Bowhill

SECOND WORKSHOP ON TECHNICAL ASPECTS OF MST RADAR
May 22-25, 1984

TABLE OF CONTENTS

D1

N85-32467

1. METEOROLOGICAL AND AERONOMICAL REQUIREMENTS FOR MST RADAR NETWORKS (Keynote Paper)

M. A. Geller

Laboratory for Planetary Atmospheres, Code 964
NASA/Goddard Space Flight Center
Greenbelt, MD 20771

INTRODUCTION

MST radar are phase coherent radars that measure the amplitude and Doppler shift of radio waves that are scattered back to the receiving antennas. For a monostatic system, the line-of-sight projection of the wind vector is obtained if one assumes that the atmospheric scatterers are being swept along with the wind velocity. The three-dimensional wind is then derived either by using multiple beams or by beam swinging. The turbulence intensity is derived either by measuring the backscattered power or by deriving the width of the autocorrelation function for the wind. Furthermore, some information on sharp changes in the atmospheric static stability (e.g. at the tropopause) can be obtained by looking for specular reflections. In the following, we will discuss how these MST measurement capabilities can contribute to various meteorological and aeronomical research areas.

TROPOSPHERE-STRATOSPHERE EXCHANGE

We can distinguish among various types of troposphere-stratosphere interactions. There are dynamical interactions. For instance, troposphere dynamics communicate with stratosphere and mesosphere dynamics through the vertical propagation of extratropical planetary waves, tropical waves, tides, and gravity waves. Extratropical planetary waves require global measurements and thus would require a global network of radars; however, since extratropical planetary wave motions are geostrophic, satellite measurements can be used for their study. On the other hand, since equatorial wave motions are ageostrophic their motions cannot be easily derived from satellite measurements, so MST radars can play a very important role in their study. Tides and gravity waves can also be studied by MST radars since they are capable of obtaining frequ ly space wind profiles with good altitude resolution.

On the subject of troposphere-stratosphere mass exchange, tropospheric air has long been thought to enter the stratosphere in the rising air of the Hadley circulation. More recently, however, evidence has been accumulating that this is not a symmetric process but takes place in conjunction with the intense convective activity that occurs in the Indonesian-Malaysian sector in the November-March period and over the Bay of Bengal and India during the Monsoon. Extensive aircraft programs are being mounted to study this process. MST radars could study these processes if they were located properly. For instance, a meridional chain of MST radars in the tropics could study the Hadley ciculation, and a zonal chain could study the Walker circulation. It should be noted that the first "equatorial" ST radar has recently been established at an island location at 158°E and 7°N.

Several groups in the world are making plans to establish prototype ST radar networks. One such network has already been operated for about one year in Colorado by NOAA's Wave Propagation Laboratory. The Australian Bureau of Meteorology and CSIRO are planning to establish a network to enhance the prediction of cold fronts during the summer season. The Pennsylvania State University is planning a network of three ST radars to study mesoscale dynamics, and finally NOAA is considering establishing an extensive ST network throughout the middle United States to provide data for their mesoscale forecasting models.

Given that more extensive ST networks are foreseen in the near future, various issues arise. Some of these are as follows:

(1) Since ST network data can be very valuable for both operational and research purposes, how can we best ensure that valuable information on gravity wave motions, for example, are not lost in the data reduction process and that the ST network data are available to be used for research purposes.

(2) It is very important that mesoscale modelers participate in the planning of future mesoscale ST networks.

Stratospheric air is thought to descend into the troposphere in extratropical latitudes in conjunction with tropopause folding events. Some work has been done on measuring the transverse circulation around the jet stream and more could be done on this.

ST radars can also obtain climatologies of clear air turbulence and vertical velocity. There is, however, the nagging problem of the apparent paradox between radar and aircraft measurements of lower stratosphere turbulence. Meteorological aircraft data indicate that turbulence plays a negligible role in vertical constituent transport in the lower stratosphere. Radar data indicates that turbulence plays a much larger role. This apparent discrepancy needs resolution. Balloon measurements of turbulence can play a very large role in this.

SEVERE WEATHER AND FRONTS

Conventional meteorological radar only gives returns when precipitation is present. ST radar networks potentially could be used to follow the organization of severe weather in clear air before precipitation begins. Given that millimeter radars can sense clouds in the precipitation phase, a properly conceived radar network could sense the entire life cycle of mesoscale events, occurring within such a network.

GRAVITY WAVES FROM STRATOSPHERE TO MESOSPHERE

MST radars can get wind profiles with very good height and time resolution. This makes them very well suited for gravity-wave studies. So far, there have been measurements of wave spectra, wave momentum fluxes, and some process studies from selected cases. MST networks are required to measure such important wave parameters as horizontal wavelength and wave phase velocity. In interpreting MST radar data on gravity waves it is very important to be aware that gravity waves can travel thousands of km from their tropospheric source and reacn mesospheric altitudes days after being launched. This, in addition to the fact that radiative damping processes will absorb many gravity waves in the stratosphere, should be kept in mind when analyzing mesospheric gravity wave data.

GENERAL CIRCULATION OF THE MIDDLE ATMOSPHERE INCLUDING EQUATORIAL WAVES

Since the general circulation is, by definition, a global scale phenomenon, a global network of MST radars would be required to study the general circulation of the middle atmosphere in a straightforward manner. Radar data and temperature data would still be required. On the other hand, MST data from even a few stations are valuable as is evidenced by the significance of the radar measurements of meridional motions in the mesosphere. One difficulty, however, is to demonstrate the representativeness of single station measurements. This can be done by using satellite data, for example.

Single station statistics of wind profile fluctuations can be quite useful to test general circulation model simulations. Also, radar data together with satellite data can be used to look at the transition from a predominantly geostrophic to an ageostrophic regime.

One issue to which MST radars can contribute significantly is in the study of stratopsheric gravity waves. It is now appreciated that gravity waves play a very important role in the general circulation of the mesosphere, but it is not known how important a role they play in the stratosphere.

Finally, an equatorial MST radar could be used to look at the interactions between tropical waves and the mean flow.

WIND AND CAT PROFILING

As was mentioned in the introduction, MST radars provide profiles of wind velocity and turbulence. These profiles could be used operationally (e.g. near airports), could substitute for rawinsonde wind measurements in providing initial conditions for meteorological forecasts, as well as be used for research purposes.

Experience with the Colorado Wind-Profiling Network has illustrated some of the practical difficulties that are encountered with an MST radar network. These include frequency allocation problems, altitude-limitations on data acquisition, radio interference problems, site selection; and slow data processing procedures.

TROPOPAUSE HEIGHT DETERMINATION

It has been demonstrated that there is enhanced backscattered power from the tropopause for a vertically pointing beam relative to that for one pointing off-vertical due to specular reflection. These measurements can be used to obtain ground-based measurements of tropopause heights. These measurements can be quite useful. For example, such knowledge can be helpful in satellite temperature retrievals.

SYNOPTIC-SCALE DYNAMICS WITH VERTICAL VELOCITY

MST radars are unique in their ability to directly measure vertical velocities instead of deriving it indirectly as is usually done in meteorology. Experience has shown that one can statistically obtain large-scale vertical velocities at a single radar site to ± 2 cm s^{-1} with about nine hours of data during quiet times. These "quiet" times have been found to occur about 10-40% of the time depending on the terrain of the radar site. Studies have shown that radar measured vertical velocities are usually quite similar to those derived from meteorological models but have a tendency to be a bit larger than the derived vertical velocities. The reasons for this are not understood at the present time.

OPTIMIZATION OF ST RADAR NETWORKS FOR STUDIES OF ATMOSPHERIC STRUCTURE AND PROCESSES

ST networks can contribute valuable data for many studies of the atmosphere. Among these are studies of mesoscale dynamics and studies of tropospheric sources for gravity waves. It is not clear that we can define a single optimal network of all these purposes or indeed whether it is best to use a variety of network configurations with transportable ST radars to investigate phenomena with various radar spacings. We believe that studies should be carried out with portable ST systems to investigate optimal spacings. We also believe that studies with mesoscale model simulations can help in establishing

desired network configurations.

SUMMARY

Since equatorial wave motions are ageostrophic their motions cannot be derived easily from satellite measurements, so MST radars can play a very important role in their study. Tides and gravity waves can also be studied by MST radars since they are capable of obtaining frequently spaced wind profiles with good altitude resolution.

A meridional chain of MST radars in the tropics could study the Hadley circulation, and a zonal chain could study the Walker circulation.

ST radars can also obtain climatologies of clear air turbulence and vertical velocity. Balloon measurements of turbulence can play a very large role in this.

A properly conceived radar network could sense the entire life cycle of mesoscale events occurring within such a network.

In interpreting MST radar data on gravity waves it is very important to be aware that gravity waves can travel thousands of km from their tropospheric source and reach mesospheric altitudes days after being launched. This, in addition to the fact that radiometric damping processes will absorb many gravity waves in the stratosphere, should be kept in mind when analyzing mesospheric gravity-wave data.

One difficulty, however, is to demonstrate the representativeness of single station measurements. Single station statistics of wind profile fluctuations can be quite useful to test general circulation model simulations.

It is now appreciated that gravity waves play a very important role in the general circulation of the mesosphere, but it is not known how important a role they play in the stratosphere.

Experience with the Colorado Wind-Profiling Network has illustrated some of the practical difficulties that are encountered with an MST radar network. These include frequency allocation problems, altitude limitations on data acquisition, radio interference problems, site selection, and also data processing procedures.

These measurements can be used to obtain ground-based measurements of tropopause heights. These measurements can be quite useful. For example, such knowledge can be helpful in satellite temperature retrievals.

MST radars are unique in their ability to directly measure vertical velocities instead of deriving it indirectly as is usually done in meteorology, but have a tendency to be a bit larger than the derived vertical velocities. The reasons for this are not understood at the present time.

It is not clear that we can define a single optimal network of all these purposes or indeed whether it is best to use a variety of network configurations with transportable ST radars to investigate phenomena with various radar spacings.

We believe that studies should be carried out with portable ST systems to investigate optimal network spacings. We also believe that studies with mesoscale model simulations can help in establishing desired network configurations.

1.1A TROPOSPHERIC-STRATOSPHERIC EXCHANGE

C. R. Cornish

School of Electrical Engineering
Cornell University, Ithaca, NY 14853

The topic of interaction between the troposphere and stratosphere has been reviewed recently by MURGATROYD and O'NEILL (1980) and HOLTON (1983), the highlights of which are described below. Circulation in the extratropical winter stratosphere is characterized by a zonal westerly flow and planetary waves of zonal wave numbers 1 and 2, which appear to be driven by vertically propagating forced planetary waves from the troposphere. The tropospheric sources attributed to these waves are orographic forcing and differential heating. On the other hand, the easterly flow of the summer extratropical stratosphere is undisturbed as planetary waves are blocked from reaching the annual variation, transient planetary wave activity varies the mean flow, resulting in stratospheric sudden warmings, which are attributed to the breakdown of the stratospheric polar night jet and coincide with enhanced upward fluxes of eddy energy from the troposphere. In contrast, the tropical stratospheric circulation is dominated by the 26-month period quasi-biennal oscillation which is driven by wave-mean flow interactions between eastward Kelvin waves and westward Rossby waves. These Kelvin and Rossby waves are forced in the troposphere, possibly by large-scale tropical convective disturbances.

Much of the observational evidence of large scale tropospheric-stratospheric exchange has been obtained by radiosonde and satellite radiance data. So far MST radars have made minimal contributions, in part due to their recent use as a meteorological tool, intermittent operation at some facilities and sparse geographic distribution. However, as more MST facilities come on-line in more locations, the good time and height resolution data throughout the troposphere and much of the stratosphere obtainable by MST radars will enhance the detail of stratospheric and tropospheric circulations and interactions. On smaller scales MST radars have already been used to examine convective forcing from the troposphere into the stratosphere and subsequent launching of gravity waves (LARSEN et al., 1982). Observations of persistent turbulent layers in the stratosphere over Arecibo, attributable to inertial oscillations, appear to propagate away from a source region near the tropopause (SATO and WOODMAN, 1982).

While much observational and theoretical interest has been devoted to effects of the troposphere on the stratosphere, few observations have been made and little is known of stratospheric effects on the troposphere. HOLTON (1983) suggests that the QBO may affect the interannual variability of the equatorial troposphere and sudden warmings may affect high latitude regions. MURGATROYD and O'NEILL (1980) suggest that stratospheric conditions may affect the upward propagation of planetary waves and cite two possible mechanisms. One proposed by Hines is the reflection of energy from higher altitudes to the regions of planetary-wave generation in the troposphere and subsequent constructive or destructive interference. The other proposed by Bates is a sensitive connection between planetary-wave structure and horizontal heat fluxes in the troposphere and stratospheric wind profile and static stability.

In summary, MST radars offer the availability of high resolution wind data in height and time needed to observe interactions between the troposphere and stratosphere. The lack of geographic coverage (e.g. equatorial regions) and insufficient data bases at many MST facilities presently inhibit studies of large-scale interactions. At present MST radars can be used to examine smaller scale interactions.

REFERENCES

Holton, J. A. (1983), The stratosphere and its links to the troposphere, in Large-Scale Dynamical Processes in the Atmosphere, B. J. Hoskings and R. P. Pearce, eds., Academic Press, 277-304.

Larsen, M. F., W. E. Swartz and R. F. Woodman (1982), Gravity-wave generation by thunderstorms observed by a vertically-pointing 430 MHz radar, Geophys. Res. Lett., 9, 571-574.

Murgatroyd, R. J. and A. O'Neill (1980), Interaction between troposphere and stratosphere, Phil. Trans. R. Soc. Lond. A, 296, 87-102.

Sato, T. and R. F. Woodman (1982), Fine altitude resolution radar observations of the upper-tropospheric and lower-stratospheric winds and waves, J. Atmos. Sci., 39, 2539-2545.

1.2A OBSERVATIONS OF FRONTAL ZONE STRUCTURES WITH A VHF DOPPLER RADAR AND RADIOSONDES*

M. F. Larsen

Cornell University
Ithaca, NY 14853

J. Rottger**

EISCAT Scientific Association
Kiruna, Sweden

INTRODUCTION

The SOUSY-VHF-Radar is a pulsed coherent radar operating at 53.5 MHz and located near Bad Lauterberg, West Germany. Since 1977, the facility, operated by the Max-Planck-Institut fur Aeronomie, has been used to make a series of frontal passage observations in the spring and fall. Experiments in winter have been difficult because part of the transmitting and receiving array is usually covered by snow during that part of the year. Wavelengths around 6 m are known to be sensitive to the vertical temperature structure of the atmosphere (GREEN and GAGE, 1980; RASTOGI and ROTTGER, 1982). Thus, it has been possible to use radars operating at frequencies near 50 MHz to locate the tropopause. Comparisons between radar data and radiosonde data have shown that there is a large gradient in the radar reflectivity at the height where the radiosonde tropopause occurs.

An experiment carried out by ROTTGER (1979) on March 15-16, 1977, showed that the radar's sensitivity to the vertical temperature structure could also be used to locate the position of fronts. The SOUSY-VHF-Radar consists of a transmitting array, also used for receiving in some configurations, that can be scanned in the off-vertical direction but not at sufficiently low elevation angles to study the horizontal extent of structures as extended as fronts. GAGE and BALSLEY (1978), BALSLEY and GAGE (1980), ROTTGER (1980), and LARSEN and ROTTGER (1982) have reviewed UHF and VHF Doppler radar techniques and applications to atmospheric research. In the experiments described here, the radar was operated in the spaced antenna mode. ROTTGER and VINCENT (1978) and VINCENT and ROTTGER (1980) have described the method and its advantages. The transmitting array consists of 196 Yagi antennas, and the receivers are three separate arrays of 32 Yagis each. The effective antenna aperture was 2500 m^2, the applied average transmitter power was typically 20 kW, and the height resolution was 150 m. Vertical profiles of the reflectivity were obtained in each of the three receiver arrays, and it was found that besides the enhancement of the signal strength associated with the tropopause region, there was also a secondary band of enhanced reflectivities stretching downward from the upper to the lower troposphere. Comparisons between the radar data and data from a nearby radiosonde station show that the band is associated with the temperature gradients in a passing frontal zone. The vertical and horizontal velocities were also measured during the experiments, but they will not be discussed here.

The results of analyzing two events have been presented by ROTTGER (1979, 1981), ROTTGER and SCHMIDT (1981), and LARSEN and ROTTGER (1983). However, in

* Published also in Preprint Volume, 22nd Conference on Radar Meteorology, Zurich, September 10-14, 1984, 489-494.

**Presently at Arecibo Observatory, Arecibo, Puerto Rico, on leave from Max-Planck-Institut fur Aeronomie, Lindau, W. Germany.

this paper we would like to summarize a more complex data set consisting of a series of five observations of frontal structure made with the SOUSY-VHF-Radar in March 1977, March 1981, November 1981, February 1982, and April 1984. The extensive data set shows results essentially in agreement with the preliminary results. Comparison of time/height cross sections of reflectivity measured with the radar and potential refractivity gradients calculated from radiosonde data taken at a nearby location show good agreement. Therefore, we conclude that the radar is detecting the temperature structure associated with the front and that the enhancement in reflectivities is not due to precipitation or other very localized processes. Also, we have found that the radar can be used to locate the fronts consistently, even in some cases when the fronts are rather weak.

MARCH 15-16, 1977

At 0000 UTC on March 15, 1977, a low pressure center in the North Atlantic was propagating eastward toward the British Isles. The associated warm front and the trailing cold front extended southward from the center of the low. The warm front at the surface had traversed France and West Germany by 0000 UTC on March 17. Reflectivities measured with the SOUSY-VHF-Radar from 1200 UTC on March 15 to 0900 UTC on March 16 are shown in Figure 1. Cloud cover observations from two nearby meteorological observatories are shown below the reflectivities.

Of particular interest is the band of enhanced echoes stretching from 4 km altitude at 0000 UTC on March 16 to 2 km altitude at 0600 UTC. Extrapolating the slope of the band to the surface gave a time for the surface frontal passage in agreement with that derived from the weather charts. Comparison between the temperature cross section perpendicular to the front and the features seen in the radar reflectivity data showed good agreement.

MARCH 6-7, 1981

Figure 2 shows the reflectivities observed with the radar between 1200 UTC on March 6 and 0900 UTC on March 7, 1981. The contour interval is 2 dB, and the stippling indicates regions of higher reflectivity. The signal strength generally decreases with height in the troposphere but increases by 10-12 dB over a vertical distance of 0.5 km or so at the tropopause. The tropopause determinations from Hannover radiosonde data is shown by the heavy bars in the figure. The bar corresponding to 0900 UTC was actually obtained at 1200 UTC, the standard synoptic time.

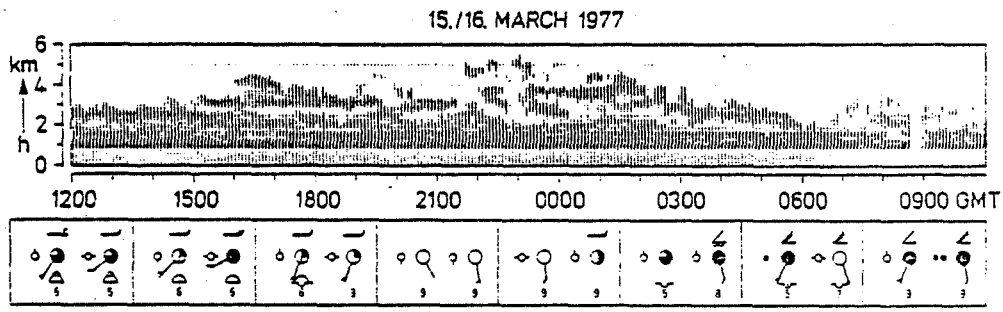

Figure 1. Radar reflectivities as a function of height and time measured by the SOUSY-VHF-Radar. Observations from the meteorological observatories at Kassel, 60 km southwest, and Hannover, 90 km north-northwest, are shown on the left and right sides of the boxes, respectively.

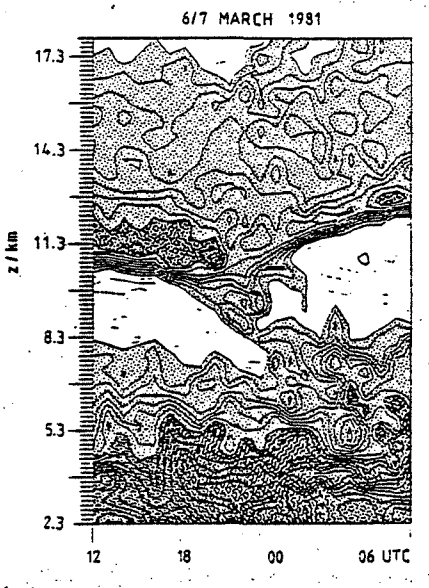

Figure 2. Radar reflectivities as a function of height and time. Contour interval is 2 dB. Stippled areas show higher reflectivities.

The feature of particular interest is the band of enhanced echo strength stretching downward from the tropopause beginning at approximately 1700 UTC. The feature is associated with a warm front that was essentially parallel to the NNW-SSE direction and propagated eastward across West Germany and past the radar. The radar reflectivity is proportional to M^2 with M given by

$$M = -77.6 \times 10^{-6} \frac{P}{T} \left\{\frac{\partial \ln\theta}{\partial z}\right\} \cdot \left\{1 + \frac{15500}{T}\left(1 - \frac{1}{2}\frac{\partial \ln q/\partial z}{\partial \ln\theta/\partial z}\right)\right\} \quad (1)$$

where P is in millibars, T is absolute temperature, θ is potential temperature, and q is the specific humidity. The contours of M^2 calculated from the Hannover radiosonde data are shown in Figure 3 with a contour interval of 4 dB. Once again, the stippled areas correspond to higher values. The agreement between the observations and the calculated values is quite good. The contours of M^2 show the increase in the height of the tropopause at 1200 UTC on March 7. Also, the enhancement of the echoes between 6.8 and 8.3 km after 0000 UTC on March 7 is apparent. There is an indication of the frontal echo band in the values of the potential refractivity at 0000 UTC as shown by the feature near 8.75 km altitude. However, the time resolution of the radiosonde data is not sufficient to show the details of the frontal zone structure.

NOVEMBER 4-10, 1981

In the first half the November 1981 observations were made over a period of more than a week. The reflectivities for the period from November 4 (Day 308) to November 10 (Day 314) are shown in Figure 4. On Day 308, the reflectivities decrease with altitude in the troposphere and then begin to increase just below the tropopause. A cold frontal band is observed after 1600 UTC and stretches upward in altitude with time as would be expected. Two warm frontal bands are evident as enhanced reflectivity regions moving downward with time. The first is observed near the tropopause at 0000 UTC on Day 309. The second is first seen at 0600 UTC on Day 310.

Potential temperatures were calculated from the Hannover radiosonde data

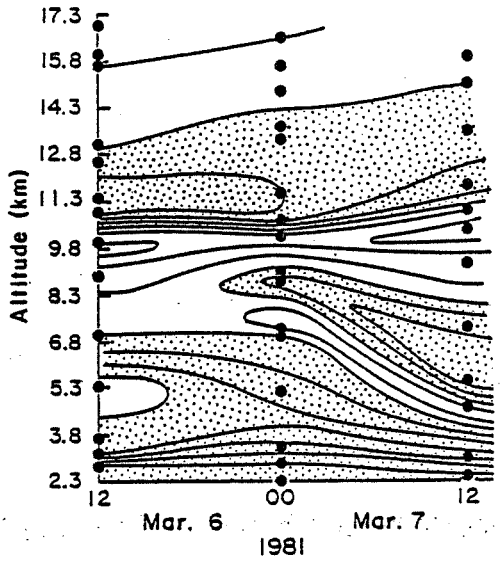

Figure 3. Gradient of potential refractive index calculated from Hannover radiosonde data for the time period corresponding to the reflectivities shown in Figure 2. Stippled areas correspond to larger values.

and have been plotted and contoured on a scale similar to that used for the reflectivities. The results are shown in Figure 5. The same general features are evident in both figures. The packing of the potential temperature contours is characteristic of the tropopause and stratosphere. The lower boundary of the packing is located at the same height as the increase in the radar reflectivities associated with the tropopause. The cold front and the second warm front show up clearly in the potential temperature data, but the first warm frontal band is not as clearly evident. However, satellite photos for this time show two distinct cloud bands.

During the time from Nov. 4 to 10, the radar site was in a region of northerly flow on the eastern side of a stationary high pressure system centered over the British Isles. The fronts that traversed the radar site were confined to the upper troposphere, as the potential temperature cross section shows.

FEBRUARY 7-9, 1982

The reflectivities measured by the radar during the period from February 7 to 9, 1982, are shown in Figure 6. Once again the stippled areas represent

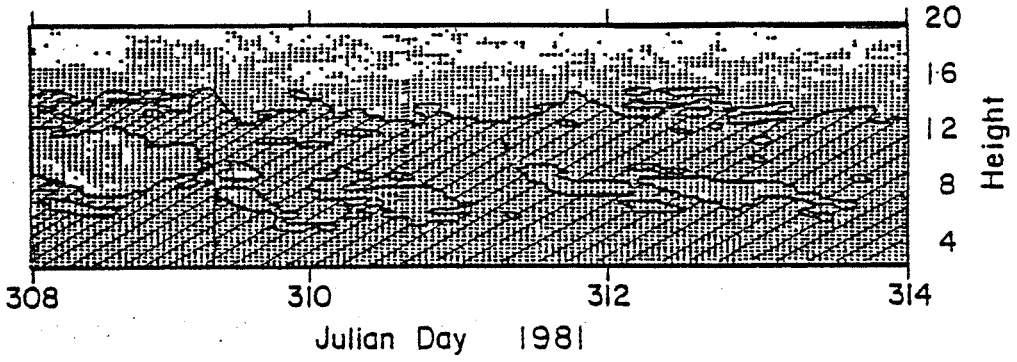

Figure 4. Reflectivities measured by the SOUSY-VHF-Radar during the period from Nov. 4 to 10, 1981.

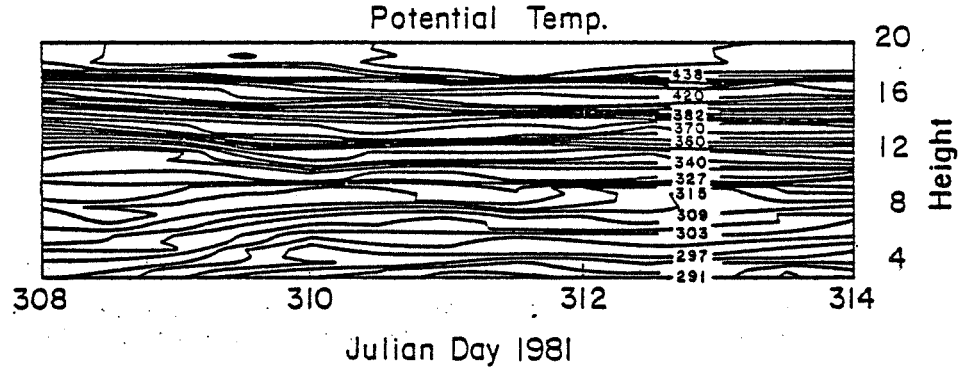

Figure 5. Potential temperatures calculated from the Hannover radiosonde data for the period corresponding to the radar reflectivities shown in Figure 4.

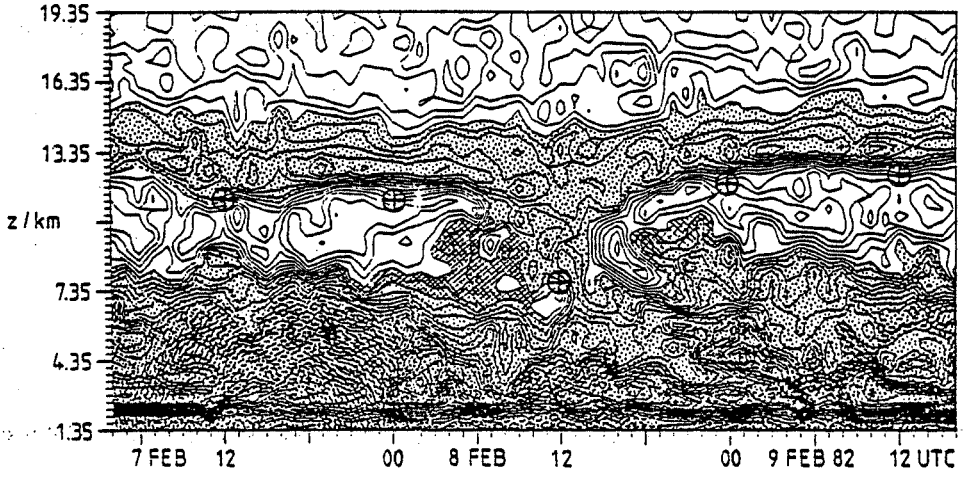

Figure 6. Same as Figure 2 but for February 7-9, 1982.

larger reflectivities. However, this time the intermediate values have been cross hatched, as well. The typical features already noted in the previous examples are present. The echo strength decreases with altitude in the troposphere, but there is an enhancement in the reflectivities in the upper troposphere associated with the temperature discontinuity that defines the location of the tropopause. The heavy circles show the tropopause height determined from the Hannover radiosonde.

Near 1200 UTC on February 8, a band of enhanced reflectivities associated with a warm front stretches downward from the tropopause. Beginning at approximately 0200 UTC on February 8, a band of intermediate reflectivities stretches upward in connection with a cold front associated with the low pressure system. The cold front for this particular event was much weaker than the warm front, and the difference in strength accounts for the difference in the magnitude of the reflectivities.

We have also calculated the potential refractive index gradient M^2 based on Hannover radiosonde data. The vertical time section is shown in Figure 7. The same features are evident in both the reflectivity and M^2 cross sections. More detailed analysis of the event is given by LARSEN and ROTTGER (1983).

APRIL 9-13, 1984

Observations were made with the SOUSY-VHF-Radar over a five day period in April 1984. From 1200 UTC on April 9 until 1200 UTC on April 11, the radar was located in a region of northerly flow on the eastern side of a stationary high pressure system. During this time a number of mesoscale disturbances with horizontal scales of 50 to 100 km developed in the region. Most did not pass the radar, but one such system was observed near 0000 UTC on April 11. The radar reflectivities are shown in Figure 8.

The signal strength showed an enchancement in the upper troposphere during the passage of the mesoscale system, but the feature is not as narrow and does not show the tilt characteristic of the other frontal passage observations that we have presented. Late in the day on April 12 a surface frontal passage took place, as shown by the weather charts and satellite photographs. The features typical of a frontal passage are clearly present in the reflectivity data beginning at about 1600 UTC on April 11. A band of enhanced echoes begins to descend from the height of the tropopause and stretches downward toward the surface. The air mass following the frontal passage then has a higher tropo-

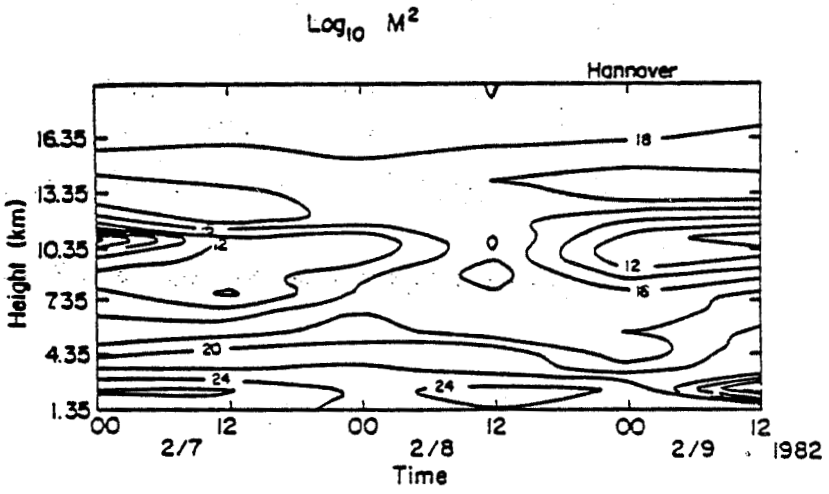

Figure 7. Same as Figure 3 but corresponding to the data shown in Figure 6.

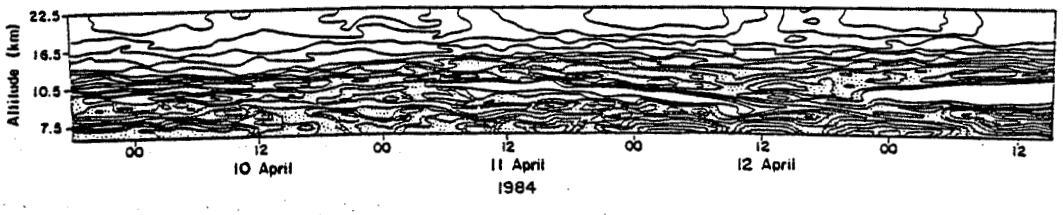

Figure 8. Same as in Figure 2 but for the period April 9-13, 1984.

pause height than the air mass prior to the frontal passage. The morphology in this event is very similar to the morphology in the other four events presented here.

CONCLUSION

Observations of five separate frontal passage events made with the SOUSY-VHF-Radar have shown that a radar operating at a frequency near 50 MHz can be used to detect the location of fronts on a routine basis. The SOUSY-VHF-Radar does not operate on a continuous basis. While the observation periods were chosen on the basis that it would be likely that a frontal passage would take place at the location of the radar, no attempt was made to choose only the strongest or most developed fronts. In fact, the front observed in April 1984 and the cold front observed in February 1982 did not have particularly strong temperature gradients.

The comparisonsbetween radar and radiosonde data have shown good agreement, indicating that the features seen in the radar reflectivity data are characteristic of the frontal temperature structure and are not associated with precipitation or local convection. That is particularly true since the separation between the radar site and the nearest radiosonde station is approximately 90 km.

REFERENCES

Balsley, B. B. and K. S. Gage (1980), The MST radar technique: Potential for middle atmospheric studies, Pure Appl. Geophys., 118, 452-493.

Gage, K. S. and B. B. Balsley (1978), Doppler radar probing of the clear atmosphere, Bull. Am. Meteorol. Soc., 59, 1074-1093.

Green, J. L. and K. S. Gage (1980), Observations of stable layers in the troposphere and stratosphere using VHF radar, Radio Sci., 15, 395-406.

Larsen, M. F. and J. Rottger (1982), VHF and UHF Doppler radars as tools for synoptic research, Bull. Am. Meteorol. Soc., 63, 996-1008.

Larsen, M. F. and J. Rottger (1983), Comparison of tropopause height and frontal boundary locations based on radar and radiosonde data, Geophys. Res. Lett., 10, 325-328.

Rastogi, P. K. and J. Rottger (1982), VHF radar observations of coherent reflections in the vicinity of the tropopause, J. Atmos. Terr. Phys., 44, 461-469.

Rottger, J. (1979), VHF radar observations of a frontal passage, J. Appl. Meteorol., 18, 85-91.

Rottger, J. (1980), Structure and dynamics of the stratosphere and mesosphere revealed by VHF radar investigations, Pure Appl. Geophys., 118, 494-527.

Rottger, J. (1981), The capabilities of VHF radars for meteorological observations, Proc. IAMAP Symp., Hamburg, Aug. 25-28, 1981, European Space Agency, ESA-SP-165, Paris, France.

Rottger, J. and G. Schmidt (1981), Characteristics of frontal zones determined from spaced antenna VHF radar observations, Preprint Vol., 20th Conf. on Radar Meteorology, Nov. 30-Dec. 3, 1981, Boston, Mass., AMS, Boston, Mass.

Rottger, J. and R. A. Vincent (1978), VHF radar studies of tropospheric velocities and irregularities using spaced antenna techniques, Geophys. Res. Lett., 5, 917-920.

Vincent, R. A. and J. Rottger (1980), Spaced antenna VHF radar observations of tropospheric velocities and irregularities, Radio Sci., 15, 319-335.

D4 N85-32470

1.3A EXCERPTS FROM THE PAPER: RESEARCH STATUS AND RECOMMENDATIONS FROM THE ALASKA WORKSHOP ON GRAVITY WAVES AND TURBULENCE IN THE MIDDLE ATMOSPHERE, FAIRBANKS, ALASKA, 18-22 JULY 1983*

D. C. Fritts[1], M. A. Geller[2], B. B. Balsley[3], M. L. Chanin[4], I. Hirota[5], J. R. Holton[6], S. Kato[7], R. S. Lindzen[8], M. R. Schoeberl[2], R. A. Vincent[9], and R. F. Woodman[10]

... 3. THEORETICAL DISCUSSION

Internal gravity waves are disturbances whose intrinsic frequencies $k(c - \bar{u})$ are smaller than the Brunt-Vaisala frequency (N). Their importance arises because:

(1) they are the major components of the total flow and temperature variability fields of the mesosphere (i.e., shears and lapse rates) and hence constitute the likely sources of turbulence;
(2) they are associated with fluxes of momentum that communicate stresses over large distances. For example, gravity waves exert a drag on the flow in the upper mesosphere. However, in order for gravity waves to exert a net drag on the atmosphere, they must be attenuated.

There are two general types of processes that seek to attenuate gravity waves -- dissipation and saturation. Dissipation is any process that is effective independent of the wave amplitude, while saturation occurs when certain wave amplitude conditions are met. Radiative damping is an example of dissipation, while convective overturning, which arises when the wave-breaking condition $|\partial T/\partial z| \sim \Gamma$ (or $u' \sim |c - \bar{u}|$) is met, is an example of saturation. The two processes are not mutually exclusive.

Saturation implies that the wave field has reached amplitudes such that either secondary instabilities (LINDZEN, 1981; DUNKERTON, 1982a) or nonlinear interactions, such as the parametric subharmonic instability (LINDZEN and FORBES, 1983), can occur, which limit further wave growth. In the atmosphere, amplitudes sufficient for saturation may result either from exponential growth with height or from the approach of a wave packet to a critical level. The saturation mechanism considered most common is the generation of convective or Kelvin-Helmholtz (KH) shear instabilities. Both instabilities were observed in the laboratory study of gravity-wave propagation by KOOP and MCGEE (1983), but

* Bull. Am. Meteorol. Soc., 65, 149-159.

1 Geophysical Institute, University of Alaska, Fairbanks, AK 99701
2 Laboratory for Planetary Atmospheres, NASA Goddard Space Flight Center, Greenbelt, MD 20771
3 Aeronomy Laboratory, National Oceanic and Atmospheric Administration, Boulder, CO 80303
4 Service d'Aeronomie du Centre Nationale de la Recherche Scientifique, Verrieres le Buisson, France
5 Geophysical Institute, Kyoto University, Kyoto 606, Japan
6 Department of Atmospheric Sciences, University of Washington, Seattle, WA 98195
7 Radio Atmospheric Science Center, Kyoto University, Uji 611, Japan
8 Department of Earth, Atmospheric and Planetary Sciences, Massachusetts Institute of Technology, Cambridge, MA 02139
9 Physics Department, University of Adelaide, Adelaide, South Australia, 5001
10 Instituto Geofisico del Peru, Sector Educacion, Apartado 3747, Lima 100, Peru

convective instabilities were found to dominate when both were possible. The local development of convective and dynamical instabilities may result in the radiation of secondary gravity waves (DUNKERTON and FRITTS, 1983); however, the most important result is the production of turbulence. Turbulence generation initially is confined to regions of dynamical or convective instability within the wave field. Following generation, turbulence may be advected away from the unstable zone, whereas the actively unstable region propagates with the wave.

The most important consequence of saturation on the dynamics of the large-scale circulation is the momentum deposition resulting from the amplitude-limiting mechanism (LINDZEN, 1981). Secondary effects produced by the turbulent layers include heat as well as constituent transport. The study by SCHOEBERL et al. (1983) suggests that the turbulent heat transport drives the mean state towards an adiabatic lapse rate. Using a quasi-linear initial-value model, WALTERSCHEID (1983) found that large-amplitude, gravity-wave saturation produces a rapid reduction in both the intrinsic phase velocity of the wave and the eddy diffusion needed to balance wave growth. There also is some heating due to wave and turbulence dissipation.

This description provides a very simplistic view of the saturation of an isolated monochromatic gravity wave. The detailed evolution of the wave field during saturation, including the production of turbulence and possible wave frequency broadening (WEINSTOCK, 1976; 1982), is not well understood. Advances in this area will have immediate consequences for observational programs. For example, to what extent can waves be partially reflected from neutrally buoyant layers produced by turbulent zones or from large velocity shears due to differential momentum deposition, and could we expect to see evidence of such reflections in the data? Reflection at an internal shock and wave scattering due to localized dissipation were observed in the numerical experiments of DUNKERTON and FRITTS (1983). Finally, there is some evidence that suggests that multiple wave interaction can lead to saturation, although this process has not been studied in detail.

The spatial and temporal variability of gravity waves entering the mesosphere is understood poorly at present. Clearly, the upward flux of waves at the stratopause is a function of the production of waves in the troposphere, their transmission, and zonal and meridional propagation (DUNKERTON, 1982b; SCHOEBERL and STROBEL, 1983). The obvious tropospheric gravity-wave sources are unstable wind shear, topography, and convection. Others may be important as well. Wind shear produces waves with phase velocities characteristic of tropospheric wind speeds, while topography generates gravity waves with a phase velocity distribution centered about zero. Of the three dominant gravity-wave sources, the phase velocity spectrum associated with convection is the least understood. However, it is reasonable to suppose that the phase speed distribution is broad and centered near tropospheric wind speeds. Characteristic scales and amplitudes, as well as the distribution and variability of the sources just mentioned are not well known at present (LINDZEN, 1983). Such information requires additional theoretical work and detailed tropospheric observations of gravity-wave forcing and structure.

The transmission of gravity waves into the mesosphere is controlled by their propagation in, and interaction with, a variable environment. Important effects include refraction, reflection, and critical-level absorption due to variations of $\bar{u}$ and N^2 with height. These variations cause changes in the vertical wavelength and group velocity of the wave and may lead to selective filtering of the gravity-wave spectrum (BOOKER and BRETHERTON, 1967; HINES and REDDY, 1967). For motions with small intrinsic frequencies, nonstationary mean flows and radiative damping also are likely to be important (FRITTS, 1982; SCHOEBERL et al., 1983). Spatial inhomogeneities of gravity-wave sources or transmissivity are likely to produce a vertical smoothing and broadening of the

zonally averaged momentum deposition, as well as the excitation of large-scale gravity waves and planetary wa.es. In order to understand the consequences of gravity-wave momentum deposition and turbulence production in the middle atmosphere, however, the morphology of the flux of gravity waves into and through the middle atmosphere must be better known. ...

... 4b. TOPICS

(1) Turbulence

Radar methods provide a powerful tool for studying turbulence in the middle atmosphere (for details, see BALSLEY and GAGE, 1980; ROTTGER, 1980). The backscattered echo power and the Doppler spectral width of the signal returns are related directly to turbulence intensity. The echo power is a direct measure of one spatial Fourier component of the refractive index variation produced by a turbulent region, while the spectral width (used with caution) is a measure of the variance of turbulence velocities.

Turbulence spatial characteristics already have been studied at a number of sites via the backscatter power structure. The presence of vertically thin, horizontally extended turbulent regions that exist for many hours has been noted in both the stratosphere and lower mesosphere (CZECHOWSKY et al., 1979; SATO and WOODMAN, 1982). While some exceptions to this general picture exist (i.e., in the high-latitude summer mesosphere), they probably can be considered typical.

Estimates of vertical diffusion can be made using statistical properties of the thin turbulent regions (WOODMAN et al., 1981). This is of particular importance in the current context, since enhanced diffusivity increases gravity wave damping and the corresponding mean flow accelerations. Estimates of stratospheric diffusion and turbulence dissipation have been obtained from the observed dispersion of rocket vapor trails (ROSENBERG and DEWAN, 1975) and from high-resolution balloon data (CADET, 1977) among other things. Current radar estimates of vertical diffusivity in the lower stratosphere suggest values that may be appreciably larger than those obtained by aircraft techniques (LILLY et al., 1974). Further measurements appear necessary to address this disparity.

The possibility of using radar systems with very good vertical resolution (tens of meters) to study the space-time structure of turbulence within the layers is exciting and should allow us to understand better the underlying generation mechanisms (i.e., dynamical and convective breaking of the waves). In this regard, the use of special rocket and balloon-borne techniques (PHILBRICK et al., 1983; BARAT, 1983) concurrent with radar observations to obtain the high-resolution structure of turbulent regions would appear important for understanding the generation mechanisms of turbulence and would enable a valuable comparison between techniques.

The use of Doppler spectral width to measure turbulence intensity has yet to be exploited fully (SATO and WOODMAN, 1982; HOCKING, 1983). Since the velocity variance is related directly to the eddy dissipation rate, it is clear that a greatly increased observational program using spectral width estimates of eddy dissipation rates would have direct relevance to the development of more accurate general circulation and mechanistic models. Energy dissipation rates also can be used to infer vertical diffusivity and heating, thus spectral width measurements may provide an alternative method of determining vertical diffusivity. Spectral width measurements, however, require a narrow radar beam and a correspondingly large antenna area.

Finally, the general characteristics of the turbulent structure profiles can be expressed in terms of the refractive index structure constant C_n^2 (TATARSKII, 1971). This parameter is useful, for example, in comparing radar,

optical, and other turbulence measurements.

(2) Gravity Waves

A significant amount of information on middle-atmosphere gravity waves already has been obtained by existing techniques. Radars can provide a detailed description of the wind field as a function of height and time. They can also produce spectral descriptions of the wind field fluctuations as a function of frequency (BALSLEY and CARTER, 1982). Lidars provide similar information for the temperature fluctuations (CHANIN and HAUCHECORNE, 1981). Data from rocket networks can reveal long-term statistics on the geographical and seasonal variation of the wave field (HIROTA, 1983). Rocket data also provide instantaneous profiles of temperature and wind (THEON et al., 1967) from which gravity wave processes can be inferred.

Two important parameters about which relatively little information has been collected are the horizontal wavelengths (λ_h) and phase velocities (c) of gravity waves. Some information on these parameters has been obtained from studies of airglow emissions and noctilucent clouds (ARMSTRONG, 1982; HERSE et al., 1980; HAURWITZ and FOGLE, 1969). Initial radar estimates of λ_h and c were made by VINCENT and REID (1983) and by FRITTS et al. (1983). VINCENT and REID (1983) also made the first direct measurements of another important quantity, the upward flux of horizontal momentum ($\overline{u'w'}$) in the mesosphere, and VINCENT (1983) used rotary spectra to obtain a lower limit on the fraction of upward-propagating, low-frequency gravity waves in the mesosphere and lower thermosphere. The latter study suggests an upward flux of energy and momentum consistent with the requirement of gravity-wave drag.

Two interpretations have been advanced to account for the low-frequency ($\omega < N$) and low (horizontal) wavenumber spectra observed in the middle atmosphere. One is that the motions are due to a spectrum of internal gravity waves analogous to the "universal" wave spectrum applied to the ocean (VANZANDT, 1982). Such a theory is consistent with both the apparent role of gravity-wave transport, drag, and diffusion in middle-atmosphere dynamics and the observed spectral character of atmospheric fluctuations. A second interpretation, based upon the theory of 2-dimensional turbulence, also appears to be consistent with certain spectral observations (GAGE, 1979; LILLY, 1983), but this theory requires the presence of propagating gravity waves as the primary coupling between the lower and middle atmosphere and is concerned primarily with the spectral distribution of kinetic energy. The actual state of the atmosphere, of course, may involve a combination of gravity waves, 2-dimensional turbulence, and other motions, with further studies needed to delineate their relative importance.

Gravity-wave observations to date have provided good preliminary information on motions, processes, and spectra using a variety of techniques. Often, however, such observations are made without knowledge of the mean velocity and static stability profiles. This is a major shortcoming (particularly the lack of $\bar{u}$) because it causes ambiguities in the determination of the characteristics and/or consequences of the wave motions that might otherwise be inferred.

5. FUTURE RESEARCH NEEDS

(a) Modeling Needs

Because they tend to be computationally efficient and allow individual processes to be studied in isolation, mechanistic models probably will continue to play a major role in the development and testing of parameterizations for gravity wave-mean flow interactions. Both the quasi-geostrophic models and the global primitive equation models will be useful tools. We anticipate, however,

that there may be less emphasis on zonally symmetric models in the future, particularly for the study of wave-mean flow interactions in the winter hemisphere. The current primitive state of knowledge of gravity-wave morphology and of the detailed physics of wave-breaking allows for a wide range of assumptions in present models. Ideally, mechanistic models that properly handle wave-mean flow interactions will provide some useful constraints on the possible characteristics of the observed wave climatology. However, there is little prospect that modeling can be in any sense a substitute for observations.

It should be cautioned that measured gravity-wave fluxes and other parameters will not be able to be used directly in middle-atmosphere models. One reason for this is that measured quantities depend on atmospheric conditions in the troposphere, stratosphere, and mesosphere that may be very different from those existing in a model. However, measurements of the global gravity-wave morphology should allow the development of schemes that can represent consistently the proper dependence of the large-scale flow on gravity-wave processes.

(b) Theoretical Needs

Theoretical studies are needed to address a number of problems that are unlikely to be solved using existing observational techniques. The most obvious of these relate to the saturation process itself. In particular, studies are needed that address the detailed mechanisms and consequences of saturation, including wave-scattering and reflection, and multiple-wave saturation, and the effects of the temporal and spatial variability of saturation. The former studies are necessary to understand the evolution of a saturating gravity-wave spectrum; the latter is needed to incorporate correctly the effects of saturation and its variability in mechanistic and general circulation models of the middle atmosphere.

Other areas in which theoretical work is needed are the identification and quantification of the dominant tropospheric sources of gravity waves and the study of wave propagation and filtering through wave-wave and wave-mean flow interactions. Theoretical studies of gravity-wave sources in conjunction with high-resolution observations may help determine the phase speed and horizontal wavelength distributions, as well as their geographical and temporal variability. These distributions are poorly known at present, but they are expected to have a major impact on the occurrence and effects of saturation in the middle atmosphere. Likewise, the propagation of gravity waves through, and their interaction with, a variable environment will influence the character and occurrence of saturation. It also is important to determine to what extent the concept of a universal gravity-wave spectrum can be applied to the atmosphere.

(c) Observational Needs

(1) Gravity wave and turbulence climatology

There is a clear need to extend our studies of the climatology of atmospheric gravity waves and turbulence. Observations of the geographical and temporal distributions of gravity-wave sources, energies, and momentum and heat fluxes, as well as turbulent diffusion, are required. The distributions of momentum fluxes ($\overline{u'w'}$ and $\overline{v'w'}$) and heat fluxes ($\overline{v'T'}$ and $\overline{w'T'}$), in particular, have direct implications for modeling the large-scale circulation and will depend on the dominant sources and the propagation of gravity waves into the middle atmosphere. Measurements of turbulent diffusion and spectral width are needed to address the rate of gravity-wave energy dissipation and the effects of diffusion in the middle atmosphere.

It is also important to address the vertical transport of energy and momentum by the full spectrum of gravity waves under various conditions. To this end, studies of low-frequency motions using rotary spectra and filtering through radiative cooling, and wave-wave and wave-mean flow interactions appear relevant.

Momentum flux, energy, turbulence intensity, and rotary spectrum measurements currently are possible with multiple-beam radar systems; heat fluxes could be determined with combinations of radars and lidars.

(2) Case studies

Case studies of nearly monochromatic wave motions providing the mean and perturbation wind fields and the distributions of vertical wavenumber would permit comparisons with theoretical models and provide evidence of important processes and interactions. Independent measurements of the associated temperature fields would permit a check on the wave parameters inferred from radar measurements. Observations of wave excitation and dissipation (or saturation) are particularly important in this regard. It also would be useful to identify the frequency of occurrence of the various gravity-wave processes and interactions thought to be important in the middle atmosphere.

One example of a useful case study is nearly monochromatic gravity-wave saturation. Saturation is associated with either $|\partial T/\partial z| \sim \Gamma$ or $|u'| \sim |c - \bar{u}|$. Because there are uncertainties in estimating c using data from a single station, however, saturation may be identified most unambiguously in measurements of the temperature structure. Because c is constant and $\bar{u}$ may change with height, $|u'|$ need not remain constant above the saturation level.

(3) Measurement of λ_h and c

Two gravity-wave parameters of particular significance are the horizontal wavelength (λ_h) and the (horizontal) phase velocity (c). They are important because they are essentially constant following the wave motion and they determine the occurrence and distribution of gravity waves in the middle atmosphere. Other relevant wave parameters, such as the intrinsic frequency ($k(c - \bar{u})$) and the vertical wavenumber ($m = 2\pi/\lambda_z$), are not constant, but depend on N^2 and $\bar{u}$. Determination of the phase speed distribution of gravity waves near their source regions in the troposphere and in the middle atmosphere would permit a quantitative assessment of the effects of filtering and wave-wave interactions as the gravity waves propagate vertically. Horizontal wavelength measurements would help establish the degree of homogeneity in the mesospheric response to gravity-wave saturation.

Estimates of λ_h and c can be obtained in certain instances with present radar and lidar systems using multiple-beam techniques. However, such estimates are subject to potentially large errors and may be biased towards relatively small-scale waves ($\lambda_h \lesssim 200$ km) because of small horizontal beam separations. It would be desirable, therefore, to make more direct radar and lidar measurements at a range of spacings from a few tens of a kilometer upwards in order to measure those wavelengths and phase velocities more relavant to middle-atmosphere dynamics. Such spacings are considerably less than those required to address the geographical distribution of gravity-wave saturation and turbulent diffusion.

(4) Measurement of mean winds

In addition to gravity-wave and turbulence measurements, long-term measurements of the mean zonal and meridional wind components in the mesosphere and lower thermosphere are required. At present, the climatology of the mean zonal

wind at these levels is not well known, especially in the tropics. The current data base for the mean meridional wind is completely inadequate. The latter is particularly important since gravity-wave drag in the mesosphere is balanced primarily by the Coriolis torque due to the mean meridional motion.

(d) Observational networks

As discussed in several of the previous sections, it would be desirable to establish networks of radar and/or lidar systems for the following reasons:

(1) The horizontal wavelengths and phase velocities of monochromatic atmospheric gravity waves can be measured more reliably by making observations from at least three spatially separated points. Because the wavelengths of longer waves cannot be determined accurately using small spacings, it will be necessary to use a range of spacings.

(2) Studies of the global morphology of gravity waves require that several such facilities be established at geographically distinct locations. Such systems should make extended observations to determine seasonal and interannual variability. The potentially important effects of orography can be examined by establishing sites near extensive mountain ranges and by comparing these results with observations taken in orographically smooth regions.

Other combinations of observing systems also would provide important information on gravity-wave propagation and dissipation processes and morphology. Colocated lidar and radar facilities, for example, would permit much more detailed observations of gravity-wave saturation in the mesosphere. Saturated wave amplitudes then could be compared directly with perturbation lapse rates for both narrow- and broad-spectrum saturation. Meteorological rockets would provide an important complement to both radar (MST or PR) and lidar facilities through the addition of mean wind, temperature, and gravity-wave structure in regions where no balloon or radar wind data are available. Such data would make studies of gravity-wave propagation and the onset of saturation possible.

One final recommendation pertains to establishing such observatories in the tropics. Extended tropical observations, particularly within a few degrees of the equator, will yield (in addition to the low-latitude gravity waves) important new information on long-period equatorial waves. These waves exist only in the tropics and comprise the major mechanism for momentum transport into the middle atmosphere in that region. ...

... REFERENCES

Armstrong, E. B. (1982), The association of visible airglow features with a gravity wave, J. Atmos. Terr. Phys., 44, 325-336.

Balsley, B. B. and D. A. Carter (1982), The spectrum of atmospheric velocity fluctuations at 8 km and 86 km, Geophys. Res. Lett., 9, 465-468.

Balsley, B. B. and K. S. Gage (1980), The MST radar technique: Potential for middle atmosphere studies, Pure Appl. Geophys., 118, 452-493.

Barat, J. (1983), The fine structure of the stratospheric flow revealed by differential sounding, J. Geophys. Res., 88, 5219-5228.

Booker, J. R. and F. P. Bretherton (1967), The critical layer for internal gravity waves in a shear flow, J. Fluid Mech., 27, 513-539.

Cadet, D. (1977), Energy dissipation within intermittent clear air turbulence patches, J. Atmos. Sci., 34, 137-142.

Chanin, M. L. and A. Hauchecorne (1981), Lidar observation of gravity and tidal waves in the middle atmosphere, J. Geophys. Res., 86, 9715-9721.

Czechowsky, P., R. Ruster and G. Schmidt (1979), Variations of mesospheric structures at different seasons, Geophys. Res. Lett., 6, 459-462.

Dunkerton, T. J. (1982a), Wave transience in a compressible atmosphere, Part III: The saturation of internal gravity waves in the mesosphere, J. Atmos. Sci., 39, 1042-1051.

Dunkerton, T. J. (1982b), Stochastic parameterization of gravity wave stresses, J. Atmos. Sci., 39, 1711-1725.

Dunkerton, T. J. and D. C. Fritts (1983), The transient gravity wave critical layer, Part I: Convective adjustment and the mean zonal acceleration, J. Atmos. Sci., in press.

Fritts, D. C. (1982), The transient critical-level interaction in a Boussinesq fluid, J. Geophys. Res., 87, 7997-8016.

Fritts, D. C., B. B. Balsley and W. L. Ecklund (1983), VHF echoes from the arctic mesosphere and lower thermosphere, Part II: Interpretations, Proceedings of the U.S.-Japan Seminar on the Dynamics of the Middle Atmosphere, Honolulu, Hawaii, 8-12 November 1982, in press.

Gage, K. S. (1979), Evidence for a $k^{-5/3}$ law inertial range in mesoscale two-dimensional turbulence, J. Atmos. Sci., 36, 1950-1954.

Haurwitz, B. and B. Fogle (1969), Waveforms in noctilucent clouds, Deep Sea Res., 16, 85-95.

Herse, M., G. Moreels and J. Clairemidi (1980), Waves in the OH emissive layer: Photogrametry and topography, Appl. Opt., 19, 355-362.

Hines, C. O. and C. A. Reddy (1967), On the propagation of atmospheric gravity waves through regions of wind shear, J. Geophys. Res., 72, 1015-1034.

Hirota, I. (1983), Climatology of gravity waves in the middle atmosphere, Proceedings of the U.S.-Japan Seminar on the Dynamics of the Middle Atmosphere, Honolulu, Hawaii, 8-12 November, 1982, in press.

Hocking, W. K. (1983), On the extraction of atmospheric turbulence parameters from radar backscatter Doppler spectra - I. Theory, J. Atmos. Terr. Phys., 45, 89-102.

Koop, C. G. and B. McGee (1983), Measurements of internal gravity waves in a stratified shear flow, Submitted to J. Fluid Mech..

Lilly, D. K. (1983), Stratified turbulence and the mesoscale variability of the atmosphere, J. Atmos. Sci., in press.

Lilly, D. K., D. E. Waco and S. I. Adelfang (1974), Stratospheric mixing estimated from high-altitude turbulence measurements, J. Appl. Meteorol., 13, 488-493.

Lindzen, R. S. (1981), Turbulence and stress due to gravity wave and tidal breakdown, J. Geophys. Res., 86, 9707-9714.

Lindzen, R. S. (1983), Gravity waves in the mesosphere, Proceedings of the U.S.-Japan Seminar on the Dynamics of the Middle Atmosphere, Honolulu, Hawaii, 8-12 November 1982, in press.

Lindzen, R. S. and J. Forbes (1983), Turbulence originating from convectively stable internal waves, J. Geophys. Res., 88, 6549-6553.

Philbrick, C. R., K. U. Grossmann, R. Hennig, G. Lange, D. Krankowsky, D. Offermann, F. J. Schmidlin and U. von Zahn (1983), Vertical density and temperature structure over northern Europe, Adv. Space Res., 2, 121-124.

Rosenberg, N. W. and E. M. Dewan (1975), Stratospheric turbulence and vertical effective diffusion coefficients, AFCRL-TR-75-0519, Air Force Cambridge Res. Labs., Hanscom AFB, Mass.

Rottger, J. (1980), Structure and dynamics of the stratosphere and mesosphere revealed by VHF radar investigations, Pure Appl. Geophys., 118, 494-527.

Sato, T. and R. F. Woodman (1982), Fine altitude resolution observations of stratospheric turbulent layers by the Arecibo 430 MHz radar, J. Atmos. Sci., 39, 2546-2552.

Schoeberl, M. R. and D. F. Strobel (1983), Nonzonal gravity wave breaking in the winter mesosphere, Proceedings of the U.S.-Japan Seminar on Dynamics of the Middle Atmosphere, in press.

Schoeberl, M. R., D. F. Strobel and J. P. Apruzese (1983), A numerical model of gravity wave breaking and stress in the mesosphere, J. Geophys. Res., 88, 5249-5259.

Tatarskii, V. I. (1971), The effects of the turbulent atmosphere on wave

propagation, National Technical Information Service, Springfield, VA, pp. 97-102.

Theon, J. S., W. Nordberg, C. B. Katchen and J. J. Horvath (1967), Some observations on the thermal behavior of the mesosphere, J. Atmos. Sci., 24, 428-438.

VanZandt, T. E. (1982), A universal spectrum of buoyancy waves in the atmosphere, Geophys. Res. Lett., 9, 575-578.

Vincent, R. A. (1983), Gravity wave motions in the mesosphere, submitted to J. Atmos. Terr. Phys.

Vincent, R. A. and I. M. Reid (1983), HF Doppler measurements of mesospheric gravity wave momentum fluxes, J. Atmos. Sci., 40, 1321-1333.

Walterscheid, R. L. (1983), Gravity wave attenuation and the evolution of the mean state following wave breakdown, Proceedings of the U.S.-Japan Seminar on the Dynamics of the Middle Atmosphere, Honolulu, Hawaii, 8-12 November 1982, in press.

Weinstock, J. (1976), Nonlinear theory of acoustic-gravity waves, I. Saturation and enhanced diffusion, J. Geophys. Res., 81, 633-652.

Weinstock, J. (1982), Nonlinear theory of gravity waves: Momentum deposition, generalized Rayleigh friction, and diffusion, J. Atmos. Sci., 39, 1698-1710.

Woodman, R. F., P. K. Rastogi and T. Sato (1981), Evaluation of effective eddy diffusive coefficients using radar observations of turbulence in the stratosphere, MAP Handbook Vol. 2, edited by S. K. Avery, pp. 363-369, (available through Aeronomy Laboratory, Dept. of Electrical Engineering, University of Illinois, Urbana, Ill.

1.3B GRAVITY WAVES FROM THE STRATOSPHERE TO THE MESOSPHERE

M. R. Schoeberl

NASA/Goddard Space Flight Center
Atmospheric Chemistry Branch, Code 964
Greenbelt, MD 20771

The propagation of gravity waves from the stratosphere to the mesosphere has important implications both for observers and those who are attempting to parameterized wave breaking in global models. As they propagate from the tropopause to their breaking level (here, assumed to be the mesosphere), gravity waves can encounter a refractive environment since the vertical group velocity is a function of the background wind. They may be focussed or scattered or dissipated before reaching the mesosphere. It is even conceivable that gravity waves may break, stop breaking, and begin breaking again at higher altitudes with a resultant loss of wave energy in the intervening region.

From a modeling viewpoint, the important concern for large-scale flows is the total upward flux of gravity wave (pseudo) momentum entering the stratosphere and mesosphere. Admittedly this quantity may show enormous spatial variations since the usual tropospheric generation processes for gravity waves (e.g. orography and thermal convection) are local. The refraction of gravity waves also presents a difficult problem for observers since waves passing through the tropopause may arrive a thousand kilometers upstream in the mesosphere. Thus, it would appear to a single station looking upward near the source point that all the gravity waves are absorbed in the stratosphere.

Since MST radars sense tropospheric and mesospheric conditions most accurately, they are ideally suited to assess the total gravity-wave flux through the tropopause and stratopause. Unfortunately, the refraction problem suggests networks of radars making coordinated measurements may be required to accurately determine the upward flux of momentum as well as the flux convergence between layers. The observational requirements needed to determine these fluxes are discussed in FRITTS et al. (1984).

REFERENCE

Fritts, D. C., M. A. Geller, B. B. Balsley, M. R. Chanin, I. Hiroto, J. R. Holton, S. Kato, R. S. Lindzen, M. R. Schoeberl, R. A. Vincent and R. F. Woodman (1984), Research status and recommendations from the Alaska Workshop on gravity waves and turbulence in the midde atmosphere, Fairbanks, Alaska, 18-22 July, 1983, Bull. Am. Meteorol. Soc., 65, 149-159.

D6

N85-32472

1.3C THE SUPPRESSION OF CONVECTIVE WAVEBREAKING BY RADIATIVE TRANSFER PROCESSES

M. R. Schoeberl

NASA/Goddard Space Flight Center
Atmospheric Chemistry Branch, Code 964
Greenbelt, MD 20771

INTRODUCTION

SCHOEBERL et al. (1983) suggested that convective wavebreaking of monochromatic gravity waves might be suppressed by radiative transfer processes if the vertical wavelength waves were sufficiently short. As the vertical wavelength or the gravity wave decreases, radiative transfer between adjacent vertical layers becomes increasingly important. This exchange can increase the radiative relaxation time scale so that the wave will no longer grow with altitude. Thus, very short vertical wavelength waves may dissipate radiatively rather than become convectively unstable. SCHOEBERL et al. (1983) showed that gravity waves with $(\bar{u}-c) < 22$ ms^{-1} ($\lambda_x = 1000$ km), and $(\bar{u}-c) < 13$ ms^{-1} ($\lambda_x = 100$ km) would be radiatively damped.

Since publication of these results, APRUZESE and STROBEL (1984) have revised the exchange coefficients used in SCHOEBERL et al. (1983). Also, CHAO and SCHOEBERL (1984) pointed out that the computation made by LINDZEN (1981) of the convective diffusion rate may be a factor of two too low as the convective adjustment processes tends to minimize the thermal transport by the wave. The purpose of this note is to revise the values given in SCHOEBERL et al. (1983). These results also suggest that the very thin turbulent layers observed by MST radars (e.g. WOODMAN, 1980) cannot be produced by the convective instability of monochromatic gravity waves with large horizontal scales.

METHODOLOGY AND RESULTS

The condition required to prevent convective wavebreaking is

$$\gamma_{diff} = \gamma_{rad} \tag{1}$$

where γ_{diff} is the diffusive damping time scale required to prevent wave growth with altitude and γ_{rad} is the radiative damping time scale. Now,

$$\gamma_{diff} = \alpha^2 D \tag{2}$$

where $$D = \frac{m(\bar{u}-c)^4}{H\,\delta^3\,N^3}, \quad \alpha = \frac{N}{\bar{u}-c}$$

D is twice LINDZEN'S (1981) turbulent diffusion (see CHAO and SCHOEBERL, 1984), and α is the vertical wave number of the gravity wave. The other terms in (2) are; H, the atmospheric scale height (7 km), N, the buoyancy frequency (2×10^{-2} s^{-1}), m, the zonal wave number ($2\pi/L$) and $\delta = (1 + k^2/m^2)^{1/2}$ where k is the meridional wave number. For simplicity we take $\delta = 1$.

For γ_{rad} we use Equation (20) from FELS (1982) which agrees with the recent results of APRUZESE and STROBEL (1984) and also includes the effect of O_3 in the IR exchange parameterization. The transcendental system (1) can then be solved numerically. Since D varies with m and γ_{rad} varies with altitude, our results for $\bar{u}$ min (c=0) are shown in Figure 1 verses L at 5 km intervals from 20 to 70 km. The values shown in Figure 1 are the magnitudes of zonal mean wind values below which convective wave breaking would not take place for a standing gravity wave. Below 20 km the exchange approximation given by FELS is not valid because of CO_2 line overlap. Above 70 km non-LTE effects domi-

nate. In the intermediate region N and H are assumed constant. The background temperature is given by the 1962 US Standard Atmosphere.

DISCUSSION

A vertically propagating gravity wave will grow in amplitude with height unless the vertical wavelength is small enough that radiative exchange between layers damps the gravity waves. The equivalent minimum phase speed in a resting atmosphere (or equivalent zonal wind speed for a stationary wave) for a gravity wave which will be so strongly damped radiatively that it will not grow with height is shown in Figure 1. These results were obtained from (2) and the FELS (1982) parameterization of IR cooling.

Obviously from Figure 1 the cutoff phase speeds are very slow, thus these wave approach periods where the inertial frequency cannot be neglected. Under such situations, full solution of Laplace's tidal equation is required; however, compared to Laplace tidal results, (2) tends to underestimate the vertical wavelength so the cutoff velocities shown in Figure 1 will be lower limits.

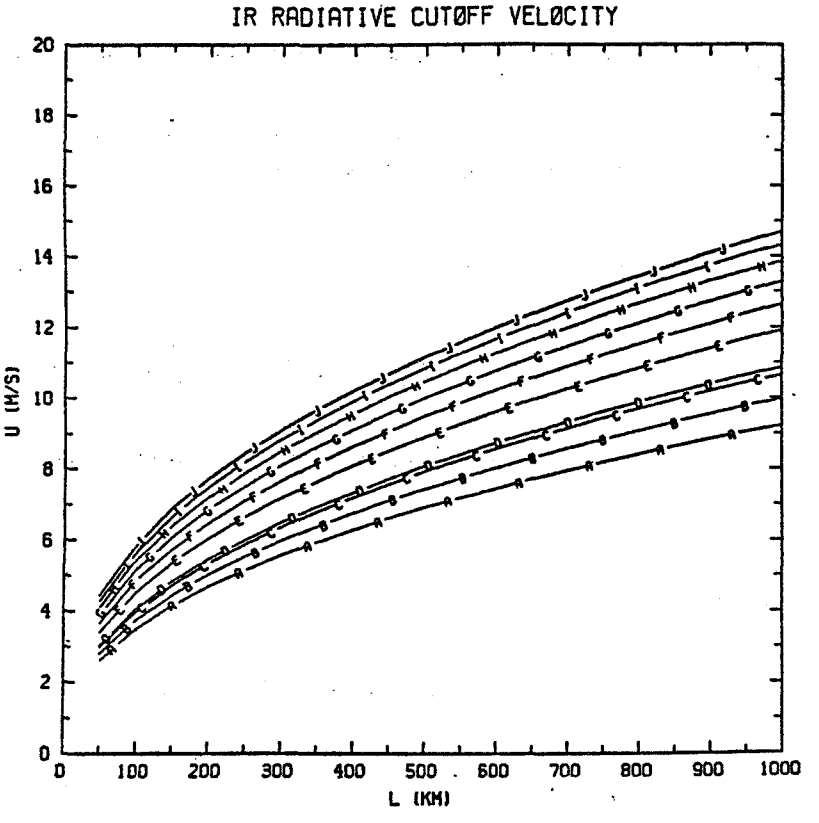

Figure 1. The minimum zonal wind possible for convective wavebreaking by a monochromatic gravity wave with zonal wavelength L and zero phase speed. The letters correspond to computations at different altitudes with 5 km increments starting at 20 km (e.g. A = 20 km, B = 25 km,..., J = 70 km). For wind values below that shown, the wave is radiatively damped so strongly that it cannot grow in amplitude with height.

REFERENCES

Apruzese, J. P., D. F. Strobel (1984), Radiative relaxation rates for individual 15 μ CO_2 lines in the upper stratosphere and lower mesosphere, J. Geophys. Res., (in press).

Chao, W. and M. R. Schoeberl (1984), A note on the linear approximation of gravity wave saturation in the mesosphere, J. Atmos. Sci., (in press).

Fels, S. B. (1982), A parameterization of scale-dependent radiative damping rates in the middle atmosphere, J. Atmos. Sci., 39, 1141-1152.

Schoeberl, M. R., D. F. Strobel and J. P. Apruzese (1983), A numerical model of gravity wave breaking and stress in the mesosphere, J. Geophys. Res., 88, 5249-5259.

Woodman, R. F. (1980), High altitude resolution stratospheric measurements with the Arecibo 2380-MHz radar, Radio Sci., 15, 423-430.

1.4A A NUMERICAL ANALYSIS OF TRANSIENT PLANETARY WAVES AND THE VERTICAL STRUCTURE IN A MESO-STRATO-TROPOSPHERE MODEL

Ke-Su Zhang and T. Sasamori

Department of Atmospheric Sciences
University of Illinois
Urbana, Illinois 61801

ABSTRACT

The structure of unstable planetary waves is computed by a quasi-geostrophic model extending from the surface up to 80 km by means of eigenvalue-eigenfunction techniques in spherical coordinates. Three kinds of unstable modes of distinct phase speeds and vertical structures are identified in the winter climate state: (1) the deep Green mode with its maximum amplitude in the stratosphere, (2) the deep Charney mode with its maximum amplitude in the troposphere, and (3) the shallow Charney mode which is largely confined to the troposphere. Both the Green mode and the deep Charney mode are characterized by very slow phase speeds. They are mainly supported by upward wave energy fluxes, but the local baroclinic energy conversion within the stratosphere also contributes in supporting these deep modes. The mesosphere and the troposphere are dynamically independent in the summer season decoupled by the deep stratospheric easterly. The summer mesosphere supports the easterly unstable waves 1-4. Waves 3 and 4 are identified with the observed mesospheric 2-day wave and 1.7-day wave, respectively.

INTRODUCTION

Since the discovery of the spectacular natural phenomena of stratospheric sudden warmings, interest in planetary waves has been increasingly enhanced. After satellite observations became possible, along with previous observations by meteor radar, partial-reflection radar and rocket sounding, many transient wave activities in the upper atmosphere have been documented, such as 2-day waves in the summer mesosphere (RODGERS and PRATA, 1981), 4-day waves in the upper stratosphere (VENNE and STANFORD, 1982), the slowly moving planetary waves in the winter stratosphere and mesosphere (HARTMANN, 1976), and a wide wave spectrum in the lower stratosphere (YU et al., 1983). Some wave activities, mainly in wave 1 and 2, are intimately related to the sudden warming phenomena, which extend from the stratosphere well into the mesosphere. The planetary scale waves possess deep vertical structure in winter, but vertically decoupled in summer (LABITZKE, 1981a,b).

The purpose of the present study is to investigate those transient planetary waves based on instability theory. The growth rate, phase speed, meridional and vertical structure of unstable modes are examined for the winter and summer solstice climate states. A comparison study of stabilities for the basic states before and after the 1976/1977 sudden warming event is also discussed.

METHOD OF ANALYSIS

(a) Governing Equation

Assuming the large-scale wave motions are adiabatic and nondissipative, we use the linearized quasi-geostrophic, spherical model formulated by MATSUNO (1971):

$$\left(\frac{\partial}{\partial t} + \frac{\bar{U}}{ac}\frac{\partial}{\partial \lambda}\right)\mathcal{L}(\phi) + \frac{2\Omega}{s^2}\phi_\lambda - \frac{\phi_\lambda}{cs^2}\left[\frac{(\bar{U}c)_\theta}{ac}\right]_\theta = 4\Omega^2 a^2 \frac{\partial \omega}{\partial p} \qquad (1)$$

$$(\frac{\partial}{\partial t} + \frac{\overline{U}}{ac}\frac{\partial}{\partial \lambda})\phi_p - \frac{\phi_\lambda}{ac} U_p + S\omega = 0 \qquad (2)$$

where

$$\mathcal{L}(\phi) \equiv [\frac{1}{c}\frac{\partial}{\partial \theta}(\frac{c}{s^2}\frac{\partial}{\partial \theta}) + \frac{1}{s^2 c^2}\frac{\partial^2}{\partial \lambda^2}]\phi$$

Equations 1 and 2 are vorticity and thermodynamic equations, respectively, where λ denotes the longitude, θ the latitude, $c = \cos\theta$, $s = \sin\theta$, Ω the angular velocity of the earth, a the radius of the earth, ϕ the perturbation geopotential, U the basic zonal flow, and S the static stability.

(b) Grid Point Arrangement and Boundary Conditions

The model is discretized vertically by ten computation levels covering from the surface up to 80 km and it is referred to as an MST model (M for mesosphere, S for stratosphere and T for troposphere). The computation levels are arranged at p = 0.01, 0.04, 0.2, 1 mb in the mesosphere; at p = 3, 10, 30, 100 mb in the stratosphere and at p = 250, 750 mb in the troposphere. The vertical boundary condition $\omega = 0$ is assumed at p = 0 and p = 1000 mb. In the meridional direction the model is bounded by the fixed boundary conditions $\phi' = u' = v' = 0$ at the pole and the equator with 10° meridional mesh sizes. The grid point arrangement is shown in Figure 1.

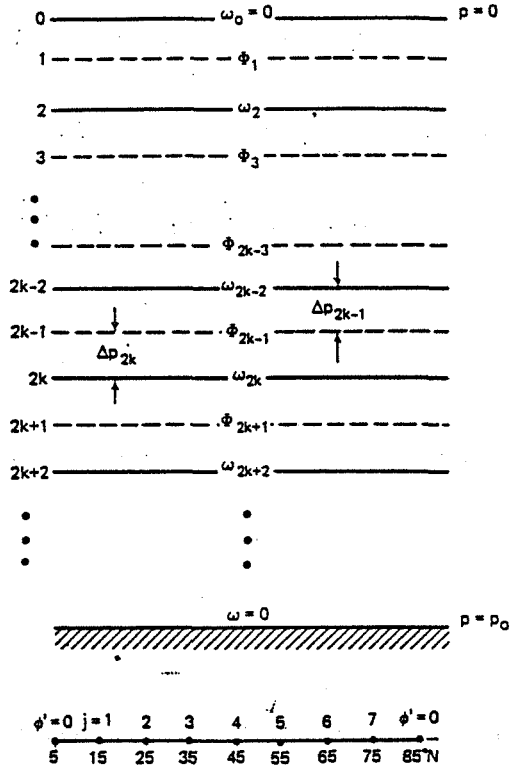

Figure 1. Vertical and meridional grid arrangement and boundary conditions used in the spherical model.

(c) Basic State Parameters

The winter and summer solstice climate basic flows are shown in Figure 2. The zonal-mean temperature field and the wind field consist of the parameter space (S, U), where the static stability is calculated from the temperature field.

(d) Normal Mode Solution

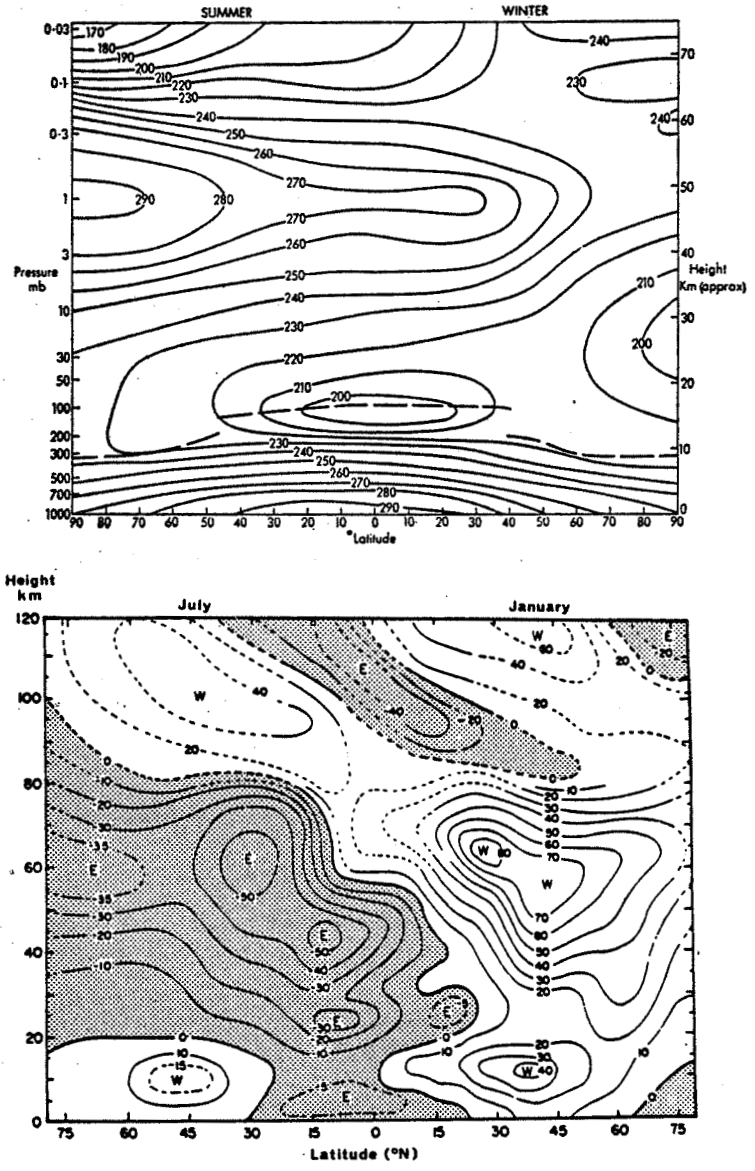

Figure 2. The solstice climate states. The upper panel is temperature (K) and the lower panel is the zonal mean wind in m/s.

We assume a normal mode solution:

$$\Phi = \Phi(\theta, p)e^{im(\lambda-ct)}$$

and calculate the phase speed C_r, growth rate $\sigma_i = mC_i$, and the eigenfunction $\Phi(\theta,p)$, where $C = C_r + iC_i$ and $\Phi = \Phi_r + i\Phi_i$ are complex numbers.

RESULTS

(a) Winter

Figure 3 shows the spectrum of the growth rates and phase speeds of the unstable waves computed for the winter basic flow. The values of α and α_s are representative for "dry" and "wet" tropospheric conditions. Both reveal the presence of three kinds of unstable modes:

1. Green mode, denoted by MST in Figure 3, for waves 1 and 2,
2. Deep Charney mode, denoted by ST in Figure 3, for wave 3, and
3. Shallow Charney mode, denoted by T in Figure 3, for waves 5-9.

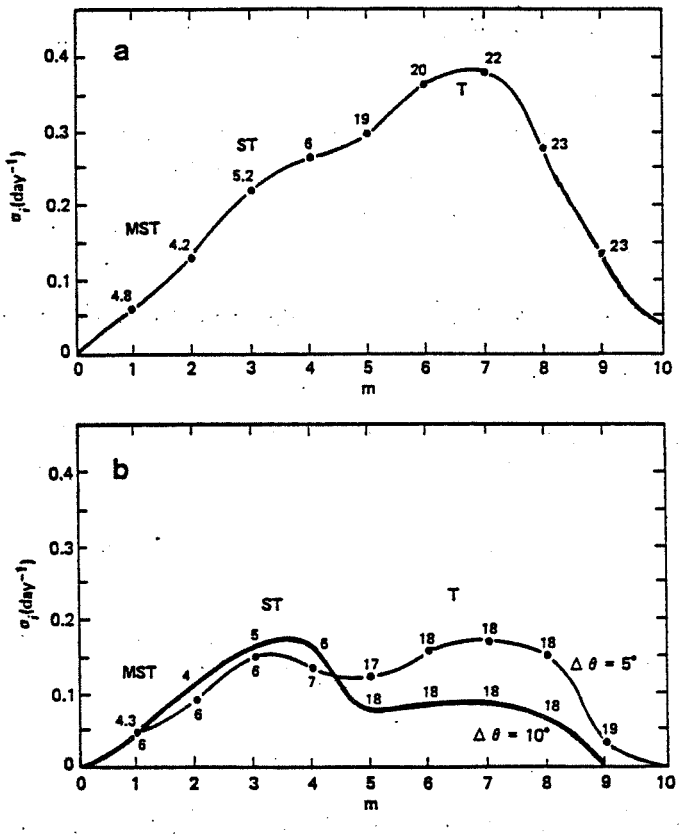

Figure 3. The growth rate (ordinate) and the phase speed at the equator (labeled in m/s) for winter solstice basic state: a) the dry troposphere; b) the moist troposphere.

The phase speeds given in Figure 3 reveal an interesting instability exchange between the slow modes (waves 1-4, including the Green mode and the deep Charney modes) and the fast modes (waves 5-9, all of which are confined to the troposphere). It implies some intrinsic relation between the phase speed and the vertical structure. The vertical wave energy fluxes (Figure 4) depict that the deep waves are vertically coupled as an entirety. They may be identified with the slowly moving waves 1, 2 and 3 in the real atmosphere.

(b) Summer

The spectra of the growth rates, phase speeds for the summer circulation are given in Figure 5. The mesospheric modes, with large negative phase speeds $C_r < 0$, and the tropospheric modes, with the positive phase speeds $C_r > 0$, exchange their stabilities at wave number 4. The computed most unstable mode is wave 3 with a period of 2 days which compares favorably with the observed 2-day wave. Figure 6 shows structures of the computed mesospheric waves with m = 1-4 and the tropospheric wave with m = 6. They are spatially separated by the easterly wind in the stratosphere. The planetary scale waves dominate in the mesosphere and the synoptic scale waves dominate in the troposphere.

VERTICAL COUPLING AND DECOUPLING

In order to understand the stability due to vertical coupling between the mesosphere, the stratosphere and the troposphere in the winter season, a case study is performed to compare the eigenmodes in the basic states before and after the 1976/1977 sudden warming event. Figure 7 shows the observed variation of geopotential amplitude for waves 1 and 2 during the warming phase.

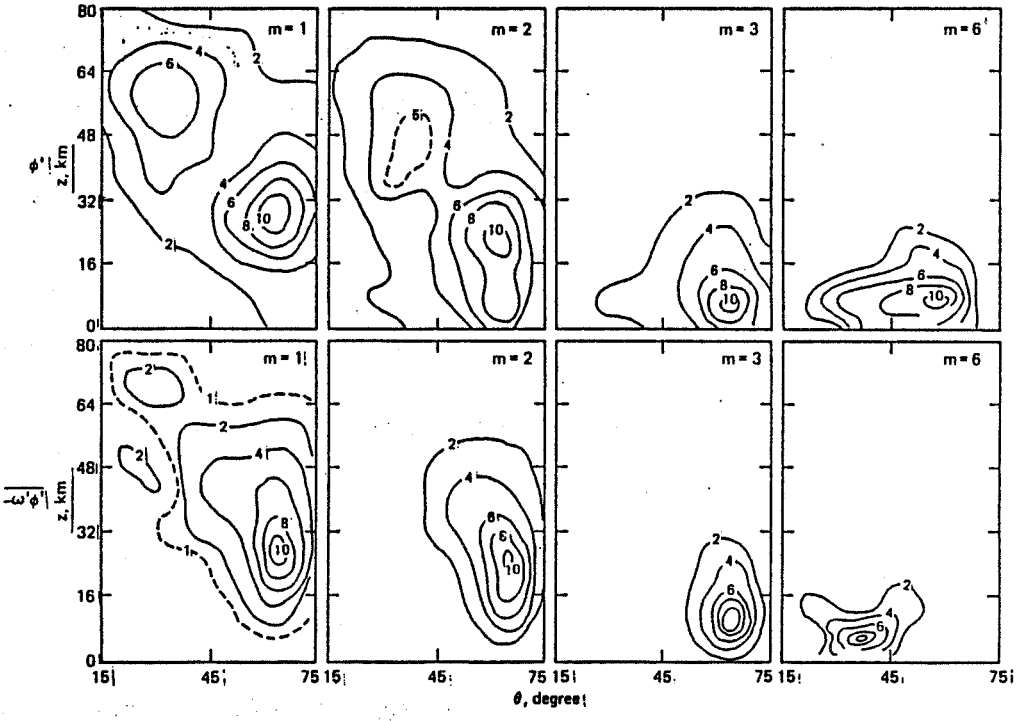

Figure 4. Geopotential eigenfunctions (upper and vertical wave energy flux (lower) in the NH winter basic flow with the "dry" troposphere. Units are arbitrary.

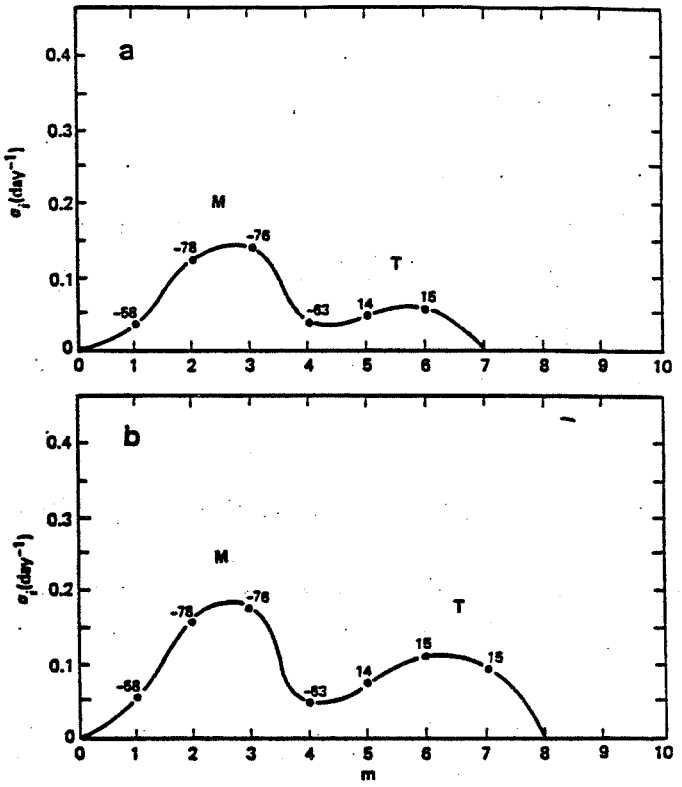

Figure 5. The growth rates (ordinate) and the phase speeds (labeled in m/s) for summer solstice basic state with a) the "dry" troposphere and b) the "moist" troposphere. m indicates the wave number, M the mesospheric mode and T the tropospheric mode.

Both waves 1 and 2 were growing during December 1976 and decreasing in January 1977. The basic flow in December 1976 is characterized by a broad, weak throughout the troposphere and the stratosphere, and in January 1977 is characterized by easterlies at high latitudes. Figure 8 summarizes the results of frequency computations for December and January.

Three significant changes occur after the sudden warming:

1. The maximum growth rate shifts from planetary scale (m = 2) to synoptic scale (m = 7) and the planetary scale waves are substantially stabilized.
2. Transition occurs from the slow modes to the fast modes at wave number 4 before the warming, but all waves change to the fast modes after it.
3. All the deep modes (MST modes and ST modes) are suppressed to the shallow, tropospheric modes after the sudden warming as shown in Figures 9 and 10.

Since the deep Green mode and the deep Charney mode have been calculated in the winter climate basic flow, we suspect that the deep modes exist in the whole season except in periods after sudden warmings, in which all deep modes are suppressed primarily by the reversed zonal flow at high latitudes.

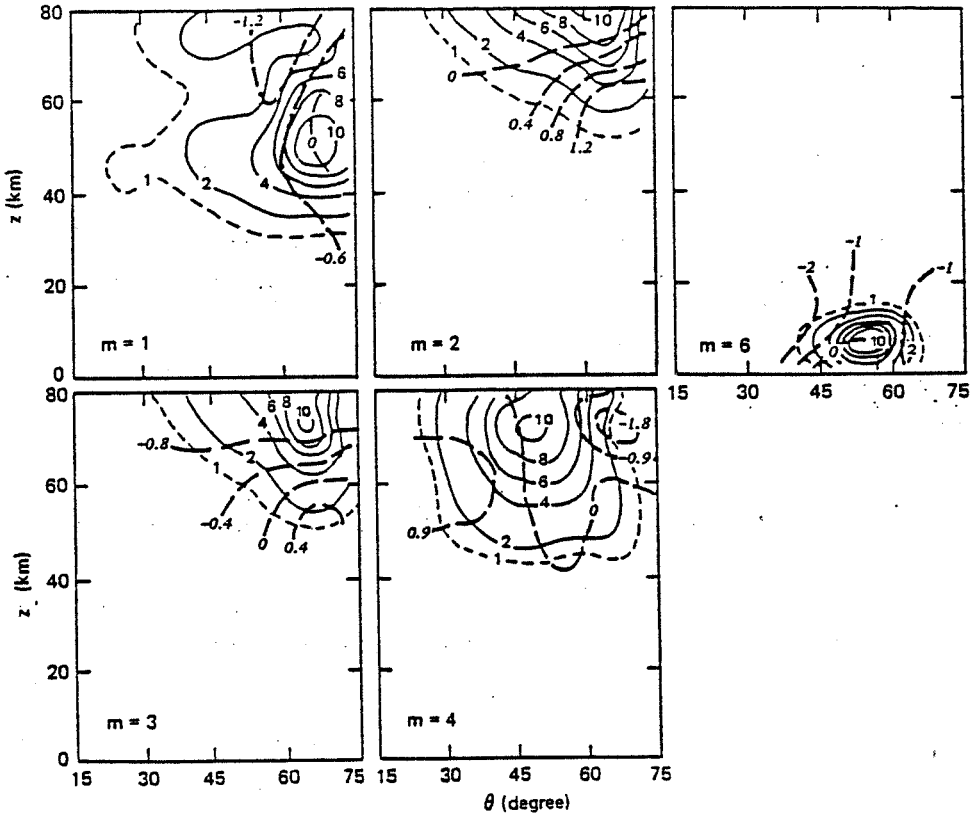

Figure 6. The geopotential eigenfunctions for waves m = 1 - 4 in the summer mesosphere, for wave m = 6 in the summer troposphere. The units of amplitude (solid line) are arbitrary. The phases (broken line) are in π radians.

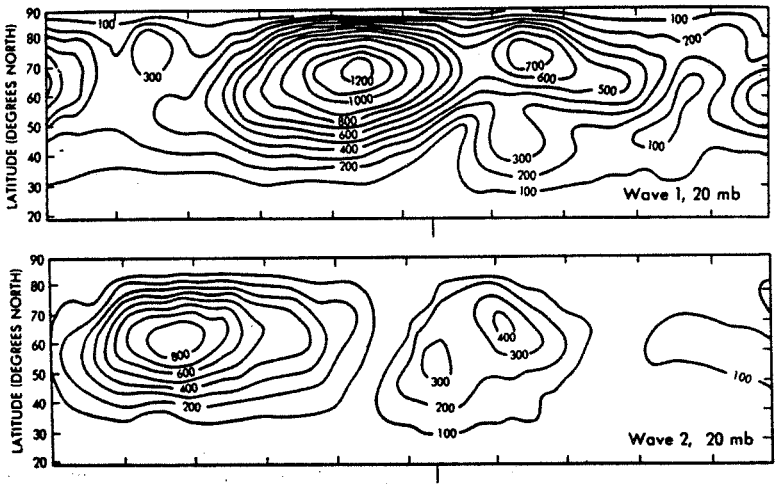

Figure 7. Latitude-time cross sections of geopotential height wave amplitude (meters) for waves 1 and 2 during the 1976/1977 sudden warming event (after O'NEILL and TAYLOR, 1978).

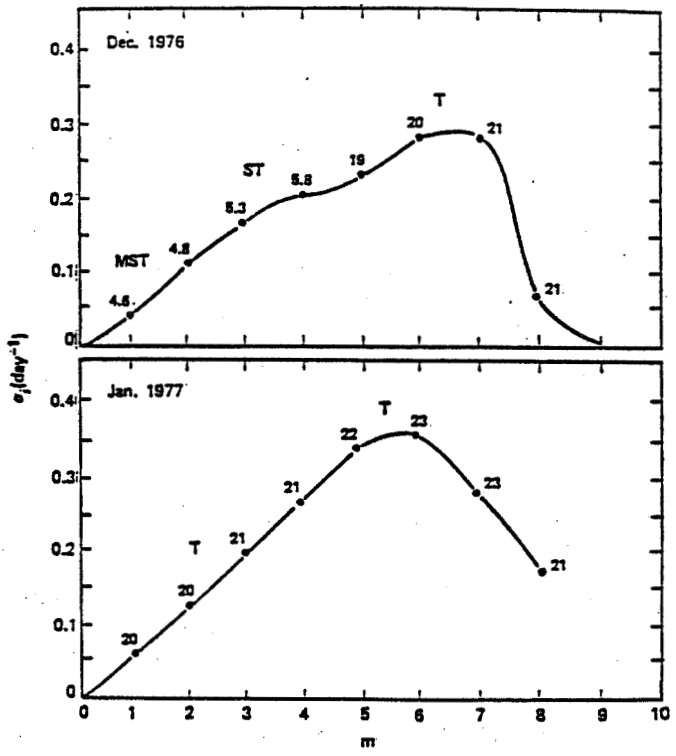

Figure 8. The growth rate (ordinate) and the phase speed at the equator (labeled in m/s) as a function of wave-number m.

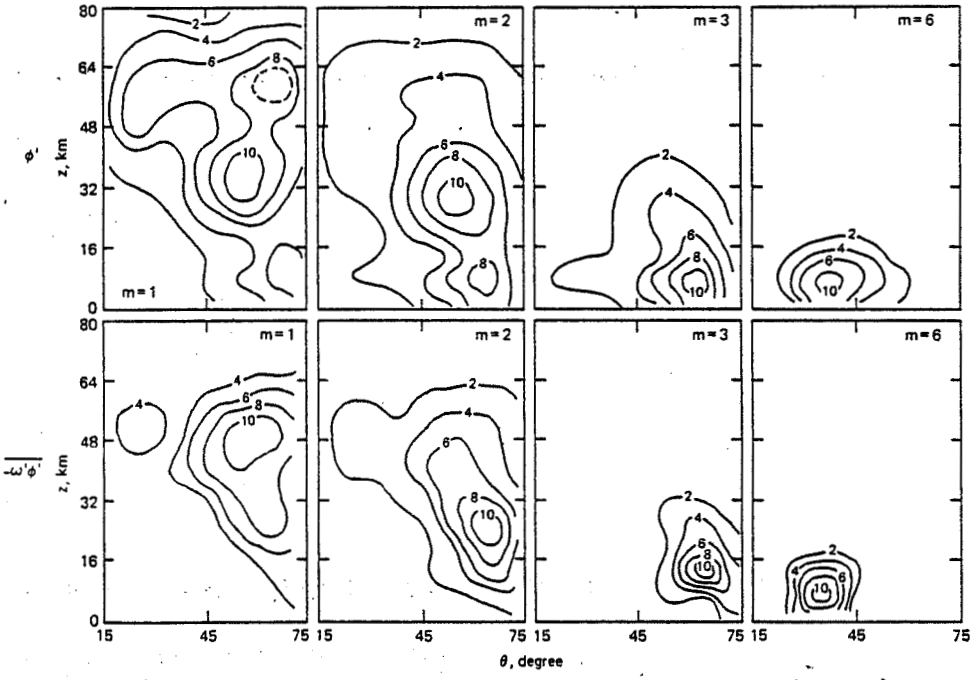

Figure 9. Geopotential (top) and wave energy flux (bottom) in December 1976. Units are arbitrary.

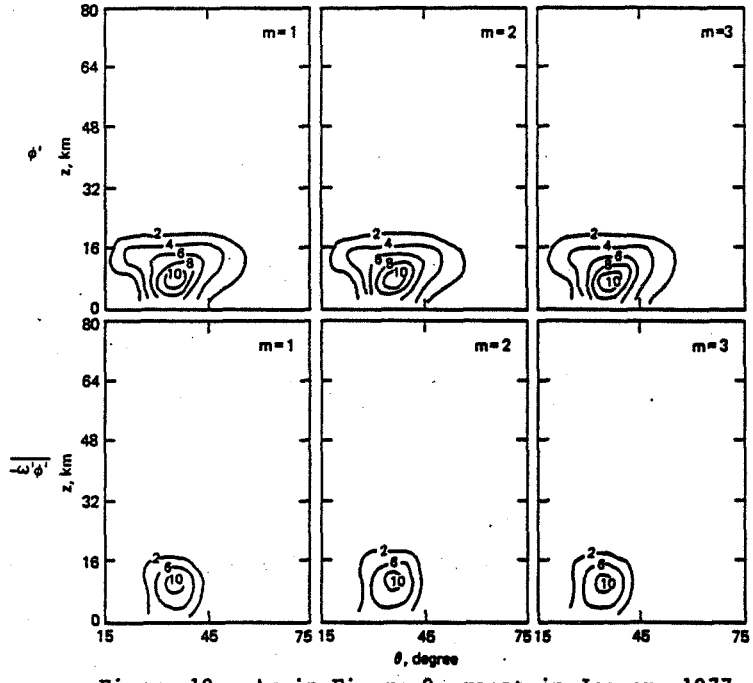

Figure 10. As in Figure 9 except in January 1977.

CONCLUSION

In conclusion, we propose a baroclinic instability for the generation of some planetary transient waves in the upper atmosphere. The usually observed transient waves 1 and 2 in the winter may have an origin of baroclinic instability in addition to the response to the external forcing. The mesosphere, the stratosphere and the troposphere are intimately coupled by the deep planetary waves in the winter circulation, while the summer circulation is vertically decoupled by the stratospheric easterly zonal wind. The computed unstable wave 3, confined to the mesosphere and the upper stratosphere, compares favorably with the observed 2-day wave.

REFERENCES

Hartmann, D. L. (1976), The structure of the stratosphere in the southern hemisphere during late winter 1973 by satellite, J. Atmos. Sci., 33, 1141-1154.

Labitzke, K. (1981a), The amplification of the height wave 1 in January 1979: A characteristic precondition for the major warming, Mon. Wea. Rev., 109, 983-989.

Labitzke, K. (1981b), Stratospheric-mesospheric midwinter disturbances: A summary of observed characteristics, J. Geophys. Rev., 86, 9665-9678.

Matsuno, T. (1971), A dynamical model of the stratospheric sudden warming, J. Atmos. Sci., 28, 1479-1494.

O'Neill, A. and B. F. Taylor (1979), A study of the major stratospheric warming of 1976-1977, Quart. J. Roy. Meteorol. Soc., 105, 71-92.

Rodgers, C. D. and A. J. Prata (1981), Evidence for a traveling 2-day wave in the middle atmosphere, J. Geophys. Res., 86, 9661-9664.

Venne, D. E. and J. L. Stanford (1982), An observational study of high-latitude stratospheric planetary waves in winter, J. Atmos. Sci., 39, 1026-1034.

Yu, W.-B., R. L. Martin and J. L. Stanford (1983), Long and medium-scale waves in the lower stratosphere from satellite-derived microwave measurements, J. Geophys. Res., 88, 8505-8511.

1.4B GENERAL CIRCULATION OF THE MIDDLE ATMOSPHERE

M. R. Schoeberl

NASA/Goddard Space Flight Center
Atmospheric Chemistry Branch, Code 964
Greenbelt, MD 20771

In both the tropical and extratropical regions there are a large number of dynamical problems which can be addressed by MST radars. The distinct advantage the MST radar has over rocket observations is continuous data acquisition. Without a doubt, the time-space spectrum of the mesospheric flow field is rich in high frequency motions associated with gravity waves rather than turbulent (random) fluctuations, and these events are particularly amenable to analysis with continuous data sets. In addition to the high frequency motions there are longer period fluctuations in the upper stratosphere and mesosphere wind fields which; combined with temperature fields derived from satellite data or lidars, can greatly enhance our knowledge of the upper atmosphere.

Previously, it had been thought that the mesosphere, like the stratosphere, contained very large-scale waves (which propagated up from the stratosphere) and intermittent turbulent fluctuations associated with local shear or convective instabilities. However, HODGES (1969) and LINDZEN (1967) pointed out that the likely source for the turbulent field is the convective breakdown of vertically propagating gravity waves. The theoretical requirement of a large vertical flux of momentum carrying gravity waves for the mesospheric mean circulation models (LINDZEN, 1981), and the indirect observational evidence of a large zonal mean meridional wind which would require a huge drag on the zonal flow (possibly hundreds of meters per second per day) to balance the Coriolis torque both indicate that a large flux of gravity waves from the troposphere does penetrate to mesospheric heights. It further suggests that the dynamics of the mesosphere may be much more complex than previously thought, as the stress on the local flow, set up by the breaking gravity wave, could produce an entire sub-spectrum of Rossby and gravity waves which are free to propagate laterally and vertically to other regions. For example, consider a mountain wave which penetrates to the mesosphere. The convective breakdown of this wave produces a stationary torque and a secondary circulation which would generate a train of Rossby waves much like the barotropic wave trains observed in the troposphere as well as secondary gravity waves.

In addition to the subspectrum of forced disturbances, the turbulent fluctuations produced by the convective breakdown of the gravity wave can have a profound effect on the heat and constituent transport in the mesosphere. The depth of the turbulent layer determines the mixing scale for fast transport of constituents as well as potential temperature. Since the mesosphere is a radiatively stable region, the mixing due to turbulence produces a downward flux of heat and tends to push the mesospheric lapse rate toward adiabatic. Thus the total production of turbulence and the depth of the turbulent layers is a relevant question to the thermodynamic budget of the mesosphere. Unfortunately, a single MST radar site is not adequate to determine the "climatology of turbulence" as there could be as much spatial variation in the turbulent field as there is in the surface orography.

The upward flux of momentum by small-scale waves has been measured by dual-beam radars (e.g. VINCENT and REID, 1983). But the dual-beam radar lacks precision in measuring the momentum flux due to large horizontal scale gravity waves and it may be difficult to separate the momentum transport by waves from the transport of the basic shear momentum by the turbulent field. In other words, there may be a local redistribution of momentum due to the effect of

turbulence on the mesospheric shear not associated with a flux of momentum from the troposphere.

In the equatorial zones, the dynamics of large-scale flows can be reduced to a two-dimensional problem (height and longitude). DUNKERTON (1982) has suggested that the mesopause semiannual oscillation could be induced by gravity waves. Unfortunately, the observations of the semiannual oscillation are not tremendously reliable and verification of the theory is difficult. A series of MST radars located along the equator would provide important input into our understanding of the dynamics of the tropical mesosphere.

To summarize, the MST radar can have tremendous impact on our understanding of the general circulation of the mesosphere and upper stratosphere. Single stations linked into networks could provide both continuous spatial and temporal information on medium and large scale waves in the mesosphere as well as the local climatology of turbulence. Multibeam stations can provide data on the vertical flux of momentum by small-scale (gravity) motions. Additional discussion of the impact of the MST radars on our understanding of the general circulation is discussed in FRITTS et al. (1984).

REFERENCES

Dunkerton, T. (1982), J. Atmos. Sci., 39, 2681-2690.
Fritts, D. C., M. A. Geller, B. B. Balsley, M. L. Chanin, I. Hirota, J. R. Holton, S. Kato, R. S. Lindzen, M. R. Schoeberl, R. A. Vincent and R. F. Woodman, (1984), Bul. Am. Meteorol. Soc., 65, 149-159.
Hodges, R. R., J. Geophys. Res., 74, 4087-4090.
Lindzen, R. S. (1967), Q. J. R. Meteorol. Soc., 93, 18-42.
Lindzen, R. S. (1981), J. Geophys. Res., 86, 9707-9714.
Vincent, R. A. and M. Reid (1983), J. Atmos. Sci., 40, 1321-1333.

1.5A PERFORMANCE OF THE COLORADO WIND-PROFILING NETWORK

R. G. Strauch, K. B. Earnshaw, D. A. Merritt,
K. P. Moran and D. W. van de Kamp

National Oceanic and Atmospheric Administration
325 Broadway, Boulder, CO 80303

The Wave Propagation Laboratory (WPL) has operated a network of radar wind Profilers in Colorado for about 1 year. The network consists of four VHF (50-MHz) radars and a UHF (915-MHz) radar located as shown in Figure 1. The Platteville VHF radar was developed by the Aeronomy Laboratory (AL) and has been operated jointly by WPL and AL for several years. The other radars were installed between February and May 1983. The radars, their remotely controlled operation, and their data processing are described by STRAUCH et al. (1984). In this paper we summarize our experiences with these radars and discuss some general aspects of tropospheric wind measurements with Doppler radar.

RANDOM SAMPLE CONSENSUS AVERAGE

In examining the performance of the Colorado Wind-Profiling Network it is important to understand how the data are acquired and averaged. The VHF radars at Fleming, Lay Creek, and Cahone have identical characteristics and operating procedures, as described by STRAUCH et al. (1984). One part of the data processing that is not fully described in that reference is the method used to average data for hourly wind profiles. This averaging is performed as follows for the VHF radars:

Twenty-four observations are made of the (u,v) wind components at each height during a total data acquisition time of about 48 min: twelve measurements are made with a 3-μs pulse duration, and twelve are made with a 9-μs pulse. The u and v components are measured simultaneously. The short pulse or "Low" mode is used to measure winds as close as possible to the surface and extending to about 9 km MSL (the sites are located at about 1.5 km MSL). Data are sampled at range intervals of two-thirds of the pulse width; heights from about 4 to 9 km are observed with both pulses. Figure 2 shows how the time is shared between the two modes of operation. Data acquisition starts on the hour and lasts for about 48 min; 2 min are required to analyze the data and the last 10 min of the hour are used for telephone (dial-up) communications with the network. Figure 3 shows the details of how the time is spent during each mode.

Following the 48-min observation period, the u and v components for each height are averaged using the random sample consensus method (FISCHLER and BOLLES, 1981). The mean radial velocities of the twelve observations at each height are examined to find the largest subset of data points whose mean radial velocities are within two Doppler spectral points of each other. The total number of spectral points in the Doppler velocity spectrum is 64; the window of acceptable data is, therefore, one-sixteenth of the total radial velocity interval. If the largest subset is four or more, the average of this subset is taken as the mean radial velocity during the 48-min observation period. If the largest subset is less than four, the data are discarded and no wind component is computed for that height. If there is more than one subset with the same (largest) number of data points, then the subset containing measurements closest to the end of the data-acquisition period is accepted. Both the u and v components must yield an acceptable subset to calculate wind speed and direction. The width of the velocity window corresponds to a horizontal wind speed of 7.3 m/s for the 3-μs pulse mode and 8.7 m/s for the 9-μs mode. This algorithm has proved effective for rejecting data contaminated by aircraft and for rejecting data when the signal-to-noise ratio is so low that the set of twelve estimates

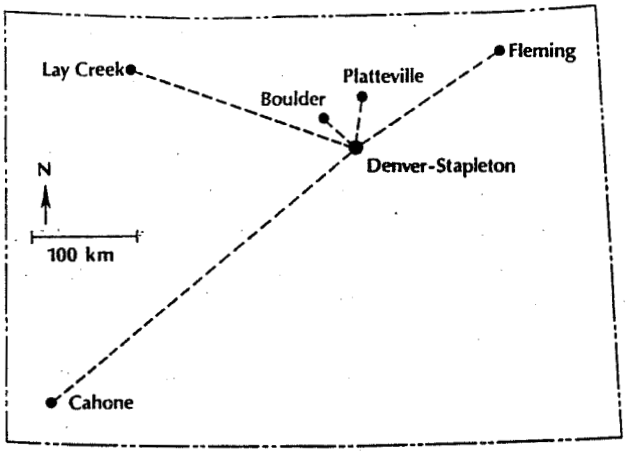

Figure 1. Location of radar wind Profilers. Data are transmitted by telephone to a control computer located at the WSFO at Denver.

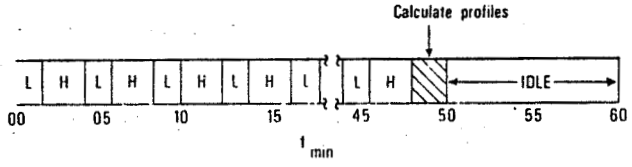

Figure 2. Hourly sequence of wind observations with 3-μs pulses (L) and 9-μs pulses (H). The idle period is for network communications.

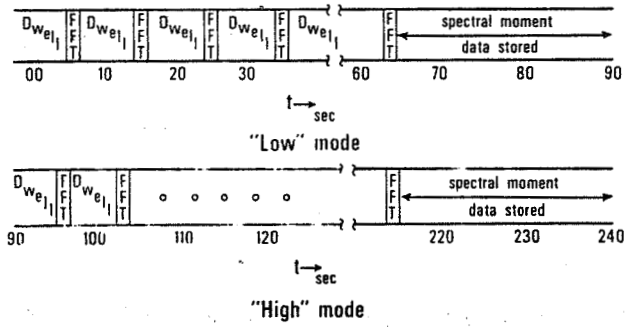

Figure 3. Details of temporal averaging during the 3-μs ("LOW") mode and 9-μs ("HIGH") mode of operation.

of radial velocity are essentially uniformly distributed over the Nyquist velocity interval.

To see how this algorithm functions in the case of no atmospheric signal, and because an analytic solution for the probability of occurrence of the largest subset was not obvious, we simulated the performance. The probability p that exactly k values will be in the data window is the following:

k	p (largest subset = k)
0	0
1	0.007
2	0.413
3	0.463
4	0.104
5	0.013
6	0.001
7	0.001

The probability is zero that the largest subset is zero because the algorithm centers the window on each measured data point to count the subset. The probability that the largest subset is greater than seven is too low to measure by simulation. If the input is noise, the probability that the largest subset is four or more is 0.119; if estimates of both u and v are made in noise, the probability of obtaining a "valid" wind estimate is 0.014. When the radar attempts to measure winds at heights where the atmospheric signal is too weak to detect, the largest subset is usually two or three; this indicates that the radial velocity estimates are uniformly distributed, as they must be for this algorithm to function properly.

VHF RADAR PERFORMANCE

The Colorado Network radars have demonstrated that continuous hourly averaged wind profiles could be provided by a national network of radars with automated and unattended operation. Figure 4 shows a sample of the hourly averaged winds measured by the VHF radar at Fleming. (Some of the problems that are apparent with the data from 0600 to 1500 GMT on Feb. 24, 1984, are discussed below.) The details that can be observed during events such as frontal passages give a temporal and spatial picture of the flow fields that is not presently available to the operational meteorologists. Whether this picture can lead to improved weather forecasting is a question that must be answered before an operational network is pursued; however, the interest in such data by commercial aviation is obvious.

An important question in the design of a tropospheric wind Profiler is that of sensitivity: given a desired height resolution, an averaging time for the wind data, the maximum height desired, and the fraction of the time the winds must be measured, how sensitive must the radar be? For VHF radars the answer to this question determines the average transmitted power and effective antenna area required. The VHF radars in the Colorado Network have a power-aperture product of 10^6 W-m^2: 400 W of average transmitted power and a 50 m x 50 m antenna. Figure 5 shows the percentage of time the Bay Creek radar was able to measure hourly winds as a function of height. The squares are the data points for the 3-μs pulse mode, and the circles are the data for the 9-μs mode. Both the u and v wind components passed the random sample consensus test, described in the first section, for the percentage of time shown (as a function of height). The data are from 450 profiles (for each pulse mode) obtained from Nov. 12 to Dec. 12, 1983. We do not have these statistical results from all the data; in general, we expect the same trend as shown in Figure 5, but the rapid decrease in height coverage that starts at about 16 km (9-μs mode)

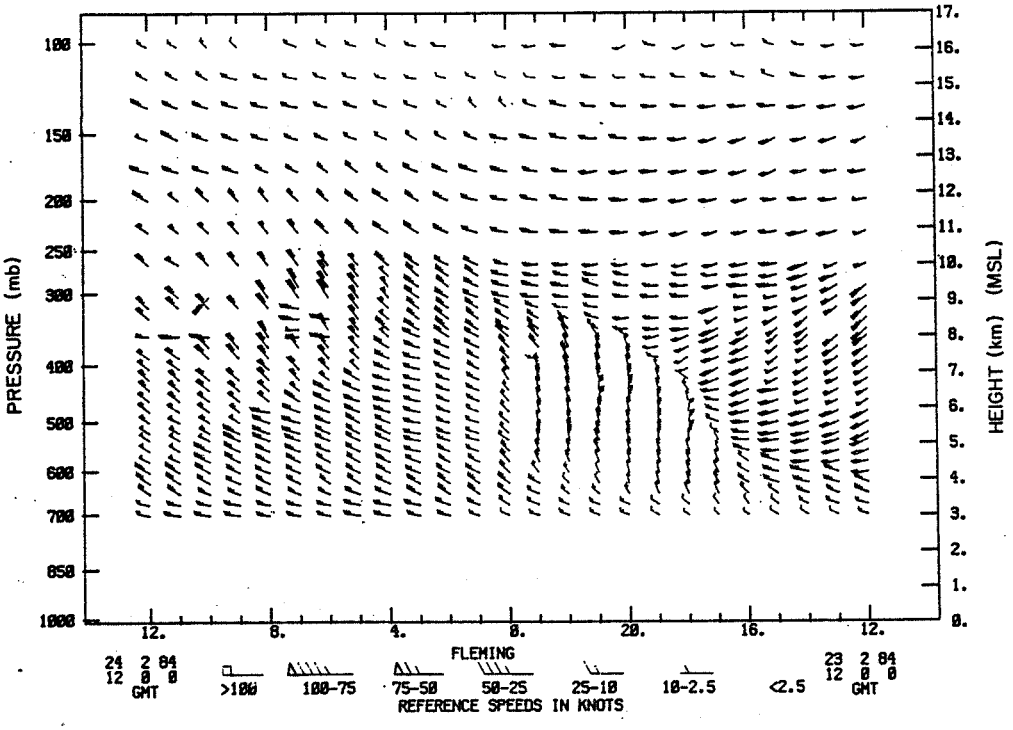

Figure 4. Sample of hourly averaged winds measured by the 6-m wavelength radar at Fleming.

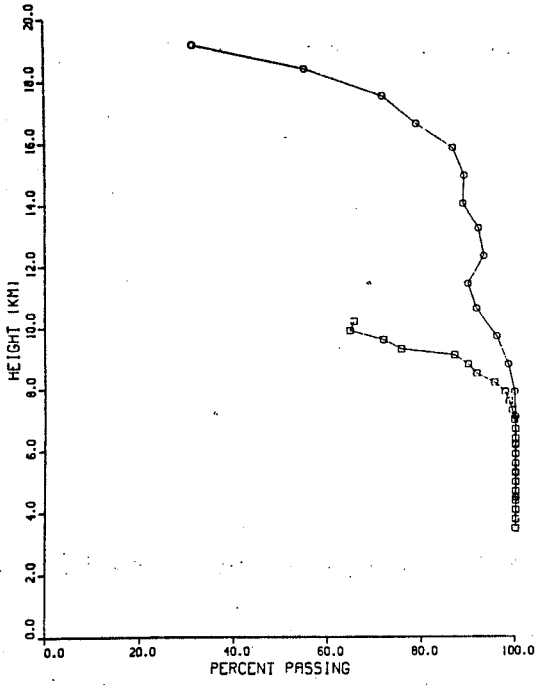

Figure 5. Percentage of time the 6-m radar at Lay Creek was able to measure wind profiles with a 3-μs pulse (squares) and a 9-μs pulse (circles). Power aperture product is the same for both modes. Data shown are from 450 profiles measured from Nov. 12 to Dec. 12, 1983. Twelve profiles are measured during each hour; four or more must pass the consensus test.

for the winter data will probably start at about 14 km for summer data. The decrease in percentage coverage at about 12 km is due to signal dropout in the core of a jet stream that was over the Network during this period. No systematic data analysis has been performed to sort out the different meteorological regimes.

Figure 6 shows what percentage of the data would have passed the random sample consensus if the algorithm had required that 8 or more of the 12 observations be in the largest subset. The decrease in percentage at about 5 km altitude (3-μs mode) is probably a result of moving clutter, such as automobile traffic, which would tend to cause the data system to select a false velocity, whereas fixed clutter is rejected (to a large extent) by the data processing. Figure 7 shows the percentage of the u (squares), v (circles), and both u and v (triangles) components that pass the consensus. We believe the difference in the u and v data reflects the difference in radar sensitivity (separate transmitters, receivers, and antennas) rather than a difference in radar reflectivity.

The accuracy of the wind measurement is difficult to assess because there is no reference or standard available for comparison. We believe the major limitation on the accuracy of the hourly averaged winds lies in the assumption that the vertical winds averaged over an hour are negligible. If the vertical winds are negligible, then a worst-case accuracy can be found by examining the data-averaging algorithm; if we have but four measured data points in the largest subset, and they are uniformly distributed over the velocity window, then the variance of the consensus-averaged u or v will be $\approx 1.3\ m^2/s^2$. In general, the variances of u and v will be less than $1\ m^2/s^2$ because there

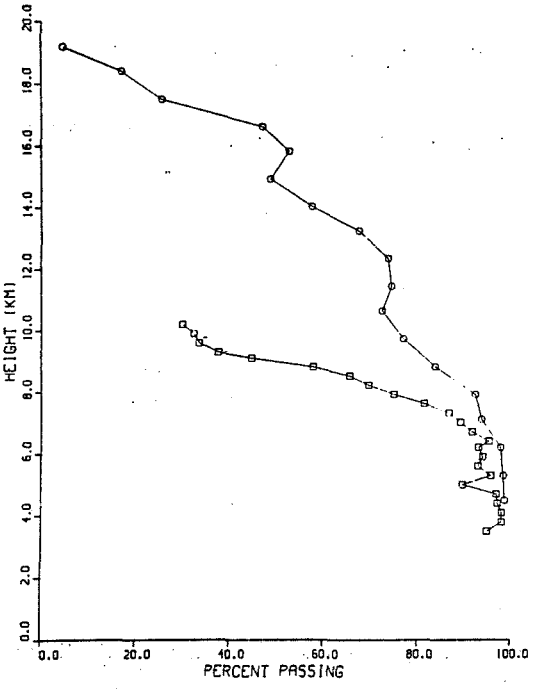

Figure 6. Same as Figure 5 but 8 or more of the 12 profiles must pass the consensus test.

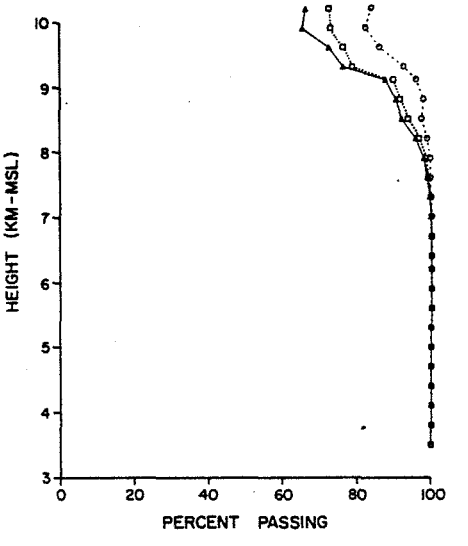

Figure 7. Percentage of time the 6-m radar was able to measure u (squares), v (circles) and both u and v (triangles) with the 3-μs mode. Same data as in Figure 5. Four or more must pass the consensus test.

are usually more than four estimates in the average and they are not uniformly distributed in the window. The spatial and temporal consistency of the wind profiles indicates that the variance of the estimates of hourly averaged winds is much less than 1 m^2/s^2.

VHF RADAR PROBLEMS

Some of the problems encountered with the VHF radars in the Colorado Network are associated with the particular hardware implementation we used and some are the result of VHF operation.

Problems associated with VHF operation:

(1) Frequency allocations are difficult to obtain at VHF. The frequency allocation for the Colorado Network is on a noninterference basis with another user.

(2) Even when frequency allocations are obtained, the authorized bandwidth limits the height resolution of the radar. The bandwidth authorized for the Colorado Network is 400 kHz, so the best height resolution is about 400 m.

(3) The weakest signal that can be detected by the VHF radars is about -145 dBm. It is difficult to avoid interference from the many communications systems that operate at nearby frequencies. We have had occasional interference problems with all our VHF systems.

(4) A remote site with an acre or more of level ground is required. We selected our VHF radar sites in rural Colorado to be at least 10 miles from small towns or airports; sites were relatively easy to find, and all the sites are relatively free from moving clutter. However, the remote locations can lead to problems with primary power and telephone service. The radar site at Lay Creek has had very unreliable power; power outage occurred several times per week during the thunderstorm season. The computer at that site had to be modified so it could be reset by telephone. (All systems self-start after power failure unless the power remains off for more than 30 min; if this happens the computer must be reset.) The site near Craig has also had telephone problems; when telephone service is interrupted, rural locations are the last to be restored. Note in Figure 4, for example, data for the 3-μs mode was lost during telephone transmission at 1500 GMT on Feb. 24, 1984.

Problems related to our particular hardware:

(1) The minimum height that can be measured in the 3-μs pulse mode is about 1.7 km AGL. It should be possible to measure winds below 1 km AGL, but the combination of recovery time of the transmit/receive switch and switching transients limits the minimum height.

(2) The power-aperture product of 10^6 $W\text{-}m^2$ does not always permit hourly wind measurements at all heights of interest. In particular, the core of the jet stream is a region of poor signal-to-noise ratio where signal dropout occurs. Note the data dropout at about 300 mb from 0600 to 1600 GMT on Feb. 24, 1984, in Figure 4. Whether this is a serious problem that needs to be corrected by increased average transmitted power or increased antenna aperture must be determined by the users.

(3) Colinear-coaxial dipole arrays provide a low-cost, large-aperture

antenna. Their radiation patterns are not of high quality, and antenna sidelobes have caused some problems. The enhanced echo observed with VHF zenith-pointing radars can sometimes be strong enough to be observed through an antenna sidelobe. This spurious signal from the zenith, if it is strong enough, can cause the velocity estimate for that height to be near zero. We believe this is the explanation for the group of wind vectors that show only west winds near 300 mb from 0600 to 1400 GMT on Feb. 24, 1984 (Figure 4). The north-pointing antenna measured almost zero radial velocity. The signal-to-noise ratio of the turbulence echo is low in this region (note the dropouts discussed above), so it could be smaller than the specular signal observed through an antenna sidelobe. The main lobe of the antenna points 15 degrees off-zenith; a pointing angle change to direct an antenna pattern null toward zenith could reduce the number of times this occurs. Other spurious echoes occur occasionally, but their origin cannot always be identified. A higher-quality illumination pattern would no doubt eliminate some of them.

(4) We have operated the radars at remote stations (one site is an 8-h drive from the laboratory) in an unmanned and automated mode. The remote locations cause maintenance problems, particularly with hardware that has not been through development and tests for long mean times between failures. Most of our problems are associated with high-voltage/vacuum-tube transmitters; the problems are easy to correct and the radar is usually returned to operation a short time after someone reaches the site. We have relatively unskilled local people available to correct problems that can be diagnosed by telephone, and they have been very valuable in saving time and travel. However, successful operation of a network of Profilers that operate unmanned requires that skilled personnel make routine visits for preventative maintenance; in our year of operation we have responded to problems rather than trying to prevent them.

All of the problems associated with our particular hardware implementation can be solved, so we conclude that a network of VHF wind Profilers is feasible provided that the fundamental constraints of frequency allocations, bandwidth, and interference, imposed by VHF operation, do not unduly compromise the measurement objectives.

UHF RADAR OPERATION

The 915-MHz (33-cm wavelength) radar was installed near the Weather Service Forecast Office at Denver's Stapleton International Airport in January of 1983. Unlike the remote VHF radars, which have been operated in the same mode since they were built, the UHF radar has operated in many different modes for special experiments and comparisons with other instruments. When it is used for wind profiling, the data processing and signal averaging are the same as for the VHF radars. The UHF radar uses pulse widths of 1-, 3-, and 9-μs with corresponding average power-aperture products of 1.1×10^4, 2.6×10^4, and 4.5×10^4 W-m^2. Observation of u, v, and w wind components is sequential, not simultaneous. Hourly averages of 12 observations are made in each antenna position and with each pulse width.

Figures 8-10 illustrate the height coverage of the UHF radar. These figures show the results of 415 profiles (for each pulse width) acquired from Nov. 5 to Nov. 23, 1983. Circles show the north antenna data, squares show the east data, and triangles show the percent of the profiles where both the north and east data passed the consensus. Figure 8 shows data for the 1-μs pulse mode with a largest subset required of 5 or more of the 12 observations. The

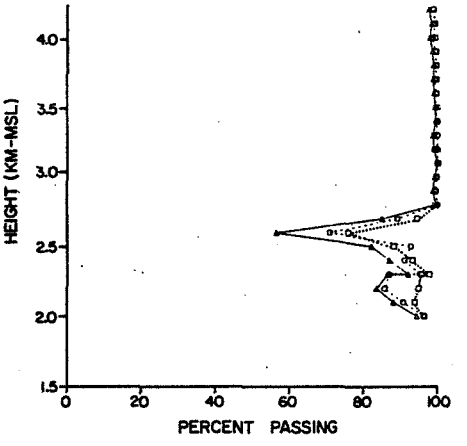

Figure 8. Percentage of time the UHF radar was able to measure hourly averaged winds in the 1-μs pulse mode. East component (squares), north component (circles), and both components (triangles) passed the consensus test with 5 or more of 12 profiles in the largest subset. Data are from 415 profiles obtained Nov. 5 to Nov. 23, 1983.

radar is located at 1.6 km MSL; the first range gate is about 350 m AGL. Data are sampled every two-thirds of a microsecond or about every 100 m in height to about 4.3 km MSL. The consensus algorithm shows the problems caused by clutter in the lowest eight range locations (1.9-2.7 km MSL). The abrupt decrease in percentage passing at 2.6 km is caused by traffic on a nearby interstate highway; moving clutter cannot be eliminated in the Doppler spectrum as readily as fixed clutter. The signal-to-noise ratio of the atmospheric scatter is higher at these lower altitudes than it is at the upper heights where the winds are measured nearly all the time. The clutter is strong enough to impair the ability of the radar to measure winds in the lowest 1.1 km AGL. Figure 9 shows the 3-μs pulse data when the largest subset required is eight or more. Figure 10 shows the corresponding data for the 9-μs pulse mode. The increased height coverage with 9-μs pulses as compared with the height coverage with 3-μs pulses is much less pronounced for the UHF radar than for the VHF radar

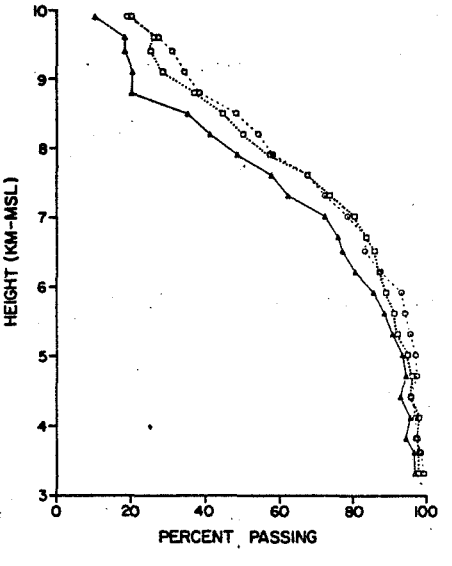

Figure 9. Same as Figure 8 except the data are obtained with a 3-μs pulse and a largest consensus requirement of 8 of 12 profiles.

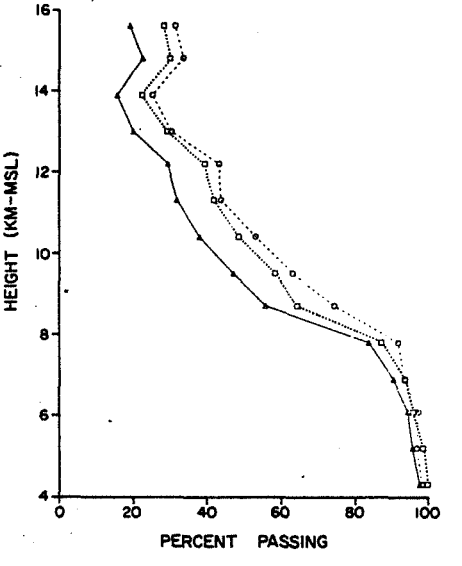

Figure 10. Same as Figure 8 except the data are obtained with a 9-μs pulse and a largest consensus requirement of 8 of 12 profiles.

(Figures 5 and 6). At the 60% passing level, the 9-μs pulse mode only increased the height coverage by about 1 km for the UHF radar. For the UHF radar the power-aperture product of the 9-μs mode is 6 dB greater than the 3-μs mode, but for the VHF radars it is the same so the height coverage difference is all the more dramatic. We believe the failure of the increased sensitivity of the 9-μs mode to increase the height coverage of the UHF radar is an indication that the inner scale of turbulence is less than half the radar wavelength at 10 km MSL or below in at least some meteorological conditions. The 33-cm radar can measure winds to 14 km MSL in some cases, but its wavelength may be too short for routine tropospheric coverage. We are comparing the reflectivity profiles of the 33-cm radar with those measured by a colocated 10-cm radar to attempt to identify how the inner scale of the inertial subrange limits the measurement height at these two wavelengths.

UHF RADAR PROBLEMS

Problems associated with using UHF radar for wind profiling:

(1) The height coverage of the UHF radar may be limited more by the scattering mechanism than by sensitivity (power-aperture/noise temperature) considerations.

(2) Clouds and precipitation detected from antenna sidelobes can be stronger than the refractive turbulence signal from the main lobe. Although this has no doubt occurred with our 33-cm radar, we do not have a procedure to identify when it happens.

Problems encountered that are related to our particular UHF hardware implementation:

(1) A major airport is an extremely poor choice for a site for a sensitive clear-air radar. The ground clutter in the lowest 1.1 m height impairs our ability to measure winds close to the surface. The clutter power does not saturate the receiver or data system, so it would be much more tolerable if it was not caused partly by moving targets (automobiles, aircraft taxiing and flying).

(2) The only component failures in a year of operation are the mechanical rf switches that select the antenna pointing direction. They are being replaced with another type of switch with a longer rated life time.

(3) The maximum power-aperture product available is 8×10^4 W-m^2; the height coverage expected with this radar is less than expected with the VHF radars.

(4) The UHF radar uses the same data processing as used with the VHF radars. However, the VHF radars require 5 or 6 s to acquire the time series of radar returns needed to calculate a 64-point Doppler velocity spectrum whereas the UHF radar acquires the same data in about two-thirds of a second. (The dwell time is proportional to the radar wavelength.) Therefore, software power spectral analysis does not represent a serious overhead time (about 1 s) for the VHF radars, but it seriously reduces the incoherent integration time available for the UHF radar.

(5) A zenith-pointing antenna position is included in the UHF radar, because the scattering from hydrometers can exceed that from refractive turbulence, and therefore a correction for particle fallspeeds must be made during precipitation. The correction has not been implemented.

(6) We have observed occasional interference from other transmitters. A request has been made to shift transmitted frequency to between 910 and 915 MHz to solve this problem.

WIND MEASUREMENTS WITH FIXED-BEAM DOPPLER RADAR

The radar wind Profilers in the Colorado Network are fixed-pointing systems with two or three pointing directions. The two-beam systems have orthogonal viewing directions at 15 degrees off-zenith; the three-beam systems also have a zenith-pointing position. The choice of elevation angle and the method of wind measurement is discussed by STRAUCH et al. (1984).

The meteorological assumptions needed to measure hourly averaged horizontal wind profiles with a two-beam system are (a) the errors cause by vertical velocity will be negligible; and (b) the horizontal wind components, measured at separated volumes in space, are representative of the mean wind at the radar location. Vertical velocity at the measurement volume causes an error in the measured horizontal wind component of $w \tan \Theta_e$ (m/s) where w is the vertical wind and Θ_e is the elevation pointing angle. For the Colorado radars we must assume $w < 0.25$ m/s for an hourly average if the error in the horizontal component is to be less than about 1 m/s. The representativeness assumption applies when the horizontal components are combined and said to be the vector wind at the radar location. The difference in the wind at the measurement volume and at the radar is (grad u_i) (h) cotan Θ_e where h is the measurement height and grad u_i is the mean gradient of the wind component in the direction that the component is translated. Gradients normal to the translation direction do not enter into the wind calculations; nevertheless, a tacit assumption of a locally uniform wind field underlies the two-beam measurement technique. It is important to note that vertical wind causes errors in the measured horizontal wind components. Horizontal gradients do not introduce an error in the horizontal wind component at the measurement location. In some applications the wind components would be assigned to their actual locations so there would be no error from horizontal gradients.

The meteorological assumptions needed to measure hourly averaged winds with a three-beam system are that horizontal gradients of w will cause negligible errors and that the wind components measured at separated volumes can be combined to form a vector wind. Horizontal wind accuracy of about 1 m/s requires that (grad w) (h) cotan Θ_e be less than 0.25 m/s. The assumption of a locally uniform wind field is unchanged with the addition of a third beam. The third beam adds relatively little to the ability of the radar to measure hourly averaged horizontal winds. The zenith beam provides a direct measurement of w, and it measures the temporal scale of vertical fluctuations so it can indicate the temporal averaging period needed to reduce vertical motion contamination of horizontal measurements. The two-beam system will have significant errors in the measured horizontal components if the period of vertical velocity perturbations is long compared with the averaging time; the three-beam system allows a correction for this long-term vertical motion but only if the spatial wavelengths of w are large compared with the separation of the measurement volumes. Correction of the horizontal winds for vertical motion on a short-term basis (wind components are measured every 2 min in the VHF systems) does not seem possible because the measured vertical motion cannot be related to the vertical motion where the horizontal winds are measured without some knowledge of the spatial wavelengths of w. Perhaps the greatest value of the zenith beam is that at VHF the vertical beam can measure the height of the tropopause (GAGE and GREEN, 1982), while at shorter wavelengths the vertical beam can allow a correction for fallspeed of particles in widespread precipitation.

CONCLUSIONS

The Colorado Wind-Profiling Network operates continuously and unattended; it automatically measures hourly average vertical profiles of the horizontal wind and sends these data to a central control computer. Experience with the radars has shown that an operational network of wind Profilers is feasible. We believe that this network could use radar wavelengths in the range of 0.7 to 7 m (40 to 400 MHz). The wavelength choice would depend on available frequency allocations and the data requirements.

ACKNOWLEDGEMENTS

The cooperation and assistance of the Atmospheric Dynamics Group of the Aeronomy Laboratory are gratefully acknowledged. The VHF radar techniques we have exploited were developed in that group by Ben Balsley, Warner Ecklund, and Dave Carter. Tony Riddle has assisted us in processing Platteville data, and Judy Schroeder obtained the statistics on radar coverage.

REFERENCES

Fischler, M. A. and R. C. Bolles (1981), Random sample consensus: A paradigm for model fitting with application to image analysis and automated cartography, Commun. Assoc. Comput. Mach., 24, 381-395.

Gage, K. S. and J. L. Green (1982), An objective method for determination of tropopause height from VHF radar observations, J. Appl. Meteorol., 21, 1159-1163.

Strauch, R. G., D. A. Merritt, K. P. Moran, K. B. Earnshaw and D. van de Kamp (1984), The Colorado wind-profiling network, J. Oceanic Atmos. Tech., in press.

N85-32476
49

1.6A VERTICAL TRANSPORT IN THE ATMOSPHERE - MEASUREMENT CAPABILITIES AND REQUIREMENTS OF VHF RADARS

J. Rottger*

EISCAT Scientific Association
981 27 Kiruna, Sweden

Mass exchange, mixing or transport in the atmosphere involves reversible processes, i.e. any kind of organized motions such as wave and large-scale flows, and nonreversible processes, i.e. molecular and turbulent diffusion. Without evaluating in detail the relative efficiency of these processes, it shall be attempted here to summarize those phenomena which can be qualitatively (and eventually also quantitatively) observed with VHF radars. We will only consider mixing in the vertical direction, since this appears to be the essential part of transport processes to which VHF radars can contribute better understanding. We will first briefly discuss mixing processes in the troposphere and thereafter also outline possible contributions of VHF radars to study the mass exchange processes between the troposphere and stratosphere. Transport in the middle atmosphere will be briefly summarized, since it is in principle similar to transport in the lower atmosphere.

The troposphere is the portion of the neutral atmosphere which is more likely to be convectively unstable than other altitude regions. Essentially, the vertical transport in the troposphere is due to the convection processes, namely, thunderclouds. As shown in Figure 1a (from WALLACE and HOBBS, 1977), up- and downdrafts transport substantially and very efficiently air masses between the bottom and top of the troposphere. In Figure 1b (from ROTTGER, 1980) observations with a VHF radar during the passage of a thundercloud are shown. These depict the turbulent velocity σ_W, the echo power P (consistent with the radar reflectivity), and the mean vertical velocity W. The rise of the upper limit of the power level from about 7 km to 10 km altitude indicates the rise of the cloud top up to the tropopause. Mean upward velocities were almost 10 m s^{-1} and fluctuating velocities several m s^{-1}. The qualitative similarity between Figure 1a and Figure 1b unveils the capabilities of VHF radars to investigate the dynamics of these convective processes and it is proposed that more work should be done for deducing qualitative results on entrainment and detrainment of air masses in and around the thunderclouds as well as on vertical exchange of air masses.

The vertical transport due to convection is very pronounced in the tropical regions, which essentially drives the mean global circulation. As shown in Figures 2a and 2b (from REITER, 1975), the (vertical) flow pattern changes consistently with latitude and season. Since VHF radars exhibit a unique capability to measure vertical velocities, a continuous operation of a chain of VHF radars along a meridian would be a suitable contribution to monitor the mean vertical transport.

Another process, gaining vertical mixing, is active turbulence generated by shear instability. Pronounced regions of this clear-air turbulence are associated with velocity shears in jet streams. An example of this kind of turbulence is shown in Figure 3, depicting the vertical velocity fluctuations measured with a VHF radar (from ROTTGER and SCHMIDT, 1981). The intense vertical velocity fluctuations (between 00 UTC and 09 UTC in the height region 8-12 km) occurred in connection with a jet stream associated with a warm front pas-

*presently at Arecibo Observatory, Arecibo, Puerto Rico, on leave from Max-Planck-Institut fur Aeronomie, Lindau, W. Germany

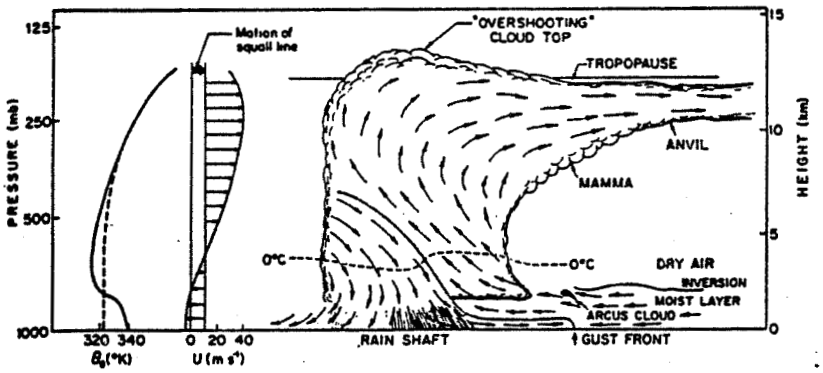

Figure 1a. Schematic description of a cumulonimbus tower (from WALLACE and HOBBS, 1977).

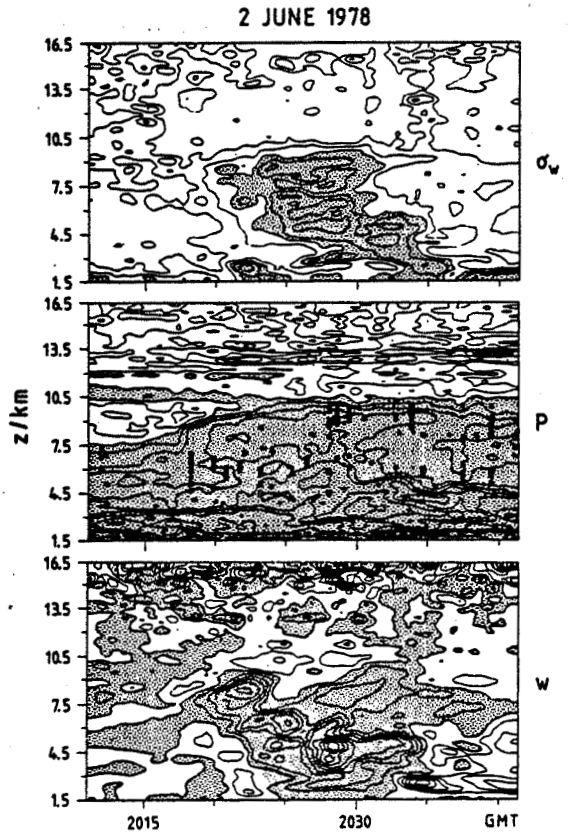

Figure 1b. Contour plots of vertical velocity W, power P and velocity fluctuations σ_W observed during the overhead passage of a thundercloud. The contour levels of W are drawn in steps of 1 m s^{-1}, the gray shaded areas are upward velocities. The contour steps of P and 4 dB, and 2 m s^{-1} for σ_W (from ROTTGER, 1980).

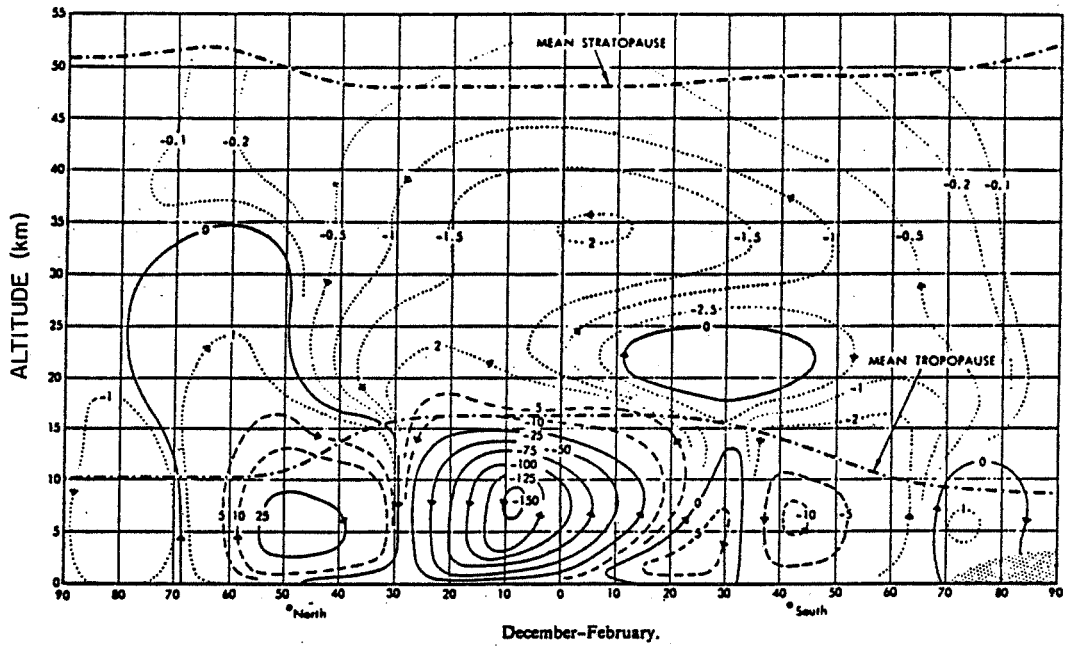

Figure 2a.

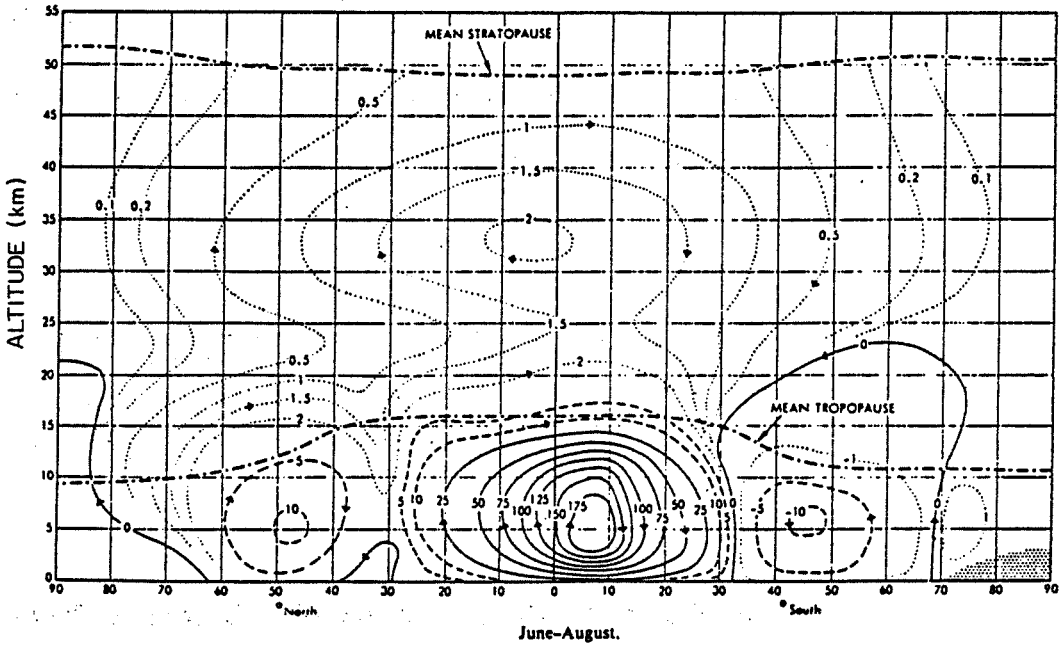

Figure 2b. Mean meridional circulation (from REITER, 1975).

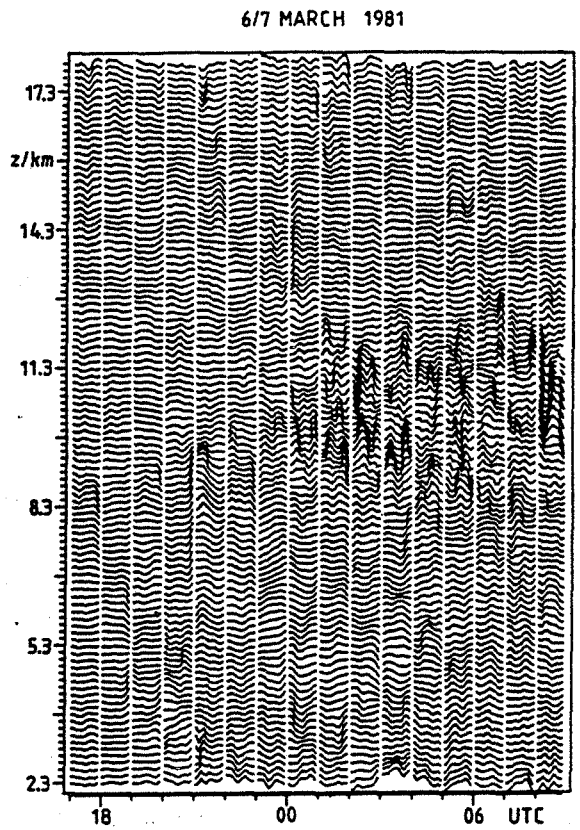

Figure 3. Time series of vertical velocity (W) fluctuations during 10-min periods, following each full hour. One unit of the z-axis is Δz = 150 m, and also corresponds to $W = 0.4 \text{ m s}^{-1}$ (from ROTTGER and SCHMIDT, 1981).

sage. This is explained by the series of Figures 4a-4d (from LARSEN and ROTTGER, 1982). The mechanism of Kelvin-Helmholtz instability generating the clear-air turbulence was intensively investigated with VHF radars (e.g., RUSTER and KLOSTERMEYER, 1983). It is envisaged that further efforts will take place such as the continuous monitoring of vertical velocity fluctuations with VHF radars to get an improved statistical climatology of clear-air turbulence, its connection to synoptic-scale disturbances, and the associated vertical transport (see example of Figure 5 (from ECKLUND and GAGE, 1981)).

Convergences and divergences in synoptic-scale disturbances result in changes of the flow pattern also in the vertical direction. This apparently occurs around the jet stream and was measured with VHF radars (e.g., GAGE et al., 1980), and also on larger scales due to nonhorizontal flow of warm and cold air in the frontal systems, occurring in connection with synoptic-scale disturbances. This is shown in Figure 4b where the vertical velocity changes its direction before and after the passage of the front. In further VHF radar observations one evidently has to evaluate more distinctly this kind of synoptic-scale vertical velocity and its impact on large-scale vertical transport. A very promising attempt has already been made by NASTROM (1984).

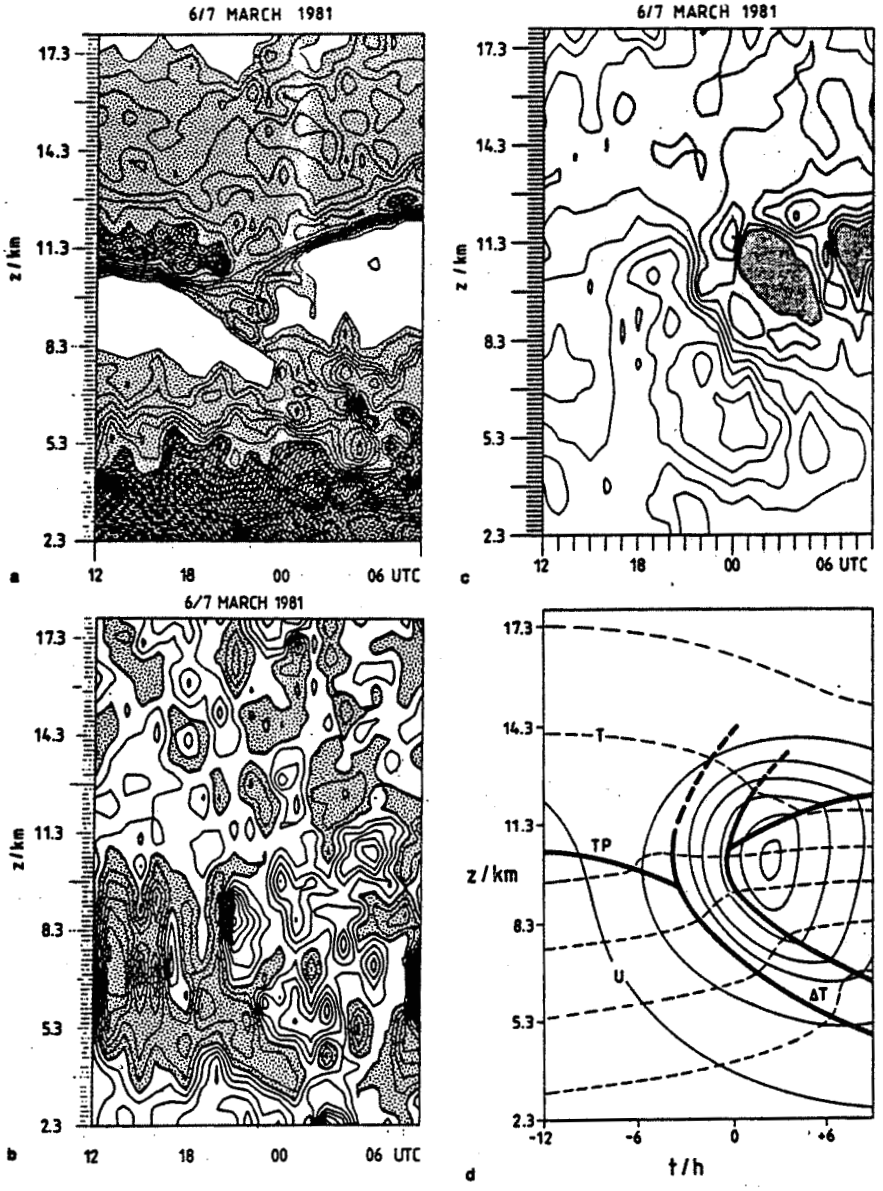

Figure 4. (a) Reflectivity contour plot. Difference between contour lines is 2 dB. Intensity of shading corresponds to intensity of echoes. (b) Contour plot of vertical velocities. Shading indicates downward velocity. The interval between contours is 7.5 cm/s. (c) Contour plot of wind speed with a contour interval of 2.5 m/s. Shading indicates speeds greater than 20 m/s. The heavy stippled areas correspond to missing wind data due to undersampling. (d) Thermal structure and wind near fronts adapted from PALMEN and NEWTON (1969). The heavy line-labeled TP corresponds to the tropopause. The dashed lines are the isotherms, and the solid lines are the isotachs. The jet is located on the warm side of the front just below the tropopause (from LARSEN and ROTTGER, 1982).

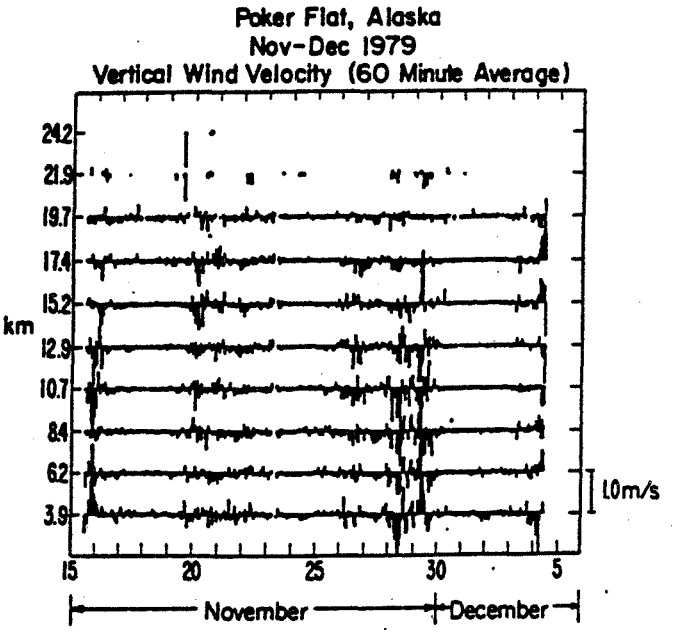

Figure 5. Twenty-one-day record of hourly averaged vertical velocities (from ECKLUND and GAGE, 1981).

The preceding examples were yet only discussed in terms of transport in the troposphere. As demonstrated by the VHF radar observations presented in Figure 6, the troposphere is more turbulent (larger fluctuations of vertical velocity W in the troposphere below ≈10 km) and wave structures occur in the more stable stratosphere. These are obviously two regions of different stability, separated by the boundary of the tropopause. The exchange of air masses between the troposphere and the stratosphere is fairly important since it means transport through a region of strongly increasing stability, namely, the tropopause. There are basically the following processes responsible for the mass transfer between the stratosphere and troposphere (REITER, 1975):

(1) the seasonal adjustment in the height of the mean tropopause level,

(2) organized large-scale horizontal and vertical motions expressed by the mean meridional circulation,

(3) large-scale eddy transport, mainly in jet stream regions, and

(4) mesoscale and small-scale eddy transport across the tropopause.

All of these processes can be understood by studying the preceding figures. REITER (1975) estimated that about 40% of the vertical transport is due to the Hadley cell circulation in the tropics, although vertical velocities in mid- and higher latitudes are also nonnegligible (e.g., Figure 8). One has also to consider that overshooting cumulonimbus towers (penetrative convection) transport tropospheric air into the stratosphere. Approximately 20% of mass exchange is caused by large-scale eddies of synoptic-scale disturbances and associated tropopause breaks (compare Figure 7 with the VHF radar observations presented in Figures 4), which can representatively be detected with VHF radars. About 10% of mass flux is estimated to be due to the seasonal changes of the

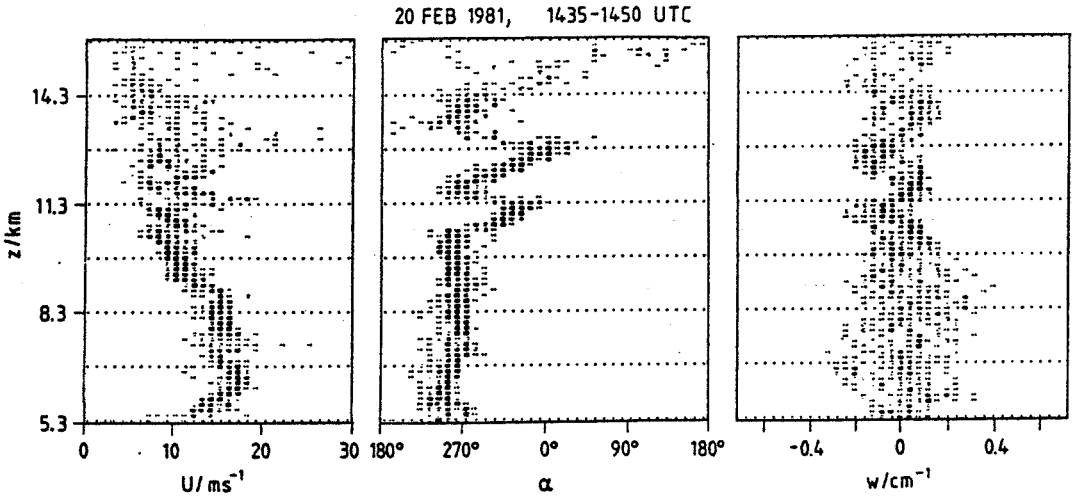

Figure 6. Wind speed U and direction α and vertical velocity W in the troposphere and lower stratosphere measured with a VHF radar.

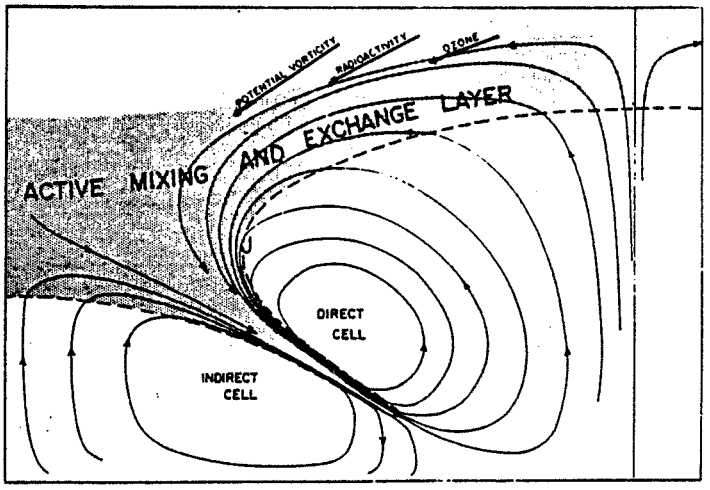

Figure 7. Vertical cross-section of a tropopause break (after REITER, 1975). The shaded zone corresponds to the region where stratospheric air intruded into the upper troposphere.

tropopause height, which also can be monitored continuously by VHF radars (e.g., Figure 8). Although REITER (1975) estimated that small-scale and mesoscale turbulent diffusion contributes only very insignificantly to the vertical transport, investigations of WOODMAN et al. (1981) resulted in a different conclusion. It is also worthwhile to study if and how much the wave motions observable with the VHF radars (e.g., Figure 6 and Figure 8b) contribute to vertical transport.

GELLER (1979) has reviewed the dynamics of the middle atmosphere including all scales of motions from the mean zonal flow down to small-scale turbulence.

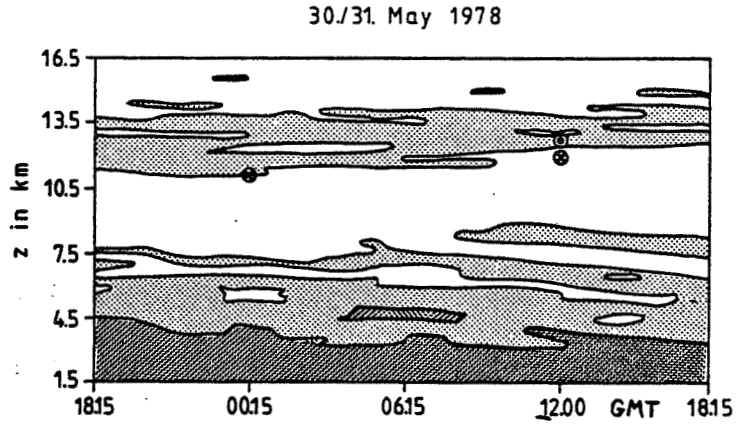

Figure 8a.

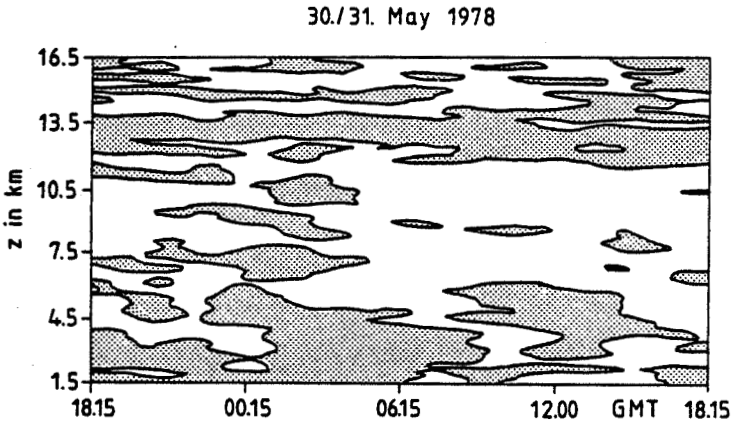

Figure 8b. (a) Tropopause measured with radiosondes (⊗) and by means of VHF radar reflectivity, which also indicates downward-sloping frontal zones in the tropopause (upper diagram). In the lower diagram (b) the corresponding mean upward (shaded) and downward velocity, measured with the SOUSY-VHF-Radar, are shown.

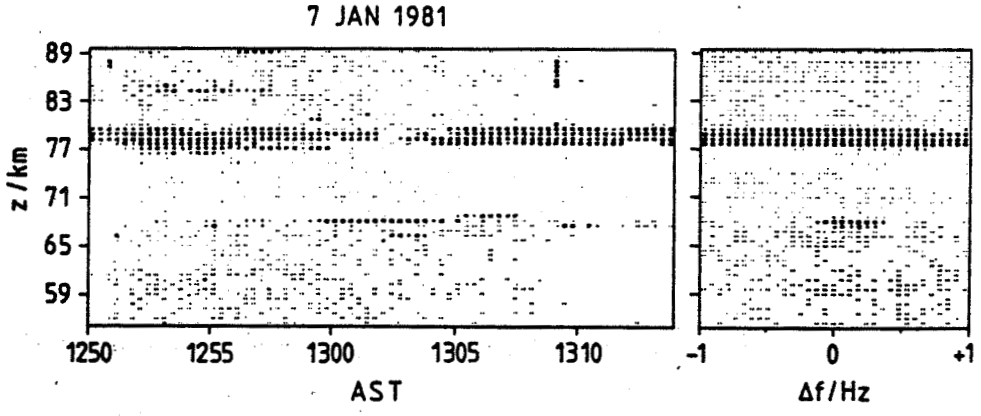

Figure 9. Mesospheric turbulence layers (left diagram) and their spectra, measured with a VHF radar at the Arecibo Observatory.

There is strong evidence now that gravity-wave motions and turbulence give rise to enhanced diffusion in the middle atmosphere (essentially in the mesosphere), and VHF radars are very suitable tools to study these phenomena. One obtains statistics of occurrence (see Figure 9) as well as turbulence intensity and velocity fluctuations from the Doppler spectra (see for instance ROTTGER et al., 1979; HOCKING, 1983; and many other papers referenced therein).

REFERENCES

Ecklund, W. L. and K. S. Gage (1981), Gravity wave activity in vertical winds observed by the Poker Flat MST radar, Geophys. Res. Lett., 8, 285-288.

Gage, K. S., J. L. Green and T. E. VanZandt (1980), Use of Doppler radar for the measurement of atmospheric turbulence parameters from the intensity of clear-air echoes, Radio Sci., 15, 407-416.

Geller, M. A. (1979), Dynamics of the middle atmosphere, J. Atmos. Terr. Phys., 41, 683-705.

Hocking. W. K. (1983), On the extraction of atmospheric turbulence parameters from radar backscatter Doppler spectra - I. Theory, J. Atmos. Terr. Phys., 45, 89-102.

Larsen, M. F. and J. Rottger (1982), VHF and UHF Doppler radars as tools for synoptic research, Bull. Am. Meteorol. Soc., 63, 996-1008.

Nastrom, G. D. (1984), Detection of synoptic-scale vertical velocities using an MST radar, Geophys. Res. Lett., 11, 57-60.

Reiter, E. R. (1975), Stratospheric-tropospheric exchange processes, Rev. Geophys. Space Phys., 13, 459-474.

Rottger, J. (1980), Development of refractivity structures during anti-cyclonic weather conditions, Preprint Vol. 19th Conf. on Radar Meteorol., 593-598, publ. by Am. Meteorol. Soc., Boston, MA.

Rottger, J. and G. Schmidt (1981), Characteristics of frontal zones determined from spaced antenna VHF radar observations, Preprint Vol. 20th Conf. on Radar Meteorol., 30-37, publ. by Am. Meteorol. Soc., Boston, MA.

Rottger, J., P. K. Rastogi and R. F. Woodman (1979), High-resolution VHF radar observations of turbulence structures in the mesosphere, Geophys. Res. Lett., 6, 617-620.

Ruster, R. and J. Klostermeyer (1983), VHF radar observations of a Kelvin-Helmholtz instability in a subtropical jet stream, Geophys. Astrophys. Fluid Dynamics, 26, 107-116.

Wallace, J. M. and P. V. Hobbs (1977), Atmospheric Science - An Introductory Survey, Academic Press, New York.

Woodman, R. F., P. K. Rastogi and T. Sato (1981), Evaluation of effective eddy diffusive coefficients using radar observations of turbulence in the stratosphere, Handbook for MAP Vol. 2, edited by S. K. Avery, 363-369. publ. by SCOSTEP Secretariat, Univ. of Illinois, Urbana, IL.

1.7A. COMPARISON OF TROPOPAUSE ALTITUDE DETERMINATION BY THE PLATTEVILLE RADAR, SUNSET RADAR AND THE NWS RAWINSONDE

J. L. Green and K. S. Gage

Aeronomy Laboratory
National Oceanic and Atmospheric Association
Boulder, CO 80303

INTRODUCTION

During the month of March, 1981 the Sunset and Platteville Radar and Platteville Radar were operated primarily with vertical antenna beams. These radars are both VHF ST (Stratosphere-Troposphere) radars. The separation between them was 63 km, the Sunset site located in the foothills of the Rocky mountains and the Platteville site was in the plains, just east of the mountains. Both radars were operated continuously for about three weeks with a time resolution of a few minutes. Both made measurements in the 4-20 km altitude interval with an altitude sampling of 1.2 km.

The purpose of this paper is to compare the estimation of the altitude of the tropopause by these two radars with the altitude of the tropopause derived from standard NWS rawinsondes. The results of vertical wind measurement for the two radars was presented in a earlier paper (BALSLEY et al., 1981) and a comparison of the reflectivities was presented in (GAGE et al., 1983).

DESCRIPTION OF EXPERIMENT

The two radar systems used in this experiment are located near the towns of Sunset and Platteville, CO. Their relative locations are indicated on the map in Figure 1. Note that the site alignment is approximately east-west, i.e., in line with the prevailing wind pattern. An outline of the profile of the ground surface altitude on the line between the two sites appears at the bottom of Figure 1. The location of both sites relative to the continental divide and the beginning of the plains region is evident: Sunset is located in the foothills close to the divide, while Platteville is situated in more of a plains environment. Line-of-sight between the two radars is about 63 km.

System parameters for both Sunset and Platteville are given in Table 1. Both systems are pulsed, VHF Doppler radars operating at intermediate power levels which use phased arrays comprised of lines of coaxial-cable dipoles. More complete descriptions can be found for Sunset in GREEN et al. (1979) and for Platteville in ECKLUND et al. (1979). The Sunset and Platteville systems are similar, the main difference is that the Sunset beam can be steered electronically, while the Platteville beams are fixed.

In this experiment both radar systems operated almost exclusively with vertically directed beams, the exception being that Sunset performed a three-position scan every 12 hours to measure the horizontal wind field as well. This procedure did not cause an appreciable deterioration of the vertical data.

Data from both systems were processed in similar ways to afford the best comparison. The time resolution in the present data set has been standardized by appropriate computer averaging. Both radars were sampled at altitude intervals of 1.2 km. The Sunset radar used a vertical resolution of 1 km and the Platteville radar used a vertical resolution of 2.4 km.

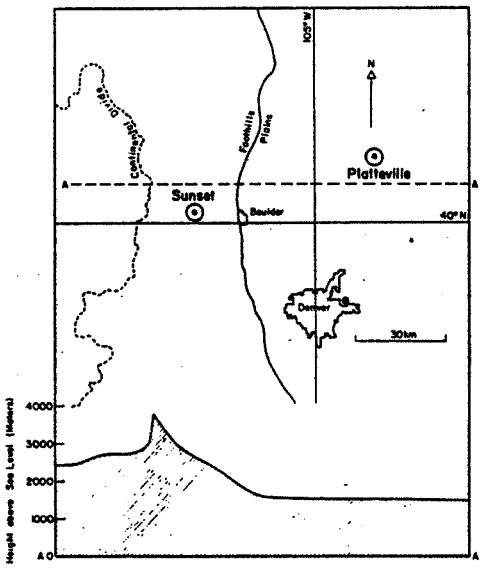

Figure 1. Map of the experimental area.

Table 1. Radar system parameters

		Platteville	Sunset
Transmitter	Frequency	49.920 MHz	40.475 MHz
	Peak pulse power	15 kW	50 kW
	Average power	133 W	1.0 kW
	Pulse width	16 μs	7 μs
	Pulse rate	555 Hz	5.4 KHz
Receiver	Noise figure	∿ 3 dB	∿ 3 dB
	Bandwidth	Matched to pulse width	Matched to pulse width
	Filtering (range gate)	Bessel	Gaussian
Antenna	Area	10^4 m^2	3.6×10^3 m^2
	Beamwidth (two-way)	∿ 2°	∿ 4.6°
	Direction	Vertical	Vertical (occasionally oblique)
	Efficiency	.39	.30
Processing	Coherent averaging	256 pulses (digital)	210 pulses (analog)
	Spectral resolution	64 points	256 points
	Doppler spectral bandwidth	1.1 Hz	12.8 Hz

RESULTS

Figure 2 shows typical vertical profiles of S/N observed by both radars. The difference in the vertical resolutions of the radars is evident in the greater detail shown in the Sunset curve. The increase in sensitivity of the Platteville radar because of its longer pulse length is evident in its greater altitude range.

An objective technique for determining tropopause altitudes was presented in GAGE and GREEN (1982). This technique was used to determine tropopause altitude from both the Sunset Radar and Platteville Radar data sets. Figure 3

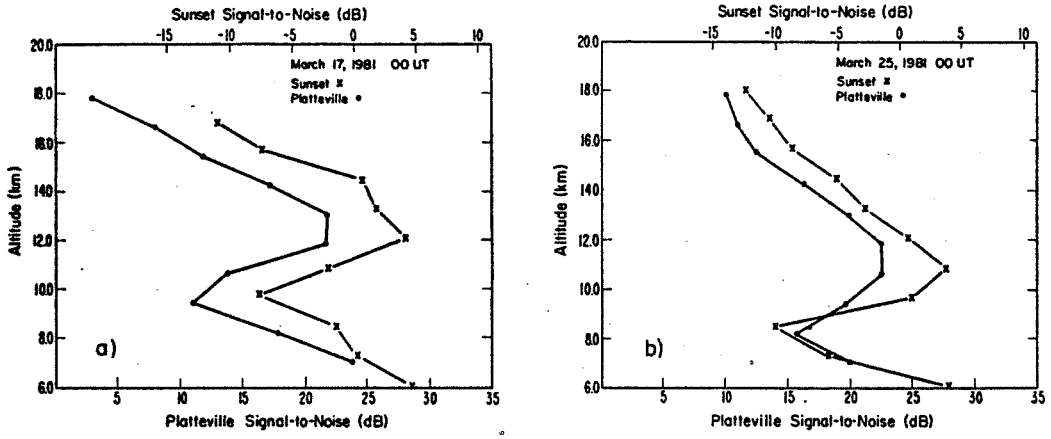

Figure 2. Vertical profiles of signal-to-noise ratio observed by the Sunset and Platteville radars (a) 00 UT 17 March 1981; (b) 00 UT 25 March 1981.

compares a time series of tropopause altitudes determined from both radars and the corresponding NWS Denver rawinsonde data.

In Figure 3, it can be seen that the tropopause altitude determined from the data from each of the two radars are in about the same agreement with each other as with that determined from the rawinsonde data. At the times when poor agreement is evident, the altitude of the tropopause is changing rapidly leaving open the possibility that the observed difference is real.

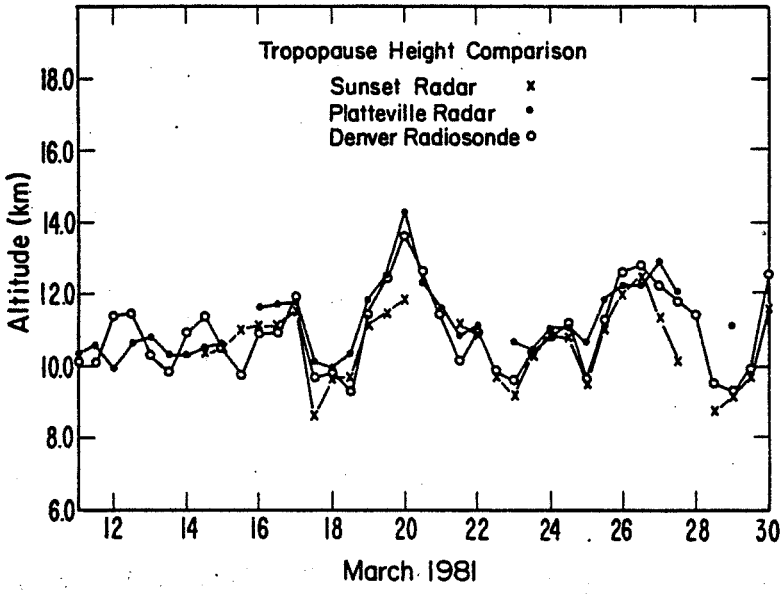

Figure 3. Comparison of tropopause heights determined from Sunset and Platteville radar data with tropopause heights determined from routine NWS Denver soundings.

REFERENCES

Balsley, B. B., J. L. Green, W. L. Ecklund, W. L. Clark, R. G. Strauch and A. C. Riddle (1981), Joint observations of gravity wave activity in vertical winds in the troposphere and lower stratosphere over a 63 km baseline obtained with clear air VHF radars at Platteville and Sunset, Colorado, Preprint Vol., 20th Conf. on Radar Meteorology, 110-115, Am. Meteorol. Soc., Boston.

Ecklund, S. L., D. A. Carter and B. B. Balsley (1979), Continuous measurement of upper atmospheric winds and turbulence using a VHF Doppler radar: Preliminary results, J. Atmos. Terr. Phys., 41, 983-994.

Gage, K. S. and J. L. Green (1982), An objective method for the determination of tropopause height from VHF radar observations, J. Appl. Meteorol., 21, 1150-1154.

Gage, K. S., J. L. Green, B. B. Balsley, W. L. Ecklund, R. G. Strauch and K. J. Ruth (1983), Comparison of Radar Reflectivities between the Sunset and Platteville ST radars, Preprint, Vol., 21st Conf. on Radar Meteorology, Am. Meteorol. Soc., Boston.

Green, J. L., K. S. Gage and T. E. VanZandt (1979), Atmospheric measurements by VHF pulsed Doppler radar. IEEE Trans. Geosci. Elec., GE-17, 262-280.

1.8A SYNOPTIC-SCALE DYNAMICS WITH VERTICAL VELOCITY

G. D. Nastrom

Control Data Corporation
Box 1249
Minneapolis, MN 55440

BACKGROUND

Radar measurements of all three of the atmospheric velocity components by the MST technique date from all the pioneering work of WOODMAN and GUILLEN (1974). The radar horizontal velocities have been compared with other standard measurements, such as radiosonde winds, in a number of studies and are now finding widespread acceptance within the meteorological community for research and operational forecasting purposes (e.g. LARSEN and ROTTGER, 1982; CARLSON and SUNDARARAMAN, 1982; LARSEN, 1983). Perhaps the single most interesting report recently is that the MST profiler winds are turning out to be one of the most useful pieces of data for predicting upslope snowfalls (SCHLATTER, 1984) in the cold-season forecasting study of the PROFS Program (REYNOLDS, 1983). By contrast, the vertical velocities measured by MST radars have received relatively little attention, despite the facts that direct continuous measurement of vertical velocity is unique (i.e., it cannot be done with radiosondes) and that the vertical velocity is intimately linked with the dynamics of the atmosphere.

Indeed, for many forecasting applications the vertical velocity is the single most important variable, yet it is usually inferred indirectly from other dynamical variables. The ST radars now available have the potential to change this situation, and the next section reviews some of the results from vertical velocity measurements which have direct application in synoptic-scale dynamics.

In the third section I consider some of the remaining research questions which should be addressed before plans are made to fully exploit this technology. In the final section, I discuss a few potential applications of this technology for synoptic-scale analysis and forecasting.

SYNOPTIC-SCALE RESULTS ON VERTICAL VELOCITY

By synoptic-scale, we mean those motion systems that operate on scales from several hundred to a few thousand kilometers, and will focus attention on them while realizing that there is interaction among motion systems of all scales. For example, jet stream and frontal systems are usually considered synoptic-scale features, but the principal benefits of vertical velocity measurements in these cases seem to lie in understanding their interaction with smaller scales. As reviewed by GAGE (1983), jet streams are a locus for turbulence and internal gravity wave activity, and ST radars are helping to define the interaction processes at work there. Also, LARSEN and ROTTGER (1982) have reviewed the application of ST radar data, including vertical velocities, to the study of frontal passage events. Again, a primary use of the vertical velocity data appears to be in studying the mesoscale processes along the frontal boundary. However, the vertical velocity data may have application on a larger scale as well, as seen next.

Figure 1 (from LARSEN and ROTTGER, 1982) shows the sequence of events during a warm frontal passage at SOUSY. The vertical velocity ahead of the front is clearly upward on the average, while that behind the front is downward, as expected. Eyeball averaging the values in Figure 1b gives mean magnitudes on the order of 10 - 20 cm s^{-1}, up or down, which are not at all unreasonable compared with classical models (PALMEN and NEWTON, 1969).

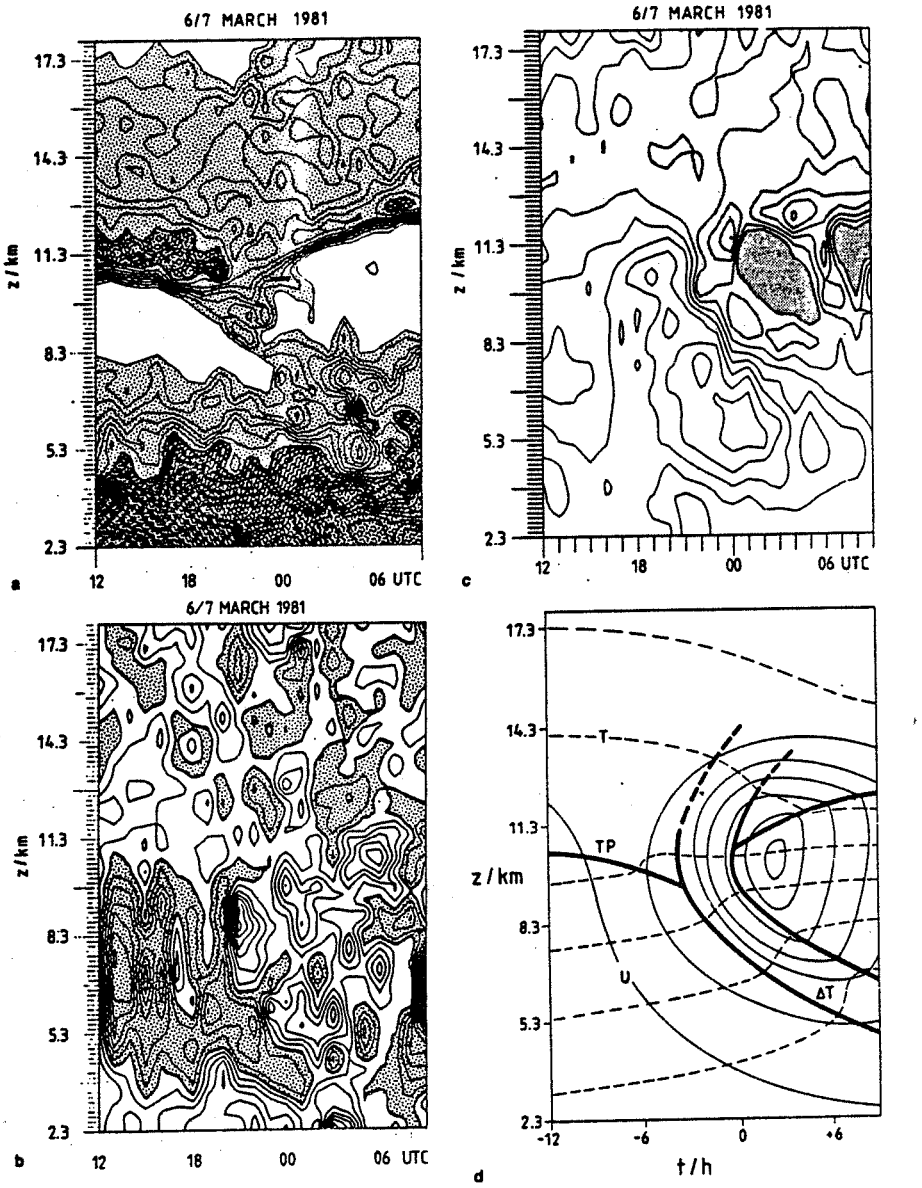

Figure 1. Frontal passage at SOUSY radar (after LARSEN and ROTTGER, 1982). (a) Reflectivity; interval 2 dB. (b) Vertical velocity; interval 7.5 cm/s; shading indicates downward. (c) Wind speed; interval 2.5 m/s; stippled is missing. (d) Classical frontal model.

Time average values of the ST measured vertical velocity in Alaska, Colorado and France have been compared with vertical velocities computed by the adiabatic, kinematic, and quasi-geostrophic omega equation methods by NASTROM (1984) and NASTROM et al., (1984). Some of the results (e.g. Figure 2) are very encouraging, and suggest that the ST radar data can provide reliable estimates of the synoptic-scale vertical velocity over a station. The success of these comparisons under general synoptic conditions has not yet been demonstrated, however, due to the siting of the available ST radar stations. All radars are located in or near rough, mountainous terrain. It has been established (ECKLUND et al., 1982; NASTROM et al., 1984) that flow over mountains increases the variance of the vertical velocity, and may induce standing lee waves. This meteorological "noise" can swamp the synoptic-scale signal at times as shown in Figure 3 from Platteville, Colorado. Note that Platteville is east of the Rockies. In the two panels in the lower right of Figure 3, the wind was strong and from the west, and the comparison is poor; in the two panels in the lower left, the wind was from the east, across the plains, and the comparison is good. In the top four panels, the statistical standard error of the mean (SE) is given by $SE = \sigma/\sqrt{N}$, where σ is the standard deviation and N is the number of independent observations. When the winds are from the east, over the plains, σ is relatively small; SE is then small enough that the visual comparison looks encouraging. The important point is that, at Platteville, the radar can measure the synoptic-scale vertical velocity with acceptable error limits under certain conditions.

There were three ST radars installed for ALPEX, in France near the mouth of the Rhone (BALSLEY et al., 1983), in a triangular array about 5 km on a side. When the wind was from the south, off the sea, these radar results also compared well qualitatively with each other and with the indirectly computed vertical velocities (Figure 4). Although the quantitative comparisons are not always perfect, the values fall within statistical error limits. Based on the available results, it appears that ST radars can provide reasonable estimates of the synoptic-scale vertical velocity.

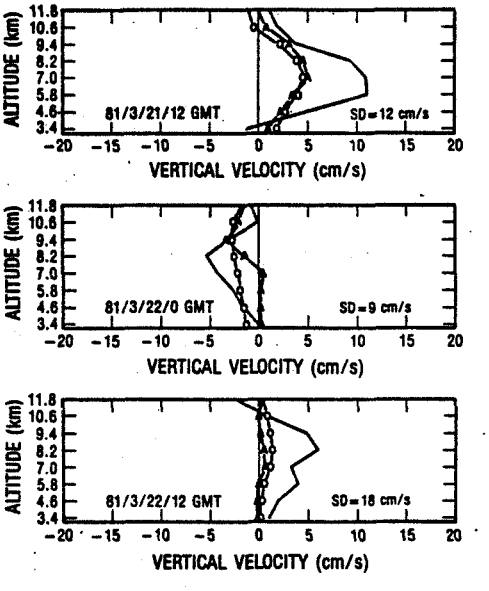

Figure 2. Vertical velocity at Platteville radar (after NASTROM, 1984). Solid line is 9-hour radar average, A is from adiabatic method, O is from omega equation.

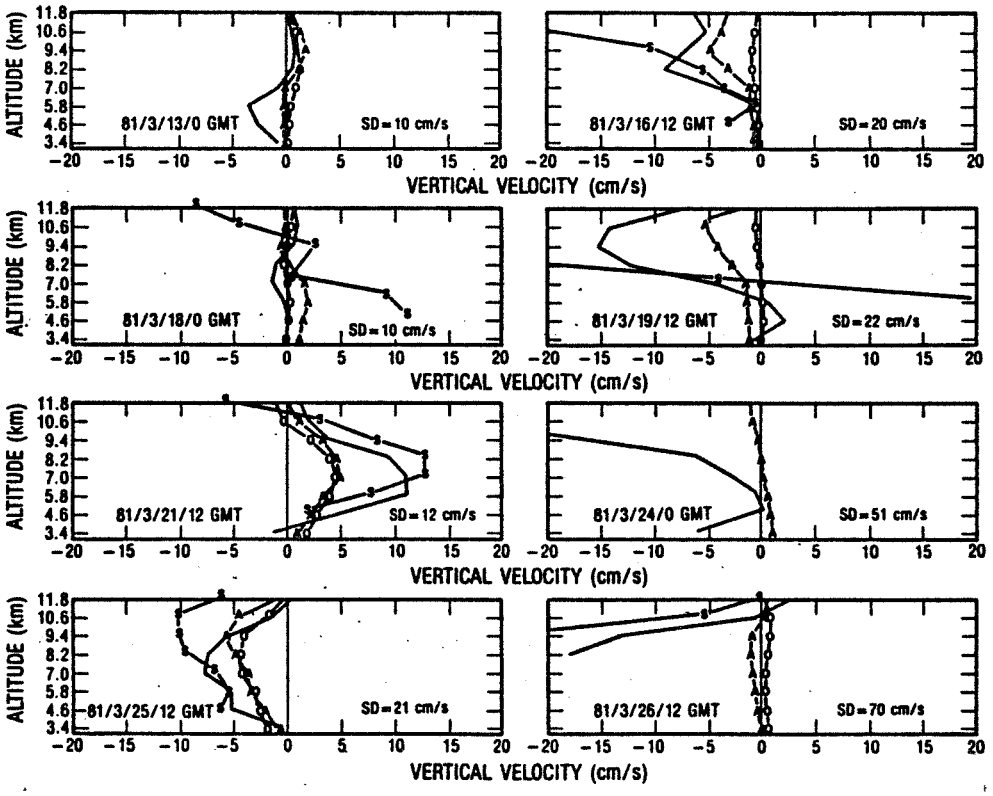

Figure 3. As is Figure 2; S is Sunset radar 9-hour average.

In order to generalize the above results, an ST radar(s) should be sited in the central plains for several months. The measured vertical velocities should be compared with indirectly computed vertical velocities and with proxy indicators of vertical motion such as weather radar echoes and satellite cloud pictures. If this technology were demonstrated under general conditions, it would surely be accepted and used by the meteorological community. It could, for example, enhance the usefulness of major research efforts such as the upcoming STORM project.

EXAMPLES OF APPLICATIONS

When established, this technology could also enhance operational synoptic-scale analysis and forecasting. For example, a number of "rules of thumb" used by forecasters are rooted in the dynamical equations for vertical motion (e.g., strong positive vorticity advection aloft; low level convergence/high level divergence). If a forecaster could monitor the vertical velocity field in real time, his successful warnings would be improved. It is during the critical zero to six hour time frame where credible forecasts of severe weather have the greatest impact on protecting life and property, and it is precisely in this time frame where continuous observations of the vertical velocity can help a station forecaster the most. Under current procedures, the raw radiosonde data are available an hour or two after the scheduled file time (00Z or 12Z), but centralized analyses of vorticity, divergence, or the most simple NWP model forecasts are not available for several hours. Then, for the next 12 hours the forecaster can only "adjust" these products based on the weather actually being

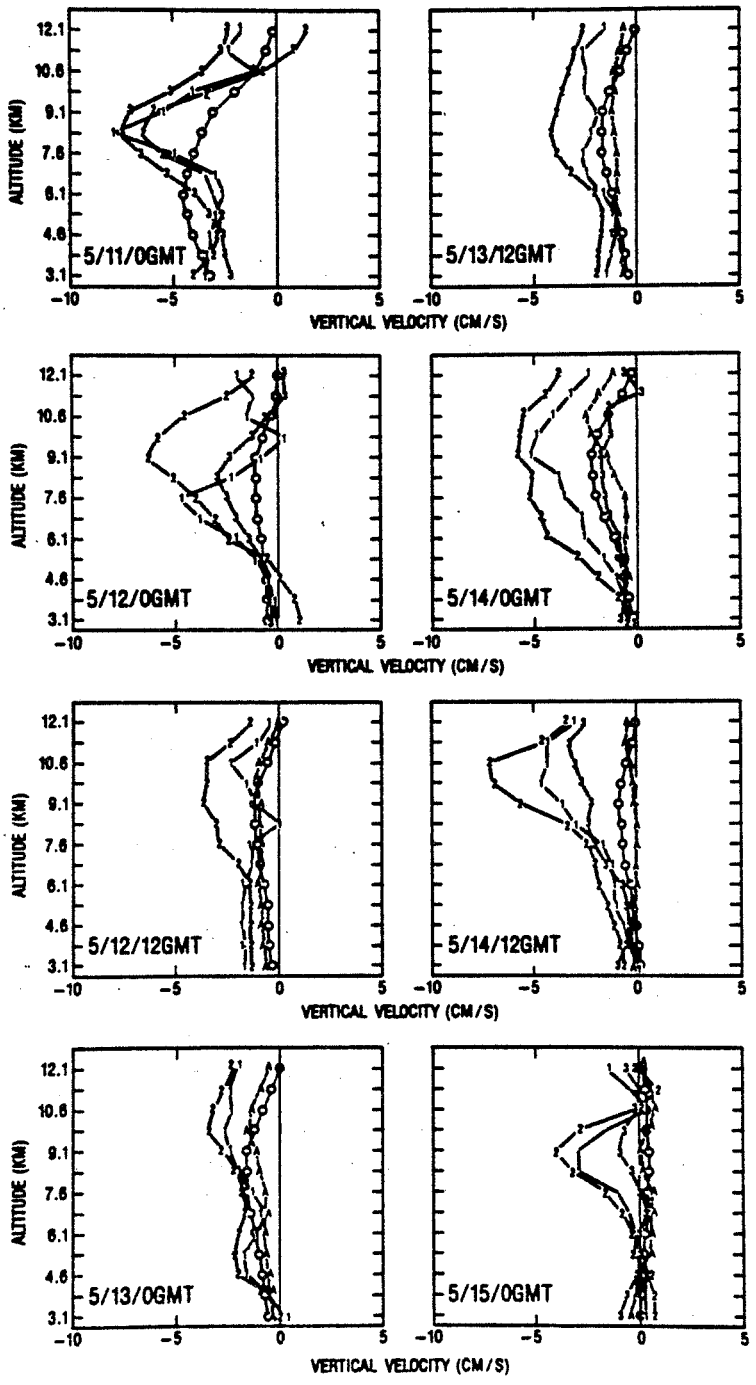

Figure 4. As in Figure 2, except radar data from 3 sites in France (ALPEX).

observed. With continuously available vertical velocity profiles he could monitor storm movement and development in real time -- the nowcasting approach. The application of vertical velocity data would extend beyond the single station forecaster to centralized use also.

On a centralized scale, the horizontal and vertical velocity data from a network of ST radars could be used to initialize and update regional NWP models (limited-area or window models). Present NWP are formulated to run without vertical velocity data because it is not available; they could be recast to take advantage of this new information, and might be improved in the process.

Of course, measurements of the synoptic-scale vertical velocity should also be useful for research purposes. A single station could provide time histories of the vertical motion in baroclinic storm systems, and over a period of months would permit more realistic descriptive models to be formulated. A network of ST radars might be used to estimate diagnostic variables such as fluxes of heat, momentum, or mass: or, perhaps more importantly, measurements of the vertical velocity would permit us to estimate other variables, such as diabatic heating rates, now only indirectly computed.

The list of possible applications for synoptic-scale purposes could be longer and another list of meso-scale applications could be given. However, I believe the case is already firmly made for anticipating the possible benefits of direct measurement of the synoptic-scale vertical velocity.

SUMMARY

In summary, results from ST radars in Colorado and France strongly suggest that the synoptic-scale vertical velocity can be detected. Before plans are made to exploit this capability in major field programs, the vertical velocity should be checked under more general conditions than previously possible -- perhaps with a brief experiment in the central plains states. Once convincingly demonstrated under general conditions, this new technology will improve our ability for synoptic-scale analysis and forecasting in both single station and centralized operations.

REFERENCES

Carlson, H. C. and N. Sundararaman (1982), Real-time jetstream tracking: National benefit from an ST radar network for measuring atmospheric motions, Bull. Am. Meteorol. Soc., 63, 1019-1027.

Ecklund, W. L., K. S. Gage, B. B. Balsley, R. G. Strauch, and J. L. Green (1982), Vertical wind variability observed by VHF radar in the lee of the Colorado Rockies, Mon. Wea. Rev., 110, 1451-1457.

Balsley, B. B., M. Crochet, W. L. Ecklund, D. A. Carter, A. C. Riddle and R. Garello (1983), Observations of vertical motions in the troposphere and lower stratosphere using three closely-spaced ST radars, Preprints, 21st Conf. on Radar Meteorology, Am. Meteorol. Soc., Boston.

Gage, K. S. (1983), Jet stream related observations by MST radars, Handbook for MAP Vol. 9, 12-21, SCOSTEP Secretariat, Univ. IL, Urbana, IL 61801.

Larsen, M. F. and J. Rottger (1982), VHF and UHF doppler radars as tools for synoptic research, Bull. Am. Meteorol. Soc., 63, 996-1008.

Larsen, M. F. (1983), Can a VHF doppler radar provide synoptic wind data? A comparison of 30 days of radar and radiosonde data, Mon. Wea. Rev., 111, 2047-2057.

Nastrom, G. D. (1984), Detection of synoptic-scale vertical velocities using an MST radar, Geophys. Res. Lett., 11, 57-60.

Nastrom, G. D., W. L. Ecklund, and K. S. Gage (1984), Direct measurement of synoptic-scale vertical velocities using clear-air radars, Submitted to Mon. Wea. Rev.

Palmen, E. and C. Newton (1969), Atmospheric Circulation Systems: Their Structure and Interpretation, Academic Press, New York, 603 pp.

Reynolds, D. W. (1983), Prototype workstation for mesoscale forecasting, Bull. Am. Meteorol. Soc., 64, 264-273.

Schlatter, T. (1984), personal communication.

Woodman, R. F. and A. Guillen (1974), Radar observations of winds and turbulence in the stratosphere and mesosphere, J. Atmos. Sci., 31, 493-505.

1.8B PRACTICAL USE OF A TROPOPAUSE HEIGHT DETERMINATION ALGORITHM ON AN MST RADAR DATA SET

A. C. Riddle, K. S. Gage* and B. B. Balsley*

CIRES/NOAA, University of Colorado, Boulder, CO 80309
*Aeronomy Laboratory, NOAA, Boulder, CO 80303

The possibility of detecting tropopause height from vertical incidence clear-air radar returns was demonstrated by GAGE and GREEN (1979). Following theoretical analysis by GAGE et al. (1981) an objective method for tropopause height determination was presented by GAGE and GREEN (1982). That method was adapted for use as a computer algorithm by RIDDLE et al. (1983). In this paper, we report further progress on an improved algorithm. It will be shown that this improved algorithm substantially reduces the number of misidentified tropopauses, while at the same time, increases the number of correctly identified tropopauses. Some of the problems of the algorithm will be identified and suggestions made for further improvement.

METHOD

It has been shown (GAGE and GREEN, 1982) that, for the purpose of determining tropopause height, the reflected power from a vertically directed ST radar is given by

$$P_r = \alpha \left[P \left(\frac{dT}{dz} + \Gamma\right)/T^2\right]^2 f(r) \qquad (1)$$

where r indicates range, P, T, z and Γ have the usual meteorological significance. The "constant" α conceals many physical parameters (such as radar wavelength) that do not vary during the experiment and some parameters (such as transmitter power) which may vary (slowly) with time. The function f(r) includes range dependent factors which are discussed below.

In previous studies, there has been some question as to whether the form of f(r) should be r^{-2} or r^{-4} (e.g. BALSLEY and GAGE, 1981). Either functional form could be shown to be a good fit to some data. While RIDDLE et al. (1983) have shown that use of either form does not appreciably affect performance of the tropopause height algorithm, further examination reveals that one form works well on certain data sets while the other form works better on other data sets. Hence, if the algorithm were allowed to choose the form of f(r), improved results might follow. GAGE et al. (1984) have suggested that perhaps it is not so much the reflection mechanism but variations in the vertical wave number spectrum of radio refractivity that determines the appropriate form. They suggest that an appropriate form for f(r) might be $r^{-2}e^{-r/r_*}$ where r_* is a scale height. Thus, for the purposes of the current investigation, we have chosen for f(r) the form

$$f(r) = r^{-2}10^{-nr} \qquad (2)$$

and allowed the algorithm to choose the appropriate value for n. We note that over the small range of heights considered by the algorithm, there is little difference between power law and exponential forms; the important detail is that the form is now allowed to vary from one data set to another.

The new algorithm was derived in the following manner. First, it is noted that near the tropopause we have

$$P = P_o e^{-(r-r_o)/H} \qquad (3)$$

where $P = P_o$ at some reference range r_o and H is the scale height. Combining Equations (1), (2), and (3) we have

$$\log(P_r) = \log(\alpha P_o^2/T^2) - \log(r)^2 + 0.868(r_o - r)/H - nr + \log(\frac{dT}{dz} + \Gamma)^2 \qquad (4)$$

Now, to the extent that H and T are almost constant near the tropopause, the first three terms on the right-hand side of Equation (4) are either constant or have known r dependence, the fourth term is linear in r and the final term is nonlinear in r and varies with $(dT/dz + \Gamma)$. The first four terms vary rather slowly with r. In contrast, the nonlinear term is relatively constant below the tropopause, above which $dT/dz = -6$ or $-7 Km^{-1}$ and then changes abruptly at the tropopause, above which $dT/dz \geq -2 Km^{-1}$. As in the earlier algorithm, we first locate the transition region in which dT/dz changes from ~-6 or -7 to ~0. Then using data above that region, where dT/dz is assumed to be 0, the linear trend is fitted (simultaneously fitting the constant terms also). Finally, the height at which $dT/dz = -2 Km^{-1}$ is determined. This is the radar tropopause.

RESULTS

This new algorithm has been applied to the relatively continuous data set from the Poker Flat MST radar for 1981 and 1982. Early in this period, vertical soundings were taken only every 12-15 minutes, but by the end of 1982, such data were available about every 4 minutes. For each hour that data were available, the median signal strength at each range gate (range gate separation = 2.25 km) was computed. The algorithm was applied to these 1-hour medians. Typical results are shown in Figure 1 where the tropopause height, determined from balloon soundings at Fairbanks in August 1982, is plotted together with the Poker Flat radar tropopause for the hour before and the hour after the nominal balloon time.

In Figure 2 we show the results of a similar comparison using the entire data set. For each month, the mean difference between the radar tropopause height and the balloon tropopause height is plotted in the middle panel below

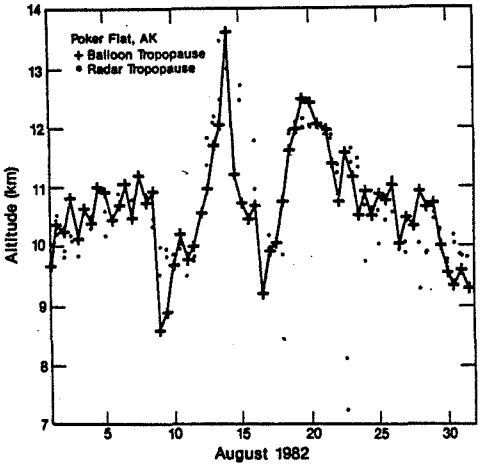

Figure 1. A comparison of balloon tropopause heights at Fairbanks and radar tropopause heights at Poker Flat, Alaska for most of the month of August 1982. The radar tropopause is plotted for both the hour before and the hour after the nominal balloon time.

the standard deviation of the same quantity from that mean. If the balloon tropopause is regarded as the standard for comparison, then the standard deviation can be regarded as the rms error of the radar tropopause determinations. This rms error ranges from 0.5 to 0.8 km and the mean error is between ±0.65 km. These results are better than those achieved with the previous algorithm for which the rms error ranged from 0.7 to 1.0 km (RIDDLE et al., 1983) for portions of the same data set. More impressive, however, is the increase in the number of cases for which useful determination of tropopause height can be made and the decrease in the number of cases in which very bad determinations (defined as errors > 3 km) are made. This improvement is summarized in Table 1 in which the number of useful determination and bad determinations are expressed as a percentage of potential determinations in each month for the cases $f(r) = r^{-2}$, r^{-4} and the new algorithm.

Examination of Table 1 shows that, taken over the whole 2-year data set, the useful determinations increase from 78% to 88%, while at the same time, the bad determinations decrease from 6% to 1%.

It should be noted that the above results were obtained using a data base that was not designed to examine tropopause height. The times for which determinations were not made include periods for which the data format was not appropriate, as well as equipment down time. A dedicated instrument would have reduced the nondeterminations by better scheduling of down time and avoidance of interfering experiments. Also, the instrumental parameters, especially the 2.25-km range spacing, could have been chosen better. Future dedicated systems, designed in part for routine tropopause height determinations, could achieve much better results.

DISCUSSION

An algorithm has been developed which can routinely determine tropopause heights from MST/ST radar observations with good accuracy, however, there is room for improvement. Some suggestions for further improvement are outlined below.

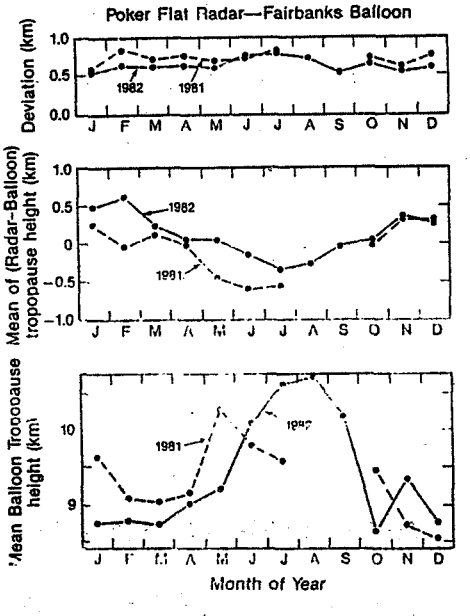

Figure 2. A comparison of balloon tropopause heights at Fairbanks and radar tropopause heights at Poker Flat, Alaska for 1981 and 1982. Monthly average results are plotted. Each balloon tropopause was compared with the radar determination for the hour before and the hour after nominal balloon time.

Table 1

	r -2		r -4		r -2 10^{-nr}	
	% valid determination	% bad determination	% valid determination	% bad determination	% valid determination	% % bad determination
1981						
January	87	7	86	8	94	1
February	81	1	81	1	99	0
March	74	0	72	3	76	0
April	92	4	95	2	92	2
May	53	32	76	9	85	3
June	61	25	76	9	87	0
July	88	0	88	0	85	3
October	80	0	81	1	82	0
November	47	0	46	1	95	0
December	43	2	41	4	89	0
1982						
January	90	2	83	11	92	0
February	74	2	62	14	76	0
March	--	--	--	--	81	0
April	93	1	90	3	89	0
May	93	2	94	0	94	1
June	94	2	97	0	97	2
July	68	14	66	16	82	3
August	66	14	78	2	80	5
September	82	9	92	0	90	2
October	81	4	77	6	85	0
November	84	9	81	12	92	0
December	89	2	85	5	90	1
OVERALL	77	6	79	5	88	1

The first concern is the annual variation of the mean error in radar-determined tropopause height. This variation is out of phase with the mean tropopause height as is shown on the lower panel of Figure 2. While it is possible that there is a physical source for the mean radar tropopause height error, we suspect that there is a more basic source for the error. The balloon tropopause at Fairbanks cycles almost exactly between two of our range gates (8.4 km and 10.7 km), which are at the top and bottom of the lower panel of Figure 2. Now, as one can see in the scatter plots of Figure 3, there appears to be a marked tendency for the radar tropopause algorithm to make determinations midway between the heights of the range gates. This property of the algorithm would tend to overestimate heights just above a range gate and underestimate those just below a range gate. This would produce an error out of phase with the actual heights for the Fairbanks data, as is observed. Unfortunately, we do not yet have data from another site with a different relationship of tropopause height to sample height with which to test this hypothesis. If this effect is indeed an artifact of the algorithm, it can be reduced by taking radar samples at closer intervals. Alternatively, it might be substantially removed by fitting the error to some cyclic function and subtracting this fitted function from the derived height.

Examination of the data shows two types of problems caused by the radar itself. One problem is due to the fact that the radar return currently saturates the receiver at the lower heights so that the apparent signal strength is much reduced over the actual value at 3.9 km and is often reduced at 6.2 km. This effect adds another knee in the signal vs height curve so that when the true tropopause is high, the algorithm sometimes mistakes this false knee for the knee caused by the tropopause. This effect produces may of the "bad" tropopause determinations, predominantly in summer when the tropopause is high. In winter, when the tropopause often goes below 8 km, the effect modifies the tropopause knee causing a high radar determination. This problem can be solved by increasing the dynamic range of the signal processor or by reducing peak power of the transmitter.

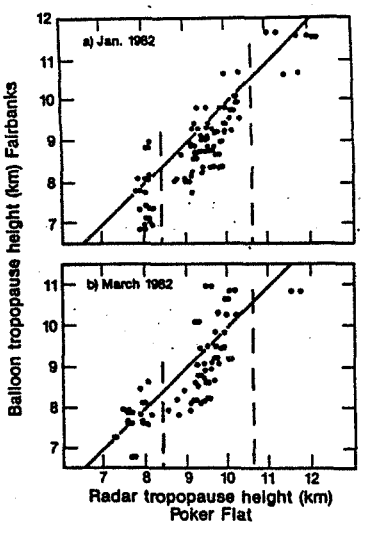

Figure 3. A scatter plot comparison of balloon heights at Fairbanks and radar tropopause determinations at Poker Flat, Alaska. Each balloon tropopause was compared with the radar determinations for the hour before and the hour after nominal balloon time. The vertical dashed lines show the heights of the radar range gates.

A second problem was caused by the use of the radar in modes which did not produce significant echoes above the 12.9-km range. Sometimes, this was due to low transmitted power, sometimes to radar component failure, and sometimes because of instrument parameter settings not being appropriate. This situation, when it occurred, hampered determination of tropopause height when the tropopause was high (usually summer). However, this problem is also easily overcome. Routine observations to 24 km at Poker Flat are now the norm and even with simpler lower-powered radars, such as the one at Platteville or the ones used in the ALPEX experiment, 16-20 km echoes are received regularly.

ACKNOWLEDGEMENTS

Thanks are due to D. Carter, W. Ecklund, P. Johnston, and S. Smith without whose efforts none of these data would have been collected.

REFERENCES

Balsley, B. B. and K. S. Gage (1981), On the vertical incidence VHF backscattered power profile from the stratosphere, Geophys. Res. Lett., 8, 1173-1175.

Gage, K. S. and J. L. Green (1979), Tropopause detection by partial specular reflection with very high frequency radar, Science, 203, 1238-1240.

Gage, K. S., B. B. Balsley and J. L. Green (1981), Fresnel scattering model for the specular echoes observed by VHF radar, Radio Sci., 16, 1447-1453.

Gage, K. S. and J. L. Green (1982), An objective method for determination of tropopause height from VHF radar observations, J. Appl. Meteorol., 21, 1159-1163.

Gage, K. S., W. L. Ecklund and B. B. Balsley (1984), A modified Fresnel scattering model for the parameterization of Fresnel returns, Paper 2.3A, this volume.

Riddle, A. C., K. S. Gage and B. B. Balsley (1983), An algorithm to monitor continuously the tropopause height using a VHF radar, 21st Conf. on Radar Meteorology, Am. Meteorol. Soc., Boston.

2. SOME RECENT DEVELOPMENTS IN THE INTERPRETATION OF MST RADAR RETURNS FROM CLEAR AIR
(Keynote Paper)

C. H. Liu

Department of Electrical and Computer Engineering
University of Illinois at Urbana-Champaign
Urbana, Illinois 61801

MST radar returns from clear air come about through the interaction of electromagnetic waves with the inhomogeneous structures of refractive index in the atmosphere. In order to interpret the data correctly to obtain information concerning the dynamics of the atmosphere, one must first know how the various refrative index structures can affect the propagation and scattering of the radio waves. This can be achieved through theoretical and model studies. On the other hand, in order to carry out realistic theoretical studies, realistic models of the inhomogeneous structures of the atmospheric refractive index are needed. These are available only through observational data. Therefore the close interplays between theoretical and observational investigations are essential in making progress in this area. In this paper, we shall present some results on certain aspects of the problem with emphasis on those that may lead to new developments.

THEORETICAL CONSIDERATION OF THE SCATTERING PROCESS

The classical scattering formula in the form of Booker-Gordon results in general is derived under several assumptions. These are: (1) the inhomogeneous structures of refractive index are weak so that only single scattering needs to be considered; (2) the linear dimension of the scattering volume determined by the radar beam width and pulse length, and the characteristic scale of the irregularities are small compared to the dimension of the Fresnel zone so that the phase incoherence of the scattered fields within the scattering volume can be neglected; (3) the range is sufficiently large so that far-field approximation can be used; (4) the scattering volume is large enough to contain sufficiently large number of irregularities; and (5) the irregular structures are characterized by a homogeneous random field so that integration over the scattering volume can be related to the power spectrum of the irregularities.

Recently, effects of multiple scattering on backscattered radar signals have been studied by FANTE (1982) and YANG and YEH (1984). The results are applicable to cases where the refractive index fluctuations are strong to cause multiple scattering by the probing radar wave. In most MST radar applications, these effects probably are not important. What is important in atmospheric applications is the possible violation of assumptions (2) to (5) for many MST radar configurations. Realizing the possibility that the radar beam size may be comparable to the Fresnel zone dimension, LIU and YEH (1980) modified the classical Booker-Gordon formula. Since the structures in the atmosphere are highly anisotropic with large horizontal dimensions, the Fresnel zone dimension may be smaller than the horizontal coherence distance of the irregular structure. DOVIAK and ZRNIC (1983) derived more general formulae to take this into account by expanding the phase term in the scattering integral to second order. They also derived a criterion to distinguish between Fraunhofer and Fresnel scatter approximations. These general formulae are applicable to most MST radar applications under the assumption that the irregular structures are properly characterized statistically by a homogeneous random field. However, as the range resolution of operating MST radars improve, assumptions (4) and (5) may become invalid. The problem of whether the echo power depends on pulse length or the square of the pulse length underlines the importance of this point

(GAGE et al., 1981). It was shown (FARLEY, 1983; LIU, 1983; HOCKING and ROTTGER, 1983) that if many layers exist in the scattering volume such that statistical description is valid, the scattered power should depend linearly on the pulse length. Other forms of the dependence will result if the scattering volume does not contain sufficient irregularity layers such that they can be characterized statistically, or the homogeneous random field characterization of the irregularities is not valid. These results have been demonstrated to be consistent with the experimental results obtained by GREEN (1983). To correctly describe the scattering/reflection processes involved when the statistically homogeneous characterization of the scatterers breaks down, one needs to generalize the existing theoretical work to include the effects of the distribution of layers, the finite scattering volume, etc. It is conceivable that numerical modeling involving the Monte Carlo type of simulation may be able to contribute to the progress along this direction.

PARAMETERIZATION OF FRESNEL RETURNS

Ever since the experimental observation of enhanced specular-like returns of MST radars at vertical incidence (GAGE and GREEN, 1978; ROTTGER and LIU, 1978), there have been continuing efforts to understand the mechanism and to parameterize the echo power in terms of atmospheric parameters (GAGE et al., 1981; ROTTGER, 1983). In order to carry out the parameterization, assumptions on the scattering/reflection targets have to be made. Assuming a statistical power spectral characterization of the layers, it is possible to relate the echo power to the meteroological data from rawinsonde (GAGE et al., 1981). ROTTGER (1984), on the other hand, proposed to make use of the specific behavior of the correlation function of the returned signal when the radar beam is vertical to separate the specular component from the scatter component. In many cases, the correlation function can be separated into three parts. The first part is the fast drop between zero and the next time lag corresponding to the effects due to uncorrelated noise. The second part is the smooth decrease of the correlation function at small time lags up to a few seconds. This is viewed as due to random scattering. The last part is the slow decay of the correlation up to many tens of seconds. This is due to the specular component of the return. These three parts can be separated by a parameter-fitting scheme, and used to approximately estimate the scattered contributions to the total received echoes. More accurate estimates of the different contributions can be obtained if we have better understanding of the scattering process. This can be achieved through a modeling.

CORRELATION BETWEEN ECHO POWER AND COHERENCE TIME

A positive correlation between the strength of the echo power and the coherence time of the received signal has been observed in many MST radar experiments (RASTOGI and BOWHILL, 1976; ROTTGER and LIU, 1978; WAND et al., 1983; ROYRVIK, 1984). This is quite intriguing. If the echoes are due to scattering from turbulence, then from statistical theory of scattering, the signal power should be proportional to the variance of the refractivity fluctuation. On the other hand, the coherence time of the returned signal is inversely proportional to the spectral width of the signal which is directly related to the variance of the fluctuation of the radial velocity, hence, the strength of the turbulence. Therefore, if there is a direct relation between the variance of the refractivity fluctuations and the velocity variance, one should expect a negative correlation between the echo power and the coherence time (P/C). The fact that in many cases this is opposite to what has been observed, indicates that further investigation of the scattering mechanisms is needed.

ROTTGER and LIU (1978) related the observed positive P/C correlation to the specular partial reflection process due to layered structures when the radar was

looking vertically. This will not apply to the tropospheric data reported by WAND et al. (1983) for low-elevation observations, where they also found that the spectral width of the signal is proportional to the layer thickness. RASTOGI (1983) proposed the idea of turbulent layer broadening by entrainment to explain the data.

Recently, in anattempt to interpret the mesosphere data, ROYRVIK (1984) proposed to re-examine the relation between the variance of the refractivity and the velocity variance.

Currently, our understanding of the various mechanisms that cause the radar echoes is still not complete and a definitive explanation of the observed P/C correlation is not available. On the other hand, this phenomenon does provide us with important information that can be applied to verify proposed models of scattering/reflection processes.

SIGNAL STATISTICS

It has long been recognized that by studying the statistics of the returned radar signal, certain detailed information about the targets can be extracted (RASTOGI and HOLT, 1981; ROTTGER, 1980). Signal statistics include the distributions of the intensity and the phase; the distribution of angle of arrival; the spectra of intensity and phase, etc. Ultimately the signature of the signal itself should be investigated.

Using the signal signature, the Doppler spectrum and the distributions of the intensity and the in-phase and quadrature components of the signal, SHEEN et al. (1984) studied the vertical radar returns from the troposphere and lower stratosphere. They found that the spectral width and the Nakagami m-coefficient for the intensity distribution can be used to characterize the scattering/reflection processes. When the returned signal comes from independent scatterers or reflectors which are distributed in space with rms separations greater than one wavelength and moving with different velocities, then the intensity of the received signal will have the classical Rayleigh distribution with $m \approx 1$. If a dominant specular component exists in the signal, the distribution will have an m-coefficient greater than one, satisfying the Rice Nakagami distribution. Therefore signals with broad Doppler spectra and an m-coefficient close to unity characterize scattering by anisotropic turbulence or multiple thin layers. The majority of the data are found to be of this type. There are almost no cases, however, where the m-coefficient is substantially greater than unity. On the other hand, signals with narrow Doppler spectrum and an m-coefficient close to 1/2 are found in many cases. By modeling, it is shown that these features are consistent with returns from single diffusive layers causing focusing and defocusing of the signals. This indicates that reflections from single layers do occur. The layers, however, are invariably undulating. Therefore, more than one specularly reflected ray will come into the rather broad radar beam, interacting with each other, giving rise to the observed signal signature.

In many cases, the Doppler spectra exhibit several sharp spikes indicating that they may come from different "sub-reflectors" moving at different radial velocities. ROTTGER (1984) proposed to study this phenomenon by measuring the statistics of the angle of arrival. He pointed out that more about the nature of the targets can be learned from this study.

BUOYANCY WAVES AS ORIGIN OF REFRACTIVE INDEX FLUCTUATIONS

VANZANDT and VINCENT (1984) proposed the displacement associated with the low-frequency internal gravity waves acting on the background gradient of refractivity may be the cause of the horizontally stratified laminae of

refractive index that produce enhanced VHF radar echoes near the zenith. A model spectrum for the displacement corresponding to the modified Garrett and Munk spectrum was used to compute the angular dependence of the radar cross section. They proposed an experimental test for the model.

If the refractive index fluctuations are caused by spectra of buoyancy waves, the wave-associated velocity fluctuations will be seen as wind velocity fluctuations. Indeed, VANZANDT (1982) first proposed a universal buoyancy wave spectrum to interpret the observed mesoscale wind fluctuations in the atmosphere. MST radars have been used to study the velocity spectra (BALSLEY and CARTER, 1982). Since MST radar measures the line-of-sight Doppler velocity, it senses the components of the wave-associated velocities along the radar beam direction. Because of the polarization relations relating the different wave-associated velocity components, the observed line-of-sight velocity will depend on the wave frequency and wave number as well as the observation geometry. Therefore, the observed velocity spectrum will be different from the original wave spectrum. For example, if the radar is in an exact zenith direction, the radar is only sensitive to vertical velocity fluctuations. As the wave frequency $\omega \to 0$, the waves will propagate almost in the vertical direction. Since the buoyancy waves are transverse waves, there will be no vertical velocity component associated with these very low frequency waves. Therefore, in the vertical observation mode of the radar the low frequency portion of the wave spectrum is suppressed. As $\omega \to \omega_b$, the Brunt Vaisala frequency, the waves propagate almost horizontally and the wave-associated velocity is almost completely vertical. Therefore the wind fluctuation spectrum observed by vertical radar will be the same as the wave spectrum in the neighborhood of ω_b. This example indicates how the observation geometry can affect the interpretation of the observed wind velocity fluctuation spectra in terms of gravity-wave spectra.

If the radar observation geometry is oblique, the relation between the observed wind fluctuation spectrum and the buoyancy wave spectrum is more complicated. This relation has been studied by SCHEFFLER and LIU (1984). Because of the angular dependence of the relation, it is possible to design experiments to test the assumption that buoyancy waves are the causes of mesoscale wind velocity fluctuations, as well as the origin of refractive index fluctuations in the atmosphere.

REFERENCES

Balsley, B. B. and D. A. Carter (1982), The spectrum of atmospheric velocity fluctuations at 8 km and 86 km, Geophys. Res. Lett., 9, 465-468.

Doviak, R. J. and D. S. Zrnic (1983), Fresnel zone considerations for reflection and scatter from refractive index irregularities, Handbook for MAP, Vol. 9, 83-87, S. A. Bowhill and B. Edwards (eds.), Univ. of Illinois, Urbana-Champaign.

Fante, R. L. (1982), Generalization of the Booker-Gordon formula to include multiple scattering, Radio Sci., 17, 980-987.

Farley, D. T. (1983), Comments on "Fresnel Scattering", Handbook for MAP, Vol. 9, 71-72. S. A. Bowhill and B. Edwards (eds.), Univ. of Illinois, Urbana-Champaign.

Gage, K. S. and J. L. Green (1978), Evidence for specular reflection from monostatis VHF radar observations of the stratosphere, Radio Sci., 13, 991-1001.

Gage, K. S., B. B. Balsley and J. L. Green (1981), A Fresnel scattering model for the specular echoes observed by VHF radar, Radio Sci., 16, 1447-1453.

Green. J. L. (1983), Range gate dependence of specular echoes, Handbook for MAP, Vol. 9, 73-77, S. A. Bowhill and B. Edwards (eds.), Univ. of Illinois, Urbana-Champaign.

Hocking, W. K. and J. Rottger (1983), Pulse length dependence of radar signal strengths for Fresnel backscatter, Radio Sci., 18, 1312-1324.
Liu, C. H. and K. C. Yeh (1980), Scattering of VHF and UHF radar signals from the turbulent air, Radio Sci., 15, 277-282.
Liu, C. H. (1983), Interpretation of MST radar returns from clear air, Handbook for MAP, Vol. 9, 49-56, S. A. Bowhill and B. Edwards (eds.), Univ. of Illinois, Urbana-Champaign.
Rastogi, P. K. (1983), Spectral characteristics of the MST radar returns, Handbook for MAP, Vol. 9, 105-113, S. A. Bowhill and B. Edwards (eds.), Univ. of Illinois, Urbana-Champaign.
Rastogi, P. K. and S. A. Bowhill (1976), Scattering of radio waves from the mesosphere, J. Atmos. Terr. Phys., 38, 449-462.
Rastogi, P. K. and O. Holt (1981), On detecting reflections in the presence of scattering from amplitude statistics with application to D-region partial reflections, Radio Sci., 16, 1431-1443.
Rottger, J. (1980), Reflection and scattering of VHF radar signals from atmospheric refractivity structure, Radio Sci., 15, 259-276.
Rottger, J. (1983), Parameterization of Fresnel returns, Handbook for MAP, Vol. 9, 286-288, S. A. Bowhill and B. Edwards (eds.), Univ. of Illinois, Urbana-Champaign.
Rottger, J. (1984), Signal statistics of the radar echoes, angle of arrival statistics, this volume.
Rottger, J. and C. H. Liu (1978), Partial reflection and scattering of VHF radar signals from the clear atmosphere, Geophys. Res. Lett., 5, 357-360.
Royrvik, O. (1984), Interpretation of radar returns from the mesosphere, this volume.
Scheffler, A. O. and C. H. Liu (1984), Observation of gravity wave spectra in the atmosphere using MST radars, submitted to Geophys. Res. Lett.
Sheen, D. R., C. H. Liu and J. Rottger (1984), A study of signal statistics of VHF radar echoes from clear air, to be submitted.
VanZandt, T. E. (1982), A universal spectrum of buoyancy waves in the atmosphere, Geophys. Res. Lett., 9, 575-578.
VanZandt, T. E. and R. A. Vincent (1984), Is VHF Fresnel refractivity due to low frequency buoyancy waves? Handbook for MAP, Vol. 9, 78-80, S. A. Bowhill and B. Edwards (eds.), Univ. of Illinois, Urbana-Champaign.
Wand, R. H., P. K. Rastogi, B. J. Watkins and G. B. Loriot (1983), Fine Doppler resolution observations of thin turbulence structures in the tropo-stratosphere at Millstone Hill, J. Geophys. Res., 99, 3851-3857.
Yang, C. C. and K. C. Yeh (1984), Effects of multiple scattering and Fresnel diffraction on random volume scattering, to appear in IEEE Trans. on Antenna and Prop.

ISSUES AND RECOMMENDATION

ISSUES:

1. Parameterization of Fresnel Returns:
   (a) Is the statistical description of the process satisfactory?
   (b) Can anisotropic turbulence explain both the aspect sensitivity and absolute power of the echoes?
   (c) Dependence of $E_\zeta(k,z)$ — spectrum of displacement.

2. Echo Power -- Coherence Time Correlation:
   (a) Relation between $\sigma_{\text{refractive index}}$ and σ_{velocity} in the troposphere, stratosphere and mesosphere.
   (b) The issue may contain key information about targets.

3. Angle-of-Arrival Statistics:
   (a) What can be learned from them?
   (b) Requirements

RECOMMENDATION:

Recommend future experimenters to include absolute power and refractive index gradient information in their publications; whenever possible, simultaneous in situ measurements and radar observations should be carried out.

Important for modeling and checking scattering-reflection processes.

D15 N85-32481

2.1A MORPHOLOGY OF THE SCATTERING TARGETS: FRESNEL AND TURBULENT MECHANISMS

O. Royrvik

Department of Electrical and Computer Engineering,
University of Illinois
Urbana, IL 61801

INTRODUCTION

Refractive index fluctuations cause coherent scattering and reflection of VHF radio waves from the clear air in the altitude region between 0 and approximately 90 km. Similar echoes from the stratosphere/troposphere and the mesosphere are observed at UHF and MF/HF frequencies, respectively. The nature of the refractive index fluctuations has been studied for many years without producing a clear consensus on what mechanism causes them. It is believed that the irregularities can originate from two different mechanisms: turbulent mixing of the gradient of refractive index, and stable horizontally stratified laminae of sharp gradients in the refractive index.

In order to explain observations of volume dependence and aspect sensitivity of the echo power in the MST region, a diversity of submechanisms has been proposed. They include isotropic and anisotropic turbulent scattering, Fresnel scattering and reflection, and diffuse reflection (Figure 1).

Isotropic turbulent scattering is believed to cause a majority of the clear-air echoes observed by MST radars. Echoes showing no apparent aspect sensitivity are expected to be of this type. The mechanism requires active turbulence mixing of a preexisting gradient in the refractive index profile.

Anisotropic turbulent scattering also requires active turbulence mixing of a gradient in the refractive index profile. At the larger scales, turbulence must be anisotropic in the direction of the shear velocity, resulting in anisotropic scattering at radio wavelengths comparable to these large turbulent irregularities. At some unknown smaller scale, the irregularities are expected to become isotropic.

Fresnel reflection, also called partial reflection, results when a radio signal encounters a single sharp, horizontally stratified ledge in the refractive index. If perfect stratification is assumed, reflected signals would be received only from the vertical direction.

Fresnel scattering is similar to Fresnel reflection except that it consists of multiple stratified layers reflecting individually with random phase. This concept has been introduced to explain the pulse length dependence of some aspect-sensitive echoes.

Diffuse reflection results from a corrugated layer of sharp changes in the refractive index. The concept was introduced to explain observations showing significant amounts of radar scattering from large off-vertical angles in layers that are believed to be horizontally stratified.

TURBULENCE

The subject of turbulence is a very involved one, and no clear consensus exists as to what signatures radar echoes from turbulent layers should have. Some of the questions arising from interpretation of turbulent scattering of radio waves will be considered below.

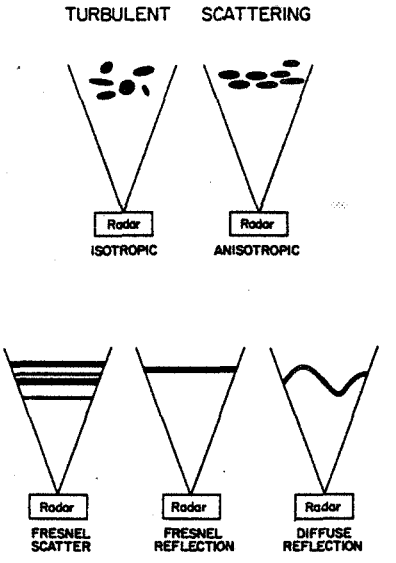

Figure 1. Diagram depicting different forms of irregularities causing VHF radar echoes in the MST regions.

(a) Aspect Sensitivity

In order to simplify considerations of shear-layer turbulence, it is usually assumed that turbulent irregularities at scales smaller than the outer scale of turbulence are statistically isotropic (TENNEKES and LUMLEY, 1972) and should therefore scatter radio waves isotropically. However, it is recognized that individual turbulent irregularities are not isotropic and that they have a tendency to be aligned along the direction of the shear flow velocity. In fact, STEWART (1969) and others have shown from experiments that anisotropy extends throughout the inertial subrange and well into the dissipation subrange of turbulence. This might indicate that isotropic scattering from shear-layer turbulence is more an abnormality than a normal state of affairs.

It seems likely, therefore, that aspect sensitivity would decrease with decreasing radar wavelength until isotropy is obtained, perhaps inside the dissipative subrange. Thus it appears that aspect sensitivity is not a good discriminator between partial reflection and scattering from shear-layer turbulence.

(b) P/C Correlation

In radar signals scattered from clear air, there exists a relationship between signal correlation time and echo power. In some regions of the atmosphere the correlation is positive, whereas it is negative in other regions. It is believed that negative P/C correlation is a manifestation of turbulent scattering (ROTTGER, 1980). RASTOGI and BOWHILL (1976) attempted to explain the positive P/C correlation as resulting from stronger turbulence occurring in narrower layers. However, LIU and YEH (1980) have shown that the effect of narrowing a turbulent layer is not enough to cause positive P/C correlation. Thus FUKAO et al. (1980) and ROTTGER (1980) have suggested that positive P/C correlation may be a manifestation of partial reflections from horizontally stratified layers. In the mesosphere, however, it is difficult to see how

stable layers of widths less than 3 m can be maintained, since the inner scale of turbulence tends to be larger than 3 m. Positive P/C correlation may, however, be explainable if an approach similar to that of BOLGIANO (1968) is taken. In the mesosphere, positive or negative P/C correlation is obtained when the radar wavelength is within the inertial or dissipative subrange of turbulence, respectively. However, this approach requires slowly varying shear-layer turbulence that is compared to the mixing time within the turbulent layer.

(c) Turbulent Spectra

It has generally been taken for granted that the radar Bragg wavelength must be within the dissipative subrange of turbulence in order for the radar to observe scattering from turbulent irregularities (CRANE, 1980). RASTOGI and BOWHILL (1976) estimated that the inner scale of turbulence in the mesosphere is larger than 3 m. Nevertheless, radar echoes from clear air are readily received on 50 MHz all the way up to about 90 km. Recent rocket data now show that the inner scale of turbulence in the upper mesosphere is almost one order of magnitude larger than the radar Bragg wavelength (ROYRVIK and SMITH, 1984). The large but finite negative gradient of the wave number spectrum in the dissipative subrange provides enough irregularities to cause scattering at frequencies as high as 50 MHz. Only in the lowest part of the mesosphere will a 50-MHz radar operate within the inertial subrange of the spectrum.

(d) Convective Instability

Whereas turbulence causing radar returns of VHF is usually considered to be caused by layers of strong velocity shears, it may also be of the convective instability type. BALSLEY et al. (1983) have argued that convective instabilities resulting from breaking gravity waves may cause a major fraction of the radio-wave scattering in the high-latitude winter mesosphere. Some recent Langmuir probe data from high-latitude winter mesosphere have shown that the inner scale of turbulence is considerably smaller than that measured at the equator, possibly indicating a difference between shear-layer and convective-instability turbulence.

PARTIAL REFLECTION

While the nature of radar echoes due to partial reflection is fairly easy to understand, it is more difficult to explain the stability and short vertical scale height of layers reflecting radio waves at VHF frequencies. This is particularly true for the mesosphere. Stratified layers reflecting VHF radio frequencies must be horizontally stratified over at least one Fresnel zone (several hundred meters in the mesosphere). The change in the refractive index must be a fraction of 1% within a vertical distance that is small compared to the radio wavelength. At VHF frequencies, that means one meter or less. In the mesosphere the refractive index is due to the ambient electron density. It is clear that such a sharp and limited ledge in the electron density cannot be generated by the natural production and loss mechanisms of the ionization (HAUG et al., 1977). Even if they could be generated, they would disappear within a few tens of seconds due to diffusion.

BOLGIANO (1968) has suggested that turbulence acting on a gradient in the refractive index would generate sharp stratified ledges at the boundary of the active turbulent region. These boundary ledges might then cause partial reflections of the radio waves. Although this appears to be a feasible mechanism for the troposphere/stratosphere region, it is unlikely that it can generate stratified layers in the mesosphere capable of reflecting at VHF frequencies all the time the radio wavelength is equal to or smaller than the inner scale of turbulence.

VANZANDT and VINCENT (1983) have suggested that the stratified layers in the troposphere/stratosphere can be formed by a spectrum of buoyancy waves with very short wavelengths and near-horizontal phase surfaces acting on a gradient of refractive index. A detailed evaluation of this mechanism has not been made since it has not been possible to observe waves with wavelengths as short as a few meters.

Some of the mechanisms associated with radar echoes at VHF from the MST region have been considered, and some of the problems with each mechanism have been pointed out. It seems fairly well documented that turbulence generates a large fraction of refractive index structures responsible for scattering of the VHF radio waves. As for other mechanisms (for instance. buoyancy waves of vertical wavelength equal to the radar Bragg wavelength), no definitive answer is available. However, even horizontally stratified laminae of refractive index may be generated by turbulence. so a generalized turbulence theory may provide all the answers.

ACKNOWLEDGMENT

The work described was supported by the National Aeronautics and Space Administration under grant NSG 7506.

REFERENCES

Balsley, B. B., W. L. Ecklund, and D. C. Fritts (1983), VHF echoes from the high-latitude mesosphere and lower thermosphere: Observations and interpretations, J. Atmos. Sci., 40, 2451.

Bolgiano, R., Jr. (1968), Winds and Turbulence in the Stratosphere, Mesosphere and Ionosphere, (Edited by K. Rawer), pp. 371-400, North-Holland Amsterdam.

Crane, R. K. (1980), A review of radar observations of turbulence in the lower stratosphere, Radio Sci., 15, 177.

Fukao, S., T. Sato, R. M. Harper and S. Kato (1980), Radio wave scattering from the tropical mesosphere observed with the Jicamarca radar, Radio Sci., 15, 447.

Haug, A., E. V. Thrane. K. Bjorna. A. Brekke and O. Holt (1977), Observations of unusually strong partial reflections in the auroral D-region during an absorption event, J. Atmos. Terr. Phys., 39, 1333.

Liu, C. H. and K. C. Yeh (1980), Scattering of VHF and UHF radar signals from the turbulent air, Radio Sci., 15, 277.

Rastogi, P. K. and S. A. Bowhill (1976), Scattering of radio waves from the mesosphere - 2. Evidence for intermittent mesospheric turbulence. J. Atmos. Terr. Phys., 38, 449.

Rottger, J. (1980), Reflection and scattering of VHF radar signals from atmospheric refractivity structures, Radio Sci., 15, 259.

Royrvik, O. and L. G. Smith (1984), Comparison of mesospheric VHF radar echoes and rocket-probe electron concentration measurements, J. Geophys. Res., submitted.

Stewart, R. W. (1969), Turbulence and waves in a stratified atmosphere, Radio Sci., 4, 1269.

Tennekes, H. and Lumley, J. L. (1972), A First Course in Turbulence, The MIT Press, Cambridge, MA.

VanZandt, T. E. and R. A. Vincent (1983), Is VHF Fresnel reflectivity due to low frequency buoyancy waves? Handbook for MAP, Vol. 9, 78-80. S. A. Bowhill and B. Edwards (eds.), Univ. of Illinois, Urbana-Champaign.

2.2A SIGNAL STATISTICS OF THE RADAR ECHOES - ANGLE-OF-ARRIVAL STATISTICS

J. Rottger*

EISCAT Scientific Association
981 27 Kiruna, Sweden

The statistical characteristics of radar echoes were investigated by several groups since the early days of VHF radar observations. Essentially, the power, amplitude and phase distributions as well as the distribution of power as a function of frequency (power spectrum analysis) were studied extensively. This led to a better, but not yet exhaustive, understanding of the processes leading to the VHF radar echoes from the lower and middle atmosphere, and it is now fairly well established that volume scattering as well as Fresnel scattering and reflection occur.

It was noted earlier that Doppler spectra, measured with a vertical antenna beam, are characterized by essentially two different kinds of distributions (e.g., ROTTGER, 1980; GAGE et al., 1981), one has a very narrow and the other a broad spectral width. The former is accepted as due to reflection whereas the latter is due to scattering. It can happen that both kinds of spectra are observed simultaneously, as shown in Figure 1. Superimposed on a fairly broad Gaussian signal spectrum, very narrow signal spikes are evident. The spikes can be even more distinctly seen in the spectra of Figure 2, computed for a 6-times shorter integration period (80 s).

Since the height resolution during these experiments was 150 m and the signal amplitude changed drastically between adjacent range gates (Figures 2 and 3), it is very unlikely that these echoes are due to volume scattering. They are rather due to reflection from a thin sheet or step in refractivity, being much narrower than the range gate of 150 m (reference also HOCKING and ROTTGER, 1983). The spikes in the spectra of Figure 2, however, cannot be explained by reflection from a flat and smooth discontinuity. The sheet must be rather tough or corrugated, and reflection from several subregions of the sheet is expected, as shown in Figure 5. Because the spikes occur at different Doppler frequencies, the subreflectors have to be assumed to move with different radial velocities.

To experimentally verify this reasonable assumption, it is proposed to measure the angle of arrival of the different signal returns. One can here make use of the essential advantage that the spikes can be filtered in frequency (called Doppler sortening or sharpening). By means of the cross-spectrum analysis with the interferometer technique (measuring phase differences between spaced antennas, as described in the paper "Improvement of vertical velocity measurements" by J. Rottger, Chapter 3, this volume), their angle of arrival can be measured. This will allow determination of the distribution of the angles of arrival. Knowing the Doppler shift and the arrival angle of the whole set of returns (sorted by Doppler frequency, i.e., radial velocity) yields a set of $n = 1,\ldots,N$ equations (N = number of evaluable spikes):

$$V_{rn} = V'_{rn} + U_o \cos \delta^*_n + W_o \sin \delta^*_n .$$

The solution (e.g., regression analysis) will lead to the mean horizontal and vertical velocities, the tilt and the aspect sensitivity of the illuminated area. It also would support the hypothesis that the reflecting sheet is

*presently at Arecibo Observatory. Arecibo, Puerto Rico, on leave from Max-Planck-Institut fur Aeronomie. Lindau, W. Germany

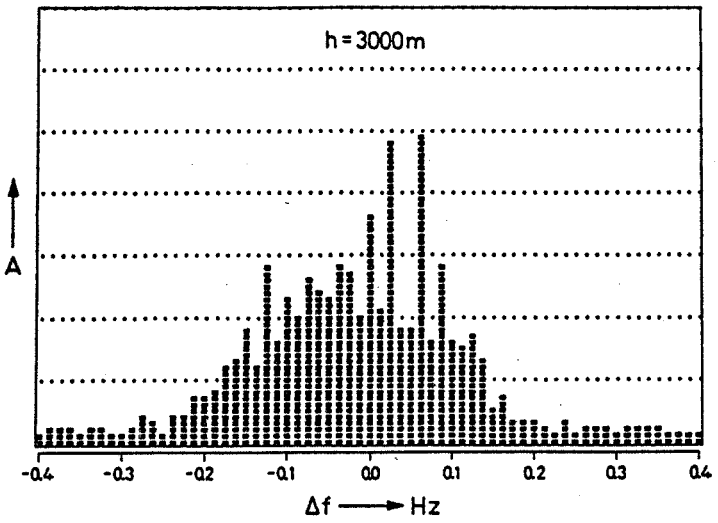

Figure 1. Doppler spectrum of signal measured with vertical antenna beam and 150 m height resolution, averaged over 8 min (from ROTTGER, 1980).

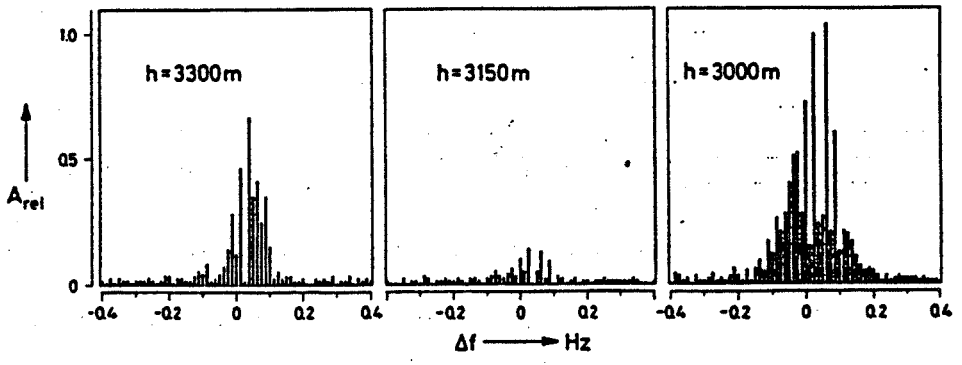

Figure 2. Doppler spectra computer from an 80 s time series.

corrugated. The determination of the mean velocities by this method also allows testing of Brigg's hypothesis (1980) that the Doppler beam-swinging method (DBS) is in principle similar to the spaced antenna-drifts method (SAD).

Measuring the variation of the arrival angle distribution as a function of time will also allow testing of the hypothesis (GAGE et al., 1981) that the specular reflection point moves with respect to different phases of gravity waves which may modulate the reflecting sheet. There may even be atmospheric waves of different periods involved in this process, as indicated in Figures 3 and 4. The amplitude time series in Figure 3 shows evident oscillations at periods of about 10 s, which may be because of a Benard cellular structure of the reflecting sheet moving through the radar beam, causing focussing and defocussing (SHEEN et al., 1984), and correspondingly also changes of the arrival angle (to be experimentally proved). The long-period (≈10 min) oscillation seen in the Doppler spectra of plot of Figure 4 also causes a varia-

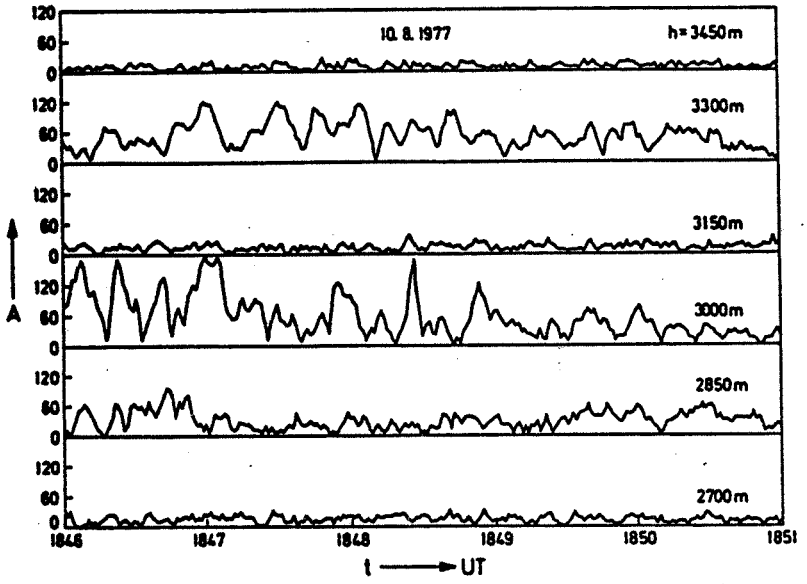

Figure 3. Amplitude time series for different height range gates.

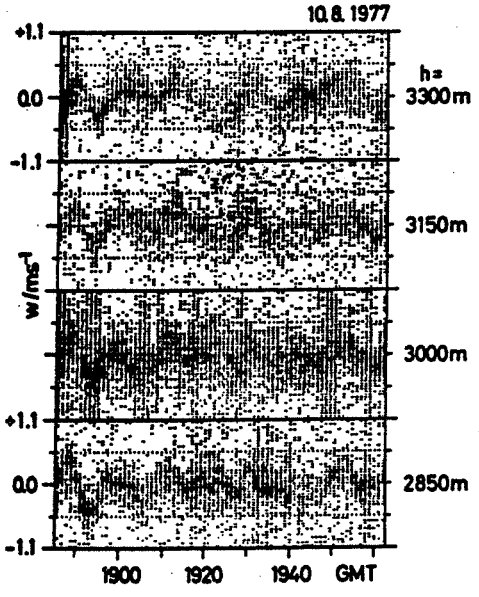

Figure 4. Doppler spectra plots (from ROTTGER, 1980).

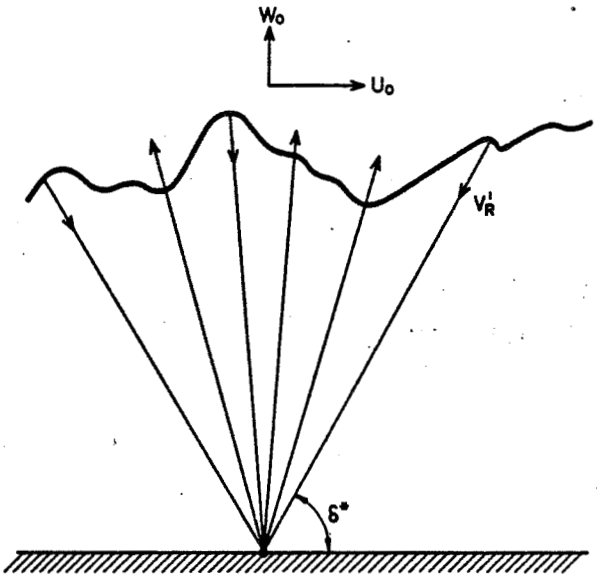

Figure 5. Reflections from sub-areas of a corrugated sheet of refractive index change, moving with the mean horizontal velocity U_o and the mean vertical velocity W_o; additionally a random (turbulent) component v_R' (due to fluctuations of U_o and W_o) is assumed.

tion of the signal amplitude. The period of the amplitude variation would be half the period of the velocity oscillation if the specular point moves out of the antenna beam (GAGE et al., 1981), but it should be equal to the wave's velocity period for focussing/defocussing. A long-period variation of the amplitude is also evident in Figure 3. The measurement of the distribution of arrival angles will yield additional information on these two effects.

REFERENCES

Briggs, B. H. (1980), Radar observations of atmospheric winds and turbulence: a comparison of techniques, J. Atmos. Terr. Phys., 42, 823-833.

Gage, K. S., D. A. Carter and W. L. Ecklund (1981), The effect of gravity waves on specular echoes observed by the Poker Flat MST radar, Geophys. Res. Lett., 8, 599-602.

Hocking, W. K. and J. Rottger (1983), Pulse length dependence of radar signal strengths for Fresnel backscatter, Radio Sci., 18, 1312-1324.

Rottger, J. (1980), Reflection and scattering of VHF radar signals from atmospheric refractivity structures, Radio Sci., 15, 259-276.

Sheen, D. R., C. H. Liu and J. Rottger (1984), A study of signal statistics of VHF radar echoes from clear air, to be submitted.

2.3A A MODIFIED FRESNEL SCATTERING MODEL FOR THE PARAMETERIZATION OF FRESNEL RETURNS

K. S. Gage, W. L. Ecklund and B. B. Balsley

Aeronomy Laboratory
National Oceanic and Atmospheric Administration
Boulder, CO 80303

ABSTRACT

This paper presents a modified Fresnel scatter model and compares the revised model with observations from the Poker Flat, Alaska, radar, the SOUSY radar and the Jicamarca radar. The modifications to the original model have been made to better account for the pulse-width dependence and height dependence of backscattered power observed at vertical incidence at lower VHF. Vertical profiles of backscattered power calculated using the revised model and routine radiosonde data show good agreement with observed backscattered power profiles. Relative comparisons of backscattered power using climatological data for the model agree fairly well with observed backscattered power profiles from Poker Flat, Jicamarca and SOUSY.

INTRODUCTION

Since the first observations at vertical incidence of enhanced specular-like echoes at lower VHF (GAGE and GREEN, 1978; ROTTGER and LIU, 1978), there has been considerable debate and controversy concerning the nature of the scattering/reflection mechanism responsible for these echoes. As discussed in GAGE and BALSLEY (1980), the enhanced echoes obtained at vertical incidence by VHF radars might be attributed to some combination of anisotropic turbulence scatter, Fresnel reflection from regions of strong refractive index gradients, and from Fresnel scattering from a volume filled with stable laminae of radio refractive index coherent transverse to the probing wave. Subsequently, GAGE et al. (1981) presented a model for Fresnel scattering which enabled the parameterization of radar echoes using ordinary rawinsonde data as input. While this model seemed to simulate the dependence of echo magnitude with stability, it did not properly account for the pulse-width dependence of the observed echoes (HOCKING and ROTTGER, 1983; GREEN et al., 1983). Also, it now appears that the height-dependence (BALSLEY and GAGE, 1981) was not properly accounted for in the original model. This paper presents a modified Fresnel scattering model which takes into account the contributions of FARLEY (1983), LIU (1983) and DOVIAK and ZRNIC (1984) as well as HOCKING and ROTTGER (1983) and hopefully corrects these deficiencies. The revised model is compared to observations of the Poker Flat, Alaska MST radar as well as the SOUSY radar located in the Federal Republic of Germany and the Jicamarca radar located in Peru.

A MODIFIED FRESNEL SCATTER MODEL

As originally presented in GAGE et al. (1981) the Fresnel scatter model assumed a coherent scattering from the half-wavelength Fourier component of the refractivity structure directed along the beam. This procedure was justified by GAGE et al. (1981) in order to account for a pulse length squared $(\Delta r)^2$ dependence of backscattered power which was observed in early VHF radar studies of specular echoes (GREEN and GAGE, 1980). Subsequent studies, however, have shown that a $(\Delta r)^1$ dependence is more typical (GREEN et al., 1983). Theoretical arguments in favor of a linear dependence on Δr have been advanced by HOCKING and ROTTGER (1983), LIU (1983) and FARLEY (1983). Clearly, the Fresnel scattering model must be modified to account for this.

Under conditions of stable stratification gradients of radio refractivity tend to be concentrated in thin layers that are horizontally coherent. Under these circumstances it is appropriate to consider the backscattered power P_r that arises from a partial reflection process. This is given by the radar equation

$$P_r = \frac{\alpha^2 P_T A_e^2}{4 r^2 \lambda^2} |\rho|^2 \tag{1}$$

where P_T is transmitted power (per pulse), A_e is effective antenna area, α is an efficiency factor, r is the range to the target, λ is radar wavelength and $|\rho|^2$ is a power reflection coefficient which depends upon the refractivity structure in the volume of the atmosphere being observed. The conventional approach to partial or Fresnel reflection is to determine the reflection coefficient deterministically based on a particular gradient structure. Since the detailed structure of individual layers is unknown, this approach is of limited value for the real atmosphere. More importantly, if the backscattered power were due to a single thin layer, there would be no Δr-dependence. The implication of the observed increase in backscattered power with Δr is clearly that the volume is filled with many thin layers. Furthermore, the reflectivity of this layered structure is greatly enhanced in hydrostatically very stable regions of the atmosphere.

The reflection coefficient pertinent to a medium filled with horizontally layered structure can be determined in the context of a one-dimensional scattering problem following LIU (1983) and FARLEY (1983). The voltage reflection coefficient ρ is given by

$$\rho = \frac{1}{2}\int_{-\ell/2}^{\ell/2} \frac{dn}{dz}\, e^{-2kiz}\, dz = ik \int_{-\ell/2}^{\ell/2} n(z) e^{-2ikz}\, dz \tag{2}$$

where ℓ is the thickness of the region of layered structure and $k(= 2\pi/\lambda)$ is radar wavelength.

When the layered structure which gives rise to the specular echoes is the result of vertical displacement due to either turbulence or waves, it is appropriate to replace n in Equation (2) by the generalized potential refractive index n (OTTERSTEN, 1969). Then, Equation (2) can be re-expressed as

$$\rho = \frac{1}{2}\int_{-\ell/2}^{\ell/2} M e^{-2kiz}\, dz = ik \int_{-\ell/2}^{\ell/2} n e^{-2ikz}\, dz = ik \int_{-\ell/2}^{\ell/2} \Delta n\, e^{-2ikz}\, dz \tag{3}$$

where $M = dn/dz$ is the gradient of generalized refractive index and Δn is the fluctuating component of refractivity. The power reflection coefficient pertinent to a radar observing at vertical incidence with a probing pulse of length Δr is

$$|\rho|^2 = k^2 \int_{-\Delta r/2}^{\Delta r/2} dz_1 \int_{-\Delta r}^{\Delta r} d(z_1 - z_2)\, \langle \Delta n(z_1) \Delta n(Z_2) \rangle\, e^{-2ik(z_1 - z_2)} \tag{4}$$

which leads to

$$|\rho|^2 = k^2 \cdot \Delta r \cdot \Phi_n(2k)$$

where $\Phi_n(k)$ is the vertical wave number spectrum of generalized potential radio refractive index

$$\Phi_n(k) = \int_{-\infty}^{+\infty} d(z_1 - z_2) \, \langle \Delta n(z_1) \, \Delta n(z_2) \rangle \, e^{-2ik(z_1 - z_2)} \tag{6}$$

For purposes of modeling the backscattered power in a way that can be evaluated from meteorological data it is convenient to introduce the mean gradient of generalized potential index of radio refractive index

$$M \equiv -77.6 \times 10^{-6} \frac{P}{T} \left(\frac{\partial \ell n \, \theta}{\partial z}\right) \times \left[1 + \frac{15{,}500q}{T} \left(1 - \frac{1}{2} \frac{\partial \ell n \, q/\partial z}{\partial \ell n \, \theta/\partial z}\right)\right] \tag{7}$$

where P is atmospheric pressure in millibars, T is absolute temperature, θ is potential temperature [$\theta \equiv T(1000/P)^{2/7}$], and q is specific humidity. M(z) and $\Phi_n(k)$ are related through the spectrum of vertical displacements $E_\zeta(k)$ (VANZANDT and VINCENT, 1983).

$$\Phi_n(k) = E_\zeta(k) \, \bar{M}^2 \, . \tag{8}$$

Combining Equation (8) with Equation (5) we find

$$|\rho|^2 = K^2 \cdot \Delta r \cdot E_\zeta(2k) \, \bar{M}^2 \tag{9}$$

and defining

$$F(2k;z)^2 \equiv 4k^2 \cdot E_\zeta(2k,z) \tag{10}$$

we obtain

$$|\rho|^2 = \frac{1}{4} \cdot \Delta r \cdot F(2k,z) \, \bar{M}^2 \, . \tag{11}$$

For generality in Equation (10) and Equation (11) we have indicated an altitude dependence for F and E_ζ. Substitution of Equation (11) in Equation (1) leads to the backscattered power

$$P_r = \frac{\alpha^2 \, P_t \, A_e^2 \, \Delta r}{16 \, r^2 \, \lambda^2} \left[\bar{M} \, F(2k,z)\right]^2 \tag{12}$$

The height dependence of P_r can tell us much about the height dependence of F and E_ζ. To investigate the height dependence of P_r, it is necessary to consider the height dependence of each factor in Equation (12). Since

$$P_r \propto \frac{\bar{M}^2 \, E_\zeta}{r^2} \propto \frac{[\rho_{air}(z)]^2 E_\zeta}{r^2} \tag{13}$$

it is clear that the height dependence of P_r is dominated by the $\rho_{air}^2(z)$ factor implicit in $\bar{M}^2$.

If $E_\zeta(k)$ were due to a spectrum of vertically propagating waves that conserved their energy, it would follow that $E_\zeta \propto \rho_{air}^{-1}$ and $P_r \propto \rho_{air}(z)/r^2$. If however, the growth with altitude of E_ζ were limited by some saturation process, E_ζ would become independent of altitude and $P_r \propto \rho_{air}^2(z)/r^2$.

BALSLEY and GAGE (1981) explored the height dependence of P_r and found that it decreased more rapidly than $\bar{M}^2/z^2$. Indeed, they reported the observed $P_r \propto \bar{M}^2/z^4$ and suggested that this might be the result of

reflection from structures limited in their horizontal dimensions (by their horizontal coherency length) to a fraction of Fresnel zone. As pointed out by DOVIAK and ZRNIC (1984) there is no reason for the horizontal dimensions of the reflecting region to be limited by the horizontal coherency length. If, indeed, the height dependence observed by BALSLEY and GAGE (1981) is real, it must be explained in some other way. One way to explain this height dependence would be to account for it in the height dependence of $E_\zeta(k,z)$. In what follows we have supposed that

$$E_\zeta(k,z) \propto e^{-z/z_*} \tag{14}$$

where z_* is a scale-height. Up to about 20 km the exponential fall-off approximates z^{-2}, but at higher altitudes the exponential fall-off is increasingly more rapid. The exponential dependence has been adopted here because it fits the data very well, especially at the higher heights, as will be shown below.

An exponential fall-off of $E_\zeta(k)$ is not easily explained, however at the meter scales pertinent to VHF radar studies it would not be surprising if viscous damping and turbulence processes played an important role. In the remainder of this paper we adopt the exponential dependence of $E_\zeta(k,z)$ and set

$$F(2k,z)^2 = F_1^2(\lambda)e^{-z/z_*} \tag{15}$$

where $F_1(\lambda)$ corresponds to the value of "F" used in GAGE et al. (1981). With this change we obtain the backscattered power

$$P_r = \frac{\alpha^2 P_t A_e^2 \Delta r}{16 r^2 \lambda^2} [\bar{M} F_1(\lambda)]^2 e^{-z/z_*} \tag{16}$$

for the modified Fresnel scattering model.

Following GAGE and GREEN (1978) it is convenient to define a normalized received power S_v by

$$S_v \equiv 10^{17} P_r(\text{watts}) \left\{\frac{r(m)}{10^3 m}\right\}^2 \tag{17}$$

which when combined with Equation (16) leads to

$$S_v = 10^{17} \frac{\alpha^2 P_T A_e^2}{16 \lambda^2 10^3 m} \left(\frac{\Delta r}{10^3 m}\right) \{M F(\lambda)\}^2 e^{-z/z_*} \tag{18}$$

In the following section we compare S_v calculated according to Equation (15) with observed values of S_v.

COMPARISON OF SOME POKER FLAT MST RADAR OBSERVATIONS WITH THE MODIFIED FRESNEL SCATTERING MODEL

The calculated values of S_v presented here have been made under the assumption that the generalized potential refractive index M is determined in the upper troposphere and stratosphere by its dry part:

$$M_d = -77.6 \times 10^{-6} \frac{P}{T} \frac{\partial \ln \theta}{\partial z} \tag{19}$$

where P is atmospheric pressure in mb, T is absolute temperature in Kelvins, θ is potential temperature in Kelvins and z is altitude in meters. M_d is easily calculated for each significant level of the radiosonde soundings. Typically, there are several significant levels for each radar range gate. The

individual values of M_d are then weighted according to the thickness of each significant level and averaged together to give $\overline{M_d}$ corresponding to each range gate. Of course, the larger the range gate the more effective will be the smoothing of the $\overline{M_d}(z)$ profile. The data reported in this section were taken at Poker Flat, Alaska in the fall of 1979 when one-quarter section (100 m x 100 m) of the final antenna was phased to look vertically. During this period a single transmitter was used with peak power of about 55 kW. Most of the data were obtained with 15 μs pulses (Δr = 2.25 km) but a limited sample of data was also taken with 5 μs pulses (Δr = .75 km).

A comparison of modeled and observed S_y for the Poker Flat MST radar is contained in Figures 1 through 4. The model calculations make use of the routine radiosonde soundings at Fairbanks which are launched about 40 km from the MST radar site at Poker Flat. The model profiles were calculated using $F_1(\lambda) = 8 \times 10^{-3}$ and $\alpha = 0.5$ in Equation (15).

Figure 1 contains a comparison of the modified Fresnel scattering model with Poker Flat radar observations taken on 13 September 1979 with .75 km height resolution. The radar observations are an average of two hours of data which bracket the time of the balloon launch in Fairbanks. The overall agreement in the magnitude and shape of the two profiles is excellent. We do not attach too much significance to the agreement in the upper troposphere (in this case below about 10 km) since we expect that, in the less stable environment of the troposphere, turbulent processes are dominant.

A second example of the agreement between modeled and observed profiles of S_y for the Poker Flat radar using .75 km height resolution is contained in Figure 2. In this case the overall agreement in magnitude is not quite so good but the agreement in shape of the two profiles is excellent. Even some of the detailed structure evident in the observed profile is reproduced in the model profile.

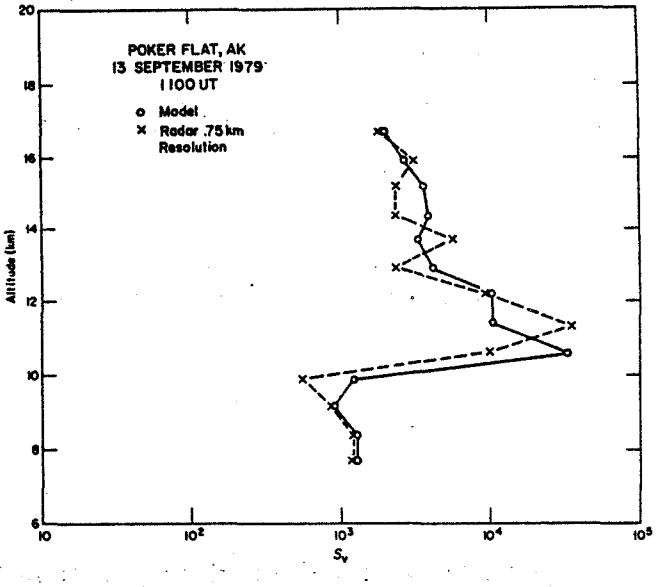

Figure 1. Comparison of calculated and observed fine-resolution profiles of normalized backscattered power for 13 September 1979.

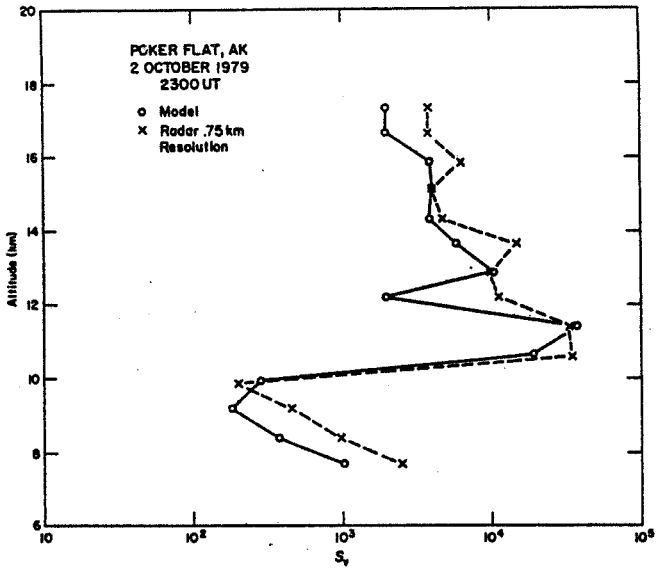

Figure 2. Comparison of calculated and observed fine-resolution profiles of normalized backscattered power for 2 October 1979.

Only a very limited sample of data was available at .75 km resolution from the Poker Flat MST radar during the Fall of 1979. However, nearly continuous coarse-resolution data were available during this period (2.25 km resolution). Two examples of comparisons obtained during this period are contained in Figure 3 and Figure 4. The most obvious change in comparison to the fine resolution profiles is the increase in backscattered power. The change in Δr in the modified version of the model accounts very well for this observed change in backscattered power. The coarse resolution profiles show low values of backscattered power in the troposphere with a significant increase in the lower stratosphere followed by a systematic decrease with altitude due mainly to decreasing atmospheric density. Both comparisons show very good agreement with the modified Fresnel scattering model. Note that the tropopause on 6 November 1979 was unusually high. Also note that both model and observed coarse-resolution profiles contain much less structure than is found in the fine-resolution profiles.

CLIMATOLOGICAL MODEL COMPARISONS WITH OBSERVATIONS

The modified Fresnel scatter model can be used with climatological data to examine the altitude dependence of this process. This procedure is similar to that followed in BALSLEY and GAGE (1981) but here we use a different approach to the height dependence as explained above. Figure 5 contains the results of these model calculations.

Figure 5a compares the relative backscattered power calculated using our modified ("exponential") Fresnel scatter model with a set of observations made in October-November 1979 using the Poker Flat, Alaska, MST radar (BALSLEY et al., 1980) (note that all comparisons with observtions shown in this section are relative). The model profile is calculated using 60°N climatological data (U.S. Standard Atmosphere Supplement, 1980). The agreement is comparable to that found by BALSLEY and GAGE (1981) using an assumed z^{-4} dependence.

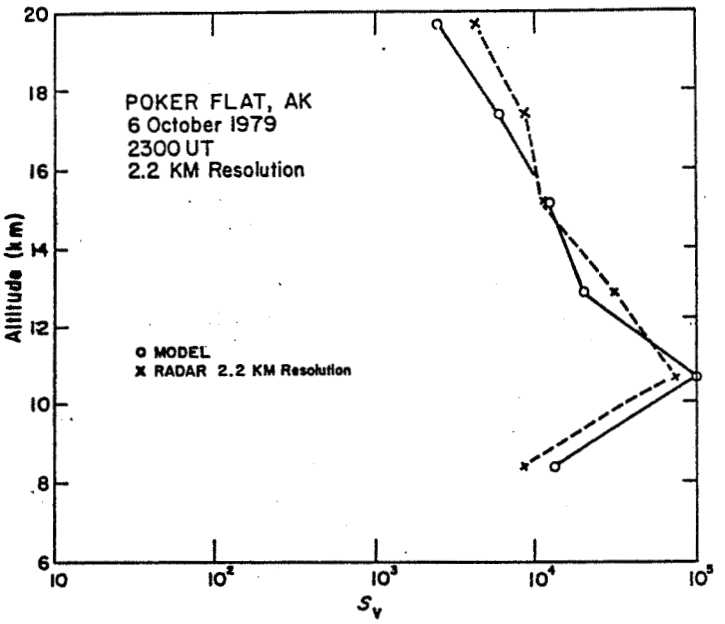

Figure 3. Comparison of calculated and observed coarse-resolution profiles of normalized backscattered power for 6 October 1979.

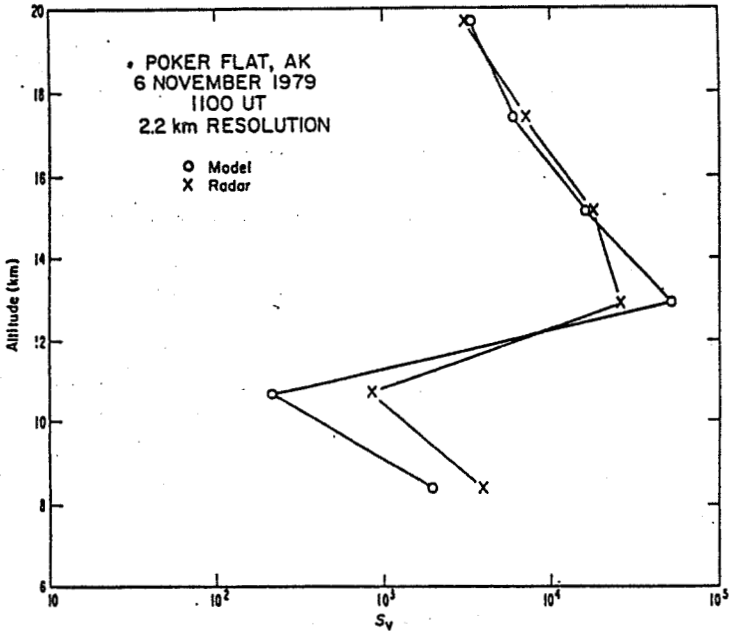

Figure 4. Comparison of calculated and observed coarse-resolution profiles of normalized backscattered power for 6 November 1979.

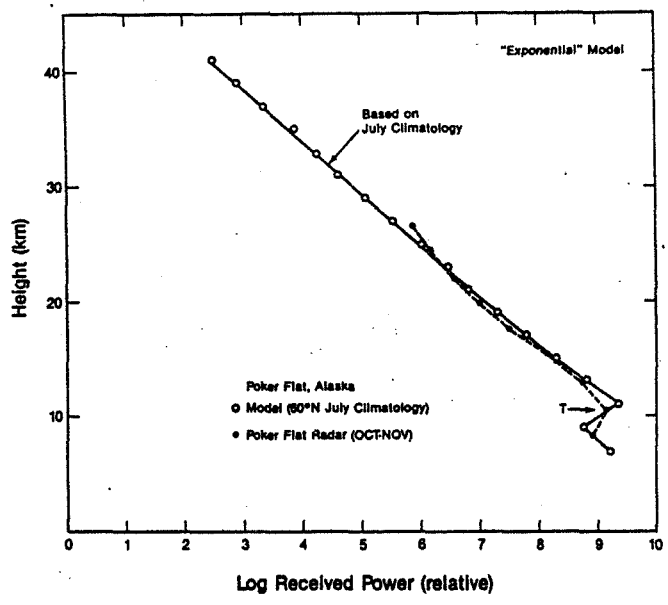

Figure 5(a).

Figure 5. Comparisons of observed profiles of backscattered power from three radars with theoretical profiles calculated from the U. S. Standard Atmosphere Supplement (1966): (a) Poker Flat, Alaska MST radar (b) Jicamarca radar (BALSLEY, 1978), and (c) SOUSY radar, Federal Republic of Germany (RUSTER et al., 1980).

Shown in Figure 5b is a comparison of the modeled backscattered power profile calculated using climatological data for 15°N with observations of the Jicamarca radar located at 12°S near Lima, Peru. The overall fit of the new model profile to the observed backscattered power profile is a considerable improvement over the old model (BALSLEY and GAGE, 1981). This result is especially significant since the observations in this case cover most of the stratosphere. As a third example we compare in Figure 5c a climatological calculation for 45°N with observations from the SOUSY radar (RUSTER et al., 1980). Again, the comparison is significantly improved over the earlier results.

CONCLUSIONS

In this paper we have formulated a modified Fresnel scattering model which permits the parameterization of VHF radar echoes obtained at vertical incidence in terms of routinely measured atmospheric parameters. It is assumed the radar observing volume is filled by a collection of transversely coherent, horizontally stratified, stable laminae of radio-index of refraction. The revised model assumes that the layered structure is randomly distributed as discussed in HOCKING and ROTTGER (1983). It also assumes an exponential decrease with altitude in the magnitude of the vertical displacement spectrum. While the exponential decrease in the vertical displacement spectrum is somewhat surprising, it is not too unreasonable at the meter scales pertinent to VHF radar probing since at these scales turbulence and viscous effects are expected to be important. With these changes the Fresnel scattering model simulates very well the observed profiles of backscattered power as seen by several MST radars.

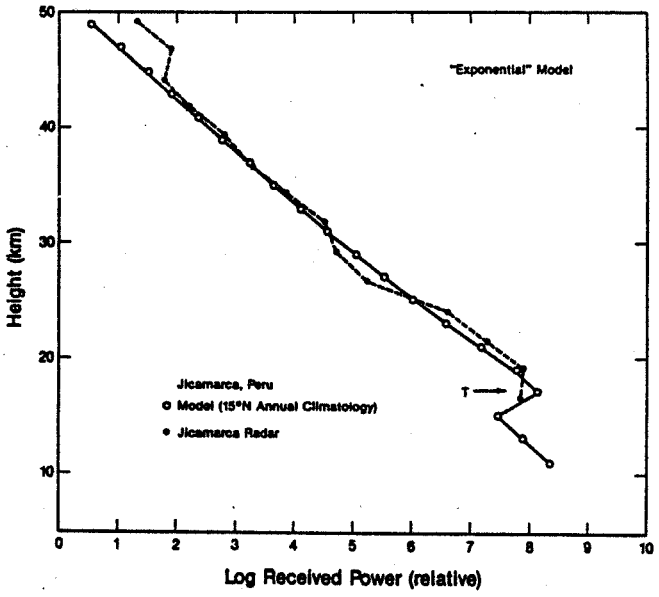

Figure 5(b).

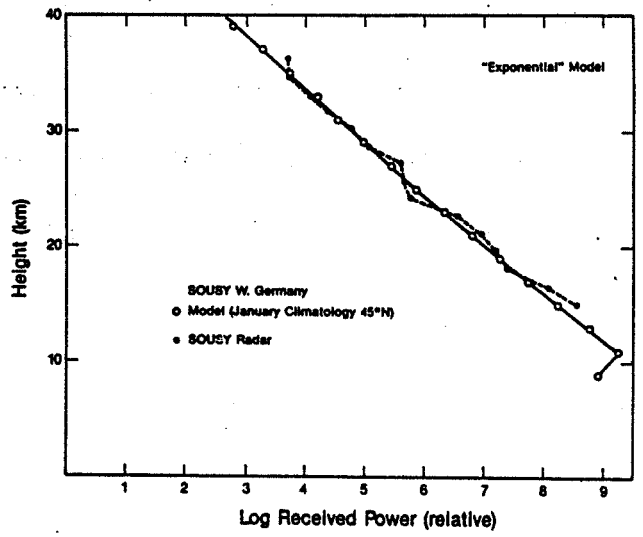

Figure 5(c).

REFERENCES

Balsley, B. B. (1978), The use of sensitive coherent radars to examine atmospheric parameters in the height range 1-100 km, Preprints, 18th Conf. on Radar Meteorology (Atlanta) AMS, Boston, 190-193.

Balsley, B. B. and K. S. Gage (1981), On the vertical incidence VHF backscattered power profile from the stratosphere, Geophys. Res. Lett., 8, 1173-1175.

Balsley, B. B., W. L. Ecklund, D. A. Carter and P. E. Johnston (1980), The MST radar at Poker Flat, Alaska, Radio Sci., 15, 213-223.

Doviak, R. J. and D. S. Zrnic (1984), Reflection and scatter formula for anisotropically turbulent air, Radio Sci., (in press).

Farley, D. T. (1983), Comments on "Fresnel Scatter", Proc. Workshop on Technical Aspects of MST Radars, Handbook for MAP, Vol. 9, SCOSTEP Secretariat, Univ. Illinois, Urbana, IL, 71-72.

Gage, K. S. and J. L. Green (1978), Evidence for specular reflection from monostatic VHF radar observations of the stratosphere, Radio Sci., 13, 991-1001.

Gage, K. S. and B. B. Balsley (1980), On the scattering and reflection mechanisms contributing to clear air radar echoes from the troposphere, stratosphere, and mesosphere, Radio Sci., 15, 243-257.

Gage, K. S., B. B. Balsley and J. L. Green (1981), A Fresnel scattering model for the specular echoes observed by VHF radar, Radio Sci., 16, 1447-1453

Green, J. L., B. B. Balsley and K. S. Gage (1983), A reexamination of the pulse-length dependence of backscattered power observed by VHF radars at vertical incidence, Preprints, 21st Conf. on Radar Meteorology (Edmonton) AMS, Boston, 141-143.

Green, J. L. and K. S. Gage (1980), Observations of stable layers in the troposphere and stratosphere using VHF radar, Radio Sci., 15, 395-405.

Hocking, W. K. and J. Rottger (1983), Pulse-length dependence of radar signal strengths for Fresnel backscatter, Radio Sci.

Liu, C. H. (1983), Interpretation of MST radar returns from clear air, Proc. Workshop on Technical Aspects of MST Radar, Handbook for MAP, Vol. 9, SCOSTEP Secretariat, Univ. Illinois, Urbana, IL, 1247-1249.

Ottersten, H. (1969), Mean vertical gradient of potential refractive index in turbulent mixing and radar detection of CAT, Radio Sci., 4, 1247-1249.

Rottger, J. and C. H. Liu (1978), Partial reflection and scattering of VHF radar signals from the clear atmosphere, Geophys. Res. Lett., 5, 357-360

Ruster, R., P. Czechowsky and G. Schmidt (1980), VHF-radar measurement of dynamical processes in the stratosphere and mesosphere, Geophys. Res. Lett., 7, 999-1002.

U.S. Standard Atmosphere Supplements (1966), Prepared by ESSA, NASA, USAF. Available from U.S. Government Printing Office, Washington, D.C.

VanZandt, T. E. and R. A. Vincent (1983), Is VHF Fresnel reflectivity due to low frequency buoyancy waves? Preprint Vol., 21st Conf. on Radar Meteorology, Sept. 19-23, 1983, Edmonton, Alberta, Canada, AMS, Boston, MA.

D18

2.4A OBSERVATIONS OF MESOSPHERIC TURBULENCE BY ROCKET PROBE AND VHF RADAR

O. Royrvik and L.G. Smith

Aeronomy Laboratory
Department of Electrical and Computer Engineering
University of Illinois
Urbana, IL 61801

INTRODUCTION

Irregularities in the refractive index result in coherent backscattering of VHF radar signals from the mesosphere (WOODMAN and GUILLEN, 1974). There are two well-known characteristics of the scattered radar signal which appear to be particularly relevant to the scattering mechanism. The scattered signal is aspect sensitive so that a stronger echo is received when the radar antenna is pointed vertically than when it is pointed off-vertical (FUKAO et al., 1980). This aspect sensitivity is altitude dependent. Correlation between the echo power and the signal correlation time (P/C correlation) is also altitude dependent. A strong positive correlation is present in the lower mesosphere, changing to negative above about 75 km.

FUKAO et al. (1980) and others have suggested that radar echoes from the lower mesosphere may be caused by partial reflection from stratified layers modulated by gravity waves or turbulence, thus causing the observed amount of off-vertical scatter. In the upper mesosphere, however, where the scattering is isotropic, it is generally assumed that turbulence is the only mechanism generating refractive index fluctuations.

THRANE et al. (1981) compared irregularities in ion density data from a probe to echo power observed by a 2.75 MHz radar near Tromso, Norway. They concluded that the data were consistent with radio waves scattered from homogeneous, isotropic turbulence from 70 to 95 km. HOCKING and VINCENT (1982) have also presented data from a similar set of experiments performed at Woomera, Australia. They, however, concluded that partial reflections from horizontally stratified steps in the electron concentration play an important role in causing the radar echoes, at least up to an altitude of 85 km.

Here we compare data obtained simultaneously from rocket-borne Langmuir probes and from a 50 MHz MST radar. Rockets carrying Langmuir probes were launched from Punta Lobos in Peru during the CONDOR campaign of February-March 1983. In support of these rocket experiments, the Jicamarca VHF radar obtained data in the mesosphere and upper E-region.

OBSERVATIONS

The rocket (Nike Orion 31.028), launched on 27 February 1983, observed some irregularities in a narrow altitude region around 86 km. The echo power map obtained by the Jicamarca radar between 10:16 LST and 11:56 LST is shown in Figure 1. Note that the data recording system was operated intermittently during the one-hour period prior to the rocket launch. The mesospheric region showed scattering in a narrow layer initially located at 79 km and largely stationary at that altitude for at least one hour prior to the rocket launch at 11:33 LST. The scattering was so localized in altitude that it appeared in only one range gate indicating a thickness of at the most 3 km. Immediately prior to the rocket launch the scattering region moved upwards to cover both the 79 km and the 82 km range gates.

The relative electron density irregularity ($\Delta N/N$) profile in different frequency bands observed by the rocket on the up leg is shown in Figure 2.

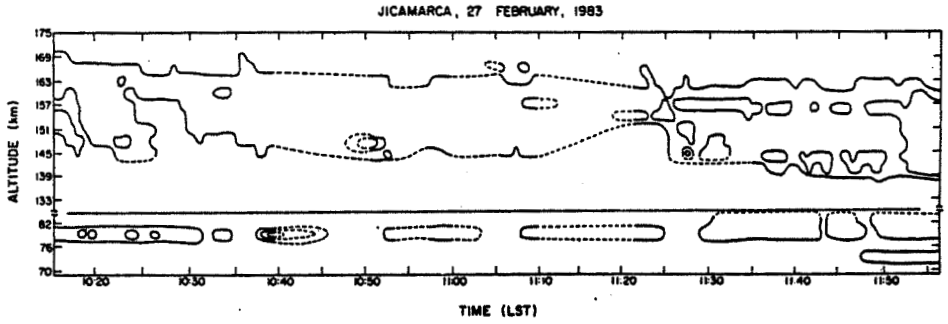

Figure 1. Jicamarca radar echo power map from February 27, 1983 between 10:15 and 11:56 LST. Data from the upper mesosphere (70-82 km) and the upper E region (133-175) were recorded intermittently. The power level visually observed during times of no data are indicated by the broken contours. Contour levels indicate signal-to-noise levels of 1, 5 and 10. Note the break in the altitude scale between 82 and 133 km.

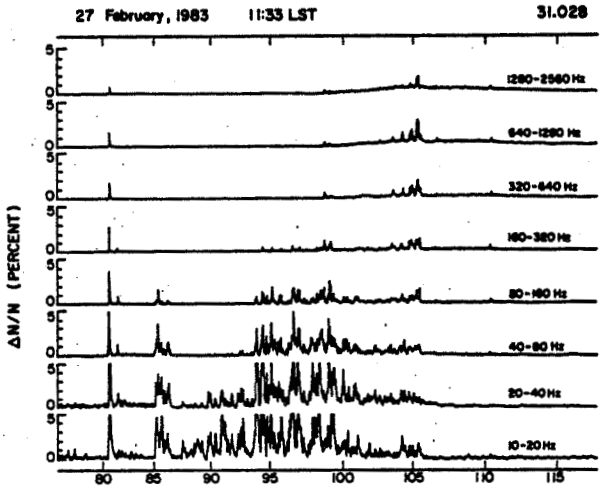

Figure 2. Relative electron density variations in different frequency bands in the altitude region 75 to 115 km for the rocket (Nike Orion 31.028) launched on 27 February 1983. The signal is filtered by narrow band filters and rectified. The peaks at 81 and 82 km are attributed to instrumental effects.

The electrojet region is clearly visible between about 90 km and 106 km. In addition, there appears to be a narrow region of irregularities at about 86 km. The altitude of the irregularities is higher than the scattering layer observed by the Jicamarca radar. However, the horizontal distance separating the two observations and the observed altitude change in the radar data at the time of the rocket launch makes it reasonable to argue that the same layer was observed in the two data sets.

RADAR DATA

The P/C correlation was calculated for the February 27 data set and was found not to be negative but showed distinct, unexplained, features as can be seen in Figure 3. Notice that the short-lived increase in echo power at 11:31 LST at the 79 km altitude is accompanied by a steady increase in correlation time that lasts until the scattered power has decreased to its pre-enhancement level. Other short-lived bursts of scattered power are accompanied by similar unexplainable behavior of the signal correlation time. Typical correlation time seen in Figure 3 is about 0.3 s. In particular this is true for both the two altitude ranges 79 and 82 km at the time of the rocket launch.

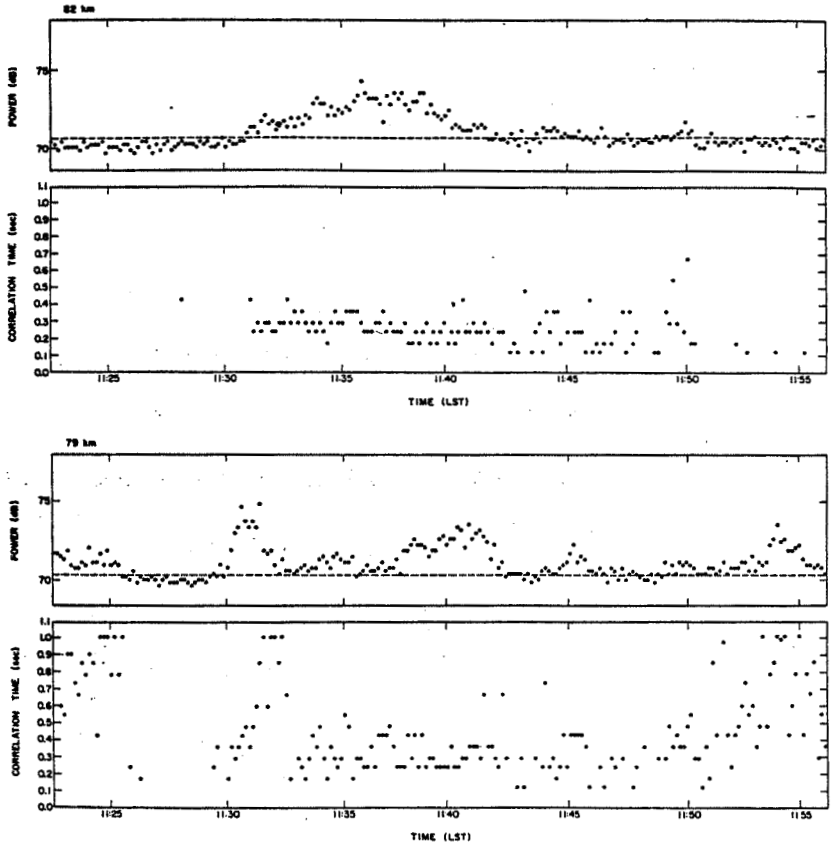

Figure 3. Jicamarca radar signal power and signal correlation time for the 79 and 82 km altitude bins between 11:23 and 11:56 LST on 27 February 1983. Time resolution is about 10 s. Correlation time is calculated when the ratio between the zero and first lag in the autocorrelation function is less than 10.

The present experiment which used only two antenna sections spaced in the east-west direction could detect vertical velocity variations in the east-west direction only by use of the interferometer method (ROYRVIK, 1983). Some examples of vertical velocity differences were found in the present data set and two examples are presented in Figure 4. There is a phase shift accompanying the shift in frequency across the spectral peaks. The east-west size of these structures can be roughly estimated from the total phase shift (ROYRVIK, 1983) and in the present case the size is about 600 m. It has been suggested (ROYRVIK, 1983) that the observations of differential vertical velocities are manifestations of Kelvin-Helmholtz vortices and thus presumably are related to the development of turbulent layers.

ROCKET DATA

The rocket data of $\Delta N/N$, considered here, came from the high-gain channel of the fine-structure probe experiment. Detailed examination of the record between 70 km and 90 km show a single region of irregularities between 85.0 and 86.4 km. The two peaks at 81 and 82 km, visible in Figure 2, are attributed to instrumental effects. Spatial power spectra of the relative density fluctuations were calculated from 2048 data points covering a spatial range of about 600 meters. It is clear that the spectral power of three meter irregularities (500 Hz) is close to or below the noise level even in the region of strong irregularities at 86 km. We thus depend on interpolation of the spectrum of longer wavelengths to calculate the scattered power at the three meter wavelength. The first three spectra in Figure 5 cover the 1400 meter vertical extent of the region of enhanced irregularities. The last spectrum is apparently the noise-level spectrum from the region immediately above the layer of irregularities. At frequencies above 200 Hz (corresponding to 7.5 m spatial wavelength) the spectra are below noise level, but below this

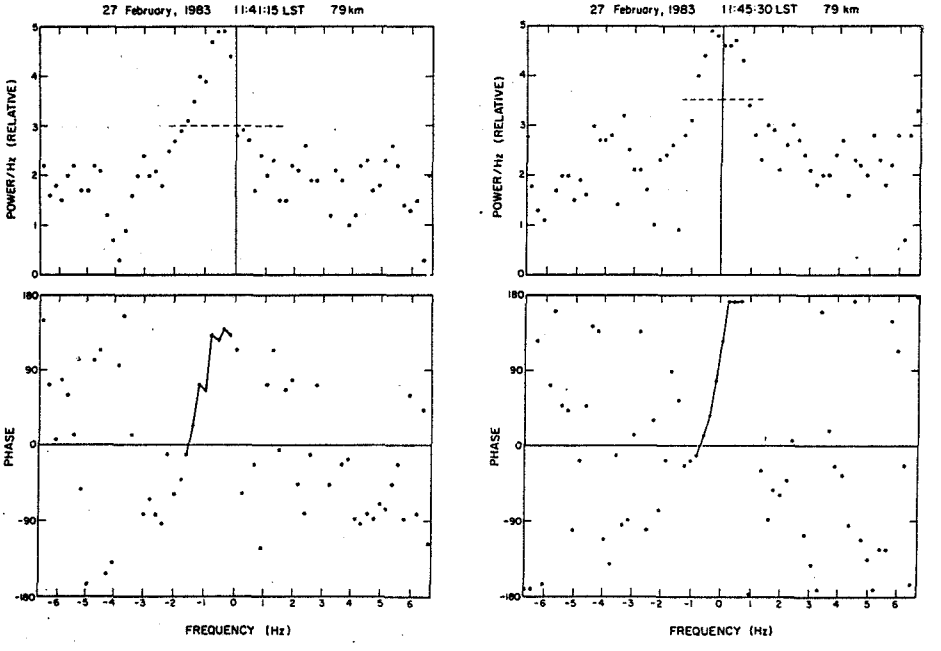

Figure 4. Jicamarca radar cross spectra from 11:41:15 LST and 11:45:30 LST on 27 February 1983. The broken line in the power spectra indicates an upper estimate of the noise level. The phases of the spectral components exceeding this noise level have been joined by a solid curve.

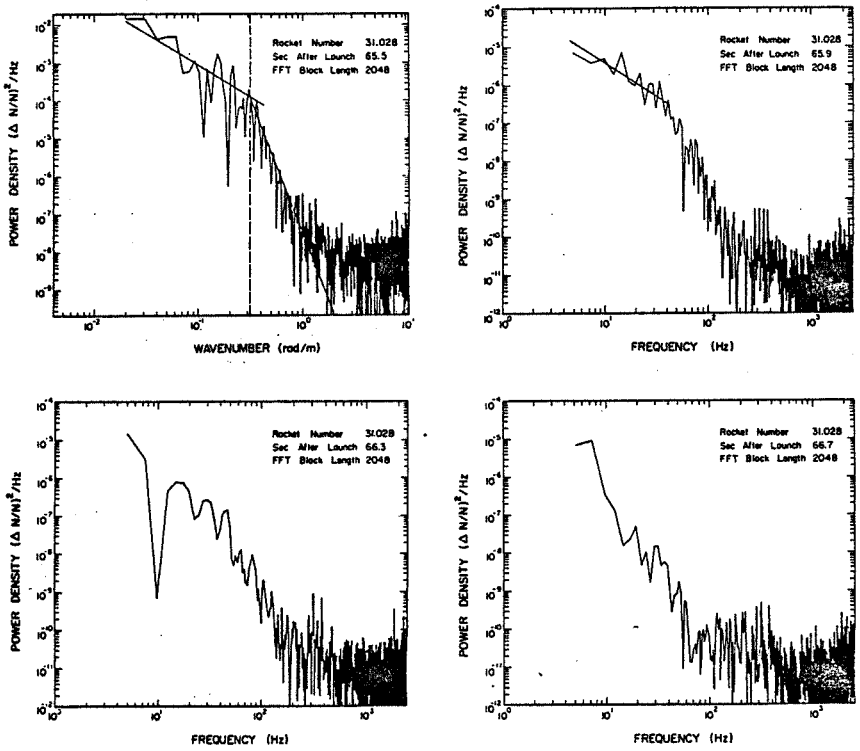

Figure 5. Spectra of relative electron density variations ($\Delta N/N$) in the scattering layer observed by the probe experiment on 27 February 1983 between 85.2 and 86.6 km altitude. The first spectrum has been shown in units of wavelength assuming a rocket velocity of 1.5 km. The three remaining spectra are in units of Hz. The last spectrum is from a region of no detectable turbulence.

frequency there is a marked increase in power above the noise level. This is consistent with the irregularity profiles shown in Figure 2.

Turbulence theory (TATARSKII, 1971) predicts a spectral index of -5/3 in the inertial subrange of turbulence. Figure 5 shows, however, that there is a noticeable break in the spectral slope at about 50 Hz corresponding to a wavelength of about 30 m. At lower frequencies (longer wavelengths) the spectral slope -5/3 fits the observed spectra quite well. At higher frequencies (shorter wavelengths) the spectral slope is much steeper, apparently close to a slope of -7.

DISCUSSION

Several comparisons can be made between the VHF radar data and the rocket electron-density measurement. The most straightforward is to compare the radar scattering cross section per unit volume (σ) measured by the radar to the cross section calculated from the spectrum of irregularities observed by the rocket. We adopt the formula for the radar reflectivity from VANZANDT et al., (1978)

$$\sigma = \frac{9\pi}{2} \frac{c\, k_B\, B\, (T_c + T_{rx}/\alpha)}{\alpha\, P_t\, F_r\, A} \left(\frac{r}{\Delta r}\right)^2 \left(\frac{S}{N}\right) \qquad (1)$$

where c is the velocity of light and k_B is the Boltzmann's constant. The definitions and values of the radar parameters are given in Table 1. From Figure 1 it is seen that the signal-to-noise ratio ($\frac{S}{N}$) varies between 1 and 10 in the altitude range around 80 km. If we assume what seems to be a typical S/N ratio of 2 for the time of the rocket launch we calculate:

$$\sigma = 2 \times 10^{-18}\ m^{-1}$$

We have used $A = 4.2 \times 10^4\ m^2$ since only two quarter-sections of the antenna were used for reception.

To calculate the reflectivity resulting from the rocket irregularity data we start with the formula given by OTTERSTEN (1969)

$$\sigma(k) = \frac{\pi^2}{2} k^4 \phi_n(\underline{k}) \tag{2}$$

where k is the wave number and $\phi_n(\underline{k})$ is the spectrum representing the three dimensional refractive index field. The rocket experiment, however, measures the one-dimensional relative variation in the electron density $S_N(k)/N^2$ and we will have to modify (2). The relationship given by WOODMAN and GUILLEN (1974) relates the spectra of the refractive index and the spectra of electron density variations ($\phi_N(\underline{k})$) as

$$\phi_n(\underline{k}) = \frac{f_p^4}{4 f^4} \frac{\phi_N(\underline{k})}{N^2} \tag{3}$$

Here f_p is the plasma frequency and f is the frequency of the probing radio wave. So, for the mesosphere, we get

$$\sigma(\underline{k}) = \frac{\pi^2}{2} k^4 \frac{f_p^4}{4 f^4} \frac{\phi_N(\underline{k})}{N^2} \tag{4}$$

Note that $\phi_N(\underline{k})$ is a three-dimensional spectrum, whereas the one measured by the rocket is a one-dimensional spectrum. OTTERSTEN (1969) has discussed this conversion in detail and if the spectra are isotropic and follows the negative power law one can substitute for $\phi_N(\underline{k})$

$$\phi_N(\underline{k}) = -(n) \frac{1}{4\pi} k^{-2} S_N(k) \tag{5}$$

where $S_N(k)$ is the one-dimensional spectrum measured by the rocket. By substituting (5) into (4) we end up with the appropriate relationship between the radar reflectivity and the rocket irregularity spectrum

$$\sigma(k) = -n \left(\frac{\pi}{8}\right) k^2 \frac{f_p^4}{4 f^4} \frac{S_N(k)}{N^2} \tag{6}$$

The question of isotropic irregularity spectrum cannot be independently determined in this case, however, we feel justified in assuming isotropy since previous radar experiments (COUNTRYMAN and BOWHILL, 1979, FUKAO et al., 1980, and and ROYRVIK, 1983) have shown isotropic coherent scattering of VHF radio waves at and above 80 km in the mesosphere.

It is clear from Figure 5 that the spectral component at 3 m (k = 2.1 rad/m) is below the noise level, however, fitting of a power law with spectral index n = -7 gives an estimated power of 3×10^{-10} $(\Delta N/N)^2$ m/rad. This value when substituted into (6) gives

$$\sigma = 4 \times 10^{-18}\ m^{-1}$$

in good agreement with the value calculated from the radar data.

According to elecmentary isotropic turbulence theory (TENNEKES and LUMLEY, 1972) the energy dissipation rate can be related to turbulent velocity and to the scale size of the turbulence through

$$\varepsilon \sim v^3/l \tag{7}$$

For stationary turbulence it must be assumed that the energy dissipation rate is equal to the rate of energy input at the largest scale of turbulence so that $\varepsilon \sim V_B^3/L_B$. HOCKING (1982) has discussed this point and suggested the relationship

$$\varepsilon \approx 2.9\ \overline{v^2}\ f_B \tag{8}$$

where f_B is the Brunt-Vaisala frequency (in Hz) and v is the horizontal rms velocity. The total rms value of the line-of-sight velocity variations can be obtained from the Doppler spectrum of the scattered signal through the equation

$$V_z = \frac{\lambda}{2} f_{1/2}\ (2 \ln 2)^{-1/2} \tag{9}$$

where $f_{1/2}$ is the half width of the spectrum (BRIGGS, 1980). It is important to verify that the spectral width is due to turbulence rms velocities only, and do not contain contributions from a host of other phenomena. This has been done.

The correlation half-time, which is the quantity calculated is quite variable at least for the 79 km range gate (Figure 3), however for the 82 km range time it is fairly stable at about 0.3 s giving a half width of the Doppler spectra of about 0.6 Hz. Substituting this value into equation (9) we calculate

$$V_z = 2.2\ m/s.$$

TENNEKES and LUMLEY (1972) have suggested that due to the anisotropy at the largest scales of turbulence the vertical rms velocity is a factor $\sqrt{2}$ smaller that the horizontal rms velocity. We use this assumption when calculating the energy dissipation rate from equation 8, and get $\varepsilon = 0.05\ W\ kg^{-1}$.

The inner scale of turbulence (Kolmogorov microscale) $\eta = (\nu^3/\varepsilon)^{1/4}$ is related to the energy dissipation rate (ε) and the kinematic viscosity (ν). Using values from the U.S. Standard Atmosphere model for the kinematic viscosity we get $\eta = 3.15$ m at 85.5 km. According to TENNEKES and LUMLEY (1972) the velocity spectrum will be in the inertial subrange if $k_\eta < 1$ and in the dissipation subrange for $k_\eta > 1$. Thus it is expected that the change-over between a $-5/3$ power law spectrum and a much steeper spectrum will occur at $k = 0.31\ m^{-1}$. This value is marked in Figure 5 and appears to be in good agreement with the observed change in the spectral slope.

Finally, we can compare the outer scale of turbulence, or the turbulent layer thickness, estimated from the two data sets. For the radar data we use the equation

$$L_B \sim 1.1\ \bar{v}/f_B = 800\ m$$

where f_B is the Brunt-Vaisala frequency corresponding to a period of 5 min. The 800 m layer thickness compares reasonably well with the 1.4 km region of irregularities observed with the rocket as shown in Figure 2. The difference

may be due to the horizontal difference separating the two observation volumes, but it may also be due to the fact that turbulence close to the outer scale L_B is not isotropic and the rms velocity observed in the vertical antenna is not identical to the shear velocity across the turbulent layer.

SUMMARY AND CONCLUSIONS

Data from the Jicamarca VHF radar and from a Langmuir probe fine-structure on a Nike Orion rocket launched from Punta Lobos, Peru have been compared. A single mesospheric scattering layer was observed by the radar. The Langmuir probe detected irregularities in the electron-density profile in a narrow region between 85.2 and 86.6 km. It appears from a comparison between these two data sets that turbulence in the neutral atmosphere is the mechanism generating the refractive index irregularities.

ACKNOWLEDGMENT

The work described was supported by the National Aeronautics and Space Administration under grant NGR 14-005-181.

REFERENCES

Briggs, B. H. (1980), Radar observations of atmospheric winds and turbulence: a comparison of techniques, J. Atmos. Terr. Phys., 42, 823-833.

Countryman, I. D. and S. A. Bowhill (1979), Wind and wave observations in the Mesosphere using coherent-scatter radar, Aeronomy Report, No. 80, Aeron. Lab., Dep. Elec. Eng., Univ. ILL., Urbana-Champaign.

Fukao, S., T. Sato, R. M. Harper and S. Kato (1980), Radio Wave scattering from the tropical mesosphere observed with the Jicamarca radar, Radio Sci., 18, 447-457.

Hocking, W. K. (1982), On the extraction of atmospheric turbulence parameters from radar backscatter Doppler spectra - I. Theory., J. Atmos. Terr. Phys., 45, 89-102.

Hocking, W. K. and R. A. Vincent (1982), A comparison between HF partial reflection profiles from the D-region and simultaneous Langmuir probe electron density measurements, J. Atmos. Terr. Phys., 44, 843-854.

Ottersten, H. (1969), Atmospheric structure and radar backscattering in clear air, Radio Sci., 4, 1231-1253.

Royrvik, O. (1983), VHF radar signals scattered from the equatorial mesosphere, Radio Sci., 18, 1325-1335.

Tatarskii, V. I., (1971), The effects of the turbulent atmosphere on wave propagation, Israel Program for Scientific Translations Ltd., U.S. Dept. of Commerce, NTIS. Springfield, VA 22151.

Tennekes, H. and J. L. Lumley (1972), A First Course in Turbulence, MIT Press, Cambridge.

Thrane, E. V., B. Grandal, R. Fla and A. Brekke (1981), Fine structure in the ionospheric D-region, Nature, 292, 221-223.

VanZandt, T. E., J. L. Green, K. S. Gage and W. L. Clark (1978), Vertical profiles of refractivity turbulence structure constant: Comparison of observations by the Sunset Radar with a new theoretical model, Radio Sci., 13, 819-829.

Woodman, R. F. and A. Guillen (1974), Radio observations of winds and turbulence in the stratosphere and mesosphere, J. Atmos. Sci., 31, 493-505.

2.5A INTERPRETATION OF RADAR RETURNS FROM THE MESOSPHERE

O. Royrvik

Aeronomy Laboratory
Department of Electrical and Computer Engineering
University of Illinois
Urbana, IL 61801

INTRODUCTION

Since the first study of VHF radar signals from the mesosphere by WOODMAN and GUILLEN (1974) it has been clear that neutral atmosphere turbulence play a central role in generating the refractive index irregularities that backscatter the radio waves. It is generally believed (HARDY, 1972; ROTTGER, 1980, LIU and YEH, 1980) that an increase in the turbulent energy dissipation rate will result in a decrease in signal correlation time and an increase in scattered signal power. Thus, in turbulence-generated radar echoes a negative correlation between echo power and signal correlation time is expected (LIU and YEH, 1980). We will in the following adopt the notation P/C correlation for this relationship.

It has become apparent that the P/C correlation changes as a function of altitude (RASTOGI and BOWHILL 1976b; HARPER and WOODMAN, 1977). The P/C correlation is negative in the upper part of the mesosphere as expected of turbulence-generated irregularities, whereas it is largely positive in the lower mesosphere. Similar changes in the P/C correlation have also been observed in the stratosphere/troposphere region (ROTTGER and LIU, 1978). RASTOGI and BOWHILL (1976a,b) attempted to explain the positive P/C correlation observed in the lower mesosphere in terms of stronger turbulence occurring in narrower layers. However, LIU and YEH (1980) have argued that the effect of a narrowing layer is not strong enough to cause the positive P/C correlation. Instead ROTTGER and LIU (1978) suggested that the positive P/C correlation is a manifestation of partial reflection from stratified layers of refractive index gradient.

Partial reflection would explain another observational fact, namely that the scattered signal is aspect sensitive in the lower part of the mesosphere with maximum echo power coming from the vertical direction (FUKAO et al., 1980). On the other hand, perfect stratification would result in partial reflection of the radar waves, and no signal should be observed if the radar probing direction was oblique to the vertical. Since radar echoes, although reduced from that received from the vertical direction, are observed at very oblique angles it has been suggested that stratified layers modified by turbulence is needed to explain the observations from the lower mesosphere.

We shall examine the turbulence theory and assumptions made in previous studies and show that the scattered signal from the mesosphere is compatible with this theory if reasonable assumptions are made. We will show that under situations of stable turbulence the P/C correlation is positive if the radar Bragg wavelength (λ_r) is within the inertial subrange. Finally we will compare the results of the calculations to VHF radar data.

THEORY OF TURBULENCE

Turbulent motions in a fluid like the atmosphere are described by the Navier-Stokes equations, an unclosed set of nonlinear equations with no known general solution. Considerable work has gone into finding special solutions based on assumptions about, and observations of, the physical state of turbu-

lence. One of the assumptions usually made is that the turbulence is isotropic at all scales substantially smaller than the largest (outer) scale. A general understanding of turbulence has emerged (TATARSKII, 1971; TENNEKES and LUMLEY, 1972); however, the resulting equations that describe the turbulent spectra are more a result of limited physical insight and assumptions than of strict mathematical analysis, and thus should be carefully compared to experimental results.

In the inertial subrange of turbulence the velocity and irregularity spectra, $E(k)$ and $E_\theta(k)$, respectively, are given by TATARSKII (1971), and TENNEKES and LUMLEY (1972) as follows

$$E(k) = \alpha\, \varepsilon^{2/3}\, k^{-5/3} \tag{1}$$

and

$$E_\theta(k) = \beta N\, \varepsilon^{-1/3}\, k^{-5/3} \tag{2}$$

Here $\alpha = 1.5$ and $\beta = 0.5$ are experimentally determined constants, N is a variable related to the source of the refractive index gradient and ε is the turbulent energy dissipation rate. Note that both spectra follow the $-5/3$ power law in wave number k. The inner scale of the two spectra are defined separately as $\eta = (\nu^3/\varepsilon)^{1/4}$ and $\eta_\theta = (\gamma^3/\varepsilon)^{1/4}$, respectively. Here ν is the kinematic viscosity and γ the thermal diffusivity. For simplicity we shall assume $\nu \sim \gamma$ so that the inner scale (Kolmogorov microscale) of the spectra are equal.

In the dissipation subrange of turbulence the spectral forms are different and given by TENNEKES and LUMLEY (1972) as

$$E(k) = \alpha\, \varepsilon^{2/3}\, k^{-5/3}\, \exp[-3/2\, \alpha\, (k\eta)^{4/3}] \tag{3}$$

and

$$E_\theta(k) = \beta\, N\, \varepsilon^{-1/3}\, k^{-5/3}\, \exp[-3/2\, \beta\, (k\eta_\theta)^{4/3}] \tag{4}$$

for the velocity and irregularity spectra, respectively. For a discussion of the validity range of these spectra see TENNEKES and LUMLEY (1972). In what follows only dimensional analysis will be made.

A first inspection of equation (1) and (3) which determines the line-of-sight velocity variations at the Bragg wavelength indicate a continuously increasing velocity as a function of an increase in ε, both in the dissipation and the inertial subranges. However, the radar signal correlation time observed at one radar wavelength is related to the sum of all velocity fluctuations at wavelengths larger than the Bragg wavelength. As the scattering irregularities move around, their motions are affected by all turbulent cells of size larger than the Bragg wavelength. Thus we have the relationship between the radar rms velocity v and the turbulent velocity spectrum

$$\langle v^2 \rangle \propto \int_{k_L}^{k_r} E(k)\, dk \tag{5}$$

Here k_r is the radar Bragg wave number and k_L is the wave number corresponding to the outer scale of turbulence which is given by TENNEKES and LUMLEY (1971) as

$$L \propto \frac{V^3}{\varepsilon} \tag{6}$$

V is the shear velocity-difference across the turbulent layer. Assuming that there is an inertial subrange and that $k_B >> k_L$ we get by integrating equation (5) and substituting equation (6)

$$< v^2 > \propto \varepsilon^{2/3} k_L^{-2/3} \propto V^2 \tag{7}$$

Equation (7) shows that v is directly proportional to the velocity difference across the turbulent layer. Rearranging equation (6) we get

$$\varepsilon \propto V^2 \frac{V}{L} . \tag{8}$$

For further simplification we need to find a relationship between velocity difference and the layer thickness L.

The Richardson number is defined as

$$R_i = \omega_B^2/(dV/dz)^2$$

where ω_B is the Brunt-Vaisala frequency, and the average R_i across the turbulent layer is $R_i = \omega_B^2/(V/L)^2$. The critical Richardson number for onset of turbulence is known experimenatlly to be $R_i = 1/4$. The Brunt-Vaisala frequency is also a constant at a given altitude so that the ratio V/L is a constant and equation (8) reduces to

$$\varepsilon \propto V^2$$

and thus from (7) and (8) we get

$$V \propto \varepsilon^{1/2} \propto T^{-1} \propto \nu \tag{9}$$

here T is the signal correlation time. Since the line-of-sight rms velocity is proportional to the square root of the energy dissipation rate, and the signal correlation time is inverse proportional to the rms velocity, we conclude that the signal correlation time is proportional to $\varepsilon^{-1/2}$ regardless of whether the Bragg wavelength is in the inertial or dissipation subrange.

To calculate the relationship between radar echo power and energy dissipation rate we first need to consider the factor N in equations (2) and (4). To do so we need physical insight in the meaning of N. N is a measure of the dissipation of refractive index fluctuations. Assuming for the time being that the refractive index fluctuations are due to temperature (θ) variations and following TATARSKII (1971) we have

$$N = \gamma \frac{\partial \theta}{\partial z} \frac{d\theta}{dz}$$

In a steady state N is also a measure of the combined heat sources of a turbulent region. In considering equation (2) both TATARSKII (1971) and HARDY (1972) assumed a constant overall temperature gradient through the turbulent layer. However, the effective thermal diffusion coefficient (γ) changes order of magnitude with the onset of turbulence, so to maintain a constant temperature gradient it is required that the source of the turbulent irregularity structures (N) change as a function of ε. This leads to the following relation between the radar scattering cross section σ and ε given by HARDY (1972)

$$\sigma = \varepsilon^{2/3} .$$

This indicates a positive correlation between radar echo power and turbulent energy dissipation and led ROTTGER (1980) to conclude that a negative P/C correlation existed in the inertial subrange. However, the requirement that the source of temperature fluctuations changes in order to keep up with the

changing turbulent energy dissipation rate seems physically unreasonable. It seems much more reasonable to assume that the source is independent of the turbulence. In this case N is independent of ε and onset of turbulence produces a decrease in temperature gradient across the turbulent layer to compensate for the increase in effective diffusion. Thus inside the inertial subrange we get from equation (2) the following relationship

$$E_\theta(k_r) \propto \varepsilon^{-1/3}. \tag{10}$$

For a backscatter radar that operates at a fixed frequency with Bragg wave number k_r, it can be shown that the scattered power $P(k_r)$ is proportional to $E_\theta(k_r)$ (OTTERSTEN, 1969). Combining equations (9) and (10) gives the relationship $P \propto T^{2/3}$. Thus we find that there should be a positive correlation between radar echo power and signal correlation time if the radar Bragg wavelength is within the inertial subrange of the turbulent spectrum.

If, on the other hand, the radar operates in the dissipative subrange of the turbulence spectrum we have to examine equation (4) to obtain the relationship between the energy dissipation rate and the spectral power E_θ. Substituting for η_θ in equation (4) and again assuming that N is a constant we get

$$E_\theta(k_r) \propto \varepsilon^{-1/3} \exp(-K \varepsilon^{-1/3}) \tag{11}$$

where K is a constant. Considering equation (11) we conclude that if the radar Bragg wavelength is sufficiently inside the dissipative subrange, an increase in energy dissipation rate will result in an increase in radar echo power since the exponential term will overpower the power term. Thus considering equations (9) and (11) we conclude that there will be a negative P/C correlation if the radar Bragg wavelength is within the dissipative subrange of the turbulent spectrum.

DISCUSSION

In the previous section it was pointed out that turbulent theory as presented by TATARSKII (1971), and TENNEKES and LUMLEY (1972) can easily explain both positive and negative P/C correlation in VHF radar data provided the source of the refractive index variations (N) is a constant independent of the turbulent energy dissipation rate. The equations were developed on the assumption of isotropic and homogeneous shear layer turbulence.

RASTOGI and BOWHILL (1976b) have estimated that the Jicamarca VHF radar operates at a Bragg wavelength (3 m) that is within the dissipative subrange throughout the mesosphere, and recent comparison between Jicamarca radar data and rocket electron-density data (ROYRVIK and SMITH, 1984) have shown that this is true for a turbulent layer located at an altitude of 86 km. However, Royrvik and Smith also noted that the inertial subrange of the spectrum extended to higher wave numbers than estimated by RASTOGI and BOWHILL (1976b). Thus we would expect a negative P/C correlation in the altitude region around 85 km as observed by several investigators (HARPER and WOODMAN, 1977; COUNTRYMAN and BOWHILL, 1979; FUKAO et al., 1980, and ROYRVIK, 1983).

In order to determine if the positive P/C correlation observed in the lower mesosphere (RASTOGI and BOWHILL, 1976b; COUNTRYMAN and BOWHILL 1979, FUKAO, et al. 1980 and ROYRVIK, 1983) is caused by the radar Bragg wavelength being in the inertial subrange of the irregularity spectrum, we have recalculated the range of the inner scale of turbulence that can be expected in the mesosphere. In doing so we have calculated the turbulent energy dissipation rate (ε) from the signal correlation time; and the inner scale of turbulence η from ε and the kinematic viscosity ν taken from the U.S. Standard Atmosphere model. Outer limits on correlation time have been estimated from data available from the Jicamarca radar (RASTOGI and BOWHILL, 1976b; HARPER and WOODMAN, 1977;

COUNTRYMAN and BOWHILL, 1979; FUKAO et al., 1980 and ROYRVIK, 1983). The resulting limits on the inner and outer scales of turbulence have been plotted in Figure 1. It appears that for strong turbulence the Jicamarca radar Bragg wavelength will be in the inertial subrange of turbulence below about 70 km, and positive P/C correlation should be expected for this altitude range at least part of the time.

This result is only partly satisfying since positive P/C correlation has been observed as high as 75 km in a region where $k_\eta < k_r$. It should be noted, however, that equations (3) and (4) are valid only for $k_\eta << k_r$ and the changeover from negative to positive P/C correlation may occur not at $k_\eta = k_r$ but at $Ak_\eta = k_r$ where A is a factor somewhat larger than 1. Another possible source for the discrepancy is that the kinematic viscosity given by the U.S. Standard Atmosphere is somewhat overestimated and thus has reduced the estimate of k_η in the lower mesosphere.

Additional support for this theory comes from HF partial-reflection data from the 2.6-MHz Urbana radar. Correlation between scattered power and signal correlation time is positive throughout the D region as can be seen in Figure 2. This is as expected of turbulent scattering since the Bragg wavelength for this radar (~56 m) is within the inertial subrange at least up to 90 km. The situation has been summarized in Figure 3 which shows the spectra of irregularities for two different energy dissipation rates.

So although there is a small discrepancy between observations and the calculations in this paper we feel justified in concluding that the turbulent model as described here correctly predicts positive and negative P/C correlation in the lower and upper mesosphere, respectively.

The model of turbulent scattering of radio waves suggested here is very similar to a model suggested by BOLGIANO (1968) in which very strong turbulence results in a layer of nearly uniformly mixed refractive index bordered by two sharp ledges. Very little is known about the shape of these ledges; however,

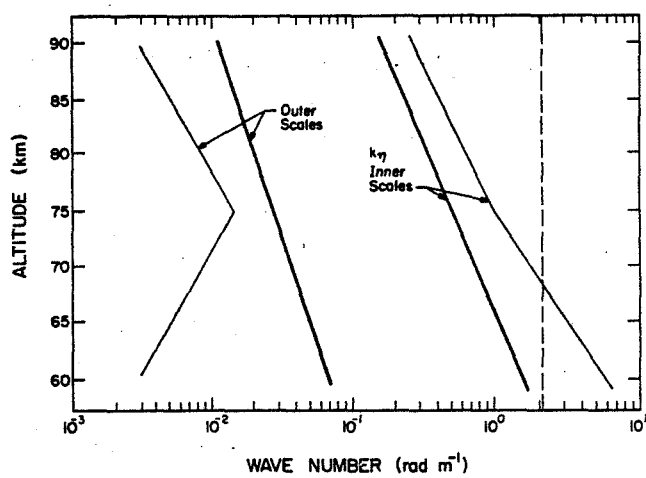

Figure 1. Profiles of inner and outer scales of turbulence in the mesosphere for two extremes of energy dissipation rates. The maximum and minimum energy dissipation rates were calculated from the maximum variation in signal correlation time at each altitude.

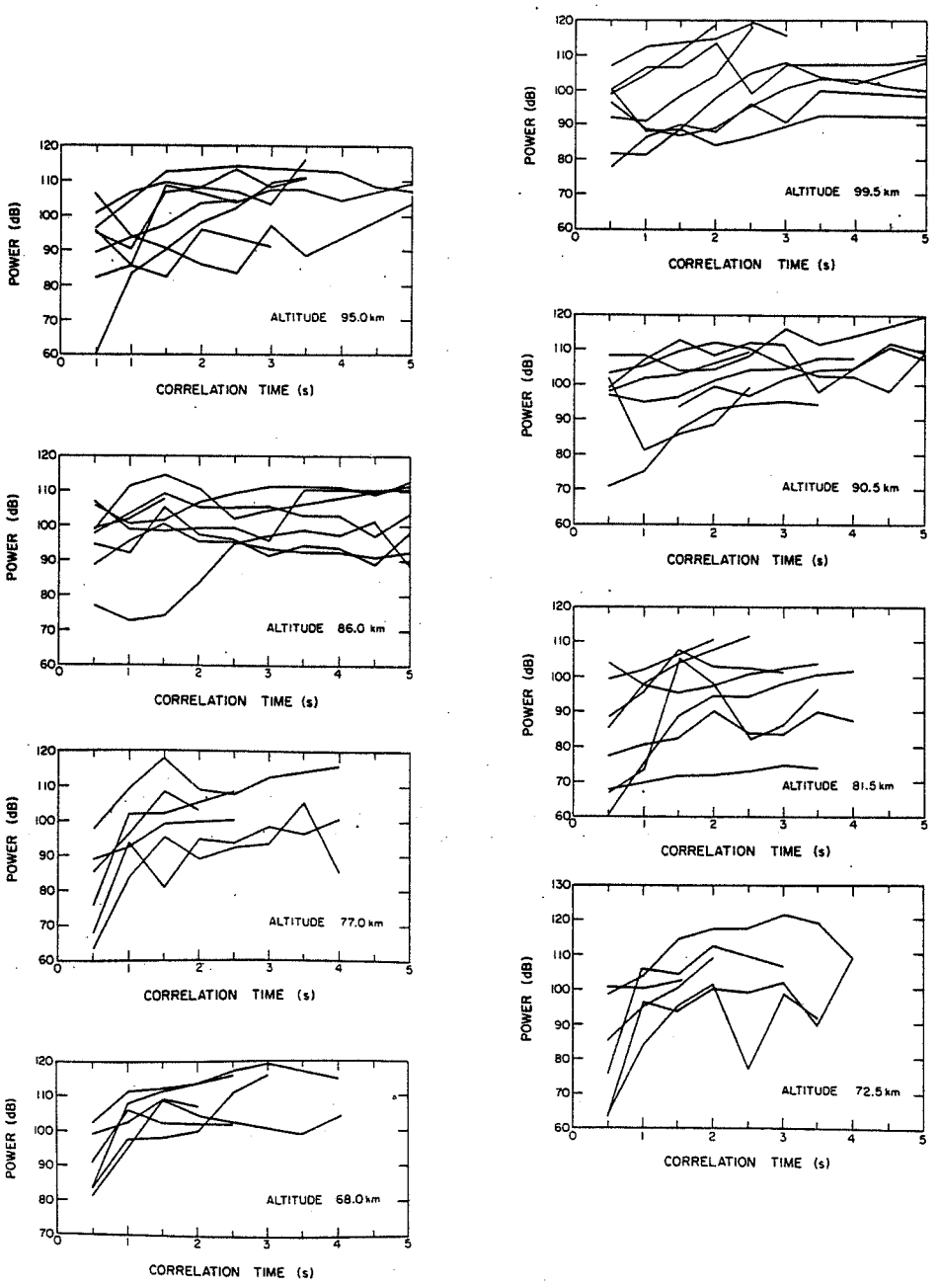

Figure 2. Correlogram of echo power versus signal correlation time for the Urbana 2.6-MHz partial-reflection radar for data obtained on 24-26 April 1982. Each curve represents from four to seven hours of data.

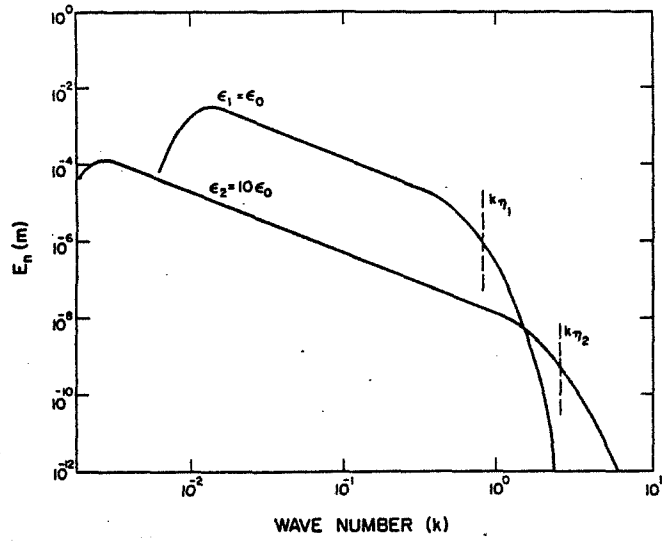

Figure 3. Schematic representation of refractive index irregularity spectra for two different energy dissipation rates.

it seems reasonable to assume that at Bragg wavelengths equal to, or smaller than, the inner scale of turbulence no additional radar echo will be received (ROTTGER et al., 1979). On the other hand if the Bragg wavelength is a substantial fraction of the outer scale of turbulence these ledges may cause partial reflection that come in addition to the scattering from the turbulent layer itself. This may be the reason for observations made at MF/HF frequencies by HOCKING and VINCENT (1982) and others.

REFERENCES

Bolgiano, R., Jr. (1968), Winds and Turbulence in the Stratosphere, Mesosphere and Ionosphere, (Edited by K. Rawer), pp. 371-400, North-Holland, Amsterdam.

Countryman, I. D. and S. A. Bowhill (1979), Wind and wave observations in the mesosphere using coherent-scatter radar, Aeron. Rep. No. 89, Aeron. Lab., Dep. Elec. Eng., Univ. of Illinois, Urbana.

Fukao, S., T. Sato, R. M. Harper and S. Kato (1980), Radio wave scattering from the tropical mesosphere observed with the Jicamarca radar. Radio Sci., 15, 447-457.

Hardy, K. R. (1972), Studies of the Clear Atmosphere Using High Power Radars, Remote Sensing of the Troposphere, Chap. 14 edited by V. E. Derr. NOAA. U. S. Department of Commerce, Washington, D.C.

Harper, R. M. and R. F. Woodman (1977), Preliminary multiheight radar observations of waves and winds in the mesosphere over Jicamarca, J. Atmos. Terr. Phys., 39, 959-963

Hocking, W. K. and R. A. Vincent (1982), Comparative observation of D region HF partial reflection at 2 and 6 MHz, J. Geophys. Res., 87, 7615-7624.

Liu, C. H. and K. C. Yeh (1980), Scattering of VHF and UHF radar signals from the turbulent air, Radio Sci., 15, 277-282.

Ottersten, H. (1969), Radar backscattering from the Turbulent clear atmosphere. Radio Sci., 4, 1251-1255.

Rastogi, P. K. and S. A. Bowhill (1976a), Scattering of radio waves from the

mesosphere 1. Theory and observations, J. Atmos. Terr. Phys., 38, 399-411.

Rastogi, P. K. and S. A. Bowhill (1976b), Scattering of radio waves from the mesosphere, 2. Evidence for intermittent mesosphere turbulence. J. Atmos. Terr. Phys., 38, 449-462.

Rottger, J. (1980), Reflection and scattering of VHF radar signals from atmospheric refractivity structures, Radio Sci., 15, 259-276.

Rottger, J. and C. H. Liu (1978), Partial reflection and scattering of VHF radar signals from the clear atmosphere, Geophys. Res. Lett., 5, 359-360.

Rottger, J., P. K. Rastogi and R. F. Woodman (1979), High-resolution VHF radar observations of turbulence structures in the mesosphere, Geophys. Res. Lett., 6, 617-620.

Royrvik, O., (1983), VHF radar signals scattered from the equatorial mesosphere, Radio Sci., 18, 1325-1335.

Royrvik, O., and L. G. Smith (1984), Comparison of mesospheric VHF radar echoes and rocket probe electron-concentration measurements, J. Geophys. Res., submitted.

Tatarskii, V. I. (1971), The effects of the turbulent atmosphere on wave propagation, U.S. Dep't. of Commerce, National and Technical Information Services, Springfield, VA.

Tennekes, H. and J. L. Lumley (1972), A First Course in Turbulence, MIT Press, Cambridge and London.

Woodman, R. F. and A. Guillen (1974), Radar observations of winds and turbulence in the stratosphere and mesosphere, J. Atmos. Sci., 31, 493-503.

2.6A RADAR ECHOES AT 2.66 AND 40.92 MHz FROM THE MESOSPHERE

O. Royrvik

Aeronomy Laboratory
Department of Electrical and Computer Engineering
University of Illinois
Urbana. IL 61801

INTRODUCTION

Radars operating in the frequency range from 1 to 60 MHz have been used extensively during the last decades to study the ionospheric D region. Some progress has been made in understanding the mechanism that cause the reflection/scattering of the transmitted radio waves although some problems remain to be solved. THRANE et al. (1981) compared rocket measurements of ion density irregularities to radar echo observations at 2.75 MHz and concluded that the received radar signal was due to scattering from isotropic and homogenous turbulence in the altitude region between 70 and 95 km. HOCKING and VINCENT (1982) on the other hand, compared scattering cross section at two frequencies, 2 and 6 MHz. and suggested that the radar echo from the region below 80 km was in part due to partial reflection from stratified layers.

It is well known that the VHF scattering cross section is aspect sensitive in the D region below about 75 km. whereas it tends to be isotropic at higher altitudes (COUNTRYMAN and BOWHILL, 1979; FUKAO et al. 1980; ROYRVIK 1983). FUKAO et al. suggested this to be the result of a mixture of scattering and reflection at the lower altitudes, and pure isotropic scattering at higher altitudes. However. ROYRVIK (1983) studying Doppler spectra of the mesospheric echoes. suggested that the aspect sensitive part of the signal is due to scattering from anisotropic turbulence. ROTTGER et al (1979) rejected partial reflection of VHF radio waves from ledges in the refractive index bordering a turbulent region (BOLGIANO. 1968) because the inner scale of turbulence in the mesosphere is larger than the radar Bragg wavelength.

Positive correlations between scattered signal power and signal correlation time (P/C-correlation) have been observed by VHF radars in the lower mesosphere by FUKAO et al. (1980) who concluded that it might be an additional indication of partial reflection from stratified layers (ROTTGER and LIU. 1978). In the upper mesosphere where the P/C correlation for the VHF signals is negative, it is believed that the scattering is caused by isotropic turbulence. Recently, however, ROYRVIK (1984) has argued that steady-state shear-induced turbulence should result in a positive P/C-correlation if the Bragg wavelength is within the dissipative subrange of turbulence.

The Aeronomy Laboratory Field Station at the University of Illinois contains a 41-MHz MST radar (MILLER et al. 1978) and a 2.66-MHz partial-reflection antenna radar (RUGGERIO and BOWHILL, 1982). Initially these two radars used the same computer for data acquisition, and thus simultaneous runs were not possible. Recently. however. a set of microcomputers have been adapted for separate data collection from the two radars (RUGGERIO and BOWHILL, 1982). Several simultaneous runs have been made in order to compare both measured horizontal velocities and variations in scattered power measured by the two radar systems. The results of the wind measurements have been reported by RUGGERIO and BOWHILL (1982). Here we will report some preliminary results from comparison of the radar scattering cross section at the two radar frequencies.

EXPERIMENTAL TECHNIQUE AND CALIBRATION

The Urbana MST radar operates at a frequency of 40.92 MHz in a pulsed, monostatic mode. Peak transmitted power is 1.4 MW in 20 μs pulses. Pulse repetition frequency is 400 Hz. The transmitting/receiving antenna consist of a rectangular array of 1008 half-wave dipoles with a physical aperture of 11000 m^2. The receiving system consists of a transmit/receive switch, a blanker/preamplifier and a receiver with IF frequency of 5.5 MHz. Autocorrelation functions with twelve 1/8 s lags of the complex received signal are calculated on line and stored every minute in 20 altitude bins spaced 1.5 km apart.

The partial-reflection radar operates on a frequency of 2.66 MHz with a peak transmitted power of 3.5 kW. Pulse length is 25 μs and pulse repetition frequency is 200 Hz. Separate transmitting and receiving antennas are used. The transmitting antenna consists of a 60 half-wave dipole array. The receiving antenna consists of an almost identical array which is divided into four sections. The signal strength from each section is separately detected for use in a spaced antenna experiment. Scattered signal power for each antenna, and horizontal wind velocities are estimated and recorded every minute in eight altitude ranges spaced 4.5 km apart, i.e., a slight undersampling in altitude (RUGGERIO and BOWHILL, 1982).

Both radars were calibrated so that absolute scattering cross section could be estimated from the echo strength. The nature of this calibration is different for the two radars and will be outlined in the following sections. The 41-MHz scattering cross section is calculated from the radar equation in the form given by VANZANDT et al. (1978)

$$\eta = \frac{9\pi}{2} \frac{ck\,B\,(T_c + T_{rx}/\alpha)}{\alpha\,P_t\,F_r\,A_e} \left(\frac{r}{\Delta r}\right)^2 \left(\frac{S}{N}\right) \qquad (1)$$

Here the signal-to-noise ratio S/N is measured directly from the autocorrelation function, r is the range of the scattering volume, and c is the velocity of light. The remaining constants are defined, and values given in Table 1. The noise temperature (T_{rx}) of the receiving system was measured by a noise diode to approximately 90 K°. This is reasonable considering that the manufacturer of the preamplifier quotes a 1-dB noise figure and a 20-dB gain. Measurement of the antenna efficiency factor (α) gave a value of 0.35. This value is considerably better than that measured by ALLMAN and BOWHILL (1976) and approximately equal to the value predicted with a preamplifier inserted immediately following the transmit/receive switch. Considering the uncertainties involved in equation (1) it is estimated that the scattering cross section can be measured to within a factor of two.

At 2.66 MHz the sky noise temperature (T_c) is highly variable and cannot be used as a convenient reference to compare the scattered power. Thus the partial-reflection radar was calibrated against nighttime F-layer reflection using the equation

$$P_r = \frac{\alpha^2 P_t A_e^2}{4\lambda^2 r^2} |\rho|^2 = X \frac{|\rho|^2}{r^2} \qquad (2)$$

Here X is a constant including all radar parameters. X can be found by measuring P_r at night and assuming that the nighttime F-layer reflection is total, i.e., $|\rho|^2 = 1$. Initial calibration of the partial-reflection radar was out during a 2-hour run around midnight between May 3 and 4, 1984. From this experiment we calculated $X = 1.27 \times 10^{27}$. The scattering cross section per unit volume can then be calculated from the equation

Table 1

λ	wavelength	1.3 m
m	samples coherently integrated	24
P_t	peak pulse power	1.4 MW
α	efficiency of radar antenna	0.35
A	effective antenna area	1.1×10^4 m^2
Δr	range resolution	2×10^3 m
f	radar frequency	41 MHz
F_r	pulse repetition frequency	400 Hz
B	bandwidth of integration filter	8 Hz
T_c	cosmic noise temperature	10^4 °K
T_{rx}	receiver noise temperature	90 °K

$$\eta = \frac{|\rho|^2}{\Delta r} = P_r \frac{r^2}{X \Delta r} \tag{3}$$

Use of equation (3) as opposed to (2) assumes volume scattering, an assumption that may be debated. However, VINCENT and BELROSE (1977) from a study of 2.66-MHz radar signals found that the majority of echoes were due to incoherent scattering from a number of irregularities.

Calibration of the 2.66-MHz radar is inherently more difficult than calibrating the 41-MHz radar. Consequently, the uncertainties in the measurements of the scattering cross section are larger at 2.66 MHz; perhaps as large as a factor of five.

OBSERVATIONS

Several days of simultaneous observations by the two radars were made in late April and early May 1984. Some problems with the partial-reflection data recording system were encountered, however, a total of approximately 24 hours of data were recorded. Both radars were obtaining scattered power profiles between approximately 60 and 90 km altitude. Observations of the real time display showed that there usually were one or two scattering layers in both radars. The altitude of the layers in the two radars seemed to agree most of the time, but there also were occasions when the scattered power profiles looked quite different. Most importantly, perhaps, was the fact that the short period (~1 min) time variations in the amount of scattered power did not appear to be related in the two radars even in layers that were clearly occupying the same altitude region. This made data comparison quite difficult. However, as a preliminary comparison, data were chosen from times when the temporal variations were small.

Examples of scattered power as observed by the two radars are given in Figures 1 and 2. Four different sets of data have been compared on the assumption that the echoes are due to turbulent scatter. The comparison

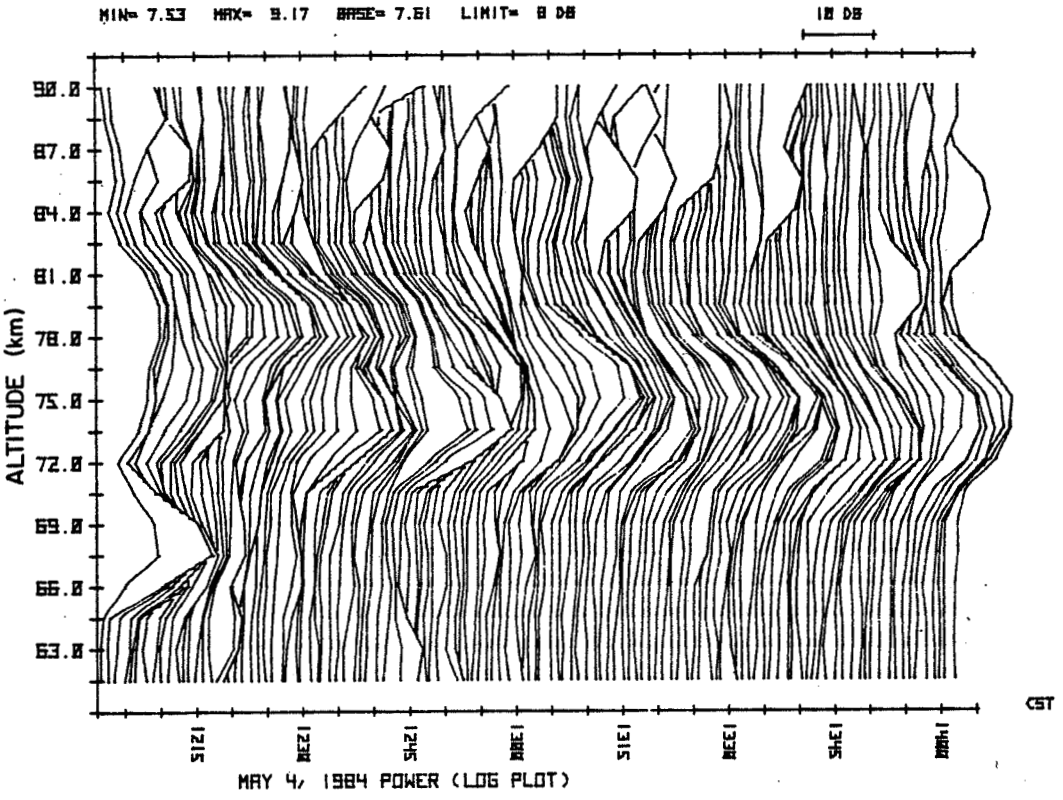

Figure 1. Scattered power profiles from the 41-MHz radar, May 4, 1984.

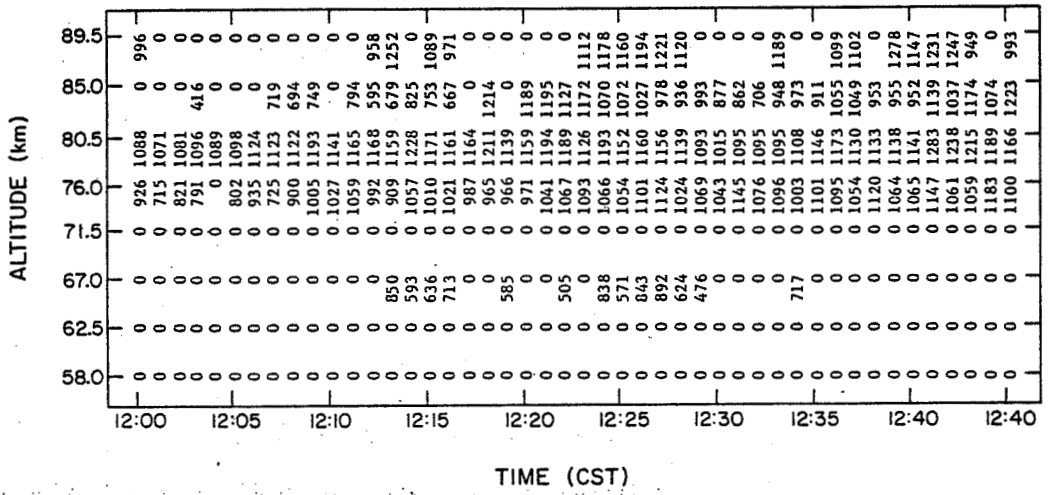

Figure 2. Map of scattered power from the 2.67-MHz radar in dB x 10), May 4, 1984. Zeros indicate time and altitudes where correlation time is less than one time lag in the correlation function. This represents noise level.

involves several steps as explained in the following sections.

For each data set the scattering cross section observed at 2.66 MHz is taken as a reference. Then the corresponding scattering cross section for the 41-MHz radar was calculated from the equation

$$\eta = 6.18 \times 10^2 \left(\frac{P}{kT}\right)^2 C_R^2 \, C^{-4} \, \lambda^{11/3} \qquad (4)$$

obtained from GAGE and BALSLEY (1980). However, this equation assumes that the radar Bragg wavelength is within the inertial subrange of turbulence. RASTOGI and BOWHILL (1976) have indicated that the Bragg wavelength of a VHF radar is in the dissipative subrange of turbulence in the mesosphere. ROYRVIK and SMITH (1984) showed spectra of turbulent irregularities that confirmed this and indicated that the spectral slope in the dissipative subrange is close to -7.

We now assume that the discrepancy between the observed cross section for 41 MHz and the cross section calculated using equation (4) is due to the rapid falloff of the irregularity spectra in the dissipative subrange. The amount of discrepancy observed should be a function of the inner scale of turbulence. The inner scale of turbulence needed to explain the discrepancy in each case is found at the intersection between the lines with slopes -5/3 and -7 in Figure 3. These values, plus additional values, of the inner scale as a function of altitude have been plotted in Figure 4 along with an estimate of the limiting values of the inner scale. As can be seen, these estimated values are reasonable indicating that the radar echoes at both 2.66 and 41 MHz are due to scattering from the same layer of turbulence-generated irregularities. Note in particular that the scattering cross section of the 41-MHz radar is never significantly above the value predicted from the 2.66-MHz cross section if turbulent scatter is assumed.

A continuation of this work will include calculation of signal correlation

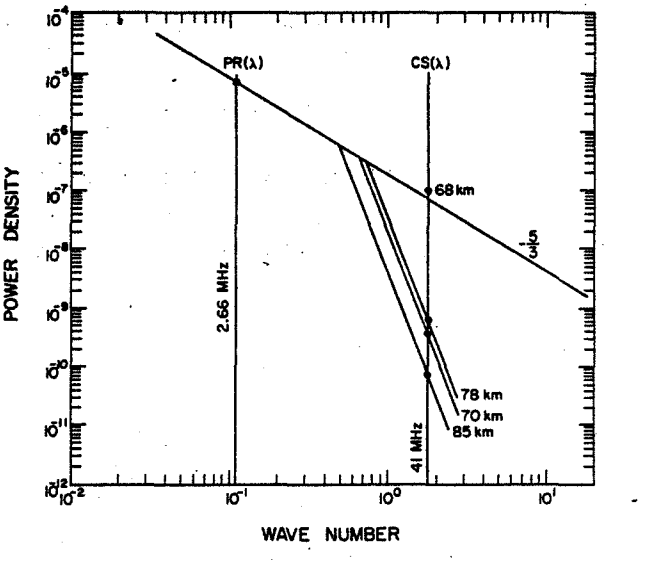

Figure 3. Spectra of scattering irregularities with the 2.67-MHz radar cross section as reference. The figure only gives information of the relative cross section between the radars.

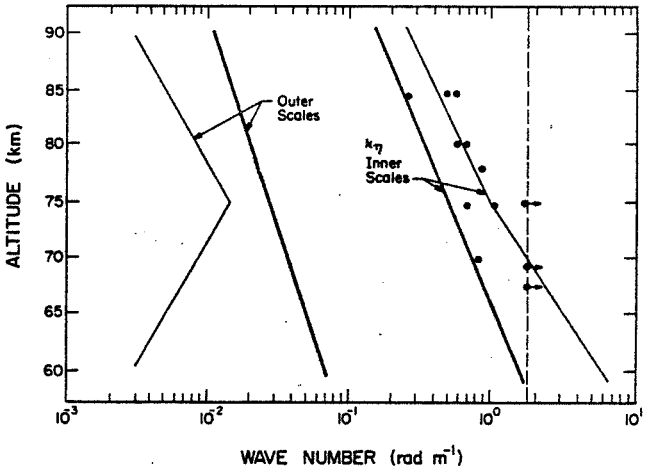

Figure 4. Limits of inner and outer scales of turbulence calculated from signal correlation times at the Jicamarca 50-MHz radar. The solid dots indicate deduced inner scales of turbulence. The dots with arrows indicate that the inner scales are equal to or smaller than the 41-MHz Bragg wavelength.

time. and estimates of energy dissipation rate as a function of altitude. This will allow independent estimates of the inner scale of turbulence that can be compared to the values shown in Figure 4. A particularly interesting study would be the comparison of the time variations of the scattering cross sections in the two radars at altitudes where the 41-MHz radar operates within the dissipative subrange of the turbulent spectrum (ROYRVIK, 1984).

REFERENCES

Allman. M. E. and S. A. Bowhill (1976), Feed system design for the Urbana incoherent-scatter radar antenna, Aeron. Rep. No. 71, Aeron. Lab., Dept. Elec. Eng., Univ. Ill., Urbana-Champaign.

Bolgiano, Jr., R. (1968), The General Theory of Turbulence. Turbulence in the Atmosphere Winds and Turbulence in Stratosphere, Mesosphere and Ionosphere, (edit. by K. Rawer), North-Holland, Amsterdam.

Countryman. I. D. and S. A. Bowhill (1979), Wind and wave observations in the mesosphere using coherent-scatter radar. Aeron. Rep. No. 89, Aeron. Lab., Dept. Elec. Eng., Univ. of Ill., Urbana-Champaign.

Fukao, S., T. Sato, R. M. Harper and S. Kato (1980), Radio wave scattering from the tropical mesosphere observed with the Jicamarca radar, Radio Sci., 15, 447-457.

Gage. K. S. and B. B. Balsley (1980), On the scattering and reflection mechanisms contributing to clear air radar echoes from the troposphere, stratosphere, and mesosphere, Radio Sci., 15, 243-257.

Hocking, W. K. and R. A. Vincent (1982), Comparative observations of D region partial reflections at 2 and 6 MHz, J. Geophys. Res., 87, 7615-7624.

Miller, K. L., S. A. Bowhill, K. P. Gibbs, and I. D. Countryman (1978), First measurements of mesospheric vertical velocities by VHF radar at temperate latitudes. Geophys. Res. Lett., 5, 939-942.

Rastogi, P. K. and S. A. Bowhill (1976), Scattering of radio waves from the mesosphere, 1, Theory and observations, J. Atmos. Terr. Phys., 38, 399-411.

Rottger. J., and C. H. Liu (1978), Partial reflection and scattering of VHF radar signals from the clear atmosphere, Geophys. Res. Let., 5, 357-360.

Rottger, J., P. K. Rastogi and R. F. Woodman (1979), High-resolution VHF radar-observations of turbulence structures in the mesosphere. Geophys. Res. Lett., 6, 617-620.

Royrvik, O., (1983), VHF radio signals scattered from the equatorial mesosphere. Radio Sci., 18, 1325-1335.

Royrvik, O. (1984), Interpretation of radar returns from the mesosphere. Paper 2.5, this volume.

Royrvik, O. and L. G. Smith (1984), Comparison of Mesospheric VHF radar echoes and rocket-probe electron concentration measurements. J. Geophys. Res. in press.

Ruggerio. R. L. and S. A. Bowhill (1982), New advances in the partial-reflection-drifts experiment using microprocessors. Aeron. Rep. No. 106, Aeron. Lab., Dept. Elec. Eng., Univ. of Ill., Urbana-Champaign.

Thrane. E. V., B. Grandal. T. Fla and A. Brekke (1981), Fine structure in the ionospheric D-region, Nature, 292, 221-223.

VanZandt. T. E., J. L. Green, K. S. Gage and W. L. Clark (1978), Vertical profiles of refractive turbulence structure constant: Comparison of observations by the Sunset Radar with a new theoretical model. Radio Sci., 13, 819-829.

Vincent. R. A. and J. S. Belrose (1977), The angular distribution of radio waves partially reflected from the lower ionosphere. J. Atmos. Terr. Phys., 40, 35-47.

2.6B USEFULNESS OF MULTIFREQUENCY MST RADAR MEASUREMENTS

P. K. Rastogi and J. D. Mathews

Department of Electrical Engineering and Applied Physics
Case Western Reserve University
Cleveland, OH 44106

INTRODUCTION

Scattering of radio waves from atmospheric refractive-index irregularities induced by turbulence was invoked almost four decades ago to explain the characteristics of signals received on VHF/UHF ionospheric and tropospheric forward-scatter links (WIESNER, 1960). Due to the bistatic geometry of these links a slender, horizontally extended, common volume or cell is formed in space. The principal contribution to scattering arises from refractive-index fluctuations in this volume at the Bragg wave number $\underset{\sim}{k}_B = \underset{\sim}{k}_i - \underset{\sim}{k}_s$ corresponding to the difference of the incident and scattered wave propagation vectors. The length scale corresponding to the Bragg wave number is $2\pi/k_B = \lambda/(2 \sin\theta/2)$, where θ is the angle between $\underset{\sim}{k}_i$ and $\underset{\sim}{k}_s$. For backscatter, $\theta = 180°$ and the Bragg wave number corresponds to the length scale $1/2\lambda$ for a radio wavelength λ (BOOKER and GORDON, 1950; BOOKER, 1956).

Since the early days of scatter-propagation research, it has been realized that multifrequency measurements offer the possibility of monitoring the spectrum of refractive-index fluctuations at several distinct Bragg wave numbers (WIESNER, 1960; BLAIR et al., 1961; BOLGIANO, 1963). A quantitative interpretation of such measurements has led to a critical reexamination of the role of turbulence in producing these fluctuations (BOLGIANO, 1958; BOLGIANO, 1960; WHEELON, 1959,1960; HILL and BOWHILL, 1976).

In recent years, multiple-frequency MST radar capabilities have become available at several sites around the world at frequencies ranging from HF, through VHF to UHF. It has been surmised that the use of more than one frequency in probing the middle-atmosphere regions should help resolve several issues pertaining to the scattering mechanism (LIU, 1983). These issues are briefly re-examined in this note. The implications of the radar equation are discussed in the next section. The two following sections consider the problems arising due to layered structure of turbulence and the choice of frequencies most suitable for multifrequency measurements, respectively.

IMPLICATIONS OF THE RADAR EQUATION FOR MULTIFREQUENCY MEASUREMENTS

The radar equation for a uniform random medium with refractive-index fluctuations n relates the received signal power (P_s) to the transmitted power (P_t), the antenna parameters (e.g., its physical aperture A), range (R), range resolution (ΔR), and a radar reflectivity (η) for the medium. For narrow-beam monostatic radars, the radar equation can be written in several different forms. A simple form following ROTTGER (1980) is

$$P_s = \frac{P_t L A \Delta R \eta}{4\pi R^2} \qquad (1)$$

where the factor L accounts for the system losses. The reflectivity η for a homogeneous, isotropic field of fluctuations is obtained as

$$\eta = 1/2\pi^2 \, k_B^4 \, \Phi_n (k_B) \tag{2}$$

where $\Phi_n (k_B)$ is the three-dimensional spectrum of refractive-index fluctuations, evaluated over a spherical shell of radius k_B in phase space. For small-scale fluctuations in the inertial range or beyond, $\Phi_n (k)$ is related to the refractive index structure constant C_n^2

$$\eta = 0.033 \, C_n^2 \, k^{-11/3} \exp[-k^2/k_m^2] \tag{3}$$

with $k_m = 5.91/\ell_o$, and ℓ_o the inner scale of turbulence. These results have been discussed by ISHIMARU (1978) and TATARSKII (1971).

Several conditions are essential for obtaining equations (1) and (2). It is assumed that the radar cell lies in the far field of the antenna. Refractive index (and other) fluctuations in the medium must be homogeneous and isotropic, and the medium is assumed to entirely fill the beam and the radar cell. Single scattering and quasi-static approximations must also hold. The numerical coefficient in equation (1) depends on the antenna radiation pattern, and ΔR is a rectangular approximation to the convolution of the pulse shape with receiver-system impulse response.

A strong motivation for multifrequency experiments is the possibility of measuring the form of the spectrum $\Phi_n(k)$ at several Bragg wave numbers through signal power measurements. It should be emphasized that such measurements require absolute radar calibration for each frequency. The current approaches and problems in such calibrations were briefly discussed at the previous workshop (BOWHILL, 1983).

CONSEQUENCES OF LAYERED TURBULENCE STRUCTURES

The assumptions of homogeneity and isotropy of refractive-index fluctuations, and that they fill the radar beam and the radar cell, are most readily violated in the presence of turbulent layers. These layers have indeed been observed throughout the middle atmosphere (WOODMAN and RASTOGI, 1984; ROTTGER et al., 1979).

The first consequence of layered turbulence is that there is a range of wave numbers in the vicinity of k_B that contribute to scattering. This range Δk_B depends inversely on the layer thickness L_T (RASTOGI and BOWHILL, 1976)

$$\Delta k_B \sim \frac{2\pi}{L_T} \tag{4}$$

This produces a smearing of the underlying spectrum in the vicinity of k_B. The extent of this smearing depends on the distribution of refractive-index variance in the layer, and can be quite serious for a normal layer thickness of 100 m (Figure 1).

The second consequence of layered turbulence is due to quasi-specular or diffused reflections that are produced from the edges of these layers. HOCKING and ROTTGER (1983) have considered modifications to the radar equation due to this effect.

To minimize the effect of layered turbulence in multifrequency experiments it is important to keep the common volume fixed. This requires that the antennas be scaled with frequency to give the same beam widths, and in addition, the pulse shape, receiver system impulse response and range delays be kept identical for all frequencies.

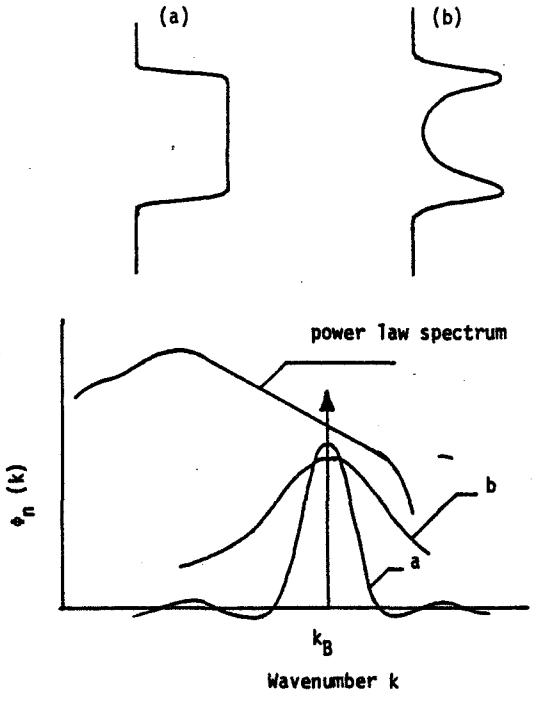

Figure 1. Two possible distributions (a) and (b) of refractive-index variance across a thin layer. The arrow shows the ideal Bragg filter at wave number k_B for an infinite scattering volume. The shapes labelled (a) and (b) show the Bragg filters corresponding to the distributions above. The power law spectrum is only a plausible form for $\Phi_n(k)$.

CHOICE OF FREQUENCIES

The range of frequencies currently available for MST radars is ~3 MHz to well above 1 GHz. Only the HF and lower VHF radars are sensitive to turbulent fluctuations in the mesosphere. Sensitive UHF radars can be used to probe the D-region ionization (MATHEWS, 1984). The widest choice of frequencies is available at EISCAT and Arecibo.

Figure 2 shows schematically the Bragg length scales associated with several radars. Also shown in this figure are the energy spectra associated with strong and weak turbulence in the troposphere and mesosphere. The form of these spectra are qualitative and no distinction is made between energy spectra and the spectra of refractive-index fluctuations.

In the mesosphere, the Bragg length scale for VHF radars is comparable to the inner scale of turbulence. For this reason two VHF radars with a frequency spacing of a few MHz can provide useful information about the spectra associated with small-scale turbulence. The use of a UHF radar in addition can provide information about D region electron-densities and their gradients that is vital for interpreting the behavior of VHF returns.

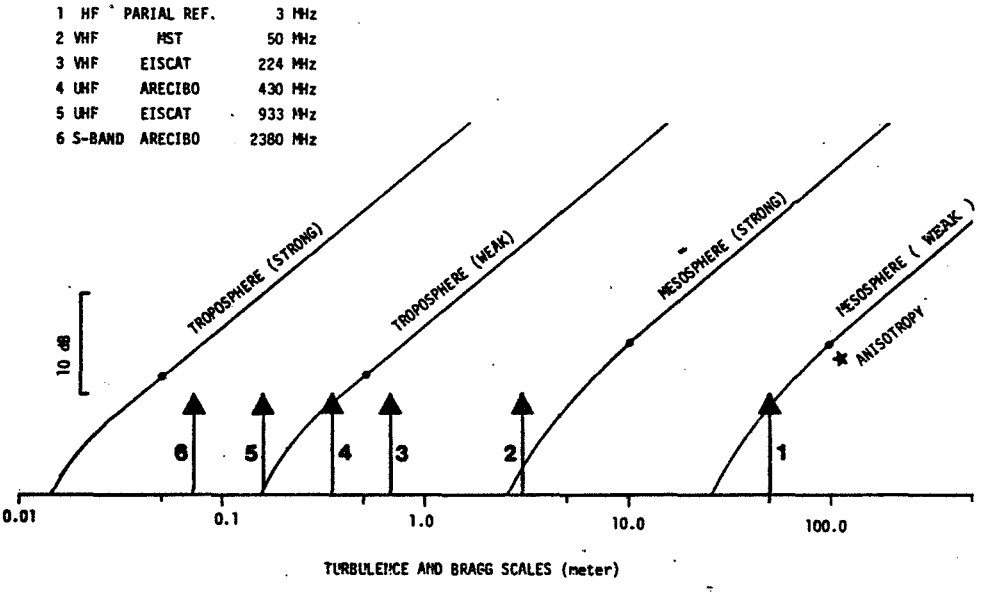

Figure 2. Bragg length scales ($\lambda/2$) for six backscatter radars are shown by the arrows. Tropospheric and mesospheric spectra for strong and weak (by 10,000 times) turbulence have been superimposed. The form of these spectra are qualitative and no distinction is made between energy spectra and spectra of refractivity fluctuations. Dots show a length scale that is 5 x the wavelength associated with the turbulence inner scale. At smaller length scales, the inertial-range form is invalid. At Bragg scales $\gtrsim$50 m, anisotropy effects become significant.

HF radars usually lack a fine altitude resolution (typically 3 km or worse). The X- and O-mode returns suffer, however, different attenuations and their corresponding propagation vectors k_x and k_o become significantly different in the upper D region. For this reason, a range-time cross-correlation analysis of several closely spaced HF frequencies will complement the conventional partial-reflection experiments (RASTOGI and HOLT, 1981).

In the vicinity of the tropopause, the turbulence inner scale is just a few centimeters. Two widely separated frequencies (e.g., 224 MHz and 933.5 MHz for the EISCAT radars) offer the possibility of detecting large variations in the intensity of turbulence through their effect on the inner scale.

In some cases, especially with VHF radars, it may be possible, even advantageous, to use two rather closely spaced frequencies. This would allow the use of the same radar at two frequencies with only a slight degradation in performance.

A careful reexamination of the frequency dependence of the turbulence and refractive-index spectra, and of scattering from thin turbulent layers is essential for interpretation of multifrequency measurements.

REFERENCES

Blair. J. C., R. M. Davis and R. C. Kirby (1961), Frequency dependence of D-region scattering at VHF, J. Res. NBS, 65D, 417-425.

Bolgiano, R. (1958), The role of turbulent mixing in scatter propagation. IRE Trans., AP-6, 161-168.

Bolgiano, R. (1960), A theory of wavelength dependence in ultrahigh frequency transhorizon propagation based on meteorological considerations. J. Res. NBS, 64D, 231-237.

Bolgiano, R. (1963), The role of radio wave scattering in the study of atmospheric microstructure. Electromagnetic Scattering, ed. M. Kerker. MacMillan Co., 261-267.

Booker, H. G. (1956), A theory of scattering by nonisotropic irregularities with application to radar reflections from the aurora. J. Atmos. Terr. Phys., 8, 204-221.

Booker, H. G. and W. E. Gordon (1950), A theory of radio scattering in the tropospherre. Proc. IRE, 38, 410-412.

Bowhill, S. A. (1983), Design considerations for MST radar antennas. Handbook for MAP, Vol. 9, S. A. Bowhill and B. Edwards (eds.), 447-455.

Hill, R. J. and S. A. Bowhill (1976), Small-scale fluctuations in D-region ionization due to hydrodynamic turbulence. Aeron. Rep. No. 75, Aeron. Lab., Dept. Elec. Eng., Univ. Ill., Urbana-Champaign.

Hocking, W. K. and J. Rottger (1983), Pulse length dependence of radar signal strengths for Fresnel backscatter. Radio Sci., 18, 1312-1324.

Ishimaru, A. (1978), Wave Propagation and Scattering in Random Media, Academic Press, New York, 572.

Liu, C. H. (1983), Interpretation of MST radar returns from clear air. Handbook for MAP, vol. 9, S. A. Bowhill and B. Edwards (eds.), 49-56.

Mathews, J. D. (1984), The incoherent scatter radar as a tool for studying the ionospheric D-region, submitted to J. Atmos. Terr. Phys.

Rastogi, P. K. and S. A. Bowhill (1976), Scattering of radio waves from the mesosphere - 2. Evidence for intermittent mesospheric turbulence. J. Atmos. Terr. Phys., 38, 449-462.

Rastogi, P. K. and O. Holt (1981), On detecting reflections in presence of scattering from amplitude statistics with applications to D-region partial reflections, Radio Sci., 16, 1431-1443.

Rottger, J. (1980), Reflection and scattering of VHF radar signals from atmospheric refractivity structures, Radio Sci., 15, 259-276.

Rottger, J., P. K. Rastogi and R. F. Woodman (1979), High resolution VHF radar observations of turbulence structures in the mesosphere. Geophys. Res. Lett., 6, 617-620.

Tatarskii, V. I. (1971), The effects of turbulent atmosphere on wave propagation, Nat. Tech. Inf. Serv., 472 (translated from the Russian).

Wheelon, A. D. (1959), Radio wave scattering by tropospheric irregularities, J. Res. NBS, 63D, 205-233.

Wheelon, A. D. (1960), Relation of turbulence theory to ionospheric forward scatter propagation experiments. J. Res. NBS, 64D, 301-309.

Wiesner, J. B. (1960), Radio transmission by ionospheric & tropospheric scatter - A report of the It. Tech. Adv. Com., Proc. IRE, 48, 4-29.

Woodman, R. F. and P. K. Rastogi (1984), Evaluation of effective eddy diffusive coefficients using radar observations of turbulence in the stratosphere. Geophys. Res. Lett., 11, 243-246.

3. RELATIONSHIP OF SPACED ANTENNA AND DOPPLER TECHNIQUES FOR VELOCITY MEASUREMENTS
(Keynote Paper)

R. A. Vincent

Department of Physics
University of Adelaide
Adelaide, South Australia 5001

INTRODUCTION

The Doppler, spaced-antenna and interferometric methods of measuring wind velocities all use the same basic information -- the Doppler shifts imposed on backscattered radio waves -- but they process it in different ways. The Doppler technique is most commonly used at VHF since the narrow radar beams are readily available. However, the spaced antenna (SA) method has been successfully used with the SOUSY and Adelaide radars. At MF/HF the spaced antenna method is widely used since the large antenna arrays (diameter > 1 km) required to generate narrow beams are expensive to construct. Where such arrays of this size are available then the Doppler method has been successfully used (e.g. Adelaide and Brisbane). In principle, the factors which influence the choice of beam pointing angle, the optimum antenna spacing will be the same whether operation is at MF or VHF.

Many of the parameters which govern the efficient use of wind measuring systems have been discussed at previous MST workshops (e.g. ROTTGER, 1983; STRAUCH, 1983; HOCKING, 1983; FARLEY, 1983). In the following some of the points raised by these workers and others are summarized.

SPACED ANTENNA TECHNIQUES

The SA method uses 3 or more antennas to sample the moving diffraction pattern produced by backscatter from a given range from the atmosphere. The pattern can be decomposed into Fourier components which are formed by interference between signals scattered at complementary angles to the zenith (Figure 1). The differential Doppler shifts induced by the horizontal velocity u, cause the pattern to move with velocity 2u (BRIGGS, 1980).

Usually only 3 antennas are used, arranged in the form of an equilateral triangle since the symmetry is less likely to introduce a bias in determining the velocity. The auto- and cross-correlation functions of the signals are computed (Figure 2) in order to determine the pattern velocity. The three time delays of the maxima of the cross correlation functions between the three pairs of spaced antennas give the apparent velocity. This is an overestimate of the actual (true) velocity since random motions etc. will cause the pattern to change as it moves. The so-called full correction analysis (FCA) is used to correct for these changes as well as for the anisometry of the pattern. The FCA makes use of such information as the lag at which the autocorrelation function is the same as the instaneous correlation between 2 spaced antennas.

Obviously, if the antennas are too closely spaced then the errors become large and experimentally it is found that the corrected ('true') velocity is too small. On the other hand if the spacing is too large then random changes in the pattern can dominate over the translational effects (e.g. ROYRVIK, 1983) and the correlation values are so small that the analysis breaks down. On pragmatic and experimental grounds it is found that the optimum spacing is where the average zero lag correlation is about 0.5.

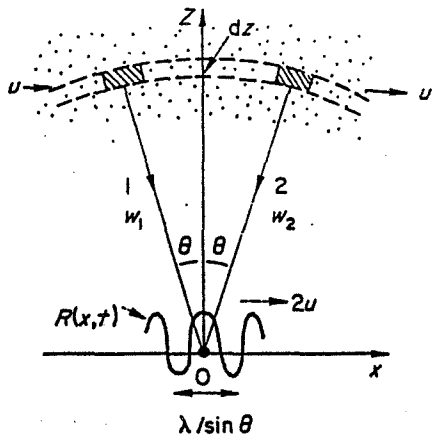

Figure 1. Two-dimensional radar situation with a uniform wind u in the x direction (after BRIGGS, 1980).

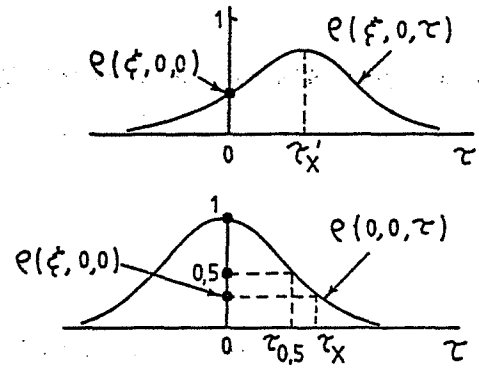

Figure 2. The cross- and autocorrelation functions of the signals from two antennas separated along the x direction by a distance ξ.

The mean pattern size and hence the distance at which the mean correlation is about 0.5 is determined by the angular distribution of the backscattered energy. In turn, this angular distribution is determined by the polar pattern of the transmitting and the receiving antennas as well as the angular distribution imposed by the nature of the scattering irregularities. It is possible to show (BRIGGS and VINCENT, 1973) that the complex spatial correlation function as a function of spacing α (in wavelengths) is

$$\rho(\alpha) = \int_0^\infty R(s)\, S(s)\, T(s)\, s^2\, J_0\,(2\pi\alpha s)ds$$

where R(s) and T(s) are the receiver and transmitter power polar diagrams, respectively, and S(s) is the angular distribution of backscattered power; all are evaluated as a function of $s = \sin\theta$ where θ is zenith angle and circular symmetry is assumed. J_0 is the zero order Bessel function.

At MF/HF, the antenna polar diagrams are usually broader than the irregularity angular distributions so that it is usually the latter (half power-half widths $\sim\theta_0 \sim$ 2-20°) which determine ρ(α). It may be expected that since θ_0 varies as a function of height and time that ρ(α) will also be variable but on average it is found that spacings of the order of 150-200 m (α ~ 1-1.5λ) are optimum for radio frequencies near 2 MHz.

At VHF the antenna polar diagrams are of the order of a few degrees in

width i.e. comparable in width to the angular spectra of the irregularities (θ_0 ~ 1-5°). The minimum spacing may be computed for a given R(s) and T(s) by assuming isotropic scatter (S(s) ~ 1). At Adelaide, with a transmitter beam having a half width of θ_T ~ 1.6° it is found that this minimum spacing is 5λ (about 30 m at a frequency of 50 MHz) but in practice it is found that a mean spacing of about 50 m (α ~ 9λ) is optimum for the troposphere. Incidentally, this implies a mean θ_0 ~ 2°.

Despite the narrowness of the angular spectra of backscatter from the lower mesosphere at MF and from the lower atmosphere at VHF, it is found experimentally that the SA method gives reliable measurements of the wind velocity. In each case it is found that the importance of random changes in producing temporal changes in the signals are small compared with those changes caused by movement of the pattern. This may not always be true in the mesosphere when working at VHF and with narrow beam antennas. In this case the random motions may become dominant leading to a breakdown in the SA analysis (ROYRVIK, 1983).

DOPPLER TECHNIQUES

It is, in principle, quite straightforward to measure the vertical wind component w by using a vertically pointing beam. The horizontal wind components must, however, be estimated by projecting the radial velocity v_r measured along a beam offset at an angle θ from the vertical, onto the horizontal plane. STRAUCH (1983) has summarized the factors which determine the optimum value of θ.

Among those factors which favor the use of a small angle θ are: (a) the desire to make use of the aspect sensitivity of the scatterers which gives enhanced power from near the zenith; (b) the effects of horizontal variations in the wind field are reduced; (c) the r^{-2} effect is minimized.

On the other hand if θ is large then: (d) errors in v_r translate into smaller errors in the horizontal velocity; (e) the effects of the vertical velocity is less pronounced and (f) the influence of the aspect sensitivity on effective beam direction is less important if θ is large.

Probably (f) is the key factor. As ROTTGER (1983) emphasizes, the effective beam pointing direction is determined by the product of the beam pattern and the angular distribution of the scatter. The effective beam zenith angle is smaller than the physical angle and the horizontal velocity component is underestimated. This can be a serious problem when using antennas with relatively broad beams (θ_H > 3°). For example, at Adelaide with a beam angle of θ_H > 4.5° it is found that the horizontal velocity can be up to a factor of 2 too small when the physical pointing angle is 12°. In principle, this factor can be allowed for if θ_0 is known (e.g. WHITEHEAD et al. 1983) but this probably entails measurements of the scattered power at more than one angle and of course θ_0 will change with height and time so that only a statistical analysis can be used. Overall, Strauch recommends an angle of θ = 15° for VHF studies of the lower atmosphere. At this angle the scatter from isotropic irregularities is presumed to overcome the anisotropic scatter.

RADAR INTERFEROMETRY

The radar interferometer exploits the Doppler information inherent in coherent spaced antenna measurements. Cross spectral analysis of the signals received at separated antennas can be used to locate and track irregularities while Doppler sorting can be used to discriminate against multiple targets -- provided they have different radial velocities (FARLEY et al., 1981). PFISTER (1971) seems to have been the first to use this method in a study of gravity

motions in the E-region. This method seems to have merit for studying spatial variations in the wind field.

In another variation of this method, ROTTGER and VINCENT (1978) digitally 'steered' the lobes of an interferometer formed from widely spaced antennas in order to study the fine structure and horizontal tilts of refractive index irregularities. This method has significant potential for correcting for the "vertical" velocities induced by these tilted irregularities.

DISCUSSION

The intrinsic errors in each velocity determination by either the Doppler or SA methods are determined by such factors as the signal-to-noise ratios and the record lengths. Expressions have been derived for the rms error of a line-of-sight Doppler velocity by, for example, DOVIAK et al. (1979). The precision of SA velocities has not been as rigorously determined but, provided the random changes are small the error is determined by the accuracy to which τ_x' (Figure 2) can be measured. The fractional error is independent of wind speed because the width is narrower for larger velocities (small lag) and becomes broader as the velocity becomes smaller (large lag). For either technique the velocity measurements can be improved by averaging the power spectra (Doppler) or the unnormalized cross correlation functions (SA). However, this process can only be carried out for durations which are short compared with the time for significant changes in the mean wind.

Another factor limiting the precision of horizontal wind determinations is the "noise" imposed by unresolved vertical velocities. Since the Doppler and SA methods utilize the same information, it may be expected that they will be affected in the same way by such factors as spatially and temporally varying vertical velocities. Significant short-period vertical velocities such as those encountered in the mesosphere where rms amplitudes ~1-2 ms^{-1} are possible can lead to difficulties in estimating the mean zonal wind. BOWHILL (1983) estimates that averaging times of an hour are required for Doppler measurements of $\bar{u}$ but that the effects can be minimized by using tilt angles of 10°. ROYRVIK (1983) has shown that the differential velocities caused by vertical velocities which vary in the horizontal will be interpreted as horizontal motions by the SA method. The importance of this effect is not yet clear since the SA method is not as easy to model as the Doppler technique.

In summary, the choice of operating parameters for a given radar will be determined by compromise between a number of opposing factors. What is optimum for one height range (e.g. the lower atmosphere) may not be the most suitable for another height (e.g. the mesosphere).

REFERENCES

Bowhill, S. A. (1983), Proceedings of Workshop on Technical Aspects of MST Radar, Handbook for MAP, Vol. 9, SCOSTEP Secretariat, Dep. Elec. Eng., Univ. IL, Urbana, 235.

Briggs, B. H. (1980), J. Atmos. Terr. Phys., 42, 823.

Briggs, B. H. and R. A. Vincent (1973), Aust. J. Phys.

Doviak, R. J., D. S. Zrnic and D. S. Sirmans (1979), IEEE, 67, 1522.

Farley, D. T., H. M. Ierkic and B. G. Fejer (1981), J. Geophys. Res., 86, 1467.

Hocking, W. K. (1983), Proceedings of Workshop on Technical Aspects of MST radar, Handbook for MAP, Vol 9, SCOSTEP Secretariat, Dep. Elec. Eng., Univ. IL, Urbana, 171.

Pfister, W. (1971), J. Atmos. Terr. Phys., 33, 999.

Rottger, J. (1983), Proceedings of Workshop on Technical Aspects of MST Radar, Handbook for MAP, Vol. 9, SCOSTEP Secretariat, Dep. Elec. Eng., Univ. IL, Urbana, 150.

Rottger, J. and R. A. Vincent (1978), Geophys. Res. Lett., 5, 917.
Royrvik, O. (1983), Radio Sci., 18, 461.
Strauch, R. G., Proceedings of Workshop on Technical Aspects of MST Radar, Handbook for MAP, Vol. 9, SCOSTEP Secretariat, Dep. Elec. Eng., Univ. IL, Urbana, 232.
Whitehead, J. D., W. R. From, K. L. Jones and P. E. Monro (1983), J. Atmos. Terr. Phys., 45, 345.

SUMMARY AND RECOMMENDATIONS

OPTIMUM POINTING ANGLE: There are a number of factors which determine the choice of the off-zenith pointing angle for Doppler velocity measurements. At frequencies near 50 MHz the main factor is the strong aspect sensitivity of the scattering which can cause the effective pointing direction to be smaller than the physical beam direction. There is consensus that zenith pointing angles of 10 to 15° are suitable for tropospheric, stratospheric and mesospheric studies. At these angles however, signals received through sidelobes pointing near the zenith may become significant. Such signals can be distinguished by their signature in the Doppler spectra and so their contribution should be rejected by the use of appropriate algorithms at the analysis stage.

OPTIMUM SPACINGS FOR SA MEASUREMENTS: The receiving antennas should be separated by distances comparable to the mean pattern scale (i.e., the separation where the zero-lag correlation is 0.5 on average. A MF/HF separation of about 1.0 to 1.5λ have proved satisfactory. At VHF, the scale will be determined in general by the use of the transmitting antenna and the angular distribution of the backscattered signals. While it is possible to calculate the spacing, the optimum spacing has to be determined experimentally. For a radar with a transmitting antenna with a 3° beam, a spacing of about 50 m has been found to be satisfactory.

RECOMMENDATION: Noting that there are some uncertainties associated with the vertical velocities measured by MST radars working in the lower VHF range where specular reflections are important and noting that for radars working at UHF such echoes are not observed, it is recommended that comparative studies of vertical velocities be made as soon as possible with co-located VHF and UHF radars and other suitable techniques such as lidar. Where practicable, interferometric techniques should be used to remove the effects of any tilts in the specularly reflecting surfaces.

RECOMMENDATION: It is noted that the aspect sensitivity at zenith angles smaller than 10 - 15° causes the effective antenna pointing direction to be closer to the zenith than the physical pointing direction. This effect will be most important for wide beams and will give errors in estimating the horizontal wind velocity. Investigations to obtain estimates of the likely errors and how they can be minimized are necessary.

3.1A A SIMPLE MODEL FOR TESTING THE EFFECTS OF GRAVITY-WAVE-PRODUCED VERTICAL OSCILLATIONS OF SCATTERING IRREGULARITIES ON SPACED-ANTENNA, HORIZONTAL DRIFT MEASUREMENTS

C. E. Meek and I. M. Reid

Institute of Space and Atmospheric Studies
University of Saskatchewan
Saskatoon, Canada

INTRODUCTION

It has been suggested that the velocities produced by the spaced antenna partial-reflection drift experiment may constitute a measure of the vertical oscillations due to short-period gravity waves rather than the mean horizontal flow. The contention is that the interference between say two scatterers, one of which is traveling upward, and the other down, will create a pattern which sweeps across the ground in the direction (or anti-parallel) of the wave propagation. Since the expected result, viz. spurious drift directions, is seldom, if ever, seen in spaced antenna drift velocities, this speculation is tested in the following model.

MODEL

Figure 1 illustrates the geometry of the model, which is very similar to that developed by WRIGHT and PITTEWAY (1978). Forty point scatterers are placed randomly within the aperture of the antenna system. Amplitudes are summed at all receiver antennas every 0.5 s, after which the scatterers are moved according to:

$$\vec{V}_i = \vec{U} + \vec{V}_{gw} \cos(\omega t + \vec{k}\cdot\vec{r}_i), \quad \vec{r}_i = 0.5\vec{V}_i + \vec{r}_i$$

where i refers to the i^{th} scatterer. The amplitudes are also varied randomly in a staggered fashion, a complete update takes place over 7 samples. If a scatterer moves out of the aperture in the horizontal direction, it is replaced by one at the opposite side; if it moves out vertically, it is not included in the amplitude summation until it re-enters. At 50 m/s, the whole pattern would be replaced in 10 min. "Records" are 5 min in length.

Simulations were done for several values of GW perturbation velocity and periods, and a range of azimuth angles. The background flow was 50 m/s eastward.

DISCUSSION AND CONCLUSIONS

It can be seen from Table 1 that the drift directions are very close to the mean background flow (90°). The true velocities are low, possibly because the model does not fit the analysis assumptions (viz. Gaussian spatial and decay time correlations). The major effect of the GW is to lower the characteristic time in the pattern.

Another test (not shown) with the aperture and GW wavelength reduced by 1/2, but the same rf wavelength, did exhibit major perturbations in the correlations and resulting drift velocities which are not yet understood. The distortion of the correlations caused at least half the data to be rejected on the basis of the normalized time discrepancy -- that is, the correlation peaks did not indicate a pattern motion. The effect appears to depend on the relation between the aperture and the radio wavelength. If so, then the results found in the present model (λ = 135 m, antenna beam = 20°) can be scaled to VHF (λ ~ 6 m) by reducing the beam width to 4° (the difference in range between the

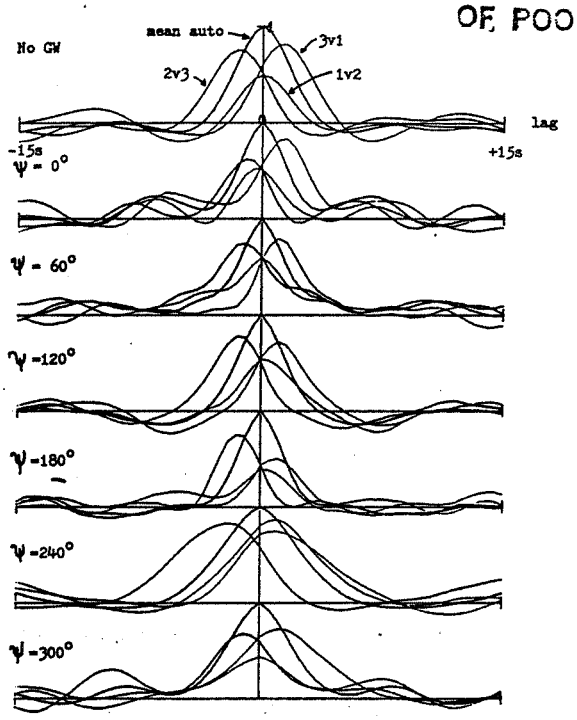

Figure 1. Geometry of scattering model.

center and edge of the scattering layer is made the same number of wavelengths).

Consequently, although the velocities may be perturbed by gravity waves, no spurious values (depending only on the GW) are expected, and this is what is found in practice.

An expansion of the model to simulate MF doppler experiments is planned for the future.

REFERENCE

Wright, J. W. and M. L. V. Pitteway (1978), Radio Sci., 13, 189.

Table 1. Results of drift analysis for various azimuth angles and wavelengths of gravity waves.

Gravity wave			Drift analysis							
V_{gw} (m/s)	λ_{gw} (Km)	Azim. E of N	V_{ap} (m/s)	ϕ_{ap} EofN	V_{tr} (m/s)	ϕ_{tr} EofN	τ_c (sec)	A (m)	B (m)	tilt EofN
-	-	-	54	103°	47	89°	3.6	163	129	53°
GW period = 5.2 min										
5	20	0°	55	91	45	88	3.6	153	140	73
5	20	60	59	88	47	90	3.4	178	162	168
5	20	120	57	93	45	88	3.3	163	148	42
5	20	180	57	87	42	89	2.6	127	112	97
5	20	240	58	91	50	86	3.6	150	129	68
5	20	300	61	100	49	89	3.1	163	127	67
20	20	0	72	96	47	84	2.0	160	129	41
20	20	60	59	87	41	93	2.8	176	149	158
20	20	120	84	98	37	79	1.6	167	119	43
20	20	180	70	98	38	98	2.0	180	140	9
20	20	240	74	91	37	92	1.8	167	136	1
20	20	300	72	93	38	87	2.0	161	142	31
GW period = 10.1 min										
20	60	0	63	74	48	71	2.7	153	144	39
20	60	60	67	91	48	87	2.6	173	155	22
20	60	120	61	99	46	97	2.8	157	144	19
20	60	180	62	103	43	107	2.3	136	121	123
20	60	240	45	118	34	98	4.2	270	162	42
20	60	300	67	84	37	86	2.8	188	134	88

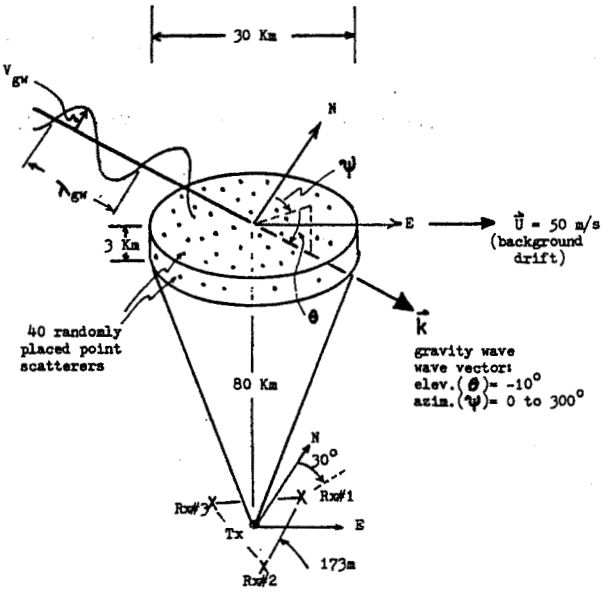

Figure 2. Auto- and cross-correlations for V_{gw} = 20m/s, λ_{gw} = 60 km. period = 10.1 min, for the data used in Table 1.

3.1B POTENTIAL ADVANTAGES OF THE SPACED ANTENNA METHOD FOR OPERATIONAL WIND PROFILING

J. Rottger*

EISCAT Scientific Association
P.O. Box 705
S-98127 Kiruna, Sweden

M. F. Larsen

School of Electrical Engineering,
Cornell University
Ithaca, NY 14853

INTRODUCTION

The problem of very short-range forecasting is twofold. It is necessary to understand the processes that are being forecasted, and data appropriate to the scale of interest has to be generated. Coherent VHF and UHF radars are being used for operational wind profiling and are providing part of the solution to the data-acquisition problem (LARSEN, 1983). The Profiler system operated by the Wave Propagation Laboratory at NOAA has already shown great promise (STRAUCH, 1981; STRAUCH et al., 1982). As a result, plans are being considered for expanding the network of radars to cover a larger area of the country.

The Profiler uses what is commonly referred to as the Doppler method for measuring winds. Two beams are pointed off-vertical, and the Doppler shift of the echo determines the line-of-sight velocity. The velocity components along the beams are then translated to horizontal wind components. While there is no doubt that the Doppler method is adequate for wind profiling, we want to discuss a number of possible advantages of the spaced antenna (SA) method for operational wind profiling. There is virtually no difference in cost between the two types of systems. However, there may be some significant advantages of the SA method, particularly when smaller radars are being considered. Since any Profiler network is still only in the planning stage, now is the time to consider the various alternatives.

DESCRIPTION OF THE TWO TECHNIQUES

The Doppler method uses the same antenna array for transmitting and receiving. The array is phased in such a way that the beams point at some angle off vertical. The Doppler shift of the received signal is then proportional to the line-of-sight velocity, V' in the right-hand-side of Figure 1. Two beams pointing in different directions have to be used, together with the assumption that the vertical velocity is negligible, to determine the two horizontal wind components. The three-dimensional vector wind velocity can be determined uniquely only if three beam directions are used. The spaced antenna method (see ROTTGER, 1981 for a detailed description), shown in the left-hand-side of Figure 1, uses one transmitter array and three closely spaced receiving arrays with all beams pointing vertically. The three receiving antennas may be separated from the transmitting antenna, but more efficient is a configuration in which each third of the transmitting array is used as a separate receiving array. The horizontal velocities are calculated using the time lags at which the cross-correlations of the signals received in the various antennas maximize. The spaced antenna method essentially tracks the propagation of a perturbation in the refractive index across the distance separating the receiving antennas. The vertical velocity is calculated from the Doppler shift.

---

*presently at Arecibo Observatory, Arecibo, Puerto Rico, on leave from Max-Planck-Institut fur Aeronomie, Lindau, W. Germany.

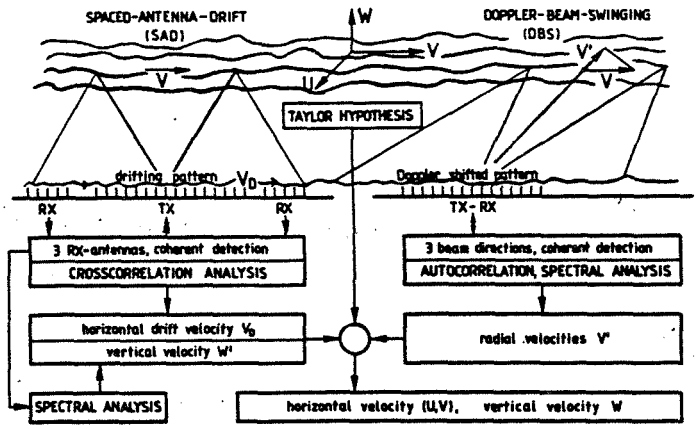

Figure 1. Schematic of the spaced antenna and the Doppler method for measuring the three-dimensional velocity in the troposphere, stratosphere, and mesosphere.

An objection to the spaced antenna method that is often heard is that the technique gives incorrect wind measurements when the medium is strongly affected by wave activity. In that case the scattering is primarily from the refractive index structure associated with the wave fronts, and the measured velocity is the phase of the waves rather than the true wind velocity. However, BRIGGS (1980) has shown rigorously that the Doppler method and spaced antenna method are, in fact, equivalent. Both techniques scatter from the same variations in the medium. Therefore, the effect of wave structures is equally a problem with the Doppler method and the SA method. There is no reason to expect that the latter will give poorer results on that account.

AN EXPERIMENT TO COMPARE THE TWO TECHNIQUES

The SOUSY-VHF-Radar is one of the few radars at present where a comparison between the Doppler technique and the spaced antenna technique can be carried out directly. The configuration of the antenna system is shown in Figure 2. The large antenna can be used for both transmitting and receiving in the Doppler mode. The three smaller antennas can also be used as spaced receivers in combination with the large transmitting array. In October 1979, an experiment was carried out with this radar to compare the two measurement techniques.

The spaced antenna wind measurements can be made either by cross correlating the received power at the three receiving antennas or by cross correlating the complex amplitudes. The latter approach retains the phasing information and gives better results because it is consistent with the process of coherently integrating the signals. Figure 3 showns the resulting comparison. It is clear that the complex amplitude cross correlation provides data over a greater height range than the simple power cross correlation. Especially, the region between 8.2-km and 9.7-km altitude and the lower stratospheric heights should be compared.

It is well known that signals at VHF have a strong angular dependence near the zenith. Specular reflections or Fresnel scattering associated with the stable temperature stratification in the atmosphere produce enhanced echoes at vertical incidence. The echo strength decreases rapidly, by as much as 10 dB (GREEN and GAGE, 1980), at even a few degrees off vertical. The spaced antenna

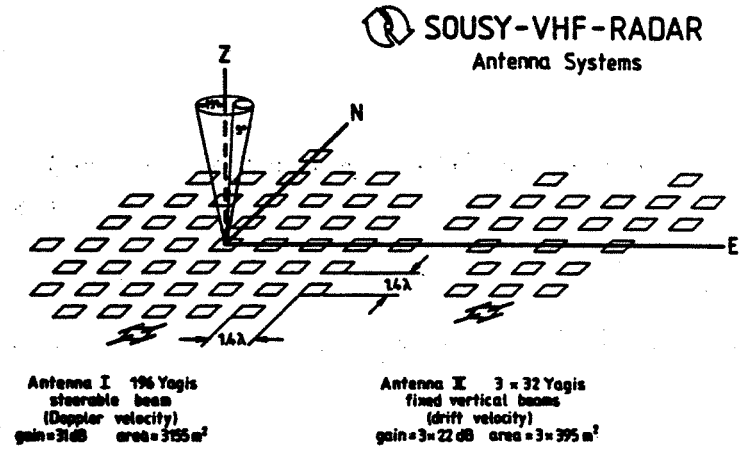

Figure 2. Antenna systems of the SOUSY-VHF Radar (from ROTTGER 1981). Antenna I is the smaller system of 3 x 32 four-element Yagi antennas which are used in the spaced antenna mode for reception when the large array of 196 Yagis is used for transmission.

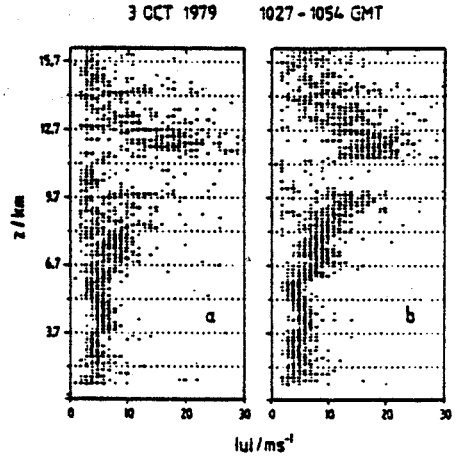

Figure 3. Height profiles of drift speed deduced from (a) power cross correlation and (b) complex amplitude cross correlation.

technique makes maximum use of this effect since all the beams are pointed vertically, producing a higher signal-to-noise ratio at those heights where the winds are measured. The Doppler method does not take advantage of the effect since the beams have to be pointed off vertical to make the wind measurements.

The strong angular dependence of the reflectivities does pose a potential problem for the Doppler technique when small antenna arrays are used. There are generally practical limitations on how far off vertical the beams can be pointed, and, of course, the beam width increases as the dimension of the antenna array decreases. When the beam width is wide, the received signal is really a convolution of the antenna pattern and the angular dependence of the echo strength, as shown in Figure 4. The result is that the apparent look angle is different than the real look angle, and the horizontal winds tend to be underestimated. The effect is critical when the vertical pointing direction is within the main lobe of the radiation pattern.

The effect is shown in the experimental results presented in Figure 5. Figure 5a shows the velocity profile derived from the complex cross correlation of the spaced antenna signals. Simultaneous aircraft wind measurements, shown by the open circles, indicate good agreement between the two independent wind measurements. Panel b shows the vertical velocity profile which could only be measured with the VHF radar. Figure 5c gives the velocity profile derived from the Doppler method using a beam pointed 7° off vertical and shows very good agreement with the spaced antenna method. However, the beam width of the large array is 5°, and when the beam is pointed at only 3.5° off vertical, there is a significant contribution from the vertical direction. The resulting wind profile is much poorer since it has broader scatter and underestimates the velocities.

DISCUSSION

The data from the October 1979 experiment are not conclusive, but they do indicate that there may be certain advantages in using the spaced antenna method, particularly for systems with small dimensions of the type likely to be used in operational wind profiling. Problems associated with the aspect sensitivity only arise when the beam width is large. It is, in fact, likely that when larger systems are used, there is little difference between the two techniques since the beam widths are small then. Therefore, the SOUSY comparison may not fully show the advantages of the spaced antenna method for small tropospheric sounding systems, and further comparison should be carried out in the future.

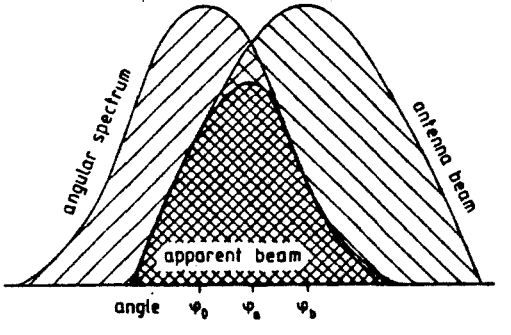

Figure 4. Formation of an apparent beam direction.

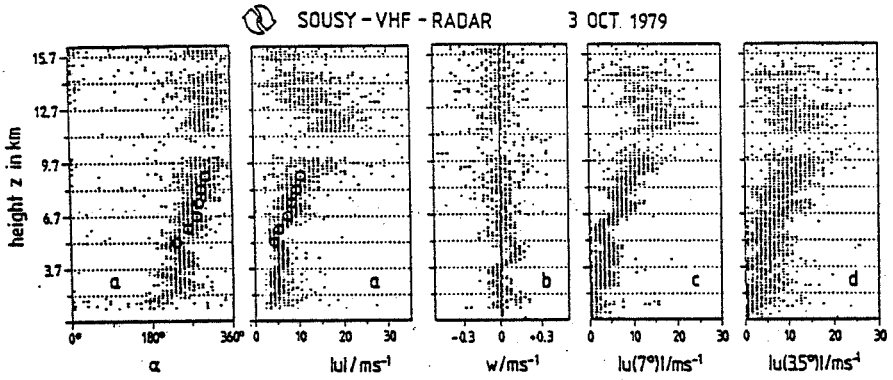

Figure 5. Height profiles of (a) wind direction and wind speed measured with the spaced antenna method and comparison with aircraft winds shown by the open circles, (b) vertical velocity, and (c) wind speed measured with the Doppler method using a beam pointing at 7° and (d) 3.5° off vertical.

REFERENCES

Briggs, B. H. (1980), Radar observations of atmospheric winds and turbulence: a comparison of techniques, J. Atmos. Terr. Phys., 42, 823-833.

Green, J. L. and K. S. Gage (1980), Observations of stable layers in the troposphere and stratosphere using VHF radar, Radio Sci., 15, 395-406.

Larsen, M. F. (1983), The MST radar technique: Requirements for operational weather forecasting, Handbook for MAP Vol 9, 3-11, SCOSTEP Secretariat, Univ. IL, 1406 W. Green St., Urbana, IL.

Rottger, J. (1981), Investigations of lower and middle atmosphere dynamics antenna drifts radars, J. Atmos. Terr. Phys., 43, 277-292.

Strauch, R. G. (1981), Radar measurement of tropospheric wind profiles, Preprints, 20th Conference on Radar Meteorology (Boston), AMS, Boston, 430-434.

Strauch, R. G., M. T. Decker, D. C. Hogg (1982), An automatic profiler of the troposphere, Preprints, AIAA 20th Aerospace Sciences Meeting, (Orlando, Fla.), American Institute of Aeronautics and Astronautics, New York.

3.2A CRITERIA FOR OPTIMUM SPACING OF SPACED ANTENNAS

C. E. Meek

Institute of Space and Atmospheric Studies
University of Saskatchewan
Saskatoon, Canada

INTRODUCTION

There are many factors affecting the spaced antenna drift results, only one of which is antenna spacing. Generally, good results are obtained at MF for receiver antenna spacings of 1-1.5 λ, and at VHF (e.g. SOUSY) for spacings ~6λ. Since one of the factors, local atmospheric/ionospheric conditions, are difficult to predict, this paper will be restricted to a short discussion of relevant factors, and methods for comparing various antenna/analysis configurations.

"Optimum" may mean different things; for example;

(1) the most accurately determined lags for peak cross correlation
(2) the most consistent wind vectors, e.g. for small time differencces
(3) the least biased speed determination, based on theoretical considerations
(4) the most wind vectors
(5) the most accurate winds (by comparison with another "accepted" technique)
(6) the fastest wind vectors, i.e. shortest record lengths.

These may depend to a greater or lesser extent on the experimental system parameters, such as:

(1) transmitter antenna aperture
(2) transmitter pulse width and power
(3) receiver antenna aperture (physical size)
(4) receiver antenna spacing (including possible rf coupling)
(5) sampling rate and raw data integration
(6) record length
(7) noise level
(8) type of correlation (amplitude, hybrid bit-amplitude, or bit)
(9) rejection criteria (lower limit on acceptable peak correlation, normalized time discrepancy)
(10) analysis method; apparent or true velocity, and type of analysis (e.g. graphical, Gaussian fit to correlations, 6 point methods).

Some of these latter, pertaining to antenna systems, are discussed next.

EXPERIMENTAL FACTORS

Apparent velocity (V_{ap}) depends just on the lags, t_{max}, for peak cross correlation between receiving arrays, whereas true velocity, V_{tr}, accounts for average pattern scale and elongation as well as pattern decay rate (characteristic time). Larger pattern scales lead to wider correlations, and longer decay times to greater peak correlations. Because of statistical fluctuations, the t_{max} are less accurately determined for wide cross correlations, and it may be necessary to increase the absolute lag to reduce these errors (by increasing the antenna spacing, for example).

The transmitter beam width has a theoretical effect on the ground pattern scale, but in practice larger scales are found at Adelaide (wide beam) than at

Saskatoon (narrow beam); so it is likely the effective beam width is usually determined by the aspect sensitivity of the scattering process (although receiver spacing and analysis also seem to play a role). Increased transmitter pulse width and power lead to greater signal-to-noise ratio. Tests at Saskatoon for ~1 hr of data showed no obvious difference in quality (NTD distribution) between 20 μs and 50 μs pulse data, although the latter produced more data (presumably because good scattering layers were spread over several height gates).

The important characteristics of the receiving antennas: spacing, physical size, and rf coupling including any coupling in the feeder cables), can bias the measured speeds and pattern characteristics. A two-hour data set using the "Y" antenna array (Figure 1) at Saskatoon was analysed for both large (2λ) and small (1.2λ) spacing. Figure 2 shows that there is no significant bias between speeds, however larger pattern scales and characteristic times were found for the large spacing. A similar result was found in a comparison between the 1.2λ and a separate 1λ array over several weeks of daytime data.

Physical size of the antenna array implies a spatial average, in some way of the ground pattern. If the space between different receiving arrays is filled with antenna elements, a simple 1-D calculation with a rigid pattern, Gaussian correlation function, and the unrealistic condition that all scattered power arrives in phase, shows that the measure V_{ap} ($V_{ap} = V_{tr}$ in this case) can be too low by ~7%, independent of pattern scale. A similar 2-D simulation (but non-rigid pattern) supports this figure. The reason appears to be that the average correlation is weighted towards the higher values of correlation due to elements in different arrays which are close to each other; and so the "effective" receiver spacing is actually smaller than that used to calculate the velocity. The 2-D simulation also shows that pattern scales are

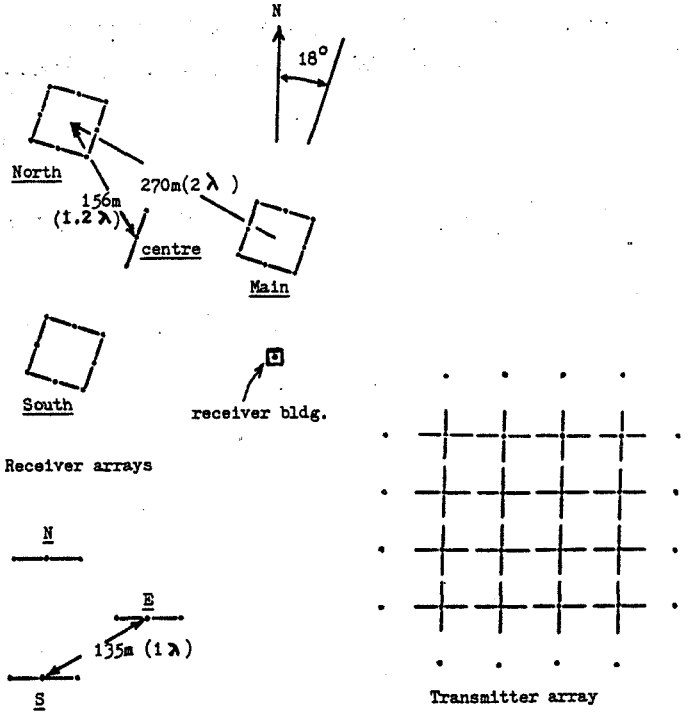

Figure 1. Antenna systems, main site (Saskatoon).

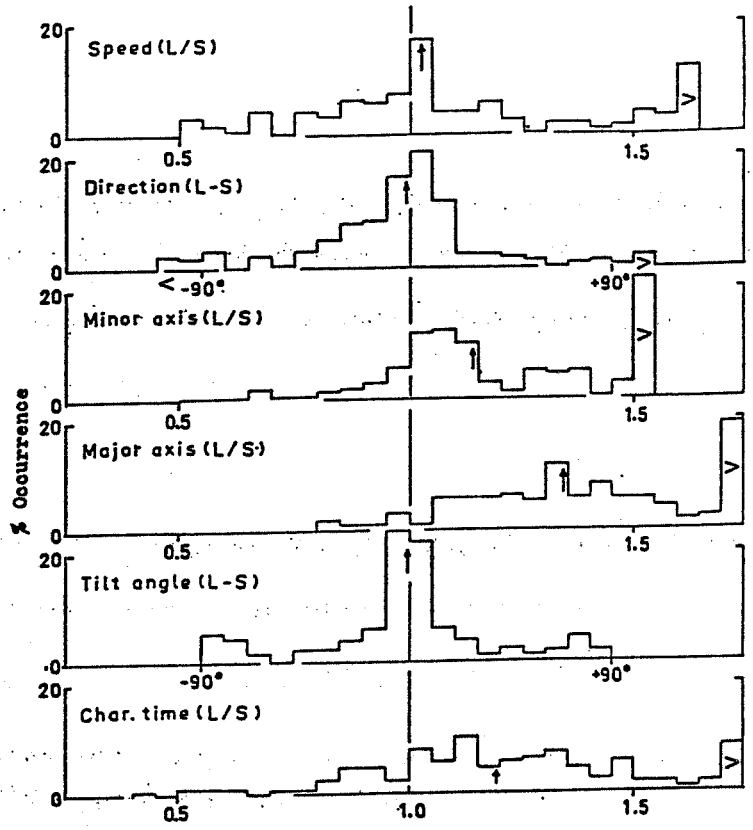

Figure 2. Comparison between FCA parameters for large spacing (2λ) and small spacing (1.2λ) arrays.

larger for a "filled" aperture antenna system (by ~20%), but the characteristic times are virtually unaffected (possibly because of the unrealistic condition on phase).

Coupling of antenna elements may be a problem, particularly at MF where the spacing is of the order of the rf wavelength; however, the 1-λ array (see Figure 1) mentioned previously, where the single dipole elements are not arranged for optimum isolation (-16dB coupling between two elements, phase shift unknown) shows negligible bias on the measured speeds in Figure 3. (The isolation between elements of the 1.2-λ array is better than 40 dB). A simulation for <u>in-phase</u> coupling of -20 dB shows that the measured speeds should be too high by ~20%, the pattern scales too high by ~30% and the characteristic times too low by ~5% on the average, depending on the input pattern characteristics. None of these, except the last, is seen in the 1-λ array data, and this might be due to spacing.

These simulations have yet to be done for complex amplitudes; however it is first necessary to investigate whether antenna elements hooked directly in parallel (as is the usual practice) add amplitudes in the same way as a power combiner.

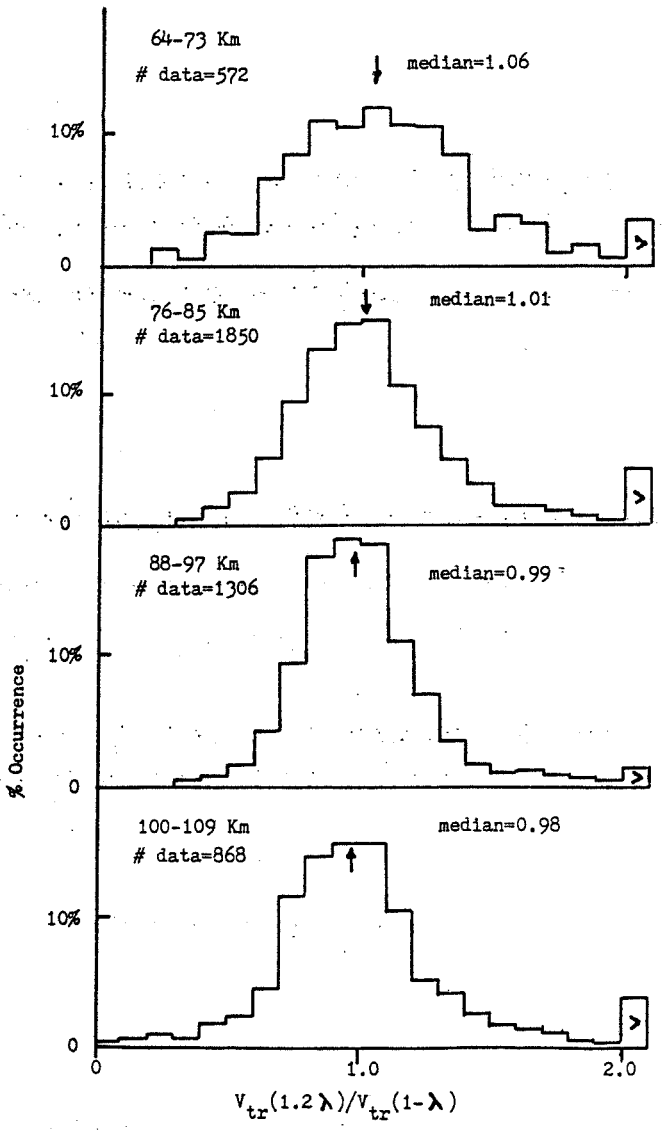

Figure 3. Speed comparison between the 4-antenna, 1.2-λ array and the 1-λ array. Selected days in Jan-Feb 1984. Bit correlation used in real-time analysis. 10 μs transmitter pulse.

METHODS FOR COMPARING DIFFERENCES IN LOCATION/HARDWARE/SOFTWARE

The most useful parameter is the normalized time discrepancy, NTD. If t_{max} are the lags for peak cross correlation for the i^{th} receiver pair, and the receiver pair vectors form a closed loop, the $\Sigma\, t_{max} = 0$ for a moving pattern. Distribution of the NTD,

$$NTD = \left|\Sigma t_{max_i}\right| \Big/ \Sigma \left|t_{max_i}\right|$$

are useful for comparing with the random t_{max} case, or with other antenna/analysis configurations. An example is shown in Figure 4. The NTD distribution depends on ionospheric conditions as well as spacing (which affects the magnitude of peak correlation), and defines the "quality" of the data (i.e. the fraction of the t_{max} data which may be attributed to moving patterns. In general, the larger the receiver spacing, the worse the NTD distribution -- since some of the "wanted" peaks fall below the magnitude of spurious peaks.

Other useful distributions are the angle difference and the normalized vector difference, $|(\bar{V}_1 - \bar{V}_2)/(\bar{V}_1 + \bar{V}_2)|$, where the wind vectors are closely separated in height or time, which are a "consistency check" on the data. These are found to depend strongly on the NTD distribution (although there is no direct theoretical connection) and so do not add much information when comparing basic experimental parameters.

CONCLUSIONS

The best advice for anyone setting up an MF radar system is to try an initial receiver antenna spacing of 1-1.5λ (using single dipoles and light masts), determine how much of the data is acceptable through the NTD distribution, and if too much is lost then adjust the spacing accordingly, based on examination of the cross correlations.

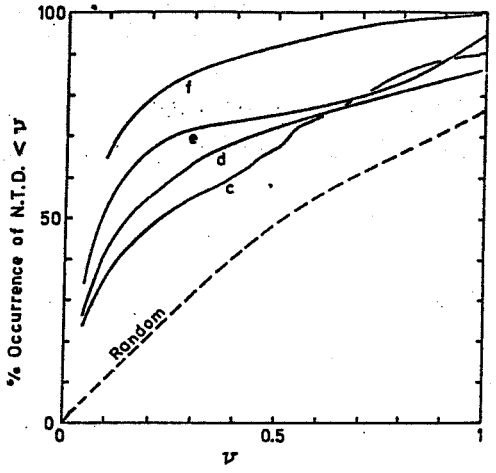

Figure 4. NTD distributions for small amounts of data for Saskatoon (c=2λ array, d=1.2λ array), Adelaide (f) and Ottawa (e).

926

3.3A ANISOTROPY OF THE PERMITTIVITY FIELD INFERRED FROM ASPECT-SENSITIVE RADAR ECHOES*

A. T. Waterman

STARLAB, Stanford University
Stanford, CA 94305

This paper attempts to draw some quantitative conclusions regarding the anisotropy of the clear-air back-scattering mechanism based on the measured variation of echo power with zenith angle. The measurements were made by the SOUSY group of the Max Planck Institute for Aeronomy at Lindau, FRG, (ROTTGER et al., 1981; WATERMAN and CZECHOWSKY, 1983). They installed their 47-MHz transmitter and antenna feed in the 300-meter diameter reflector at Arecibo. The resulting 1.7-degree beam was stepped successively through seven 1.7-degree intervals from 1.7 to 11.7 degrees in zenith angle, obtaining about four minutes of data at each setting. This procedure was carried out in an eastward pointing azimuth and in a northward pointing azimuth, the entire set of measurements consuming an hour and twenty minutes. Range resolution was 150 meters.

Figure 1 shows received echo power vs actual height (corrected for slant range) for the seven zenith angles; the data cover two ranges of height intervals, selected for good signal-to-noise ratio and freedom from other complications. The variation of signal with zenith angle is apparent, particularly in the layer at 16.8 km and even more strongly around 14 km.

Figure 2 is an example of the aspect sensitivity at 13.9 km for the eastward looking azimuth. The discrete measured values of echo power at the seven zenith angles are connected by straight line segments, while the smooth curve is a least-mean-squares fit to these data using a specific model of anisotropic scattering.

The specific anisotropic scattering model was taken from GAGE and BALSLEY, (1980) who used the Booker-and-Gordon scattering concept (BOOKER and GORDON, 1950) as modified by STARAS (1955) to take possible anisotropy into account. It leads to an expression for the volume scattering reflectivity which can be written as

$$\eta = \frac{B}{(\sin X)^2 + R^2 (\cos X)^2} . \qquad (1)$$

B is an amplitude constant, X is the zenith angle, and R is the quantity related to the anisotropy. If there is anisotropy in the vertical only, and the permittivity field is horizontally isotropic, then

$$R = \frac{\ell_z}{\ell_x} \qquad (2)$$

where ℓ_z is the vertical axis in the correlation ellipse of the permittivity field and ℓ_x is its horizontal axis. If there is anisotropy in the horizontal as well as the vertical, the interpretation of R becomes more complicated, since the horizontal anisotropy ellipse has a minor axis ℓ_y and a major axis ℓ_x as well as an orientation angle ϕ measured from east:

$$R = \left(\frac{\ell_z}{\ell_x}\right) \sqrt{\frac{1 + (\tan \phi)^2}{1 + (\ell_y/\ell_x)^2 (\tan \phi)^2}}$$

* A more detailed account of this analysis is given in "Measurements of Anisotropic Permittivity structure of upper troposphere with clear-air radar", A. T. Waterman, T.-Z. Hu, P. Czechowsky and J. Rottger, to appear in Radio Science.

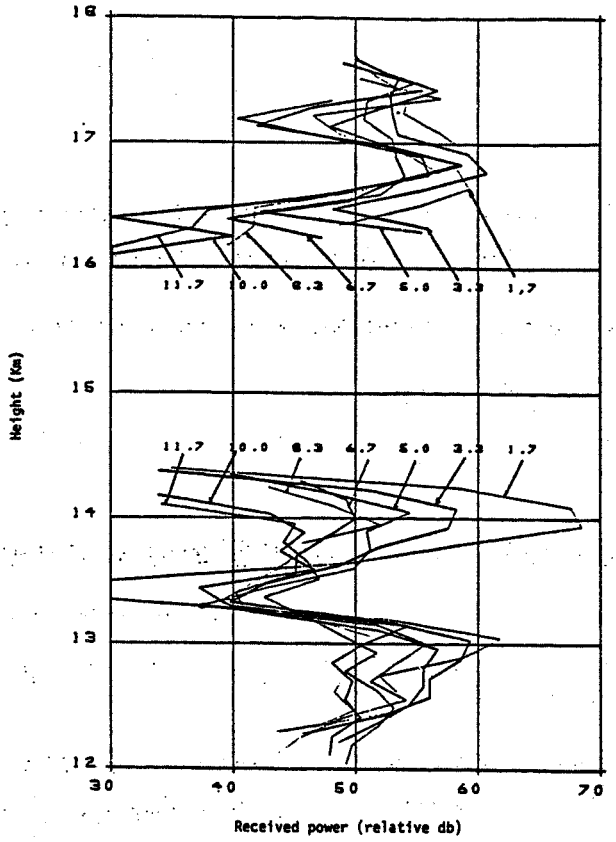

Figure 1. Backscattered power vs height for seven zenith angles (marked, in deg) and eastward azimuth.

From the measurements, the reflectivity as a function of zenith angle X is determined, and the values of B and R giving the least-mean-squares fit are found. This is done for each height for both eastward and westward azimuths, yielding R_E and R_N. (The values of B provide redundant information in this model). The three desired quantities, vertical anisotropy ℓ_z/ℓ_x, horizontal anisotropy ℓ_y/ℓ_x, and orientation ϕ, cannot be uniquely determined from the measurements -- a third azimuth would be needed -- but limits within which these quantities must lie can be found. They are shown in Figure 3.

The right-hand column of Figure 3 shows vertical anisotropy (ℓ_z/ℓ_x) as a function of height. Here the two curves are the upper and lower bounds within which the anisotropy must lie. Remember that the ℓ-ratios here are minor-to-major-axis ratios, so that low values represent greater anisotropy. (Unity implies isotropy). Except for the region around 13.3 to 13.5 km, a clear vertical anisotropy prevails.

The left-hand column of Figure 3 shown the upper bound on this anisotropy ratio for the horizontal structure -- that is, the atmosphere is at least as anisotropic as the values given by this curve, and may be more so. Associated with this measure of the structure is the orientation of the major axis of the horizontal anisotropy ellipse. The limits within which it must lie are shown by the shaded areas in the center portion of the figure. At low elevations it

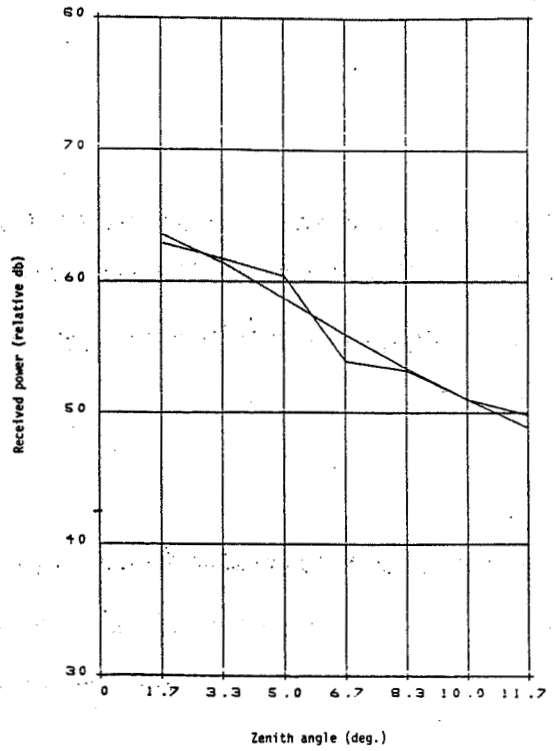

Figure 2. Aspect sensitive backscattered power at 13.9 km. R = 0.1.

starts out with an orientation aligned within ± 30 degrees of east-west. At about 12.5 km it swings around to a more nearly north-south orientation, etc.

Owing to the small amount of data and limitations in the nature of the data, one should not draw too many conclusions from these results. Nevertheless, it is clear that some form of anisotropy exists here, and this analysis is one attempt to put it on a quantitative basis.

REFERENCES

Booker, H. G. and W. E. Gordon (1950), A theory of radio scattering in the troposphere, Proc. IRE, 401-412.

Gage, K. S. and B. B. Balsley (1980), On the scattering and reflection mechanisms contributing to clear air radar echoes from the troposphere, stratosphere, and mesosphere, Radio Sci., 15, 243-257.

Rottger, J., P. Czechowsky and G. Schmidt (1981), First low-power VHF radar observations of tropospheric, stratospheric and mesospheric winds and turbulence at the Arecibo Observatory, J. Atmos. Terr. Phys., 43, 789-800.

Staras, H. (1955), Forward scattering of radio waves by anisotropic turbulence, Proc. IRE, 1374-1380e.

Waterman, A. T. and P. Czechowsky (1983), Upper tropospheric structures observed with VHF radar at Arecibo, ESA-SP-194, 89-94.

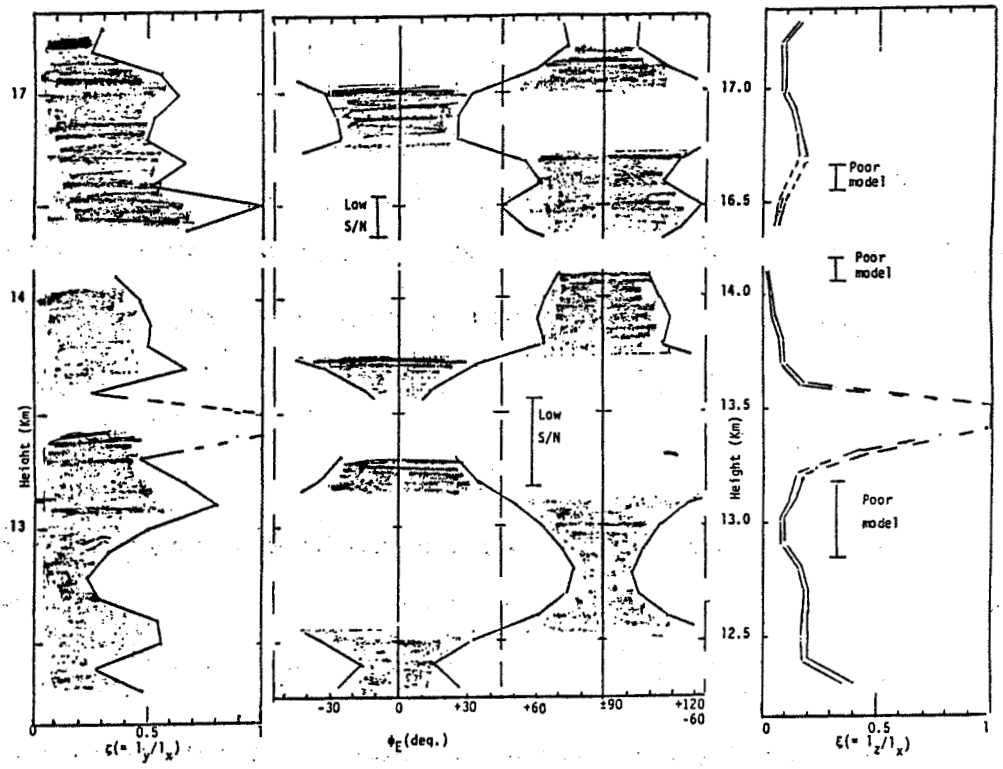

Figure 3. Degree ζ and orientation ϕ_E of horizontal anisotropy; degree of vertical anisotropy ξ. Shaded areas show permissable range of values. Low values of ζ and ξ are most anisotropic.

3.4A ACCURACY OF VELOCITY AND POWER DETERMINATION BY THE DOPPLER METHOD

J. Rottger*

EISCAT Scientific Association
981 27 Kiruna, Sweden

THE REQUIRED SUPPRESSION OF ANTENNA SIDELOBES NEAR THE MAIN LOBE

When designing an MST radar antenna one has to trade between the choices to optimize the effective aperture or to optimize the sidelobe suppression. An optimization of the aperture increases the sensitivity. Suppression of sidelobes by tapering attenuates undesirable signals which spoil the estimates of reflectivity and velocity. Generally, any sidelobe effects are equivalent to a broadening of the antenna beam. The return signal is due to a product of the antenna pattern with the varying atmospheric reflectivity structures. Thus, knowing the antenna pattern, it is in principle possible to find the signal spectra, which, however, may be a tedious computational and ambiguous procedure.

For vertically pointing main beams the sidelobe effects are efficiently suppressed because of the aspect sensitivity. It follows that sidelobes are a minor problem for spaced antenna methods. However, they can be crucial for Doppler methods, which need off-vertical beams. If a sidelobe is pointing towards the zenith a larger power may be received from the vertical than off-vertical directions, but quantitative estimates of this effect are not yet known.

To get an error estimate of sidelobe effects with an off-vertical main beam we discuss the following 1-dimensional example. This yields a reasonable estimate since the sidelobe closest to zenith, in the plane in which the main beam is steered, mostly dominate the errors.

Assume that the antenna pattern $P(\delta)$ in the plane in which the main beam is tilted is given by Figure 1. Let P_1 be the power gain of the main lobe at the zenith angle δ_1, and P_2 the power of the sidelobe at δ_2. The aspect sensitivity, given by $\alpha(\delta)^2$, changes the actual antenna pattern to an apparent antenna pattern, sketched by the dashed lines. It alters the direction and the power of the antenna lobes. For the following estimates we do not consider the apparent beam direction and we confine to the power in the main lobe at δ_1 and the first sidelobe at δ_2. The other sidelobes (at δ_2', δ_3' and δ_3) are reasonably suppressed by the aspect sensitivity and are not considered here. To get a worst estimate we also do not consider the doubling of sidelobe suppression for reflection and assume a one-way beam only (scattering).

From the Doppler spectrum $P(\omega)$ of the radar returns we get the average power

$$\overline{P} = \int P(\omega)\, d\omega,$$

and the average Doppler frequency

$$\overline{\omega} = \frac{\int \omega\, P(\omega)\, d\omega}{\overline{P}}$$

Assuming that the radar detected structures move with a velocity U in the plane of Figure 1, we would measure Doppler frequencies $\omega_1 = (-4\pi\, U \sin \delta_1)/\lambda_0$ and $\omega_2 = (-4\pi\, U \sin \delta_2)/\lambda_0$, and average (normalized) powers P_1 and P_2 through the main beam at δ_1 and the sidelobe at δ_2. Since the contribution from the main- and the sidelobe cannot be separated, we obtain the incorrect

*presently at Arecibo Observatory, Arecibo, Puerto Rico, on leave from Max-Planck-Institut fur Aeronomie, Lindau, W. Germany

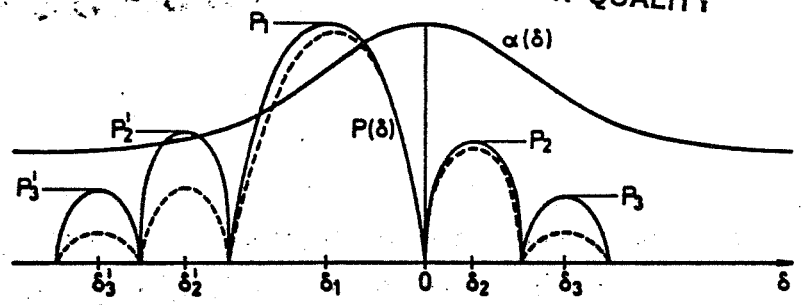

Figure 1. Schematic antenna pattern $P(\delta)$ in the vertical plane as function of zenith angle δ. The main lobe with power gain P_1 is tilted off the vertical at an angle δ_1. Sidelobes are shown at angles δ_2, δ_2', δ_3, δ_3'. The antenna pattern is weighted (dashed lines) by the aspect sensitivity $\alpha(\delta)$.

estimates

$$\bar{P} = a_1 P_1 + a_2 P_2,$$

$$\bar{\omega} = \frac{\bar{\omega}_1 a_1 P_1 + \bar{\omega}_2 a_2 P_2}{a_1 P_1 + a_2 P_2}$$

where $a_1 = \alpha(\delta_1)$ and $a_2 = \alpha(\delta_2)$.

If one would neglect the sidelobe effects, one measures the signal power ($\hat{=}$ radar reflectivity) and velocity with fractional errors

$$\Delta\bar{P} = \frac{\bar{P} - a_1 P_1}{a_1 P_1} = \frac{a_2 P_2}{a_1 P_1},$$

$$\Delta U = \frac{\bar{\omega} - \bar{\omega}_1}{\bar{\omega}_1} = \frac{a_1 P_1 + a_2 P_2 \cdot \sin \delta_2 / \sin \delta_1}{a_1 P_1 + a_2 P_2} - 1.$$

Using for example $\delta_1 = 9°$, $\delta_2 = -4.5°$ (without considering the apparent beam direction), $P_1 = 1.0$, $P_2 = 10^{-2}$ (for a worst estimate of -20 dB two-way-beam sidelobe suppression), and $a(\delta) = 1$ dB/degree corresponding to $a_1 = 1.3 \cdot 10^{-1}$ and $a_2 = 3.6 \cdot 10^{-1}$, yields $\Delta\bar{P} = 2.8 \cdot 10^{-2}$ and $\Delta U = -4.3 \cdot 10^{-2}$. This means that the power would be overestimated by 2.8%, and the horizontal velocity would be underestimated by 4.3%. A similar computation will yield the error estimates for the spectral width. Since δ and $P_{1,2}$ are known, instrumental parameters and $a(\delta)$ is fairly well known from observations, $\Delta\bar{P}$ and ΔU can be used for correction, which will yield a very reasonable estimate of $\bar{P}$ and U. It, thus, may appear to be more feasible to apply corrections which have to take into account the two-dimensional pattern than use tapering. However, situations may occur (e.g., strongly tilted, reflecting layers) which would lead to substantial contributions through antenna sidelobes. These situations need special attention during the data analysis. To minimize the problems with tilted layers, it is recommended to swap the main beam direction, viz. measure at zenith directions δ_1 and $-\delta_1$, when applying the Doppler beam swinging method. A more reliable estimate of the tilt, however, can be deduced with the interferometer technique.

D28

3.4B IMPROVEMENT OF VERTICAL VELOCITY MEASUREMENTS

J. Rottger*

EISCAT Scientific Association
981 27 Kiruna, Sweden

Vertical velocities are assumed to be measurable with vertically pointing antenna beams. An exact horizontal levelling and good phase calibration of the radar antenna system can yield real main-beam directions which do not significantly differ from calculated patterns. It is, thus, anticipated that antenna beams can be pointed exactly vertically. Because of area size and near-field limitations, VHF radar antennas have typically beam widths of more than several degrees.

It is known that most of the reflectivity structures detected by vertically beaming VHF radars in the troposphere, stratosphere and lower mesosphere are aspect-sensitive. It cannot a priori be assumed that these structures are exactly horizontally stratified, they are rather inclined according to the atmospheric flow pattern in which they are embedded. This flow pattern is mostly not exactly horizontal. We have collected a few examples to support this statement.

In synoptic-scale disturbances the isopleths of temperature and humidity are inclined and correspondingly the isopleths of the vertical gradient of the potential refractive index are inclined, too. This is shown in Figure 1 which compares the radiosonde-deduced and the VHF radar-deduced results obtained during the successive passages of a cold front and a warm front. Another illustrative example of passage of a warm front is shown in Figure 2 which very clearly indicates layers sloping downwards and upwards with time. Since these disturbances propagate and have lifetimes of a day or more, layers ascending or descending with time over a fixed (radar) location have to be tilted. Typical tilt angles of these frontal structures are a fraction of a degree to some degree.

Whereas synoptic-scale disturbances have characteristic horizontal scales of some 1000 km and vertical scales of the height of the troposphere (≈ 10 km), the corresponding baroclinicity (tilt angle) is fairly small but not negligible. For illustration of tilted cross section see also Figure 4. Larger tilt angles occur in smaller scale disturbances such as orographically influenced flow patterns, namely mountain lee waves (Figure 3). Here tilt angles of several degrees or more can occur.

This generally holds for any kind of gravity waves. For example, it was pointed out by GAGE et al. (1981) that the specular reflection point changes its direction with respect to the vertical antenna beam at different phases of a gravity wave (Figure 5). This results in a modulation of the radar return power if the radar beam is narrower than the offset range of the direction to the specular point (2, 4). It can also result in defocussing (1) or focussing (3) for wider antenna beams. More crucial, it changes the direction of incidence, and even with an exactly vertically oriented antenna beam the ray direction is off-vertical. This has an obvious effect on the measurement accuracy of the vertical velocity. The possible error can be reduced by applying a technique to measure the incidence angle and correct the estimated horizontal and vertical velocities.

---

*presently at Arecibo Observatory, Arecibo, Puerto Rico, on leave from Max-Planck-Institut fur Aeronomie, Lindau, W. Germany.

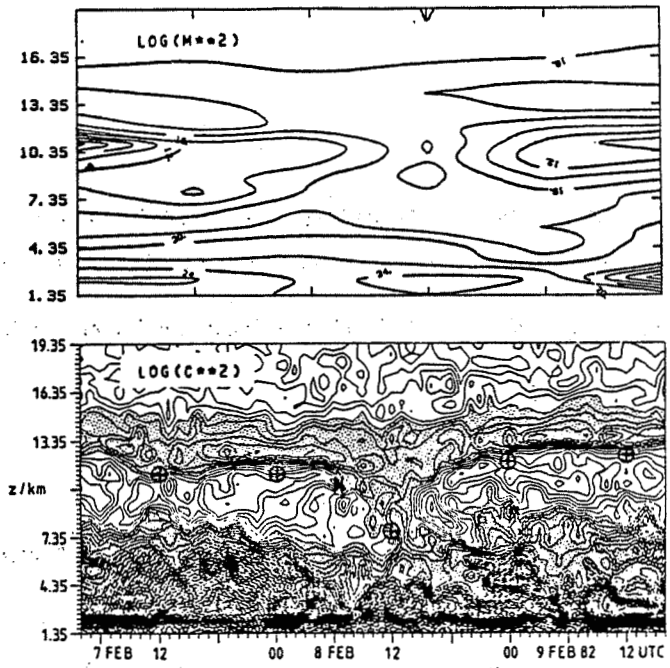

Figure 1. Logarithms of the vertical gradient of potential refractive index M^2, deduced from radiosonde data, and of the corresponding effective reflectivity C^2, measured with a vertically beaming VHF radar (from LARSEN and ROTTGER, 1983).

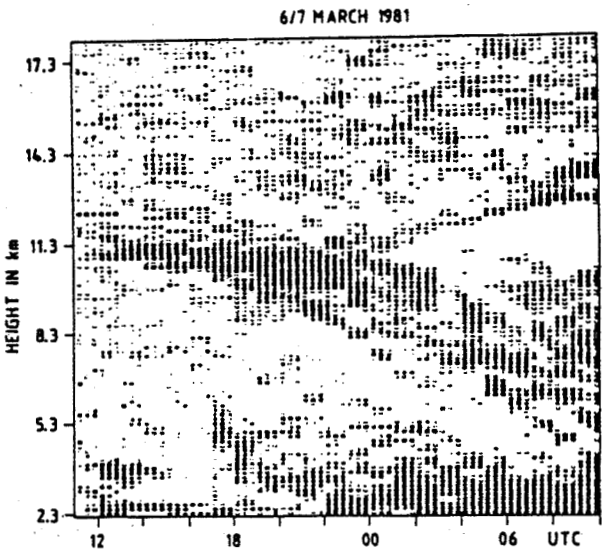

Figure 2. Modified (mean profile subtracted) height-time intensity plot showing sloping layers of enhanced radar reflectivity due to frontal boundaries and tropopause (after ROTTGER, 1981), observed with the SOUSY-VHF Radar.

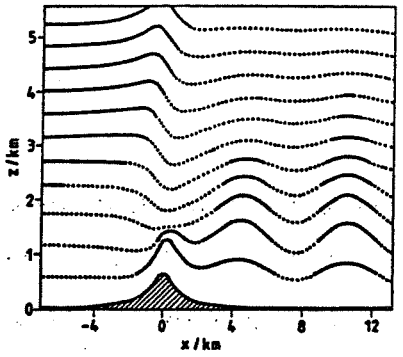

Figure 3. Displacement of streamlines of lee waves, resulting in equivalent structures of the potential refractive index.

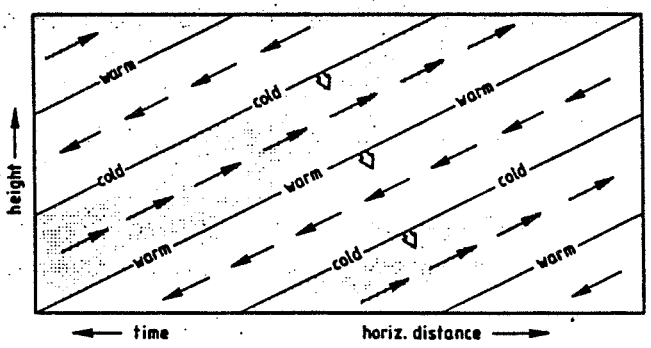

Figure 4. Idealized cross section for internal gravity wave (after HOLTON, 1972).

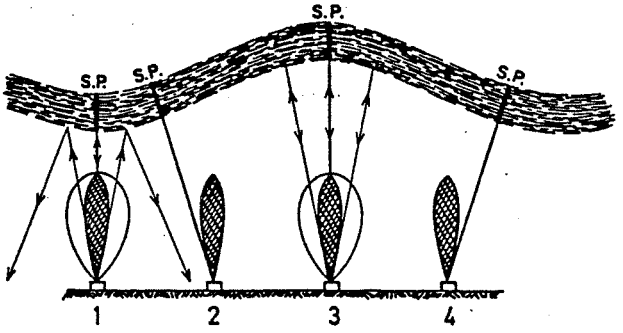

Figure 5. Schematic diagram showing changes in the specular point with respect to the vertical angenna beam at different phases of the gravity wave (after GAGE et al., 1981). Additionally, wide beam widths are inserted to show the effect of focussing (3) and defocussing (1).

The Doppler and the spaced antenna drifts method do not separately evaluate the spatial distribution of the phases of the field pattern at the ground. With the spaced antenna set-up the amplitudes and the phases can be measured. Combining in a suitable procedure the complex signals from different antennas is in a wide sense the application of the interferometer technique. In the first spaced antenna measurements with VHF radars, ROTTGER and VINCENT (1978) and VINCENT and ROTTGER (1980) applied this method to measure the angular spectrum of tropospheric returns. The vertical velocity measurements can also be improved by using a spaced antenna interferometer. The basic principle of the technique is sketched in Figure 6. Let us assume diffuse reflection from a rough surface or structure S which is sufficiently far from the radar antenna and which is slightly tilted to the horizontal by an angle δ'. This structure moves with a velocity given by the horizontal component U and the vertical component W. A radar with vertically pointing antenna A_o with beam width larger than δ' measures the radial velocity

$$V' = W^* - U^* = W \cdot \cos \delta' - U \cdot \sin \delta'.$$

Thus, even when knowing the horizontal velocity U, the vertical velocity is still incorrect if δ' is unknown.

The reflected signal can also be received at two separate antennas A_1 and A_2, and the complex cross-correlation function ρ_{12} be computed. Its amplitude $|\rho_{12}|$ and phase ϕ_{12} are sketched in the lower part of Figure 6. From the displacement τ_{12} of the maximum of $|\rho_{12}|$ and the horizontal sepa-

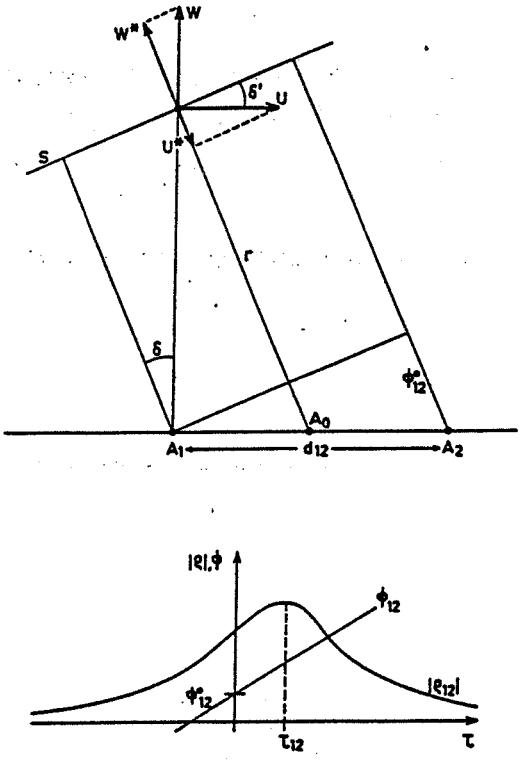

Figure 6. The principle of phase measurements at antennas A_1 and A_2, and determination of time delay τ_{12}.

ration d_{12} of the receiving antennas, the apparent velocity $V_a = d_{12}/2\tau_{12}$ is calculated with the spaced antenna drifts method. We assume here for simplification that $V_a = U$ (instead of V_a, the true velocity has to be calculated according to full correlation analysis). The radial velocity is calculated from the time derivative of ϕ at $\tau = 0$:

$$V = \lambda/4\pi \cdot d\phi\,(o)/dt.$$

The tilt angle δ', which is similar to the incidence angle δ, is

$$\delta' = \arcsin(\phi_{12}(o) \cdot \lambda/2\pi d_{12}.$$

This yields the corrected vertical velocity

$$W = (V' + V_a \sin\delta)/\cos\delta.$$

For a typical ratio $U/W = 100$ and $\delta = 0.6°$, for example, the vertical velocity estimate would be incorrect by a factor of 2 (0.5) if this correction were not applied. The angle δ' is equivalent to the inclination of the reflecting structures. Its average can give an estimate of the inclination of isentropic surfaces (baroclinicity), which is evidently of interest for meteorological applications (GAGE, 1983).

The phase lag between two antennas can also be introduced instrumentally, either by including a delay line between the antennas and the receiver or by adding a phase lag to the complex signal samples received at the different antenna channels. In the first case (preselected beam direction) the signals from both antennas would be added in an analogue coupler, and in the second case (post-selected beam direction) the digital samples would simply be added as vectors during data processing. This procedure is equivalent to electrically swinging the beam to different angles δ. The addition (distribution) of signals from (to) different antenna modules is used to swing the receiver (transmitter) beam of a phased array. For separate transmission and receiving antennas, the transmitter antenna beam can be kept fixed and the receiving antenna beam be swung by post-selection as long as the angle δ is narrower than the beam of the transmitter antenna. The advantage of this latter method is the post-selection of all possible angles δ, whereas the former method preselects an angle which cannot be changed after the data were taken. Of course, this method is easily extendable from the explained 1-dimensional example to a 2-dimensional application as well as to an array of more than two antenna modules.

This radar interferometer method not only allows the measurement of the horizontal wind components by the Doppler method, but also the tilt, the aspect sensitivity and the horizontal phase velocity and wavelength of atmospheric waves (see ROTTGER, 1983).

Another application, which originally was used to study ionospheric plasma turbulence (FARLEY et al., 1981), was recently applied also to MST radars to trace discrete structures, such as blobs of turbulence moving through the antenna beam (ROTTGER and IERKIC, in preparation). By making use of a cross-spectrum analysis and observing the change of δ and V' as a function of time, not only the location of the blobs but also their vertical and horizontal velocities can be measured more accurately (see also paper 2.2A by ROTTGER, this volume).

The measurements of δ and its temporal variations are very useful to avoid erroneous interpretations that the radial velocities measured with vertical antenna beams are really vertical velocities.

REFERENCES

Farley, D. T., H. M. Ierkic and B. G. Fejer (1981), Radar interferometry: A new technique for studying plasma turbulence in the ionosphere, J. Geophys. Res., 86, 1467-1472.

Gage, K. S. (1983), On the measurement of vertical velocity by MST radar, Proceedings of Workshop on Technical Aspects of MST Radar, Handbook for MAP, Vol. 9, SCOSTEP Secretariat, Dep. Elec. Eng., Univ. Il, 215-226.

Gage, K. S., D. A. Carter and W. L. Ecklund (1981), The effect of gravity waves on specular echoes observed by the Poker Flat MST radar, Geophys. Res. Lett., 8, 599-602.

Holton, J. R. (1972), An introduction to Dynamic Meteorology, Academic Press, New York.

Larsen, M. F. and J. Rottger (1983), Comparison of tropopause height and frontal boundary locations based on radar and radiosonde data, Geophys. Res. Lett., 10, 325-328.

Rottger, J. (1981), The capabilities of VHF radars for meteorological observations, ESA SP-165, 143-148 (publ. by European Space Agency, Paris).

Rottger, J. (1983), Determination of vertical and horizontal wavelengths of gravity waves, Proceedings of Workshop on Technical Aspects of MST Radar, Handbook for MAP, Vol. 9, SCOSTEP Secretariat, Dep. Elec. Eng., Univ. Il, Urbana. 262-268.

Rottger J. and R. A. Vincent (1978), VHF radar studies of tropospheric velocities and irregularities using spaced antenna techniques, Geophys. Res. Lett., 5, 917-920.

Vincent, R. A. and J. Rottger (1980), Spaced antenna VHF radar observations of tropospheric velocities and irregularities, Radio Sci., 15, 319-335.

3.4C ANTENNA INDUCED RANGE SMEARING IN MST RADARS

B. J. Watkins and P. E. Johnston*

Geophysical Institute
University of Alaska
Fairbanks, Alaska 99701

INTRODUCTION

There is considerable interest in developing ST and MST radars for higher resolution to study small-scale turbulent structures and waves. At present most ST and MST radars have resolutions of 150 meters or larger, and are not able to distinguish the thin (40 - 100 m) turbulent layers that are known to occur in the troposphere and stratosphere, and possibly in the mesosphere. However the antenna beam width and sidelobe level become important considerations for radars with superior height resolution.

The objective of this paper is to point out that for radars with range resolutions of about 150 meters or less, there may be significant range smearing of the signals from mesospheric altitudes due to the finite beam width of the radar antenna. At both stratospheric and mesospheric heights the antenna sidelobe level for linear equally spaced phased arrays may also produce range aliased signals.

To illustrate this effect we have calculated the range smearing functions for two vertically directed antennas, (1) an array of 32 coaxial-collinear strings each with 48 elements that simulates the vertical beam of the Poker Flat, Alaska, MST radar, and (2) a similar, but smaller, array of 16 coaxial-collinear strings each with 24 elements. Figure 1 shows the one-way antenna pattern for the Poker Flat vertical antenna. The main lobe has a two-way beam width of 2.2 degrees. The smaller antenna has a two-way beam width of 4.4 degrees.

CALCULATION OF RANGE SMEARING FUNCTIONS

Referring to Figure 2, a thin turbulent layer is illustrated by the thick horizontal line. For a vertically directed antenna, R1 is the vertical range to the turbulent layer. However, because the antennas have a finite beam width with sidelobes, some energy is transmitted at an angle θ to the main lobe direction. The received power from the direction θ has a strength that depends on the antenna pattern, and originates from a range R2 = R1 + X. Therefore a function F(x) can be derived for a particular antenna that represents the variation of returned signal power as a function of distance (x) above a thin layer. For a thick turbulent layer, or multiple layers, the total radar echo response will be a convolution of the turbulence layer structure with the function F. This function is also height dependent, therefore, for illustrative purposes we will present calculations for heights of 85 and 15 km in the mesosphere and lower stratosphere, respectively.

MESOSPHERE

Figure 3 shows the range smearing function for the Poker Flat, Alaska, MST radar vertical beam antenna. Figure 4 is the same data covering only the first 100 meters that results from the main antenna lobe. The observed mesospheric signals in Alaska are frequently 20 dB or more above the minimum detectable level. These strong signals will be smeared in range up to 100 meters or possibly more for extremely strong signals.

---

*Also with NOAA Aeronomy Laboratory, Boulder, CO.

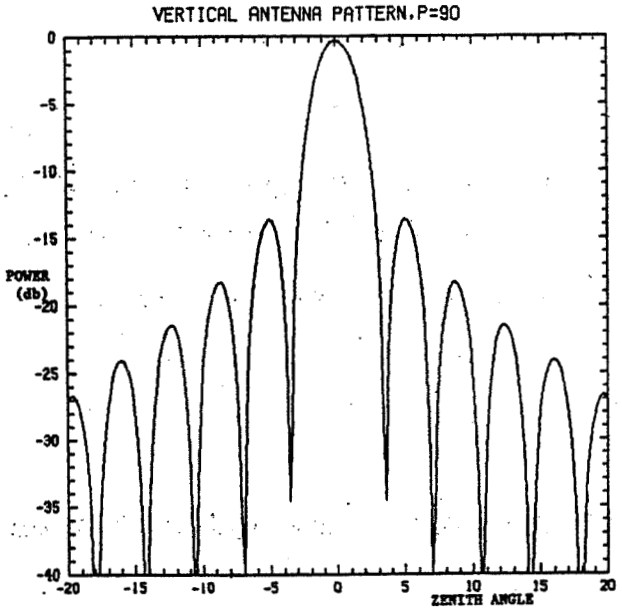

Figure 1. Radiation pattern for a square array of 32 coaxial-collinear stings each containing 48 elements.

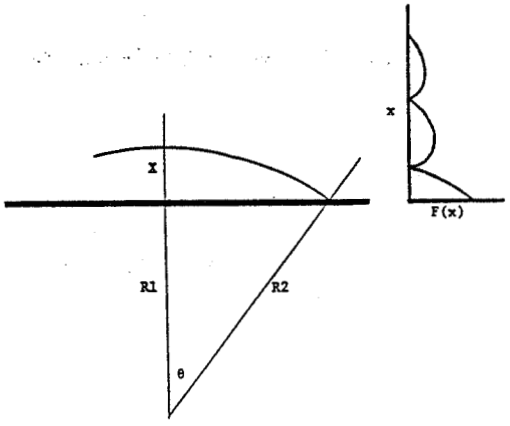

Figure 2. Geometry of two paths to a turbulent layer and the range smearing function F(x).

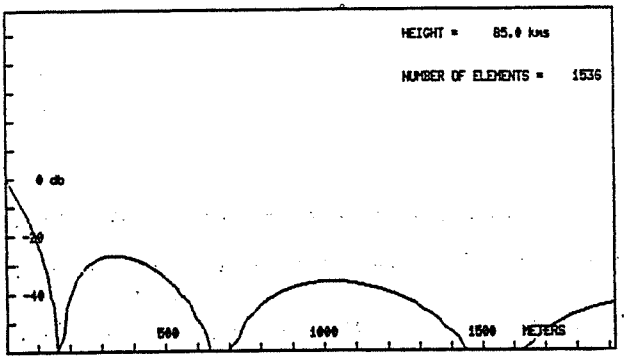

Figure 3. The range smearing function at a height of 85 km for an antenna composed of 32 coaxial-collinear strings each with 48 elements.

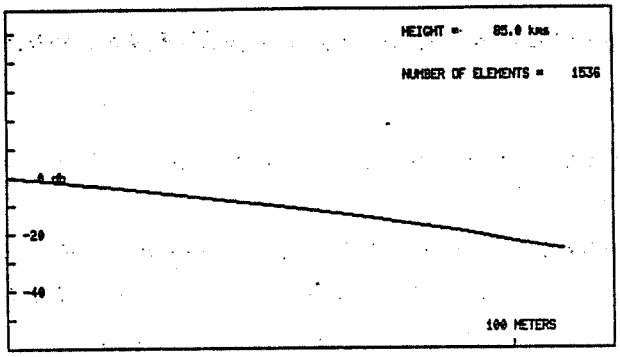

Figure 4. The same data as Figure 3 but only showing the first 100 meters.

With regard to the sidelobes, a very strong turbulent layer that produces signal returns more than 27 dB above the detectable limit will produce detectable signals at a distance of about 350 meters above the strong layer (see Figure 3). These range-aliased signals due to the first sidelobe are admittedly weak compared to the strong layer that produces them, but their magnitude may still be comparable with real turbulent layers at other heights.

For the smaller antenna (Figure 5) the situation is much worse. Range smearing due to the main antenna lobe extends more than 300 meters for signals stronger than about 20 dB above the detectable limit. If the signals are very strong (i.e. > 27 dB) the first antenna sidelobe may contribute signals from about 1100 to 1700 meters above the strong turbulent layer.

STRATOSPHERE

There is little problem with range smearing due to the main antenna lobe at low altitudes. Figure 6 for the Poker Flat antenna at 15 km altitude indicate less than 20 meters range spread which is probably a negligible error for most present or planned ST radars. However the smaller antenna shows more spreading (Figure 7); for an ST radar with such an antenna, a narrower beam antenna would be beneficial if high resolution is desired.

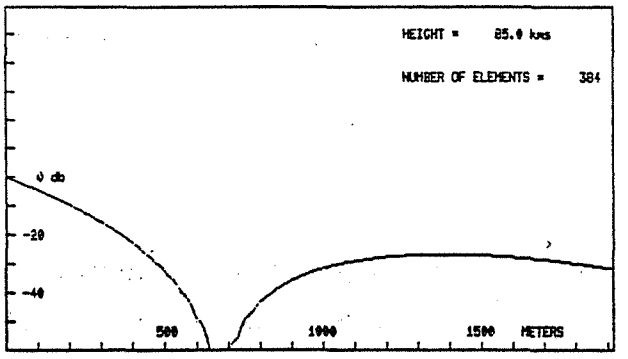

Figure 5. The range smearing function at a height of 85 km for an antenna composed of 16 coaxial-collinear strings each with 24 elements.

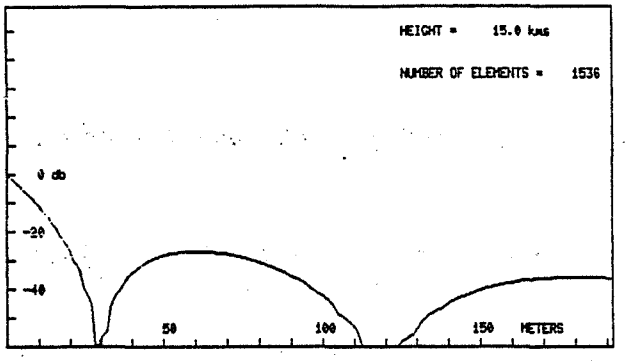

Figure 6. The range smearing function at a height of 15 km for an antenna composed of 32 coaxial-collinear strings each with 48 elements.

Concerning the sidelobes, the same problems exist in the stratosphere/troposphere as was discussed above for the mesosphere. It has been established from radar observations (WOODMAN, 1980), and balloon and smoke trail experiments (GOOD et al., 1982a,b) that tropospheric and stratospheric turbulence occurs in thin layers typically 30 - 100 meters thick separated vertically about 100 - 200 meters apart.

The balloon data frequently indicate variations of turbulence levels > 20 dB. It is likely that if new radars are designed with sufficient resolution to discriminate these thin intense turbulent layers, then antenna sidelobes may contribute to the returned signals.

SUMMARY

It is suggested that finite width of the radar antenna main lobe may produce range smearing that is important for high resolution MST radars, especially at mesospheric heights. For an extremely turbulent layer, the returned signals may be strong enough that the first antenna sidelobe is important.

Our calculations relate to vertically directed beams. For off-vertical antenna directions the problem is more severe.

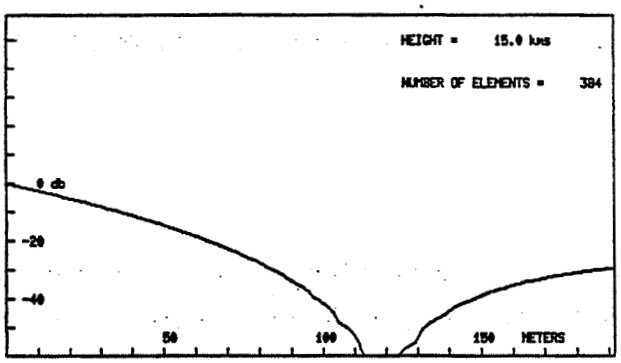

Figure 7. The range smearing function at a height of 15 km for an antenna composed of 16 coaxial-collinear strings each with 24 elements.

We suggest that in the design of future high resolution MST radars consideration be given to obtaining as narrow an antenna beam as is practical. The average power-aperture product determines the radar sensitivity; therefore it may be preferable to invest more in the antenna (to obtain a larger aperture and narrower antenna beam) than in a high power transmitter.

The simple inexpensive linear equally spaced arrays (e.g., coaxial-collinear antennas) have first sidelobes that may be too large for high resolution studies. Sidelobe reduction is possible by utilizing nonequal spacing or a tapered power distribution. For example, the UK MST radar (BOWMAN et al., 1983) utilizes a Dolph-Chebychev power distribution to partially suppress sidelobes.

REFERENCES

Bowman, M. R., V. J. G. Brown, D. Eccles, A. J. Hall and J. W. King (1983), Design study for a United Kingdom MST radar, Rutherford Appleton Lab.

Good, R. E. and A. F. Quesada (1982a), Probability distribution of turbulent layer thickness in the stratosphere, Trans. Am. Geophys. Union, 63, May.

Good, R. E., J. H. Brown, A. F. Quesada, B. J. Watkins and G. B. Loriot (1982b), Intercomparison of C_n^2 profile measurement techniques; Optical Society of America, Tucson, Arizona.

Woodman, R. F. (1980), High-altitude-resolution stratospheric measurements with the Arecibo 2380 MHz Radar. Radio Sci., 15, 423.

3.5A EFFECTS OF LINE-OF-SIGHT VELOCITY ON SPACED-ANTENNA MEASUREMENTS

O. Royrvik

Aeronomy Laboratory
Department of Electrical and Computer Engineering
University of Illinois
Urbana, IL 61801

INTRODUCTION

Horizontal wind velocities in the upper atmosphere, particularly the mesosphere, have been measured using a multitude of different techniques. Most techniques are based on stated or unstated assumptions about the wind field that may or may not be true. In this brief paper we will point out some problems with the spaced antenna drifts (SAD) technique that usually appear to be overlooked. These problems are not unique to the SAD technique; very similar considerations apply to measurement of horizontal wind using multiple-beam Doppler radars as well.

Simply stated, the SAD technique relies on scattering from multiple scatterers within an antenna beam of fairly large beam width (BRIGGS, 1980). The combination of signals with random phase gives rise to an interference pattern on the ground. This pattern will drift across the ground with a velocity twice that of the ionospheric irregularities from which the radar signals are scattered. By using spaced receivers and measuring time delays of the signal fading in different antennas, it is possible to estimate the horizontal drift velocities. Although the technique is quite simple in principle, the numerical calculations are plagued by a high degree of statistical uncertainties because small variations from an assumed model can give large errors in the estimated velocity.

It is to be understood that the SAD technique ultimately relies on differential line-of-sight velocities to calculate the horizontal wind. The differences are due to changing line-of-sight components of the horizontal wind as a function of changing look angle within the finite beam width of the antenna. A radar with an infinitely narrow transmitting antenna beam width can never be used as a SAD radar. Although much can be said about the problems of implementing a SAD radar system, we shall limit ourselves to considering interpretation of the results under ideal conditions of no system noise. That is, we shall assume we can accurately measure the drift velocity of the interference pattern over the ground, and consider what motions in the scattering layer may give rise to this drift velocity.

DISCUSSION

As already mentioned, only the line-of-sight velocity of a scattering irregularity will give rise to a drifting interference pattern (Figure 1). Calculation of the horizontal drift velocity of the scattering irregularities therefore requires that two assumptions be made. These are (1) the horizontal wind component is everywhere the same within the radar volume, and (2) the vertical wind component is small and everywhere the same within the radar volume. Any violations of these assumptions will result in errors in the estimated horizontal wind velocity. A short mathematical derivation of the result of relative motion within the radar volume was given by ROYRVIK (1983). The contribution to this error from motions of different scales will be discussed.

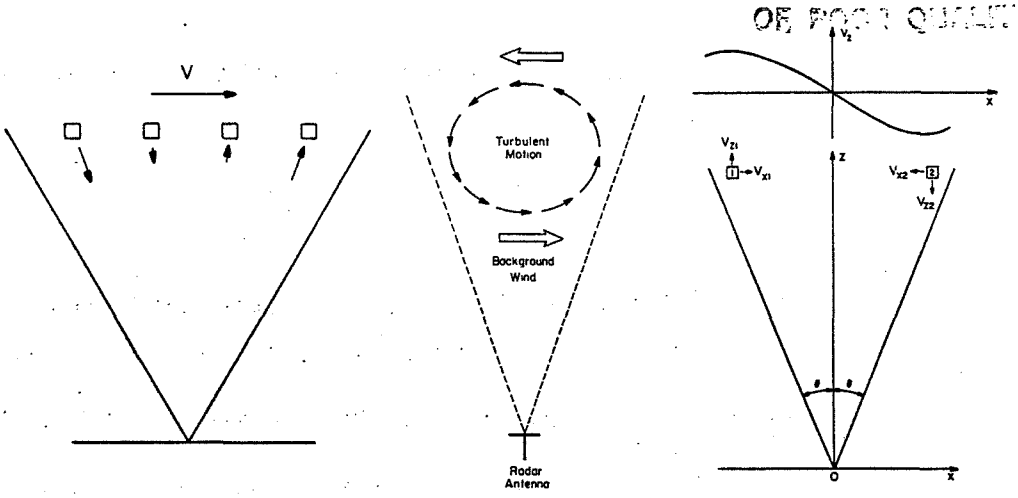

Figure 1. Schematics showing the differential wind velocities within a SAD radar scattering volume. Idealized vortex motion that may result from a wind shear (center); Radar situation with two scattering irregularities moving under the influence of a short-wavelength gravity wave (right).

(a) Differential Horizontal Motion

The average horizontal wind within a radar scattering volume which is limited by the antenna beam width in the horizontal direction and the range gate in the vertical direction, is due to oscillations with long horizontal wavelengths. The oscillations are caused mainly by long-period gravity waves and tides. Horizontal winds of the order of tens of meters per second are expected to result from these oscillations. In comparison, horizontal winds resulting from short-wavelength, short-period oscillations have amplitudes of only a few meters per second. Thus, even if these oscillations have horizontal wavelengths comparable to the horizontal dimension of the scattering volume, the error in the calculated horizontal velocity would not be more than 10% which in most cases is less than could be expected from statistical errors. Therefore we will not consider differential horizontal wind further.

(b) Differential Vertical Motion

The assumption that the vertical wind velocity is uniform throughout the radar volume does not hold true in most circumstances. There are three different length scales that can contribute to these vertical velocity differences. On the smallest scale are the turbulent velocity oscillations, which are considered to be randomly distributed throughout the scattering volume. They do not contribute to the measurement of the horizontal velocity in a systematic way; however, they contribute indirectly to the random error because increase in turbulent velocity will decrease the signal correlation time, which again makes the horizontal velocity more difficult to calculate (ROYRVIK, 1983). As the correlation time decreases, the irregularity pattern changes faster while drifting across the ground from one receiving antenna to another. Thus making the time sequences observed by the antennas become more dissimilar, and the time lag between them become more difficult to measure.

Vertical velocities that change systematically in the horizontal direction within the radar volume will contribute a large systematic error to the calculated horizontal velocity (ROYRVIK, 1983). The reason is that the SAD tech-

nique relies on changing line-of-sight velocity within the antenna beam; but, since it has no way to determine if the contribution is from horizontal or vertical wind, it assumes that there is a horizontal wind component only. If there is a differential wind component, however, it contributes much more efficiently to the line-of-sight velocity than does the horizontal wind and can contribute large errors. An antenna beam with angular half width of 10° is a factor of 5 more sensitive to vertical velocity differences than horizontal wind.

There are two different mechanisms that can generate differential vertical velocities with the required horizontal wavelength of one to twenty kilometers in the mesosphere. At the shorter end of this scale there are the organized motions resulting from overturning Kelvin-Helmholtz vortices with estimated horizontal wavelengths from a few hundred meters to a few kilometers. Differential vertical velocities of as much as 5 m/s may be generated. For a large antenna having very narrow beam width with cross section of 1 to 3 km in the mesosphere matching the dimensions of the vortices, this mechanism may account for calculated horizontal velocities of hundreds of meters per second. At the other end of the spectrum (10 km or more) short wavelength gravity waves will contribute to the calculated horizontal velocity. Doppler radars have shown that short-period waves in the mesosphere typically have amplitudes of 1-5 m/s, and the estimated horizontal wavelengths of these waves are from 20 km and upwards. Such waves combined with an antenna beam width of approximately 10° will give rise to oscillations in the estimated horizontal wind of 10-50 m/s. This error is of the same order of magnitude as the actual horizontal wind resulting from the tidal oscillations.

SUMMARY

From this discussion it should be evident that short-period oscillations observed by the SAD technique do not necessarily reflect oscillations in the horizontal velocity in the mesosphere. For oscillations with periods of one hour or more, the vertical velocity is very small compared to the horizontal velocity. The horizontal wavelength will also be large compared to the horizontal dimension of the radar volume. In this case the assumption of uniform wind within the scattering volume is valid, and the horizontal wind velocity can be measured accurately to within the statistical limitations of the SAD technique.

We conclude that the effect of vertical line-of-sight velocities is to preclude measurements of short-period horizontal wind oscillations.

ACKNOWLEDGMENT

This work was supported by the National Aeronautics and Space Administration under grant NSG 7506.

REFERENCES

Briggs, B. H. (1980), Radar observations of atmospheric winds and turbulence: A comparison of techniques, J. Atmos. Terr. Phys., 42, 823.

Royrvik, O. (1983), Spaced antenna drift at Jicamarca, mesospheric measurements, Radio Sci., 18, 461.

D31

3.6A INTERFEROMETER APPLICATIONS OF VHF RADARS*

J. Rottger**

EISCAT Scientific Association
Box 705
S-98127 Kiruna, Sweden

INTRODUCTION

Using a spaced antenna setup of a VHF radar, the spatial distribution of amplitudes and phases of the radar echoes from the troposphere, stratosphere and mesosphere can be measured. Combining in a suitable analysis procedure the complex digital samples from the different receiving antennas is consistent with the radar interferometer method. In addition to the well-known parameters measured with the commonly applied Doppler and drifts methods, i.e., reflectivity and mean and fluctuating velocity, the interferometer technique allows to measure the angular spectrum of the returns. It gives supplementary useful information on wave and turbulence structures and on the baroclinicity of the detected structures as well as improves the accuracy of the vertical velocity measurements.

This technique, which was first applied with the spaced antenna system of the SOUSY-VHF-Radar in W. Germany, as well as some first examples of results are described here. These comprise the measurements of the horizontal and vertical velocities of the mean flow as well as of turbulence structures, the aspect sensitivity and the tilt of layers from which the baroclinicity can be estimated. Particularly, results of interferometer measurements of the vertical and horizontal phase velocities and wavelengths of gravity waves in the stratosphere are displayed. The latter results are also discussed in terms of the generation and propagation of these waves.

RADAR INTERFEROMETRY

The interferometer technique is most extensively used in radio astronomy (e.g., KRAUS, 1966). It is also applied in the radar technique (e.g., WOHLLEBEN and MATTES, 1973). Under special conditions it was also employed in radar investigations of the ionosphere (e.g., PFISTER, 1971; FARLEY et al., 1981; WHITEHEAD et al., 1983), although only Farley et al. used the name "radar interferometry". First attempts to apply it to VHF radar investigations of the lower and middle atmosphere were reported by ROTTGER and VINCENT (1978), VINCENT and ROTTGER (1980), ROTTGER (1983) and ROYRVIK (1983). The commonly utilized methods in the MST/VHF radar operations are the Doppler (beam swinging) method and the spaced antenna (drifts) method. Although in both methods the amplitudes and phases of the signals are recorded (coherent detection), an evaluation of the spatial variations of the phases of the radar echoes (radar interferometry) is not accomplished.

The Doppler method uses different preset beam directions (obtained either by appropriate positioning of a dish antenna or by fixed instrumentally implemented phasing between submodules of a phased-array antenna system). Combining the radial Doppler velocities measured at different beam directions yields the

---

* To be published also in: Preprint Volume, American Meteorological Society, 22 Conference on Radar Meteorology, Zurich, Switzerland, 1984.

**Presently at Arecibo Observatory, Arecibo, Puerto Rico, on leave from Max-Planck-Institut fur Aeronomie, Lindau, W. Germany.

total bulk velocity vector of the moving scatterers. If one does receive the radar signal with two different (spatially separated) antenna systems as shown in Figure 1, and inserts a suitable phase shift $\Delta\phi$ to the recorded data one can point the receiving antenna beams to different positions without changing the hardware (insertion of phase differences before taking the data). This kind of interferometer method we may call "postset beam direction". Whereas the method of "preset beam direction" (i.e., the commonly applied Doppler method) uses mostly the same fixed beam direction for transmission and reception and therefore does not allow a change of beam direction after the data were recorded, the method of "postset beam direction" has to use a fixed transmitter beam with beam width broader than the steering angles of the receiver beams. However, the (receiver) beam direction of the latter method can still be varied (within the limit of the transmitter beam width) after the data are recorded on tape. It has to be noted here that both these methods work for reflection from small or extended targets as well as for volume scattering. Because the beam widths of the transmitter and receiver antennas are equal in the preset beam direction method, it yields a better signal-to-noise ratio than the postset beam direction method where part of the transmitter energy is lost because the receiver antenna beam picks out only a portion of the wide transmitter antenna beam. However, the postset method has other advantages since it allows to scan (simultaneously) the total area illuminated by the transmitter beam and thus yields improved information (high spatial and temporal resolution) on the atmospheric structure detected by the radar. The example in Figure 1 indicates a wave-like structure overhead the radar antennas, which can be scanned not only at the indicated positions, but (provided the receiver antennas are suitably configurated) also at positions in between, yielding the radial velocities and reflectivities as a function of incidence angle (angular spectrum).

The configuration of the radar interferometer array can be computed in a way similar to the standard procedure of antenna theory. Assume that N individual antenna elements with equal spacing d are horizontally lined up to form a multi-element array. In the array far-field $r>(Nd)^2/\lambda$, where λ is the radar wavelength, the antenna polar diagram is

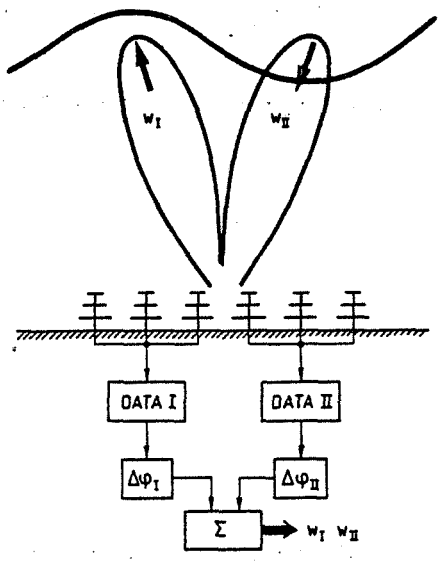

Figure 1. Principle of postset beam steering.

$$E(\delta) = \sum_{n=1}^{N} E_n(\delta)\exp(i(2\pi d\sin\delta(n-1)/\lambda + \Delta\phi_n)), \quad (1)$$

where $E_n(\delta)$ is the pattern of an individual element, δ is the zenith angle and $\Delta\phi_n$ is the relative phase placed on this element. Since $E_n(\delta)$ does not vary considerably in our applications (small δ), we assume $E_n(\delta) = E_n$ = const, and $\phi_n(\delta) = 2\pi d\sin\delta(n-1)/\lambda$. Equation (1) can be written as

$$E(\delta) = \sum_n E_n \exp\,(i(\phi_n(\delta) + \Delta\phi_n)) \quad . \quad (2)$$

The integral of (2) over δ is proportional to the complex signal C_n which is measured at the antenna n. For $\Delta\phi_n = 0°$ and $d < \lambda$ the antenna system has a main lobe at $\delta = 0°$ (zenith) with width $\delta_B = \arcsin(\lambda/Nd)$. The direction of the main lobe δ_o can be changed by applying a linearly progressing phase $\Delta\phi_n$ from element to element:

$$\Delta\phi_n = 2\pi d\sin\delta_o(n-1)/\lambda\,. \quad (3)$$

Note, that in the radar inferometer application $\Delta\phi_n$ is inserted during the data processing procedure. Also grating (side) lobes occur in this application for $d > \lambda$, which have to be suitably suppressed.

Whereas this method of beam steering works principally for hard targets (reflecting structures) and for soft targets (scattering structures) it can in a basically similar way also be used to measure the incidence or zenith angle of reflecting discrete structures or small blobs or patches of turbulence irregularities and to correct velocity estimates. This is briefly sketched in Figure 2.

Let us assume that diffuse reflection takes place from a rough surface or structure S which is slightly tilted to the horizontal by an angle δ'. This structure shall move with a velocity given by the horizontal component U and the vertical component W. A radar with vertically pointing transmitting antenna A_o with beam width larger than δ' measures the radial velocity

$$V' = W^*-U^* = W\cos\delta'-U\sin\delta'. \quad (4)$$

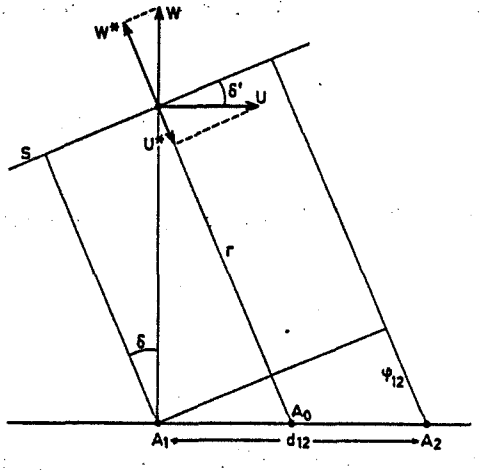

Figure 2. Principle of measuring incidence angle δ.

Thus, even when knowing (i.e., measuring by other means) the horizontal velocity U, the vertical velocity is still incorrectly measured, if δ' is unknown (ROTTGER, 1981).

When we apply the interferometer technique with n=2 antennas A_1 and A_2, we can compute the complex cross correlation function of the signals measured at A_1 and A_2. Its phase at zero lag (τ=0) is $\Delta\phi_{12}$, which yields the tilt or incidence angle

$$\delta' = \arcsin (\Delta\phi_{12}\lambda/2\pi d_{12}). \quad (5)$$

Measuring the horizontal velocity U with the spaced antenna drifts method and the radial velocity V' from the time derivative of the correlation function near zero

$$V' = d\phi/d\tau \; \lambda/4\pi, \quad (6)$$

we obtain the corrected vertical velocity

$$W = (V'+U\sin\delta)/\cos\delta. \quad (7)$$

This method (ROTTGER, 1984) can be refined by applying a complex cross spectrum analysis (FARLEY et al., 1981), which allows to improve the signal-to-noise ratio and to discriminate (by means of Doppler sorting) between separate discrete scatterers or reflectors in the beam which move with different velocities.

This radar interferometer method allows not only the measurements of the horizontal wind component (when pointing the receiver beams as done in the preset beam direction Doppler method) but also the tilt or inclination (baroclinicity) and the aspect sensitivity of reflecting structures. It is also suitable for gravity wave investigations as described in a later section, as well as will allow to measure the momentum flux, i.e., the cross product between U and W as done by VINCENT and REID (1983) with preset beam directions.

EXPERIMENT AND DATA ANALYSIS

The interferometer investigations were done by analysing a data set taken in an earlier experiment carried out from 3-14 September 1980 with the SOUSY-VHF-Radar. The radar was operated at 53.5 MHz with 500 kW pulse peak power and 4% duty cycle. Since this experiment concentrated on the stratosphere and mesosphere, an 8-bit complementary code with 10-µs bit length was used, providing a range resolution of 1.5 km at the maximum average power 20 kW. The lowest recorded height was 13.5 km and the spaced antenna method was applied using the 196 Yagi system for transmission and the 3x32 Yagi system for reception (Figure 3). The data were coherently preintegrated over 1/6 s, yielding an effective sampling rate of 1/2 s for the 3 spaced antennas. Since the earlier data analysis (ROTTGER, 1981) showed a fairly pronounced wave activity in the stratosphere, the interferometer analysis was applied to a part of this data set in order to test the applicability of the method and to gain a more profound insight into the gravity wave phenomena.

We first had to compute the optimum interferometer antenna pattern E, resulting from the combination of the spaced antenna setup E_R, the transmitter antenna pattern E_T and the aspect sensitivity A. This was done by just combining two spaced antenna modules (3-1, 3-2 or 2-1) at a time which is equivalent to a two-element interferometer with quasi-continuous aperture distribution. It allows to steer the interferometer beam in an E-W direction, 26° E of N and 26° W of N. Taking into account the positions of single Yagis of the spaced antenna system (fed with equal phase for each module), equation (1)

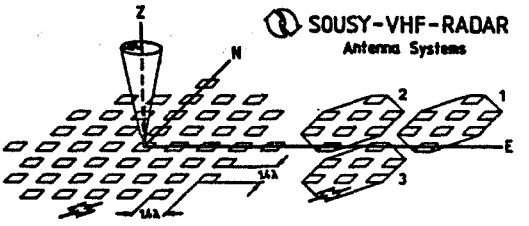

Figure 3. Antenna system with main antenna (3155 m^2 area) and three spaced antenna modules (3x395 m^2 area) pointing vertical. Distance between centres of spaced antennas was 24 m (2-1) and 28 m (3-1,3-2).

was used with n=2 to calculate E_R. The aspect sensitivity was assumed as A=2 dB/degree. The total interferometer pattern then becomes:

$$E = E_R \cdot E_T \cdot A.$$

By varying the phase difference $\Delta\phi$ between two modules, the maximum difference between the two interferometer lobes closest to the zenith was searched for. The optimum suppression of this simple 2-element interferometer configuration was found to be 6 dB. Integrating the antenna pattern over δ from -6° to +6° yields an apparent interferometer beam direction $\bar{\delta}$=1.2° for the combinations 3-2 and 3-1. The corresponding $\Delta\phi$ then was used to transform the complex data recorded with antenna 3, 2 and 1, which are available on tape. After complex summation (Figure 1 and equation (1)), the procedure was applied to calculate the first moment of the Doppler spectrum, respectively the radial velocity W*, which in the following treatments is reasonably assumed to be equal to W.

OBSERVATIONS

In Figure 6 of ROTTGER (1981) a series of quasi-vertical velocity data is shown which was obtained measuring with one antenna. The observed velocity oscillations at periods of 4-6 minutes are clearly repeated in Figure 5 of this paper. These results were obtained by combining the data of antenna 3 and 1 after introducing phase shifts $\mp\Delta\phi$. As described in the preceding section this corresponds to tilting the interferometer beam ±1.2° off the vertical direction. The average horizontal probing distance at these tilt angles is about 800 m at 20 km altitude. It is clearly seen that this tilting results in a phase shift of the wave-like oscillations in Figure 5. The curves with open circles correspond to a tilt in direction 3-1 (about N) and the closed circles in direction 1-3 (about S). The phase delay of the wave structure was not so pronounced when observing with antennas 3-2/2-3, and it was not observed with 2-1/1-2. We, thus, conclude that we observed a wave propagating into the direction around 26° E of N.

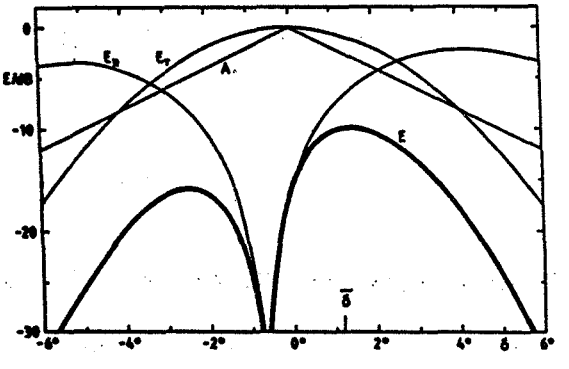

Figure 4. Optimum interferometer pattern E, resulting from pattern of transmitter antenna E_T, spaced antenna E_R and aspect sensitivity A.

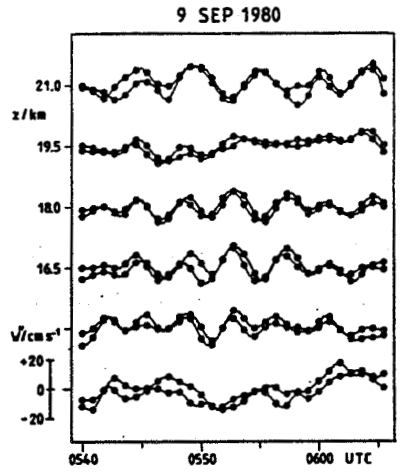

Figure 5. Radial velocity time series, measured with interferometer beam tilted to zenith angles 1.2° N (open circles) and 1.2° S (closed circles) for range gates at altitudes z.

These observations can be improved by a more quantitative approach which results in the data displayed in Figure 6. Here we have shown the average phase difference between the oscillations of the radial quasi-vertical velocity observed with different beam directions. The notations N32, S32, N31, S31 indicate the directions (N or S) to which the antenna combinations 3-2 and 3-1 were tilted. The phase angle ϕ_w was calculated by a cross spectrum analysis of the quasi-vertical velocity time series over a time interval of 90 min from 0446-0616 UT. The cross spectrum analysis yields also the coherence of two time series. Since the observed oscillations are not monochromatic but cover a band corresponding to about 4-6 min period (ROTTGER, 1981), the average phase difference ϕ_w was calculated by a weighted average using the coherence as a weighting function. This procedure suppressed noisy velocity fluctuations and filtered out the period band of about 4-6 min.

It is evident from Figure 6 that the phase difference ϕ_w changes its sign when steering the interferometer from the northward to the southward tilt. The absolute phase difference was in the range of about 5°-15°. There are obviously some fluctuations superimposed on these estimates of ϕ_w. These are partly because of the nonstationary wave oscillations, their nonmonochromatic nature and also due to the fact that the interferometer sidelobe (positioned at about opposite zenith direction of the main lobe, Figure 4) is suppressed by only 6 dB. This obviously yields spurious contributions from the opposite direction. It is also likely that the reflectivity structures are slightly

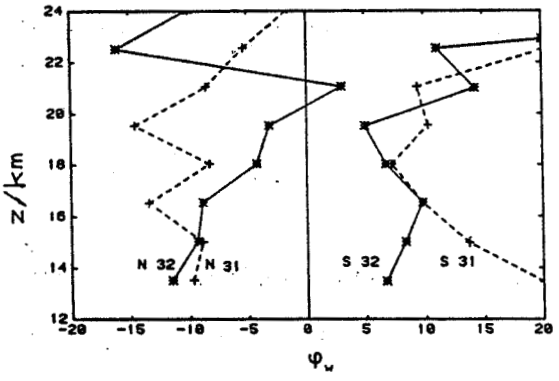

Figure 6. Phase difference ϕ_w of radial velocity oscillation, measured with beams tilted to N and S.

tilted with respect to the horizontal (due to the wave modulation), which results in a change of incidence angle (and aspect sensitivity model in Figure 4) and consequently of the measured radial velocity. Principally, however, the results of Figure 6 prove that the applied interferometer method is consistent with the expectations.

Not only fluctuating or oscillating radial velocities can be evaluated with this method but also the average vertical and horizontal velocity. We have briefly outlined the deduction of the average vertical velocity in a previous section and it was discussed also by ROTTGER (1981), and we will describe here the approach to measure the horizontal velocity with the interferometer setup. Even at small off-zenith angles, the component of the horizontal velocity is not negligible and can be measured. When averaging over 90 min with the interferometer beam at the same positions N32,... as described earlier, we measure the mean radial velocity $\overline{V}'$ (Figure 7). It is again noticed that also $\overline{V}'$ has a different sign with the beam towards N and S. If the method is correct, the difference $\Delta=\overline{V}'(N)-\overline{V}'(S)=0$. The single stars and crosses in Figure 7 indicate Δ for the antenna configurations 3-2 (*) and 3-1 (+). The residual Δ of less than 0.1 ms^{-1} is acceptably smaller than $\overline{V}'$.

The average U_R obtained with 3 antenna combinations can be transverted into the horizontal velocity vector because we know the tilt angle δ. This yields the average wind speed U_o and direction α_o (Figure 8). The subscript i denotes the values deduced with the described interferometer technique and the subscript D the values deduced with the spaced antenna drift method (ROTTGER, 1981). The similarity of these radar results with radiosonde data (⊠) gains a very reliable confidence that the interferometer method is applicable and practical.

WAVES AND TURBULENCE

Combining the results of the cross spectrum analysis of the wave events shown in Figure 5, the horizontal wave vector, respectively, horizontal phase speed V_p, wavelength λ_h and propagation direction α_p can be estimated. The analysis also yields the mean amplitude of the vertical velocity W and the mean period T of the wave. Results are shown in Figure 9. In this diagram additionally the horizontal width b of the volume probed with the applied beam

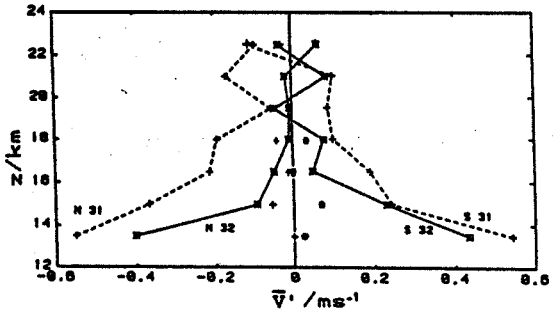

Figure 7. Average radial velocity $\overline{V}'$, measured with beams tilted to N and S.

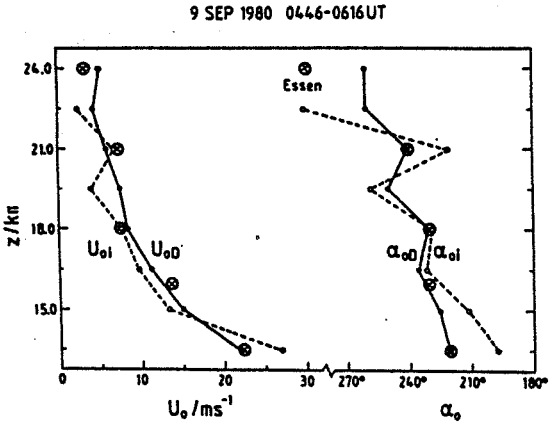

Figure 8. Average wind speed U_o and direction α_o measured with interferometer (I) and spaced-antenna drifts (D) compared with radiosonde data from Essen (⊠).

widths is indicated. It is much smaller than the horizontal wavelength λ_h. The vertical wavelength λ_z of the gravity wave events is found by cross spectrum analysis of adjacent altitude gates. Since we observed coherent wave events only over a few kilometers height range (ROTTGER, 1981) and the phase differences with height are not too pronounced, the measurement of the vertical wavelength is not too consistent. The vertical wavelength and mean period change with altitude which also makes the determination of λ_z difficult.

Knowing the horizontal wave vector from the described measurements, one can find the horizontal phase velocity V_p (with respect to the fixed observer) and the propagation direction α_p of the wave event. These are shown in Figure 10, where additionally the average background wind speed U_o and its direction α_o are inserted. We can summarize the results of the analysis of these wave events observed in the lower stratosphere:

(1) The horizontal wavelengths are about 10-20 km and increasing with height,
(2) The vertical wavelengths are 2-3 times larger than the horizontal wavelengths,
(3) The wave periods increase with altitude from about 250 s to 300 s,
(4) The mean vertical velocity amplitude increases with height from about 8 cm s^{-1} to 10 cm s^{-1},
(5) The direction of wave propagation is almost constant with altitude,
(6) The phase speed of waves is about 40 ms^{-1} and constant with altitude, it is several times larger than the mean wind above 15 km altitude,
(7) The phase speed and direction are similar to wind speed and direction close to the lowest height observed (~13.5 km),
(8) The wave phases propagate downward,
(9) From (7) and (8) it is deduced that these waves are probably generated in wind shear regions close to 13.5 km altitude.

Average vertical velocities connected with synoptic scale disturbances were analysed by ROTTGER (1981). It was estimated that they are some 10 cm s^{-1} in the lower stratosphere and can be determined with an accuracy of about 20% if one does not correct for possible tilts. Qualitative analyses of baroclinicity in the troposphere indicated tilt angle changes during frontal passages, but quantitative investigations are still under way. The aspect sensitivity (angular spectrum) and tilt (incidence) angles were also measured by VINCENT and ROTTGER (1980).

Incidence angle variations can be either explained by varying tilt angles of extended reflecting structures or by turbulence blobs moving through the

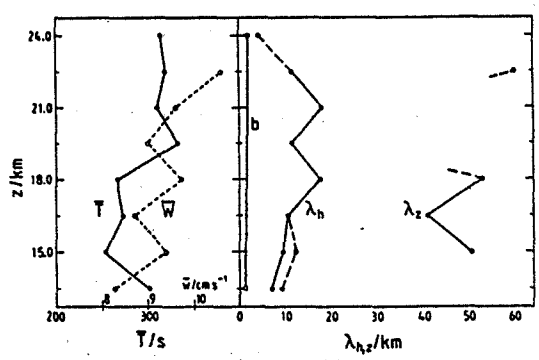

Figure 9. Height profiles of average period $\bar{T}$, quasi-vertical velocity $\bar{W}$, horizontal (λ_h) and vertical (λ_z) wavelengths.

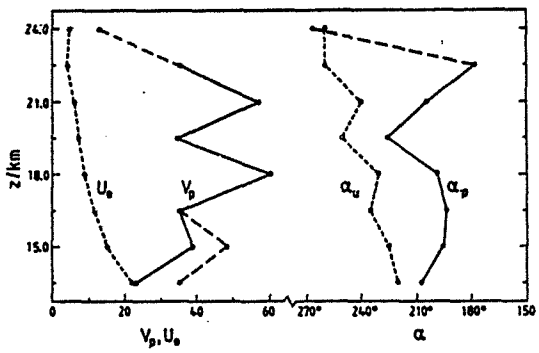

Figure 10. Phase speed V_p and propagation direction α_p of waves, and mean wind speed U_o and direction α_o.

antenna beam. The latter case may occur in the mesosphere as suggested by ROTTGER et al. (1979). To test this hypothesis we have analysed a similar event which is displayed in the height-time-intensity plot of Figure 11. It shows a fairly thin and short-lived structure at about 65 km altitude after 0710 UT. Analysing this event with the cross spectrum interferometer technique yielded the results displayed in Figure 12 (see IERKIC and ROTTGER (1984) for details). Here P_1, P_2 and P_3 are the power spectra measured over 40 s at the three different spaced antennas. They clearly show a change of Doppler shift from positive values at the beginning to negative values at the end of the event. In the lower diagrams the coherence C_{13} and phases ϕ_{13} of signals measured at antennas 1 and 3 are displayed. It is evident that the phases changed as a function of time, which would not be expected if the scattering target would have remained overhead and moved down and up in the radar beam, according to the Doppler shift. The only explanation of these observations is that a small scattering blob was in the antenna beam, moving with vertical and horizontal velocity. This analysis evidently proves the great advantage in applying the interferometer technique to avoid misinterpreting the velocity measurements, by assuming only a vertical velocity component inferred from the Doppler spectra.

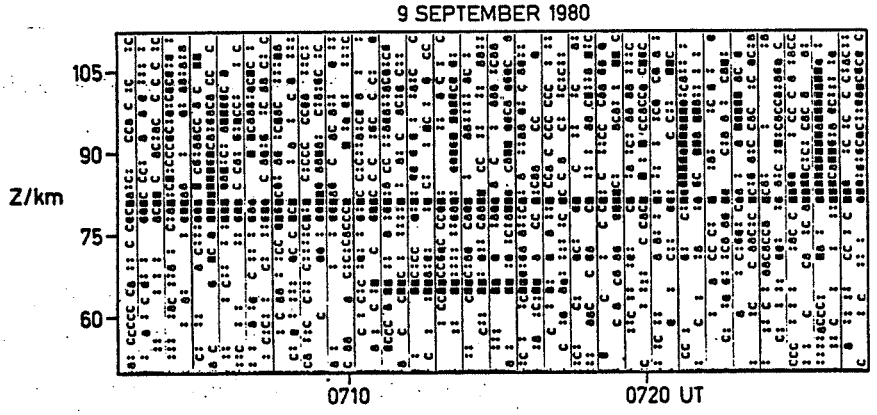

Figure 11. Height-time-intensity plot of mesospheric signals.

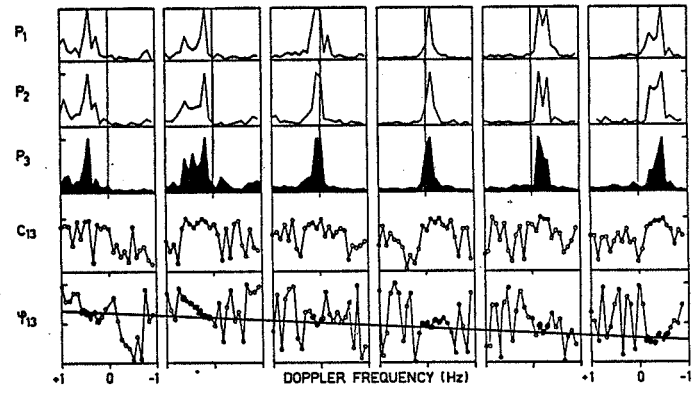

Figure 12. Power spectra P coherence C_{13} and phase ϕ_{13} of the mesospheric signal at z = 65 km. The straight line connects significant phase estimates at high coherence.

In summary we recognize that the application of the interferometer technique to MST/VHF radars is feasible and yields additional and very essential information on atmospheric structures and dynamics.

REFERENCES

Farley, D. T., H. M. Ierkic and B. G. Fejer (1981), Radar interferometry: A new technique for studying plasma turbulence in the ionosphere, J. Geophys. Res., 86, 1467-1472.

Kraus, J. D. (1966), Radio Astronomy, McGraw-Hill, New York.

Ierkic, H. M. and J. Rottger (1984), Mesospheric measurements of irregularity patches using a three-antenna interferometer, paper 3.6B, this volume.

Pfister, W. (1971), The wave-like nature of inhomogeneities in the E-region, J. Atmos. Terr. Phys., 33, 999-1025.

Rottger, H. and R. A. Vincent (1978), VHF radar studies of tropospheric velocities and irregularities using spaced antenna techniques, Geophys. Res. Lett., 5, 917-920.

Rottger, J. (1981), Wind variability in the stratosphere deduced from spaced antenna VHF radar measurements, Preprint volume 20th Conf. on Radar Meteorology, Boston, Am. Meteorol. Soc., 22-29.

Rottger, J. (1983), Techniques for measurements of horizontal and vertical velocities; Determination of horizontal and vertical wavelengths of gravity waves, Handbook for MAP, Vol. 9, 150-163; 262-267, SCOSTEP Secretariat, Dep. Elec. Computer Eng., Univ. IL, Urbana.

Rottger, J. (1984), The MST radar technique, Handbook for MAP, Vol. 13, 187-202, SCOSTEP Secretariat, Dep. Elec. Computer Eng., Univ. IL, Urbana.

Rottger, J., P. K. Rastogi and R. F. Woodman (1979), High-resolution VHF radar observations of turbulence structures in the mesosphere, Geophys. Res. Lett., 6, 617-620.

Royrvik, O. (1983), VHF radar signals scattered from the equatorial mesosphere, Radio Sci., 18, 1325-1335.

Vincent, R. A. and I. M. Reid (1983), HF Doppler measurements of mesospheric gravity wave momentum fluxes, J. Atmos. Sci., 40, 1321-1333.

Vincent, R. A. and J. Rottger (1980), Spaced antenna radar observations of tropospheric velocities and irregularities, Radio Sci., 15, 319-335.

Whitehead, J. D., W. R. From, K. L. Jones and P. E. Monro (1983), Measurements of movements in the ionosphere using radio reflections, J. Atmos. Terr. Phys., 45, 345-351.

Wohlleben, R. and H. Mattes (1973), Interferometrie in Radioastronomie und Radartechnik, Vogel-Verlag, Wurzburg.

3.6B MESOSPHERIC MEASUREMENTS OF IRREGULARITY PATCHES USING A 3-ANTENNA INTERFEROMETER

H. M. Ierkic

Arecibo Observatory
P. O. Box 995
Arecibo, Puerto Rico

J. Rottger*

EISCAT Scientific Association
P.O. Box 705
S-98127 Kiruna, Sweden

We have isolated three very interesting events of mesospheric radar returns to illustrate the potential of a three-antenna interferometer in the study of the neutral atmosphere. The first plot (Figure 1) shows contour plots of echo intensity and the presence of irregularities in isolated and well-defined regions. These measurements were carried out using the SOUSY radar in the Harz mountains in Germany, on September 9, 1980. The system frequency is 53.5 MHz. Local time is 2 hours in advance of Universal time. The irregularities wavelength is 2.81 m and the three arms of the interferometer were sampled with 167 ms of time difference.

To provide precise estimates of vertical velocities, the measured (radial) Doppler shift has to be corrected to subtract the contribution due to the horizontal motions. For near-vertical observations (zenith angle less than about 10°) it is readily shown that the rate of change of the measured phases are related to the velocities V_{ew}, V_{ns} (in the East-West and North-South directions, respectively) as indicated

$$V_{ew} \approx \frac{r}{kl} \dot{\rho}_{12} \; ; \; V_{ns} \approx - \frac{r}{kl} (\dot{\rho}_{13} + \dot{\rho}_{23})$$

with $l \approx 24.1$m, k the radar wave number, r the range (or height) and $\dot{\rho}$ the rate of change of the phase of the signals arriving at the antennas specified by the different subscripts. The geometrical arrangement of the antennas which constitute the interferometer is shown in Figure 2. The signals, after decodification, are Fourier analyzed and multiplied to form the spectrum and cross-spectrum (e.g. FARLEY et al., 1981).

Selected but representative examples of spectra and cross-spectra (coherency and phase) are presented in Figures 3a-c. All the transforms are averaged by 40 s and they have a rang of ±1 Hz with a frequency resolution of 0.083 Hz. There are some observations on the data that are worth bringing out. Figure 3a (event I) shows clearly a continuous change of Doppler shift with time and also illustrates frequency aliased spectra. The coherency maximizes within the energy containing frequency ranges and the corresponding computed phase changes, increasing steadily. Event II (Figure 3b) is more complex because it shows double-peaked spectra. From the graphs of phase it is clear that the opposite Doppler shifts are associated with physically separate regions of the atmosphere (about 4 km apart). In this example we can appreciate the great resolving capability of the interferometer. Figure 3c (event III) presents sharp and well-defined spectra and includes all (3) combinations of cross-spectra. From the high values of the coherency it can be deduced that the echoes are coming from horizontally localized regions or "blobs" (ROTTGER, 1983). The horizontal velocities for each event can be estimated measuring the rate ot change of the phases. From the data, Table 1 was constructed for the horizontal velocities.

*presently at Arecibo Observatory, Arecibo, Puerto Rico, on leave from Max-Planck-Institut fur Aeronomie, Lindau, W. Germany

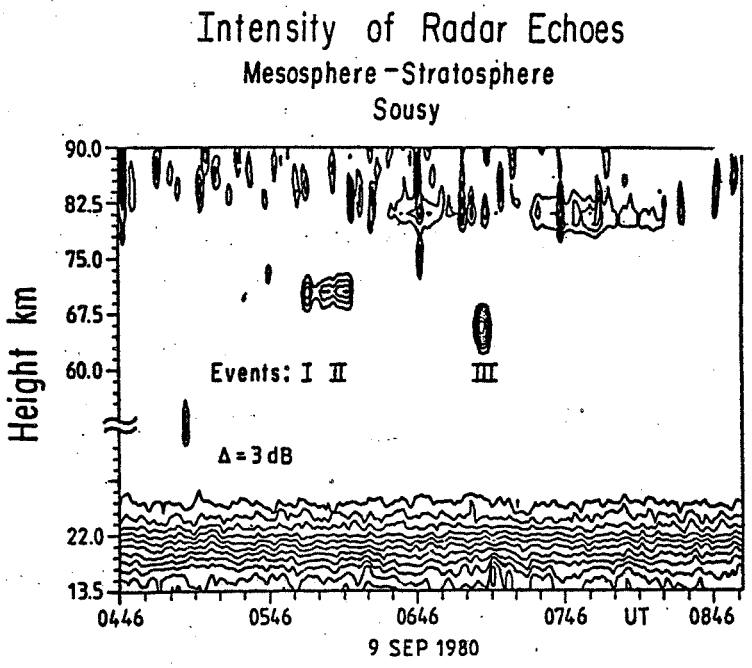

Figure I. Contour plots of the intensity of mesospheric backscattered signals. Three events are distinguished for further study.

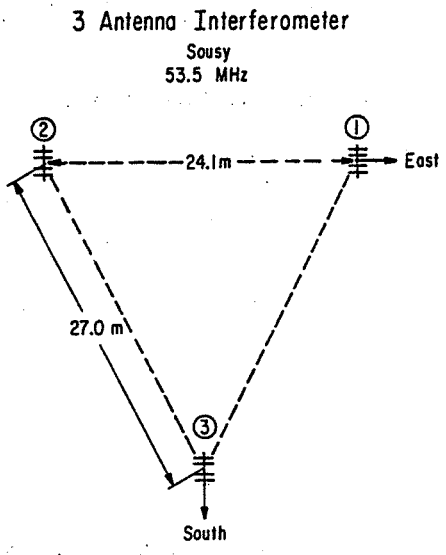

Figure 2. Geometrical configuration of SOUSY interferometer system.

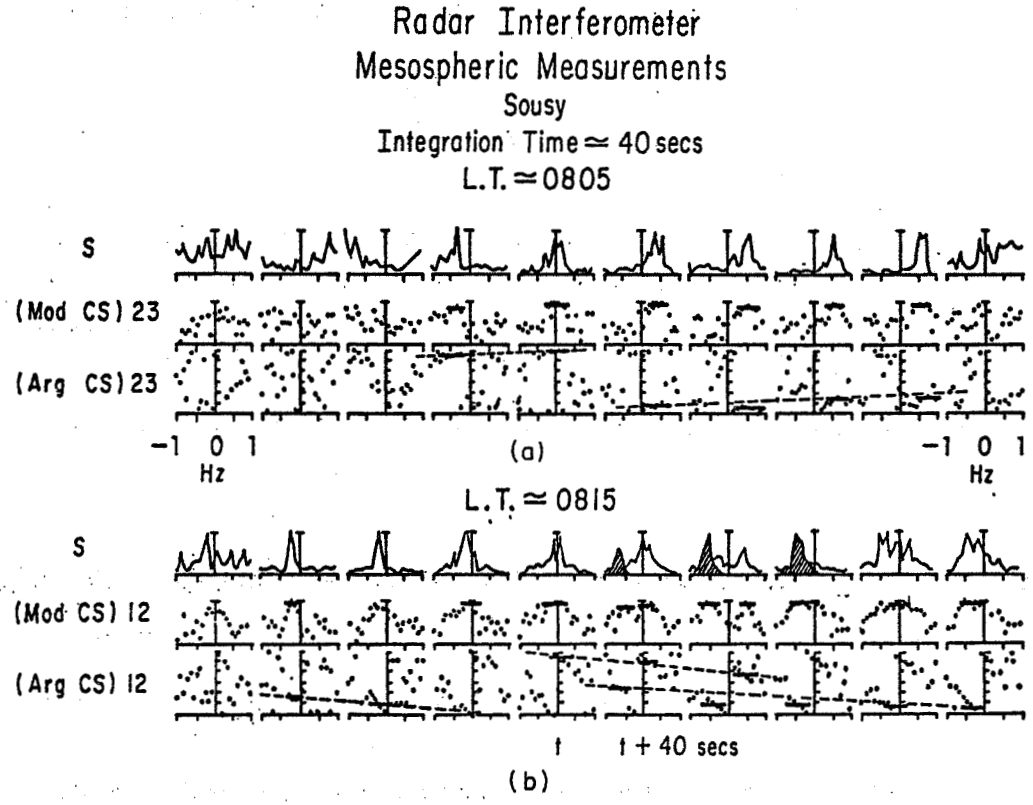

Figure 3. Measurements of spectra (s) and cross spectra (cs).
(a) Example with frequency aliased spectra.
(b) Example with double peak spectra.

Table 1.

Event	V_{ew} (m/s)	V_{ns} (m/s)	Time (LT)
I	15.4	4.7	~0803
II	30.8	15.4	~0815
III	24.2	7.8	~0915

Knowledge of the horizontal component of the velocity and of the radial (line-of-sight) velocity allows for an unambiguous estimate of the vertical component. For the data at hand and during the time that the "blobs" were observable the vertical Doppler shift changed from negative to positive in a reasonably linear fashion (to first order) and with the following parameters where T_s time within sight, V_v vertical velocity, $\dot{V}_v$ rate of change of the vertical velocity. The events tabulated in Table 2 occur within a vertical extent between 3 and 4.5 km. The third event is characterized because it has the largest values of the intensity of the echoes as well as of the coherency of the cross-spectra.

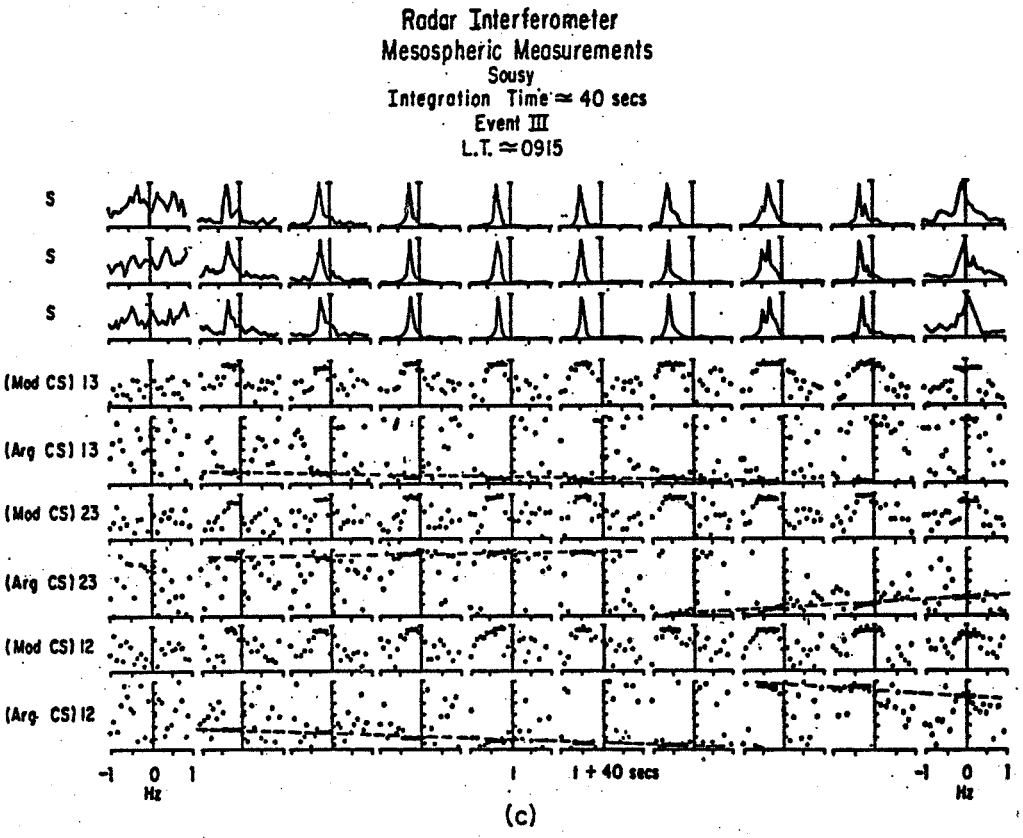

Figure 3(c). Measurements of spectra (s) and cross spectra (cs). Example of a "compact" backscattering region.

Table 2.

Event	T_s(min)	V_v(m/s)	$\dot{V}_v$(cm/s^2)
I	5.0	-3.9 → 2.2	2.0
II	4.3	-2.5 → 2.8	2.4
III	5.7	-1.9 → 1.0	0.8

The technique used here makes possible some understanding of the morphology of the scattering medium. In fact the data suggest that patchy regions ("blobs") fairly localized (to within about 3 km) exist. Moreover these blobs are carried away by (or they ride on) prevalent winds and waves. The origin of the blobs has not been investigated yet, but some preliminary notions are worth mentioning. They could result from short-scale turbulence due to the breaking of solitary waves. It is interesting to note that irregularities were observed always when the blobs were lifted upward, soon to be pushed downward. Another possibility relies on the presence of ("frozen") local deviations in the value of the index of refraction relative to the spatial average. This last interpretation is, in a sense, analogous to the well-known ionospheric holes phenomena.

Figure 4 presents, for the data analyzed, the (two-dimensional) horizontal trajectories followed by the irregularities. Event II is composed of two sub-events with geometrical separation of about 4 km. A more extended data base will be necessary to establish the frequency of occurrence of the events here described as well as their spatial distribution. This will allow better characterization of the physical picture presented and also will help to decide if estimates of the vertical profiles of the velocities are feasible.

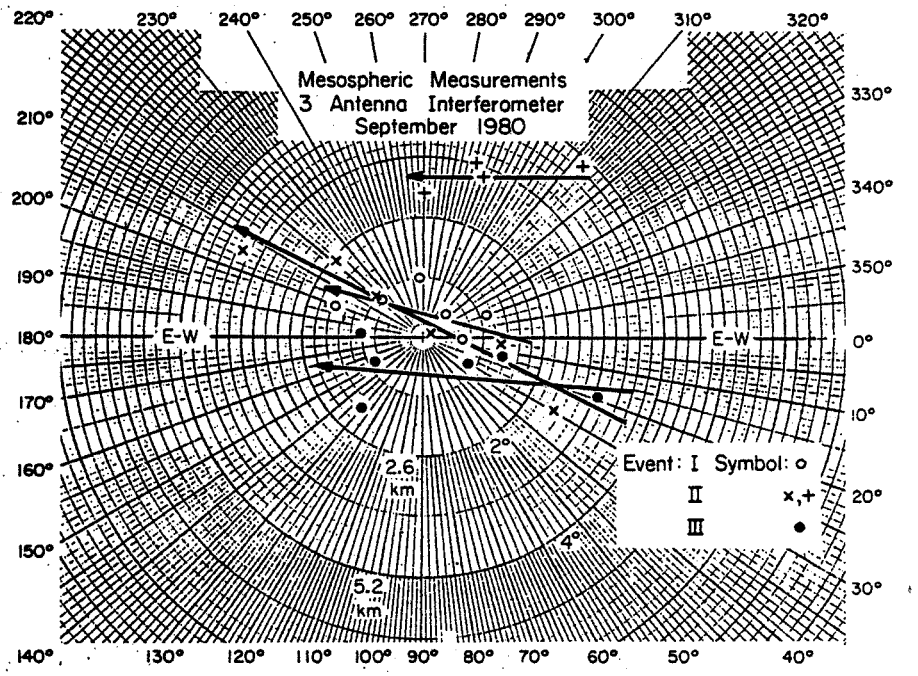

Figure 4. Horizontal trajectories of observed irregularity patches.

REFERENCES

Farley, D. T., H. M. Ierkic, and B. G. Fejer (1981), Radar interferometry: A new technique for studying plasma turbulence in the ionosphere, J. Geophys. Res., 86, 1467.

Rottger, J. (1983), Techniques for measurements of horizontal and vertical velocities, Proceedings of Workshop on Technical Aspects of MST Radar, Handbook for MAP, Vol. 9, SCOSTEP Secretariat, Dep. Elec. Eng., Univ. IL, Urbana, 150-163.

4. TECHNIQUES FOR THE STUDY OF GRAVITY WAVES AND TURBULENCE (Keynote Paper)

M. R. Schoeberl

NASA/Goddard Space Flight Center
Laboratory for Planetary Atmospheres, Code 964
Greenbelt, MD 20771

INTRODUCTION

Probably one of the most important achievements MST radars can make toward increasing our understanding of the dynamics of the atmosphere is to determine the exact relationship between the generation of turbulence and the sources of high shear or convectively unstable flows. An important theoretical tool through which we can begin to understand spontaneous generation of turbulence is the gravity-wave-breaking model. In this model, large amplitude gravity waves produce local regions where the Richardson number ($N^2/[U_z]^2$) is less than 1/4 thus giving rise to turbulent flows. Thus the appearance of turbulent layers can often be interpreted as a breaking-gravity-wave signature.

Even though the techniques for studying gravity waves and turbulence may be quite different (and historically have resulted in somewhat separate bodies of literature), it is clear from the wave-breaking model that the phenomena are intimately linked. The techniques for measurements of gravity wave flow fields and turbulent regions by MST radar should show cognizance of some of the theoretical questions raised by the wave-breaking model.

(a) Determination of Turbulent Structures

Preliminary efforts have been made to categorize turbulent phenomena observed by high power radars (e.g., ROTTGER et al., 1979). Turbulent patches often appear as distinct layers which agrees well with the monochromatic gravity-wave-breaking model. Single bursts of turbulence are more enigmatic, however. They may result from superposition of gravity waves or other unknown processes. More work can be done toward classifying and expanding the turbulent layer morphology. How fast do the layers grow; what is their depth; how long do they persist; what is their frequency of occurrence; and can they be associated with gravity-wave events?

(b) Spectral Measurements of Wind Fluctuations

Initial attempts have been made to measure the energy spectrum associated with the horizontal motions (CARTER and BALSLEY, 1982). They found that the power law dependence showed -5/3 behavior suggestive of Kolgomorov's inertial subrange for turbulent motions. This result is reasonable for smaller scale eddies, but one would not expect theories of homogeneous turbulence to apply necessarily to the larger scale convective motions touched off by gravity-wave passage. Furthermore we would, *a priori*, not expect the gravity-wave spectrum itself to exhibit the -5/3 behavior. The fluctuation spectrum may "break" at larger wave numbers toward a different power law behavior as predicted by saturation theories of gravity waves or it may not exhibit any tendency at all. Clearly, important information on small-scale processes can be gained by measurement of the spectrum.

(c) Measurements and Interpretation of the Heat and Momentum Flux

Probably the greatest impact MST radars can have on our understanding of the general circulation is an accurate measurement of the climatology of the

upward flux of momentum into the mesosphere ($\overline{u' w'} + \overline{v' w'}$) and the vertical convergence of that flux. The transport of heat by the turbulence induced by breaking waves is also of critical importance but can probably only be measured using an MST radar-lidar configuration.

Using a clever multibeam configuration VINCENT and REID (1983) have directly measured the momentum flux and found a surprising amount (1/3) of the transport in the high frequency gravity-wave field. This momentum flux may also include local transport of momentum by turbulent eddies acting on the basic shear which, of course, would not contribute to the net deceleration of the mesosphere. This may be the source of the momentum transport associated with high frequency motions.

In order to separate local transport of momentum from the upward flux of (psuedo) momentum from the troposphere, the layer fluxes should be carefully evaluated. It may also be possible to separate turbulent transport of momentum from transport by waves using the dispersion relations as a "wave transport" criteria.

(d) Relationship Between Isolated Turbulent Regions to the General Turbulent Background

As alluded to in the previous sections, the average turbulent background can produce important transports of heat, momentum and constituents. Some observers report semipermanent regions of turbulence in the upper mesosphere. How is this turbulence maintained (if a background level indeed exists)? Are there special locations for the formation of permanent turbulent layers?

(e) Determination of Vertical and Horizontal Wavelengths of Gravity Waves and Their Spectral Measurements

The development of a climatology of gravity waves in the mesosphere and stratosphere is most critical to our understanding of the circulation of that region. Information on both the horizontal wavelengths and relative frequencies are needed to determine the fluxes of momentum. Several methods are currently being used to determine directly the horizontal wavelengths including coincident spatial measurements and multibeam techniques.

The relative frequency of the gravity wave can be determined from the vertical wavelength via the dispersion relation or by independent measurement of the phase speed and background wind. The amplitude spectrum verses vertical and horizontal wave number is also useful since this can be theoretically related to the momentum transport. In addition to the local climatology of gravity waves, a global climatology is needed, and MST measurements need to be made at a variety of sites and under various conditions (e.g., summer, winter, etc.). To reiterate, since the origin of turbulence in the middle atmosphere can be linked to wave breaking, the study of gravity wave passage and subsequent turbulence formation leads to insight into both processes.

SUMMARY AND RECOMMENDATIONS

The study and measurement of gravity waves and the study of turbulence are not separate topics. The development and generation of low Richardson number flows which produce turbulent fields occurs through the saturation and/or interaction of gravity waves. It is the turbulent eddies from which the MST echo is derived. Thus it is important to determine if the "frozen turbulent field in a background flow" approximation is a valid assumption or whether the radar is measuring a property of the turbulent generation mechanism (i.e., the wave).

High power radars in the GHz frequencies have the capability of studying turbulence generation. Especially interesting are the detection of K-H CAT's eye structures. These structures are differentiated from other turbulence systems (e.g., convection) by their aspect ratio between the vertical and horizontal scale (about 1:6 ideally). Unfortunately the K-H billows cannot be detected until fully developed and thus the theory from which the aspect ratio is derived may no longer apply.

Another approach to studying both the turbulent and gravity-wave field is the compilation of spectra. Spectra are useful in a number of circumstances: first, the existence of spectra for the random fluctuation differentiates the kind of turbulent approximation and the mixing processes which may be important. For example, if the spectrum is characteristic of 2-d turbulence (horizontal) then vertical mixing is minimized. Also, 2-d turbulent spectra implies transfer of energy to large scales from smaller ones. If such transfer exists then turbulent energy may be transferred back to the gravity-wave motions.

Second, a buoyancy wave spectra contains implicit information about the distribution of energy within the gravity-wave field. The buoyancy wave spectra could be separated from the 2-d turbulence spectra by an examination of the fluctuations of the vertical velocity (2-d turbulence shows no vertical motion fluctuations). Unfortunately, nature may not be so reasonable as to present a pure 2-d turbulent field so it may, in practice, be difficult to separate the two spectra. It was also suggested that energy partitioning might be used to discriminate between the buoyancy spectra and the 2-d spectra. But this may also be difficult in practice. The buoyancy (gravity) wave spectra may also be hard to measure accurately without knowledge of the background wind, so to correct the observed frequency to the intrinsic frequency.

Finally, there have been a number of proposals that a universal gravity-wave spectrum exists in the atmosphere in analogue to the Garrett-Munk oceanic spectra. Independent constructions of spectra at various MST sites could yield important information on the global morphology or universality of spectra.

In contrast to the statistical approach of spectra construction, identification and measurement of individual gravity waves helps us understand forcing mechanisms and local polarization of gravity waves. Unfortunately, the identification of single monochromatic events with spaced receivers seems to be very difficult as gravity waves of different wave number and phase speed are often superimposed. Stratospheric measurements have been made only under the most ideal conditions when lee wave contamination was minimal.

The average momentum fluxes due to gravity waves and turbulent mixing of shear is somewhat easier to determine than the identification of individual waves. Furthermore, this quantity is probably most useful to large-scale modelers. However, care must be exercised in the measurement method so that bias toward certain wavelength gravity waves is not made. Mesospheric results indicate that most of the momentum flux is carried by high frequency short-scale gravity waves in summer, but larger scale planetary waves may contribute during winter.

Finally, it was pointed out that measurement of turbulent diffusion coefficients from radars can be misleading as turbulence is generated by breaking gravity waves between stable layers so the mixing is restricted to short vertical distances.

RECOMMENDATIONS

1. To study the generation of turbulence both the vertical and horizontal resolution need to be improved. This type of study can have a direct impact

on the measurements made by MST radars. Vertical resolution of 100 m in the mesosphere and 10 m in the stratosphere and troposphere, and horizontal beam widths of 1° - 2° as well as limited integration times (10-20 s) are required. Doppler velocities resolution of 10 cm s^{-1} is needed.

2. The measurement of the fluctuation of different types at different altitudes, and location is needed. More theoretical work needs to be done to determine to what extent the spectra are due to forcing, weak wave interaction, strong wave interaction or can be characterized by two-dimensional turbulence. Since there is some indication of an anisotropic gravity-wave spectrum (more upward propagating waves than downward propagating waves) do the analogies to oceanic spectrum still hold up?

3. Attempts to define and observe individual gravity waves should continue. Of particular interest is the distribution of gravity-wave intrinsic frequencies (background flow corrected frequencies) by horizontal wave number at different sites. We should also try to determine major sources of gravity waves.

4. Momentum flux measurements at different locations should be made both in the stratosphere and mesosphere and over varying topography and climatic conditions. A global morphology of the momentum flux and mean wind field ($\overline{u}$, $\overline{v}$, $\overline{w}$) would be very useful.

4.1A DETERMINATION OF BILLOWS AND OTHER TURBULENT STRUCTURES

P. K. Rastogi

Department of Electrical Engineering and Applied Physics
Case Western Reserve University
Cleveland, OH 44106

INTRODUCTION

Billows are regular, wave-like arrays of cross-flow vortices that develop in stratified oceanic or atmospheric flows with large shear. Atmospheric billows can become manifest through condensation. Billows are frequently seen in their characteristic cloud forms in the lower atmosphere. Under suitable viewing conditions, billows can also be seen in noctilucent clouds that form near the polar mesosphere during the summer months. Excellent examples of these cloud forms have been catalogued by SCORER (1972).

Other turbulent structures -- related to billows -- are the Kelvin-Helmholtz instability (KHI) and cat's eye structures that occur in fully developed turbulent shear flows. Shear flows may contain perturbations at many different horizontal wavelengths and vertical scales. Realistic theoretical models have been constructed to study the stability and growth of these perturbations. For the purpose of this note, it will suffice to point out that, as the local gradient Richardson number Ri is reduced below a value of about 0.25, the most rapidly growing perturbations have a wavelength (λ) that is $\sim 2\pi$ times the initial thickness, h (TURNER, 1973; GOSSARD and HOOKE, 1975). As the layer becomes completely mixed, it may eventually acquire a thickness $H \sim 5h$ (SCORER, 1969; WOODS and WILEY, 1972). Stages in the growth of a shear-flow instability have been outlined by SCORER (1969), THORPE (1969), WOODS (1969) and READINGS (1973).

In this note we outline the extent to which billows and KHI have been observed in the atmosphere, principally with the use of radars. Most of these observations are confined to the troposphere. Suggestions are made for improved radar experiments that are required to detect these structures at higher altitudes.

BILLOW OBSERVATIONS IN THE ATMOSPHERE

High-power radars operating at GHz frequencies have a sufficiently fine spatial and temporal resolution to detect billows of $\sim$100-200 m thickness. Early radar observations of billow structures and KHI in the troposphere were reported by HICKS and ANGELL (1968), and HARDY and KATZ (1969).

ATLAS et al. (1970) have used a 2.9 GHz FM-CW radar, with a height resolution of $\sim$1 m, to observe the details of growth of a KHI in the boundary layer at 300-400 m, and its eventual decay into clear-air turbulence. JAMES and BROWNING (1981) have used a similar radar, with a $\sim$30 m range resolution and Doppler capability, to observe the development of secondary billows of 350 m wavelength on primary billows of 4.2 km wavelength at heights of 7-8 km.

VHF radars operating at a typical frequency of 50 MHz have a better altitude coverage ($\sim$5-25 km and 60-90 km), but their poor spatial resolution (typically 2-5 km in the vertical and horizontal directions) usually smears the fine structure in the shear regions. Few VHF radars make use of phase-coding and decoding techniques to achieve an improved height resolution of $\sim$150 m. UHF radars provide a narrow beam, and therefore an improved horizontal resolution. In either case, the horizontal resolution is often impaired by the

integration time (∿1 min) and depends on the wind speed. For these reasons VHF and UHF radars have provided only limited evidence for billow structures in the middle atmosphere, and most of these observations are below the tropopause.

ROTTGER and SCHMIDT (1979) have used VHF observations with 150-m resolution and 30-m spacing to detect a Cat's eye structure at 4.5-km altitude. UHF observations with 150-m resolution at Arecibo (see e.g., RASTOGI, 1981) show vaguely defined large-vortex structures and bifurcating layers of turbulence in the troposphere.

In the above experiments the Doppler resolution is usually inadequate to resolve differential motions in a radar cell. WAND et al. (1983) have improved the radial velocity resolution to 4 cm s^{-1} in a UHF radar experiment, and have used this capability to detect the evolution of a KHI and a braided structure in the troposphere.

Radars, and other techniques e.g., balloon-borne sensors, have been ineffective in detecting the evolution of billow structures in the stratosphere, though estimates of CAT layer thickness are more readily obtained (BARAT, 1982; WOODMAN and RASTOGI, 1984). The CAT layer thickness can also be inferred in the mesosphere (∿0.1 to 1 km) using high-resolution VHF radars (ROTTGER et al., 1979). ROYRVIK (1983) has used an interferometric method with the Jicamarca VHF radar to infer that rotating, vortex-like, structures may occur in the mesosphere.

SUGGESTIONS FOR IMPROVED RADAR EXPERIMENTS

The existing VHF and UHF radars have provided scant results on the characteristics of billow structures in the atmosphere, due mainly to their poor vertical, horizontal and temporal resolution. It is clear that the thickness of fully grown CAT regions is usually less than 1 km.

To observe the growth of billows and KHI in CAT regions in the stratosphere and mesosphere, it is therefore necessary to:

1. Improve the vertical resolution to ∿100 m (or less) with the use of phase codes and decoding techniques,

2. reduce the horizontal smearing by limiting the beam width to 1°-2°,

3. reduce the horizontal smearing by limiting the integration time to 10-30 s, and

4. improve the Doppler resolution to ∿10 cm s^{-1} (or less) by spectral analysis of longer series of samples.

REFERENCES

Atlas, D., J. I. Metcalf, J. H. Richter and E. E. Gossard (1970), The birth of CAT and microscale turbulence, J. Atmos. Sci., 27, 903-913.

Barat, J. (1982), Some characteristics of clear-air turbulence in the middle stratosphere, J. Atmos. Sci., 39, 2553-2564.

Gossard, E. E. and W. H. Hooke (1975), Waves in the Atmosphere, Elsevier, 456

Hardy, K. R. and I. Katz (1969), Probing the clear atmosphere with high power, high resolution radar, Proc. IEEE, 57, 468-480.

Hicks, J. J. and J. K. Angell (1968), Radar observations of breaking gravity waves in the visually clear atmosphere, J. Appl. Meteorol., 7, 144-121.

James, P. K. and K. A. Browning (1981), An observational study of primary and secondary billows in the free atmosphere, Q. J. Royal Meteorol. Soc., 107, 351-365.

Rastogi, P. K. (1981), Radar studies of gravity waves and tides in the middle atmosphere: a review, J. Atmos. Terr. Phys., 43, 511-524.

Readings, C. J. (1973), The formation and breakdown of Kelvin-Helmholtz billows (working group report), Boundary Layer Meteorol., 5, 233-240.

Rottger, J., P. K. Rastogi and R. F. Woodman (1979), High-resolution VHF radar observations of turbulence structures in the mesosphere, Geophys. Res. Lett., 6, 617-620.

Rottger, J. and G. Schmidt (1979), High-resolution VHF radar sounding of the troposphere and stratosphere, IEEE Trans. Geosci. Elect., GE-17, 182-189.

Royrvik, O. (1983), VHF radar signals scattered from the equatorial mesosphere, Radio Sci., 18, 1325-1335.

Scorer, R. S. (1969), Billow mechanics, Radio Sci., 4, 1299-1308.

Scorer, R. S. (1972), Clouds of the World, David and Charles, Newton, Eng., 176.

Thorpe, S. A. (1969), Experiments on the stability of stratified shear flows, Radio Sci., 4, 1327-1331.

Turner, J. S. (1973), Buoyancy Effects in Fluids, Cambridge U. Press, 368.

Wand, R. H., P. K. Rastogi, B. J. Watkins and G. B. Loriot (1983), Fine Doppler resolution observations of thin turbulence structures in the tropostratosphere at Millstone Hill, J. Geophys. Res., 88, 3851-3857.

Woodman, R. F. and P. K. Rastogi (1984), Evaluation of effective eddy diffusive coefficients using radar observations of turbulence in the stratosphere, Geophys. Res. Lett., 11, 243-246.

Woods, J. D. (1969), On Richardson number as a criterion for laminar-turbulent-laminar transition in the ocean and atmosphere, Radio Sci., 4, 1289-1298

Woods, J. D. and R. L. Wiley (1972), Billow turbulence and ocean microstructure, Deep Sea Res., 19, 87-121.

D35

4.2A SPECTRAL MEASUREMENTS OF TURBULENCE AND GRAVITY WAVES

K. S. Gage

Aeronomy Laboratory
National Oceanic and Atmospheric Administration
Boulder, CO 80303

Recently, it has become widely recognized that gravity waves play an important role in determining the large-scale circulation of the middle atmosphere (FRITTS et al., 1984). This realization has come about, in large measure, from the realization that Rayleigh friction plays an important role in the dynamics of the middle atmosphere. Since Rayleigh friction is intimately related to the saturation of vertically propagating gravity waves, an understanding of the saturation process has become a focal point for theoretical studies (FRITTS, 1984; WEINSTOCK, 1984).

With the advent of MST radar studies of the middle atmosphere, it has become possible to determine the spectrum of horizontal atmospheric velocity fluctuations over the range of scales which comprise the gravity-wave spectrum (BALSLEY and CARTER, 1982; LARSEN et al., 1982). It has been suggested (VANZANDT, 1982; DEWAN, 1979) that these spectra are comprised of buoyancy waves. However, the interpretation of these spectra is controversial as will be discussed below.

It has long been recognized (HODGES, 1967; BRETHERTON, 1969) that turbulence can result from the breaking of vertically propagating waves. This small-scale turbulence draws its energy from the internal wave field and, at the same time, provides a sink for internal wave energy. But there is another kind of "turbulence" that ought to be considered. This "turbulence" is the quasi-two-dimensional turbulence that occupies the same range of scales as the internal wave spectrum (GAGE, 1979; LILLY, 1983, LARSEN, 1983). Since it is associated with a reverse cascade of energy, it requires a small-scale energy source, and breaking waves would appear to provide the source that is required.

The relation between waves, quasi-two-dimensional turbulence, and ordinary small-scale three-dimensional turbulence can be examined more easily in the lower atmosphere than in the middle atmosphere. One reason for this is that, in the lower atmosphere, aircraft observations can be used to help understand the nature of the frequency spectra observed by MST radar. The results of several studies (LILLY and PETERSEN, 1983; NASTROM and GAGE, 1983) have recently shown that the aircraft spectra of horizontal velocity near the tropopause is very similar to Taylor-transformed frequency spectra of horizontal velocity obtained by radar. In addition, the aircraft also measures temperature and comparison of temperature and velocity spectra can aid in the interpretation of the nature of the observed spectra (GAGE and NASTROM, 1984).

MST radars can also be used to help understand the nature of the observed spectra. For example, vertical velocity spectra have been observed (ROTTGER, 1981; BALSLEY et al., 1983; ECKLUND et al., 1983) to be quite flat under "quiet" conditions and to fall off rapidly at periods less than the Brunt-Vaisala period. These features are strongly suggestive of a spectrum of internal gravity waves. If the spectrum of vertical motions is interpreted as an internal wave spectrum, it is possible to determine the magnitude and shape of the horizontal velocity spectrum of gravity waves and compare this spectrum with the observed spectrum of horizontal velocity fluctuations (GAGE and NASTROM, 1984).

Further clues to the nature of the observed horizontal and vertical velocity spectra may be obtained by studying the altitude variation of the horizontal and vertical spectra. It may be possible, for example, to demonstrate an increase in turbulent kinetic energy at altitudes where waves dissipate. In any event, such studies should elucidate the mechanisms by which the middle atmosphere is coupled to the lower atmosphere and clarify the role of gravity waves in this process.

Summary of issues to be resolved:

* Does there exist a "universal" spectrum of internal waves in the atmosphere analogous to the Garrett-Munk spectrum in the ocean?

* What are the sources and sinks of the atmospheric internal wave spectra? How do their dynamics differ from the dynamics of oceanic internal waves?

* Are the horizontal velocity spectra due to internal waves, quasi-two-dimensional turbulence, or some other cause?

* What is the altitude dependence of wave/turbulence spectra?

* What is the interrelationship of wave spectral amplitude, turbulence intensity, and the magnitude of the horizontal velocity spectra as a function of altitude?

* How are the joint dynamics of wave/turbulence processes best described as they relate to the coupling of the lower and middle atmosphere?

Spectral measurements needed:

* Comparisons of vertical and horizontal velocity spectra and their altitude variation.

* Climatological studies of vertical and horizontal velocity spectra.

* Comparisons of radar-derived spectra with spectra determined by other techniques.

* Vertical velocity spectra need to be obtained from flat terrain to determine the dependence of vertical velocity spectra on topography.

REFERENCES

Balsley, B. B. and D. A. Carter (1982), The spectrum of atmospheric velocity fluctuations at 8 km and 86 km, Geophys. Res. Lett., 9, 465-468.

Balsley, B. B., M. Crochet, W. L. Ecklund, D. A. Carter, A. C. Riddle and R. Garello (1983), Observations of vertical motions in the troposphere and lower stratosphere using three closely-spaced ST radars, Preprint vol., 21st Conf. on Radar Meteorology, Edmonton, Alta., Sept. 19-23, 1983.

Bretherton, F. P. (1969), Waves and turbulence in stably stratified fluids, Radio Sci., 4, 1279-1287.

Dewan, E. M. (1979), Stratospheric wave spectra resembling turbulence, Sci., 204, 832-835.

Ecklund, W. L., B. B. Balsley, M. Crochet, D. A. Carter, A. C. Riddle and R. Garello (1983), Vertical wind speed power spectra from the troposphere and stratosphere obtained under light wind conditions, Proceedings of Workshop on Technical Aspects of MST Radars, Handbook for MAP, Vol. 9, SCOSTEP Secretariat, Dep. Elec. Eng., Univ. Il, Urbana, 269.

Fritts, D. C. (1984), Gravity wave saturation in the middle atmosphere: A review of theory and observations, Rev. Geophys. Space Phys. (in press).

Fritts, D. C., M. A. Geller, B. B. Balsley, M. L. Chanin, I. Hirota, J. R. Holton, S. Kato, R. S. Lindzen, M. R. Schoeberl, R. A. Vincent and R. F. Woodman (1984), Research status and recommendations from the Alaska Workshop on gravity waves and turbulence in the middle atmosphere, Bull. Am. Meteorol. Soc., 65, 149-159.

Gage, K. S. (1979), Evidence for $K^{-5/3}$ law inertial range in mesoscale two-dimensional turbulence, J. Atmos. Sci., 36, 1950-1954.

Gage, K. S. and G. D. Nastrom (1984), On the spectrum of atmospheric velocity fluctuations and their interpretation, Paper 4.2-D, this volume.

Hodges, R. R., Jr. (1967), Generation of turbulence in the upper atmosphere by internal gravity waves, J. Geophys. Res., 72, 3455-3458.

Larsen, M. F. (1983), The MST radar technique: a tool for investigation of turbulence spectra, Proceedings of Workshop on Technical Aspects of MST Radar, Handbook for MAP, Vol. 9, SCOSTEP Secretariat, Dep. Elec. Eng., Univ. Il., Urbana, 250-255.

Larsen, M. F., M. C. Kelley and K. S. Gage (1982), Turbulence spectra in the upper atmosphere and lower stratosphere between 2 hours and 40 days, J. Atmos. Sci., 39, 1035-1041.

Lilly, D. K. (1983), Stratified turbulence and the mesoscale variability of the atmosphere, J. Atmos. Sci., 40, 749-761.

Lilly, D. K. and E. Petersen (1983), Aircraft measurements of atmospheric energy spectra, Tellus, 35A, 379-382.

Nastrom, G. D. and K. S. Gage (1983), A first look at wavenumber spectra from GASP data, Tellus, 35A, 383-388.

Rottger, J. (1981), Wind variability in the stratosphere deduced from spaced antenna VHF radar measurements, Preprint vol., 20th Conf. on Radar Meteorology, Boston, MA, November 30 - December 3, 1981, 22-29.

VanZandt, T. E. (1982), A universal spectrum of buoyancy waves in the atmosphere, Geophys. Res. Lett., 9, 575-578.

Weinstock, J. (1984), Gravity wave saturation and eddy diffusion in the middle atmosphere, submitted to J. Atmos. Terr. Phys.

4.2B GRAVITY-WAVE SPECTRA IN THE ATMOSPHERE OBSERVED BY MST RADAR

A. O. Scheffler and C. H. Liu

Department of Electrical and Computer Engineering
University of Illinois
Urbana, IL 61801

Recently, based on data from radiosonde. Doppler navigation, hot-wire anemometer and Jimsphere balloon, VANZANDT (1982) proposed a universal spectrum of atmospheric buoyancy waves. The possible existence of such a universal spectrum clearly will have significant impact on several areas in the study of the middle atmosphere dynamics such as the parameterization of sub-grid scale gravity waves in global circulation models; the transport of trace constituents and heat in the middle atmosphere, etc. Therefore, it is important to examine more global wind data with temporal and spatial resolutions suitable for the investigation of the wave spectra. MST radar observations offer an excellent opportunity for such studies (BALSLEY and CARTER, 1982).

In using wind velocities measured from MST radars to investigate the gravity-wave spectra, it is important to realize that radar measures the line-of-sight velocity which, in general, contains the combination of the vertical and horizontal components of the wave-associated particle velocity. Starting from a general oblique radar observation configuration, applying the dispersion relation for the gravity waves, we relate the spectrum for the observed fluctuations in the line-of-sight gravity-wave spectrum through a filter function (SCHEFFLER and LIU, 1984). The consequence of the filter function on data analysis will be discussed. Because of the good range resolution in many existing MST radars, it is possible to obtain two-dimensional spectra from observed data. The interpretation is, however, complicated by the fact that most observations were carried out in the oblique mode. Transformation formulae will be presented to relate the observed two-dimensional k_z'-ω spectra to the k_z-ω spectra, where k_z' is the wave number along the radar beam direction while k_z is the wave number along the vertical direction. Some observational results are presented in Figures 1, 2, 3, and 4.

REFERENCES

Balsley, B. B. and D. A. Carter (1982), The spectrum of atmospheric velocity fluctuations at 8 km and 86 km, Geophys. Res. Lett., 9, 465-468.

Scheffler, A. O. and C. H. Liu (1984), Observations of gravity wave spectra in the atmosphere by MST radar, submitted to Geophys. Res. Lett.

VanZandt, T. E. (1982), A universal spectrum of buoyancy waves in the atmosphere, Geophys. Res. Lett., 9, 575-578.

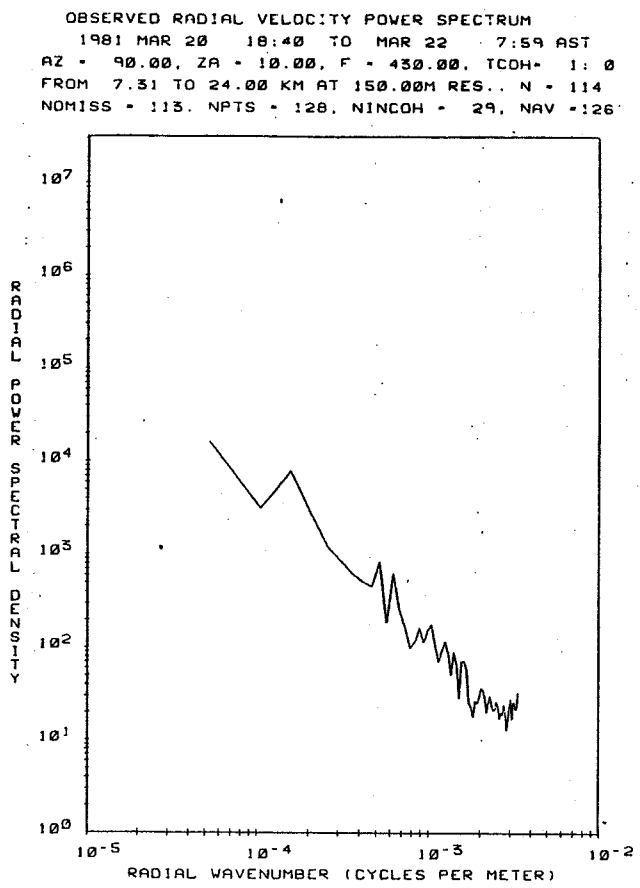

Figure 1. Wind fluctuation spectra observed by a radar operating obliquely assuming the wave-associated spectrum behaves as $f^{-5/3}$. The solid curve corresponds to $\theta_B = 15°$. The dotted curve corresponds to $\theta_B = 5°$.

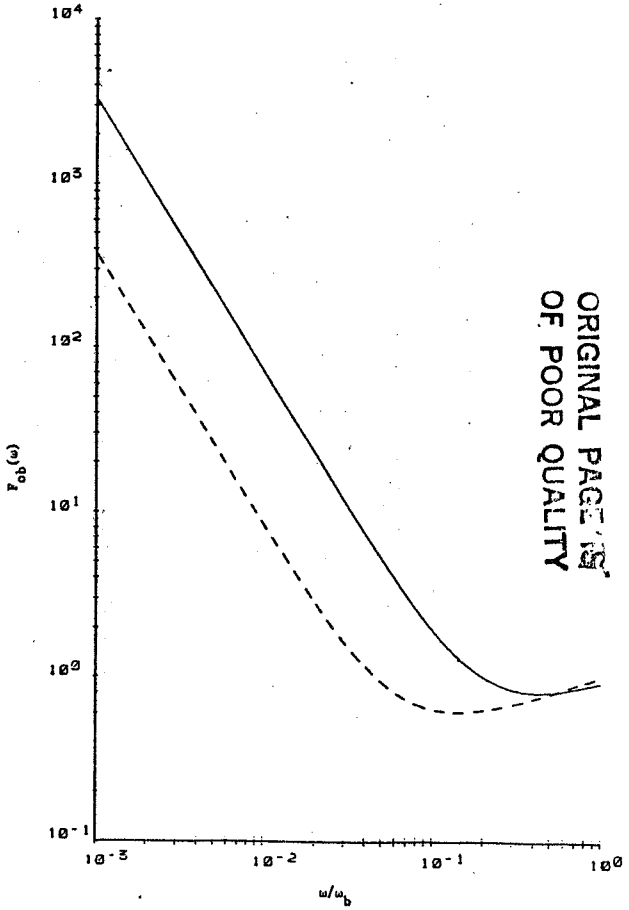

Figure 2. Observed wind fluctuation inverse wavelength spectrum by oblique radar with $\theta_B = 10°$. Spectrum is the average of 29 spectra computed from velocity profiles that were coherently integrated for a period of 1 hour. Total data et covered 35 hours.

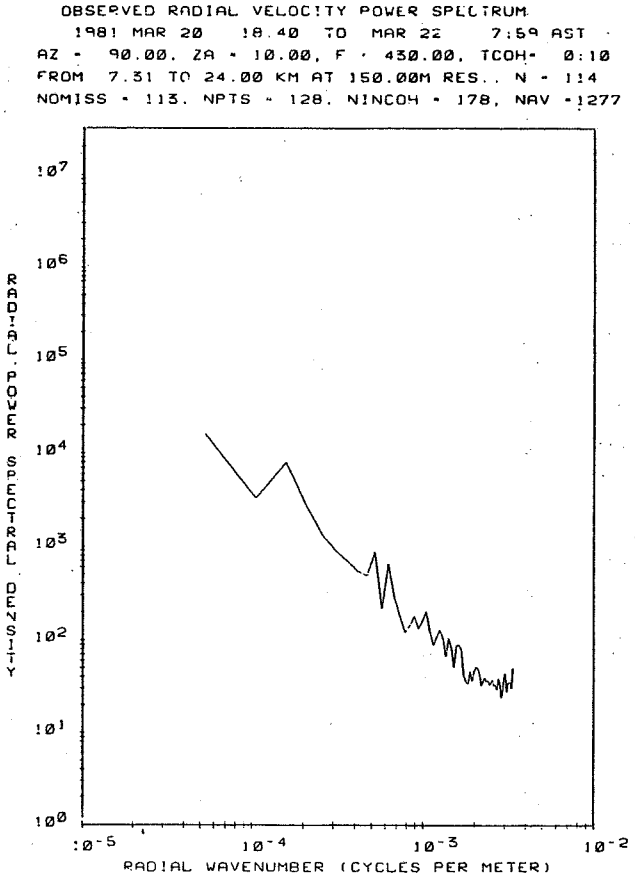

Figure 3.. Observed wind fluctuation inverse wavelenght spectrum for the same radar data as in Figure 2, except the spectrum is the average of 178 spectra computed from velocity profiles that were coherently integrated for 10 min periods.

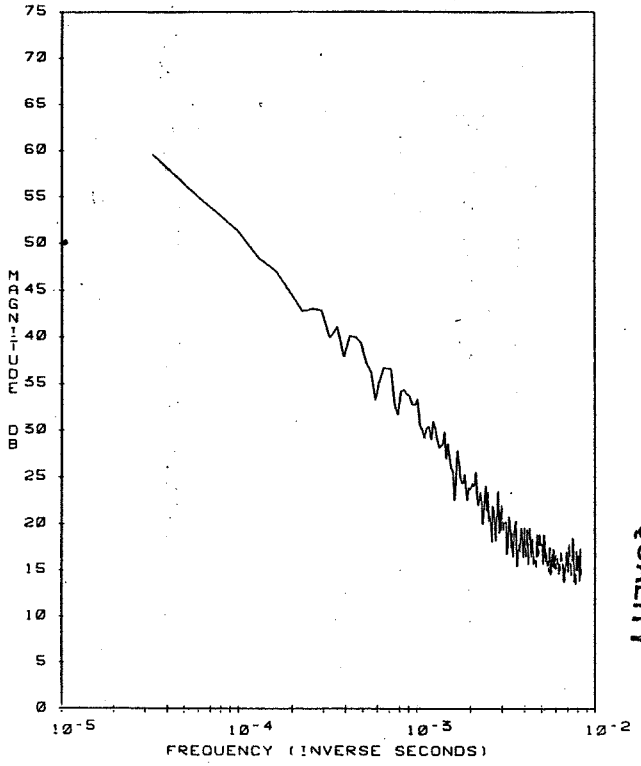

Figure 4. Observed wind fluctuation frequency spectrum by oblique radar with $\theta_B = 10°$. Spectrum is the average over 6 range heights. The spectra at each range height is the average of 4 consecutive spectra in time.

4.2C HIGH RESOLUTION EVIDENCE FOR THE GARRETT-MUNK SPECTRUM OF STRATOSPHERIC GRAVITY WAVES

E. M. Dewan, N. Grossbard, A. F. Quesada and R. E. Good

Air Force Geophysics Laboratories
Hanscom AFB, MA 01731

Vertical profiles of scalar horizontal winds have been measured at high resolution (10 m) in the 13 to 37 km region of the stratosphere (DEWAN et al., 1984a,b). This resolution (at that range of altitude) represents the state-of-the-art, and is unique. The technique used smoke trails laid by rockets in the stratosphere, and were taken by AFGL at Wallops Island, VA, White Sands Missile Range, NM, and Ft. Churchill, Canada, in the 1977-78 time period. Two or three cameras were used to give the time-lapse photographs. Our goal was to ascertain whether or not the internal waves of the stratosphere behave consistently with the Garrett-Munk model which was originally created for oceanic internal waves. Five profiles of horizontal wind are presented in Figures 1 through 5; their power spectral densities (PSDs) are shown superposed on Figure 6, and their average is shown on Figure 7. It is found that (1) they closely fit a straight line on a log-log graph even to wavelengths as small as 40 m, and (2) the average slope is -2.7 .2 (standard error = 0.1). We conclude that (1) stratospheric internal waves obey the Garrett-Munk model for vertical wave numbers, (2) there is not statistically significant evidence for a break in the curve at high wave numbers when due allowance is made for aliasing effects, and (3) the power density level of the spectra are almost equal on a log-log scale in spite of the difference in time, season, and geographical location.

REFERENCES

Dewan, E. M., N. Grossbard, A. F. Quesada, and R. E. Good (1984a), Spectral analysis of 10 m resolution scalar velocity profiles in the stratosphere, Geophys. Res. Lett., 11, 80-83.

Dewan, E. M., N. Grossbard, A.F. Quesada, and R. E. Good (1984b), Correction, Geophys. Res. Lett., 11, 624.

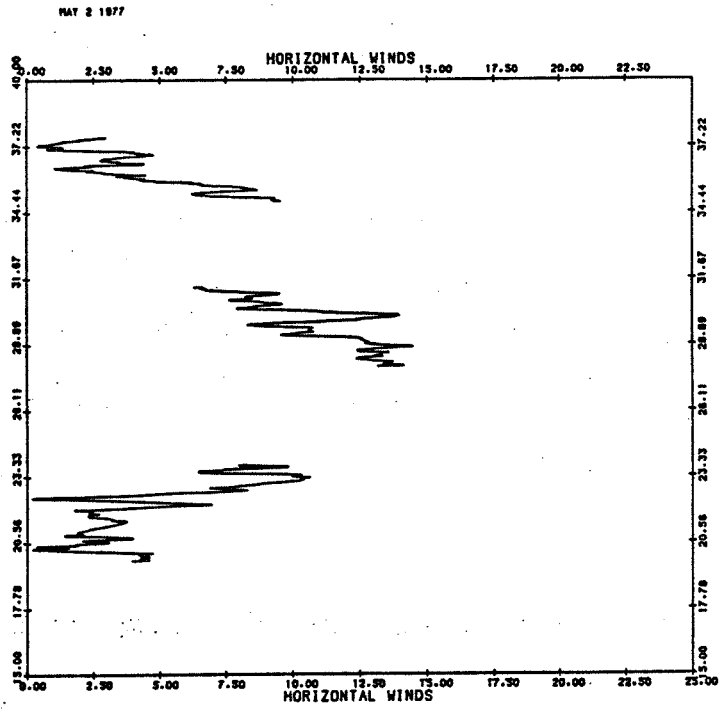

Figure 1. Profile of horizontal winds, May 2, 1977.

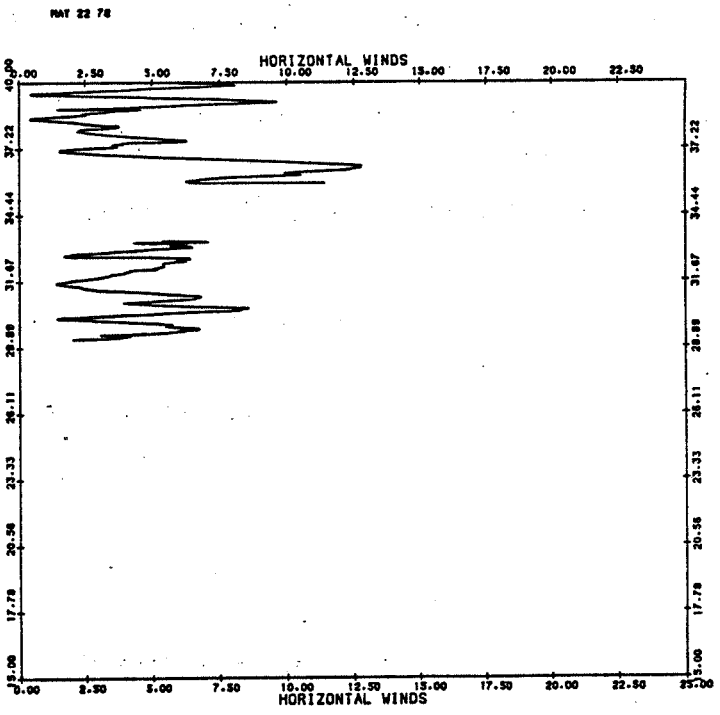

Figure 2. Profile of horizontal winds, May 22, 1978.

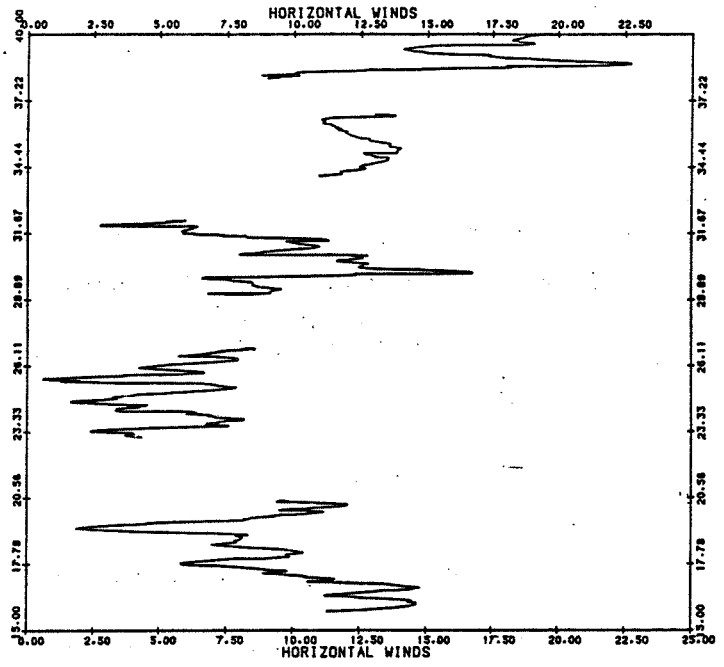

Figure 3. Profile of horizontal winds, September 12, 1978.

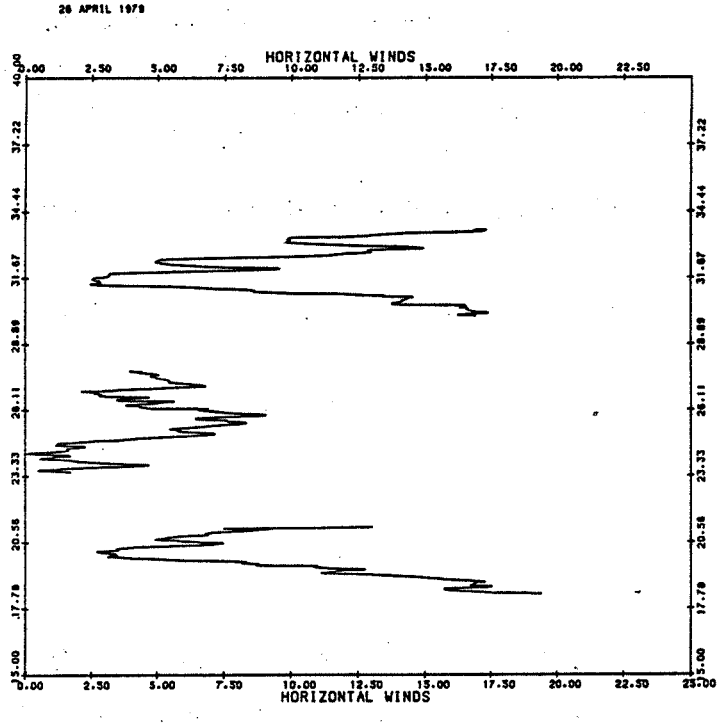

Figure 4. Profile of horizontal winds, April 26, 1979.

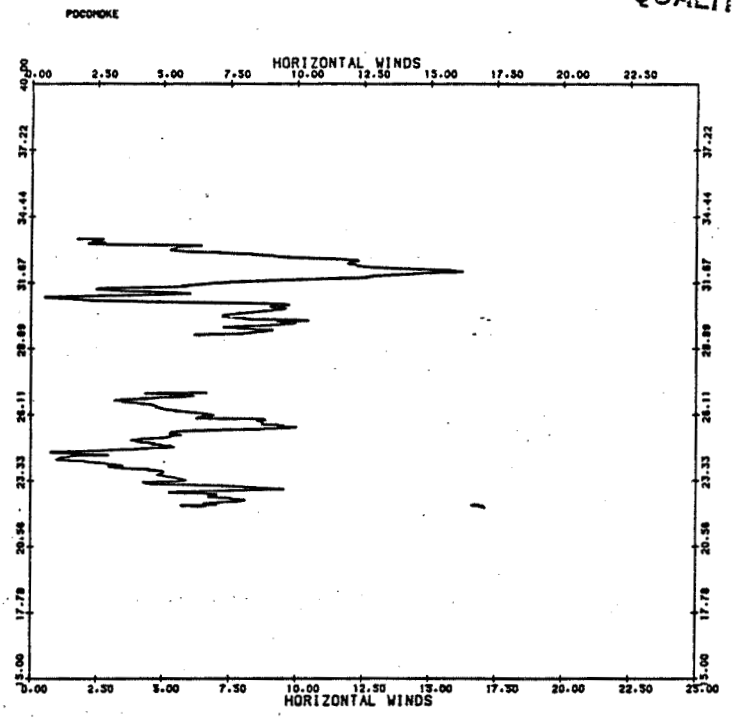

Figure 5. Profile of horizontal winds, Pocomoke.

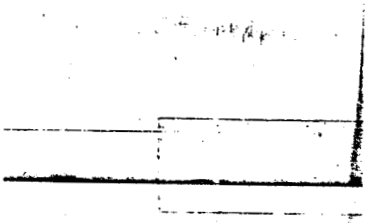

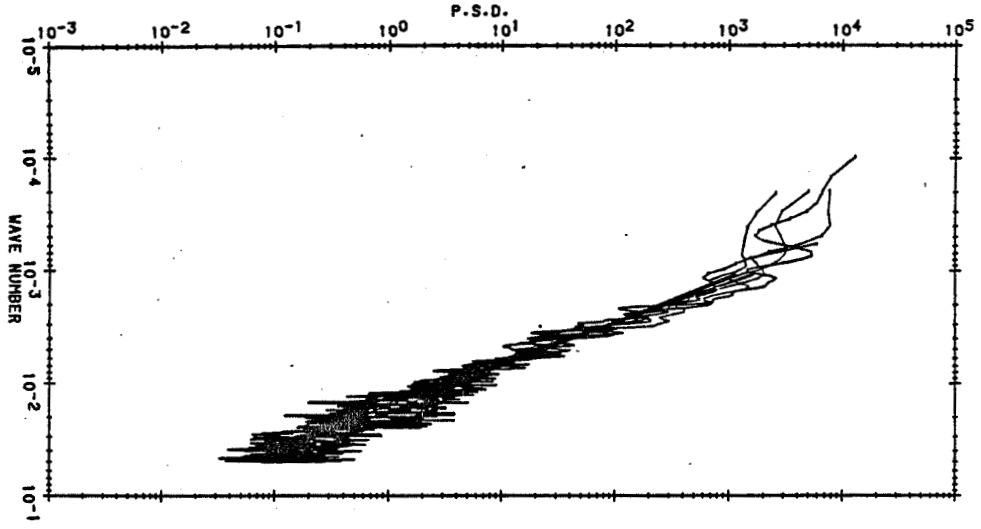

Figure 6. Superposed power spectral densities of all profiles.

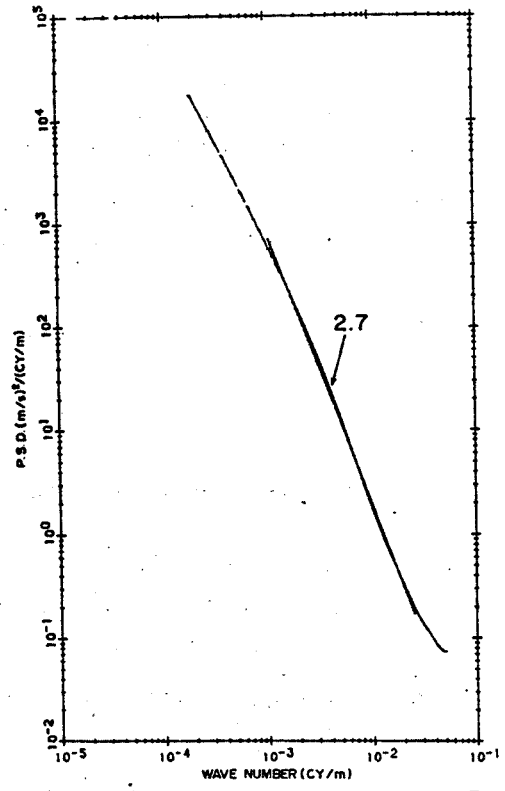

Figure 7. Averaged power spectral densities of all profiles.

4.2D ON THE SPECTRUM OF ATMOSPHERIC VELOCITY FLUCTUATIONS SEEN BY MST/ST RADAR AND THEIR INTERPRETATION

K. S. Gage

Aeronomy Laboratory
National Oceanic and Atmospheric Administration
Boulder, CO 80303

G. D. Nastrom

Control Data Corporation
P. O. Box 1249
Minneapolis, MN 55440

ABSTRACT

We consider the observations of the spectrum of atmospheric motions over the range of periods from a few minutes to many hours that have been made with ST/MST radars in the past five years. This range of periods includes the periods associated with buoyancy waves and the scale of atmospheric motions often referred to by meteorologists as the mesoscale. We consider both the spectra of horizontal and vertical velocities and examine their interpretation in terms of buoyancy wave theory and turbulence theory. To help in interpreting these spectra we present some recently determined aircraft wave number spectra.

INTRODUCTION

In recent years it has become possible to observe continuously the atmospheric wind field above a particular location using clear-air Doppler radars. These radars are referred to here as ST/MST radars although they are increasingly being called "wind profilers" by meteorologists. Several studies have been made of wind variability in the troposphere and stratosphere using the Sunset and Platteville ST radars in Colorado, the Poker Flat MST radar in Alaska and the SOUSY MST radar in the Federal Republic of Germany, besides brief campaigns elsewhere.

Time-series analysis of wind records measured by clear-air Doppler radar have yielded spectra of the horizontal and vertical winds. The frequency spectra of the horizontal wind typically possess an $f^{-5/3}$ dependence while the frequency spectra of the vertical velocity is rather flat with a sharp fall-off at periods below the Brunt-Vaisala period. Although it is fairly clear that the vertical velocity spectra are due to waves, the horizontal velocity spectra have been attributed to quasi-two-dimensional turbulence by some authors and to a spectrum of internal (buoyancy) waves by others.

In order to explore the nature of the radar-observed spectrum of horizontal wind we make use of velocity spectra in the wave number domain obtained recently from spectral analysis of a large set of aircraft winds obtained during the Global Air Sampling Program (GASP). In addition to the GASP horizontal wind spectra we also make use of the temperature spectra obtained from the GASP data set. As a final diagnostic tool we compare the consistency of the horizontal velocity spectra with the radar-observed vertical velocity spectrum under the hypothesis that both spectra are due to a common spectrum of internal waves.

SPECTRA OBSERVED BY ST/MST RADARS

During the past five years several authors have examined the spectral properties of the atmospheric wind field using ST/MST radars. GAGE and CLARK (1978) studied the wind variability observed by the Sunset radar during a jet stream passage. ROTTGER (1981) presented a study of stratospheric wind

variability using the spaced-antenna technique. BALSLEY and CARTER (1982) and LARSEN et al. (1982) presented spectra determined from wind measurements of the Poker Flat radar. The Balsley-Carter spectra for zonal velocity at 8 km and 86 km are reproduced in Figure 1. They show a clear $f^{-5/3}$ dependence down to the smallest scales measured after correction for contamination by vertical velocities near the Brunt-Vaisala period.

The spectrum of vertical velocity can similarly be determined from time-series analysis of radar-measured vertical velocities. ROTTGER (1981) presented the first spectra of vertical velocity. Vertical velocity spectra were subsequently determined from an array of vertically looking ST radars used in France during ALPEX (BALSLEY et al., 1983; ECKLUND et al., 1983). Figure 2 contains the vertical velocity spectra determined from the ALPEX data together with a vertical velocity spectrum determined from Poker Flat data. As we shall show below, the spectrum of vertical velocity is useful in the quest to differentiate waves from turbulence.

INTERPRETATION

In this section we briefly summarize the theoretical arguments which form the basis of the two interpretations which have been offered to explain the spectra presented here.

(a) Quasi-Two-Dimensional Turbulence

The general theory for two-dimensional turbulence has been presented by KRAICHNAN (1967) and KRAICHNAN and MONTGOMERY (1979). In the atmosphere, of course, turbulence is not strictly two-dimensional as pointed out by CHARNEY (1971). According to Charney energy should be distributed equally between the

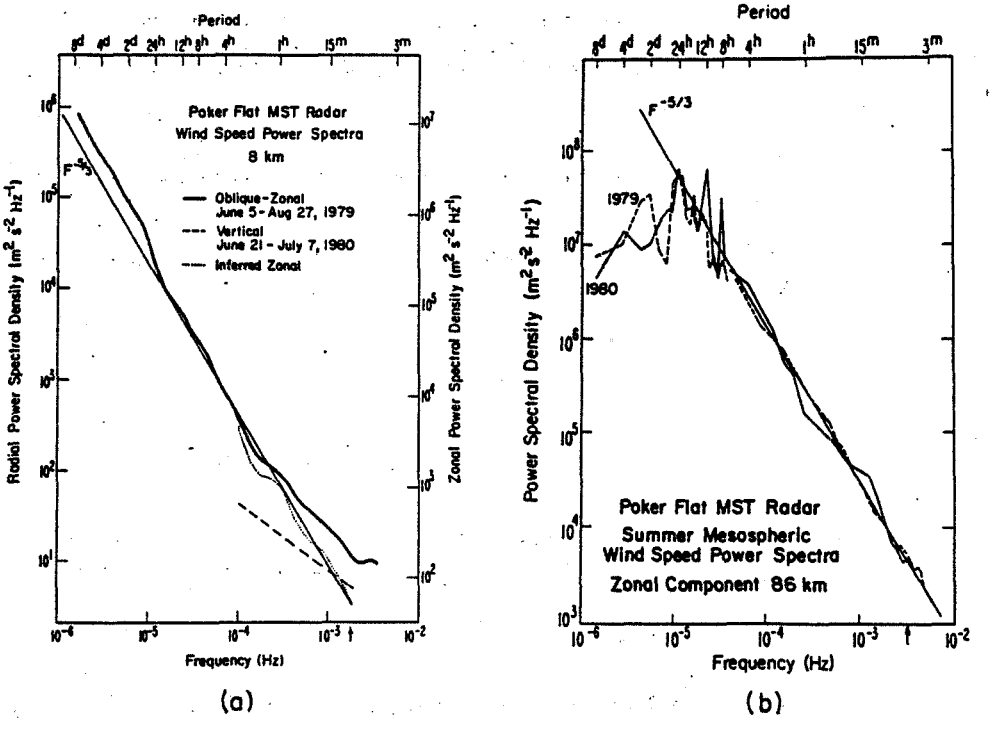

Figure 1. Power spectrum of the zonal wind observed at Poker Flat, Alaska, radar: a) 8 km and b) 86 km (BALSLEY and CARTER, 1982).

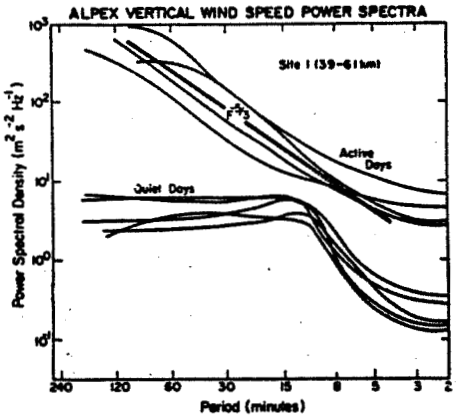

Figure 2. Power spectra of vertical velocity for quiet and active periods observed in southern France during ALPEX (BALSLEY et al., 1983).

two components of horizontal kinetic energy (zonal and meridional) and potential energy. Kraichnan showed that two inertial ranges are pertinent to turbulence in two dimensions: a k^{-3} enstrophy cascading range at scales smaller than the scale of energy insertion and a $k^{-5/3}$ reverse energy cascading inertial range at scales larger than the scale of energy insertion. GAGE (1979) suggested that this theory of turbulence might explain the observed mesoscale spectra if there were two sources of atmospheric turbulence kinetic energy: a large-scale one and a small-scale one as shown schematically in Figure 3. LILLY (1983) explored these ideas in more detail and concluded that only a few percent of small-scale energy would need to be reverse cascaded to larger scales in order to explain the observed mesoscale spectra.

The turbulence theory invokes dimensional arguments to determine the spectral shape within the two inertial ranges. For the enstrophy cascading range the spectrum has the form

$$E(k) = \alpha_1 \eta^{2/3} k^{-3} \tag{1}$$

where η is the enstrophy cascade rate and α_1 is a universal constant. For the reverse energy cascading range

$$E(k) = \alpha_2 \left(\frac{dE}{dt}\right)^{2/3} k^{-5/3} \tag{2}$$

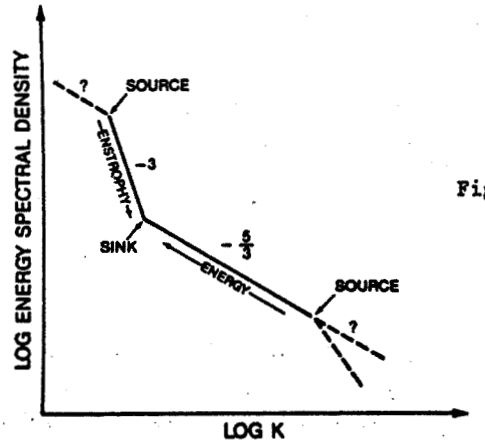

Figure 3. Schematic two-dimensional turbulence spectrum (LARSEN et al., 1983).

where dE/dt is the rate of energy insertion at the small-scale source and α_2 is also a universal constant. While the turbulence theory is formulated in the spatial domain, spectral shape of frequency and wave number spectra should be identical to the extent that the Taylor transformation is valid, as discussed below.

(b) Internal Wave Spectra

The development of a dynamical theory for a spectrum of internal waves has proceeded rapidly over the past decade. GARRETT and MUNK (1972, 1975) pioneered this effort by showing how diverse observations of ocean spectra could be given a unified treatment by hypothesizing that they were all due to different sampling strategies of a common spectrum of internal waves. A central element of the theory is that the waves obey the dispersion relation

$$\left(\frac{\omega}{N}\right)^2 = \frac{k_H^2}{k_H^2 + k_z^2} \qquad (3)$$

In Equation (3) k_H and k_z are horizontal and vertical wave numbers, ω is the angular frequency ($\omega \equiv 2\pi/\tau$; where τ is the period) and N is the Brunt-Vaisala or buoyancy frequency ($N^2 = g/\theta\ \partial\theta/\partial z$; where g is gravitational acceleration and θ is potential temperature and z is the vertical coordinate). This dispersion relation dictates the relative contribution of wave energy to vertical and horizontal velocity components as a function of frequency. Briefly, the u-, v-, and w-spectra are related through polarization relations and each is a universal function of frequency when scaled by the Brunt-Vaisala frequency N. Kinetic energy is supposed to be distributed equally between the two horizontal velocity components and the horizontal kinetic energy is supposed to equal the potential energy.

As the theory has been developed for the ocean, and ω^{-2} spectrum is pertinent to horizontal velocities and temperature or vertical displacement. An ω^0 spectrum for vertical velocity with sharp cutoffs at inertial and buoyancy frequencies is consistent with this picture. The k_x and k_z spectra are related to the above through the dispersion relation. In particular, k_x spectra have a k^{-2} power law dependence out to a transition wave number k_* and beyond that a $k^{-2.5}$ dependence.

The theory of Garrett and Munk depends upon the empirical fitting of observed spectra. While this was done successfully for the ocean and has been tested extensively, only recently has a serious attempt been made to extend the theory to the atmosphere. VANZANDT (1982) showed that it was possible to extend the internal wave description of velocity spectra to the atmosphere with only apparently minor modifications. The modifications required included a change in spectral slope from -2 for the ocean to -5/3 for the atmosphere.

WAVE NUMBER SPECTRA FROM GASP AIRCRAFT DATA

As mentioned above, a complete description of atmospheric fluctuation spectra requires analysis in the spatial domain as well as the temporal domain. In many ways the internal wave spectra are best described in the temporal domain while turbulence theory is predicted on a spatial description. Within the context of turbulence theory it is conventional to relate spatial and temporal properties through a Taylor transformation. This transformation simply assumes that all scales of turbulence fluctuations move with the same advection velocity. This aspect of the subject has been explored in some detail by BROWN and ROBINSON (1979). These authors were able to show the validity of the Taylor transformation on scales of order 500-1000 km from an examination of eastern European rawinsonde data.

The GASP data permit an examination of atmospheric spectra over scales ranging from a few km to nearly 10,000 km. Thus, there is an overlap of scale sizes in the GASP wave number spectra with earlier large-scale spectral analyses e.g., CHEN and WIIN-NIELSEN (1978), BOER and SHEPHERD (1983). The data collection phase of GASP was conducted during 1975-1979, with meteorological and trace constituent data automatically recorded with instruments placed aboard Boeing 747 airliners in routine commercial service. Wind data were taken from the onboard computer, which was linked to the inertial navigation system, and have a random error of five percent of the reported value. There are 6945 flights in the GASP data set, with over 0.6 million observations. All GASP data are archived at the National Climatic Center, Asheville, North Carolina.

Figure 4 shows the spectra of zonal and meridional winds over the range of wavelengths from 150 to 4800 km. Tropospheric spectra and stratospheric spectra are contained in Figure 4a and 4b, respectively. These spectra were obtained by analysis of the longest flights at constant altitude in the GASP data set. GASP data were recorded at five minute intervals (75 km intervals at a nominal ground speed of 250 ms^{-1}) at all times during flights above 6 km; about 80 percent of the data fall in the altitude range 9-13 km.

Several features of the wave number spectra of Figure 4 are worth noting. At wavelengths larger than 500-700 km the spectral slope approaches k^{-3}. At wavelengths less than about 500 km the spectral slope is close to $k^{-5/3}$. The spectral amplitude is nearly the same for the zonal and meridional components of velocity and the magnitude of the spectra vary little between the troposphere and the stratosphere. A more detailed analysis of the GASP data, including a limited sample of high-resolution data, has recently been prepared (NASTROM and GAGE, 1984).

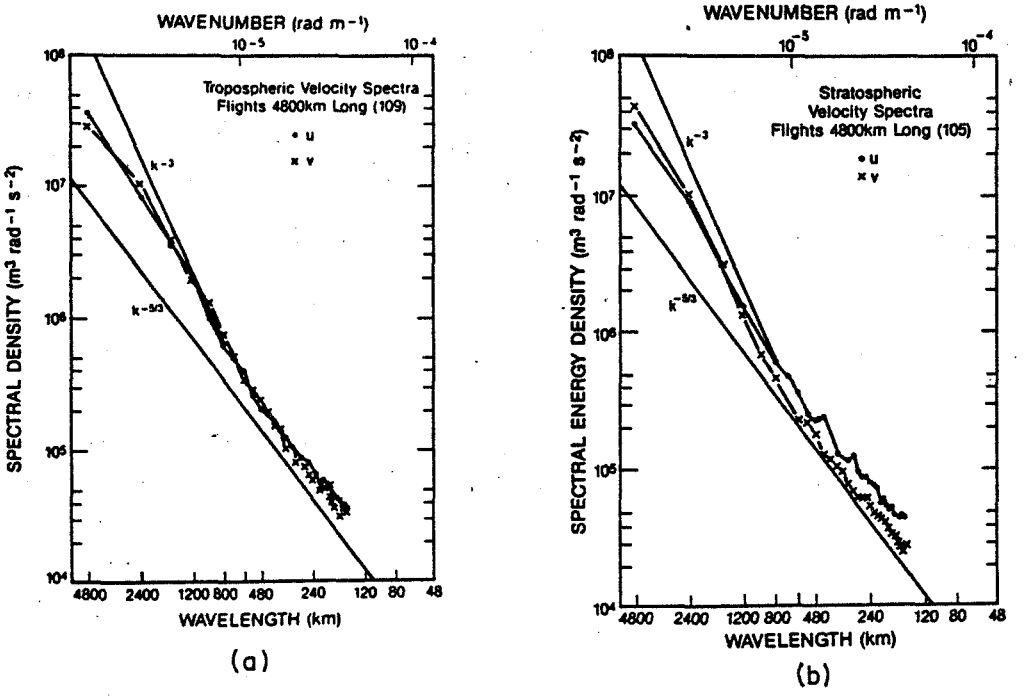

Figure 4. Horizontal velocity spectra determined from GASP flights at least 4800 km long: a) troposphere and b) stratosphere.

COMPARISON OF WAVE NUMBER SPECTRA DETERMINED BY AIRCRAFT WITH FREQUENCY SPECTRA DETERMINED BY RADAR

The radar-observed frequency spectra of horizontal velocity can be compared with aircraft-observed wave number spectra by applying the Taylor transformation to the frequency spectra. Such a comparison is shown in Figure 5 which has been adapted from LILLY and PETERSEN (1983). In this figure the Taylor-transformed Balsley-Carter spectrum is compared with the GASP wave number spectrum of Figure 4. Throughout the atmospheric mesoscale the two spectra agree very well, both exhibiting a -5/3 slope. While the agreement seen here is entirely consistent with expectations for turbulence it does not rule out the possibility the spectrum is comprised of internal waves or due to some other process. Indeed, the shape and magnitude of these spectra are in reasonable accord with the model internal wave spectra of VANZANDT (1982).

COMPARISON OF GASP KINETIC AND POTENTIAL ENERGY SPECTRA

According to turbulence theory (CHARNEY, 1971), there should be an equipartitioning between each of the two components of horizontal velocity and potential energy. That is, for turbulence, kinetic energy should be about twice the potential energy. For a spectrum of waves there should be equipartitioning between the total kinetic energy and potential energy. An examination of the ratio of kinetic to potential energy therefore can be used to help to differentiate between waves and turbulence.

The potential energy spectrum $\Phi_{P.E.}$ is related to the temperature spectrum $\Phi_{\theta\theta}$ by

$$\Phi_{P.E.} = \frac{N^2}{\left(\frac{\partial\theta}{\partial z}\right)^2} \cdot \frac{1}{2} \Phi_{\theta\theta} = \frac{g^2}{2N^2\theta^2} \Phi_{\theta\theta} \qquad (4)$$

Wave number spectra of potential temperature from GASP data are presented in Figure 6. Note that the magnitude of the potential temperature spectrum is significantly larger in the stratosphere than in the troposphere. The reason for this is the larger hydrostatic stability in the stratosphere.

The potential temperature spectra contained in Figure 6 have been converted to potential energy spectra by use of Equation (4). The factor $g^2/2N^2\theta^2$ used to convert tropospheric and stratospheric spectra were 4 and 1.5, respectively. Potential energy spectra obtained in this way are compared with

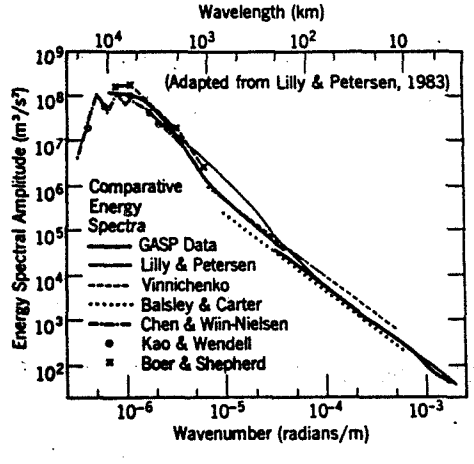

Figure 5. Composite horizontal energy spectra showing comparison of aircraft wave number spectra with Taylor-transformed radar frequency spectrum (adapted from LILLY and PETERSEN, 1983).

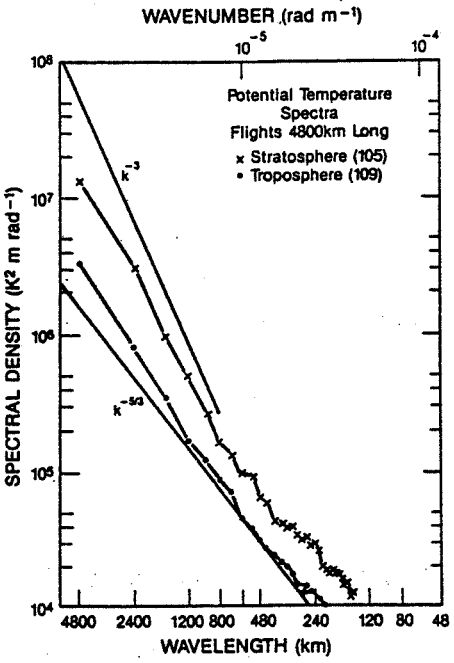

Figure 6. Potential temperature spectra in the troposphere and stratosphere from GASP aircraft flights at least 4800 km long.

the kinetic energy spectra obtained on the same flights in Figure 7. For both the troposphere and the stratosphere the comparisons in Figure 6 show a ratio of potential to kinetic energy closer to 2 than 1 over much of the spectrum. While this result favors the turbulence interpretation, it cannot be considered conclusive because of the uncertainty in the value of $g^2/2N^2\theta^2$ used to convert the potential temperature spectrum to a potential energy spectrum (GAGE and NASTROM, 1984).

COMPARISON OF RADAR OBSERVED HORIZONTAL AND VERTICAL VELOCITY SPECTRA

Most of this paper has been concerned with the interpretation of the horizontal velocity frequency spectrum observed by radar in the light of a recent study of wave number spectra obtained from aircraft observations. These comparisons have shown that the observed spectra are quite similar in the wave number and frequency domains. While these results support the turbulence interpretation they do not rule out the wave interpretation. In this section we compare the horizontal and vertical velocity spectra observed by radar to determine their consistency with the idea that these spectra are both due to internal waves. From the comparison of horizontal velocity spectra presented in Figure 5 it can be seen that these spectra are fairly universal. Not so much is known about the universality of the vertical velocity spectra although they would necessarily be fairly universal if both the horizontal and vertical spectra were due to waves.

Before examining the consistency of atmospheric spectra of horizontal and vertical velocities, it is useful to review the situation in the ocean where both horizontal and vertical spectra are thought to be due to internal waves. Figure 8 contains a comparison of vertical velocity spectra and horizontal velocity spectra from the ocean (ERIKSEN, 1978). These spectra are fairly universal in accord with the Garrett-Munk theory. The horizontal spectrum $E_H(\omega)$ can be expressed in terms of the vertical spectrum $E_V(\omega)$ using the model equation (ERIKSEN, 1978):

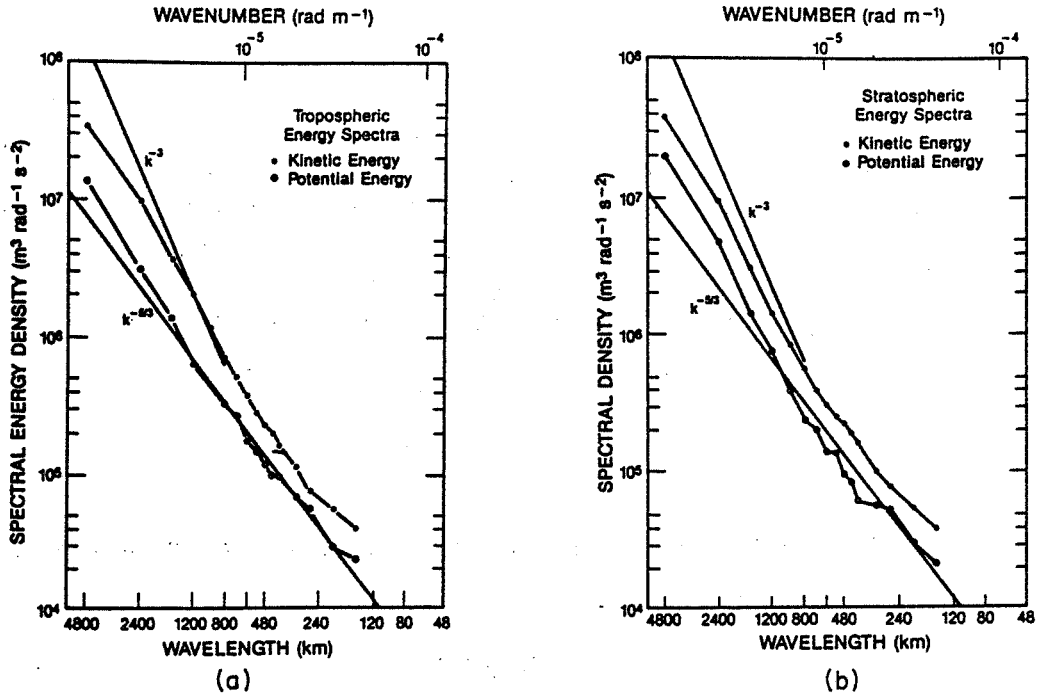

Figure 7. Kinetic and potential energy spectra from GASP aircraft flights at least 4800 km long: a) troposphere and b) stratosphere.

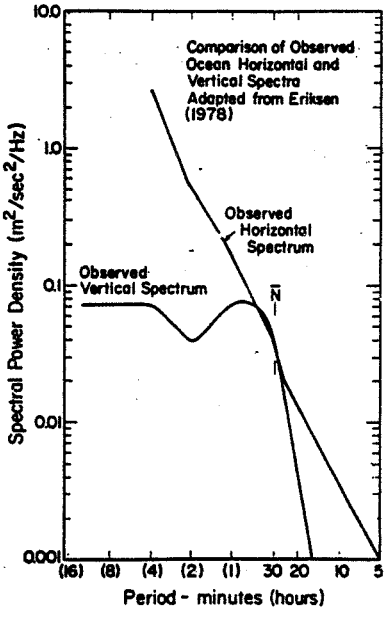

Figure 8. Internal wave spectra of horizontal and vertical velocity in the ocean (adapted from ERIKSEN, 1978).

$$E_H(\omega) = \left[\frac{N^2 - \omega^2}{\omega^2}\right]\left[\frac{\omega^2 + f^2}{\omega^2 - f^2}\right] E_V(\omega) \qquad (5)$$

where f is the coriolis frequency [$f \equiv 2\Omega \sin$ (latitude); Ω is the earth angular velocity].

Figure 9 contains a comparison of horizontal and vertical spectra observed by the radar. Starting with the vertical spectrum the dashed curve determines the location of the horizontal internal wave spectra that would be consistent with the polarization relations. The observed atmospheric spectra of horizontal velocity are shown for comparison. The fact that the magnitude of observed spectra exceeds the magnitude of the calculated wave spectra, and that the slope of the observed horizontal spectra differs significantly from the calculated wave, spectra strongly suggests that different processes are responsible for the horizontal and vertical spectra. Of course, this analysis has been made with horizontal and vertical spectra taken at different locations. To the extent that the spectra are universal this does not matter. However, the analysis should be repeated with simultaneous, co-located determinations of horizontal and vertical velocity spectra.

CONCLUDING REMARKS

In this paper we have examined the nature of the horizontal velocity spectra observed by MST/ST radar. By comparison with the aircraft-determined wave number spectra we conclude that the radar and the aircraft observe the same spectrum of atmospheric motions. Furthermore, the magnitude and shape of the Taylor-transformed radar spectra are comparable to the magnitude and shape of the aircraft wave number spectra. Finally, these spectra are in reasonable accord with expectations from quasi-two-dimensional turbulence. An examination of kinetic and potential energies deduced from the aircraft spectra shows spectral energy is partitioned equally between the two horizontal components of velocity and potential energy as expected for turbulence theory.

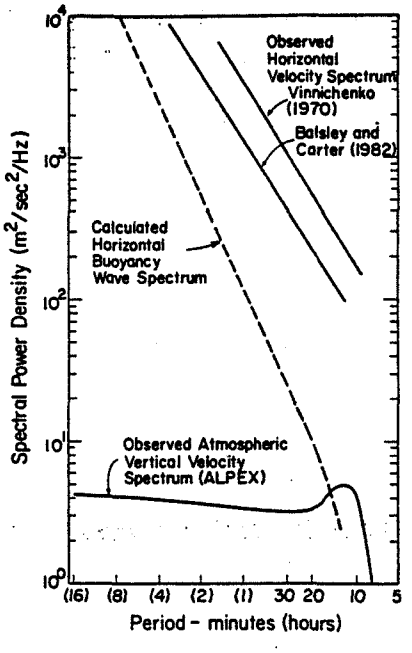

Figure 9. Comparison of observed horizontal velocity spectra in the atmosphere with horizontal spectra of internal waves (dashed line) determined from Equation (5) and observed vertical velocity spectrum.

A comparison of the energy levels and shapes of horizontal and vertical velocity spectra show that the magnitude of atmospheric spectra of horizontal velocity are too large to be consistent with the magnitude of the vertical velocity spectrum, assuming both spectra are due to waves. The spectral slope of the horizontal velocity spectrum is also inconsistent with the slope anticipated for a spectrum of internal waves given the observed shape of the vertical velocity spectrum.

Taken together these results strongly suggest that the radar spectra of vertical and horizontal velocities are indicative of different processes. They suggest that internal waves and quasi-two-dimensional turbulence are both important in determining the observed velocity spectra. The MST/ST radar observations should help in sorting out the complementary roles of waves and turbulence in middle atmospheric dynamics.

REFERENCES

Balsley, B. B. and D. A. Carter (1982), The spectrum of atmospheric velocity fluctuations at 8 km and 86 km, Geophys. Res. Lett., 9, 465-468.

Balsley, B. B., M. Crochet, W. L. Ecklund, D. A. Carter, A. C. Riddle and R. Garello (1983), Observations of vertical motions in the troposphere and lower stratosphere using three closely-spaced ST radars, Preprint Vol., 21st Conf. on Radar Meteorology, Sept. 19-23, 1983, Edmonton, Alta, Canada, 148-152.

Boer, G. J. and T. G. Shepherd (1983), Large-scale two-dimensional turbulence in the atmosphere, J. Atmos. Sci., 40, 164-184.

Brown, P. S. and G. D. Robinson (1979), The variance spectrum of tropospheric winds over Eastern Europe, J. Atmos. Sci., 36, 270-286.

Chen, T.-C. and A. Wiin-Nielsen (1978), Non-linear cascades of atmospheric energy and enstrophy, Tellus, 30, 313-322.

Charney, J. G. (1971), Geostrophic turbulence, J. Atmos. Sci., 28, 1087-1095.

Ecklund, W. L., B. B. Balsley, M. Crochet, D. A. Carter, A. C. Riddle and R. Garello (1983), Vertical wind speed power spectrum from the troposphere and stratosphere obtained under light wind conditions, Workshop on Technical Aspects of MST Radar, Handbook for MAP, Vol. 9, SCOSTEP Secretariat, Dep. Elec. Eng., Univ. Il, Urbana, 269.

Eriksen, C. C. (1978), Measurements and models of fine structure, internal gravity waves, and wave breaking in the deep ocean, J. Geophys. Res., 83, 2989-3009.

Gage, K. S. (1979), Evidence for $k^{-5/3}$ law inertial range in mesoscale two-dimensional turbulence, J. Atmos. Sci., 36, 1950-1954.

Gage, K. S. and W. L. Clark (1978), Mesoscale variability of jet stream winds observed by the Sunset VHF Doppler radar, J. Appl. Meteorol., 17, 1412-1416.

Gage, K. S. and G. D. Nastrom (1984), Theoretical interpretation of atmospheric wavenumber spectra of wind and temperature observed by commercial aircraft during GASP, manuscript in preparation.

Garrett, C. and W. Munk (1972), Space-time scales of internal waves, Geophys. Fluid Dyn., 2, 225-264.

Garrett, C. and W. Munk (1975), Space-time scales of internal waves: A progress report, J. Geophys. Res., 80, 291-297.

Kraichnan, R. H. (1967), Inertial ranges in two-dimensional turbulence, Phys. Fluids, 10, 1417-1423.

Kraichnan, R. H. and D. Montgomery (1979), Two-dimensional turbulence, Reports on Progress in Physics, 43, 547-619.

Larsen, M. F., M. C. Kelley and K. S. Gage (1982), Turbulence spectra in the upper troposphere and lower stratosphere between 2 hours and 40 days, J. Atmos. Sci., 39, 1035-1041.

Lilly, D. K. (1983), Stratified turbulence and the mesoscale variability of the atmosphere, J. Atmos. Sci., 40, 749-761.

Lilly, D. K. and E. Petersen (1983), Aircraft measurements of atmospheric energy spectra, Tellus, 35A, 379-382.

Nastrom, G. D. and K. S. Gage (1983), A first look at wavenumber spectra from GASP data, Tellus, 35A, 383-388.

Nastrom, G. D. and K. S. Gage (1984), A climatology of atmospheric wavenumber spectra observed by commercial aircraft, submitted to J. Atmos. Sci.

Rottger, J. (1981), Wind variability in the stratosphere deduced from spaced antenna VHF radar measurements, Preprint Vol., 20th Conf. on Radar Meteorology, Boston, November 30-December 3, 1981, 22-29.

VanZandt, T. E. (1982), A universal spectrum of buoyancy waves in the atmosphere, Geophys. Res. Lett., 9, 575-578.

D39

N85-32505

4.3A USE OF THE VAD TECHNIQUE AND MEASUREMENTS OF MOMENTUM FLUX IN THE STRATOSPHERE AT ARECIBO

C. R. Cornish and M. F. Larsen

School of Electrical Engineering
Cornell University
Ithaca, NY 14853

The Arecibo 430-MHz radar was used in the velocity-azimuth display (VAD) mode to obtain radial velocity measurements at 16 azimuth directions from which the three-dimensional wind field and momentum flux can be calculated. The radar was operated on a nearly continuous basis for a seven-day period in May of 1982 and the elapsed time between start and finish of a VAD scan was approximately 35 minutes. Radial velocities were measured in the upper troposphere and lower stratosphere (6-24 km) with at height resolution of 150 meters at a zenith angle of 15 deg.

Vertical and horizontal velocities are calculated from the sums and differences, respectively, of radial velocity pairs, i.e., at azimuth directions AZ and AZ + 180 degrees. Momentum flux at a particular azimuth is calculated by taking the difference between the square of radial velocities at AZ and AZ + 180 degrees in a manner first described by VINCENT and REID (1983). It should be noted that measurements of radial velocity pairs are not simultaneous but are time delayed by approximately 15-25 minutes. This period, the time required to rotate the antenna feed and take measurements at AZ and AZ + 180°, effectively limits sampling of velocities and momentum fluxes to longer period gravity waves and planetary waves. In the following presentation only the radial velocities in the principal (zonal and meridional) directions have been used. Future analysis will utilize the full 16-direction VAD from which the velocities and momentum fluxes are calculated by a least squares fit method.

Using the aforementioned technique velocities and momentum fluxes have been calculated and spectrally analyzed. Shown in Figures 1, 2 and 3 are the time series over the seven-day period and calculated spectra of the horizontal (U = zonal, V = meridional) velocities, vertical velocity (W = vertical), and momentum fluxes (Z = zonal, M = meridional), respectively, at an altitude of 14.49 km. Because of the gapped and unevenly spaced nature of the velocity time series, a DFT routine was used to calculate the spectra. To obtain an estimate of the error introduced by the uneven spacing, a sinusoidal signal composed of three sine waves with periods of 38.1, 70 and 130 hours was spectrally analyzed at the same uneven time spacing and is displayed in Figures 1-3 by the dotted curve labeled "F". The 38.1-hour period corresponds to the inertial period at Arecibo (18 deg , 21 min N). The two longer periods correspond to oscillations identified in the zonal and meridional velocities, most likely planetary wave modes. The effect of the uneven spacing is to introduce significant errors into the high frequencies (periods < 20 hours), while lower frequencies are credible.

Examination of the spectra in Figure 3 reveals that momentum flux can be identified with certain wave modes. In particular, the zonal momentum flux is significant at the inertial period with noticeable contributions at longer planetary wave periods. So far, only relative amplitudes of the spectral components of the waves have been determined; the uneven weighting of the gapped data series makes absolute values difficult to estimate until the weighting function is determined and deconvolved.

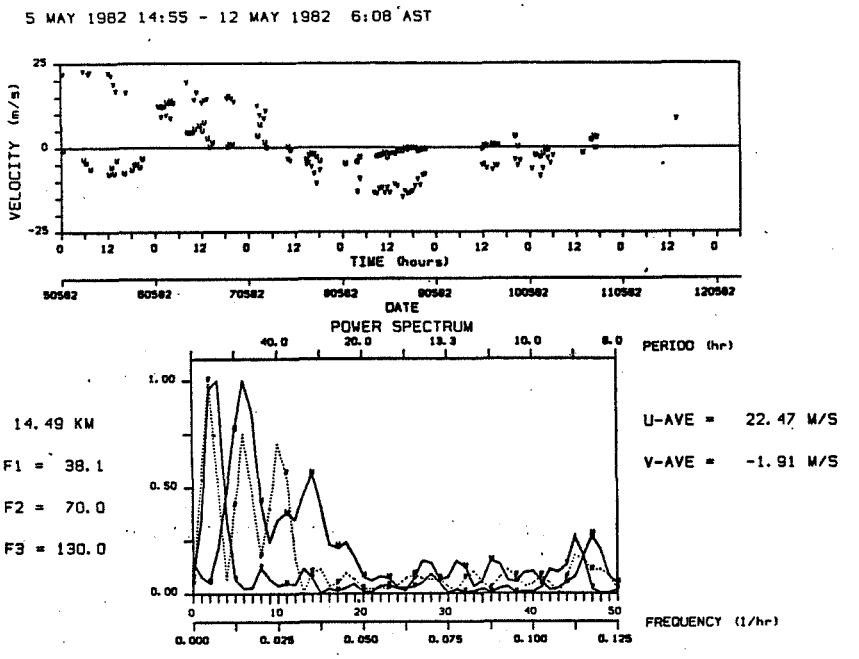

Figure 1. Zonal (U) and meridional (V) velocity time series and spectra at 14.49 km.

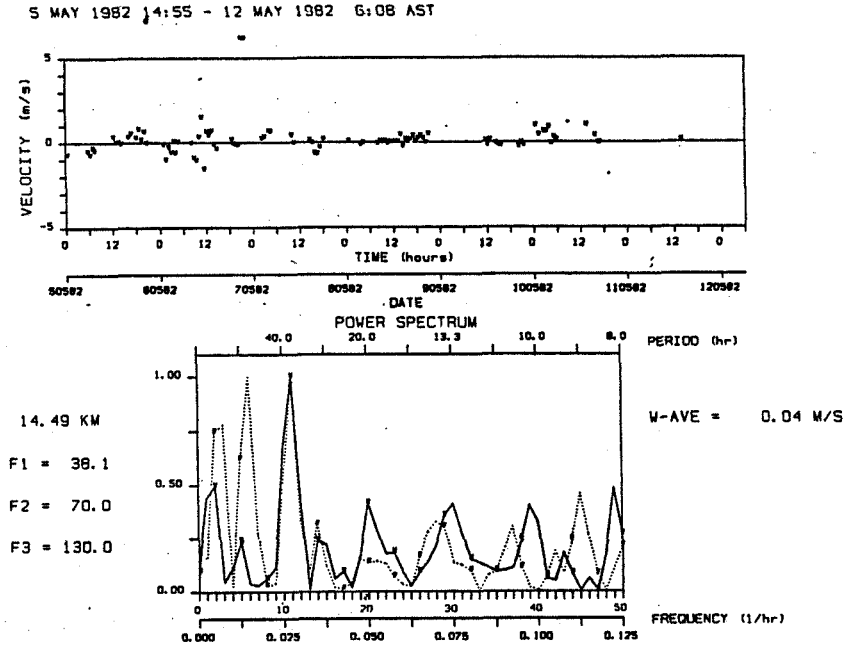

Figure 2. Vertical velocity (W) time series and spectra at 14.49 km.

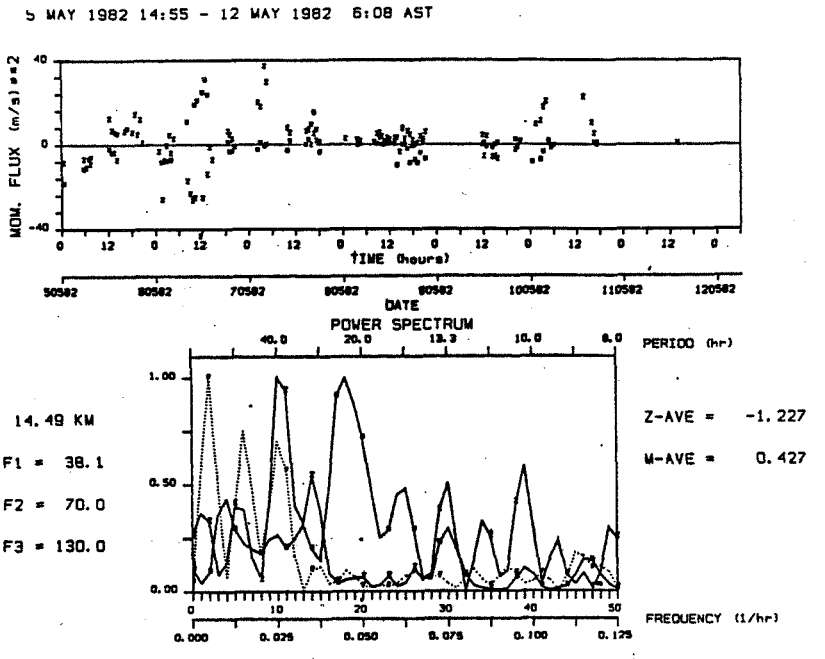

Figure 3. Zonal (Z) and meridional (M) momentum fluxes at 14.49 km.

Ongoing analysis of this data set includes determination of the various wave modes by means of identification of period, polarization of the horizontal wind, and vertical and horizontal wavelengths. Estimates of the magnitude of momentum flux at these longer periods and comparison to momentum fluxes at shorter gravity wave periods obtained after high pass filtering will provide insight into the relative contributions by the various modes. Studies of the variation of momentum flux with height at various periods will demonstrate which modes are depositing momentum into the stratosphere and which are relatively transparent to the stratosphere.

REFERENCE

Vincent, R. A. and I. M. Reid (1983), HF Doppler measurements of mesospheric gravity wave momentum fluxes, J. Atmos. Sci., 40, 1321-1333.

4.4A RELATIONSHIP OF ISOLATED TURBULENT REGIONS TO THE GENERAL TURBULENT BACKGROUND

R. G. Roper

School of Geophysical Sciences
Georgia Institute of Technology
Atlanta, GA 30332

The atmosphere below 100 km is often referred to as the homosphere; the region above, the heterosphere. In the homosphere, constituents are mixed, and average molecular weight is constant. In the heterosphere, diffusive separation occurs, and species tend to fractionate; average molecular weight decreases with height. Mixing in the homosphere has as its source dynamical (wind) energy.

Against this background turbulence, intermittent enhancements of turbulent intensity are observed. Some of these enhancements are long lived -- for example, a turbulent layer at approximately 86 km altitude seems to be almost a permanent feature of the (global?) daytime D region, as observed by partial reflection and MST radars. This may well be a delineation of the mesopause level, since long-term radio meteor studies have shown $\sim$ 85 km to be the break-point between thermospheric circulation above, and mesospheric circulation below. Rocket-released chemical trails are also characterized by turbulent sheets interleaved by laminar layers in which the diffusion coefficient is not much larger than molecular. (The prevalent practice of plotting vertical diffusion coefficients which are less than molecular does not really make much sense -- one of the basic definitions of turbulence is that it is characterized by a diffusion coefficient much larger than molecular.) If the observed turbulent layers remain at constant height, then vertical mixing is severely inhibited. Most models propose an eddy diffusion profile which varies smoothly with height -- such a profile is observed for about one in ten chemical trail releases in the mesopause and lower thermosphere.

In terms of long-term monitoring, the best estimates of height/time profiles of turbulent intensity come from the height/time profiles of signal strengths from ST radars in the lower atmosphere, and MST and partial-reflection radars in the mesosphere. In the stratosphere, Fresnel reflection is observed from stable refractivity structures whose "tilt" is related to baroclinic disturbances.

Correlations between vertical shear in the horizontal wind, presumably the source of turbulent energy, and the existence of turbulent layers have not proved conclusive. However, once a turbulent sheet is formed (perhaps by the breaking or nonlinear interaction of gravity waves), the hysterisis inherent in the formation and dissipation of turbulent structures could mean that the sheet is advected a considerable distance from its source before dissipating. Such a mechanism should be observable from the Colorado Wind Profile Network.

D41

N85-32507

4.4B ESTIMATION OF VERTICAL DIFFUSION FROM OBSERVATIONS OF ATMOSPHERIC TURBULENCE LAYERS

D. C. Fritts

Geophysical Institute
University of Alaska
Fairbanks, AK 99701

There have been numerous studies addressing the turbulent diffusion in the stratosphere and mesosphere during the last two decades. The motivation for such studies was the need for an understanding of the thermal and constituent structure of the middle atmosphere. Observational estimates of the horizontal and/or vertical diffusion were obtained using chemical release, rocket vapor trail, aircraft, balloon, and radar techniques (ZIMMERMAN and CHAMPION, 1963; KOCHANSKI, 1964; REES et al., 1972; LILLY et al., 1974; ROSENBERG and DEWAN, 1975; CADET, 1977; VINCENT and STUBBS, 1977; MANSON et al., 1979; SATO and WOODMAN, 1982; FRITTS, 1984). Typical estimates of vertical diffusion near the mesopause ranged from $\sim$200 to 600 $m^2 s^{-1}$. During the same period, a number of theoretical studies were performed to infer the level of vertical diffusion needed to account for observed constituent profiles (JOHNSON and WILKINS, 1965; COLEGROVE et al., 1966; CUNNOLD et al., 1980; ALLEN et al., 1981; APRUZESE et al., 1984). These estimates were for the most part near 100 $m^2 s^{-1}$. Thus, there appears to be a discrepancy between the level of vertical diffusion required for the dissipation of gravity wave and tidal motions on the one hand and for the maintenance of observed temperature and constituent profiles on the other. The purposes of the present contribution are to outline a possible explanation of this discrepancy and to suggest the measurements that may help verify this explanation.

The theory relies upon laboratory and atmospheric observations that suggest that the saturation of internal gravity waves via either convective or dynamical instabilities results in the generation of thin layers of turbulence which act to mix the local environment (CADET, 1977; KOOP, 1981; SATO and WOODMAN, 1982; WAND et al., 1983; PHILBRICK, private communication, 1983). Provided that these turbulent regions remain associated with the unstable portion of the wave field (as observed), it is then appropriate to examine the consequences of a turbulent diffusion that varies throughout the wave field in a systematic manner. Such an approach was taken in the study by FRITTS and DUNKERTON (1984). The results of that study and their implications for atmospheric observations will be described here.

The evolution of the wave and mean fields in the middle atmosphere are described by the nonlinear, viscous momentum and thermodynamic energy equations and the continuity equation. Using the continuity equation, the mean and perturbation potential temperature equations may be written

$$\overline{\theta}_t + (\overline{w'\theta'})_z = (\overline{\nu\theta}_z + \overline{\nu'\theta_z'})_z \tag{1}$$

and

$$\theta_t' + \overline{u}\theta_x' + w'\overline{\theta}_z + u'\theta_x' + w'\theta_z' - (\overline{w'\theta'})_z = (\nu'\overline{\theta}_z + \overline{\nu}\theta_z' + \nu'\theta_z' - \overline{\nu'\theta_z'})_z + (\overline{\nu}_h\,\theta_x' + \nu_h'\,\theta_h')_x \quad , \tag{2}$$

where subscripts denote differential and ν_h is the horizontal component of turbulent diffusion assumed proportional to ν. Then, consistent with the laboratory observations by KOOP (1981), we assume a symmetric distribution of

turbulent diffusion with a maximum at the point at which the total potential temperature is minimum (negative for convective instability). The total potential temperature may be written as

$$\theta_z = \bar{\theta}_z (1 + \alpha \cos \phi) \tag{3}$$

where ϕ is the phase function

$$\phi = kx + mz - kct \tag{4}$$

and α is a measure of wave amplitude ($\alpha > 1$ for convective instability).

We now multiply (2) by θ', average horizontally, and note that all triple correlations are small by virtue of the assumed negative correlation of ν' and θ_z'. Solving $\overline{w' \theta'}$, assuming steady-state saturation, and substituting into (1) yields, after some manipulation,

$$\bar{\theta}_t = \frac{\partial}{\partial z} \left(\overline{\nu\theta}_z + 2 \overline{\nu'\theta_z'} + \frac{\bar{\nu}}{\bar{\theta}_z} \overline{\theta_z'^2} + \frac{\bar{\nu}_h}{\bar{\theta}_z} \overline{\theta_x'^2} \right) . \tag{5}$$

Alternatively, if we write

$$\nu = \nu_o f(\cos \phi) \tag{6}$$

and define a positive coefficient

$$\beta \equiv - \frac{\overline{\nu \cos \phi}}{\bar{\nu}} \tag{7}$$

then (5) becomes

$$\bar{\theta}_t = \frac{\partial}{\partial z} \left\{ (\overline{\nu\theta}_z) \left[1 - 2\alpha\beta + \frac{\alpha^2}{2} \left(1 + \frac{k^2}{m^2} \frac{\bar{\nu}_h}{\bar{\nu}} \right) \right] \right\} . \tag{8}$$

This expression relates all of the wave and turbulence contributions to the mean turbulence flux of potential temperature. In particular, we note that both wave and turbulence fluxes include a countergradient diffusion term due to the occurrence of a maximum turbulent diffusion in regions of minimum θ_z. These countergradient terms reduce the total down-gradient flux of heat (and constituents) expected on the basis of a uniform turbulent diffusion.

The magnitude of this effect can be illustrated by assuming a distribution for turbulent diffusion of the form

$$\nu = \nu_o \left(\frac{1 - \cos \phi}{2} \right)^n \tag{9}$$

for $n \geq 0$ so that

$$\beta = \frac{n}{n + 1} \tag{10}$$

The magnitudes of the turbulence and total (wave plus turbulence) fluxes are shown for various values of n (and negligible $\bar{\nu}_h$) in Figure 1 with dashed and solid lines, respectively. Note that even for relatively small n (broad distributions of turbulent diffusion), the countergradient terms results in an appreciable reduction of the total flux expected for a uniform turbulent diffusion (with $n = 0$). In the case where ν and ν_h contribute equally to the down-gradient wave flux, it is possible to show that, while the reduction of the total flux may be significant, the total flux remains down-gradient for all α and $n \geq 0$ (FRITTS and DUNKERTON, 1984). Additionally, this theory predicts

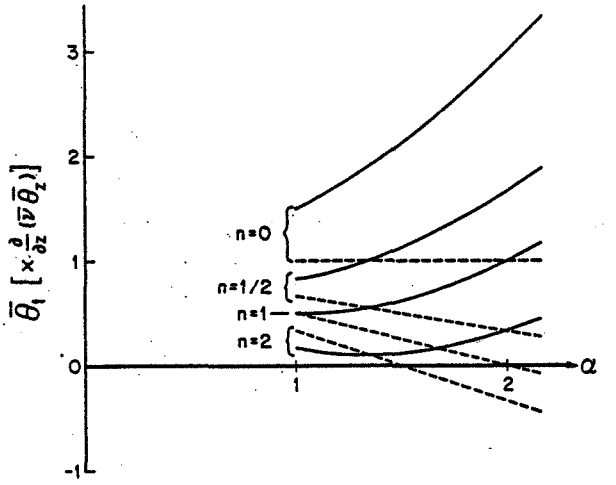

Figure 1. Variation of the turbulent (- - -) and net (——) rate of change of mean potential temperature normalized by the turbulent transport of the mean for the case of a vertical turbulent diffusivity alone. Note that even small values of n cause significant reductions in the net flux.

Prandtl numbers in the mean and perturbation equations much larger than unity for nonuniform turbulent diffusion, as anticipated by CHAO and SCHOEBERL (1984).

These results imply that, while a large turbulent diffusion may be required for the dissipation of gravity wave and tidal motions, a substantially smaller effective diffusion may act to mix mean gradients of potential temperature and constituents. The reason is that intense turbulence (and diffusion) is expected in precisely those regions of the gravity-wave field in which the total gradients of potential temperature and constituents are small or opposite to those of the mean state. Thus, it may not be sufficient to infer a mean vertical diffusion by assuming an average level of turbulence applied to the mean state. It may be necessary, instead, to infer the effective vertical diffusion from observations of the intensity and distribution of turbulent layers as well as the thermal structure. Such measurements could resolve the discrepancy between the level of turbulence required to dissipate observed wave motions and that needed to explain middle atmosphere constituent distributions.

REFERENCES

Allen, M., Y. L. Yung and J. W. Waters (1981), Vertical transport and photochemistry in the terrestrial mesosphere and lower thermosphere (50-120 km), J. Geophys. Res., 86, 3617-3627.

Apruzese, J. P., D. F. Strobel and M. R. Schoeberl (1984), Parameterization of IR cooling in a middle atmosphere dynamics model; 2. Non-LTE radiative transfer and the globally averaged temperature of the mesosphere and lower thermosphere, submitted to J. Geophys. Res.

Cadet, D. (1977), Energy dissipation within intermittent clear air turbulence patches, J. Atmos. Sci., 34, 137-142.

Chao, W. C. and M. R. Schoeberl (1984), A note on the linear application of gravity wave saturation in the mesosphere, J. Atmos. Sci. (in press).

Colegrove, F. D., F. S. Johnson and W. B. Hanson (1966), Atmospheric composition in the lower thermosphere, J. Geophys. Res., 71, 2227-2236.

Cunnold, D. M., F. N. Alyea and R. G. Prinn (1980), Preliminary calculations concerning the maintenance of the zonal mean ozone distribution in the northern hemisphere, Pure Appl. Geophys., 118, 329-354.

Fritts, D. C. (1984), Gravity wave saturation in the middle atmosphere: A review of theory and observations, Rev. Geophys. Space Phys. (in press).

Fritts, D. C. and T. J. Dunkerton (1984), Fluxes of heat and constituents due to convectively unstable gravity waves, submitted to J. Atmos. Sci.

Johnson, F. S. and E. M. Wilkins (1965), Thermal upper limit on eddy diffusion in the mesosphere and lower thermosphere, J. Geophys. Res., 70, 1281-1284.

Kochanski, A. (1964), Atmospheric motions from sodium cloud drifts, J. Geophys. Res., 69, 3651-3662.

Koop, C. G. (1981), A preliminary investigation of the interaction of internal gravity waves with a steady shearing motion, J. Fluid. Mech., 113, 347-386.

Lilly, D. K., D. E. Waco and S. I. Adelfang (1974), Stratospheric mixing estimated from high-altitude turbulence measurements, J. Appl. Meteorol., 13, 488-493.

Manson, A. H., C. E. Meek and R. J. Stening (1979), The role of atmospheric waves (1.5 hr - 10 days) in the dynamics of the mesosphere and lower thermosphere at Saskatoon (52°N, 107°W) during four seasons of 1976, J. Atmos. Terr. Phys., 41, 325-335.

Rees, D., R. G. Roper, K. H. Lloyd and C. H. Low (1972), Determination of the structure of the atmosphere between 90 and 250 km by means of contaminant releases at Woomera, May 1968, Phil. Trans. R. Soc., 271, 631-666.

Rosenberg, N. W. and E. M. Dewan (1975), Stratospheric turbulence and vertical effective diffusion coefficient, Environ. Res., 535, Air Force Cambridge Res. Labs.

Sato, T. and R. F. Woodman (1982), Fine altitude resolution observations of stratospheric turbulent layers by the Arecibo 430 MHz radar, J. Atmos. Sci., 39, 2546-2552.

Vincent, R. A. and T. J. Stubbs (1977), A study of motions in the winter mesosphere using the partial reflection drift technique, Planet. Space Sci., 25, 441-455.

Wand, R. H., P. K. Rastogi, B. J. Watkins and G. B. Loriot (1983), Fine Doppler resolution observations of thin turbulence structures in the tropo-stratosphere at Millstone Hill, J. Geophys. Res., 88, 3851-3857.

Zimmerman, S. P. and K. S. W. Champion (1963), Transport processes in the upper atmosphere, J. Geophys. Res., 68, 3049-3056.

4.5A MOMENTUM FLUX MEASUREMENTS: TECHNIQUES AND NEEDS

D. C. Fritts

Geophysical Institute
University of Alaska
Fairbanks, AK 99701

The vertical flux of horizontal momentum by internal gravity waves is now recognized to play a significant role in the large-scale circulation and thermal structure of the middle atmosphere. This is because a divergence of momentum flux due to wave dissipation results in an acceleration of the local mean flow towards the phase speed of the gravity wave. Such mean flow accelerations are required to offset the large zonal accelerations driven by Coriolis torques acting on the diabatic meridional circulation. Thus, a detailed observational knowledge of momentum flux climatology and variability is essential to a more complete understanding of the role of gravity waves in middle atmosphere dynamics.

Ideally, the momentum flux due to a random field of gravity waves would be determined from simultaneous and co-located measurements of vertical and horizontal velocities made with high vertical and temporal resolution. In practice, however, such measurements are not possible at present and other techniques must be employed. Vertical and approximate horizontal wind measurements can be made using Doppler radars with vertical and oblique beam orientations, but high frequency oblique motions are badly contaminated by vertical velocities and large phase errors occur for horizontal wavelengths that are not much larger than typical beam separation distances. Thus, such systems are only suited for measurements of momentum fluxes due to wave motions with large horizontal wavelengths ($\lambda_h \gtrsim 200$ km). These problems can be avoided, in principle, by using a phase-coherent, spaced antenna system to infer co-located horizontal and vertical motions (FRITTS et al., 1984). Another approach which does not rely on individual horizontal and vertical velocity measurements is that of VINCENT and REID (1983). This technique provides an estimate of the momentum flux in the plane of two Doppler radar beams inclined at equal and opposite angles off vertical based on the average rms velocities observed. Because all of these techniques depend on the velocity fluctuations about some mean, however, the contribution to the momentum flux due to quasi-stationary waves is likely to be largely excluded in each. In general, the wave periods for which a particular measurement applies are those that are less than the data collection interval.

Other more general problems with existing systems relate to spatial and temporal resolution; if these are not sufficiently fine, then observed motions may be aliased to other (larger) scales or overlooked altogether. Fortunately, we do not expect motions with small vertical wavelengths ($\lambda_z \lesssim 4$ km) to contribute significantly to the momentum flux and divergence on theoretical grounds (LINDZEN, 1981). On the other hand, high-frequency gravity wave motions ($T \lesssim 20$ min), which may account for significant momentum fluxes, may be excluded or substantially reduced by excessive temporal averaging.

Relatively little is known at present about the distribution and variability of gravity-wave momentum flux in the middle atmosphere, yet these determine, to a large extent, the gross features of the middle atmosphere circulation and structure. The distribution of momentum flux depends on a variety of factors. Perhaps the most significant are (1) the strength and location of important gravity wave sources (wind shear, topography, convection, etc.), (2) the filtering and evolution of the gravity-wave spectrum due to wave-

turbulence, wave-wave, and wave-mean flow interactions, and (3) the characteristics of those gravity waves that contribute most to drag and diffusion processes.

Both gravity wave sources and filtering contribute to the temporal and geographic variability of wave amplitudes, scales, and fluxes and may act to polarize the gravity-wave spectrum and align the momentum flux in preferred directions. Significant topographic sources are quite localized on a global basis, and wind shear and convective sources tend to be rather transient in nature. Of the primary gravity wave sources, wind shear and topography are expected to lead to wave spectra that may be strongly polarized, whereas convection is likely to produce a more isotropic distribution of gravity waves. The recent studies by SCHOEBERL and STROBEL (1984) and DUNKERTON and BUTCHART (1984) suggest that filtering processes can also act to modulate or polarize a gravity-wave spectrum anti-parallel to the local mean flow. A tendency for gravity waves in the middle atmosphere to be polarized has been noted by HAURWITZ and FOGLE (1969), HERSE et al. (1980), MANSON et al. (1981), and VINCENT and REID (1983), among others.

Of major importance in the study of the gravity wave and momentum flux distributions in the middle atmosphere are the characteristics of those motions that contribute most to saturation processes. This is because gravity waves with small propagation angles ($\lambda_x \gg \lambda_z$) and/or small vertical wavelengths (small intrinsic phase speeds $c-\bar{u}$) may propagate or be advected large distances horizontally between sources in the lower atmosphere and regions of strong dissipation in the stratosphere or mesosphere. Such propagation would tend to homogenize the wave field in the middle atmosphere, independent of geographically local sources and filtering effects. On the other hand, gravity waves with large propagation angles ($\lambda_x \gtrsim \lambda_z$) and large vertical wavelengths will reach the stratosphere and mesosphere rapidly, relatively unattenuated, and in close proximity to the source or filtering environment that determined the wave character. In this case the momentum flux distribution in the middle atmosphere would reflect the spatial variability of the underlying atmosphere. On the basis of the observed spectrum of atmospheric wave motions (CARTER and BALSLEY, 1982), it appears possible that the transport of momentum could be accomplished primarily by relatively high-frequency gravity waves (FRITTS, 1984), consistent with the observations of VINCENT and REID (1983) and SMITH and FRITTS (1983). Other observations suggest that the saturation of gravity waves at a wide range of scales is a nearly continuous process throughout the middle atmosphere (SATO and WOODMAN, 1982; PHILBRICK et al., 1983; BALSLEY et al., 1983; VINCENT, 1984).

Because of the considerable uncertainties regarding the momentum flux distribution in the middle atmosphere, many types of observations are required. Those observations that appear to be important in light of the above discussion include:

(1) the mean geographical and seasonal distributions of momentum flux (and divergence) throughout the middle atmosphere,

(2) those gravity wave scales and frequencies that contribute most to momentum transport,

(3) the degree and causes of polarization and variability of the gravity-wave spectrum, and

(4) the response of the middle atmosphere to changes in momentum flux divergence caused by variable gravity wave sources or filtering conditions.

Studies that address these topics will make important contributions to our knowledge of the role of gravity waves in middle atmosphere dynamics.

REFERENCES

Balsley, B. B., W. L. Ecklund and D. C. Fritts (1983), VHF echoes from the high-latitude mesosphere and lower thermosphere: Observations and interpretations, J. Atmos. Sci., 40, 2451-2466.

Carter, D. A. and B. B. Balsley (1982), The summer wind field between 80 and 93 km observed by the MST radar at Poker Flat, Alaska (65°N), J. Atmos. Sci., 39, 2905-2915.

Dunkerton, T. J. and N. Butchart (1984), Propagation and selective transmission of internal gravity waves in a sudden warming, J. Atmos. Sci. (in press).

Fritts, D. C. (1984), Gravity wave saturation in the middle atmosphere: A review of theory and observations, Rev. Geophys. Space Phys. (in press).

Fritts, D. C., M. A. Geller, B. B. Balsley, M. L. Chanin, I. Hirota, J. R. Holton, S. Kato, R. S. Lindzen, M. R. Schoeberl, R. A. Vincent and R. F. Woodman (1984), Research status and recommendations from the Alaska workshop on gravity waves and turbulence in the middle atmosphere, Bulletin of the AMS, 65, 149-159.

Haurwitz, B. and B. Fogle (1969), Waveforms in noctilucent clouds, Deep Sea Res., 16, 85-95.

Herse, M., G. Morells and J. Clairemidi (1980), Waves in the OH emissive layer: Photogrametry and topography, Appl. Optics, 19, 355-362.

Lindzen, R. S. (1981), Turbulence and stress due to gravity wave and tidal breakdown, J. Geophys. Res., 86, 9707-9714.

Manson, A. H., C. E. Meek and J. B. Gregory (1981), Gravity waves of short period (5-90 min), in the lower thermosphere at 52°N (Saskatoon, Canada); 1978-1979, J. Atmos. Terr. Phys., 43, 35-44.

Philbrick, C. R., K. U. Grossmann, R. Hennig, G. Lange, D. Krankowsky, D. Offermann, F. J. Schmidlin and U. von Zahn (1983), Vertical density and temperature structure over Northern Europe, Adv. Space Res., 2, 121-124.

Sato, T. and R. F. Woodman (1982), Fine altitude resolution observations of stratospheric turbulent layers by the Arecibo 430 MHz radar, J. Atmos. Sci., 39, 2546-2552.

Schoeberl, M. R. and D. F. Strobel (1984), Nonzonal gravity wave breaking in the winter mesosphere, Dynamics of the Middle Atmosphere, J. R. Holton and T. Matsuno, eds., Terra Scientific Publishing Co., Tokyo, 45-64.

Smith, S. A. and D. C. Fritts (1983), Estimation of gravity wave motions, momentum fluxes and induced mean flow accelerations in the winter mesosphere over Poker Flat, Alaska, Proceedings of the 21st Conf. on Radar Meteorology, Edmonton, 104-110.

Vincent, R. A. (1984), Gravity wave motions in the mesosphere, J. Atmos. Terr. Phys. (in press).

Vincent, R. A. and I. M. Reid (1983), HF Doppler measurements of mesospheric gravity wave momentum fluxes, J. Atmos. Sci., 40, 1321-1333.

4.5B TROPOSPHERIC GRAVITY WAVES OBSERVED BY THREE CLOSELY SPACED ST RADARS

D. A. Carter*, B. B. Balsley*, W. L. Ecklund*,
M. Crochet**, A. C. Riddle***, and R. Garello***

*Aeronomy Laboratory, National Oceanic and Atmospheric Administration
Boulder, CO 80303

**L.S.E.E.T., "LaGiponne" Boulevard des Armaris
Toulon 83100, France

***CIRES, University of Colorado
Boulder, CO 80309

INTRODUCTION

In the spring of 1982 a cooperative U.S.-France clear-air radar experiment was carried out on the southern coast of France during the ALPEX (Alpine Experiment) program. Three relatively small vertically directed 50-MHz ST radars were set up with spacings of about 5-6 km. Figure 1 shows the location and configuration of the radars, while Table 1 gives the system parameters. The three radars were operated concurrently for a period of about 6 weeks with 1-minute temporal and 750-m height resolution. Doppler spectra were computed at each site and tape recorded for later analysis. An examination of the temporal and spectral characteristics of the vertical velocity fluctuations has been presented by BALSLEY et al. (1983). One of the principal purposes of the experiment was to examine the horizontal and vertical properties of gravity waves in the lower atmosphere. In this report we will describe the techniques used and the first results from this wave study.

Examples from the ALPEX data set displayed in Figure 2 show the highly variable nature of the vertical wind velocity fluctuations. This variability was directly related to the background wind conditions. For example, during April 30, an active period of strong (30-40 m/s) northerly Mistral winds, the vertical velocities often reached 2 m/s with dominant periods of several hours. On the other hand, during quiet periods of weak horizontal winds (less than 5-10 m/s) such as occurred on May 14, the vertical winds showed fluctuations of less than 10-20 cm/s, sometimes with noticeable oscillations near the Brunt-Vaisala period (around 10 minutes). Most days, like May 10, for example, were between these extremes, with horizontal winds around 10-20 m/s and vertical fluctuations which were broadband and variable. There were also a very few instances of monochromatic wave events, such as on May 25, which generally occurred with rather low (<10 m/s) background horizontal winds.

WAVE ANALYSIS

With vertical velocity observations from three locations, the horizontal characteristics (wavelength, phase velocity, and propagation direction) can be determined for waves of any frequency by measuring the phase of that frequency component at each station. Equivalently, phase differences between all station pairs can give the same information. Two methods were used in this anlaysis to determine those phase differences: cross-correlation functions and coherence spectra.

For nearly monochromatic wave events a cross-correlation function was computed, which gave a time delay between each station pair. As an example, the cross-correlation functions for a 100-minute interval on May 25 are shown in Figure 3. For this particular period, the correlation is extremely good. The

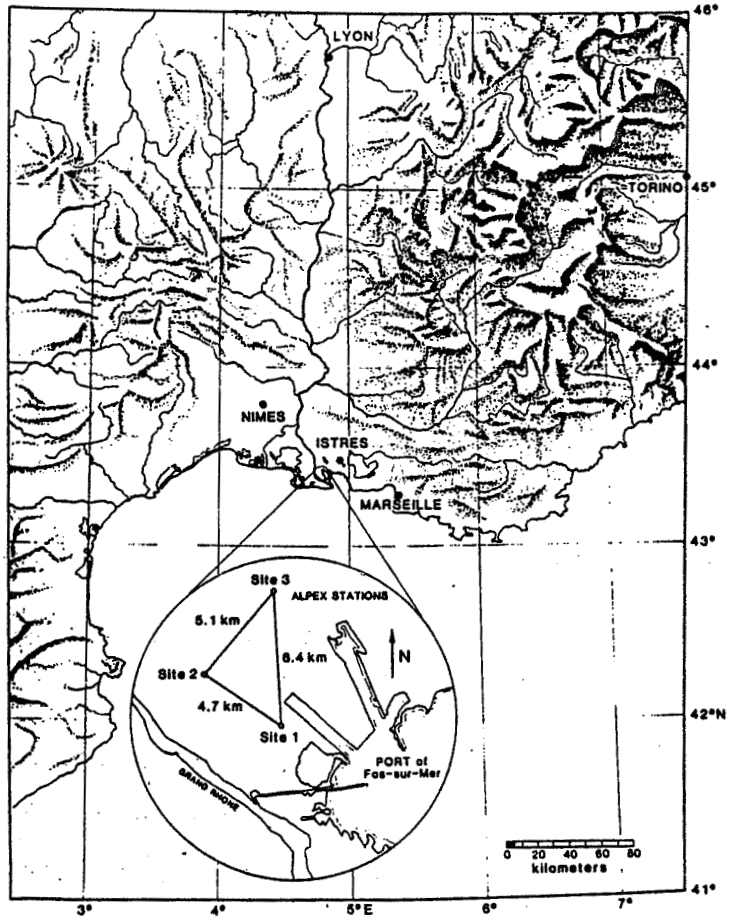

Figure 1. Plan view of the three-station ALPEX radar experiment. Inset shows details of site locations.

Table 1

SITE	FREQUENCY (MHz)	ANTENNA DIMENSIONS	AVERAGE TRANSMITTED POWER	PULSE WIDTH	HEIGHT RESOLUTION	TIME RESOLUTION
1	49.640	(70 x 100)m^2	$\sim$ 200 w	5 μs	750 m	$\sim$ 1 min
2	49.920	(70 x 100)m	$\sim$ 200 w	5 μs	750 m	$\sim$ 1 min
3	48.850	(70 x 50)m	$\sim$ 200 w	5 μs	750 m	$\sim$ 1 min

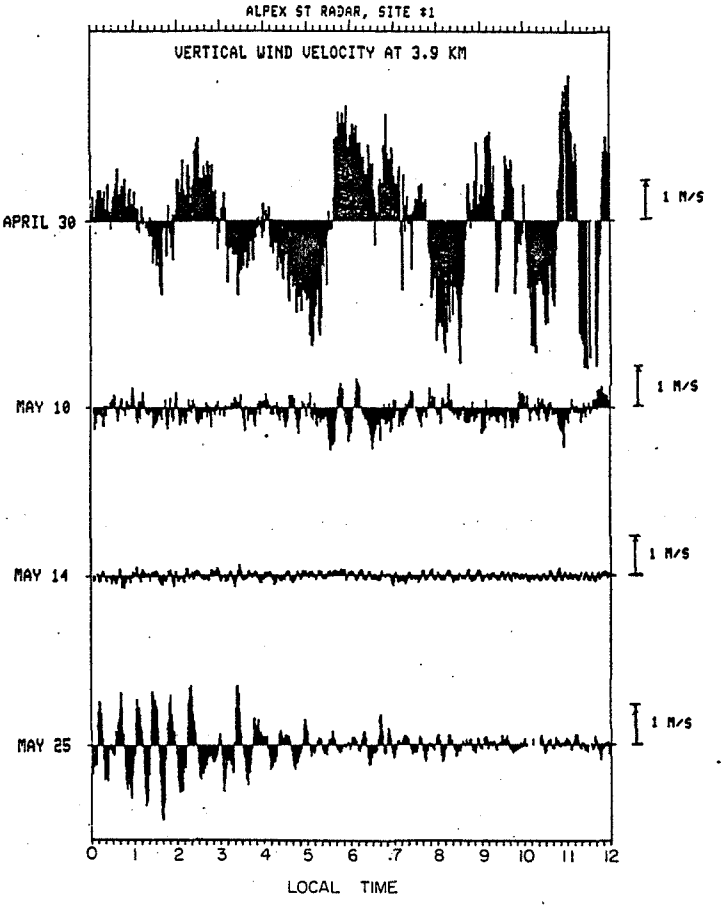

Figure 2. Examples of the vertical velocity at 3.9 km from Site 1 for 12-hour periods on four different days.

wave has a period of about 25 minutes. By using the local maximum that is closest to zero time lag in each function, the wave can be shown to have a horizontal wavelength of about 15 km and to be coming from an azimuth of about 350°.

Table 2 shows the wave parameters derived from cross-correlation analyses for other times of nearly monochromatic waves. Also given are the mean wind magnitude and direction at the altitude of the wave as determined by sounding balloons launched at six-hour intervals by the French Meteorological Service at Nimes (also shown in Figure 1). Except for May 22, the other events were not nearly as strongly sinusoidal as on May 25, but occasionally a wave-like oscillation would pop up long enough to compute a correlation function. The wave periods ranged from 15 to 60 minutes and the computed horizontal wavelengths were between 7 and 20 km. Two wave directions are given for May 22 since the time lag between two of the radars was about half a wave period and thus it could not be determined which station was leading the other. Such spatial aliasing is, of course, a possiblity for any of the other waves, but only the unaliased wave solutions are shown.

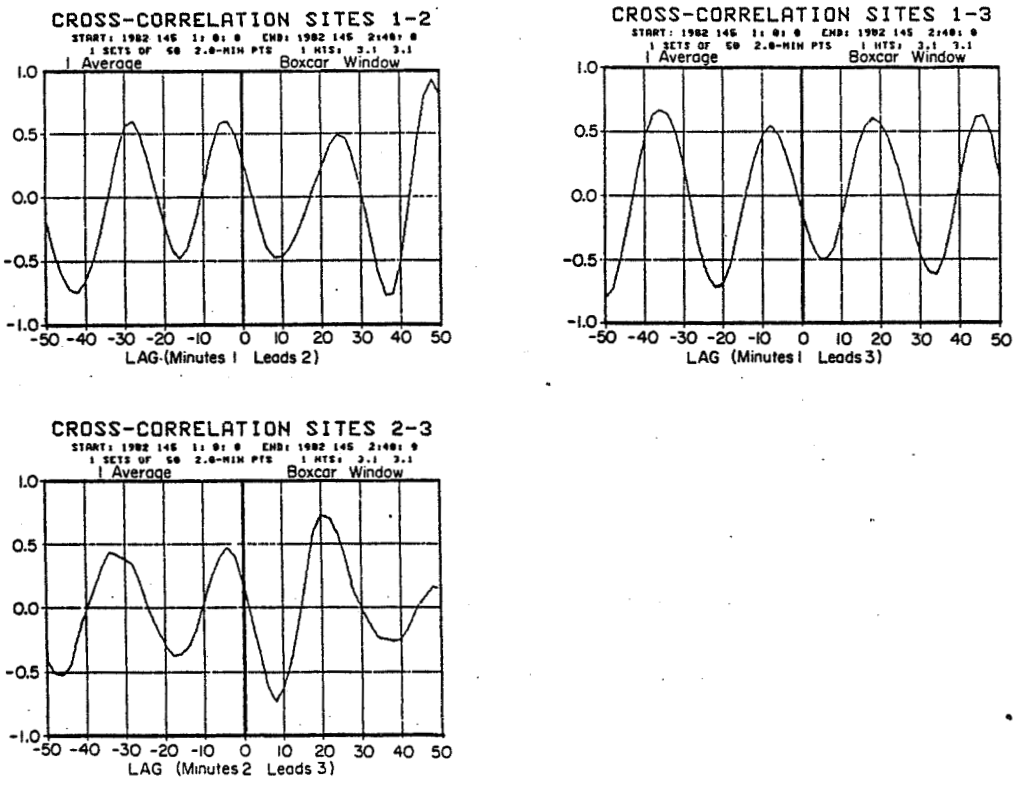

Figure 3. Cross-correlation functions computed between the three pairs of radar sites at 3.1 km for 0100-0240 local time on May 25, 1982.

Table 2. Waves derived from cross-correlation analysis.

Time		Height	Wave Period	Horizontal Wavelength	Wave Direction	Wind Direction	Wind Speed
April 25	0600-0800	4-5 km	30 min	10 km	200°	0-20°	10-15 m/s
May 2	1400-1600	4-5 km	60 min	15 km	170°	300°	15-20 m/s
May 9	1500-1700	4 km	40 min	12 km	330°	240°	15-20 m/s
May 10	2200-0200	4-5 km	40 min	20 km	320°	~270°	5-10 m/s
May 11	1700-1820	4 km	20 min	15 km	90°	200°-240°	5-10 m/s
	1800-1900	7-8 km	20 min	18 km	110°	200°-240°	5-10 m/s
May 22	0100-0200	4 km	15 min	7 km	270° or 80°	300°-340°	5-10 m/s
May 25	0100-0240	3-4 km	25 min	15 km	350°	340°	10 m/s

The cross-correlation function works well on monochromatic waves, but for the rather broadband fluctuations that were usually observed, the cross correlation gives no information on the individual frequencies present. A spectral analysis was needed to find any waves hidden in the typical vertical velocity fluctuations. For any time series a Fourier transform could be computed to derive an amplitude and phase value for each Fourier component. But this computation produces phases for uncorrelated noise as well as waves and does not distinguish between the two. A coherence spectrum, however, can give an indication of how well correlated or coherent a particular frequency component is between two time series.

The coherence spectrum is essentially the normalized magnitude of the complex cross spectrum of two time series (see BENDAT and PIERSOL, 1966). To be meaningful, the complex cross spectrum must be averaged over several data sets. If the relative phase at a given frequency varies randomly between successive complex cross spectra, the normalized magnitude (the coherence) of the average will approach zero. On the other hand, if there is a coherent signal running through all the data sets, then the cross phase will be constant, the complex cross spectra will add in phase, and the coherence will approach a value of one.

In the search for waves, the coherence analysis was applied to the entire ALPEX data set. Typically, a cross spectrum was computed between each pair of stations using a data set of 256 1-minute velocity points to which a Hanning window had been applied (SAUNDERS and HAMRICK, 1982). The complex cross spectra were averaged in time over data sets which were overlapped 50% (with a Hanning window, these data sets are 83% independent (HARRIS, 1978)). Cross spectra from several tropospheric heights were also averaged together.

A coherence spectrum and a cross-phase spectrum (phase of the cross spectrum) was computed between each of the three station pairs. Only those frequency components whose coherence met or exceeded the 1% significance level were used to compute wave parameters. The 1% significance level (the coherence above which uncorrelated signals should reach only 1% of the time) is defined by

$$\sqrt{1 - (0.1)^{1/(n-1)}}$$

where n is the number of cross spectra averaged (JULIAN, 1975). The cross phases for bands of frequencies with significant coherences were then used to calculate the horizontal wave parameters.

The results of the coherence analysis were mixed. On very active, high wind days, such as April 30 shown in Figure 2, there were no significant coherences. This result is in agreement with the impression that the strong vertical fluctuations were due to lee wave structures which would have no consistent phase relationship between radars throughout a day. In general, the very quiet days also had poor coherences, although there were some significant exceptions (such as May 14 shown in Figure 2). Although fluctuations near the Brunt-Vaisala period could be discerned in the time series, the coherent wave periods, if there were any at all, tended to be around 30-60 minutes. This implies that the correlation distance of the Brunt-Vaisala oscillations was usually less than about 5 km. Most of the data sets that showed significant coherences were moderately active days with background winds around 10-20 m/s. Table 3 lists the results from those periods which met the coherence criterion.

Figure 4 shows an example of the coherence spectra for May 14. The dashed line represents the 1% significant level. Note that the coherences for all three station pairs are significant between 2×10^{-4} and 5×10^{-4} Hz (about 30 and 80 minute periods) and that the coherence between sites 1 and 2 is much higher at low frequencies than the coherences involving site 3.

Table 3. Waves derived from coherence spectral analysis.

Time		Height	Wave Period (min)	Horizontal Wavelength	Wave Direction	Wind Direction	Wind Speed
April 25	0000-0630	3-6 km	40-80	10-15 km	220°-270°	0°-45°	10-15 m/s
	0800-1430	3-6 km	20-25	10-15 km	200°-230°	0°-45°	10-15 m/s
April 27	0000-1100	3-6 km	30-60	10-15 km	∿270°	30°-60°	10-20 m/s
May 2	1400-2400	3-7 km	30-90	10-15 km	∿130°	∿310°	15-20 m/s
May 3	0000-0900	3-7 km	25-40	8-12 km	∿140°	270°-300°	10 m/s
May 10	0000-2400	3-6 km	35-45	∿15 km	∿330°	240°-270°	10-20 m/s
May 14	0000-2400	3-6 km	30-60	20-40 km	∿200°	variable	<5 m/s

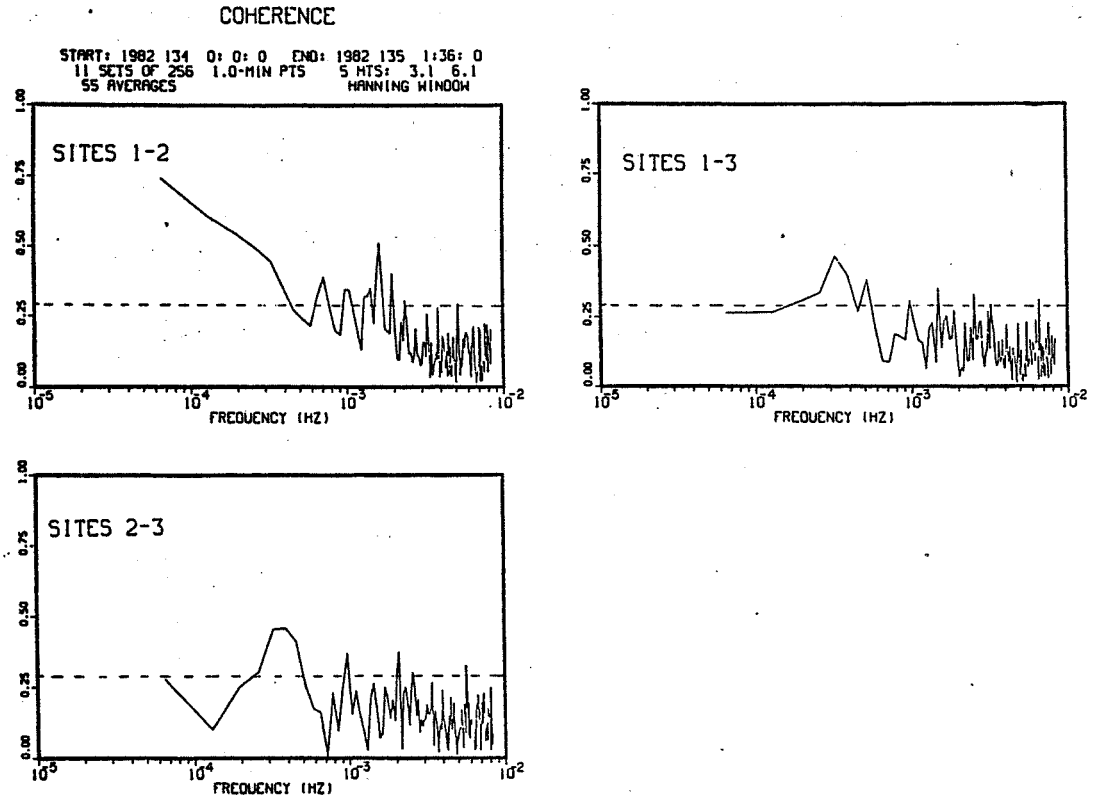

Figure 4. Coherence spectra for May 14, 1982. The spectra were averaged over 25 hours and 5 height ranges between 3 and 6 km. The dashed line is the 1 percent significance level.

Figure 5 gives the phases corresponding to the coherences in Figure 4. The dashed curve in Figure 5 represents the phase differences that would occur for waves propagating at 13 m/s from an azimuth of 230° for all periods between about 15 minutes and 2 hours. The observed phases follow this general curve even at wave frequencies where the coherences did not reach the 1% significance level. This was fairly common during other days also; the cross phases appeared to be able to give good wave determinations even with marginally good coherences.

A comparison can be made between the cross-correlation results shown in Table 2 and the coherence results in Table 3 for three common days, April 25, May 2, and May 10. The wave directions derived from cross correlations of short periods of sinusoidal oscillations agree well with those determined from the coherence analysis over a longer time period.

It must be noted here that good coherences and consistent cross phases do not necessarily imply a wave. Turbulent structures that are "frozen" into the mean wind and are advected past the radars will produce a phase speed and a propagation direction equal to the horizontal wind speed and direction. For the May 14 data this is not the case, however, since the background wind was less than 5 m/s compared to a deduced wave speed of 10-15 m/s. Table 3 shows that most wave patterns derived from the coherence analysis actually had components in the opposite direction of the background wind at the same altitude.

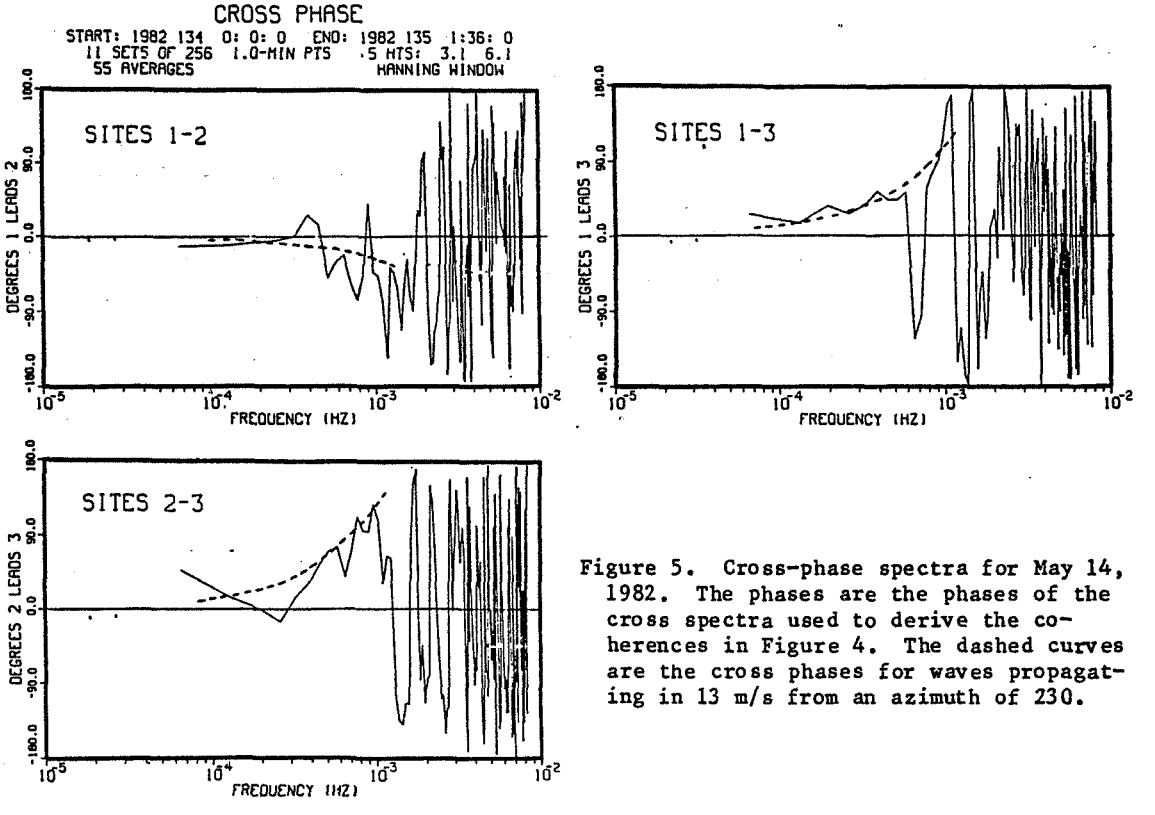

Figure 5. Cross-phase spectra for May 14, 1982. The phases are the phases of the cross spectra used to derive the coherences in Figure 4. The dashed curves are the cross phases for waves propagating in 13 m/s from an azimuth of 230.

The coherence spectral analysis was also used to examine the coherence and phase shifts between heights at each radar. The coherences were almost always very high for periods of 10-100 minutes over height separations of up to about 2 km. In nearly all cases, the phase differences between heights were essentially zero, which implies a very large vertical wavelength.

The theoretical relationship between the horizontal wavelength, λ_H, and vertical wavelength, λ_z, for an internal gravity wave is

$$\lambda_z^2 = \lambda_H^2 \cdot \frac{\omega^2}{N^2 - \omega^2}$$

where N is the Brunt-Vaisala frequency are ω, the intrinsic wave frequency is related to the observed frequency, ω_o, by

$$\omega = \omega_o - \vec{k} \cdot \vec{U}$$

where $\vec{k}$ ($|\vec{k}| = 2\pi/\lambda$) is the total wave vector and $\vec{U}$ is the mean wind. Both ω_o and λ_H remain constant through slow variations in U and N. In equation (1) ω is assumed to be much less than the inertial frequency, whose period is 17.5 hours at the ALPEX radar sites. From the above relations it can be seen that Brunt-Vaisala period waves should have infinite vertical wavelengths and longer period waves should have progressively shorter vertical wavelengths.

For a typical wave observed during the ALPEX experiment with λ_H = 15 km and period T = $(2\pi/\omega_o)$ = 30 minutes, the vertical wavelength should be about 5 km for a Brunt-Vaisala period of about 10 minutes and no background wind. An opposing mean wind, however, would Doppler shift the intrinsic frequency toward higher frequencies and thus lengthen the vertical wavelength.

Table 4 presents horizontal and vertical wavelength data for May 2 that may show evidence for gravity-wave Doppler shifting. For each observed frequency listed, the measured horizontal wavelength was used to compute the wind component in the direction of wave propagation which would be needed to produce the observed vertical wavelength. The results show a consistent picture of an opposing wind component of about 11-13 m/s that is Doppler shifting the waves to longer vertical wavelengths. (Note that the last frequency listed in Table 4 (T = 32 minutes) has an anamolous measured λ_H of 15 km. If this λ_H was more in line with the others of 10-12 km, the computed wind component would also be about -12 m/s.) Based on Nimes balloon measurements, the background wind during May 2 was approximately 15 m/s from an azimuth of 310°, yielding a component in the wave direction of -13 to -15 m/s, very close to the computed value.

Actually, this good agreement is somewhat surprising since the equations upon which the computations were based are applicable to infinite plane waves propagating under slowly varying background conditions. The Brunt-Vaisala frequency, however, changes abruptly at the tropopause, whose height (8-12 km) is much smaller than the observed vertical wavelengths. The tropospheric waves did not appear to propagate beyond the tropopause boundary and may have been trapped in the troposphere.

DISCUSSION

The wave observations described above show the usefulness of ST radars for studying gravity waves in the lower atmosphere. There were several factors, however, which limited the number of waves that could be detected and which need to be considered in the design of similar future experiments.

Table 4. May 2, 1400-2400 local time.

Wave Period	Horizontal Wavelength	Vertical Wavelength	Computed U_k
85 min	11.2 km	11 km	-11 m/s
64 min	12.3 km	17 km	-13 m/s
51 min	10.2 km	35 km	-13 m/s
43 min	10.3 km	35 km	-12 m/s
37 min	10.4 km	62 km	-12 m/s
32 min	15.1 km	00 km	-17 m/s

U_k is the component of the mean wind in the direction of the horizontal wave vector $\vec{k}_H$.

The first factor is horizontal spacing. With radar separations of roughly 5 km, waves with horizontal wavelengths less than about 10 km could be aliased and appear to have longer wavelengths. Since most observed waves had measured wavelengths around 10-12 km, it is possible that some of these were aliased. Additional stations at other spacings would increase the range of observable wavelengths.

The fact that only vertical observations were made also limited the waves that could be detected. Gravity-wave particle motion is purely vertical at the Brunt-Vaisala period and becomes totally horizontal at the inertial period. At 2-hour periods, non-Doppler shifted waves have vertical motions that are one-tenth the horizontal motion. Thus longer period waves are increasingly difficult to observe with vertical radars. This is evidenced by the typical drop in coherences between the ALPEX radars above about 1-hour wave periods. A system with oblique as well as vertical radar beams could extend the range of detectable waves to longer periods.

For vertical radars, the antenna beam may be an important factor. There were several occasions during the ALPEX experiment when the coherence between sites 1 and 2 was very good, but the poor coherences with site 3 prevented the determination of horizontal wave parameters. It can be seen from Table 1 that the site 3 antenna area was one-half that of the others and so had a wider beam width. In addition, it was necessary to operate that radar at a frequency that was 1 MHz away from the design frequency of the coaxial collinear antennas. The effect of this mismatch was to significantly increase the level of the first sidelobe. This effectively wider beam may have been more sensitive to specular reflections from off-vertical, tilted layers, which would tend to destroy the coherence of the resulting radial velocities. Thus it may be that narrow beams (at least as narrow as the $\sim 3°$ beams at sites 1 and 2) are necessary for short-period wave vertical observations.

SUMMARY

During the ALPEX experiment there were only a few instances of nearly monochromatic wave events upon which a cross correlation could be performed.

However, it appears that the coherence spectral analysis can detect waves that otherwise would have gone unnoticed. This method requires averaging over rather long time periods and/or several heights (over which the wave field must remain steady). Several periods of good coherences were observed, particularly on quiet or moderately active days. The waves derived from the coherence analysis appeared to have long vertical wavelengths. Most seemed to be propagating in a direction opposite to the background wind, which would Doppler shift gravity waves to longer vertical wavelengths. Perhaps on such relatively quiet days, where there are no obvious isolated sources for waves, the direction into the wind is a preferred direction for persisting waves. Further analysis of the waves observed during ALPEX is continuing. Future experiments with various radar configurations could significantly contribute to the understanding of gravity waves in the atmosphere.

REFERENCES

Balsley, B. B., M. Crochet, W. L. Ecklund, D. A. Carter, A. C. Riddle and R. Garello (1983), Observations of vertical motions in the troposphere and lower stratosphere using three closely-spaced ST radars, Preprint Vol., 21st Conf. on Radar Meteorology, Sept. 19-23, 1983, Edmonton, Alta., Canada. Published by the American Meteorological Society, Boston, Mass.

Bendat, J. S. and A. G. Piersol, Measurements and Analysis of Random Data, John Wiley, New York.

Harris, F. J. (1978), On the use of windows for harmonic analysis with the discrete Fourier transform, Proc. IEEE, 66, 51.

Julian, P. R. (1975), Comments on the determination of significance levels of the coherence statistic, J. Atmos. Sci., 32, 836.

Saunders, K. D. and F. C. Hamrick (1982), A note on cross spectrum and coherence calculation, J. Geophys. Res., 87, 9699.

4.5C DETERMINATION OF HORIZONTAL AND VERTICAL WAVELENGTHS OF GRAVITY WAVES IN THE MESOSPHERE BY SPACED WIND MEASUREMENTS

C. E. Meek

Institute of Space and Atmospheric Studies
University of Saskatchewan
Saskatoon, Canada

INTRODUCTION

The work reported below describes the reduction of spaced wind measurements taken over a range of heights. Briefly, the equipment used is a medium frequency radar (2.22 MHz) with one site consisting of a vertically pointing transmitter and spaced receiving antennas, and two remote receiving sites ($\sim$ 40 km distant, forming an approximately equilateral triangle) with spaced antennas. Assuming approximately horizontally stratified scatterers, horizontal winds are thus available at the corners of a triangle of side $\sim$ 20 km in the GRAVNET system. A more detailed system description was given at the 1983 Urbana MST Workshop.

HORIZONTAL WAVELENGTH AND PHASE VELOCITY

Each site has northward and eastward velocity components available for analysis. One of these components is selected and spectra are calculated for each height over a small range of heights. Cross spectra between pairs of sites are then found for each height and averaged over the height range, so that the phase differences ($\Delta\phi$) given from the cross spectra are independent. The "normalized phase discrepancy" (NOD) is defined as $|\Sigma\Delta\phi|/\Sigma|\Delta\phi|$, where the sum is done around the site pairs, and is analogous to the normalized time discrepancy used in individual determinations of wind from fading records. It indicates the "coherence" of the fluctuations at each site within the bandwidth of the spectral analysis. Consequently, it can be used for data selection. However a low NOD does not necessarily indicate the presence of a single wave, as will be shown later; it merely means that there is a well-defined oscillation at each site.

There are two ambiguities in this process. The first is in $\Delta\phi$, which could be in error by $\pm 2\pi n$, $n = 1,2\ldots$. An assumption must be made that the horizontal wavelength is at least twice as large as the array, thus restricting $\Delta\phi$ to $\pm\pi$. During data selection the further restriction is made that the $|\Delta\phi|$ be less than $\pi/2$, in order that the direction of propagation be unambiguous. A slight relaxation of these conditions is reasonable, e.g., if two of the are less than $\pi/2$ and one is greater, but NOD $\sim$ 0, the data are probably acceptable. The wide transmitter antenna beam widths used at MF are helpful in attenuating the shorter wavelength oscillations, but is is difficult to estimate this because the effective beam width depends on the scattering process.

The second ambiguity is in frequency. A 5-min data sample is used to determine the wind, giving a Nyquist frequency of 10 min. However, if the 5-min sample is assumed to be block average there is some attenuation of short-period fluctuations as shown in Figure 1.

Once the $\Delta\phi$ are found, the wavelength and direction can be found by a least squares fit to the phase differences. Each phase difference could be weighted by the appropriate coherence, but this is not done at present. Data with low NOD will give the same results regardless of weighting in any case.

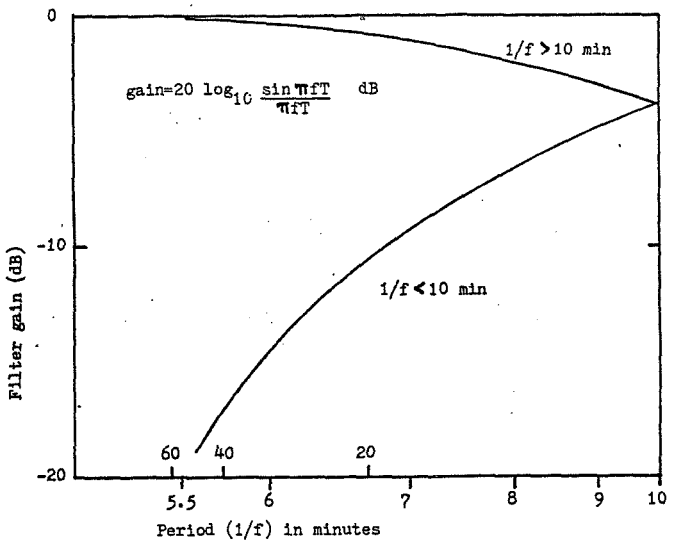

Figure 1. Attenuation due to a block fliter of length T=5 min.

Further cross checking is possible by combining N and E components for a given spectral frequency to form an elliptical oscillation at each site. For a gravity wave, the horizontal component of oscillation in the wind vector should be along the direction of propagation, consequently, the tilt angles of the ellipses should all be in this direction. In practice, because of analysis noise and other possible factors discussed later, this is seldom the case.

VERTICAL VELOCITY AND WAVELENGTH

These can be found by cross spectral analysis between different heights at the same site. The calculated phase difference at the smallest height separation, $\Delta\phi_v$ should again be between $\pm \pi/2$ to reduce doubt in the correct quadrant for the phase. This restriction can be relaxed if, for example, it is assumed that the phase velocity is always downward, or that there are no waves present with wavelength less than twice the minimum height separation. The above restriction limits the minimum acceptable wavelength to 12 km with our system (3-km transmitter pulse width). However, assuming that the scattering layers vary with height, or that there is volume scatter present over the 5- or 6-hr observing period, the shorter wavelengths should be attenuated and alleviate the problem of phase ambiguity.

Consistency in the data is checked by comparing the wavelengths (and sense, up or down) for two different height separations. As in the horizontal wave measurement, the velocity is found from the wavelength and frequency.

CONSIDERATIONS IN NUMERICAL ANALYSIS

Some of the problems encountered in analysis are low frequency resolution, particularly at periods of an hour or more, and gaps in the data sequence combined with possible sidelobes of strong spectral peaks (particularly the semidiurnal tide, which is removed before analysis).

The frequency resolution problem is to a large extent inherent in the attempted measurement. Even if the gravity wave source sends out a continuous

wave train, changes in the background wind field (especially tidal motions) will change propagation conditions over periods of several hours, so that the wave cannot be expected to be statistically stationary for longer periods of observation. Given that longer periods of observation do not help in measuring single waves, the resolution problem becomes acute at long periods. For example, a 6-hr observation period will have Fourier components at 6, 3, 2, 1.5 ... hr. When the data are tapered to reduce possible sidelobes, the resolution becomes even poorer, and waves of period say, 1-3 hr, may be combined in one spectral estimate. Higher frequency waves have smaller amplitude oscillations and run into analysis noise problems (from the individual wind determinations).

For ideal data, all values in the sequence are present, and the effect of tapering can be calculated. Gaps produce extra sidelobes which depend on the gap distribution, and it is possible that in extreme cases, tapering could do more harm that good.

These problems may be the reason that spectral peaks at the three sites (or even between N and E components at one site) are often at different frequencies; which is why methods other than spectral peak selection have been used in the choice of data.

SOME PUZZLING DATA

N and E spectral analysis for a 5-hr period are shown in Figures 2 and 3. A 10% cosine taper has been used at each end of the raw data, and the cross spectra smoothed somewhat before calculating the phase differences. The wave parameters shown have been calculated from spectral components which are above the noise level (i.e., the average amplitude between 20- and 10-min period), and have an NOD less than 0.3. The N and E spectra are quite different in places, which might be expected if the wave direction is close to N or E; and the single component spectra differ between sites, possibly due to analysis noise or gap distribution problems (each site is required to have more than 50% data existence before spectra are calculated) which are likely to cause sidelobes at different frequencies. The two periods of interest are near 2-hr and just below 1-hr period, where both components have wave parameters. Approximate parameters are shown below.

	N			E		
Period	θ	λ	V	θ	λ	V
2 hr	160°	100 km	20 m/s	350°	120 km	15 m/s
1 hr	330°	110 km	30 m/s	80°	200 km	50 m/s

The tilt angles were fairly stable around 2 hr and are shown below.

Site	Tilt (E of N)	Axial Rat(Maj/Min)
Park	120°	2.4
Drews	90°	2.2
Watson	90°	4.6

It can be seen that the wave directions given by N and E components are almost diametrically opposite for the 2-hr data, and the oscillations in wind are at right angles to both! The data are not normally quite this contradictory, but this puzzle must be explained before confidence can be placed in the rest of the results.

One possibility, which unfortunately does not appear to have a solution at present, is that there is more than one wave present in the spectral bandwidth, with possibly different speed, wavelength, and directions. If the directions are the same, then significant cancellation can occur at different sites. Table 1 shows some examples of the results expected if two waves at the same frequency

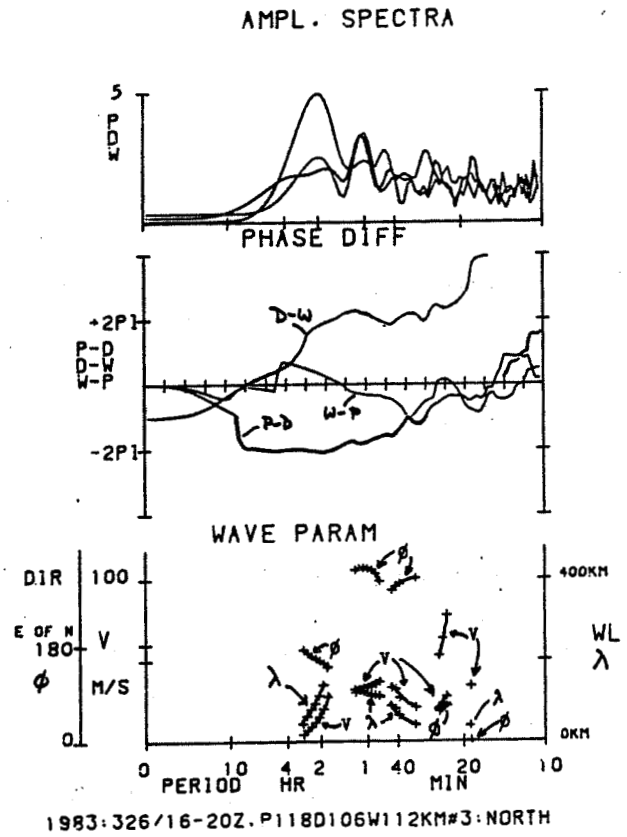

Figure 2. Results for northward component.

are summed. The amplitude of oscillation, direction of propagation (E of N), the wavelength (km) and the absolute phase (e.g., at one site) are given for each wave. The resulting N and E spectral amplitudes, tilt angle and axial ratio of the elliptical oscillation are shown for each site, and the calculated wavelength and direction for the resulting wave for separate N and E components. The NOD is by definition identically zero, since the frequency of oscillation is the same at each site.

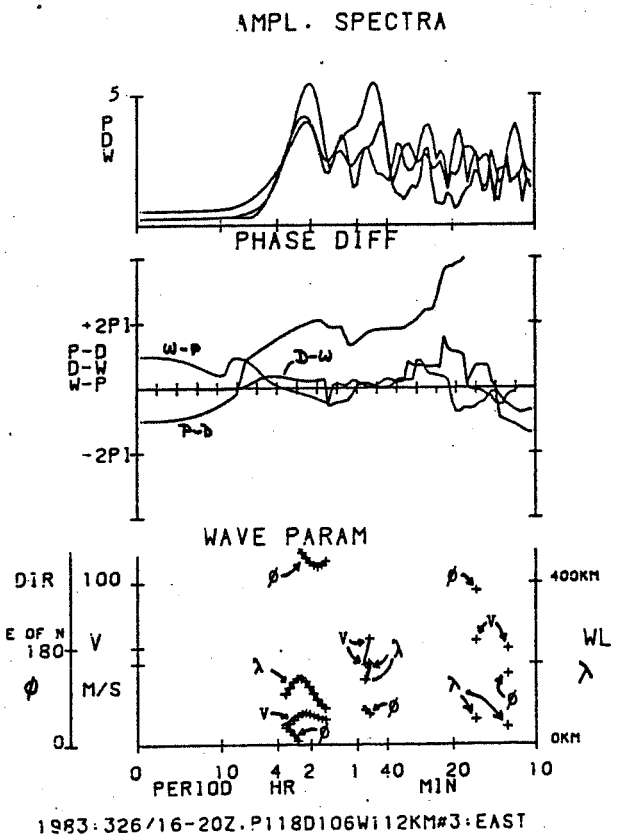

Figure 3. Results for eastward component.

Table 1. Numerical simulation of resulting wave parameters when two waves are combined in the measurement.

WAVE#1				WAVE#2				PARK				DREWS				WATSON				NCOMP			ECOMP		
M/S	DIR	WVL	PHI	M/S	DIR	WVL	PHI	AM	AE	TILT	RAT	AM	AE	TILT	RAT	AM	AE	TILT	RAT	WVL	DIR	MPD	WVL	DIR	MPD
20.	60.	300.	110.	20.	61.	100.	120.	20.	35.	61.	99.0	16.	29.	60.	99.0	19.	34.	60.	99.0	152.	61.	.00	150.	61.	.00
20.	60.	300.	110.	20.	61.	100.	140.	19.	34.	60.	99.0	14.	25.	60.	99.0	18.	32.	60.	99.0	152.	61.	.00	150.	61.	.00
20.	60.	300.	110.	20.	61.	100.	160.	18.	32.	60.	99.0	12.	20.	60.	83.4	16.	29.	60.	99.0	153.	61.	.00	150.	61.	.00
20.	60.	300.	110.	20.	61.	100.	220.	11.	20.	60.	89.2	2.	4.	60.	12.2	9.	15.	60.	56.7	173.	64.	.00	144.	61.	.00
20.	60.	300.	110.	20.	160.	100.	120.	9.	24.	110.	9.6	9.	24.	110.	7.6	17.	21.	110.	1.4	65.	171.	.00	307.	113.	.00
20.	60.	300.	110.	20.	160.	100.	140.	11.	23.	110.	3.1	9.	24.	110.	12.9	20.	19.	20.	1.1	84.	170.	.00	324.	108.	.00
20.	60.	300.	110.	20.	160.	100.	180.	18.	21.	110.	1.2	14.	23.	110.	1.9	26.	15.	20.	2.2	127.	158.	.00	372.	83.	.00
20.	60.	300.	110.	20.	160.	100.	210.	23.	17.	20.	1.4	19.	20.	110.	1.0	28.	12.	20.	5.0	145.	153.	.00	296.	42.	.00
20.	60.	300.	100.	10.	160.	100.	120.	3.	21.	87.	6.3	1.	21.	88.	49.0	12.	19.	68.	2.1	63.	54.	.00	345.	87.	.00
20.	60.	300.	110.	10.	160.	100.	160.	8.	20.	80.	2.6	5.	20.	86.	4.6	15.	17.	49.	2.2	219.	133.	.00	348.	76.	.00
20.	60.	300.	110.	10.	160.	100.	210.	15.	17.	51.	2.2	12.	18.	65.	2.0	19.	14.	37.	6.2	208.	138.	.00	265.	47.	.00

5. CRITERIA FOR SITE SELECTION AND FREQUENCY ALLOCATION (Keynote Paper)

J. Rottger*

EISCAT Scientific Association
S-981 27 Kiruna, Sweden

INTRODUCTION

During the first Workshop on Technical Aspects of MST Radar two recommendations were adopted on site and frequency selection, which first shall be repeated here; then we will make suggestions as to how to implement the recommendations, as well as summarize existing results, criteria and experiences to support the design of planned radars. Since the criteria to operate a radar will be quite different according to individual requirements of research groups, only summaries of items will be considered without aiming too strongly at their individual assessments.

(a) Recommendation on Site Selection

Although the actual interference problem will not be known until the antenna and receiver are installed, the prudent experimenter will conduct tests of interference before selecting a site. For large and expensive facilities these tests should be extensive and sensitive. A small directional antenna may be suitable to simulate sidelobe sensitivity of radars, but it should be remembered that sophisticated data-processing methods make system sensitivity extremely good; therefore it would be advisable to use (if possible) the complete data system to look for interference. These measures would certainly be called for before installing expensive, fixed sites.

(b) Recommendation on Frequency Selection

There is the difficulty of allocation of frequencies -- almost continuous use by these radars will be made when the band 40-60 MHz is allocated to other services. It was agreed that URSI should be contacted to see if they can make overtures to CCIR concerning this question.

More attention should be paid to the problem of designing MST radar antenna with lower sidelobes which will help both transmitting and receiving. This will help in the problem of MST radars interfering with each other in future.

SITE SELECTION

For selecting a location of an MST radar, one basically has to consider two general criteria, namely (a) the geophysical/meteorological phenomena which shall be investigated and (b) the operational requirements and capabilities one needs and which limitations one is able to accept.

Directions of priority of research could be towards synoptic scales (time scale of days), mesoscale (hours) or microscale (minutes). Microscale disturbances in the atmosphere are partly connected to orographic features (mountains,

---

* presently at Arecibo Observatory, Arecibo, Puerto Rico, on leave from Max-Planck-Institut fur Aeronomie, Lindau, W. Germany.

islands) and can influence considerably the accuracy and evidence of investigations of synoptic and mesoscale features. The latter are also influenced by the orography. Decision consequently has to be made to set up a radar in a mountainous or in a plain area. Of course also global climatology, i.e. research directed towards tropical, midlatitude or arctic atmosphere, will influence the selection of the radar location.

Some criteria to select a site, placing priority on optimum operation:

(1) Size of area (sufficient for antenna and equipment).
(2) Flatness and horizontal levelling, (antenna pattern accuracy).
(3) Vegetation, e.g. grass, bushes (influence maintenance of antenna).
(4) Composition of ground, e.g. rocks, soft soil, swamp, ... (influence antenna construction and reliability).
(5) Cultivated or wasteland (influences costs),
(6) Cattle or wild animals (may destruct system),
(7) Shielding by hills (avoid clutter and attenuate interference).
(8) Vicinity of next house or village (interference, security, service).
(9) Vicinity to institute or laboratory (travel, trouble shooting, maintenance).
(10) Electric power line (distance, costs to connect the system).
(11) Stability of line voltage, (reliability of operation).
(12) Water supply.
(13) Road access.
(14) Availability and cost of telephone line, (voice and data transmition).
(15) Noise interference from power line, close-by factories, roads (ignition noise).
(16) Height above sea level (pick-up of long distance groundwave interference, higher altitude permits increase of upper height to be sounded by radar).
(17) Distance from country border line (unexpected future radio interference).
(18) Costs to prepare the site and to rent and to maintain the site (duration?).
(19) Snow cover (antenna reliability and road access).
(20) Windbreaks (antenna construction).
(21) Probability of flooding.
(22) Aircraft flight routes (clutter and interference).
(23) Other close-by radio/radar systems (mutual interference).

These items may not be exhaustive but can give a guideline and were discussed and completed during the workshop discussions. The weighting of these different items has to depend on individual orientations and requirements.

A short discussion shall be added to item 7 on the clutter problem (i.e., signal returns from unwanted targets). In another paper (Paper 5.1-B, this volume) this author concludes that a shallow valley may be sufficient for shielding, even a flat plain may be acceptable, if no extraordinary conditions (e.g., very high extending mountains, buildings or radio towers in the surroundings up to several 10 km) spoil the atmospheric signal. Also seaclutter can be avoided by these means. Clutter from field-aligned ionospheric irregularities, however, can occur at locations close to the magnetic equator at near zenith angles (through the antenna main lobe) and at high latitudes at low elevation angles (through low angle sidelobes).

FREQUENCY SELECTION AND ALLOCATION

Following the early operation of the Jicamarca Radar which proved its applicability for probing the mesosphere, stratosphere and troposphere, the

following generation of radars operated in the same frequency band between 40 MHz and 55 MHz (Figure 1). Although it proved true that very efficient radar investigations of the lower and middle atmosphere can be done using these frequencies (which in the early times was strongly questioned by traditional radar meteorologists), it is not yet established that this frequency band is the optimum. Lower frequencies obviously may suffer from interference due to ionospheric propagation and a strong increase in sky noise (about inversely proportional to the square of frequency), but will allow larger antenna areas (increase of echo signal strength) and may yield stronger contributions from partial reflection. On higher frequencies the noise level decreases, improving the sensitivity and thus may allow operating with lower transmitter power and antenna gain. However, the wave number spectrum of atmospheric reflectivity is not yet known sufficiently accurately to permit a final decision which frequency may be optimum. An upper limit is obviously given by the high frequency boundary of the inertial subrange of atmospheric turbulence, determining the maximum height to be sounded. Mesospheric turbulence scatter, for instance, cannot be detected at much higher frequencies than 50 MHz, and at 430 MHz the upper height is even as low as about 30 km. It is evidently noticed also (Table 1) that all higher frequency radars (430/440 MHz, 930 MHz or 1290 MHz) use considerably higher power, although the reason is that these radars are operated mainly for incoherent scatter observations of the ionosphere. We will concentrate here on the frequency selection and allocation in the standard frequency band of MST radars in the low VHF range.

During the last World Administrative Radio Conference in 1979, worldwide frequency allocations were newly arranged and accepted. In Table 2 we have summarized the allocations between 30 MHz and 68 MHz, which are subdivided according to the worldwide Regions I, II and III (Standard of the ITU-International Telecommunications Union, see Figure 2). Except for three fairly narrow bands 30.005-30.010 MHz, 37.5-38.25 MHz, 40.66-40.70 MHz, no special allocations are furnished for scientific research purposes on an international basis. The used VHF radar frequency bands are merely allocated through national authorities, and it is evident that no legal claim can be brought forward by radar researchers to obtain a frequency allocation. The radars are permitted only to operate on the noninterference basis; i.e. they have to cease operation if interference to the primary or secondary services operating in the same band is reported. The services which most likely can be affected are the fixed and mobile (example in Table 3a), the amateur (Table 3b) and the TV broadcast service (Table 2). Fortunately, no major complaints by these services are known which would prevent VHF radar operation or even yield to decisions of national authorities to refuse issuing new licenses.

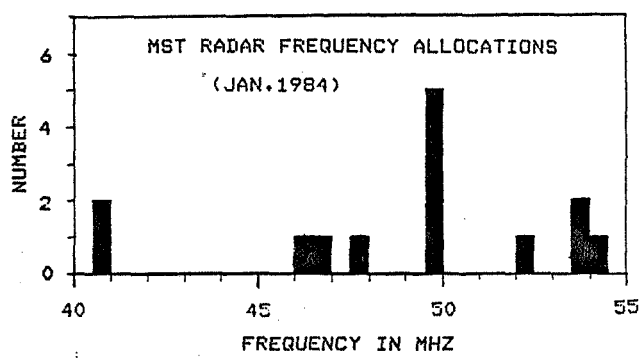

Figure 1.

C-4

Table 1. Operational and planned MST/ST/IS radars (Nov. 1983). From ROTTGER (1984).

facility	mode	lat./long. deg.	freq. MHz	ave.power kW	min.pulse width μs	duty cycle (max.)%	antenna aperture (eff.)m²	antenna beam width	antenna configuration	antenna mode	antenna steerability	status	ref.
Arecibo/Puerto Rico	IS, ST	19N,67W	430	120	1	6	50000	0.17°	circ.dish	DB	20°(m)	op	(1)
" / "	MST		46.8	1	1	2	50000	1.7°	"	DB	"	cs	
Buckland Park/Australia	(M)ST	35S,136E	54.1	0.4	7	0.7	7500	3.2°	PAC,PAY	DB,SA	15°(1)	(op)	(2)
Chung-Li/Taiwan	(M)ST	25N,121E	52	4	1	2	2500	5°	PAY	DB,SA	15°(2)	cs	(3)
EISCAT/	IS,ST	70N (67N)	933.5	250	2	12.5	520	0.6°	3 circ.dishes	DB	80°(m),tristat.	op	(4a)
North Scandinavia	IS,ST	19E (27E)	224	600	2	12.5	3300	0.6°,1.7°	cyl.dish	DB	30°,60°,20°(m)	cs	(4b)
Equatorial Pacific	ST (3x)	(0,150E)	49.8	0.2	5	(2)	(5000)	(5°)	PAC	DB	15°(2)	pl/cs	(5)
India	MST	—	45-55	60	1	2.5	20000	3°	PAC	DB	20°(2)	pl	(6)
Jicamarca/Peru	MST,IS	12S,72W	49.9	200	(1)	5	80000	1.06	PAC	DB,SA	3°(m)	op	(7)
LSEET/France	ST	43N,5E	47.8	1	2	1.7	3x2000	5°	PAC	DB	15°(2)	cs	(8)
Millstone Hill/USA	IS,ST	43N,72W	440	30	2	1.6	1640	1°	circ.dish	DB	<80°(m)	op	(9)
MU/Japan	MST,(IS)	35N,136E	46.5	50	1	5	8330	3.6°	PAY	DB,SA	30°(m)	(op)	(10)
Penn.State/USA	ST (3x)	41N,78W	48-50	1	4	2	2500	5°	PAC	DB	15°(2)	pl	(11)
Plattsville/USA	ST (4x)	40N,105W	49.8	1	4	1.7	2000	5°	PAC	DB	15°(2)	op/rt	(12)
Poker Flat/USA	MST	65N,147W	49.9	128	2	2	40000	1.4°	PAC	DB	15°(2)	op/rt	(13)
PROUST/France	ST	45N,2E	935	(~10)	4 (0.2)		2000 (95)		2 dishes	DB	bistatic	(pl)	(14)
Sondre Stromfjord/Greenland	IS,ST	67N,51W	1290	100	(1)	3	420	0.5°	circ.dish	DB	90°(m)	op	(15)
SOUSY/Germany	MST	52N,10E	53.5	24	1	4	3200	5°	PAY	DB,SA	12.5°(m)	op	(16a)
" /Norway	MST	69N,16E	53.5	8	1	4	8800	3°	PAY	DB	4.0°(2),5.6°	op	(16b)
Sunset/USA	ST	40N,106W	40.5	16	1	2.5 (16)	2200	4.4°,4.8°	PAC	DB	60°(2,m)	op	(17)
United Kingdom	MST	—	~50	12	1	5	5200	3.6°	PAY	DB	5°,10°(2)	pl	(18)
Urbana/USA	MST	40N,88W	40.9	6	10	1	2000	(<3°)	PAD	DB	1.5°(1),2.5°(2)	op	(19)

mode: IS = incoherent scatter (thermosphere, may include mesosphere)
MST = mesosphere,stratosphere,troposphere
ST = stratosphere,troposphere

antenna:
configuration: PA = phased array
PAC = phased array, coaxial-collinear dipoles
PAD = phased array, dipoles
PAY = phased array, Yagis

mode: DB = Doppler beam swinging
SA = spaced antenna (interferometer)

steerability: 15°(2) = zenith angle 15° in 2 orthogonal planes (and zenith)
15°(m) = multiple position out to 15° zenith angle (and zenith)

status: op = operational
op/rt = routine operation (continuous)
cs = under construction
pl = planned

ref.: (1) Woodman+); (2) Vincent et al., 1982; (3) Brosnahan et al.+); (4a) Röttger et al.+); (4b) Hagfors et al., 1982; (5) Balsley+); (6) Koshy+); (7) Woodman and Guillén, 1974, Woodman and Farley+); (8) Crochet+); (9) Rastogi+); (10) Kato+); (11) Peters+); (12) Strauch et al., 1983, Strauch+); (13) Balsley et al., 1980, Balsley et al.+); (14) Glass+); (15) Watkins+); (16a) Röttger et al., 1978; (16b) Czechowsky et al.+); (17) Green et al., 1975, Green+); (18) Hall+); (19) Röyrvik and Goss+)

+) = in: Bowhill (1984), Handbook for MAP 9.

Table 2. Worldwide frequency allocation plan (ITU). Capital letters denote primary services.

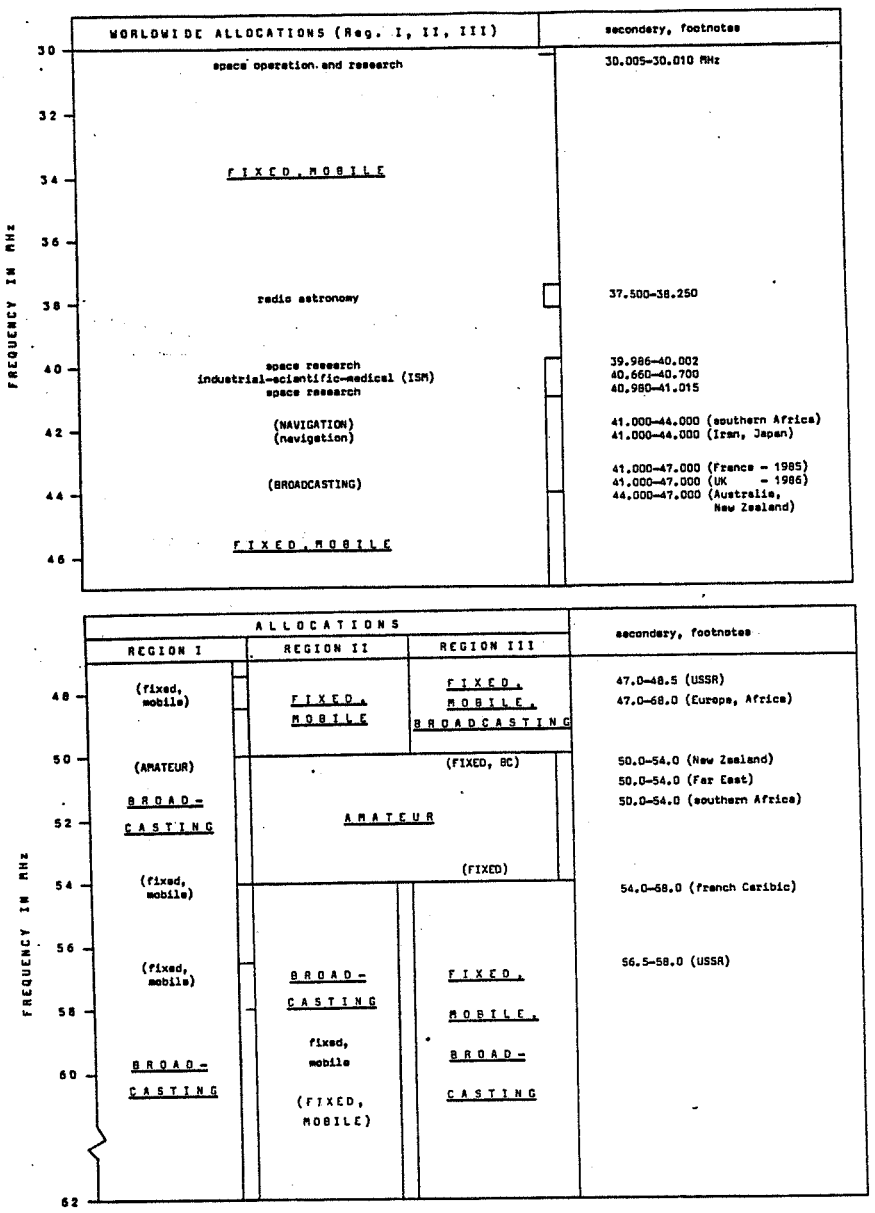

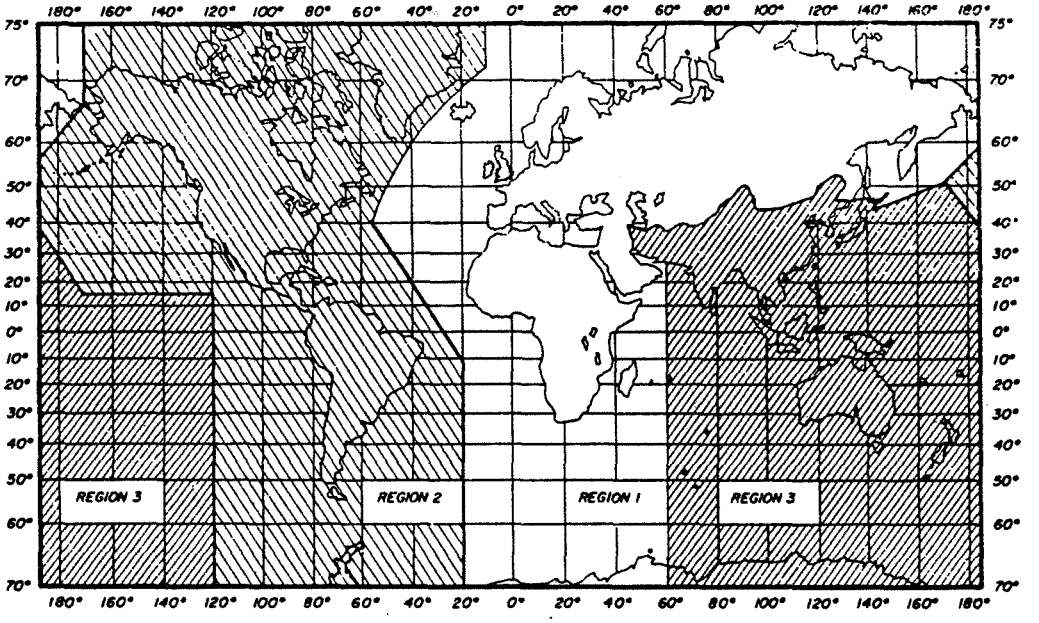

Figure 2. ITU-Regions.

Because of the fact that the VHF radars mostly cover a fairly wide bandwidth (100 kHz-2 MHz), the transmitted energy is spread out into a fairly wide frequency band, which yields less interference to narrow band operations such as those of the fixed, mobile or amateur services. Furthermore, interference is strongly suppressed because the main beam direction of VHF radars is vertical. Only a minor fraction of the energy is transmitted horizontally through the sidelobes where it could cause harmful interference to the other services. More observation has to be pointed to the fact that the radar reception will be disturbed by transmission of other services.

This problem, however, is mostly not too crucial if provision is made that the operations are properly separated in space and frequency. Since essentially ground wave propagation occurs, the field strength of interfering signals will be negligible at distances of several 10 km. However, in the lower VHF range ionospheric propagation can still occur and drastically increase the interference level. This is shown in the example of Figure 3, where the diurnal variation of frequency occupation monitored in December 1979 and January 1980 at the Arecibo Observatory is shown (after ROTTGER, 1980). Signals observed in the morning hours (06-12 AST) evidently originated through ionospheric propagation from the US mainland. The cumulative distributions of Figure 4 indicates occurrence maxima at two channels around 43 MHz and 49.5 MHz which were due to local traffic. The best choice of frequency was 46.8 MHz. It is strongly suggested to carry out similar frequency surveys before applying for a license to operate a VHF radar.

We see from Table 2 that the band 47 (54)-58 MHz is mostly covered by TV broadcast allocations (TV-band I), although partially also the fixed or mobile and the amateur service is permitted. The TV broadcast covers a much wider bandwidth than the radar operation and can be quite sensitive to interference (the video channel is much more sensitive to interference than the audio channel). In Figure 5 the required interference suppression (according to CCIR) is shown for a TV channel. It is noticed that the requirements are most strict

Table 3. a) National frequency allocation plan of United States.
b) Amateur radio band plan (50 MHz).

UNITED STATES

Band MHz 1	National Provisions 2	Government Allocation 3	Non-Government Allocation 4	Remarks 5
39.00-40.00	NC US94		LAND MOBILE	Public safety
40.00-42.00 (ISM 40.68	C 236 US94 US210 US220 0.02 MHz)	FIXED MOBILE		See Section 4.3.6 of the Manual for Channeling Plan.
42.00-46.60	NC		LAND MOBILE	42.00-42.95 Public safety 42.95-43.19 Industrial 43.19-43.69 Domestic public/Industrial/ Public safety 43.69-44.61 Land transportation 44.61-46.60 Public safety
46.60-47.00	C	FIXED MOBILE		See Section 4.3.6 of the Manual for Channeling Plan.
47.00-49.60	NC		LAND MOBILE	47.00-47.43 Public safety 47.43-47.69 Public safety/Industrial 47.69-49.60 Industrial
49.60-50.00	C	FIXED MOBILE		See Section 4.3.6 of the Manual for Channeling Plan.
50.00-54.00	AMATEUR US1		AMATEUR	
54.00-72.00	NC		BROADCASTING	Television broadcasting

AMATEUR BANDPLAN

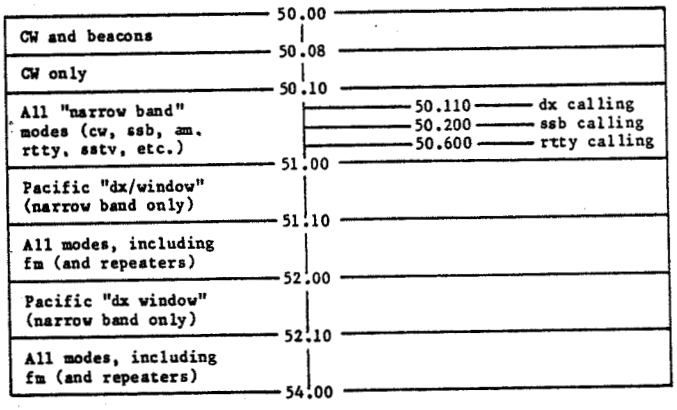

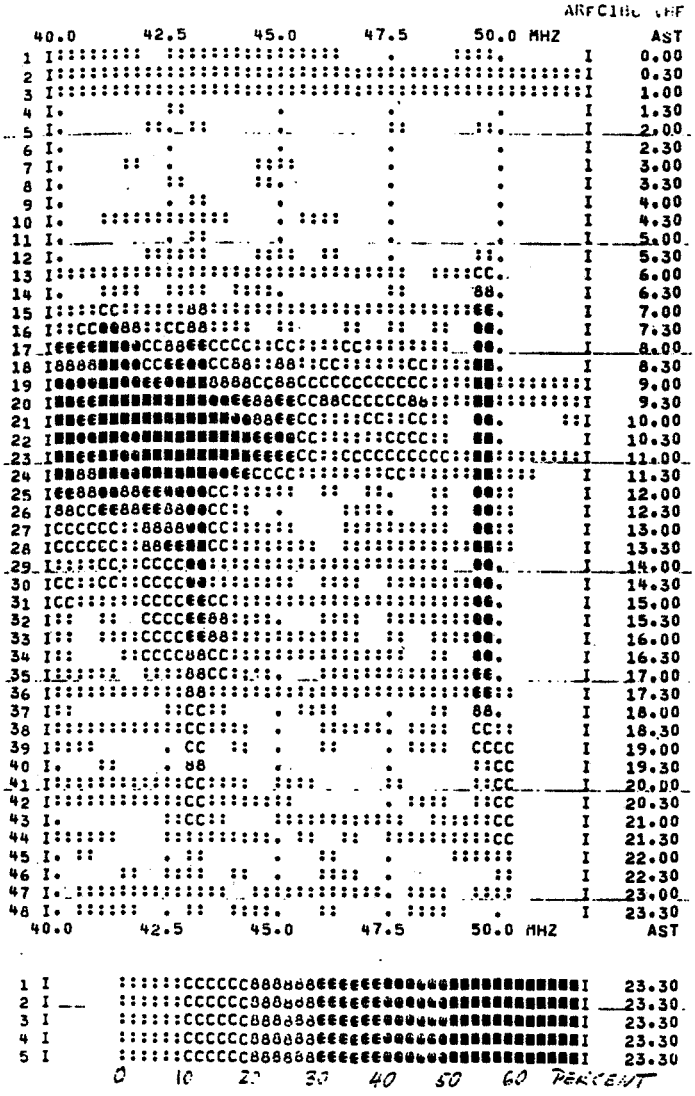

Figure 3. Occurrence of signals as function of time of day (AST) and frequency at the Arecibo Observatory in December 1979 and January 1980.

at frequencies close to the video, colour and audio carriers.

Extensive field and laboratory measurements, which were done in preparation of the licence application phase of the SOUSY-VHF-Radar in W. Germany, showed that radar operation in a TV channel is possible without causing mutual interference. It was shown that a radar operation (centrecarrier) frequency f_r = 53.5 MHz, i.e. a frequency between the colour and the audio carrier, causes the least interference to TV reception. Also a frequency just at the lower limit of a TV channel (e.g. f_r = 54.0 MHz) can be acceptable. According to the subdivision of TV-band I into channels, the video carrier frequencies

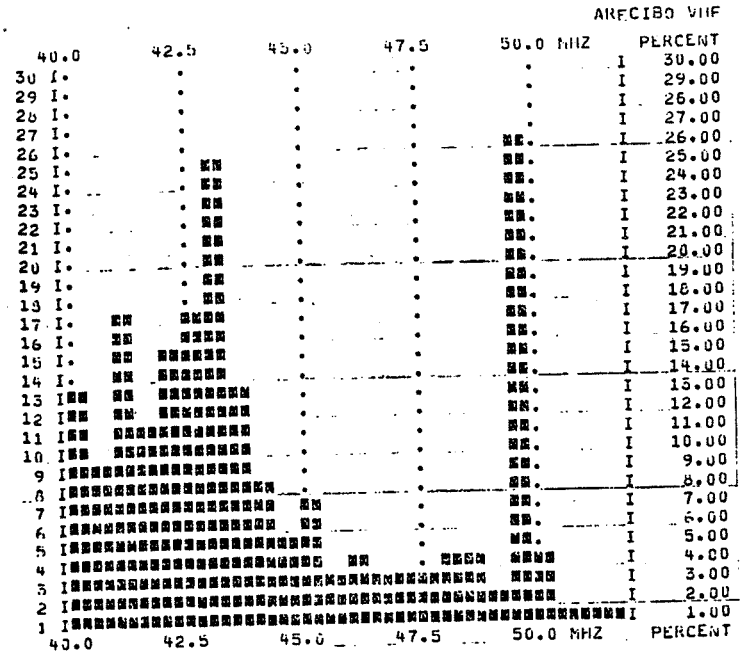

Figure 4. Cumulative distribution of interference (summary of Figure 3).

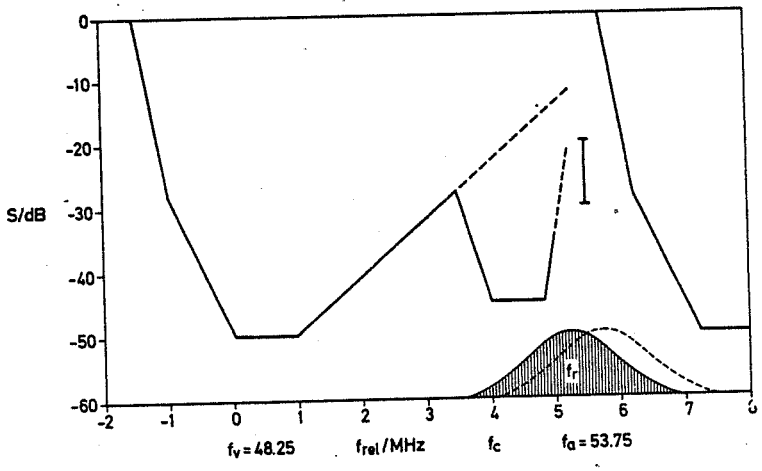

Figure 5. Interference suppression required for a TV channel (CCIR norm).

are at f_v = 48.25, 55.25 and 62.25 MHz. Radar operation (centre) frequencies $f_r = f_v + 5.25$ MHz or $f_r = f_v - 1.25$ MHz are accordingly most suitable.

Further field measurements made during the early operation of the SOUSY-VHF-Radar (f = 53.3 MHz, in a channel used by a TV-broadcast station at 160 km distance) did not indicate any interference to TV users. It even was found that the radar signal was no more detectable (because of mountain shielding and sidelobe suppression) at some 10 km distance from the radar. Occasional increases of noise level observed with the SOUSY-VHF-Radar might have been caused by increased TV field strength at the radar site during enhanced tropospheric propagation conditions. Very short-term interference (seconds to minutes duration), observed very rarely, was attributed to mobile stations in the vicinity of the radar. During summertime also TV signals from southern Europe occasionally occurred through reflection at sporadic-E layers.

REFERENCES

Balsley, B. B., W. L. Ecklund, D. A. Carter and P. E. Johnson (1980), The MST radar at Poker Flat, Alaska, Radio Sci., 15, 213-223.

Green, J. L., J. M. Warnock, R. H. Winkler and T. E. VanZandt (1975), A sensitive VHF radar for the study of winds, waves and turbulence in the troposphere, stratosphere and mesosphere, Preprint Vol. 16th Conf. on Radar Meteorol., 313-315 (publ. by Am. Meteorol. Soc., Boston, MA).

Hagfors, T., P. S. Kildal, H. J. Karcher, B. Liesenkotter, and G. Schroer (1982), VHF parabolic cylinder antenna for incoherent scatter radar research, Radio Sci., 17, 1607-1621.

Rottger, J. (1980), Utilization of the lower VHF band for radar experiments at the Arecibo Observatory, Tech. Rep. MPAe-T-00-80-01, Max-Planck-Institut fur Aeronomie, Lindau, W. Germany.

Rottger, J. (1984), The MST radar rechnique, Handbook for MAP, Vol 13, 187 232, SCOSTEP Secretariat, Dep. Elec. Computer Eng., Univ. IL, Urbana.

Rottger, J., J. Klostermeyer, P. Czechowsky, R. Ruster and G. Schmidt (1978), Remote sensing of the atmosphere by VHF radar experiments, Naturwissenschaften, 65, 285-296.

Strauch, R. G., D. A. Merritt, K. P. Moran, K. S. Earnshaw, and D. van de Kamp (1983), Tropospheric wind profiling with Doppler radar, Preprint Vol. 21st Conf. on Radar Meteorol., 118-125, (publ. by Am. Meteorol. Soc., Boston MA).

Vincent, R. A., W. G. Elford, and B. H. Briggs (1982), A VHF radar for atmosphere studies, The Australian Physicist, 19, 70-73.

Woodman, R. F., and A. Guillen (1974), Radar observations of winds and turbulence in the stratosphere and mesosphere, J. Atmos. Sci., 31, 493-505.

RECOMMENDATION

SITE SELECTION

Noticing that

(1) for a variety of meteorological investigations influences of orography are a disturbing factor,
(2) clutter and interference is mostly experienced to be minor problem,

the notion is supported

to preferably locating MST radars in flat terrain rather than in mountainous regions (excluding, obviously, research on orographic influences on meteorological phenomena).

RECOMMENDATION

FREQUENCY ALLOCATION

Noticing that

(1) Licenses to operate VHF/UHF radars are granted by national authorities in a cooperative manner, and operation has to be on a noninterference basis.
(2) Crucial interference due to radar operation has not yet been reported.
(3) The number of VHF/UHF radars used for research purposes has already increased and obviously will steadily increase, and these radars may even be included in operational meteorological systems which will increase their number explosively.

It is recommended that formal steps shall be undertaken to form a special study group of CCIR to collect experiences and define requirements and standards to facilitate negotiations with the licensing authorities and to introduce these operations officially into an internationally accepted frequency allocation scheme.

5.1A FREQUENCY AND SITE SELECTION CRITERIA FOR MST RADARS

G. D. Nastrom

Control Data Corporation
Box 1249
Minneapolis, MN 55440

The majority, if not all, MST and ST radars for which data are currently available are located in or near mountainous terrain. When measuring horizontal velocities, the terrain is a small factor, but when measuring vertical velocities. the meteorological noise induced by rough terrain can severely limit the usefulness of the observations. For example, the synoptic-scale vertical velocity is of prime importance for many meteorological purposes. but it is usually small, less than 10 cm s^{-1} or so. (Synoptic scale includes motion systems with time scales roughly from three to 24 hours). When the variance of the vertical velocity is too large. it is not possible to suitably filter the data to detect the small synoptic-scale signal with reasonable statistical confidence. It is well established that the variance of vertical velocity at all tropospheric levels is directly related to the low level wind speed during flow over rough terrain (e.g., ECKLUND et al., 1982; NASTROM et al., 1984). Also, the vertical velocity may be biased by standing lee waves during flow over rough terrain. On the other hand, our studies suggest that the synoptic-scale vertical velocity can be measured by ST radars where the terrain is smooth.

The important point is that the large-scale (synoptic-scale) vertical velocity cannot always be reliably determined from MST radar data when the underlying terrain is rough. As the vertical velocity is potentially one of the future radar site selections, taking into account the desired meteorological applications of the data as well as engineering design factors. Especially. if the synoptic-scale vertical velocity is a desired variable, the radar should not be located near mountains.

REFERENCES

Ecklund, W. L., K. S. Gage, B. B. Balsley, R. G. Strauch and J. L. Green (1982), Vertical wind variability observed by VHF radar in the lee of the Colorado Rockies, Mon. Wea. Rev., 110, 1451-1457.

Nastrom, G. D., W. L. Ecklund and K. S. Gage (1984), Direct measurement of synoptic-scale vertical velocities using clear-air radars. Submitted to Mon. Wea. Rev.

5.1B MOST DESIRABLE TERRAIN, e.g., FLAT VS VALLEY LOCATION

J. Rottger

EISCAT Scientific Association
981 27 Kiruna, Sweden

THE INFLUENCE OF GROUND REFLECTIONS ON THE ANTENNA DIAGRAM AT LOW ELEVATION ANGLES AND THEIR EFFECT ON RADAR GROUND CLUTTER AND INTERFERENCE

For obtaining an estimate it is assumed that ground reflections are similar for all (Yagi) elements of a phased array and they just change the radiation pattern of the single elements. This consequently yields a change of the radiation pattern of the entire array. It is furthermore assumed and deemed to be justified that the radiation pattern of a Yagi antenna can be treated in a good approximation for the present purpose, similar to the pattern of a single dipole, if one confines to radiation angles which are roughly perpendicular to the main beam of the Yagi antenna (e.g. at low elevation angles for vertically pointing Yagis).

Assume the geometry given in Figure 1. Antenna A is located at a height z_A above the ground. The direct path length between the antenna and the clutter target C is r_1, and the path length of the wave, reflected at R on the ground surface, is r_2. The horizontally stratified ground surface has the complex reflection coefficient ρ. The height of the clutter target above the ground surface is z_C, and the ground distance between antenna A and clutter target C is d.

Let E_o be field strength at C for free space propagation, and E_R the resulting field with ground reflection, then

$$\frac{E_R}{E_o} = \exp\left(-i\,\frac{2\pi\, r_1}{\lambda}\right) + \rho \cdot \exp\left(-i\,\frac{2\pi\, r_2}{\lambda}\right) \qquad (1)$$

where λ is the wavelength of the radar signal.

Let us assume some limiting values, which appear reasonable (λ = 6 m):

$$z_A < \lambda,\ z_C < 5\lambda,\ d > 250\lambda,$$

then $\alpha_1 \approx \alpha_2 = \alpha < 1.5°$. Ground reflection at R is within 100λ of antenna if $\alpha > 0.5°$, e.g. ground is assumed flat (inclination to the horizontal smaller than λ) out to several hundred meters from the antenna.

The reflection coefficient for horizontal polarization (propagation direction perpendicular to axis of dipole) is

$$\rho_h = \frac{\sin\alpha - \sqrt{\varepsilon_r^* - \cos^2\alpha}}{\sin\alpha + \sqrt{\varepsilon_r^* + \cos^2\alpha}}$$

and for "vertical" polarization (propagation direction in direction of dipole axis)

$$\rho_v = \frac{\varepsilon_r^* \sin\phi - \sqrt{\varepsilon_r^* - \cos^2\phi}}{\varepsilon_r^* \sin\phi + \sqrt{\varepsilon_r^* - \cos^2\phi}}$$

*presently at Arecibo Observatory, Arecibo, Puerto Rico, on leave from Max-Planck-Institut fur Aeronomie, Lindau, W. Germany.

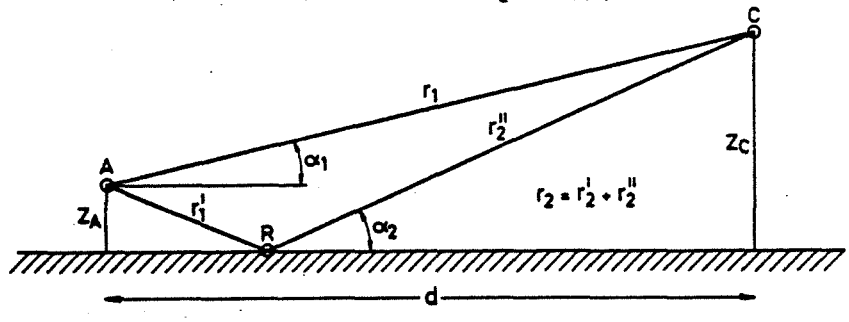

Figure 1. Geometry to calculate interference field at C of direct wave and indirect wave, reflected on the ground surface at R.

where ε_r^* is the complex permittivity given by

$$\varepsilon_r^* = \varepsilon_r - i\,60\sigma\lambda,$$

with ε_r = dielectric constant (relative), σ = ground conductivity.
For $\alpha < 1.5°$, these reduce to

$$\rho_h \approx -1,$$

$$\rho_v \approx -1.$$

(The deviation from -1 is fairly negligible for low elevation angles and reasonable ground permittivity and conductivity. Using $\rho \approx -1$ in equation (1) for $r_1 \approx r_2$ elucidates the clutter reduction!)

For $z_A < z_C \ll d$, we obtain for the two-way (radar) case

$$\frac{E_R}{E_o} = 4 \sin^2 \frac{2\pi\, z_A \cdot z_C}{\lambda \cdot d}. \qquad (2)$$

Since z_C is mostly much larger than z_A, the altitude extension of the clutter target essentially determines the clutter echo strength. Inserting the limiting values $z_A < \lambda$, $z_C < 5\lambda$, $d > 250\lambda$, equation (2) yields

$$\frac{E_R}{E_o} \lesssim 0.07 \;(\hat{=}\; -24\ \text{dB}).$$

To illustrate: The ground reflection reduces the clutter echo strength by at least 24 dB for this fairly exposed condition of a highly elevated target (e.g., top or an antenna tower at 30 m height at 1500 m distance). A tower with 10 m height would yield a clutter strength reduced by another 20 dB.

It is evident that most of the clutter contribution comes form the top part of such targets. This is because of the quadratic altitude weighting (for $z_A \cdot z_C \ll \frac{\lambda d}{2\pi}$) given by (2), and because the larger the elevation α, the more the ground reflection coefficients deviate from -1. Of course the actual clutter echo strenth depends also on the total reflection coefficient of the clutter targets (has to be integrated), which, however, may not change so strongly as the height dependence given by (2). Clutter returns from localized (point or line) targets, e.g. TV towers or buildings, will be weaker than distributed (area) targets because of their r^{-4} dependence. From equation (2) it is de-

duced that clutter returns may get fairly strong if z_C is large. This would be, for instance, the case for mountains extending up to several hundred meters or even higher altitudes. Additionally, for such extended targets only an r^{-2} dependence applies and the target reflection coefficient can be orders of magnitude larger than for single towers or buildings.

One has to keep in mind that ρ_v deviates substantially from -1 for already very small elevation angles, which is not the case for ρ_h. It follows that in direction of the dipole axis the cancellation of direct and ground reflected wave is no more efficient, except of for very grazing elevation angles.

Similar to clutter problems with elevated targets, the reverse can happen also, namely problems with an elevated antenna. Equation (2) shows that this problem can be treated in an exactly equal way. It shows that obviously very critical clutter can occur even from fairly low targets. Part of these clutter problems can be explained by the fact that the direct radiation is fairly inefficiently cancelled by the ground-reflected radiation because of the not grazing incidence angle to the earth's surface.

Equation (2), of course, also yields an estimate for interference pick-up if one assumes a transmitter (TV, broadcast, etc.) with antenna height z_C. Again, the ground-reflected signal at low elevation angles almost eliminates, or at least strongly reduces, direct signals. Equation (2) also indicates that the ground clutter suppression improves by lowering the radar antenna; the single feed elements of the antenna (or their phase centrum), however, must not be a quarter wavelength above the ground to obtain the radiation suppression at low angles.

SUMMARY

It is shown that ground reflection very effectively cancels the radiation at grazing angles ($\alpha \lesssim 5°$) because the reflected wave suffers a phase reversal during reflection. This even can suppress low sidelobes of the array pattern which may be regarded as crucial without taking into account ground reflections. The location of an array antenna at a flat ground (extending out to several 100 m) may be sufficient, but a shallow valley should generally be preferred to eliminate the low angle radiation effects. However, high extending targets, such as radio towers or mountains in the close vicinity, will still cause considerable clutter echoes, even when optimizing the antenna array for low angle radiation suppression.

6. SUMMARY OF SESSION ON OPTIMUM TRANSMITTER AND ANTENNA CONFIGURATION FOR MST RADAR

J. L. Green

Aeronomy Laboratory
National Oceanic and Atmospheric Administration
Boulder, CO 80303

It is important for persons that analyze interpret MST radar data to confer with those responsible for the hardware incorporated into these systems. Two recent examples of this necessary interaction can be cited:

(1) Dr. G. D. Nastrom has pointed out that in order to obtain the average vertical velocity related to meteorological systems, the radar antenna must be pointed with an accuracy of 0.1 degree. This is, of course, a fundamental consideration in the design of the radar antenna.
(2) The cost of editing spurious records from a radar data set may well exceed the cost of a radar antenna. This leads to a consideration of antenna sidelobe reduction to reduce the number of spurious records.

There were five papers presented in this session. Each paper led to a discussion of improvements in the MST or ST technique. These papers were:

T/R Switch Design for Short-Range Measurements by B. Yu. This was a description of a new PIN diode switch to replace the gas-discharge switch at the University of Illinois radar. This paper led to a discussion of low altitude measurements by ST radars. The conclusion was that UHF radars were better for this purpose.

Practicality of Electronic Beam Steering for MST/ST Radars by W. L. Clark and J. L. Green. This paper, presented by W. L. Clark, described a low cost relay phase shifter that could be used to steer the beam of a VHF antenna. A discussion ensued over the economics of a steered array versus the use of separate antennas for each beam position. It was concluded that if more than two beam positions were used, steering was more economical.

Increase of Antenna Area Instead of Transmitted Power by J. Rottger. This paper pointed out that the sensitivity of a radar to specular echoes (received on a vertical beam) was proportional to the antenna area squared. For this class of echoes a greater increase in sensitivity may be obtained from an increase in the antenna area than from the same increase in transmitted power.

The use of Interferometer Techniques for Beam Steering by J. Rottger. This paper proposed the use of a broad transmitted beam and an interferometer to investigate the angle of arrival of radar echoes. If the output of each interferometer element was recorded, angular investigations can be made subsequent to the actual experiment. This paper led to a discussion of the experimental possibilities of multibeam systems such as the Butler matrice. The principal limitation of these techniques was the loss of sensitivity due to the spread of the transmitted energy over a large radar volume.

Testing and Optimizing MST Coaxial-Collinear Arrays, J. M. Warnock and J. L. Green. This paper, presented by J. M. Warnock, described a method of testing and calibrating a VHF array with a movable probe and a vector voltmeter. The data obtained from these tests can be used to calculate the polar diagram of the antenna radiation and the resistive losses of the antenna. Although the

prescribed time for the end of the session precluded further discussion of this technique, this presentation may be expanded into a recommendation for further study.

RECOMMENDATION

Since coaxial-collinear antennas have come in to wide usage, and since probe measurements along a line of these dipoles indicate a decrease in radiated power, further study of this type of antenna should be made to determine the aperture efficiency of this antenna type. It may turn out that this natural tapering reduces the sidelobe response of the antenna.

6.1A T/R SWITCH DESIGN FOR SHORT-RANGE MEASUREMENTS

B. Yu

Aeronomy Laboratory
University of Illinois
Urbana, Illinois 61801

The PIN diode switch is designed to protect the receiver from burnout or damage on transmission and channel the echo signal to the receiver on reception. The transmitter peak power of Urbana Radar is a megawatt or more. The receiver must be protected firmly.

A schematic diagram of a TR-ATR switch for the Urbana Radar shown in Figure 1. The T/R switch consists of a half wavelength coaxial cavity with tuning condenser and PIN diodes.

PIN diodes UM4300 produced by Unitrode Corporation are selected for the system. Two UM4300 PIN diodes were mounted between the inner and outer conductor. The dc biasing voltage required for the PIN diodes is supplied by a control circuit. On transmission, the PIN diodes are forward biased to about 0.5 amperes. On reception, about 10 volts reverse voltage is applied to the diodes, which produces an initial reverse current to speed the recovery time.

The T/R switch characteristics were estimated by testing on the Urbana Radar. Figure 2 shows the result of testing at different peak transmitter powers from 410 kW to 1500 kW.

The next step is that we are going to mount 4 PIN diodes on a circle in coaxial line to suffer more transmitter power. The cross section of the 4 PIN diodes T/R switch is shown in Figure 3.

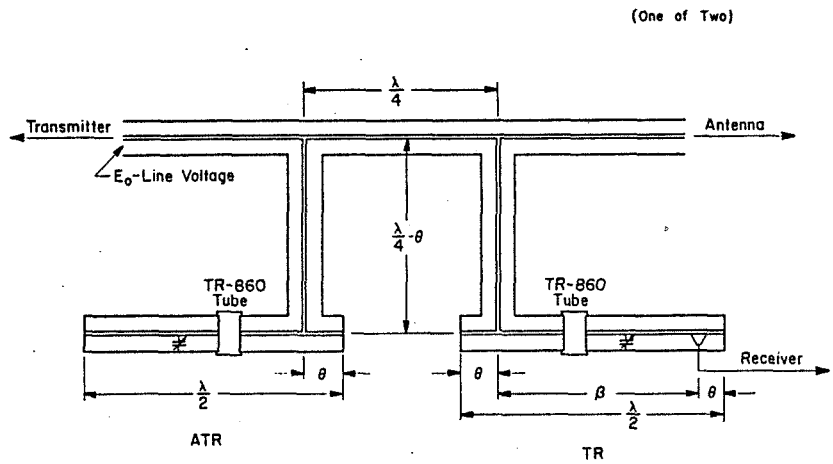

Figure 1. TR-ATR switch of the Urbana radar.

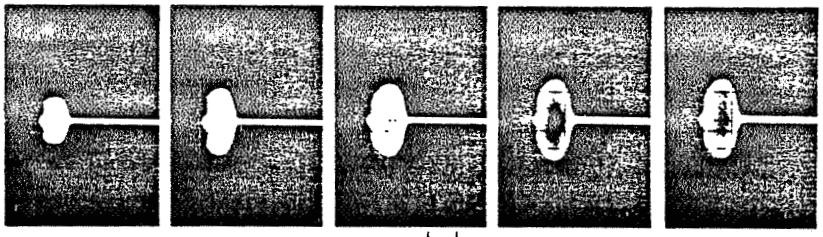

	1	2	3	4	5
Average Power	3.3 kW	5.5 kW	7.3 kW	9.8 kW	12.1 kW
Peak Power	410 kW	690 kW	910 kW	1230 kW	1500 kW
H. V.	16 kV	18 kV	20 kV	22 kV	24 kV
R. V.	17 V	23 V	27 V	30 V	31 V
Receiver Isolation	54.5 dB	54.1 dB	54.0 dB	54.3 dB	54.9 dB

Figure 2. The result of testing in different transmitter powers.

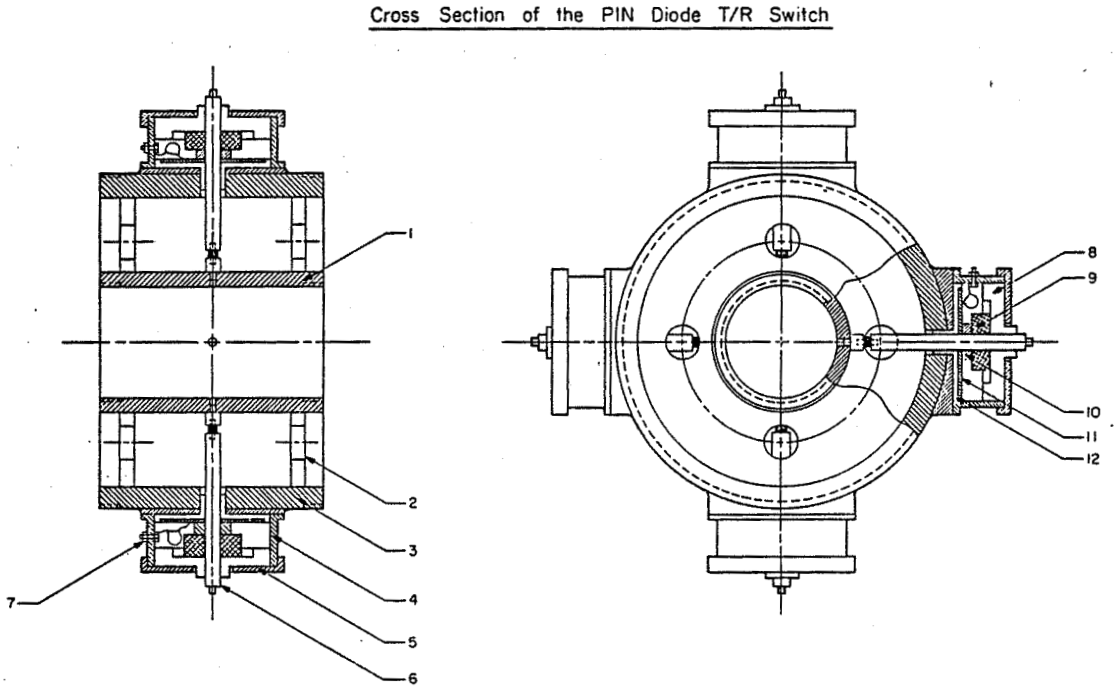

Figure 3.

6.2A PRACTICALITY OF ELECTRONIC BEAM STEERING FOR MST/ST RADARS

W. L. Clark and J. L. Green

Aeronomy Laboratory
National Oceanic and Atmospheric Administration
Boulder, Colorado 80303

INTRODUCTION

Electronic beam steering has been prominently described as complex and expensive (SKOLNIK, 1962). In this paper we describe the Sunset implementation of electronic steering, which has been in routine use since 1981, and demonstrate that such systems are, in fact, cost effective, versatile, and no more complex than fixed beam alternatives, provided three or more beams are needed.

First, as an example of the need for multibeam systems, the problem of determining accurate meteorological wind components in the presence of spatial variation is considered. Next, a cost comparison of steerable and fixed systems allowing solution of this problem is given. Then the concepts and relations involved in phase steering are given, followed by the description of the Sunset ST radar steering system. Finally, the implications are discussed, references to the competing SAD method are provided, and a recommendation concerning the design of the future Doppler ST/MST systems is made.

ESTIMATION OF METEOROLOGICAL WIND COMPONENTS

Beam pointing ST/MST radars measure the component of wind in the direction of probing. The wind components of meteorological interest (u, v, and w) are related to these radial velocity (vr) measurements by a set of linear vector equations. The vertical component, w, can be directly measured by a vertically pointing beam, but the u and v components must be obtained by solving these equations. Unfortunately, solution is possible only if a model of the local wind field is assumed.

The most often used model assumes that there is no horizontal change in the velocity components so that measurement of vr at only three beam positions is sufficient to determine u, v and w. This assumption is often not justified and leads to inaccuracies and bias in determinations of u and v (CLARK et al., 1983).

The next simplest model assumes that only the first spatial derivative of the velocity components is significant, requiring measurements of vr for a given height at seven beam positions to solve for u and v. There is a bonus for dealing with this added complexity. The necessary estimation of the first-order spatial derivatives allows estimation of the divergence and vorticity at each probed height above the radar. Thus, a seven-beam system provides not only more accurate, but additional meteorological information. A detailed consideration of optimum beam positions for solving this first-order model has been given by KOSCIELNY and DOVIAK, 1983.

The first-order model above may be inadequate in some cases. For example, under lee wave conditions a pseudo-sinusoidal model of the flow would be more appropriate in the direction of the wind. Under convective conditions, the flow can be too complex to model in a useful way. These cases will not be considered further except to note that the flexibility of electronic steering can allow use of more appropriate wind field models than a fixed-beam system.

COST COMPARISON

The biggest barrier to implementing a system capable of seven or more beam positions is probably cost. Fixed beam installations require seven separate arrays at $25,000 to $50,000 each. Electronic beam steering, coupled with time-multiplexing of beam positions, can reduce this cost to that of two orthogonal antenna arrays and the cost of the steering system. The steering system in the Sunset radar was added to two previously existing antenna arrays at a cost of about $15,000. Thus a seven-beam time-multiplexed system was implemented for less than the cost of a fixed three-beam system, and for less than 3/7 the cost of a fixed seven beam system. Furthermore, other configurations for other types of experiments can be, and often are, implemented in minutes at no further cost. The cost of transmitters and receivers is ignored because of the many possibilities for both types of system.

PHASE STEERING

Referring to Figure 1, it can be seen that when the constant phase surface of a plane wave just arrives at antenna element n with angle A to the zenith, it has the distance d(n) remaining before it reaches the last element. By adding compensating lengths of feedline to each element equal to this distance, the received signals are made to add in phase at the receiver. Thus, the gain of the antenna is made maximum for plane waves arriving at angle A and the antenna is said to point in this direction. A more detailed description of this process and approximations for the antenna pattern are presented in SKOLNIK (1962).

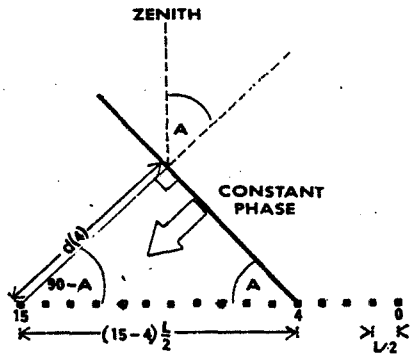

Figure 1. This is a side view of a constant-phase surface for a plane wave just reaching element 4 of a 16-element antenna array. The quantity of interest, d(4), is the distance from the surface to the last antenna element. The zenith angle of incidence is A and the freespace radar wavelength is L. The black squares represent the phaseable antenna elements spaced 1/2 L apart.

From the geometry shown in Figure 1 it is easy to develop the feedline compensating length relation

$$(1.1)... \quad d(n) = (15-n)\,(L'/2)\,\sin(A)\ [m]$$

Similarly, for a plane wave arriving from the other direction

$$(1.2)... \quad d(n) = n(L'/2)\sin(A)\ [m]$$

where

d(n) is the length of feedline to add to element n.
L' is the radar wavelength in the feedline in meters.
A is the zenith angle of the radar probing direction.
n = 0, 1, ..., 15 is the dipole number.

These relations will be used later on.

THE SUNSET ELECTRONIC PHASE STEERING SYSTEM

An electronic phase steering system, implemented in 1981, is in routine use in the Sunset radar system. The system has proven to be very reliable and yearly checks with a vector voltmeter show variability within each module to be less than a degree of phase. The system selectively steers either the north-south or east-west probing antenna to within .4 degree of any zenith angle between 0 and 45 degrees. The steering is under program control of the online computer controlling the radar and processing the return signals. Before beginning each sounding the program sets the probing direction from a sequential list of directions, input by the operator when the system is initially started. As presently implemented, up to eight positions may be in the list, which is repeatedly cycled. The operator may change this position list at any time.

The time needed to change probing directions is about a millisecond, but ground clutter removal filters have made the practicable switching rate about 30 seconds. It should be possible to remove this delay should faster cycling become important.

Power loss through the steering system is difficult to measure because it is less than 1 dB, including the harness where the element feedlines are joined. Each of the 16 phase shift modules can handle 10 kW of peak power, of 1 kW of average power at 40 MHz. This is the same capacity as that of the RG-8 cable used throughout the antenna system after the harness so that the system can handle 160 kW total peak power.

PHASE SHIFT MODULES

Each phase shift module is an aluminum box which is inserted into the feedline to a single antenna element. A mechanical relay inside the box selects connection to an element of either the north/south or east/west steering array. Eight additional mechanical relays are used to insert up to eight selected lengths of coaxial cable into the feedline as it passes through the box.

The position, 0 or 1, of each of the relays is controlled with nine TTL level control signals entering the phase module through a 25 pin D connector. When in position 1 the first phasing relay adds L'/2 meters into the feedline. The second adds L'/4, and the third L'/8, and so on geometrically till the eighth and last phasing relay adds L'/256 meters. Thus, any fraction of a wavelength that can be expressed as an eight-digit binary fraction can be inserted. The ninth relay in the box is used to select the north/south or east/west steering array.

STEERING CONTROL

The task of setting each of the 16 phase delay modules to the proper delay is handled by the main radar system computer. At the start of each sounding the desired zenith angle is converted to the appropriate 16 delays, expressed as fractions of a wavelength, Fn, using the relations

$$(3.1)\ldots \quad Fn = (n/2)\sin(a) \bmod 1,\ n=0,\ 1,\ldots,15$$

$$(3.2)\ldots \quad Fn = [(15-n)/2]\sin(A) \bmod 1,\ n=0,\ 1,\ldots 15$$

These are, of course, equations (1.1) and (1.2) where the length information has been removed; the phase modules themselves contain the length information in the form of cut cables. The mod function is used because lengths greater than a wavelength are not necessary; the goal is to keep the elements in phase, not to sample the same phase surface. The selection of (3.1) or (3.2) is determined by the sign of the zenith angle.

The control signals for the phasing relays are obtained by converting the fraction, Fn, to an eight-bit binary integer; Fn is multiplied by 256 and truncated. An additional bit is appended to select north/south or east/west steering. This operation is performed for all 16 phase shift modules and the resulting 144 bits are sent serially over coaxial cable to shift registers located near the modules. The output of these shift registers controls the relays in the modules.

DISCUSSION

Implementation of phase steering at the Sunset facility has proven to be simple, cost effective, versatile, and reliable. The radar has all the capabilities of fixed-beam systems except for simultaneous probing in two or more directions. This is an important lack, but the addition of a second transceiver could allow simultaneous probing in two directions. Furthermore, mutual interference makes difficult the probing of more than two directions simultaneously for any type of system. Finally, the added flexibility in experimental programs provided by a steerable system more than compensates for this limitation.

Only Doppler systems are considered here, but it should be noted that spaced antenna drifts (SAD) systems may be cost competitive and provide superior results in some instances. HOCKING (1983) argues strongly for this technique, while ROYRVIK (1983) describes an observed limitation. ROTTGER (1983) compares the two techniques from a theoretical standpoint.

RECOMMENDATION

Beam-swinging facilities still being designed, especially as prototypes, should include expansion to electronic steering capability in the design, even if electronic steering is not originally implemented. This will place few constraints on the design because there are many ways to achieve the necessary phasing delays and will allow later expansion to steering at minimal cost.

REFERENCES

Clark, W. L., J. L. Green and J. M. Warnock (1983), Estimating unbiased horizontal velocity components from ST/MST radar measurements, Handbook for MAP, Vol. 9, SCOSTEP Secretariat, Dep. Elec. Eng., Univ. Il, Urbana.

Hocking, W. K. (1983), The spaced antenna drift method, Handbook for MAP, Vol. 9, SCOSTEP Secretariat, Dep. Elec. Eng., Univ. Il, Urbana.

Koscielny, A. J. and R. J. Doviak (1983), An evaluation of the accuracy of some radar wind profiling techniques, Handbook for MAP, Vol. 9, SCOSTEP Secretariat, Dep. Elec. Eng., Univ. Il, Urbana.

Rottger, J. (1983), Techniques for measurement of horizontal and vertical velocities, Handbook for MAP, Vol. 9, SCOSTEP Secretariat, Dep. Elec. Eng., Univ. Il., Urbana.

Royrvik, O. (1983), Spaced Antenna Drift, Handbook for MAP, Vol. 9, SCOSTEP Secretariat, Dep. Elec. Eng., Univ. Il, Urbana.

Skolnik, M. I. (1962), Introduction to Radar Systems, McGraw Hill.

6.3A INCREASE OF ANTENNA AREA INSTEAD OF TRANSMITTER POWER

J. Rottger*

EISCAT Scientific Association
S-981 27 Kiruna, Sweden

In this short note attention shall be drawn to the fact that an extension of the antenna area may be preferred to an increase of transmitter power, if one takes into account that reflection often dominates the scatter contribution at near zenith angles. We can write the radar equation (e.g. ROTTGER, 1984):

$$P = P_a \cdot A \cdot \Delta r \, (C_r^2 + C_s^2) \cdot r^{-2}$$

with the contribution due to

reflection $\quad C_r^2 = A \cdot (F \cdot \bar{M})^2 \cdot \lambda^{-2}$

and the contribution due to

scattering $\quad C_s^2 = 0.03 \, C_n^2 \cdot \lambda^{-1/3}$,

where

- P = received echo power,
- P_a = average transmitter power,
- A = antenna area,
- r = range,
- Δr = transmitter pulse length,
- λ = radar wavelength,
- M = mean generalized refractive index gradient,
- F = calibration factor,
- C_n^2 = turbulence refractive index.

It is noticed that an increase of the antenna area A linearly increases the contribution of reflection. This is most likely to occur at vertical incidence, since M is largest in the vertical direction (leading also to the well-known aspect sensitivity). If $C_r^2 > C_s^2$, the received power P increases quadratically with the antenna area; e.g. doubling the area yields a four-fold increase of echo power, whereas a doubling of transmitter power (e.g. doubling the number of transmitters) only doubles the received power (see Figure 1). However, one has to bear in mind that these considerations hold only in the far field r_m of the antenna, i.e. $r_m > D^2/\lambda$, where D is the diameter of the antenna array. The altitude ranges at which the echo power gets weak and we have to consider improvements of sensitivity are mostly larger than 5-8 km. It follows that our considerations are valid up to antenna diameters close to 200 m for wavelengths of 6 m. On the other hand one has to bear in mind that the reflected component has to be larger than the scattered component which only holds for near zenith angles.

REFERENCE:

Rottger, J. (1984), the MST Radar Technique, Handbook for MAP, Vol. 13, 187-232, SCOSTEP Secretariat, Dep. Elec. Eng., Univ. Il, Urbana.

---

*presently at Arecibo Observatory, Arecibo, Puerto Rico, on leave from Max-Planck-Institut fur Aeronomie, Lindau, W. Germany.

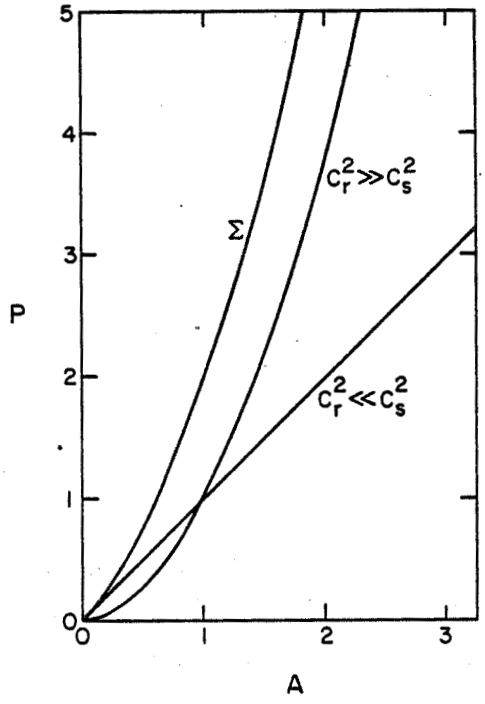

Figure 1. Dependence of power P (arbitrary units) and antenna area A (arbitrary units) for dominating scattering ($C_r^2 \ll C_s^2$) and dominating reflection ($C_r^2 \gg C_s^2$).

6.4A TESTING AND OPTIMIZING MST COAXIAL COLLINEAR ARRAYS

J. M. Warnock and J. L. Green

Aeronomy Laboratory
National Oceanic and Atmospheric Administration
Boulder, Colorado 80303

INTRODUCTION

Many clear-air VHF radar wind profilers use coaxial collinear (COCO) arrays for their antenna. A COCO array is composed of long lines of half-wave dipoles spaced one-half wavelength apart. In this paper we describe an inexpensive method of checking a COCO array and optimizing its performance by measuring and then correcting the relative rf phase among its lines at their feed point. This method also gives an estimate of the rf current amplitude among the lines. Therefore, the strength and location of the sidelobes in the H plane of the array can be estimated.

The only nonstandard equipment needed for these measurements is a probe to detect the rf signal near a radiating element. We use a short dipole 40 cm long tuned to the operating frequency by a variable inductor. Although the measurements described here were all made at the Sunset radar site, similar tests have been made at the Platteville, Craig, and Ponape radar sites, and could be made easily on any COCO array.

SUNSET RADAR ANTENNA

Figure 1 shows the distribution of rf power from the transmission feedline to each antenna element. The transmission feedline is a low-loss five-inch air dielectric; it enters a small well-screened building located in the center of the antenna where it feeds a harness. This harness divides the rf power into 16 equal parts, which are fed into 16 phase shifter boxes. The phase shifters are controlled remotely by an on-line computer. For a given tilt angle and direction, the computer selects either of two arrays and computes the phase shift required for each of the 16 phase shifters to produce the desired phase shift across the array (GREEN et al., 1984). Since a line of an array is composed of two strings of dipoles each with its own feed, the rf power output from each phase shifter is divided into half, and fed into a patch panel. This patch panel is actually one wall of the building. The antenna feedlines are attached to the panel on the outside of the building.

The antenna at the Sunset radar site is currently two colocated square arrays; one steerable in the east-west vertical plane (denoted E-W array), and the other steerable in the north-south vertical plane (denoted N-S array). Figure 2 is a plane view of the antenna. Each array is a coaxial collinear array composed of 16 lines of half-wave dipoles. These lines are spaced one-half wavelength apart, and are one-quarter wavelength above a ground plane. Physically, each line of the array consists of two strings of dipoles constructed from RG-8 coaxial cable by interchanging the inner-conductor with the braid at half wavelength intervals (BALSLEY and ECKLUND, 1972). Each string contains 12 half-wave dipoles, six on each side of its feedline, giving 24 dipoles in each line of an array.

MEASUREMENT PROCEDURE

It is important to make the measurements under conditions as close to the actual radar operating environment as possible; therefore all parts of the power distribution system and antenna elements are excited during the measurements. A signal generator feeds three watts of rf power at the operating fre-

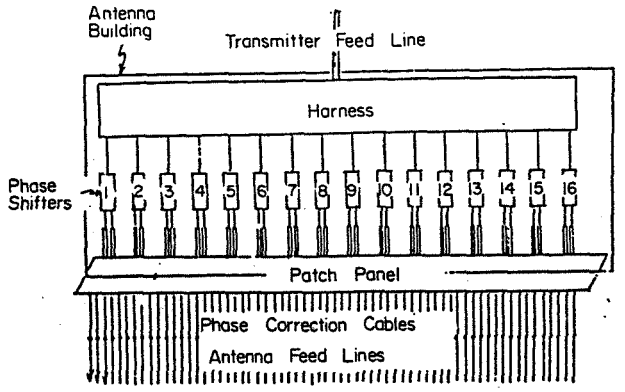

Figure 1. Schematic diagram of rf power distribution for the Sunset radar.

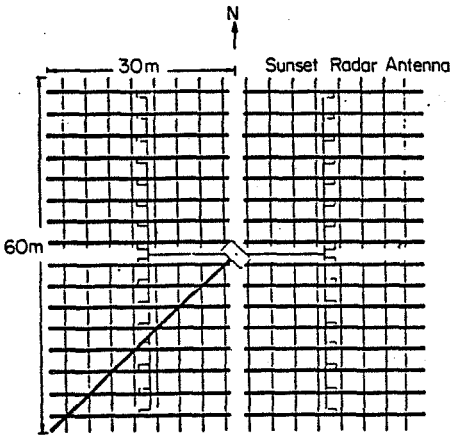

Figure 2. Plan view of Sunset radar antenna.

quency (40.475 MHz) into the front end of the transmission feedline. We place the short dipole probe a few inches from the first string of dipoles at its feedpoint. One end of a long RG-8 feedline is attached to the probe; the other end is connected to a vector voltmeter in the antenna building. We compare the rf signal from the probe with a convenient reference from the patch panel. After the amplitude and phase are measured with the vector voltmeter and recorded, the probe is moved carefully to the next string, and the measurements continued until all 32 strings of an array have been measured. Periodically, we return the probe to the first string to confirm the reproducibility of the measurements. Next we correct the relative phases among the strings by adding a correction cable to each feedline at the patch panel. Finally, we remeasure the entire corrected antenna.

RESULTS

The first, and perhaps the most useful, result is that these measurements provide a continuity test of the entire system from the transmission feedline

to the strings of dipoles. At Sunset there are more than 1500 connections in this system; defective or missing components or interchanged connections are found easily. Furthermore, periodic testing allows the performance of the system to be monitored.

Next, we compare the uncorrected and corrected antennas. Figure 3 shows three broadside antenna patterns in the H plane of the E-W array. The first pattern (Figure 3a) is computed from the measurements made before the correction cables were added. It has large broad sidelobes; the largest sidelobe is only 10 bd below the main beam. The second pattern (Figure 3b) is the corrected pattern; its sidelobes are small and narrow similar to the ideal pattern shown in Figure 3c. These sidelobes reduce considerably the radar horizon for clutter, airplanes, meteors, and other competing targets.

REFERENCES

Balsley, B. B. and W. L. Ecklund (1972), A portable coaxial collinear antenna, IEEE Trans. Antennas Propagat., AP-20, 513-516.

Green, J. L., J. M. Warnock, W. L. Clark, F. J. Eggert and K. J. Ruth (1984), Modification to the Sunset Radar to provide antenna beam steering, Preprint 20th Conference on Radar Meteorology, 1981, Boston, MA.

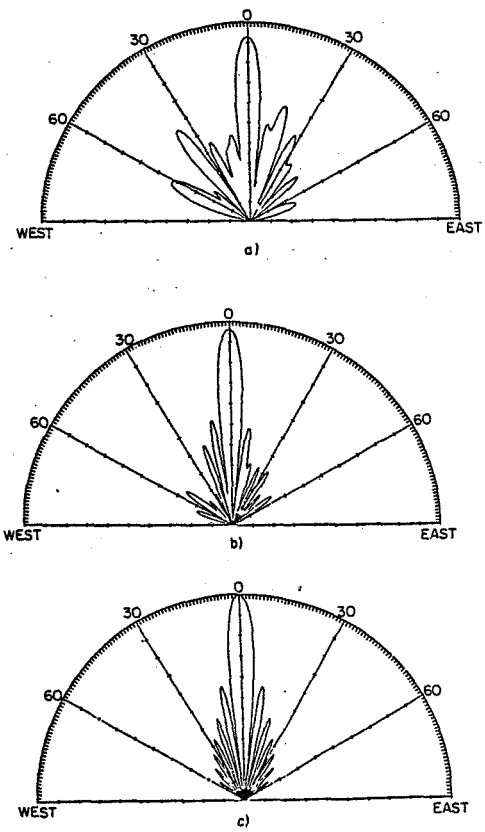

Figure 3. Broadside antenna patterns in H plane. The tick marks on the radial axis are separated by 3 dB for one-way propagation and 6 dB for two-way propagation. a) Pattern calculated from phase and relative power measured before phase correction cables are added. b) Pattern calculated from phase and relative power measured after phase correction cables were added. c) Ideal pattern.

7. OVERVIEW OF ON-LINE DATA PROCESSING FOR MST RADARS (Keynote Paper)

D. T. Farley

School of Electrical Engineering
Cornell University, Ithaca, NY 14853

INTRODUCTION

The most important aspects of the processing of MST radar data were discussed in considerable detail at the URSI/SCOSTEP Workshop of Technical Aspects of MST Radar which was held at the University of Illinois in May 1983. The papers presented at that Workshop have been published recently in the Handbook for MAP, Volume 9 (BOWHILL and EDWARDS, 1983). The concepts and conclusions presented in the many papers in this Handbook are still quite up to date, and so the aim of this paper is simply to briefly review and summarize the important points.

The analysis of the data can be divided usually into on-line and off-line portions. The on-line processing significantly compresses the data via time averages and usually produces power spectra or autocorrelation functions (ACFs). The off-line processing involves curve fitting and parameter extraction. The details of the latter depend upon the experiment, the facilities of the observatory, the types of interference that must be coped with, etc., and hence are quite variable. The goals and techniques of the on-line processing are less variable and better established, and it is these that this paper will focus on. Further details of the subjects to be discussed below are given in papers in the MAP Handbook just mentioned.

The goals of the on-line and now almost exclusively digital processing, procedures are to achieve good altitude resolution and coverage, good frequency (Doppler shift) resolution, and good time resolution, while avoiding, insofar as possible, the problems of range and frequency ambiguity (aliasing), ground clutter, and interference. Some of these goals are in conflict, of course, and compromises are necessary. In almost all cases, however, achieving optimum results requires some sort of pulse compression (or perhaps frequency stepping) and some coherent integration (voltage averaging). The first allows full utilization of the average power capability of the transmitter and the second reduces the computing requirements.

PULSE COMPRESSION BY PHASE CODING

It is easy to show that when proper processing is done, the effective signal-to-noise ratio for power, power spectrum, ACF, etc. measurements is proportional to $P_{av}\tau n^{1/2}$, where P_{av} is the average transmitter power, τ is the pulse length (or baud length for a phase coded pulse) or the inverse of the total pulse bandwidth for a chirped pulse) and the inverse of the receiver bandwidth (matched filtering), and n is the number of independent samples averaged (incoherently). For most radars the most practical way to achieve good range resolution (small τ) and still use the full power capabilities of the transmitter is through pulse compression obtained with binary phase codes. A relatively long pulse is divided up into n shorter bauds of equal length, some of which are shifted in phase by 180°. If the target remains phase coherent for a sufficiently long time, the radar echoes can be processed (decoded) in such a way that they are nearly equivalent to echoes received from a pulse of one baud length but n times the actual transmitted peak power. The compression is usually not quite perfect; the echo from a single point target would consist of weak range "sidelobes" as well as the main echo. The decoding process consists of passing the received signal through a matched filter whose im-

pulse response is the time inverse of the transmitted pulse. This amounts to cross-correlating the signal with a replica of the transmitted pulse. The codes in general use fall into a number of general classes.

(a) Barker Codes

These were first discussed by BARKER (1953) and are used extensively in incoherent-scatter measurements. The distinguishing feature of these codes is that the range sidelobes have a uniform amplitude of unity. For example, the phase coding sequence and the ACF (the voltage pattern of the decoded echo from a stationary point target) for a 5-baud Barker code are

```
          + + + - +
. . . 0 0 1 0 1 0 5 0 1 0 1 0 0 . . .
```

If the compression were perfect, only the 5 would be present in the ACF; the 1s are the unwanted range sidelobes. The maximum value of n for Barker codes, which all have this same ACF pattern, is 13. The signal-to-noise ratio in the central peak is increased by a factor n (not n^2), since the noise in each decoded sample is the sum of n independent samples.

The compression process only works if the correlation time of the scattering medium is substantially longer than the full uncompressed length of the transmitted pulse. The decoding involves adding and subtracting voltages, not powers; if the scattering centers move a significant fraction of a radar wavelength between the time of arrival of the first and last baud of the pulse, the compression process will fail. This is never a problem in practice in MST observations, but can be a problem in ionospheric studies. In fact, the correlation times in the troposphere and stratosphere are usually so long (the order of tenths of a second or longer) that more powerful compression codes can be used.

(b) Complementary Code Pairs

Although the range sidelobes for Barker codes are small, they can still cause problems in MST work because the scattering cross section decreases so rapidly with altitude (2-3 dB per kilometer). Comlementary codes completely eliminate this problem, at least in principle; they have no range sidelobes at all. The existence of these codes was first pointed out by GOLAY (1961) and is mentioned in some radar literature (RABINER and GOLD, 1975), but they are impractical for most radar applications because the targets must have very long correlation times. It was Woodman who first noticed their potential for MST work and his suggestion led to their first use in studies at SOUSY (SCHMIDT et al., 1979) and Arecibo (WOODMAN, 1980a) with 32-baud codes and 2 and 1 μs baud lengths, respectively (300 and 150 m resolution).

Complementary codes come in pairs, and the ACFs of the two pulses have the property that their range sidelobes are equal in magnitude but opposite in sign, so that if the medium stays coherent over the interpulse period (IPP), the output voltages from the pair of echoes can be added, giving complete cancellation of the sidelobes, or perfect compression. One can easily verify that the 2-baud pair (++, +−) has this property. Representing such a pair as (A, B) it is also easily shown that (AB, $A\bar{B}$), where $\bar{B}$ is the complement of B, is also a complementary pair. Hence code lengths that are any power of 2 can be constructed, and also 10 times any power of 2, it turns out. The main practical limitation on the code length is ground clutter; the lowest altitude from which useful data can be received becomes higher as the code becomes longer. The computing requirements become greater too, of course, but this is usually not a serious problem because of the availability of coherent integration, as discussed below.

(c) Complementary Sequences of Complementary Codes

If the correlation time of the medium is many times longer than the IPP, more complicated sequences with complementary properties can be devised that can reduce range ambiguity (aliasing) problems quite dramatically. Ordinarily, if the IPP is T, echoes from the altitudes h, h + cT/2, etc. are mixed together. From another point of view, the ACF of the pulse sequence has identical peaks at delays or 0, T, 2T, etc. But by transmitting cyclicly a four-pulse sequence such as A, B, A, $\overline{B}$, ... and decoding by cross correlating with A, B, A, $\overline{B}$, the first undesired peak can be pushed from T out to 2T. With longer sequences it can be pushed still farther. GONZALES and WOODMAN (1984) have used this idea in HF probing of the mesosphere with an 8-pulse sequence to eliminate problems caused by multiple reflections from the ionosphere.

(d) Quasi-Complementary Code Sets

In the real world complementary codes do not, of course, work quite as ideally as described in the previous two sections, largely because transmitters do not transmit exactly the desired waveform. So in practice there will still be range sidelobes, and some of them may be serious, but just which ones depends on the actual code used and how the transmitter happens to distort it. To cope with these practical difficulties, SULZER and WOODMAN (1984) generated a set of 48 different 32-baud codes (the computer search required some 350 hours using an FPS 120 B Array Processor!) that, when used in sequence, had substantially better sidelobe properties in actual use with the Arecibo 430-MHz radar than a simple 32-baud complementary pair. The 48-code set is also less affected by the code truncation which occurs at the lowest altitudes sampled. Unfortunately, with such a scheme there are no decoding shortcuts; each pulse must be decoded in real time as it comes in, and so only observatories with very powerful digital hardware, such as Arecibo with its assorted radio astronomy devices, can take advantage of this technique.

(e) Cyclic Codes

These are sometimes also called maximal length sequences and are a well known class of codes that repeat at intervals of $N = 2^n-1$ bauds (i.e., CW transmission) and can be generated by an n-bit shift register. The ACFs of these sequences have periodic peaks of amplitude N at intervals of N times the baud length, but are unity everywhere else. If the periodic peaks cause no range ambiguity problems, and ground clutter associated with the CW transmission is unimportant, very high compression ratios can be achieved. These requirements are often met in radar astronomy applications, where such codes are widely used, but for MST studies these codes are only useful with bistatic radar systems. WOODMAN (1980b) describes the use of cyclic codes to achieve an altitude resolution of 30 m in a bistatic measurement with the 2380 MHz radar at Arecibo, and soon 15 m resolution will be possible.

FREQUENCY STEPPING

It is possible to achieve the goals of pulse compression by manipulating the frequency rather than the phase of the transmitted signal, and it is now fairly easy to do this with a computer-driven frequency synthesizer. One can either change the frequency rapidly within a long pulse or transmit a series of short pulses at a high pulse repetition rate (PRF) with the frequency stepped cyclicly. Stepping within the pulse and suitably processing the data is just "chirping", which can also be done with analog techniques. In MST applications, however, the phase coding techniques are generally more convenient. On the other hand, using short pulses and a very high PRF to raise the average power, with frequency stepping to avoid range aliasing, can be quite useful for studies at low altitudes, where pulse compression cannot be used because of

ground clutter problems. To fully utilize the technique one may need to use several receivers.

COHERENT INTEGRATION

This is very simple and easy to implement digital filtering processes that was first applied to MST radar data by WOODMAN and GUILLEN (1974). It is a crude filter, but it often leads to an enormous reduction in subsequent computer processing requirements. Coherent integration consists of replacing N consecutive voltage samples from a given altitude by their sum, thereby reducing the number of samples which need to be processed in all subsequent operations by this factor N, which may be as large as a few hundred. Since this operation is linear it can be done before any decoding of compressed pulses is carried out (except for very long sequences of differently coded pulses; see above). Hence, as long as one can perform these additions fast enough, using special purpose hardware if necessary, the decoding and FFT or similar processing can be done with fairly inexpensive computers. Coherent integration is obviously most useful when the coherent time of the medium is at least an order of magnitude longer than the IPP.

The question that naturally arises is how large can N be? To analyze how coherent integration affects the signal, it is simplest to consider it to be made up of two separate operations: (1) filtering via a running average (a filter with a unit impulse response of duration T, where T is N times the IPP), followed by (2) sampling at intervals of T, which of course represents a drastic undersampling of the original unfiltered signal. The first operation multiplies the power spectrum of the original signal by $\sin^2 x/x^2$, where $x = \pi fT$ and f is the frequency in Hz. The sampling operation then leads to frequency aliasing, with signal power at frequencies f and $f \pm n/T$, where n is any integer, summed together. Somewhat surprisingly, perhaps, a signal spectrum which is flat before coherent integration will still be flat afterwards; the filtering and aliasing balance each other and white noise still looks white, with no tapering at the window edges. Upon reflection this result is not surprising, since the sum of n random noise samples is itself just random noise. On the other hand, a narrow signal peak with a Doppler shift of 0.44/T Hz, near the edge of the aliasing window, will be attenuated by 3 dB by the filter function, whereas a peak near the center of the spectrum will be unaffected. In other words, one should be conservative in the use of coherent integration and make sure that all signals of interest are in the central portion of the post-integration spectrum. Finally, it is perhaps worth reiterating that coherent integration is only a filtering procedure, a fairly crude one in fact. Exactly the same result (a slightly better result, actually) would be achieved (but at greater cost) by Fourier transforming the full original time series and retaining only the interesting part.

OTHER POINTS

For completeness, it may be worth including a few brief remarks about coarse quantization and spectral moments. It is possible to derive all the useful statistical information (except the total power in some cases) about the scattered signal (a Gaussian random variable) even if the quantization is very crude, e.g., determines only the sign bit in the most extreme case. With such quantization very high processing speeds are possible, particularly with special purpose hardward. A number of possible schemes and their associated correction factors and statistical efficiencies are discussed by HAGEN and FARLEY (1973). The use of coarse quantization has become less necessary as digital hardware has become faster and less expensive, but for some applications it is still necessary.

Turning to the question of spectral moments, it is well known from Fourier

transform theory that the derivatives of the ACF at the origin (zero lag) give the moments of the power spectrum. Hence from a power measurement and a complex lagged product measurement at a single short lag, it is possible to obtain the first two moments of the power spectrum as well as the total power. If the spectrum is nicely shaped, with a single fairly symmetrical peak, these moments alone give all the important information. If the spectrum is more complicated, however, as is often the case, the full spectrum is needed.

REFERENCES

Barker, R. H. (1953), Group synchronizing of binary digital systems, in Communications Theory, W. Jackson (ed.), 273-287, Academic Press, New York.

Bowhill, S. A. and B. Edwards (1983) (Editors), Handbook for MAP, Vol. 9, SCOSTEP Secretariat, Dep. Elec. Eng., Univ. Il, Urbana.

Golay, M. J. E. (1961), Complementary series, IRE Trans. Info. Theory. IT-7, 82-87.

Gonzales, C. A. and R. F. Woodman (1984), Digital correlation techniques in radio science, Radio Sci., 8, 775-784.

Rabiner, L. R. and B. Gold (1975), Theory and Application of Digital Signal Processing, Prentice-Hall.

Schmidt, G., R. Ruster and P. Czechowsky (1979), Complementary code and digital filtering for detection of weak VHF radar signals from the mesosphere, IEEE Trans. Geosci. Electron., GE-17, 154-161.

Sulzer, M. P. and R. F. Woodman (1984), Quasi-complementary codes: A new technique for MST radar sounding, Radio Sci., 19, 337-344.

Woodman, R. F. (1980a), High-altitude resolution stratospheric measurements with the Arecibo 430-MHz radar, Radio Sci., 15, 417-422.

Woodman, R. F. (1980b), High-altitude resolution stratospheric measurements with the Arecibo 2380-MHz radar, Radio Sci., 15, 423-430.

Woodman, R. F. and A. Guillen (1974), Radar observations of winds and turbulence in the stratosphere and mesosphere, J. Atmos. Sci., 31, 493-505.

SESSION SUMMARY AND RECOMMENDATIONS

A number of the points made in the 1983 Workshop were reiterated. The theory, advantages, and disadvantages of various data-processing techniques, particularly those used on line, are now pretty well agreed upon; there seem to be no serious controversies. Nevertheless, there were a number of interesting points brought out in the papers and the ensuing discussion that seem worth summarizing here.

1) J. L. Green pointed out that there may be advantages to decoding schemes that are not equivalent to matched filtering. Such schemes can substantially reduce the range sidelobes associated with Barker codes, for example, at the cost of slightly reducing the compression ratio. Of course, Barker codes are not used too much for MST radar work, but perhaps similar ideas would work with complementary codes or quasi-complementary sets? Or perhaps such procedures might eliminate the need for the quasi-complementary sets, which can only be implemented if very powerful decoding hardware is available?

2) S. A. Bowhill discussed the concept of pulse compression via frequency chirping and pointed out that in MST applications, in which the medium has a very long coherence time, it is possible to chirp by varying the frequency on a pulse-to-pulse basis, rather than within the pulse. This is like frequency stepping, except that voltages, not powers, are added after incorporating appropriate phase factors. The advantages over conventional chirping are a reduction in ground clutter and possibly better transmitter performance. The same concepts apply to phase coding also, of course, as discussed in the overview and the paper by R. G. Strauch. One must carefully compare the range

sidelobes, etc. in both cases and the ability of the transmitter to actually generate the desired pulse shape.

3) D. V. Sarwate described algorithms for generating a wide variety of sets of complementary sequences such as, for example, 8 sequences of length 7 which have the property that the sum of the 8 ACFs has no range sidelobes.

4) M. Petitdidier and J. W. Brosnahan described new high performance preprocessing hardware which is in the advance design stage and should be relatively inexpensive. Prices of digital hardware continue to drop and performance continues to rise. The biggest problem right now seems to be long delivery times for some of the crucial chips. G. Stitt and S. A. Bowhill compared various FFT device possibilities.

5) P. K. Rastogi, S. K. Avery and C. E. Meek discussed offline analysis procedures used in extracting physical parameters from conventional MST Doppler radar data, meteor radar data, and partial-reflection drift data. The problems and solutions vary considerably from technique to technique.

Turning to RECOMMENDATIONS, it was the consensus of the group that it was worth reemphasizing the recommendation of last year. Although many observatories perform quite advanced data processing, there is still room for improvement. As the cost of hardware preprocessors and small computers declines and their power increases, it is increasingly cost effective to utilize the most sophisticated techniques. As much processing as possible should be done on-line in order to compress the data and reduce the tape handling and delays associated with subsequent off-line processing.

Finally, the group urged that all spaced antenna drift (SAD) measurements should be done coherently. Forming auto- and cross correlations using only the signal power or amplitudes is considerably less effective than using full complex voltage products.

7.1A CODING SCHEMES FOR IMPROVING MST RADAR PERFORMANCE

S. A. Bowhill

Department of Electrical Engineering
University of Illinois
Urbana, IL 61801

INTRODUCTION

The performance of an MST radar can be characterized by its system sensitivity and its range resolution. The former enables Doppler velocities to be determined even in the presence of very weak structures; the latter permits study of the fine structure within a turbulent region. Unfortunately, most radar systems are limited by the peak power they can transmit, and decreasing the pulse width in an effort to improve the range resolution leads to a decrease in system sensitivity by the same ratio.

Coding of transmitted signals has as its aim an increase in the effective radar sensitivity or range resolution without an increase in the peak transmitted power. His is accomplished by spreading the power in the frequency domain, giving better range resolution, without reducing the pulse width.

Two basic techniques are used to accomplish this frequency dispersion. The first involves using a type of pseudorandom code for the phase or amplitude within a single pulse, or within a finite sequence of pulses. This approach was discussed extensively by FARLEY (1983), and is not further treated here. The second technique is to code the frequency of the transmitted signal in some way. The various possibilities are discussed below, and are compared with the pulse-coding methods.

FREQUENCY-CODING TECHNIQUES

There are three separate ways in which radar signal transmissions can be frequency-coded: pulse chirping, FM/CW, and pulse-frequency stepping.

In pulse chirping (KLAUDER et al., 1960) the radio frequency of each transmitted radar pulse is varied linearly with time during the pulse. This produces a frequency spread approximately equal to the range of frequencies scanned, assuming that to be large compared with the reciprocal of the pulse width. A decoder is then used to regenerate a pulse of width equal to the reciprocal of the bandwidth of the received pulse, in an analogous way to the decoding of a pseudorandomly coded pulse. An application of this technique to ionospheric sounding was described by WIPPERMANN and BOWHILL (1967). They used identical ultrasonic delay lines to provide the complementary dispersions required to accomplish the pulse compression.

FM/CW radar was described in its initial form by GNANALINGAM (1954), and later by BARRY and FENWICK (1964) and by FENWICK and BARRY (1965). It has provided the basis for a highly successful commercial sweep-frequency ionosonde now in wide use. It has also been used in a tropospheric sounding radar with exceptionally high resolution (RICHTER, 1969).

The principle is to generate a linear frequency sweep in a CW transmitted signal, to detect the signal coherently and to achieve range resolution by Fourier transformation of the complex amplitude recorded. Since there is no possibility of time-domain discrimination between the radar return and the direct signal from the transmitter to the receiver, the system cannot work monostatically; its best applications have been in oblique scatter soundings of the ionosphere, or in tropospheric soundings at low altitudes (GOSSARD et al., 1978).

A third possibility is the use of a combination of pulse modulation and FM coding. Here each transmitted pulse is fixed in frequency, but is displaced in frequency from its predecessor by a fixed amount. The local oscillator for the receiver is also stepped by the same amount. Consider the fate of signals scattered from successive ranges in the atmosphere. They can be thought of as spaced by the range resolution of the original pulse. The coherently detected received signal from each scattering level is recorded as the frequency steps through the allotted bandwidth. It is then Fourier transformed from the frequency domain to the time domain to give the fine structure within the scattering volume appropriate to that particular scattering level.

Of course, this technique works only if the scattering configuration of the medium remains fixed throughout the frequency-stepping procedure. It is therefore little use for incoherent-scatter sounding. However, with the relatively long correlation times appropriate for MST radars, it has distinct advantages.

SIGNAL-TO-NOISE CONSIDERATIONS

Consider a radar which can transmit radio pulses with peak power P, pulse length L, and interpulse period I. In the unmodulated mode, its power density is about P/L. Let the noise power density (at VHF, usually sky noise) be N, and suppose that the scattering target (assumed very thin in this discussion) gives a scattered power density of AP/L. Then the signal/noise ratio is AP/NL for a single pulse.

If the integration time permissible without loss of coherence is C, the number of pulses transmitted in that time is C/I. The resulting signal/noise ratio for the unmodulated pulse is CAP/INL.

Now consider the same pulse, pseudorandom-coded into n bits. The bandwidth required has now increased from 1/L to n/L, the signal/noise ratio for a single pulse is AP/nNL, and after coherent integration for time C is CAP/InNL. Of course, the range resolution has improved by a factor of n.

Finally, consider the case where the same improvement in range resolution is sought by using a frequency-stepping technique. The number of frequency steps is n, and the time taken to complete one frequency sweep is nI. Assuming the same coherence time C for the signal, coherent integration can be performed over C/nI samples. The signal/noise ratio for a single pulse is AP/NL, as in the unmodulated case. That for the coherently integrated signal is therefore CAP/InNL, the same for the pseudorandom code with the same range resolution.

The main advantage of the pseudorandom-coded pulse and the chirped pulse is that the configuration of the scattering medium is required to be fixed only for a time equal to the pulse length. In MST radar, this is not significant. Against this must be set the following advantages of the frequency-stepping method:

1) The transmitter phase and frequency are changed only during the interpulse period. Large VHF radar transmitters can cause problems when phase-coded, as discussed by HERRINGTON and BOWHILL (1983).
2) With frequency stepping, only the rf stages of the receivers need to be widened to accommodate the increased bandwidth.
3) The range-sidelobe problem of a pseudorandomly coded signal is avoided.

ACKNOWLEDGEMENT

The work described was supported by the National Aeronautics and Space Administration under grant NGR 14-005-181.

REFERENCES

Barry, G. H. and R. B. Fenwick (1965), Extraterrestrial and ionospheric sounding with synthesized frequency sweeps, Hewlett-Packard J., 16, No. 11, July.

Fenwick, R. B. and G. H. Barry (1964), Generation of frequency-sweep waveforms by direct synthesis, Tech. Rep. 99, Stanford Electronics Labs., Stanford, CA.

Gossard, E. E., R. B. Chadwick, K. P. Moran, R. G. Strauch, G. E. Morrison and W. C. Campbell (1978), Observation of winds in the clear air using an FM-CW Doppler radar, Radio Sci., 13, 285-289.

Farley, D. T. (1983), Pulse compression using binary phase codes, Handbook for MAP, Vol. 9, SCOSTEP Secretariat, Dep. Elec. Eng., Univ. IL, Urbana, 410-414.

Gnanalingam, S. (1954), An apparatus for the detection of weak ionospheric echoes, Proc. Inst. Elect. Engrs., 101 (III), 243-248.

Herrington, L. J., Jr. and S. A. Bowhill (1983), Phase modulating the Urbana radar, Aeron. Rep. 109, Aeron. Lab., Dep. Elec. Eng., Univ. IL, Urbana.

Klauder, J. R., A. C. Price, S. Darlington and W. J. Albersheim (1960), The theory and design of chirp radars, Bell System Tech. J., 39, 745-808.

Richter, J. H. (1969), High resolution tropospheric radar sounding, Radio Sci., 4, 1261-1268.

Wippermann, D. R. and S. A. Bowhill (1967), The application of pulse compression techniques to ionospheric sounding, Aeron. Rep. 16, Aeron. Lab., Dep. Elec. Eng., Univ. IL, Urbana.

7.1B ELIMINATION OF RANGE-ALIASED ECHOES IN VHF RADARS

R. G. Strauch

ERL/WPL
National Oceanic and Atmospheric Administration
Boulder, CO 80303

Very high frequency radars designed to measure tropospheric wind profiles usually detect scattering to a maximum height of about 20 km. If the antenna elevation angle is 45 degrees or more above the horizon, the maximum range of interest is less than 30 km. A VHF pulsed Doppler radar wind Profiler can, therefore, be operated at high pulse repetition rates (~5 kHz). The maximum bandwidth allowed (by frequency allocation or by the antenna) is about 0.5 MHz (at most) so a radar with uncoded pulses can operate with a duty cycle of 1 to 10%, depending on the desired height resolution. This is approximately the duty cycle allowed in many transmitters. Therefore it is often possible to operate a tropospheric-wind Profiler that utilizes all the average power available from the transmitter without the complexity of coded pulses. However the VHF radar can detect echoes from the mesosphere on occasion and, with high pulse repetition rates, these echoes will occur at the same apparent range as the tropospheric echoes of interest. These mesospheric echoes may, at times, be stronger than the tropospheric signals. The range-aliased mesospheric echoes can be greatly attenuated or effectively eliminated as described below.

First, suppose that the phase of the transmitted pulse varies randomly from pulse to pulse. This random phase occurs if the transmitter uses a pulsed oscillator instead of a pulsed amplifier, as in a microwave radar with a magnetron (oscillator) transmitter. If the transmitter uses an amplifier the phase can be varied from pulse to pulse by introducing a phase shift on a low-level reference oscillator just prior to each transmitted pulse. The phase of the reference oscillator is kept constant while all echoes from the unambiguous range interval are received. (The unambiguous range interval is 0 to cT/2 where c is velocity of propagation and T is the pulse repetition period). Then, as in a magnetron microwave Doppler radar, the signals from range-aliased targets will be incoherent and cause an increase in noise, but they will not produce a Doppler spectrum that can compete with (or be mistaken for) the tropospheric Doppler spectrum. It is possible to choose any ambiguous range interval (n $cT/2 < R < (n + 1)cT/2$) for coherent reception while targets at all other ranges are incoherent by selecting the phase of the reference oscillator used during reception to be equal to that used in previous transmitted pulses. Range-aliased signals that appear as white noise in the Doppler spectrum are much less troublesome than if they were coherent. However, because VHF radars with high pulse repetition rates can use time-domain integration of the video samples from consecutive pulses, the range-aliased echoes can be greatly attenuated or effectively eliminated rather than made incoherent (causing increased noise).

Next, let the phase of the transmitted pulse change from pulse to pulse with a pseudorandom binary code. Then signals in the range 0 to cT/2 will add in the time-domain integrator just as though the transmitter had constant phase, but range-aliased signals will add or subtract depending on the phase of the code during reception relative to the phase during transmission of a prior pulse. If the signal phase of the range-aliased targets remains constant during the time-domain integration period, the range-aliased signals will cancel if there are as many positive as there are negative elements in the code. A pseudorandom code can cancel the signals (except for at most 1 pulse) for all range-aliased intervals. If the range-aliased signals are in motion but have small velocity compared with $\pm \lambda/4MT$, where M is the number of samples averaged

in the time domain, then the cancellation of range-aliased echoes is still effective. If this were not so, one could not perform time-domain integration on the signals from the range of interest. In fact, when targets are in motion, the cancellation of the range-aliased signals is more efficient than the coherent addition of the desired signals, because in the latter case signals must remain nearly in phase throughout time MT, while in the former case cancellation occurs during subintervals of MT.

The VHF radars in the Colorado Wind Profiler Network have been designed to operate at high pulse repetition rates with uncoded pulses and to be able to reject mesospheric echoes on the basis of the above considerations. We have not as yet implemented the mesospheric echo cancelling feature.

7.1C SIDELOBE REDUCTION OF BARKER CODES

J. L. Green
Aeronomy Laboratory
National Aeronautics and Space Administration
Boulder, CO 80303

Barker codes are simple and inexpensive to implement. In the absence of large and fast computers they can be realized as simple digital preprocessors, or with the use of a delay line, can be realized as an analogue device. Assuming the process observed has an autocorrelation time that is long compared to the code length, a gain in signal to noise, G = N where N is the number of elements in the code, may be realized.

Typically Barker codes are implemented by shifting the phase of the transmitted signal by 0 or 180 degrees according to the code pattern. The known Barker codes are shown in Figure 1a. A typical detection scheme is shown in Figure 1b where the output of the radar receiver is delayed by an analogue delay line or a shift register. The signal in each element of the delay line or shift register is continuously multiplied by the code and all elements are summed.

A principal disadvantage has been the sidelobe response (FARLEY, 1983). In the case of MST or ST radar echoes where there is a dynamic range as large as 60 dB, these unwanted sidelobes cause an increase in the apparent width of atmospheric layers, or some narrow layer to appear at several altitudes. In Table 1 it can be seen that the main lobe to peak sidelobe ratio (PSR) varies from 9.54 dB, for a code of N = 3 to 22.28 dB, for a code of N = 13.

The sidelobes of a Barker code may be reduced by tapering the response of the decoder. Optimum tapers, from BLINCHIKOFF and ZEREV (1976), are shown in Table 2. This tapering is achieved by multiplying the delayed signal elements in Figure 1b by the specified coefficients rather than ±1. The results are shown in Table 1 where G and the PSR are listed for no tapering and optimum tapering. It can be seen that the sidelobe response has been greatly reduced with very little loss in G.

This tapering can be readily achieved in a digital computer with sufficient word length, but difficult to realize in an analogue filter because of the small changes in the coefficients. An alternative is to have one coefficient for A_0 and another for $A_1 \ldots A_N$. These are shown in Table 3 (BLINCHIKOFF and ZEREV, 1976). As can be seen in columns 5 and 6 of Table 3, this simplification works surprisingly well, since there is only a very small increase in the PSR and a corresponding small decrease in G.

REFERENCES

Blinchikoff, H. J. and A. I. Zerev (1976), Filtering in the Time and Frequency Domains, 353-368, Wiley, New York.

Farley, D. T. (1983), Pulse compression using binary phase codes, Handbook for MAP Vol. 9, 410-413, SCOSTEP Secretariat, Dep. Elec. Eng., Univ. IL, Urbana.

N (code Length)	Code Elements
2	+ −
3	+ + −
4	+ + − + (+ + + −)
5	+ + + − +
7	+ + + − − + −
11	+ + + − − − + − − + −
13	+ + + + + − − + + − + − +

a)

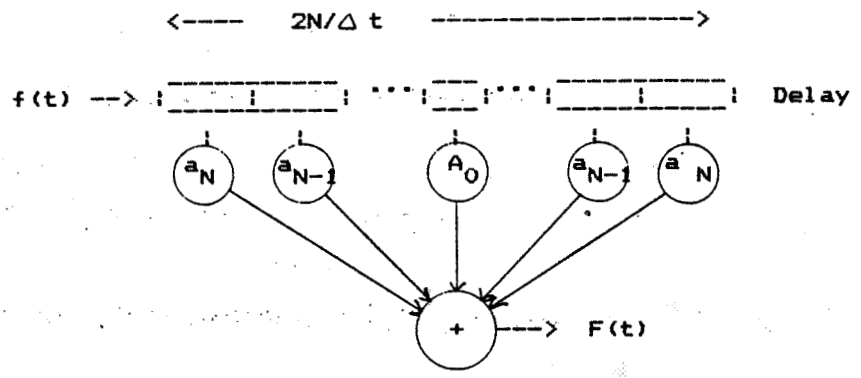

b)

Figure 1. a) Known Barker codes; b) Matched filter for Barker codes.

Table 1: Comparison of nontapered Barker code realizations to optimum, and modified tapering

	PSR			G		
N	Matched	Opt S L Suppress	Mod S. L. Suppress	Matched	Opt S L Suppress	Opt S L Suppress
3	9.54 dB	20.00 dB	20 dB	4.77 dB	4.20 dB	4.2 dB
5	13.98	25.63	25.1	6.99	6.66	6.62
7	16.90	23.00	21.58	8.45	8.15	7.55
11	20.83	25.85	23.86	10.41	10.22	10.10
13	22.28	34.79	33.98	11.14	11.03	10.99

Table 2: Optimum tap weights normalized for peak output of unity (odd tap weights are zero)

Tap	N = 3	N = 5	N = 7	N = 11	N = 13
a_0	0.4	0.22093	0.163084	0.100177	7.97249×10^{-2}
a_2	0.1	-0.023256	0.026687	0.119006	-2.391476×10^{-3}
a_4		-0.029069	0.023721	0.0111222	-2.67558×10^{-3}
a_6			0.020386	0.010267	-2.941092×10^{-3}
a_8				9.33984×10^{-3}	-3.186169×10^{-3}
a_{10}				8.348125×10^{-3}	-3.409138×10^{-3}
a_{12}					-3.60843×10^{-3}

Table 3: Realization with all tap weights equal except a_0 (all odd tap weights set to zero)

N	a_0	$a_{2..N}$	$:a_0/a_N:$	PSR	SNR
3	0.4	0.1	4	20 dB	4.2 dB
5	0.222	-0.277	8	25.1	6.62
7	0.166	0.277	6	21.58	7.25
11	0.102	0.128	8	23.86	10.99
13	0.080	-3.33×10^{-3}	24	33.98	10.99

7.1D CONSTRUCTION OF COMPLEMENTARY CODE SEQUENCE SETS

D. V. Sarwate

Coordinated Science Laboratory and the Department of Electrical and Computer Engineering
University of Illinois
Urbana, IL 61801

A set of code sequences is said to be a complementary code sequence set if the sum of the aperiodic autocorrelation functions for the sequences is zero everywhere except at the origin. This note discusses a simple construction for sets of complementary code sequences. Suppose we have a linear feedback shift register whose feedback polynomial is irreducible (PETERSON and WELDON, 1972). For example, according to the tables in (PETERSON and WELDON, 1972, Appendix C), the polynomial $x^3 + x^2 + 1$ is irreducible and corresponds to the linear feedback shift register shown below (SARWATE and PURSLEY, 1980).

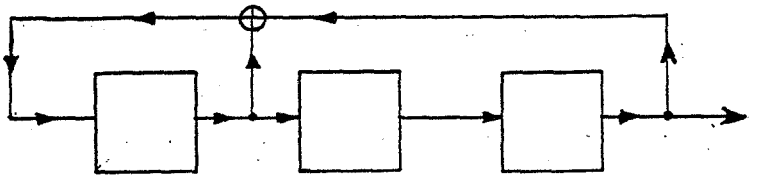

A feedback shift register with n stages produces 2^n different sequences corresponding to the 2^n initial loadings. The length (or period) of the sequences is N where $N = 2^n-1$ if the feedback polynomial is primitive, and N is a proper divisor of 2^n-1 if the polynomial is nonprimitive (PETERSON and WELDON, 1972). For example, if we choose a primitive polynomial of degree 6, we can get 64 sequences of length 63, while if we choose a nonprimitive polynomial of degree 6, we can get 64 sequences of length 21 or 9. These 2^n sequences form a complementary code sequence set. For example, the 8 sequences of length 7 generated by the shift register shown above form a complementary code sequence set. The sequences are as follows:

0000000
0011101
0111010
1110100
1101001
1010011
0100111
1001110

It will be noted that the all-zeroes sequence is always one of the sequences obtained thus. Since this may not be convenient for some applications, we consider the following modification. Choose an arbitrary binary sequence of length N and add it to all the sequences obtained from the shift register. Here, addition means bit-by-bit EXCLUSIVE OR addition of sequences. The resulting set of sequences is still a complementary code sequence set. For example, if we choose the sequence 0011010 and add it to the sequences above, we obtain the set of sequences shown:

0011010
0000111
0100000
1101110
1110011
1001001
0111101
1010100

The aperiodic autocorrelation function for a binary sequence is computed by first converting the sequence from the alphabet (0,1) to the alphabet (+1,-1) and then using the formula

$$C_x(\ell) = \sum_{i=0}^{N-\ell-1} x_i x_{i+\ell}, \quad 0 \leq \ell \leq N-1 .$$

The results of such computations for the 8 sequences are as shown below. It is clear that these sequences do indeed form a complementary code sequence set.

ℓ	0	1	2	3	4	5	6
	7	-2	-1	0	-1	0	1
	7	4	1	-2	-3	-2	-1
	7	2	3	2	1	0	1
	7	0	-1	0	3	0	-1
	7	2	-3	-2	1	2	1
	7	-2	-3	4	-1	-2	1
	7	0	1	0	-1	2	-1
	7	-4	3	-2	1	0	-1

In general, we can construct 2^{N-n} different complementary code sequence sets from a given shift register. Some of these may be more suitable for applications than others. The construction given in this note can be generalized to produce polyphase sequences also. Details are given in (SARWATE, 1983).

ACKNOWLEDGMENT

This research was supported by the Army Research Office under Contract DAAG29-81-K-0064.

REFERENCES

Peterson, W. W. and E. J. Weldon, Jr., (1982), Error-Correcting Codes, 2nd Edition, MIT Press.

Sarwate, D. V. and M. B. Pursley, (1980), Crosscorrelation properties of pseudorandom and related sequences, Proc. of the IEEE, 68, 593-619.

Sarwate, D. V., (1983), Sets of complementary sequences, Electronics Lett., 19, 711-712.

D58

7.2A PROUST RADAR: DECODING HARDWARE AND COHERENT INTEGRATION

M. Petitdidier

C.R.P.E.
4 Avenue de Neptune
94107 Saint-Maur Cedex
France

1. Characteristics

-impulsion width	:4 µs
-PRF	:140 µs
-code	:quasi complementary
-number of different codes	:as many as number of coherent integrations (64)
-number of subcodes	:20
-subcode width	:200 ns
-height resolution	:30 m

2. Device

-decoding in real time before coherent integration
-20 (number of subcodes) gates decoded in parallel but output delayed (200 ns) from one gate to the next one
-one card used for decoding and coherent integrations (Figure 1)
-number of cards: 20 identical cards + sequencer + memory card
-signal A.D.C. distributed at the same time on 20 cards. Code circulated with a time delay of 200 ns from one card to the next one

3. Advantages - limitations

-realization of one card for decoding and coherent integration and duplication for the others
-reliability of the device: one kind of spare cards
-possibility to get with the same device profile mode (600 m) or magnifier mode (30 m)
-change of altitude resolution by changing the width of the impulsion and subcodes
-limitation due to the kind of A.D.C. available for sampling frequency greater than 1 MHz, they are adjusted to one frequency only
-number of subcodes fixed

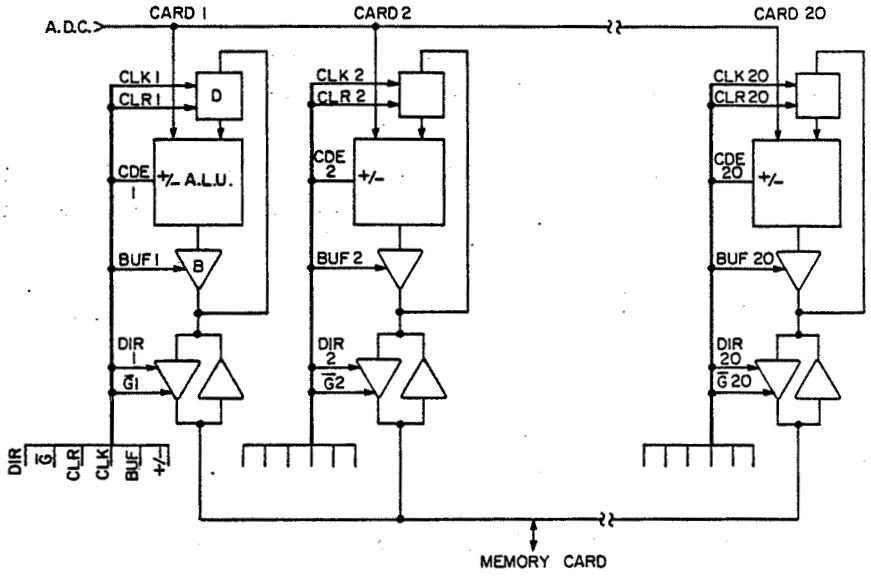

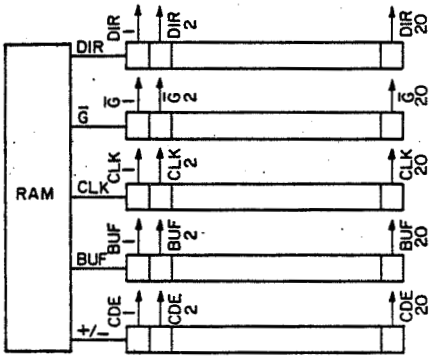

SEQUENCER: SHIFT REGISTER

7.3A A HIGH-SPEED DIGITAL SIGNAL PROCESSOR FOR ATMOSPHERIC RADAR

J. W. Brosnahan and D. M. Woodard

Tycho Technology, Inc.
P.O. Box 1716
Boulder, CO 80306

GENERAL OVERVIEW

The Tycho Technology Model SP-320 is a high-speed pipelined digital signal processing system designed around the capabilities of the Texas Instruments TMS32010 16/32-Bit Signal Processor. This device is a monolithic realization of a complex general purpose signal processor, incorporating such features as a 32-bit ALU, a 16-bit x 16-bit combinatorial multiplier, and a 16-bit barrel shifter (TEXAS INSTRUMENTS, 1983a). The SP-320 is designed to operate as a slave processor to a host general purpose computer in applications such as coherent integration of a radar return signal in multiple ranges, or dedicated FFT processing. To the main PC board may be added piggyback modules for A/D conversion and I/O interfacing (see Figure 1). Presently available is an I/O module conforming to the Intel Multichannel interface standard (INTEL CORPORATION, 1983); other I/O modules will be designed to meet specific user requirements.

The main processor board (exclusive of A/D and I/O modules) includes input and output FIFO (First In First Out) memories, both with depths of 4096 W, to permit asynchronous operation between the source of data and the host computer. This design permits burst data rates in excess of 5 MW/s.

(a) Areas of Application

The SP-320 was initially designed as a coherent integrator for atmospheric radar systems. In the course of development, it became apparent that with the addition of a few hardware features, the board could be made useful for a much broader class of mathematical and signal processing problems.

Coherent Integration for Radar. Design criteria for this application included a 1-MHz sample rate, 12 bits raw data precision, and 256 range gates. The SP-320 has a digital input data path width of 13 bits, and will support burst data rates to 5 MHz. In practice, the sampling rate is limited by the A/D conversion time required for the desired precision. For example, 12 bits in 0.5 μs is about the limit for a cost-no-object system using a single board-level converter per analog channel; a reasonable compromise is 10 bits in 1.0 μs using a hybrid A/D converter. Assuming range accumulators of 32 bits, 64 ranges can be accommodated using only the internal data memory of the TMS32010. Using external data memory, a maximum of 2048 ranges can be used. However, external range accumulators require approximately 3.6 μs for the read-add-write sequence compared to 1.4 μs for internal accumulators. Thus, for a large number of ranges, the system may become computation limited, requiring a reduction in pulse repetition frequency. Also, for a large number of ranges used in conjunction with a small number of points per integration, the system may become output limited at the processor-host interface. For a discussion of these and other performance trade-offs see (TYCHO TECHNOLOGY, INC., 1984). For the realistic case of a 1-MHz sample rate, 256 ranges, 6 parallel data channels, and a host interface capable of a DMA transfer rate of 1 W per μs, the SP-320 can support a pulse repetition period of 1 ms with any number of integration points greater than 8.

A feature of the TMS32010 that is of particular interest in the context of coherent integration is the MPYK (multiply by constant) instruction. This allows the raw data word to be multiplied by a 16-bit constant previously stored

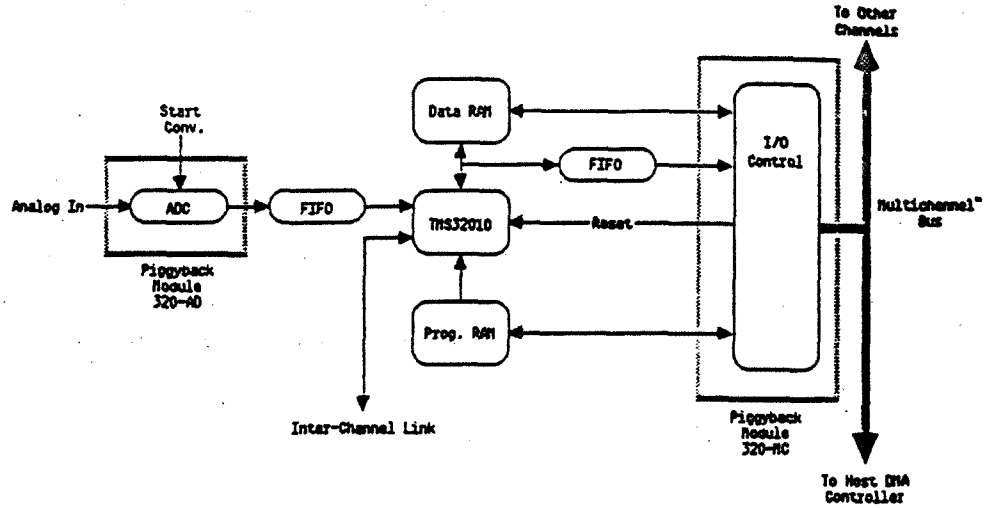

Figure 1. SP-320 overall block diagram.

in the T register with no execution time penalty compared to simply entering the raw data into the processor. The user thus may impose a window function on the integration by periodically reloading the T register from a table in program memory.

For those users who wish to implement a pre-integration pulse-pair processing algorithm, the SP-320 provides an Inter-Channel Link. This allows the processors of two associated quadrature channels to pass data words back and forth as required for complex arithmetic.

Digital Filters. The TMS32010 was designed with a strong emphasis on the efficient execution of digital filter algorithms. In particular, hardware macro instructions such as LTD allow very fast manipulation of running lists of data points. See TEXAS INSTRUMENTS (1983b), section 8, and RABINER and GOLD (1975) for more details on digital filter design. The SP-320 can be used as a fast real-time digital filter by employing the TMS32010, using only internal data memory, and the input and output FIFOs.

FFT Processing. The SP-320 supports both real-time and batch FFT processing. Maximum conversion efficiency is achieved by using straight-line code and a maximum of 64 complex points of 16 bit integer precision. See Figure 5 in MAGAR et al. (1982) for a summary of conversion times for various sizes of transforms and for both the straight-line and looped code cases. For example, a 64 point complex transform with straight-line code can be completed in 738 µs. A 1024-point transform with looped code requires 76 ms. Within the 64-point limit, the TMS32010 does not need to access external data memory, and with straight-line code can achieve conversion times that compare favorably with some dedicated FFT processors. Even with the much longer conversion times required by larger transforms and looped code (required because of the 4 kW program memory size limitation), the SP-320 may in some circumstances be a useful compromise between a hardware FFT processor and a software FFT running on a general purpose microprocessor.

HARDWARE DESCRIPTION

The SP-320 consists of a main PC board with external connections grouped on two headers. These headers mate with connectors on the two piggyback mod-

ules, the 320-AD (A/D Conversion Module), and the 320-MC (Multichannel Bus Interface). For those users who wish to design custom interfacing for the SP-320, the two headers allow direct access to the input and output FIFOs and to the program and data memories.

(a) Main Board

The TMS32010 is a "Harvard Architecture" device, i.e. the program and data memories are separate. The SP-320 implements the full 4k W addressable program memory space. The TMS32010 has 144 W of internal data memory and only 3 b of external data address. To make the SP-320 a general purpose processor, the 8 externally addressable data objects are regarded as I/O ports, and 4k W (or 2k DPW) of data memory are furnished, with auto-incrementing (or decrementing) address generation under control of the ports (see section entitled "Port Assignments").

Raw Data Input. Normal data input for real-time applications is by way of the input FIFO through header J1 using a Data Valid/Read control sequence. This input path is 12 b wide; each data word enters the TMS32010 in one instruction cycle (200 ns) by use of the MPYK instruction. A hardware switching scheme injects the current output word of the input FIFO into the constant field of the instruction. This feature may be enabled/disabled under software control to allow normal use of the MPYK instruction. Jumper settings allow the raw data word to be interpreted as either natural binary or two's complement binary. In the latter case, the data word is automatically sign-extended in the TMS32010 to 16 bits.

Data Memory. The SP-320 data memory is organized as 4096 16-bit words. However, odd and even addresses are accessed by separate I/O ports. This arrangement was determined to be optimum for implementing double precision accumulators for coherent integration. Address generation is external to the TMS32010 and address incrementing, under control of 4 bits in an increment control register, can be made to occur automatically after any or all of the following: read low word, read high word, write low word, write high word. For example, in coherent integration for radar, using double precision accumulators, one would set the increment control bit for "increment after write high word". Then, after the sequence: read low word, add, write low word, read high word, add, write high word; the data memory automatically would be incremented for the next range gate. Address, data, and control lines for block transfers to and from data memory are available at header J2.

Output FIFO. For pipelined processing, the SP-320 provides a 16 b wide by 4096 W deep output FIFO. The width (16 b as opposed to e.g. 32 b) was determined by the standard interface definitions (Multichannel, IEEE-488, etc.) in general use for scientific applications. For an application such as integration with double precision accumulators, one would program the system to write the results of the last sequence of additions to the output FIFO in low, high order instead of returning the results to data memory. The host would then be expected to transfer out the range sums at an average rate sufficient to keep up with the processor. For batch operations, the output FIFO may still be used as the output path, as an alternative to a DMA transfer out of data memory. FIFO output is available at header J2.

Program Memory. The TMS32010 executes instructions from a 16 b by 4096 W RAM which must be loaded by the host computer with TMS32010 object code. Assertion of the Reset line places the TMS32010 in an inactive state and makes the program memory address and data lines available at header J2 for block loading by the host. Upon deassertion of Reset, the TMS32010 begins execution at address 0000.

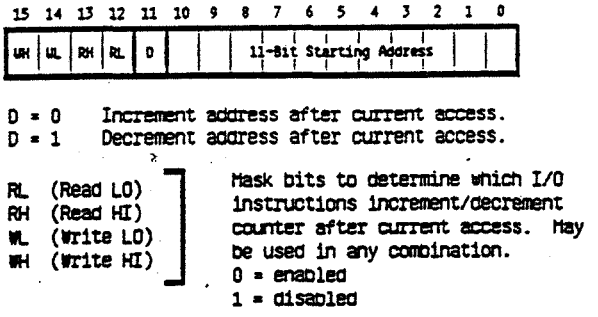

Figure 2. Format for loading data address counter.

(b) A/D Converter Module

The 320-AD piggyback module (see Figure 3) mates with J1 on the SP-320. Its main components are a Teledyne Philbrick 4860 track-hold amplifier and a Burr-Brown ADC803 analog-to-digital converter. Input voltage ranges of ±10, ±5, and 0 to -10 are jumper selectable. The converter's clock rate is adjustable, and the end-of-conversion point is jumper selectable; these features allow the module to be set up for maximum conversion speed at any precision from 8 bits to 12 bits. The output format can be jumper selected to offset binary or two's complement binary. An output latch holds the result of the last conversion while the current conversion is in process, allowing continuous pipelined operation at the maximum speed of the converter. The output latch is 16 bits wide with full sign extension, for maximum versatility in interfacing the module to devices other than the SP-320. The maximum continuous sampling rate varies from 2 MHz at a precision of 8 bits to 0.66 MHz at 12 bits (BURR-BROWN, CORPORATION, 1983).

(c) Multichannel™ Bus Interface Module

The 320-MC piggyback module mates with J2 on the SP-320. This module serves as a high-speed parallel interface between the SP-320 and a Multichannel™ bus at the Basic Talker/Listener level of compliance (see INTEL CORPORATION, 1983, section IV). The module includes counters for address generation and

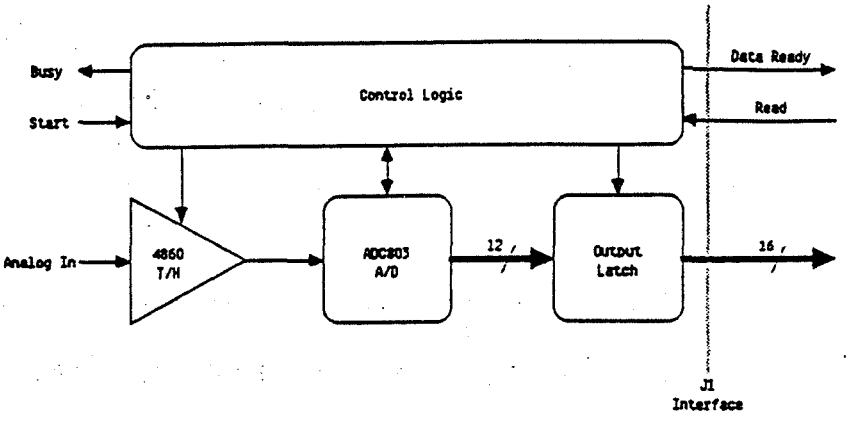

Figure 3. Block diagram of 320-AD module.

word count to support high-speed DMA transfers. Up to 15 modules may be connected to the same bus under the control of a single DMA device having Multichannel™ supervisor capabilities. All of the functions available at J2 are supported by the 320-MC as register and memory assignments. The Multichannel™ Device Number for the module is jumper selectable.

PROGRAMMING CONSIDERATION

The following hardware details have a bearing on the programming of the SP-320; they should be considered in conjunction with the TMS32010 instruction set (TEXAS INSTRUMENTS, 1983a).

(a) Port Assignments

The 8 I/O ports of the TMS32010 are decoded separately for read and write, and perform the following functions:

Port	Read Function	Write Function
0	not used	load data address counter*
1	read LO data word	write LO data word
2	read HI data word	write HI data word
3	read inter-channel link	write inter-channel link
4	read system status byte	write flag byte
5	not used	write to output FIFO
6	not used	not used
7	not used	not used

*See Figure 2 for data address counter loading format.

(b) Timing and Interrupts

The SP-320 requires that an external 40-MHz TTL level clock signal be supplied to J3 (an SMA female connector on the main PC board). Use of an external clock allows the synchronization of multiple data channels executing the same program.

Two provisions have been made to enable the system to avoid over-reading the input FIFO. The empty line of the FIFO controller is routed to the INT pin, and the Data Ready line to the BIO pin of the TMS32010 (see TEXAS INSTRUMENTS, 1983). Thus the user has the option of either checking BIO status before each data input, or using an interrupt handler to respond to the empty condition.

The flag byte (I/O port 4) has 4 user-definable bits that control on-board LEDs for diagnostic purposes. These bits are also readable at J2. The user could, for example, define one of these bits as a "task completed" indicator for batch processing and use it to initiate a host interrupt.

REFERENCES

Burr-Brown Corporation (1983), ADC803 Data Sheet, Tucson, AZ.
Intel Corporation (1983), Multibus Handbook, Santa Clara, CA.
Magar, S. S., R. Hester and R. Simpson (1982), Signal-processing μC builds FFT-based spectrum analyzer, Electronic Design, 19.
Rabiner, R. and B. Gold (1975), Theory and Applications of Digital Signal Processing, Prentice-Hall, Englewood Cliffs, NJ.
Texas Instruments (1983a), TMS32010 User's Guide, Dallas, TX.
Texas Instruments (1983b), Signal Processing Products and Technology, Dallas, TX.
Tycho, Technology, Inc. (1984). SP-320 User's Manual, Longmont, CO (in prep).

D60

7.4A HARDWARE SCHEMES FOR FAST FOURIER TRANSFORM

G. R. Stitt and S. A. Bowhill

Aeronomy Laboratory
Department of Electrical and Computer Engineering
University of Illinois, Urbana, Illinois 61801

Because of the interest in real-time FFT processing of a MST radar data, a study has been made of cost-effective approaches to hardware FFT generation. Results are summarized in Table 1. In this table, the first six entries represent previously devised hardware FFT configurations which have been described in the open literature, including the estimated number of chips used and the time required to perform a 1024-point FFT. The remaining entries in the table correspond to original designs, which presuppose the availability of a microcomputer -- an Apple II+ has been assumed -- and a modestly complicated hardware peripheral. These original designs, all of which implement a radix-4 FFT with twiddle factors, have been assigned model numbers to make them easier to refer to.

The Model 10 performs a complete FFT at one time, and is implemented using standard TTL chips. An Apple microcomputer is responsible for transferring data to a large set of input registers, and retrieving the transformed results from another set of output registers. The Model 20 is a much simpler design which calculates the value of a single butterfly output mode, and must therefore be used repeatedly by the microcomputer during the computation of a complete FFT. In order to improve throughput, the Model 30 essentially uses four Model 20s in parallel, so that all four output mode values of a single radix-4 butterfly are calculated simultaneously. Like the Model 30, the Model 40 processes an entire radix-4 butterfly at one time, but takes superior advantage of the inherent symmetry of the FFT algorithm by utilizing multiplexers and control ROMs to reduce the overall chip count.

All of the devices outlined above are inefficient from the standpoint that they require the Apple microcomputer to spend most of its time transferring data back and forth between external registers. Models 50 through 70 attempt to alleviate this problem by utilizing an external microcontroller, in these cases a Signetics 8X305. The Model 50 uses memory access (DMA) transfer of the data to be transformed to very fast external RAM, after which the microcontroller directs the flow of data between the external RAM and a Model 40. When the FFT is completed, the 8X305 DMAs the transformed results back into Apple RAM. The Model 60 eliminates the DMA steps, and 8X305 being used simply to transfer data back and forth between Apple RAM and the I/O registers of a Model 40. Lastly, the Model 70 is very similar to the Model 50, but uses a Motorola MC6844 Direct Memory Access Controller chip to perform the DMAs.

The specifications for the various processors shown in Table 1 are plotted on the graph of Figure 1. This graph indicates that those implementations which attain a relatively fast transformation time also tend to possess a relatively high chip count, regardless of the FFT algorithm chosen. Figure 1 also seems to indicate that once a particular FFT algorithm has been chosen, it may be implemented in a nearly endless variety of ways, each striking a different compromise between the characteristics of transform size and computation speed, and system size and complexity.

In Figure 1, a line has been included which possesses a slope of -1/2, and which passes through the point (1 chip, 3000 s); it can be seen that the data points fall approximately along this line. If n is the chip count of an FFT processor, and t_c is the time required by the processor to perform a 1,024-

Table 1. Specifications of various FFT processors.

TYPE	NUMBER OF CHIPS	TIME (1,024-POINT)
KOBYLINSKI et al. (1979)	≈15	15.0 s
LIU and PELED, (19759	≈950	41 μs
Mini-MAP; CSP Inc. (1982)	≈800	4.2 ms
CORINTHIOS et al. (1975)	1,800	852 μs
GROGINSKY and WORKS (1970)	≈10,000	9.11 ms
FLADUNG and MERGLER (1978)	120	28.2 ms
Compiled BASIC	5	174 s
Model 10	61,952	21.8 μs
Model 20	68	1.51 s
Model 30	225	0.441 s
Model 40	109	0.535 s
Model 50	150	48.8 ms
Model 60	153	91.7 ms
Model 70	160	41.0 ms

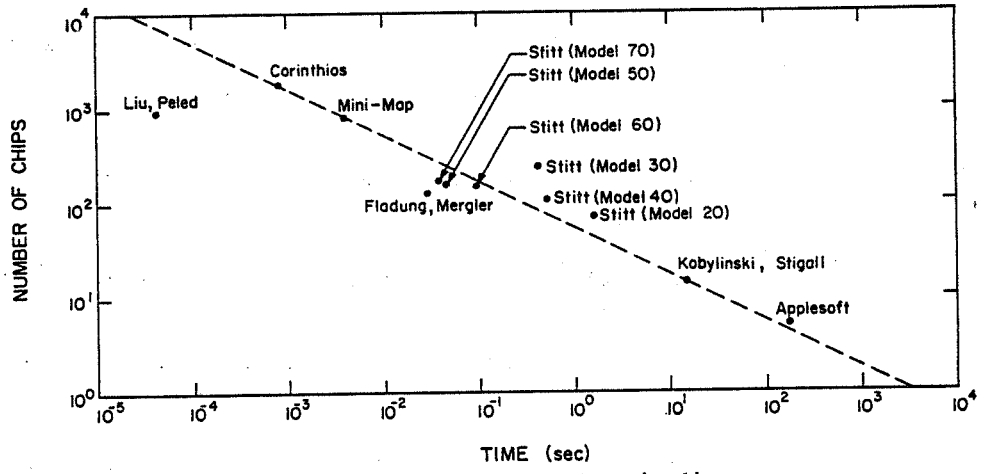

Figure 1. Figure of merit diagram.

point transform, then an equation for the line may be written in terms of these variables as follows:

$$\frac{\log n - \log 1}{\log t_c - \log 3000} = -1/2$$

$$\log n = 1/2 \log \left(\frac{-t_c}{3000}\right)$$

$$\log n^2 = \log \left(\frac{3000}{t_c}\right)$$

$$n^2 t_c = 3000$$

$$100 = \frac{300{,}000}{n^2 t_c}$$

In view of this equation, it is possible to define the following figure of merit (FM) for a FFT processor:

$$FM = \frac{300,000}{n^2 t_c}$$

With this definition, an FFT processor with specifications falling on the line will possess an FM of approximately 100. Specifications lying above this line correspond to FMs less than 100, and specifications below the line to FMs greater than 100. Clearly, a FFT processor with a high figure of merit is preferable to a processor with a low one.

The FMs corresponding to the various FFT processors in Table 1 are shown in Table 2.

The figure of merit represents one way of defining the efficiency of a particular FFT processor. By this definition, it can be seen from Table 2 that the Model 10 through Model 40 processors are fairly inefficient; as has been mentioned before, this is primarily due to the large difference which exists between the computation time of the external processor and the time required by the Apple to transfer data back and forth between itself and the processor. Models 50, 60, and 70 FFT processors introduce various forms of 8X305 based external control in an attempt to alleviate this problem; the relatively high FM values for these processors indicate that the scheme has been largely successful. At least in terms of efficiency, there appears to be little to choose between the Model 50 and 70 processors.

At present, the Model 50 processor uses fixed point arithmetic, requiring the data to be scaled before it may be transformed. Easier data handling and a wider range of data values would be possible if the Model 50 were redesigned using floating point hardware. In a similar vein, the Model 50 currently possesses no method for detecting and handling an overflow error. At the very least, some method should be provided for alerting the Apple to some incorrect transformation results. Finally the spectacular results achieved using the Liu-Peled algorithm (e.g., FLADUNG and MERGLER, 1978) suggest that a system utilizing this algorithm should be investigated.

Table 2. Figure of merit values of various FFT processors.

TYPE	FIGURE OF MERIT (FM)
KOBYLINSKI et al. (1979)	88.9
LIU and PELED, (1975)	8,110
Mini-MAP; CSP Inc. (1982)	112
CORINTHIOS et al. (1975)	109
GROGINSKY and WORKS (1970)	0.329
FLADUNG and MERGLER (1978)	739
Compiled BASIC	69.0
Model 10	3.59
Model 20	43.0
Model 30	13.4
Model 40	47.2
Model 50	273
Model 60	140
Model 70	286

ACKNOWLEDGEMENTS

Research described was supported in part by the National Aeronautics and Space Administration grant NSG 7506 and in part by the National Science Foundation grant ATM 81-20371.

REFERENCES

Corinthios, M. J. and K. C. Smith (1975), A Parallel Radix-4 Fast Fourier Transform Computer, IEEE Trans. Computers, C-24, 80.

CSP, Inc. (1982), Array Processor is small but fast, Electron. Design, 30, (13), 206.

Fladung, R. L. and H. W. Mergler (1978), High-Performance Fast Fourier Transformer, IEEE Trans. Indust. Control Instrum., IECI-25, 322.

Groginsky, H. L. and G. A. Works (1970), A pipeline fast Fourier transform, IEEE Trans. Computers, C-19, 1015.

Kobylinski, R. A., P. D. Stigall and R. E. Ziemer (1979), A microcomputer-based data acquisition system with hardware capabilities to calculate a fast Fourier transform, IEEE Trans. Acoust., Speech Signal Process., ASSP-27, 202.

Liu, B. and A. Peled (1975), A new hardware realization of high-speed fast Fourier transformers, IEEE Trans. Acoust., Speech Signal Process., ASSP-23, 543.

7.5A CRITERIA AND ALGORITHMS FOR SPECTRUM PARAMETERIZATION OF MST RADAR SIGNALS

P. K. Rastogi

Department of Electrical Engineering and Applied Physics
Case Western University
Cleveland, Ohio 44106

INTRODUCTION

The power spectra [S(f)] of MST radar signals contain useful information about the variance of refractivity fluctuations (C_n^2), the mean radial velocity (V), and the radial velocity variance (σ_v^2) in the atmosphere. When noise and other contaminating signals are absent, these quantities can be obtained directly from the zeroth, first and second order moments of the spectra (ZRNIC, 1979; WOODMAN, 1983).

In practice the spectra contain, in addition to the atmospheric returns with a Doppler frequency shift f, undesirable components such as noise, ground clutter and interference. The effect of noise is to add a "platform" to the spectra. Ground clutter is usually manifest as a strong, symmetric smeared peak at zero Doppler shift. External interference appears as spurious peaks in the spectra. Transmitter malfunction or presence of unidentifiable rf sources in the observable range of the radar may cause persistent interference at some frequency shifts. Power line harmonics may also be present on occasion.

The power spectra S(f) are usually estimated by the time-averaged periodogram [P(f)] of the coherently integrated returned signal, at N discrete frequencies over a frequency interval (-F, F). At these frequencies, P(f) is a smoothed, weighted and aliased estimate of S(f) (FARLEY, 1983; RASTOGI, 1983). Perhaps the most serious consequence of using the periodogram method is that the ground-clutter contribution is smeared and falls off slowly as f^{-2}. For strong, fading clutter this is sufficient to mask weak signals with small Doppler shifts. This problem is encountered with UHF radars at near-vertical incidence, (SATO and WOODMAN, 1982). In most other cases, the noise, clutter, and signal components are distinctly identifiable in the periodograms.

This note outlines a step-by-step procedure that can be used effectively to reduce large amounts of MST radar data-averaged periodograms measured in range and time to a parametrized form. The next two sections respectively, outline the parameters to which a periodogram can be reduced and gives the steps in the procedure, that may be followed selectively, to arrive at the final set of reduced parameters. Examples of the performance of the procedure are given in the last section, where we also comment on its use with other radars.

BASIC PARAMETERS OF A TIME AVERAGED PERIODOGRAM

The form of the time-averaged periodogram of MST radar signals is shown schematically in Figure 1, where the noise, ground clutter, Doppler-shifted signal and spurious components are also identified.

The noise platform can be parametrized by a spectral density p_N and its variance σ_N^2. The total noise power P_N corresponds to $2p_NF$. p_N and σ_N^2 should be obtained over a suitable noise window. (The terms signal and noise window refer to an appropriate frequency interval. Beyond this interval the spectrum values are set to zero.)

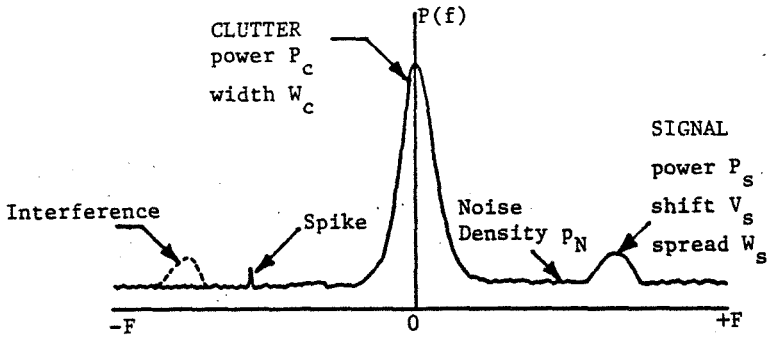

Figure 1. A typical periodogram of MST radar signals showing the clutter, noise, signal and interference component. The periodogram is measured at N discrete frequency points over an interval (-F,F).

The clutter component is symmetric about the zero frequency, and can be parametrized by the clutter power P_c and its width W_c in frequency.

To parametrize the signal component assume first that the noise and clutter contribution have been removed from the periodogram over a suitable frequency window in the vicinity of the signal peak. The signal component is then parametrized by the power P_s or the area under the signal peak, its location V_s and its frequency spread W_s. These parameters are obtained as the zeroth, first and second moment of the spectrum evaluated over the signal window.

The clutter contribution over the signal window can be removed by making use of its symmetry about the zero Doppler shift. This process also removes the noise platform. If the signal peak is well-separated from the clutter, and the clutter contribution is negligible, then the noise contribution can be removed by subtracting the noise spectral density p_n over the signal window.

The parametrization scheme outlined above requires some prior information for selecting the noise and signal windows and yields a small number of parameters: p_N, σ_N, P_N, P_c, W_c, P_s, V_s, and W_s. Originally each periodogram may contain 64-512 points. Parametrization reduces a periodogram to just 8 numbers, and thus entails a substantial data reduction.

PROCEDURE FOR PARAMETERIZATION OF PERIODOGRAMS

The outcome of an MST radar experiment is usually in the form of records, each containing periodograms averaged over a short time interval (~1/2 to 2 min) for a large number (20-200) of range cells. A typical 12-hour experiment would thus yield 10^4 to 10^5 periodograms. The step-by-step procedure discussed below is suitable for reducing the periodograms to a parametrized form using a minicomputer. It assumes the availability of two large disc storage areas, one for the unprocessed records and the other for parameters. The periodogram parameters from several experiments may be organized as a data base for subsequent analyses. The procedure has been used successfully for reducing about 600 hours of ST observations at Millstone Hill. It can be adapted with minor modifications to observations with other radars. Depending on the quality of periodograms, some steps may become redundant.

Step I: Record organization and graphical preview. The records to be processed must be organized sequentially in time without large time gaps. All the records in this sequence must correspond to the same radar pointing direction. The range cells in a record must be contiguous.

It is desirable to obtain crude prior estimates of Doppler Shifts at key ranges for selected records. Graphical displays of periodogram records are of considerable help in obtaining these estimates.

Step II: Periodogram editing, smoothing and folding. Periodogram editing involves removal of undesirable spikes using a simple despiking algorithm, based e.g. on a 3 or 5 point median filter.

Smoothing involves a circular discrete convolution with a 3-point window, e.g. a Hanning window with weights (0.25, 0.50, 0.25). If the periodogram are too noisy, a two (or even three) pass smoothing is desirable.

Folding involves the removal of ground clutter by removing that part of the periodogram that is symmetric about the center frequency. Folding also removes the noise platform.

Step III: Peak detection and tracking in range. Simple peak detection and tracking algorithms can be used to extract an initial Doppler profile from the edited periodogram records. Peak detection requires a threshold level and limiting values for the first and second difference at the peak frequency.

Once a signal peak has been unambiguously detected, it can be tracked in range by setting an ambient frequency window. The extent to which this frequency window should move between adjacent range cells can be specified on the basis of prevailing wind shear. Peak tracking in range, through a frequency window, is also effective in rejecting sporadic external interference.

Step IV: Estimating parameters. Once an initial Doppler profile has been obtained, the signal parameters discussed earlier can be obtained by computing the zeroth, first and second order periodogram moments over a signal window. To reduce the effect of smoothing, the signal parameters should be inferred from the despiked and folded periodograms. The clutter parameters are obtained from the part of the periodogram that is symmetric about the center frequency.

The noise parameters are obtained either through a noise window far removed from the Doppler profile and clutter, or from the periodogram for a distant range.

Step V: Improved estimates. The signal parameter estimates in the previous step can be improved by using the Doppler-shift information recursively. When the magnitude of Doppler shift is large and relatively steady, the signal parameters can be estimated by setting windows about the median Doppler profile. This provides a very effective means of discriminating against external interference.

EXAMPLES AND SOME COMMENTS

Figure 2 shows an example of Doppler tracking of signal peaks for two sets of periodograms observed at Millstone Hill. Figure 3 shows the development of horizontal wind field, synthesized from observations along twelve equispaced azimuths, over a ten-hour period, and illustrates the usefulness of setting up a data base.

The procedure outlined here should be useful for other VHF and UHF experiments as well. When the Doppler-shifter signal peaks are not sufficiently

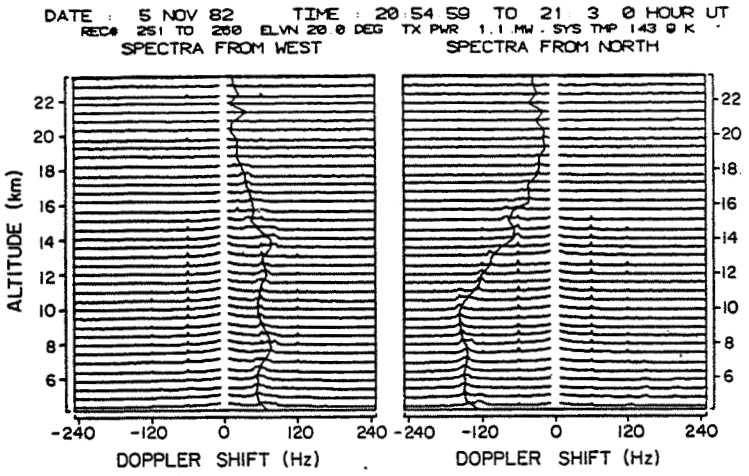

Figure 2. An example of Doppler tracking in ST radar spectra observed at Millstone Hill using the algorithms outlined in the text.

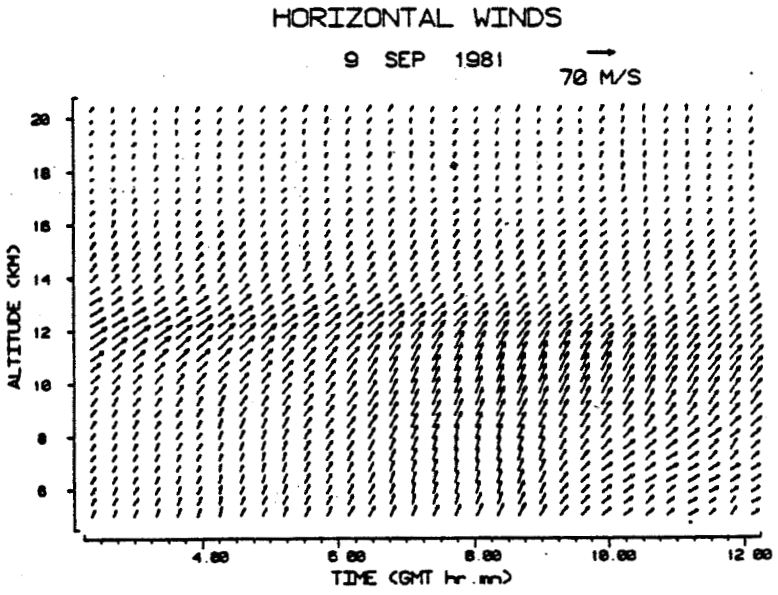

Figure 3. An example of the horizontal wind field obtained from a 12-position azimuth scan during the passage of a thunderstorm at Millstone Hill. The periodograms for each position were reduced by the method described in the text. The reduced parameters were organized as a data base and were used later to synthesize the horizontal wind field.

separated from the ground clutter, the estimates obtained by this method may be used as initial guesses for the least-squares algorithms described by SATO and WOODMAN (1982).

REFERENCES

Farley, D. T. (1983), Coherent integration, Handbook for MAP, Vol. 9, 507-508, SCOSTEP Secretariat, Dep. Elec. Computer Eng., Univ. IL, Urbana.

Rastogi, P. K (1983), A note on the use of coherent integration in periodogram analysis of MST radar signals, Handbook for MAP, Vol. 9, 509-512, SCOSTEP Secretariat, Dep. Elec. Computer Eng., Univ. IL, Urbana.

Sato, T. and R. F. Woodman (1982), Spectral parameter estimation of CAT radar echoes in the presence of fading clutter, Radio Sci. 17, 817-826.

Woodman, R. F. (1983), Spectral moment estimation in MST radars, Handbook for MAP, Vol. 9, 548-562, SCOSTEP Secretariat, Dep. Elec. Computer Eng., Univ. IL, Urbana.

Zrnic, D. S. (1979), Estimation of spectral moments for weather echoes; IEEE Trans. Geosci. El., GE-17, 113-128.

7.6A INTERPOLATION PROBLEMS IN METEOR RADAR ANALYSIS

D. Tetenbaum and S. K. Avery

CIRES
University of Colorado
Boulder, CO 80309

Meteor echoes come from random points in the observation volume, and are irregularly spaced in time. This precludes the use of FFT techniques on the raw data to give the spectrum of waves that are present. One way around this obstacle is to restrict our interest to a particular class of waves, and fit a corresponding model to the raw data. Tides can be determined this way, since we a priori know the periods: 24 and 12 hours, by definition. Even here we have to make assumptions about the spatial structure of the tides; it may be reasonable to assume that there is no horizontal variation across the observation volume, but in the vertical this is certainly not the case. If, in addition, we are interested in other types of waves which may be present and whose periods are unknown, then examining the raw line-of-sight velocities does not tell us how to modify the model, since the line-of-sight direction is not fixed. This then is the motivation for interpolation.

Interpolation takes a temporal series of line-of-sight velocities, and transforms it to a temporal series of wind velocities for each orthogonal direction, i.e. north, east, and vertical. The velocities along a given direction can then be examined readily for any waves in addition to tides.

There are different approaches to interpolation, each method having its advantages (and disadvantages). One method is to assume that the wind is constant during some fixed height/time interval, and use regression on all echoes occurring in that interval to determine the (model) constant wind. In another method, the wind is assumed to vary, in time, as a polynomial of specified degree. As before, the regression only uses echoes within a fixed time/height region. In both cases an equally spaced grid in time and height, each grid point having an associated wind vector, is obtained by marching the "interpolation region" in both time and height. The resulting grid is then ready for FFT analysis.

Another method is to regress only on clusters of echoes that are reasonably correlated. This avoids unreliable wind estimates, particularly when there are few echoes in the interpolation region, but the resulting winds are irregularly spaced in time and height.

The implicit assumption, in all the methods mentioned, is that the errors, that is, the residuals in the regression, are uncorrelated and normally distributed. This is the underlying assumption in least-squares regression, and implies that the interpolation region must be much smaller than the shortest period wavelength that we expect to see. The residuals are then attributed to instrumental error and random turbulence.

One problem with decreasing the size of the interpolation region is that fewer echoes are available for the regression and consequently the precision suffers. If the region is too large, so that it encompasses many cycles (either temporal or spatial wavelength), then we can still model the errors as uncorrelated, because the point of occurrence within the observation volume is random. In this case, however, information is lost since we have essentially filtered out the high-frequency contact. So the problem is to choose an interpolation region small enough so as not to filter out the waves that are of interest, yet not too small as to have too few echoes for a reliable estimate.

If we are trying to interpolate the wind when there are too few echoes, then there are two options. The first is to not interpolate at that point, thus leaving a gap in the time-series. If these winds are to be Fourier transformed, then the gaps must somehow be filled, preferably in such a way as not to distort the true spectrum. The second option is to increase the interpolation region so as to increase the number of echoes. This may lead to excessive smoothing, as mentioned before. So the problem is: Do we always try to interpolate a wind, resulting in a time-series with no missing values, or do we set a lowest acceptable "reliability" and treat the missing-value problem as a separate issue?

The last problem has to do with correlated errors. If there is a steady vertical shear, or, say, a trend produced by a long-period planetary wave, then the errors will always be correlated, no matter how small we choose the interpolation region. What is the effect on our estimate of the (model) wind and thus on our estimate of the tides?

To see what effect correlated errors have on the accuracy of the interpolation procedure, we have simulated a meteor radar, randomly picking the observed parameters of height, elevation, azimuth, and time of arrival. A specified wind was then projected onto the line-of-sight directions. The height, elevation, azimuth, and hourly echo rate distributions correspond to those of real echoes. Twelve hundred echoes/day were generated. Following GROVES (1959) the horizontal winds at (t_0, h_0) were computed using an interpolation box centered on (t_0, h_0) with a time width of 2 hours and a height width of 5 km. The echoes in the box were weighted inversely by the distance to the center of the box. The tidal components were then determined using a least squares curve fit.

Figure 1 is a harmonic dial showing the semidiurnal tide (at a given altitude) computed daily from 30 days of simulated meteor echoes. The specified meridional wind in this case consisted of a semidiurnal tide with a vertical wavelength of 80 km, a 3-hour gravity wave with a vertical wavelength of 5.5 km, and gaussian white noise with zero mean and a standard deviation of 25. The zonal wind was zero. For the cloud of tidal estimates shown in this figure, an error ellipse and 2-dimensional standard deviation about the true value was computed (BARTELS, 1932). This calculation was performed at all heights and the standard deviation was then plotted as a function of height as shown in Figure 2.

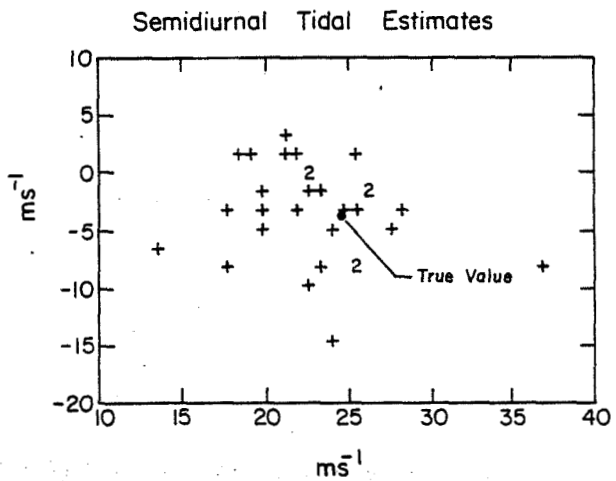

Figure 1. Harmonic dial of semidiurnal tidal estimates (Case D).

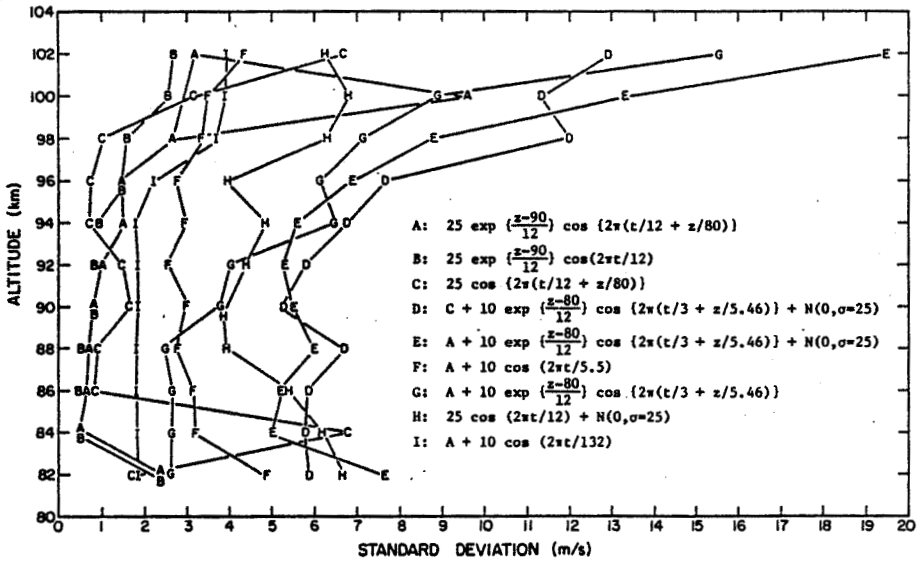

Figure 2. Standard deviation of tidal estimates for different wind fields.

From Figure 2 we can conclude that the variance of the tidal estimate will depend on the nature of the noise (correlated or uncorrelated). In the case of uncorrelated noise, the tidal variance decreases with increasing echo rate. With correlated noise (the presence of wind shears), the tidal variance is governed more by the magnitude of the wind shears. The presence of long-term trends such as planetary waves contributes less to tidal variance than gravity-wave-induced wind shears.

REFERENCES

Bartels, J. (1932), Statistical methods for research on diurnal variations, Terr. Mag. and Atmos. Elec., 37, 291-302.

Groves, G. V. (1959), A theory for determining upper-atmosphere winds from radio observations on meteor trails, J. Atmos. Terr. Phys., 16, 344-356.

7.7A PROBLEMS AND SOLUTIONS IN ANALYZING PARTIAL-REFLECTION DRIFT DATA BY CORRELATION TECHNIQUES

C. E. Meek

Institute of Space and Atmospheric Studies
University of Saskatchewan
Saskatoon, Canada

INTRODUCTION

The problem of analyzing spaced antenna drift data breaks down into the general categories of raw data collection and storage, correlation calculation, interpretation of correlations, location of time lags for peak correlation, and velocity calculation.

DATA COLLECTION AND STORAGE

The total record length required for wind analysis depends on data stationarity, and may be different at different sites (or heights, or times). Generally periods of 2-5 min are used at medium frequencies (MF) and somewhat shorter records at VHF, depending on local conditions and equipment. In real-time systems, another consideration is whether analysis can be done during data collection or not; the former is preferable since longer data sequences lead to better stability in the final wind value. Since gravity waves of short period (5-10 min) are likely to have short horizontal wavelengths, these are probably attenuated by the wide antenna beam widths employed at MF, and so the longer records are reasonable.

Raw data storage is a problem, particularly if there are a lot of height gates. It is best to have no gaps in the time sequence for the whole record, so that later correlations can use the full length, and stability will not decrease appreciably with lag. Alternately, the gaps between data blocks can be set to be an integer number of Δt (the basic sample or cycle rate), and the data interpolated later. In real-time systems the data must be broken into blocks, which are dealt with as they are collected, by accumulating partial correlations for all the lags required.

If the transmitter pulse is generated from the local power line frequency, a phase shift can move it away from locally generated interference spikes. Otherwise some sort of despiking is required on the raw data. One easy method is to replace any amplitude which is more than the sum of the adjacent amplitudes by the average of these values, a simple process in microcomputers. If despiking is not done, and the spikes are well above the signal amplitude, then spurious peaks can occur in the cross correlations.

The sample rate depends on the expected velocities. A reasonable estimate is $\Delta t = d/(2V_{max})$, where d in the antenna separation and V_{max} is the largest expected velocity. In this case the cross correlation peak furthest from zero lag would be located at approximately 1/2 lag. Data with wide cross correlations would require faster sample rates, since the peaks are less well defined in lag.

A comment should be added here on receiver gain control. The dynamic range of signals (MF) is usually ~60 dB over the mesosphere/themosphere heights. A voltage-controlled gain is usable, so that the gain can be changed with height, but if this is done in the IF stage the output will take at least one height gate to settle down (assuming that the height gates are chosen for maximum height resolution). A better way is to have a receiver with distributed outputs, each for a fixed attenuation, and select the appropriate output

for a particular gate by the signal strength. It is important to have some estimate of signal strength at each height gate in order that spurious interference, particularly teletype signals at night, can be recognized in examination of the final wind values. Such interference will be constant in all height gates, and can be rejected by choosing a height gate where no signal is expected, and setting a signal strength acceptance limit at some level above this.

CORRELATION CALCULATION

The normal definition of correlation is used with raw amplitudes, but data which has been converted to single bit amplitudes with respect to the mean must be corrected according to $\rho = \sin(\rho\pi/2)$, where ρ is the correlation value of the single bit data.

INTERPRETATION OF CORRELATIONS

Examination of the auto- and cross correlations (ACF, CCF) is invaluable, particularly at a new site or if equipment is modified, for determining data stationarity, noise problems, interference pattern effects, etc.

The basic parameters required from the correlation are the time lags for maximum CCF t_{max}, used for "apparent velocity", and peak values of the CCFs, ρ_{max}, along with the width (in lag) of the ACF, t_A, used for the "true velocity".

In theory, the sum of the t_{max}, taken in the proper sense around the receiver antenna pair vectors, should add to zero. In practice there are often multiple peaks, and even if there is only one but it is very wide, statistical fluctuations can make the accurate determination of t_{max} difficult.

There are many possible causes for multiple peaks. If the record length is too short, trends in the signal strength can cause a high correlation value at zero lag, in addition to any real peaks. A wind shear over the antenna beam width or pulse width, or any abrupt change in velocity during the record will produce a separate set of peaks for each velocity present. If these changes were smooth rather than abrupt, the result would be an average correlation function with a single peak. Other causes of multiple peaks include fringe patterns caused by interference between two or three strong reflectors.

For systems using coherent averaging, it is possible that with the high pulse rate employed, multiple reflections or scattering from, say, the F layer, could contribute "spurious" peaks to the correlations. This problem can be alleviated by making each pulse independent in phase. In any case, a method is required by which only those peaks corresponding to one pattern motion be chosen for further analysis. A simple way is to use the normalized time discrepancy ($NTD = |\Sigma t_{max}| / \Sigma |t_{max}|$) in the selection of peaks. A high value will indicate that the chosen peaks cannot refer to one pattern motion, and consequently any velocity calculated from them is meaningless.

If the correlations are very wide in lag relative to their peak location, accurate location of the peaks is difficult. One solution, termed "metacorrelation" is based on the fact that, under the assumption of a Gaussian correlation function, the ACF (ρ_A) and CCF (ρ_{ij}) have the same shape (e.g. the same width at half peak value). Thus the logarithms of these functions should be the same parbolic function but translated linearly in lag and log (ρ). An accurate value for the shift in lag can be found by lagged correlation between each log (ρ_{ij}) and log (ρ_A). The position in lag of the peak "metacorrelation" defines the best value of t_{max} (the zero-lag value of ρ_A is omitted in this process because of a possible noise spike here). Another parameter

directly available is the factor by which the original CCF's are reduced from the ACF, which gives the true value of each peak CCF, and bypasses other noise correction methods. However, these latter values were not found to be very accurate in tests.

Meteor trails are a cause of nonstationary data, and since the signal increases in all spaced antennas simultaneously, they cause wide spurious peaks in the CCFs at zero lag. If the data are converted to single-bit amplitudes in blocks, the problem is minimized because the high amplitudes during a block containing a meteor trail will be reduced to have the same significance as those without, in the conversion to binary sequences.

VELOCITY CALCULATION

Apparent velocity, V_{ap}, (which is calculated from just the t_{max} values has a theoretical disadvantage compared to "true" velocity, V_{tr}, in which possible pattern elongation and time decay are allowed. In the MF radar case (Saskatoon) V_{ap} is only ~10-20% greater than V_{tr} below ~90 km on the average, and is fairly well behaved except in cases of nonstationary data (e.g. meteor trails) where the values can be extreme; whereas V_{tr} is virtually always well behaved (although it can be biased by such things as noise level). A calculation of V_{tr} usually includes that of V_{ap}, so data can be reworked backwards to find V_{ap}.

The pattern and time decay parameters in a V_{tr} analysis are also of interest in terms of the scattering processes. Significant variations have been found in local time as well as seasonally at Adelaide and Saskatoon.

D 64

8. DATA BASE MANAGEMENT - MSTRAC
(Keynote Paper)

S. K. Avery

CIRES, University of Colorado
Boulder, CO 80309

B. B. Balsley
National Oceanic and Atmospheric Administration
Boulder, CO 80303

MSTRAC: CHRONOLOGY OF EVENTS

At the first Workshop on Technical Aspects of MST Radars held in Urbana, IL, May, 1983, a draft recommendation and initiation statement was made for a group under MAP that would serve as a forum for data exchange discussions and MST activities coordination. The name of the group is MST Radar Coordination (MSTRAC). This group has a chairman, vice-chairman, and informal representation from all current and planned MST or ST radars and from the data-user community.

In July 1983, a letter was sent to the MAP mailing list requesting a response of interest in data exchange from potential users. Several existing facilities agreed to provide a sample data set and a list of contacts was provided with the letter. Approximately ten people responded to that letter.

Following up on these requests a meeting of MSTRAC was held in Hamburg at the IAGA/IAMAP meeting in August 1983. At that meeting, the geophysical parameters to be included in the sample data tapes were determined. It was also suggested that MSTRAC compile a catalog of existing data at each of the facilities. In December 1983, a letter was sent to the facilities requesting catalog information. The response to this letter was not good.

The conclusions after one year of MSTRAC are:

1. There is a community of interested users for MST data,
2. The initial responses from observatories indicates that interest in MSTRAC is not overwhelming, probably because of time involved.
3. We need to reassess the program.

SECOND WORKSHOP SUMMARY: REASSESSMENT OF NEED

Several concerns regarding a data base were mentioned at this Workshop. Alternatives to a data base were mentioned. Many people felt that interaction between the data user and experimenter was essential and thus preferred to contact the experimenter directly. This alternative would allow the user and experimenter to design or run the radar in a mode that would provide data to answer a specific question. One major disadvantage in this route is the amount of time required of the experimenter. Obviously this interaction would be limited to a few people. As the demand for data increases, a data base would be more appropriate.

RESOURCES

Most successful data bases have resources available to the experimenter to provide data tapes to the data base in an agreed-upon format. The availability of these resources (personal and financial) will need to be addressed at some point if a data base is to be developed. Several successful data bases that might serve as models are: Atmospheric Explorer, World Data Center, Microwave Meteorological Radars. All of these data bases have a set format for the data.

Another possibility is the incoherent-scatter radar data base which has a more flexible tape format.

DATA FORMAT

Potential data formats were discussed. However, it was agreed that a further assessment of the potential users was needed. One issue of concern involving tape format was the quantity of data and the difficulty in using binary tapes at different computer facilities. ASCII or EIBCIDIC formats would involve a much greater number of tapes. Another problem in setting a tape format at this time, is that the radars are still changing experimental parameters. Sample data tapes from the facilities should be sent to users that previously requested data. These tapes should consist roughly of one-minute data points of the first three spectral moments or their equivalent in the time domain. Noise levels should also be included, if possible. These parameters were agreed upon at the Hamburg meeting. (see minutes from that meeting, Handbook for MAP, Vol. 11).

DATA CATALOG

It was suggested that we still pursue the idea of a data catalog from the facilities. MSTRAC should distribute the data catalog and reassess the data-user response. The contact person for the Colorado ST network is Dr. R. Strauch, Wave Propagation Lab., NOAA/ERL, Boulder, CO 80305, USA.

8.1A SAMPLE INTERCHANGE OF MST RADAR DATA FROM THE URBANA RADAR

S. A. Bowhill and A. Rennier

Aeronomy Laboratory
Department of Electrical and Computer Engineering
University of Illinois
Urbana, IL 61801

INTRODUCTION

As a first step in interchange of data from the Urbana MST radar, a sample tape has been prepared in 9-track 1600-bpi IBM format. It includes all Urbana data for April 1978 (the first month of operation of the radar). The 300-ft tape contains 260 h of typical mesospheric power and line-of-sight velocity data.

The tape is available at no cost from the authors at the Aeronomy Laboratory. The header file is reproduced below.

HEADER FILE

The data on this tape are provided in accordance with the MSTRAC project (MST Radar Coordination) of the Middle Atmosphere Program of SCOSTEP (Scientific Committee on Solar-Terrestrial Physics). The remaining files on this tape contain data taken at the Aeronomy Laboratory Field Station, approximately 10 km northeast of the University of Illinois at Urbana (40 deg 10 min N, 88 deg 10 min W). Transmitting frequency is 40.92 MHz and peak transmitted power is approximately 1250 kW. The transmitted pulse width is 20 μs. The antenna consists of 1008 half-wavelength dipole elements divided into three parallel sections. The ground where the antenna is located slopes 1.5 deg to the south of east, so that the on-axis antenna position is off by the same amount. The transmitter and receiver are both connected to the antenna via a gas-filled-tube transmit/receive switch. The receiver system consists of a low-noise broad-band preamplifier, a filter and a single conversion receiver with a bandwidth of 230 kHz centered around 40.92 MHz. The signal is quadrature-phase-detected, and the two components fed through a multiplexer and a 10-bit analog-to-digital converter with a conversion time of 10 microseconds. Data processing is done on a Digital Equipment Corporation PDP-15 minicomputer with a 32 k of core memory. Pulse repetition frequency is 400 Hz and 20 altitudes are sampled. Twenty-five consecutive samples from each altitude range are coherently integrated so as to give an integrated sample each 1/8 sec. Autocorrelation functions are calculated on-line with 12 lags 1/8 sec each. The correlation functions are then incoherently integrated for one minute. These one-minute averaged autocorrelation functions are stored for post-processing. Scattered power and line-of-sight velocity are calculated from the autocorrelation function and stored on floppy disk. The files on the floppy disk were used to make this tape.

Each file has the following format.

Title String	April 3, Power (Logplot)
Start Time Hours	13
Start Time Minutes	46
Number of Minutes in File	120
Minimum Value	6.28
Maximum Value	7.58
Average Value	6.53346485
Base Height (km)	57
Data Data Data Data ...	635 647 645 695 ...

Data are stored height-by-height, first minute to last. The first 120 data points correspond to minutes 1 to 120 for the altitude (base height + 1.5 km). The next 120 points correspond to minutes 1 to 120 for (base height + 3.0) km. This continues on for each height until (base height + 30) km is completed. The height resolution is 1.5 km.

Note: Data stored on this tape are 100 times greater than the actual data. This was done to allow an integer format without loss of precision. Simply divide each data value by 100 to obtain the proper values (power-bels, velocity-m/s). Additional information which may prove useful.

Label = (M, NL)
DCB = (RECFM = FB, LRECL = 80, BLKSIZE = 4000)
EBCDIC
9 Track
1600 BPI
129 Data Files

Questions concerning these data, and requests for additional data, should be made to Prof. Sidney A. Bowhill, Director, Aeronomy Laboratory, Department of Electrical Engineering, University of Illinois, 1406 W. Green Street, Urbana, Illinois 61801, USA. The remainder of this file contains a menu of the tape.

FILE	DATA	STARTTIME	DATE
1	Power	1346	4-3-78
2	Velocity	1346	4-3-78
3	Power	950	4-4-78
4	Power	1158	4-4-78
5	Power	1406	4-4-78
6	Velocity	950	4-4-78
7	Velocity	1158	4-4-78
8	Velocity	1406	4-4-78
9	Power	1206	4-7-78
10	Velocity	1206	4-7-78
11	Power	517	4-10-78
12	Power	717	4-10-78
13	Power	917	4-10-78
14	Power	1141	4-10-78
15	Power	1632	4-10-78
16	Velocity	517	4-10-78
17	Velocity	717	4-10-78
18	Velocity	917	4-10-78
19	Velocity	1141	4-10-78
20	Velocity	1632	4-10-78
21	Power	509	4-11-78
22	Power	800	4-11-78
23	Power	1000	4-11-78
24	Velocity	509	4-11-78
25	Velocity	800	4-11-78
26	Velocity	1000	4-11-78
27	Power	504	4-12-78
28	Power	704	4-12-78
29	Power	904	4-12-78
30	Power	1124	4-12-78
31	Power	1324	4-12-78
32	Power	1524	4-12-78
33	Power	1742	4-12-78
34	Velocity	504	4-12-78
35	Velocity	704	4-12-78

36	Velocity	1124	4-12-78
37	Velocity	1324	4-12-78
38	Velocity	1524	4-12-78
39	Velocity	1742	4-12-78
40	Power	514	4-13-78
41	Power	714	4-13-78
42	Power	1016	4-13-78
43	Power	1216	4-13-78
44	Power	1416	4-13-78
45	Power	1655	4-13-78
46	Velocity	514	4-13-78
47	Velocity	714	4-13-78
48	Velocity	1216	4-13-78
49	Velocity	1416	4-13-78
50	Velocity	1655	4-13-78
51	Power	537	4-14-78
52	Power	737	4-14-78
53	Power	937	4-14-78
54	Power	1151	4-14-78
55	Power	1351	4-14-78
56	Power	1551	4-14-78
57	Velocity	537	4-14-78
58	Velocity	737	4-14-78
59	Velocity	937	4-14-78
60	Velocity	1151	4-14-78
61	Velocity	1351	4-14-78
62	Velocity	1551	4-14-78
63	Power	1221	4-18-78
64	Power	1421	4-18-78
65	Power	1621	4-18-78
66	Velocity	1221	4-18-78
67	Velocity	1421	4-18-78
68	Velocity	1621	4-18-78
69	Power	504	4-19-78
70	Power	704	4-19-78
71	Power	904	4-19-78
72	Power	1113	4-19-78
73	Power	1313	4-19-78
74	Power	1513	4-19-78
75	Power	1726	4-19-78
76	Velocity	504	4-19-78
77	Velocity	704	4-19-78
78	Velocity	904	4-19-78
79	Velocity	1113	4-19-78
80	Velocity	1313	4-19-78
81	Velocity	1513	4-19-78
82	Velocity	1726	4-19-78
83	Power	518	4-20-78
84	Power	718	4-20-78
85	Power	918	4-20-78
86	Power	1156	4-20-78
87	Power	1356	4-20-78
88	Power	1556	4-20-78
89	Velocity	518	4-20-78
90	Velocity	718	4-20-78
91	Velocity	918	4-20-78
92	Velocity	1156	4-20-78
93	Velocity	1356	4-20-78
94	Velocity	1556	4-20-78
95	Power	454	4-21-78

96	Power	654	4-21-78
97	Power	854	4-21-78
98	Power	1131	4-21-78
99	Power	1331	4-21-78
100	Power	1531	4-21-78
101	Power	1741	4-21-78
102	Velocity	454	4-21-78
103	Velocity	654	4-21-78
104	Velocity	854	4-21-78
105	Velocity	1131	4-21-78
106	Velocity	1331	4-21-78
107	Velocity	1531	4-21-78
108	Velocity	1741	4-21-78
109	Power	441	4-24-78
110	Power	641	4-24-78
111	Power	841	4-24-78
112	Power	1109	4-24-78
113	Power	1509	4-24-78
114	Power	1719	4-24-78
115	Velocity	441	4-24-78
116	Velocity	641	4-24-78
117	Velocity	841	4-24-78
118	Velocity	1109	4-24-78
119	Velocity	1309	4-24-78
120	Velocity	1509	4-24-78
121	Velocity	1719	4-24-78
122	Power	444	4-25-78
123	Power	644	4-25-78
124	Power	844	4-25-78
125	Power	1054	4-25-78
126	Velocity	444	4-25-78
127	Velocity	644	4-25-78
128	Velocity	844	4-25-78
129	Velocity	1054	4-25-78

ACKNOWLEDGMENTS

The research described was supported in part by the National Aeronautics and Space Administration under grant NSG 7506 and in part by the National Science Foundation under grant ATM 81-20371.

8.2A MST RADAR DATA MANAGEMENT

G. D. Nastrom

Control Data Corporation
P. O. Box 1249
Minneapolis, MN 55440

Wind speed and direction are perhaps the most familiar variable measured with ST radars, and reporting them with the necessary accurracy should continue to be of paramount importance. But reporting only wind speed and direction denys the full capability of ST radars; it would be like reporting only the storm location with a Doppler storm-detection radar. Obviously, recording the full Doppler spectrum and all ancillary radar operating parameters would not be economical for routine operations, and some parsimony must be encouraged. On the other hand, one should not discard valuable data; an example of non-wind-speed data is given next.

One atmospheric variable which can be deduced from ST radar data other than wind speed and direction is C_n^2, related to the eddy dissipation rate. The computation of C_n^2 makes use of the transmitted power (average, or peak plus duty cycle), the range of the echoes, and the returned power (NASTROM et al., 1982). The returned power can be calibrated only if a noise source of known strength is imposed; e.g. in the absence of absolute calibration (GREEN et al., 1983), one can compare the diurnal noise signal with the galactic sky temperature. Thus to compute C_n^2 one needs the transmitter power, the returned signal as a function of height, and the returned noise at an altitude so high that it is not contaminated by any signal. Now C_n^2 relates with the amount of energy within the inertial subrange, and for many research studies it may be desirable to relate this with background flow as well as shears or irregularities on the size of the sample volume. The latter are quantified by the spectral width.

Thus, to avoid weakening the impact of ST radar data, archive recordings should include at least the wind speed and direction, returned signal, noise, and spectral width at each level plus the noise for at least one very high altitude in the neutral atmosphere.

REFERENCES

Nastrom, G. D., K. S. Gage and B. B. Balsley (1982), Variability of C_n^2 at Poker Flat, Alaska, from MST Doppler radar observations, Opt. Engr., 21, 347-351.

Green, J. L., W. L. Clark, J. M. Warnock and K. J. Ruth (1983), Absolute calibration of MST/ST radars, Preprints, 21st Conference on Radar Meteorology, Edmonton.

8.2B DATA BASE FOR THE COLORADO PROFILING NETWORK

/ D. A. Merritt

National Oceanic and Atmospheric Administration/ERL/WPL
Boulder, CO 80303

The Colorado profiling system developed by the Wave Propagation Laboratory (WPL) (HOGG et al., 1983) includes five (soon to be six) Doppler radar wind Profilers; four operate at 49 MHz (6 m) and are located at Platteville, Fleming, Lay Creek, and Cahone, and one operates at 915 MHz (33 cm) and is located at Denver. The sixth radar, now under construction, will operate at 405 MHz (UHF) and will be located at Boulder. Microwave radiometers and surface meteorological stations are at some of the radar sites. This note describes only the data base for the wind Profilers.

Each radar site has its own computer and can be controlled remotely. Information from the various sites is transmitted to Boulder by dedicated or dial-up telephone lines. Since the radar control software is driven by tables of parameters which are accessible and modifiable via remote terminal, both temporal and spatial resolutions can be changed so the host data base must be as flexible as possible. The wind profiles measured at each site are received by the data base as a time series (or "stream") of information in temporal order regardless of the operating mode of the radar. At each site (except Platteville) there can be as many as three separate horizontal wind profiles measured during the same averaging period, each with a different height resolution. In addition, the UHF sites can measure three separate vertical profiles with different resolutions during the same period. The profiles may be obtained in any order with different temporal resolution. Therefore, to maintain flexibility, the data base separates and separately stores (in temporal order) the series of profiles measured with each height resolution at each site.

The information stored for each profile is as follows:

a) For each measurement height (maximum = 32):

Wind speed	m/s	
Wind direction	deg.	(from North)
Height	km	(MSL)
Number East		(The number of individual wind profiles in
Number North		the consensus set)
Received power	dB	(not range normalized)

b) Identification information:

1. Date and time at start of data acquisition
2. Number of individual profiles used in the averaging process
3. Number of time-domain averages of radar pulses
4. Number of Doppler spectra averaged for the individual profiles
5. Pulse width (μs)
6. Pulse repetition period (μs)
7. Maximum unambiguous horizontal speed (each direction) m/s
8. First height km (MSL)
9. Number of heights
10. Height spacing km
11. Antenna selected for power information (power information is stored for only one antenna; this indicates which)

The data are stored as single precision floating point values (six or seven decimal digits of precision) as calculated and transmitted by the computers at the sites. Data can be accessed for real-time display by selecting the desired site, time, and type of data. Approximately three days of data are kept in the data base at any time; the data base is dumped to magnetic tape about every three days for permanent storage.

REFERENCE

Hogg, D. C., M. T. Decker, F. O. Guiraud, K. B. Earnshaw, D. A. Merritt, K. P. Moran, W. B. Sweezy, R. G. Strauch, E. R. Westwater and C. G. Little (1983), An automatic Profiler of the temperature, wind, and humidity in the atmosphere, J. Climate Appl. Meteorol., 22, 807-831.

D68

9.1A FURTHER DEVELOPMENTS OF EISCAT AS AN MST RADAR

J. Rottger*

EISCAT Scientific Association
S-981 27 Kiruna, Sweden

INTRODUCTION

The principal capabilities of EISCAT as an MST radar were described in an earlier report by ROTTGER et al. (1983). Since the VHF transmitter of the EISCAT system is not yet delivered, only the UHF system could be used for radar experiments. Considerable developments in the year 1983 have now strongly improved the reliability of the operations. Most of the experiments were and will be done to investigate the high latitude ionosphere and thermosphere, but some time was also devoted to observations of the lower and middle atmosphere, particularly during the MAP/WINE campaign.

Modifications and a general refurbushing of the UHF transmitter now allows its reliable and continuous operation at maximum power levels of 1.5 MW. The transmit-receive response of the system was speeded up, shifting the shortest ranges to be sampled to less than 100 μs. Essential work was also done to reduce 50 Hz-hum insertions, and oscillator sidebands are acceptably suppressed now. Fairly unique pulse modulation patterns were implemented which apply multipulse schemes. By using the multifrequency/multichannel capabilities of the EISCAT system, highest efficiency at best spatial and temporal resolution can be achieved for D- and E-region work (TURUNEN and SILEN, 1984). Although the full spectrum information of D-region incoherent scatter signals can be achieved only by pulse-to-pulse sampling, the multipulse schemes can also be used to obtain adequate velocity estimates down to 75-80 km. For troposphere and stratosphere work only the pulse-to-pulse technique is applicable. However, restrictions exist for sounding the lower atmosphere because of exceptional ground clutter and the very limited size of the result memory of the correlator (2 k). In the following part we will present some typical examples of tropospheric and mesospheric data records to elucidate capabilities and limitations of the monostatic system. Bi- or tristatic operations are not feasible for troposphere investigations (because of mountain shielding in Tromso), they were, however, done to complement velocity measurements in the mesosphere and lower thermosphere. They also can be done to probe the lower (and middle) stratosphere.

TROPOSPHERE-STRATOSPHERE OBSERVATIONS

In Figure 1 examples of real-time displays (RTGRAPH) of the complex autocorrelation functions (ACF) and the corresponding spectra are shown. The first gate is at a range r = 15 km (corresponding to 100 μs), and the separation of the gates is 1.5 km (matched to the transmitted pulse length). At the chosen elevation angle 20° the corresponding lowest altitude is z = 5.1 km and the altitude steps (altitude resolution) are 0.5 km. During these experiments 64-point ACFs were computed on-line, using a pulse-to-pulse correlator program. The size of the result memory of 2 k words (a 64 bits) limited the number of range gates to 30 (including one background noise gate) and one gate for noise calibration. The transmitter was run at about 1 MW and 1 ms (2 ms) repetition rates, corresponding to a duty cycle of 1 (0.5) % when using a 10 μs pulse on a single frequency. In order to sample the troposphere and lower stratosphere the elevation angle was set to 20°. Higher elevation angles would be more suitable; this, however, can only be done after further work to improve the transmit-receive transition has been finished.

*presently at Arecibo Observatory, Arecibo, Puerto Rico, on leave from Max-Planck-Institut fur Aeronomie, Lindau, W. Germany.

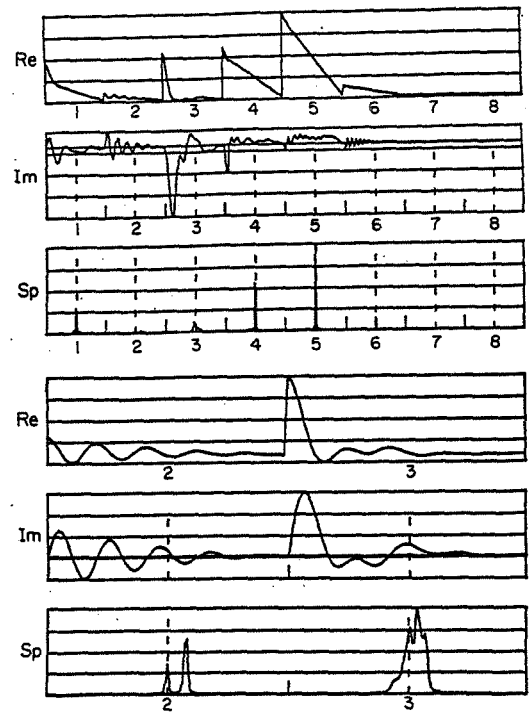

Figure 1. RTGRAPH displays of the real (Re) and imaginary (Im) part of the autocorrelation functions for different range gates (numbers) and the corresponding spectra (Sp) of echoes from short ranges (15-25 km).

The triangle shape of the real part of the ACF (e.g., gates 1, 4, 5, and 6) indicates a strong dc signal due to ground clutter, which appears as a spike at zero Doppler frequency in the spectra. The oscillating imaginary part indicates that besides the ground clutter also a signal with a Doppler shift was detected which is due to scatter from atmospheric turbulence. For elucidation of this fact two range gates with low ground clutter strength are displayed in the lower portion of Figure 1.

The ground clutter represents a very troublesome limitation to the investigations of the lower atmosphere with the monostatic UHF radar in Tromso. This clutter is obviously due to scatter/reflection from mountains. The Tromso system is in an area where high extending mountains are visible at distances from a kilometer out to several tens of kilometers. The antenna sidelobes, through which the clutter is received, cannot be suppressed. The only means would be to operate at higher elevation angles. Even then ground clutter is of considerable strength.

At 20° elevation angle the ground clutter is mostly stronger than the atmospheric signal which can be seen in Figure 2. The clutter also varies as a function of azimuth and range. The latter effect (seen also in Figure 1) is most cumbersome because the strongest clutter echo determines the attenuator setting of the receiver to avoid saturation effects. Because of the limited dynamic range of the receiver and the ADCs (8 bit), this could result in a

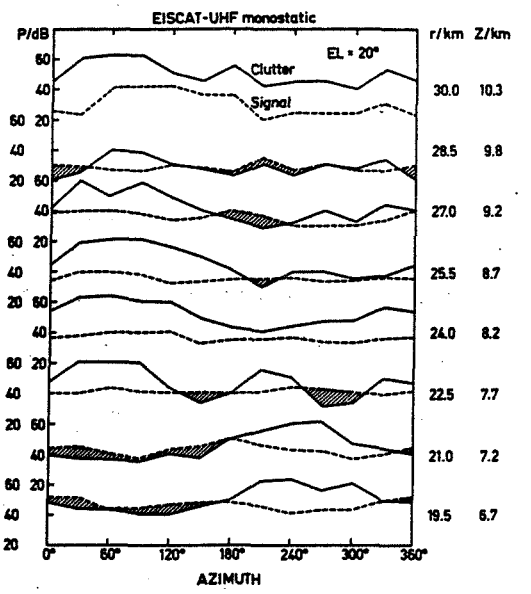

Figure 2. Ground clutter and signal power P as function of azimuth and range r. Shading indicates where the atmospheric signal was stronger than the ground clutter.

total attenuation of weak atmospheric signals, if the clutter-to-signal ratio is exceeding 48 dB.

At the relatively low average transmitter power of less than 8 kW and the 10 μs transmitter pulse, the signal-to-clutter ratio during the described operations at 20° elevation angle was not exceeding -20 dB at ranges larger than 30 km. This limited the observations to upper altitudes of about 10 km, which is the lower stratosphere in high latitudes. Using a long pulse/narrow bandwidth, lower elevation angle (i.e. longer ranges and thus less ground clutter) and almost maximum duty cycle, monostatic echoes up to heights above 20 km were recorded during EISCAT's first stratosphere experiments (ROTTGER, 1983).

The spectra shown in Figure 3 indicate another effect which complicates the analysis. This is the broadening or the modulation of the ground clutter signal. We assume that this may be either due to fading of the clutter signal or (digital) quantization noise. We do exclude a frequency or amplitude modulation of the transmitter or the receiver oscillators at these extended levels of -15 dB below the carrier signal.

Although the signal-to-clutter ratio is mostly less than one, some valuable results can be obtained which are briefly summarized in Figures 4-7. Using the VAD technique height profiles of wind velocity can be obtained and the fast real-time data acquisition allows to study high time resolution developments of clear-air turbulence. Similar measurements with the Millstone Hill Radar proved to be very useful (WATKINS and WAND, 1981; WAND et al., 1983).

OBSERVATIONS OF THE MESOSPHERE AND LOWER THERMOSPHERE

First incoherent-scatter observations of the D region were done in summer

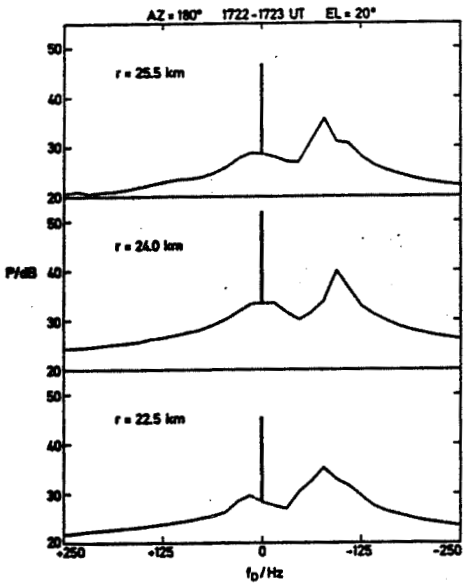

Figure 3. Doppler spectra showing ground clutter line at f_D = 0 Hz, a broadening of this line at levels of about -15 dB and the signal, shifted by about 100 Hz.

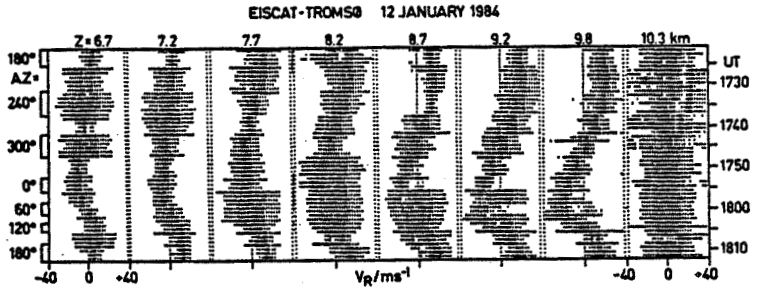

Figure 4. Velocity-azimuth-display (VAD) for altitudes z = 6.7 - 10.3 km. Note the variation of azimuth is not constant with time.

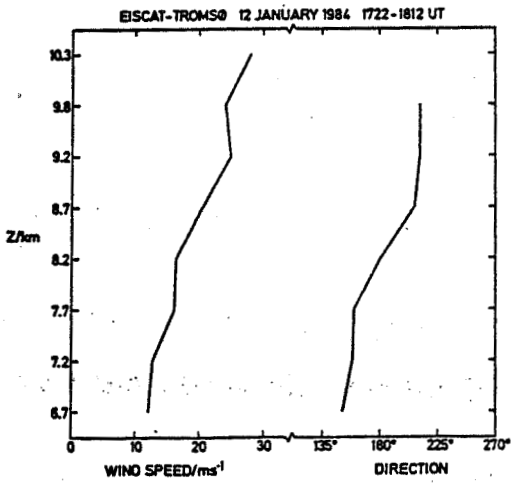

Figure 5. Wind speed and direction deduced from the VAD measurement shown in Figure 4.

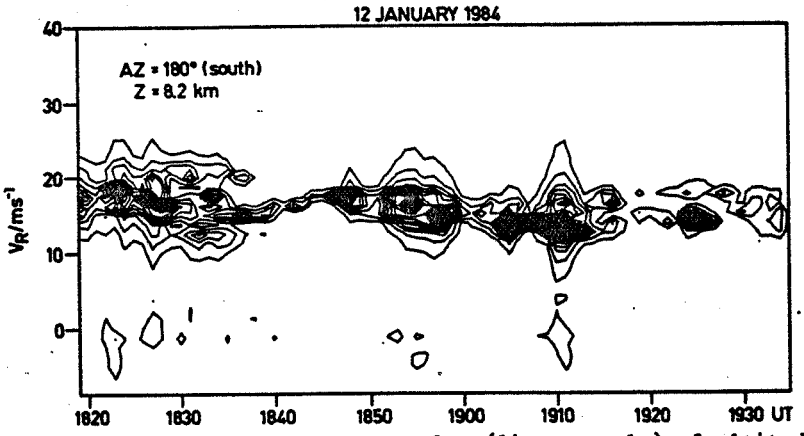

Figure 6. Spectrum contour plot (linear scale) of altitude gate z = 8.2 km, showing variability of the echo in power, Doppler shift and Doppler spread, due to intermittent clear-air turbulence carried through the radar volume.

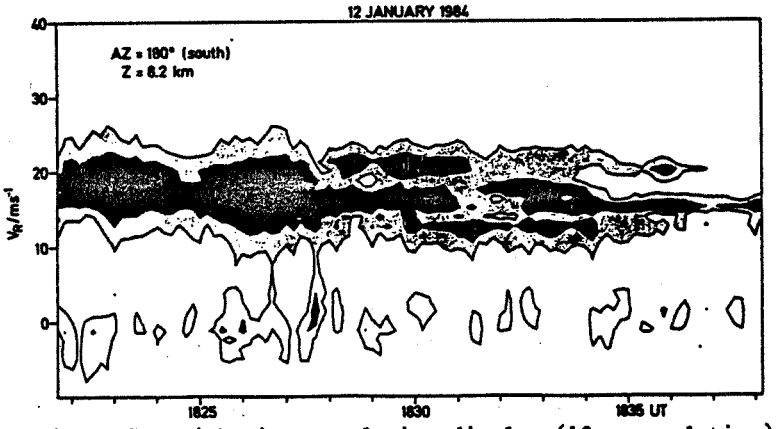

Figure 7. High time resolution display (10 s resolution) of clear air turbulence structure. Display is in logarithmic scale, where differences between contour lines are 3 dB. Note the splitting into patches with different velocities after 1830 UT.

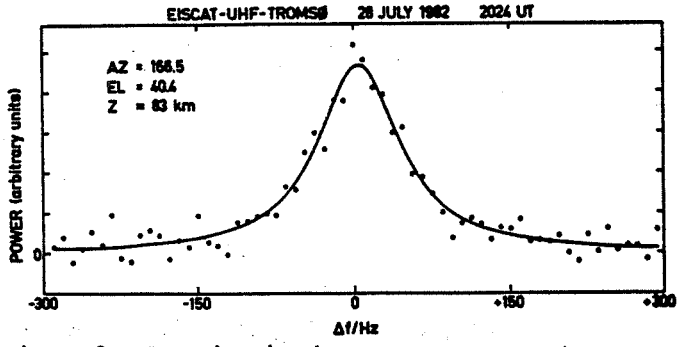

Figure 8. D-region incoherent scatter spectrum averaged over 2 min (from KOFFMAN et al., 1984).

1982 and a longer series of data were recorded during the MAP/CAMP campaign in July/August 1982. The relevant results of these campaign operations, namely electron density and wind profiles as well as mesopause temperature and negative-ion-to-electron ratios, were summarized by KOFMAN et al. (1984). In Figure 8 we show an example of an incoherent-scatter spectrum which could be obtained if high energy particle precipitation generates sufficient D-region ionization ($\gtrsim 10^{10}$ electrons per m^3), whereas the normal daylight D-region ionizations is not sufficient to yield evaluable signals. Because of the dominating collisions, the incoherent spectrum information of the D region and the lower E region up to about 110 km can be used to deduce neutral wind profiles and, under some assumptions, of the ion-neutral collision frequency, and also the neutral temperature.

The spectral width increases with height because of the decreasing collision frequency as shown in Figure 9. Above 92 km it is broader than 300 Hz. To resolve this spectrum the signal must be sampled at least at a rate of 667 μs. Applying the pulse-to-pulse sampling scheme, this rate is equal to the transmitter interpulse period (IPP). The EISCAT UHF transmitter does not allow a higher IPP than 1000 μs which places a limit to the maximum height where the pulse-to-pulse scheme can be applied. More restrictive, however, is the fact that the interpulse period must be longer than the range of the sampled gate. Since 667 μs corresponds to a range (= altitude at vertical incidence) of 100 km, the pulse-to-pulse scheme can no more be applied above about 92 km.

The altitude resolution in the region of the mesosphere and the lower thermosphere up to 130-150 km has to be of the order of some kilometer. Spectrum information above 92 km, thus, cannot be obtained with a long pulse (as possible in the F region) but only by applying multipulse schemes. It is evident that two explicitly different modulation schemes have to be used below 92 km and above 92 km. The pulse-to-pulse (< 92 km) and the multipulse (> 92 km) schemes, cannot be operated simultaneously or alternately with the present EISCAT radar controller/correlator system. However, as will be pointed out, the multipulse scheme can also be used to deduce the first spectral moment (Doppler shift to determine wind velocities) of mesospheric signals. Since the

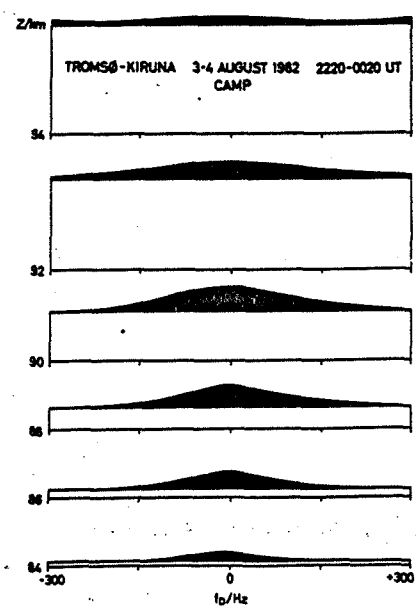

Figure 9. Average spectra (2220-0020 UT) of signals received in the bistatic mode at Kiruna during the CAMP rocket launches. The darkened area of the spectra is assumed to be due to the signal from the indicated heights, whereas the rectangular pedestal is due to signals picked up through antenna sidelobes from strong E-region ionization.

power profile (electron density) can be obtained directly from single pulse measurements, the additional application of the multipulse scheme allows to cover both the mesosphere and the lower themosphere.

Very powerful multipulse modulation schemes were recently developed by TURUNEN and SILEN (1984) and successfully applied in operations. These schemes make use of the unique multifrequency/multichannel capabilities of the EISCAT system; they allow to utilize the full applicable duty cycle at optimum range resolution and improve the significance of spectral estimates because of multichannel operation.

One of these schemes, shown in Figure 10, was used for mesosphere and lower thermosphere investigations during the MAP/WINE operations of EISCAT. This 4-pulse multipulse pattern yields the lags 1-6 of the ACF at lag increments of 40 μs. Four multipulse series are transmitted at frequencies F1, F2, F3 and F4. The EISCAT system allows to transmit on 16 frequencies at spacings of n 500 kHz around the center frequency 933.5 MHz and the reception on 8 channels, corresponding to the transmitted frequencies. The zero lag (power estimate) is obtained by using single pulses at frequencies F5 and F6.

The maximum lag of the multipulse ACF of 240 μs is obviously not sufficient to yield the full spectrum information at altitudes below about 100 km because the signal correlation time (inverse of spectral width) is longer than 240 μs. This is indicated in Figure 11 where the normalized real part ρ' of the ACFs at lags $\tau_1 = 40$ μs to $\tau_6 = 240$ μs is shown for different heights. For convenience of the display, the real part ρ' is normalized by $\rho(\tau_1)$, which is shown in relative units on the right-hand-side diagram of Figure 11. (For full ACF analysis the zero lag estimate, deduced by parabolic extrapolation, full ACF fitting or from the power profile has to be used.) In the center diagram the phase ϕ of the ACF (ϕ = arctan (Im(ACF)/Re(ACF))) is displayed. The phase derivative near zero lag is directly proportional to the Doppler shift $f_D = \phi(\tau)/2\pi\tau$. The linear phase variation at heights below 100 km indicates that we can use the phase information to deduce the Doppler shift. To improve the significance we have used all lags and calculated a weighted average

$$\bar{\phi} = \frac{\sum_{n=1}^{6} \phi(\tau_n) \cdot \rho(\tau_n)/n}{\sum_{n=1}^{6} \rho(\tau_n)}$$

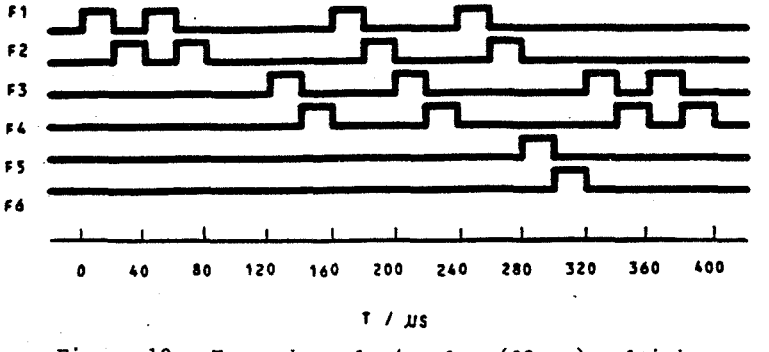

Figure 10. Four channels-4 pulse (20 μs) multiphase (F1, F2, F3, F4) and 2 channels single pulse (20 μs) at F5 and F6. Due to instrumental setting the frequencies F can be different to those noted.

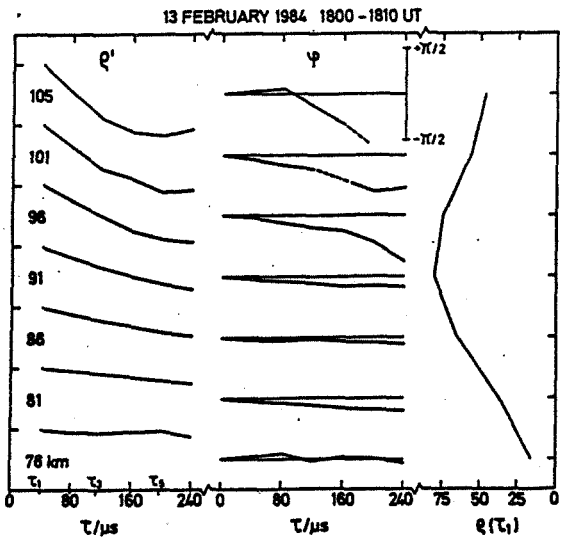

Figure 11. Normalized real part ρ' and phase ϕ of ACF, as well as the relative amplitude $\rho(\tau_1)$ of ACF at lag τ_1.

This yields a most reliable velocity estimate as long as the ACF does not cross zero.

We have used this approach to estimate preliminary velocity profiles which are shown in the Figures 12 and 13. During these operations the transmitter peak power was about 1.2 MW and the range resolution 3 km. The antenna was pointed at 33° elevation angle (corresponding altitude resolution 1.6 km) towards west (mesosphere gates north of Andenes Rocket Range) to measure the zonal wind component U and towards south to measure the meridional wind component V. Additionally the relative electron density profiles N_e' (uncalibrated) and the weighting function $\gamma = \Sigma\rho(\tau_n)$ are displayed. The relative amplitude of the weighting function is a measure for the significance of the velocity estimate. Because of the zero crossing of the ACFs, the velocity values above 100 km can be underestimated (this has to be corrected in the full spectral analysis to be applied later). The velocity profiles are additionally smoothly filtered by a five-point Hamming window. The open circles (e.g. in the V-profile measured from 1921-1930 UT on 31 Jan. 84) indicate preliminary velocity data obtained with chaff measurements (by courtesy of H. U. Widdel and U. von Zahn). The similarity of chaff and radar data, as well as the consistency of consecutive radar wind profiles, gain confidence in our method to determine mesosphere/lower thermosphere winds with the EISCAT UHF radar. In Figure 13 a time series of the zonal wind component is shown and also compared with quasi-simultaneous chaff measurements (MC8, 9, 10). The radar profiles clearly show a downward progressing wave structure with period of about 2-4 hours and vertical wavelength of 10-20 km. The wave amplitude evidently increases with altitude. However, one has to take into account that electrodynamical effects influence the structure of the measured ion drift velocity above about 110 km. A similar wave event was earlier observed with the Pokerflat MST radar in the altitude region 60-80 km (BALSLEY et al., 1983).

Finally, in Figure 14 a plot of electron density measured during a high energy particle precipitation event is shown. It proves that the sensitivity of the EISCAT UHF radar is sufficient to measure D-region (mesosphere) signals

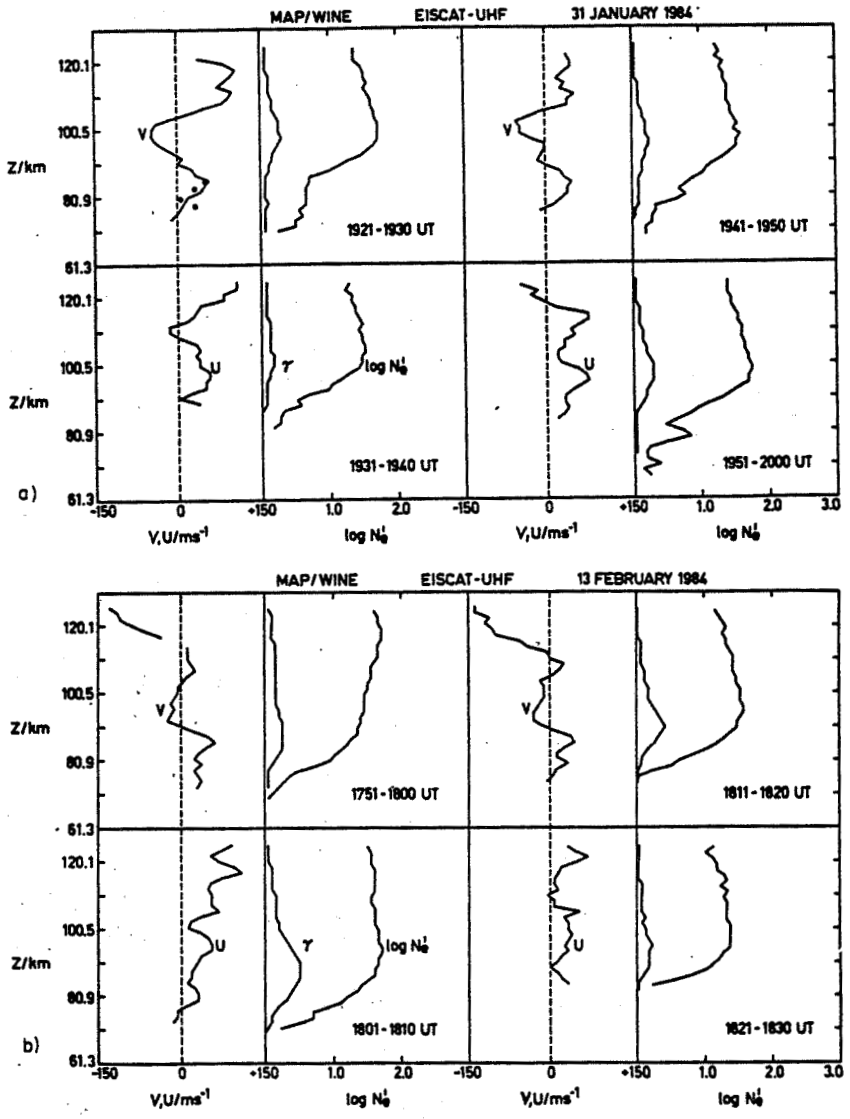

Figure 12. Profiles of zonal (U) and meridional (V) wind velocities, and relative electron density N_e' as well as the weighting function γ.

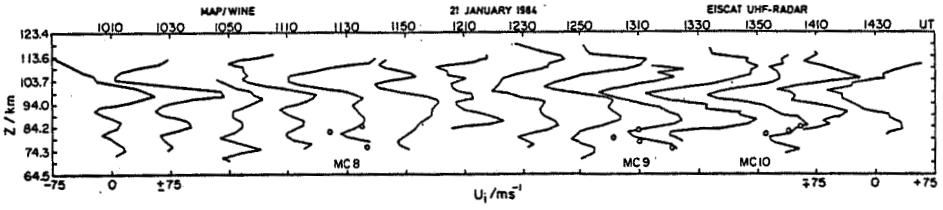

Figure 13. Time series of zonal winds. The open circles denote chaff wind data (courtesy of H. U. Widdel and U. von Zahn).

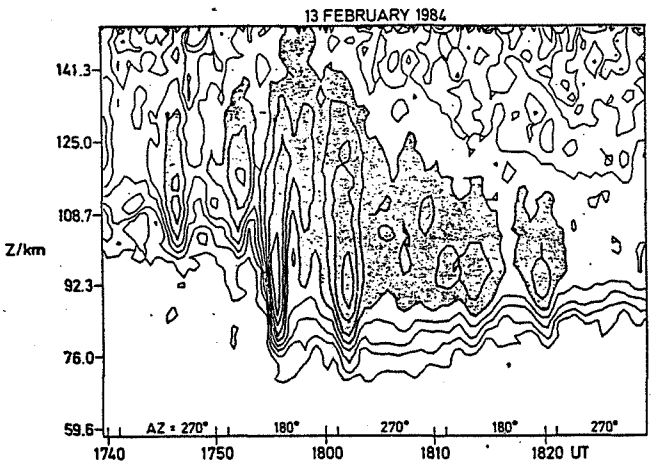

Figure 14. Electron density contour plot; the contour steps are 1.5 dB. Note the high time resolution of 30 s, which allows detection of highly variable electron density structures.

during appropriate geophysical conditions. Similar measurements at other incoherent-scatter radar facilities applying multipulse/multichannel operations for mesosphere/lower thermosphere investigations are not known yet.

I acknowledge the pleasing and very efficient cooperation with all EISCAT staff members.

The EISCAT Scientific Association is funded and operated by Centre National de la Recherche Scientifique, France, (CNRS)
Suomen Akatemia, Finland, (SA)
Max-Planck Gesellschaft, West Germany, (MPG)
Norges Almenvitenskapelige Forskningsrad, Norway, (NAVF)
Naturvetenskapliga Forskningsradet, Sweden, (NFR)
Science and Engineering Research Council, UK, (SERC).

REFERENCES

Balsley, B. B., W. L. Ecklund and D. C. Fritts (1983), Mesospheric radar echoes at Poker Flat, Alaska: Evidence for seasonally dependent generation mechanism, Radio Sci., 18, 1053-1058.

Kofman, W., F. Bertin, J. Rottger, A. Cremieu, P. J. S. Williams (1984), The EISCAT mesospheric measurements during the CAMP campaign, J. Atmos. Terr. Phys., 46, in press.

Rottger, J. (1983), Some capabilities of the EISCAT UHF radar for investigations of the stratosphere, Preprint Vol. 21st Conf. on Radar Meteorology, American Meteorological Society, Boston/USA, 100-103.

Rottger, J., M. Baron and K. Folkestad (1983), Capabilities and limitations of EISCAT as an MST radar, Handbook for MAP, Vol. 9, SCOSTEP Secretariat, Dep. Elec. Eng., Univ. Il, Urbana.

Turunen, T. and J. Silen (1984), Modulation patterns for the EISCAT incoherent scatter radar, J. Atmos. Terr. Phys., 46, (in press).

Wand, R. H., P. K. Rastogi, B. J. Watkins and G. B. Loriot (1983), Fine doppler resolution observations of thin turbulence structures in the tropostratosphere at Millstone Hill, J. Geophys. Res., 88, 3851-3857.

Watkins, B. J. and R. H. Wand (1981), Observations of clear air turbulence and winds with the Millstone Hill radar, J. Geophys. Res., 86, 9605-9614.

D69

9.2A STATUS OF THE JICAMARCA RADAR

D. T. Farley

School of Electrical Engineering
Cornell University, Ithaca, NY 14853

The capabilities of the large 50-MHz radar at Jicamarca for MST observations were discussed in some detail in Handbook for MAP Vol. 9 by Woodman and Farley. Hence the description here will be quite brief and will concentrate on recent improvements in the facility.

MAIN FEATURES

The radar is located about 20 km from Lima, Peru at longitude 76.52 W and latitude 11.56 S. It is well shielded by surrounding mountains, and most of the ground clutter is restricted to ranges of 15 km or less. The antenna consists of 18,432 half-wave dipoles (9216 crossed pairs) covering an area of 290 m by 290 m and divided up into 64 independent modules which can be individually phased and/or used as separate antennas in any way desired. The whole array can be steered about 3 degrees from the on-axis position (the limit is the beam width of the individual modules, which cannot be steered), and any polarization can be arranged. Even with this limited steerability it is straightforward to determine vector wind velocities by pointing segments of the antenna in different directions. The radar can also be used as in interferometer.

There are two sets of 50-MHz transmitters, one high power and one of lower power, and each consisting of 4 independent modules which can be used separately or combined. The high power units have a nominal power of a megawatt or more each and a duty cycle of 5-6%, but only one of the modules currently operates at this level, as is discussed more fully below. The low power units each deliver a maximum of about 60-70 kW of peak power, with a duty cycle of 2% or less and a bandwidth of up to 1 MHz (pulses as short as 1 microsecond). These can run unattended or nearly so and thus are the preferred transmitters for long experimental runs.

There are four independent receivers sharing a common local oscillator so phase comparisons between channels can be made. The output bandwidth can be selected to match pulse lengths ranging from 1 to 500 microseconds. The data-acquisition system consists of a radar controller, an 8-bit ADC system, and a Harris 100 series computer with associated tape drives and disks. The Harris does not have an array processor or a high speed floating-point arithmetic card. The high speed on-line data processing should be done in fixed point. Further details are given in the previous MAP handbook as mentioned above.

RECENT DEVELOPMENTS

The first module of the new high power transmitter designed and built by SRI International is now installed and operating well. The maximum peak power of this unit is about 1.4 MW, with a maximum duty cycle of 6% and a minimum pulse length of 1 microsecond (2 microseconds have been obtained so far). The other three modules are the originals, and pulses shorter than about 15 microseconds are seriously degraded. Furthermore, the tubes of two of these older units are far past their prime and deliver 400-500 kW of peak power at most. One of the old units, however, now has a relatively young tube (perhaps the last in the world?) obtained from Arecibo. This puts out at least 700 kW and probably can be coaxed into delivering more. Work is underway to replace the three remaining old modules with the new SRI design, but it will probably be the summer of 1985 before any of these additional new units are finished and operating.

The old digitizers and interfacing hardware at Jicamarca have now been completely replaced, leading to some improvement in speed and a great improvement in reliability. A major effort to improve the software and make it more user friendly has recently been completed also. It is now quite simple to design a rather complicated radar experiment or interleaved series of experiments, each with a different transmitting and sampling scheme. Experiments can be changed from one pulse to the next, and changes in the experiment can be made easily in real time without missing more than one or two IPPs. One computer console displays the radar pulsing and sampling parameters in a sort of "thumbwheel" format, and the user can easily change these numbers by moving the cursor to the appropriate spot on the screen and typing in the new values. With one more keystroke one initiates the revised experiment. To perform a sequence of experiments the user simply generates a series of thumbwheel displays and the appropriate commands for stepping from one to the next, and then stores these in disk files.

9.3A RECENT RESULTS AT THE SUNSET RADAR

J. L. Green, J. M. Warnock and W. L. Clark

NOAA, Aeronomy Laboratory
325 Broadway
Boulder, CO 80303

The Sunset radar is a VHF, pulsed Doppler radar located in a narrow canyon near the Sunset townsite 15 km west of Boulder, CO. This facility is operated by the Aeronomy Laboratory, ERL, NOAA, exclusively for meteorological research and the development of the MST and ST radar technique. A description of this facility can be found in the HANDBOOK FOR MAP, VOL. 9, 1983.

Recent results include a measurement of all three components of wind velocity for the Federal Aviation Administration. An example of this measurement is shown in Figure 1 (horizontal velocities) and Figure 2 (vertical velocities).

A comparison was made with a double star scintillometer located just 100 m from the center of the Sunset antenna. The scintillometer was constructed and operated by Jean Vernin, Universite of Nice, France. The importance of this comparison was that C_n^2 was simultaneously measured by two instruments that used radically different wavelengths of electromagnetic radiation and based on different physical principles. An example of this comparison is shown in Figure 3. A correction for the response of the VHF radar to water vapor is indicated on this figure by separate symbols labeled Hum Cor. Other comparisons were not as consistent in the upper troposphere as this example, but in every case there was close agreement in the lower stratosphere

PUBLICATIONS RELATED TO THE SUNSET RADAR, 1983-84

Gage, K. S., J. L. Green, B. B. Balsley, W. L. Ecklund, R. G. Strauch and K. J. Ruth (1983), Comparison of radar reflectivities between the Sunset and Platteville ST radars, Preprint Vol., 21st Cont. on Radar Meteorology, Sept. 19-23, Edmonton, Canada, 144-147.

Green, J. L., W. L. Clark, J. M. Warnock and K. J. Ruth (1983), Absolute calibration of MST/ST radars, Preprint Vol., 21st Conf. on Radar Meteorology Sept. 19-23, Edmonton, Canada, 144-147.

Green, J. L., K. S. Gage and B. B. Balsley (1983), A reexamination of the pulse length dependence of backscattered power observed by VHF radars at vertical incidence, Preprint Vol., 21st Conf. on Radar Meteorology, Sept. 19-23, Edmonton, Canada, 141-143.

Clark, W. L., J. L. Green and J. M. Warnock (1983), Estimating unbiased horizontal velocity components from ST/MST radar measurements; A case study, Handbook for MAP, Vol. 9, SCOSTEP Secretariat, Dep. Elec. Eng., Univ. Il, Urbana, 210-214.

Green, J. L. (1983), Characteristics of Sunset radar, Handbook for MAP, Vol. 9, SCOSTEP Secretariat, Dep. Elec. Eng., Univ. Il, Urbana, 320-324.

Green, J. L., J. Vernin, T. E. VanZandt, W. L. Clark and J. M. Warnock, A comparison of optical and radar measurements of C_n^2 height profiles, Preprint Vol., 22nd Conf. on Radar Meteorology, Zurich, Switzerland.

Clark, W. L. and J. L. Green (1984), Practicality of electronic beam steering for MST/ST radars, paper 6.2A, this volume.

Warnock, J. M. and J. Green (1984), Testing and optimizing MST coaxial collinear arrays, paper 6.4A, this volume.

Green, J. L. (1984), Sidelobe reduction for Barker codes, paper 7.1C, this volume.

Green, J. L. and F. S. Gage (1984), Comparison of tropopause detection by Platteville and Sunset radars and NWS Rawinsonde, paper 1.7A, this volume.

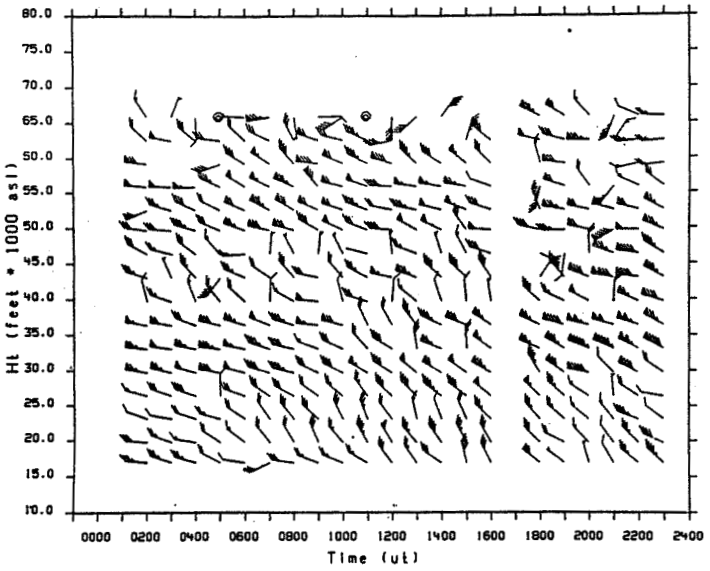

SUNSET RADAR WIND PROFILES

84/01/18 UT PL = 1049.3

Figure 1.

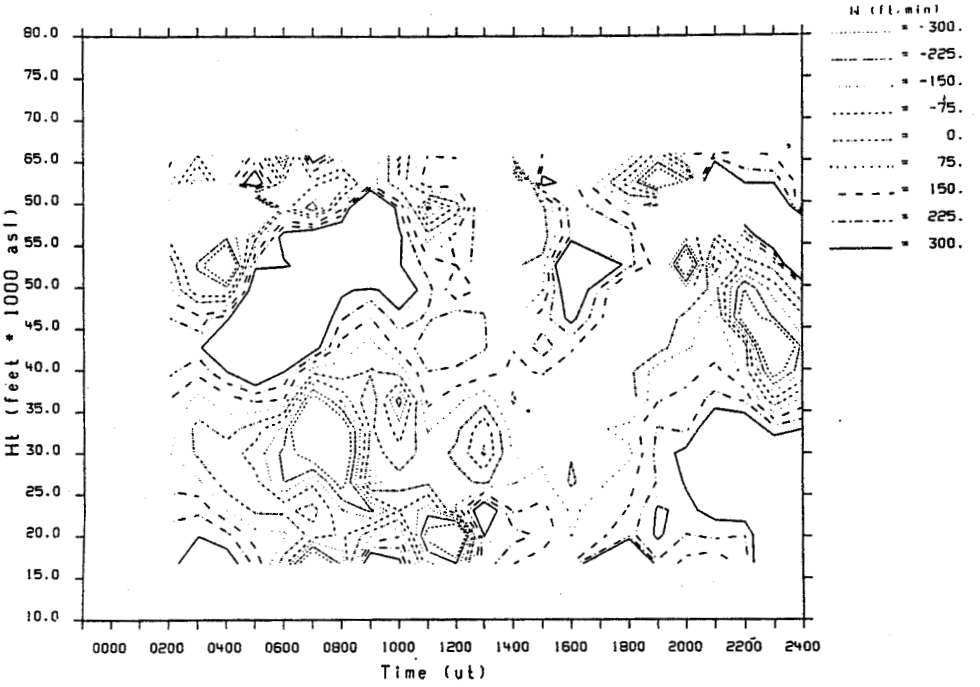

SUNSET RADAR - VERTICAL VELOCITY

84/01/18 UT PL = 1049.3

Figure 2.

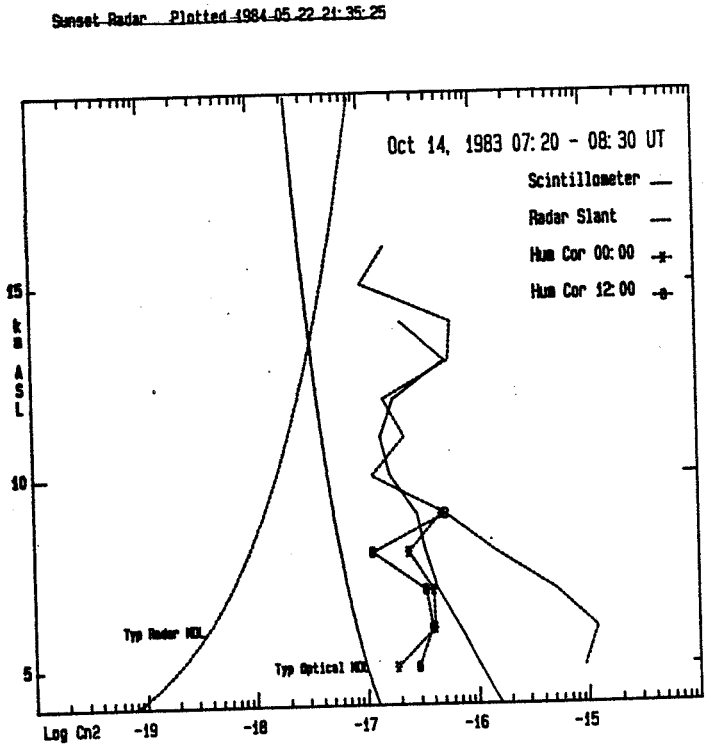

Figure 3.

9.4A THE BOOT LAKE MF IMAGING RADAR

G. W. Adams* and J. W. Brosnahan**

*Utah State University, Logan, Utah
**Tycho Technology, Inc., Boulder, CO

The Middle-Atmosphere Imaging Radar is located at the Boot Lake field site, 10 miles east of Brighton, Colorado. We operate at 2.66 MHz with a 50-kW peak pulse power in 30 microsecond pulses. Ten independent coaxial-collinear antennas (BALSLEY and ECKLUND, 1972) are used; five are parallel and run east-west, the other five are parallel and run north-south. Each antenna consists of eight half-wave dipoles. All ten antennas or a crossed pair may be used for transmission; all ten are sampled by pairs in rapid sequence for reception.

The system is now operating on a campaign basis as a Fourier interferometer by measuring the complex voltages on the ten antennas and Fourier transforming them independently. Multiple scatterers within a single range gate, now sorted by velocity, can be located individually by their phase angles. The transmitted signal cycles through four modes (N-S linear, right-hand circular, E-W linear, and left-hand circular).

The site is currently supported by the Los Alamos National Laboratory. Current investigations include studies of mesospheric and stratospheric scattering processes for the National Science Foundation, and of infrared structures and radar scattering at the mesopause for the Air Force Geophysical Laboratories.

The results presented at this conference (paper 2.5A, this volume) are the first from this experiment. Now that the software is developed, we will process several accumulated tapes of data. In addition, a measurement campaign is underway in cooperation with J. W. Meriwether and A. W. Peterson (University of New Mexico, infrared photometry and imaging). Much of our effort will focus on the analysis of these data. Our main interests in this work are the wave-like structure seen in OH(V > 1) emission, which have dimensions comparable to those observed in the radar images.

REFERENCE

Balsley, B. B. and W. L. Ecklund (1972), A portable coaxial collinear antenna, IEEE Trans. Antenna Propagat., AP-20, 513-516.

9.5A MENTOR -- ADDING AN OUTLYING RECEIVER TO AN ST RADAR FOR METEOR-WIND MEASUREMENTS

R. G. Roper

School of Geophysical Sciences
Georgia Institute of Technology
Atlanta, GA 30332

INTRODUCTION

Radar scattering from ionized meteor trails has been used for many years as a way to determine mesopause-level winds. Scattering occurs perpendicular to the trails, and since the ionizing efficiency of the incoming meteoroids depends on the cosine of the zenith angle of the radiant, echoes directly overhead are rare. ST radars normally sample within 15° of the vertical, and thus receive few meteor echoes. Even the higher powered MST radars are not good meteor radars, although Avery and coworkers have successfully retrieved meteor winds from the Poker Flat, Alaska MST radar by averaging long data intervals.

It has been suggested that a receiving station some distance from an ST radar could receive pulses being scattered from meteor trails, determine the particular ST beam in which the scattering occurred, measure the radial Doppler velocity, and thus determine the wind field. This concept has been named MENTOR (Meteor Echoes; No Transmitter, Only Receivers). This paper is a preliminary look at system requirements and possibilities.

There are a number of immediate questions to be answered, such as; If we receive a pulse scattered from an ST beam, how can we tell which beam it's from? How can we measure the Doppler velocity without access to the ST's oscillator? Can we also measure the altitude of scattering? Can we use this information to determine the wind field? In this paper we sketch one possible approach to these questions.

SITE LOCATION

Consider a typical ST radar with 3 beams; one vertical, one steered 15 degrees due North, and the third pointed 15 degrees East, as shown in Figure 1.

Many STs forego the vertical beam, and with it the ability to measure vertical winds. The MENTOR approach probably can't measure vertical winds anyhow, but viewing the third beam of an ST radar will increase the MENTOR rate by 50%. If all three ST beams use a common frequency, no additional hardware is required.

For the geometry shown in Figure 1, the best location for a MENTOR site is probably along a NE-SW line, so that the three ST beams can be seen from the MENTOR site as three separate beams with maximal separation. We will consider two MENTOR sites; one 100 km from the ST site and one 300 km from the ST site.

ST BEAM DETERMINATION

Consider a pair of MENTOR antennas defining a line normal to the MENTOR - ST axis. Let D be the spacing between the two antennas. Then the horizontal projection of the geometry is as shown in Figure 2. (This figure actually shows the horizontal projection for a MENTOR site located to the SW, rather than NE, of the ST site.) We want to choose D so that the spacing of the ST beams maps into, say, 90 degrees phase difference between this pair of MENTOR antennas.

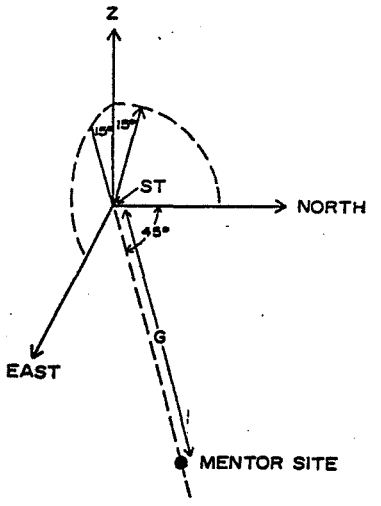

Figure 1. ST configuration and Mentor siting.

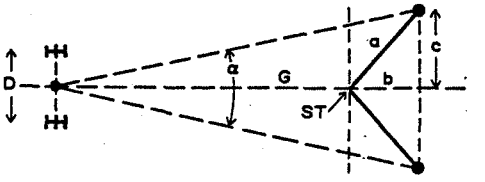

Figure 2. Beam-determination geometry.

Take the altitude region of interest to be 95 ± 15 km, and ignore effects due to the Earth's curvature. Assume an ST frequency of 50 MHz, so that λ = 6 meters. Let the ST-to-MENTOR distance be G (= either 100 or 300 km for the two strawman locations we have chosen.) Then we get

$$a = 95 \tan(15°) = 25.5 \text{ km}$$

$$b = c = a/\sqrt{2} = 18 \text{ km}$$

$$\alpha = 2 \tan^{-1}\left(\frac{c}{G+b}\right) = 17.3° \text{ (G = 100 km)}$$

$$= 6.5° \text{ (G = 300 km)}$$

$$\Delta\phi = \frac{2\pi D}{\lambda} \sin \alpha$$

Thus we find the desired spacing of the transverse pair of antennas to be 10.1 meters for the near site and 26.5 meters for the far site. With this spacing, the phase difference across the antennas will be 0 degrees if the received pulse originated in the STs vertical beam, +90 degrees if it came from the ST's North beam, and -90 degrees if it came from the ST's East beam. The range of altitudes (+/- 15 km) maps to a spread in the phase-difference values of +/- 25 degrees.

Some STs operate using different frequencies on different beams to improve beam separation. This makes beam identification easy, but means that two MENTOR channels are needed at each ST frequency for altitude determinations.

ALTITUDE DETERMINATION

For altitude determinations, we need an antenna (and receiver channel) to form a longitudinal pair with one of the first two antennas. Now consider the phase difference across this pair of antennas for an echo from thr vertical beam at an altitude z, as shown in Figure 3.

$$\Delta\phi = \frac{2\pi D}{\lambda} \sin\left(\tan^{-1}\left(\frac{Z}{G}\right)\right)$$

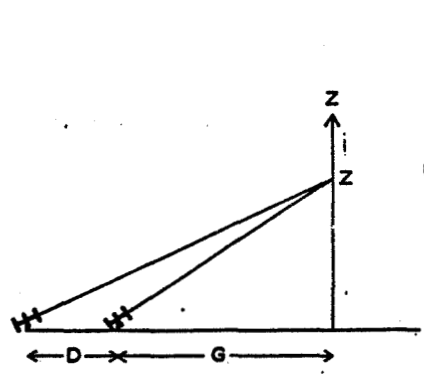

Figure 3. Altitude-determination geometry.

Thus we can choose the separation of the altitude-determining pair of antennas so that the expected range of altitudes (80-110 km) is mapped into phase differences from, say, 0 to 90 degrees. This will give an altitude resolution of 0.5 km with the anticipated MENTOR phase resolution of 1.5 degrees (slightly better or worse for the tipped beams, depending on which way they're tipped). Notice that no time-of-flight information about the pulse is needed for the altitude determination.

If it is necessary to operate the MENTOR receiver from a site such that two of the ST's beams are too closely coplanar (a projected separation of less than, say, 3 degrees), then the transverse pair of MENTOR antennas cannot discriminate between the overlapped pair of ST beams. However, if the MENTOR site is close enough to the ST site so that the regions lying between 80 and 110 km don't overlap in projection, then the longitudinal pair of MENTOR antennas can resolve the overlapped pair of ST beams. This is sketched in Figure 4. From the geometry shown,

$$x = 110 \tan (15°) = 29.5 \text{ km}$$

$$\theta_L = \tan^{-1}\left(\frac{110-80}{x}\right) = 45.5°$$

$$G_L = \frac{80}{\tan\theta_L} = 78.6 \text{ km}$$

The limiting ground distance is 78.6 km; beyond that, it would be necessary to add logic to MENTOR to determine the time-of-flight of the pulse from the ST, and use that information to determine which beam the pulse came from. We will not consider this case further.

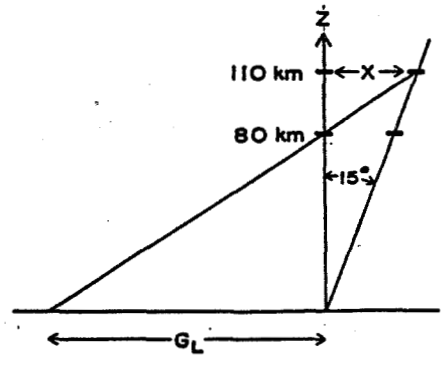

Figure 4. Limiting geometry for overlapped beams.

RADIAL DOPPLER FREQUENCY DETERMINATION

MENTOR will use, as do the ST radars, coherent detectors, so that both quadrature components of the signal (and thus amplitude and phase) are measured. This gives both the magnitude and the sign of the Doppler velocity. The problem of determining the radial Doppler velocity becomes the problem of determining $d\phi/dt$, with ϕ measured every pulse over a typical meteor-trail lifetime of 1/3 second. At the ST's pulse rate of 217 pulses/second, this will yield 72 measurements of the phase over the lifetime of the signal. If we take 150 m/sec to be a likely upper limit to the radial component of the mesospheric wind speed, then the maximum $d\phi/dt$ will be 83 degrees/pulse, which is extreme, but measureable.

REFERENCE OSCILLATOR STABILITY

The remote measurement of meteor echoes as envisaged here requires good oscillator stability for both the ST transmitter and the MENTOR receivers. Even good commercial oscillators have enough aging drift that frequent recalibration would be needed. However, commercial WWVB phase-lock receivers are available at moderate cost. Retrofitting existing STs appears to be no problem. The velocity error due to frequency instability will thus be < 1 m/sec.

WIND VELOCITY DETERMINATION

Operation of the MENTOR system will be similar to other meteor-wind radars; meteor echoes and their characterizations will be accumulated until all three beams are well sampled in as many altitude bins as possible, commensurate with the wave periods of interest. A three-dimensional wind vector can then be fitted to the data. An ST radar uses one beam that is carefully vertical, since a typical vertical velocity is overwhelmed by even a small component of the (usually) much-larger horizontal velocity. The geometry of the MENTOR system appears to preclude vertical velocity measurements, or at least to render them difficult. It is also clear that the error of the horizontal wind determination will increase as the MENTOR - ST spacing increases. The error goes as

$$\frac{\sqrt{G^2 + Z^2}}{Z}$$

so that the error will be 40% larger than the "ST equivalent" at the near site (G = 100 km) and x 3.2 larger at the far site (G = 300 km).

NETWORK POSSIBILITIES

There are two areas, Colorado and Pennsylvania, where networks of ST radars are operating (or soon will be). It is feasible to operate a single MENTOR receiving site to monitor meteor winds above a number of ST radars, provided they're all within, say, 500 km of a common site. (Received signal strength is the limiting parameter.) The Colorado network is shown in Figure 5. The ST radar sites now operating are shown as large solid circles; a likely MENTOR site is indicated. This site would give a maximum ground distance of 310 km to the furthest ST site. The differential cost for monitoring an additional ST radar, once the initial MENTOR system is installed, is expected to be small.

SUMMARY AND CONCLUSIONS

Meteor-wind measurements can be made by siting a three-channel receiver

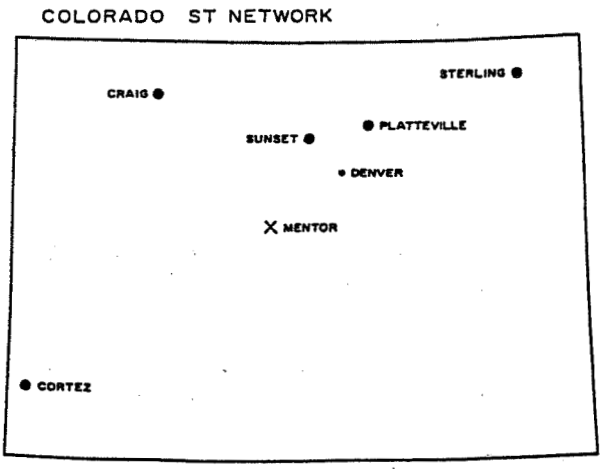

Figure 5.

some distance from an ST radar, then measuring Doppler velocities from meteor-trail scattering of the ST's pulses. Much of the gravity-wave activity in the mesosphere is thought to occur with horizontal wavelengths of 10 to 1000 km. A single MENTOR site in Colorado or Pennsylvania could add useful information over much of this range. We are working on data-rate calculations and system design.

D73

9.6A SUMMARY OF PROGRESS AT THE POKER FLAT OBSERVATORY IN ALASKA

B. B. Balsley

Aeronomy Laboratory
National Oceanic and Atmospheric Administration
Boulder, Colorado 80303

A description of the status of the Poker Flat MST Radar as of early 1983 is included in the 1983 MST Workshop Proceedings (HANDBOOK FOR MAP, VOL. 9). The following paragraphs bring that report up to date.

The Observatory continues to operate in a continuous data-taking mode, except for a three-week planned campaign experiment concurrent with the STATE rocket program during June 1983.

Constuction of the digital preprocessing system mentioned in the last status report is all but complete. This additional improvement should be operational by late summer.

The possibility of steering the array also mentioned in the last status report is being investigated. A project is underway to electronically steer the one-quarter "vertical" section of the array. Steering will be in finite steps within about ±5° of vertical. Successful testing of this modification may lead to eventually steering the entire array in this manner.

Data analysis of the data base (now more than four years in length continues with well over one dozen extramural scientific groups participating.

A partial list of this year's publications using Poker Flat results (i.e., only those publications coauthored by NOAA's Aeronomy Lab Scientists) is included below.

PUBLICATIONS RELATING TO THE POKER FLAT RADAR (SINCE MID 1983)

Balsley, B. B., W. L. Ecklund and K. S. Gage (1983), On the use of clear-air ST radars to observed winds, waves and turbulence in the troposphere and lower stratosphere, Preprint Vol., Fifth AMS Symposium on Meteorological Observations and Instrumentation, April 11-15, Toronto, Ontario, Canada, pp. 191-195.

Balsley, B. B. and A. C. Riddle, Monthly mean values of the mesospheric wind field over Poker Flat, Alaska, and a proposed polar circulation cell, submitted to J. Atmos. Sci.

Gage, K. S. and B. B. Balsley, MST radar studies of wind and turbulence in the middle atmosphere, submitted to J. Atmos. Terr. Sci.

Green, J. L., K. S. Gage and B. B. Balsley (1983), A reexamination of the pulse length dependence of backscattered power observed by VHF radars at vertical incidence, Preprint Vol., 21st Conf. on Radar Meteorology, Sept. 19-23, Edmonton, Canada, 141-143.

Luhmann, J. G., R. M. Johnston, M. J. Baron, B. B. Balsley and A. C. Riddle (1983), Observations of the high-latitude ionosphere with the Poker Flat MST radar: Analyses using simultaneous Chatanika radar measurements, J. Geophys. Res., 88, 10239-10245.

Nastrom, G. D. and K. S. Gage (1983), A brief climatology of vertical air motions from MST radar data at Poker Flat, Alaska, Preprint Vol., 21st Conf. on Radar Meteorology, Sept. 19-23, Edmonton, Canada, 135-140.

Riddle, A. C., K. S. Gage and B. B. Balsley (1983), An algorithm to monitor continuously the tropopause height using a VHF radar, Preprint Vol., 21st Conf. on Radar Meteorology, Sept. 19-23, Edmonton, Canada, 153-155.

9.7A URBANA RADAR SYSTEMS: POSSIBILITIES AND LIMITATIONS

O. Royrvik

Aeronomy Laboratory
Department of Electrical and Computer Engineering
University of Illinois
Urbana, IL 61801

INTRODUCTION

The Aeronomy Laboratory Field Station of the University of Illinois at Urbana contains three different radar systems capable of probing various regions of the atmosphere below about 100 km. These are an MST radar, a VHF meteor radar and an MF partial-reflection radar. All three radars can measure winds and waves in the ionospheric D region. The MST radar is, in addition, capable of probing the lower stratosphere and upper troposphere. A sodium (Na) LIDAR is also located at the Field Station and provides an additional way of studying winds and waves in the mesosphere by observing temporal variations in the sodium density profile.

The MST radar and the meteor radar use the same powerful 41-MHz transmitter, but separate antennas and receivers. No provisions have been made to split the power between the MST and the meteor-radar antennas, so the two systems cannot be run simultaneously. However, interlaced runs can be made in order to compare winds observed by the two systems.

The partial-reflection radar uses a separate transmitter, antennas and receiving system and can be run simultaneously with any of the other experiments.

Recently, data collection and analysis have been shifted from a single PDP-15 minicomputer to a series of 8-bit microcomputers allowing much flexibility on simultaneous runs. It should be noted, however, that the LIDAR cannot run simultaneously with the 41-MHz radars because of strong electromagnetic interference.

The three radars will be described separately, and the emphasis will be placed on recent upgrading of the different systems. A summary of the radar parameters is given in Table 1.

MST RADAR

The capabilities and limitations of the Urbana MST radar have been described by ROYRVIK and GOSS (1983) and only a short review of the general design will be given here. The radar operates at 40.92 MHz in a bistatic mode with an antenna array consisting of 1008 phased dipoles. The radar presently uses a pulse repetition frequency of 400 Hz. Coherent integration of the received signal is performed giving one coherent sample every 1/8 sec. Autocorrelation functions are calculated on line, and incoherently integrated for one minute and stored for later processing. Twenty range gates are sampled with a range separation of 1.5 km, spanning an altitude range of 30 km. By using two separate data-collecting microcomputers it is possible to obtaine data from both the stratosphere/troposphere and the mesosphere regions simultaneously.

The antenna is located on ground that slopes to the southeast by 1.5°, and the on-axis antenna beam direction is off-vertical by the same amount.

Line-of-sight Doppler velocities are calculated from the autocorrelation function, along with estimates of the signal correlation time and the scattered power. Because of the known relation between horizontal and vertical oscilla-

Table 1. Parameters of the Urbana radar systems.

	MST	Meteor Radar	Partial Reflection
Radar frequency	40.92 MHz	40.92 MHz	2.66 MHz
Peak power	1 (3) MW	1 (3) MW	50 kW
Pulse width	20 μs	20 μs	23 μs
Pulse repetition frequency	400 Hz	400 Hz	200 Hz
Receiver system bandwidth	100 kHz	100 kHz	40 kHz
Antenna			
transmitting	1008 dipoles	24 dipoles	60 dipoles
receiving	1008 dipoles	13 element yagis (4)	9 dipoles (4)

tions in internal gravity waves, we can interpret short- and long-period oscillations in the line-of-sight velocity as resulting from vertical and horizontal wind velocities, respectively (ROYRVIK and GOSS, 1983).

During the last year several upgrading projects of the MST radar have been undertaken; these will be described in the rest of this section.

(a) Transmitter

A continuous refurbishing and upgrading of the 41-MHz transmitter has resulted in a substantial improvement in peak transmitted power from a previous value of 0.7 MW to 3 MW at the present time.

A frequency-hopping technique is being investigated to increase the range resolution of the radar. A series of pulses will be transmitted, each pulse with a different radio frequency which is under the control of an Apple II microcomputer. By comparing phase differences between the different pulses in the sequence, it is possible to obtain an estimate of the location of the scatterer within the volume determined by the pulse length. This approach is similar in nature to the linear FM technique, but does not require the extensive hardware modifications necessary to implement a chirp-radar or a more conventional pulse-coding technique.

(b) Antenna

The transmit/receive antenna consists of six separately fed groups of dipoles (Figure 1). Because of the sloping ground and the orientation of the antenna, it is possible to phase the individual groups so that the antenna beam is pointing 2.5° off-vertical in the south and east directions. At the present this steering is done by manually inserting different lengths of cable in the feed lines to the different groups. This operation takes about 5 minutes and is impractical for day-to-day operation. Effort is underway, however, to implement an electromechanical switching arrangement so that the antenna beam can be switched in about one second between the four positions 2.5° to the east, 1.5° to the southeast, 2.5° to the south, and vertical. With the use of this

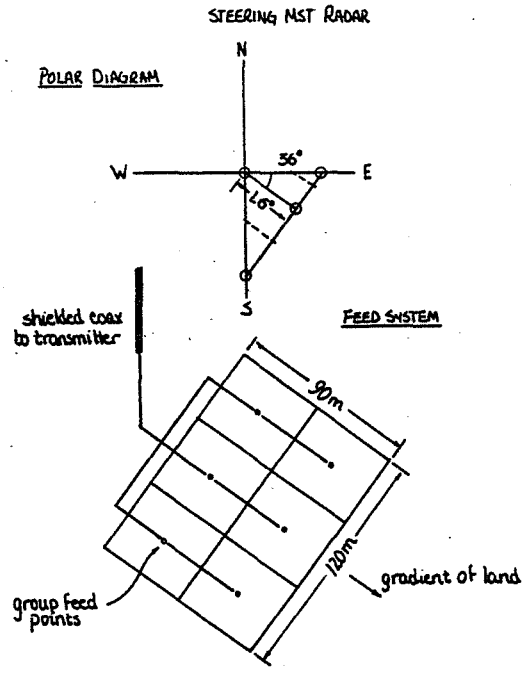

Figure 1. Schematic diagram of the MST radar antenna.

antenna beam-switching capability, it will be possible to obtain estimates of both the zonal and meridional long-period wind oscillations. The effective loss of power due to time sharing between the antenna positions will be more than made up for by the increase in transmitted power from 750 kW to 3 MW peak.

(c) Computer

Apple II microcomputers have replaced the PDP-15 as the major data-collection instrument. The two channels of the complex signal (sin, cos) is presently sampled on alternate transmitted pulses. A fast processor card is being incorporated into the microcomputer so that both channels of the complex signal can be sampled simultaneously. This improvement effectively increases the power of the radar by a factor of two.

A project is also underway to interface a fast coherent-integrator with 1 μs sample rate to the Apple allowing for better height resolution. With the transmitter capable of 2 μs pulses, the effective height resolution will be about 300 m.

(d) Transmit/Receive switch

A new T/R switch has been designed for the MST radar to allow probing of the troposphere at lower altitudes. Tests performed with one of the four gas tubes presently used, replaced by a PIN diode switch, have shown an improvement, indicating that with all four tubes replaced the radar will be able to obtain echoes as low as 4 km.

METEOR RADAR

The Urbana meteor radar (HESS and GELLER, 1976) is a very sensitive tool for studying winds and waves in the region of meteor precipitation from about 80- to 110-km altitude; it uses the powerful 41-MHz transmitter also used for the MST radar. Separate transmitting and receiving antennas are used. The transmitting antenna consists of two rows of center-fed full-wavelength dipoles. Each row contains twelve elements giving an elliptic antenna pattern. The elements are phased so that the antenna beam direction is at an elevation of 45° in the geographic north direction (HESS and GELLER, 1976). The effective east-west beam width in the meteor region is approximately 15°. The receiving antennas used in an interferometer mode to determine the azimuth and elevation angle of the reflected radar signal (Figure 2). Doppler shift, range, and phase differences between the receiving antennas give line-of-sight velocity as well as the location in space of the scattering meteor trail.

Meridional and zonal winds can be calculated from multiple meteor echoes if it is assumed that the wind is the same everywhere within the radar volumes which are limited by the antenna beam width and the effective altitude range gates. A recent test of the meteor-radar system has shown that the line-of-sight velocity and range can be measured with an accuracy of about 0.2 m/s and 500 k, respectively. However, the accuracy with which the elevation angle can be measured is quite poor, making the altitude calibration of the wind profile somewhat unreliable. Two independent phenomena appear to contribute to the problem. First, mutual coupling between the receiving antennas appears to distort the relationship between the measured phase difference and the direction of arrival of the meteor echo. Meteor echoes at greater distances from the radar appear to occur at lower altitudes. Second, due to unknown phase differences in the receiving channels, the absolute calibration of the wind profile is presently done by fitting the peak of the meteor number profile to 92 km. This procedure is suspect since it is known that the mean altitude of the ionized trail depends on the meteor velocity that changes as a function of season. For instance, the high-velocity Perseids meteors burn up before they reach an altitude of 100 km.

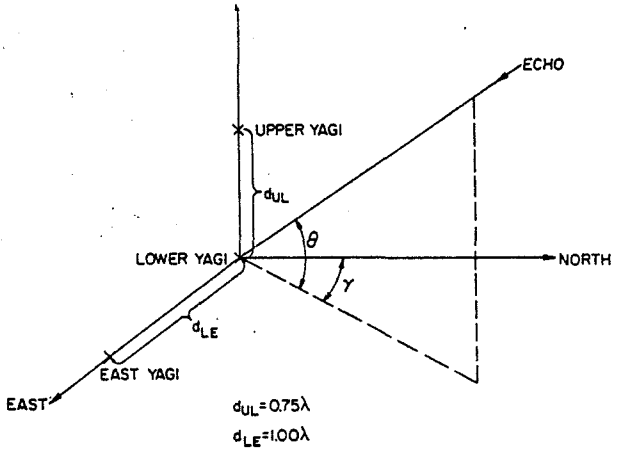

Figure 2. Meteor radar receiving antenna positioning.

An attempt is being made to upgrade the phase difference measurements and to find a simple way to calibrate accurately the altitude scale of the wind profile obtained. When this is accomplished the meteor radar will be a very powerful tool for studying horizontal winds in the meteor region. With an echo rate of several thousand meteor echoes per day, the wind can be resolved on temporal scales down to about one hour and with altitude resolution of 2 km or less.

PARTIAL-REFLECTION DRIFT RADAR

A 2.66-MHz partial-reflection radar is also located at the Aeronomy Laboratory Field Station (RUGGERIO and BOWHILL, 1982). It uses separate transmitting and receiving antennas. The transmitting antenna is a 300-m square array of crossed half-wave dipoles (Figure 3). Transmission of ordinary or extraordinary mode is under computer control and switching takes about one second. The receiving antenna is almost identical except that each quadrant of the antenna can be sampled separately to allow for spaced antenna drifts (SAD) measurements. Data collection and analysis for the SAD experiment is performed by a set of Apple II microcomputers. If differential-absorption measurements are to be performed the PDP-15 computer must be used. The system does not incorporate quadrature detection of the received signal so no vertical Doppler velocity can be measured. However, the four separate receiving channels provide redundancy in the horizontal velocity measurements.

Because of several restrictions on the SAD technique (ROYRVIK, 1983) the system suffers from limitations on the interpretation of the velocity. Although velocities are calculated every minute, it is believed that only oscillations with periods longer than one hour can be interpreted reliably as horizontal wind motions. Short-period vertical velocity variations contribute to large uncertainties in the horizontal velocity estimates. No improvement in the ability of this radar to measure horizontal wind is expected nor has been attempted. Nevertheless, the partial-reflection radar is the only operational system at Urbana presently capable of measuring zonal and meridional mesospheric wind profiles with reasonable vertical resolution.

REFERENCES

Hess, G. C. and M. A. Geller (1976), The Urbana meteor-radar system: Design, development, and first observations, Aeron. Rep. No. 74, Dep. Elec. Computer Eng., Univ. IL, Urbana-Champaign.

Royrvik, O. (1983), Spaced antenna drift at Jicamarca; Mesospheric measurements, Radio Sci., 18, 461-476.

Royrvik, O. and L. D. Goss (1983), The Urbana MST radar, capabilities and limitations, Handbook for MAP, Vol 9, 346-356, SCOSTEP Secretariat, Dep. Elec. Computer Eng., Univ. IL, Urbana-Champaign

Ruggerio, R. L. and S. A. Bowhill (1982), New advances in the partial-reflection-drifts experiment using microprocessors, Aeron. Rep. No. 106, Dep. Elec. Computer Eng., Univ. IL, Urbana-Champaign.

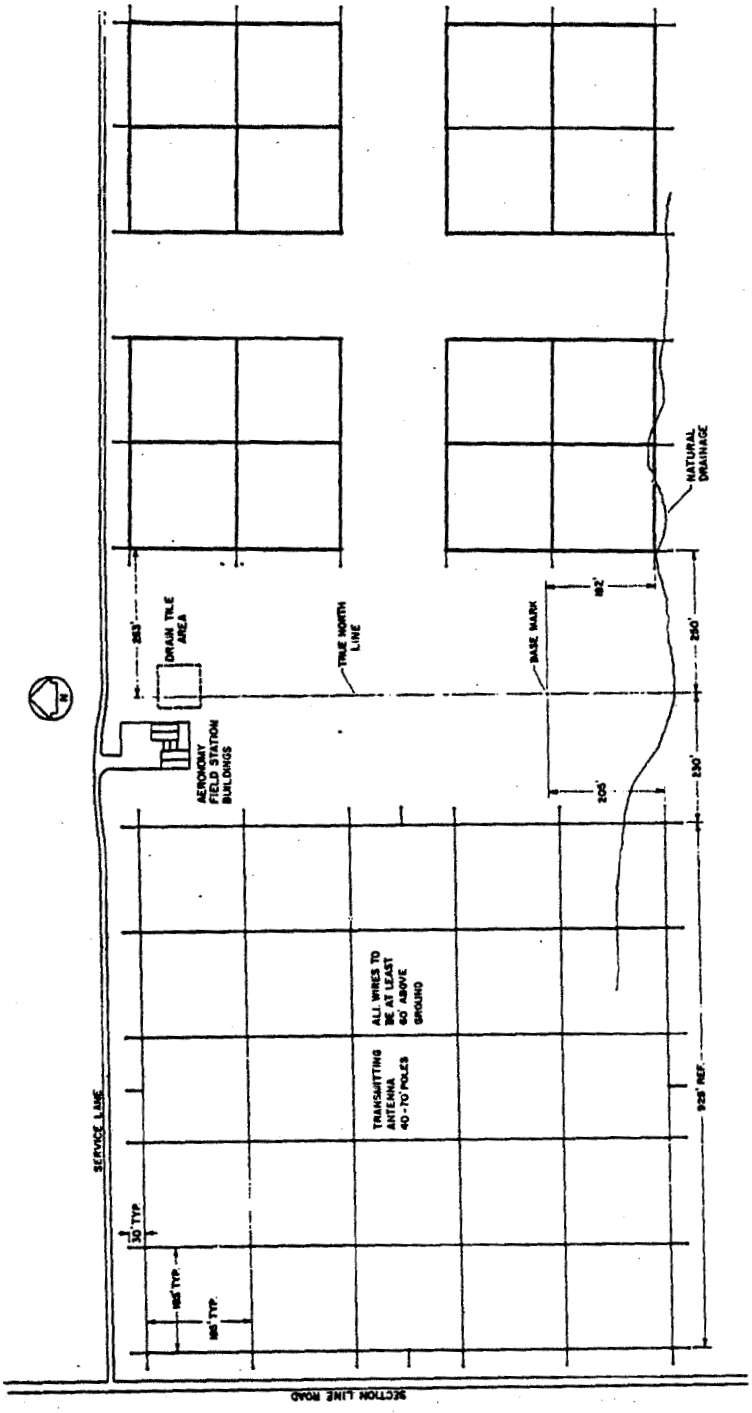

Figure 3. Schematic diagram of the MF partial-reflection radar antennas.

9.8A THE SONDRESTROM RADAR: PROGRESS AND PROPOSED UPGRADES FOR ST WORK

B. J. Watkins

Geophysical Institute
University of Alaska
Fairbanks, Alaska 99701

At the first Workshop on Technical Aspects of MST Radar, the capabilities and limitations of the Sondrestrom Radar for ST observations was presented (WATKINS, 1983). Therefore this paper will only summarize recent progress and proposed upgrades.

During the first year of operation (April 1983 to April 1984) there was only one ST experiment, mainly with the objective of evaluating the site and determining that the hardware and software were still operational after the radar's move from Alaska. The Sondrestrom site has about the same degree of ground clutter as the former Chatanika site and the data appear to be similar. The radar's operation continues to be managed by SRII with its primary use being incoherent-scatter observations of the ionosphere. The main radar parameters are summarized in Table 1.

The major limitations of the radar still exist, i.e. low average power, poor range resolution (750 m), and inadequate computer/signal processing hardware. The upgrades required to meet these deficiencies would jointly benefit the incoherent-scatter operations, therefore we are hopeful that the necessary improvements will be possible in the near future.

It is unlikely that the system could ever be operated in a continuous ST mode because of high operational costs and competition from other incoherent-scatter work. Currently there is a total of about 100 hours per month radar operation funded. Therefore any future ST experiments must be of the short campaign nature.

The radar is potentially unique because of its high operating frequency and fast fully steerable dish antenna. Although the high frequency limits the maximum attainable height to about 20 km, the time to acquire a spectrum is very short compared to a 50-MHz radar. For example, with the current maximum PRF, the time to acquire one record with no incoherent spectral averaging is 1/2 sec for a 128-point spectrum. This, coupled with the fast fully steerable disn antenna is an ideal system for studying spatial variations of turbulence structures, short-period gravity waves, etc.

Unfortunately these types of experiments have been severely compromised by the inadequate data processing system. It is not possible for the data processing to keep up with the data input in real time. Therefore a critical upgrade item is at least an array processor for enhancing the data acquisition system.

The second upgrade needed is to implement phase coding that will effectively increase the average transmitter power and therefore system sensitivity. At present the transmitter is operating at 0.13% duty cycle with 5 μs uncoded pulses. The maximum permissible transmitter duty cycle is 3%. Therefore the opportunity exists to either enhance the average power with phase coding and/or increase the resolution. So far we have not attempted to use pulses shorter that 5 μs because of weak signal returns. Although uncoded pulses longer than 5 μs do enhance the signal/noise ratio they have not been used because of the resulting loss in range resolution.

Table 1

Location	67°N 51°W
Frequency	1290 MHz
Peak Pulse Power*	3 MW
Max. Pulse Repetition Frequency*	250 Hz
Pulse Lengths*	5-10 μs
Max. Duty Cycle	3%
Antenna - Fully Steerable Dish	
Antenna Diameter	32 m
Antenna Gain	49.6 dB
Antenna Efficiency	52%
Polarization	Circular
System Temperature	100°K

*Typical values for ST observations

A third, but not as critical, need is for a higher transmitter maximum PRF, at present this is 250 Hz. The spectral folding frequency converted to an equivalent doppler velocity $\delta\mu$ is given by

$$\delta\mu = \text{PRF}\ \lambda/2$$

$$= 28.8 \text{ m/s} \qquad \text{for PRF} = 250 \text{ Hz}$$

$$\lambda = 0.23 \text{ m}$$

When the antenna is directed off-vertical in the azimuth of the wind direction the horizontal wind speed is often large enough ($\gtrsim$ 28 m/s) to produce aliassing. A maximum PRF of about 1000 Hz would be optimum.

REFERENCE

Watkins, B. J. (1983), Capabilities and limitations of the Sondrestrom radar for ST observations, Handbook for MAP, Vol. 9, SCOSTEP Secretariat, Dep. Elec. Eng., Univ. Il, Urbana, 375-380.

D76

9.9A PROGRESS AND PLANS FOR THE COLORADO WIND PROFILER NETWORK

R. G. Strauch

National Aeronautics and Space Administration/ERL/WPL
Boulder, CO 80303

Since January 1983, the Wave Propagation Laboratory (WPL) has placed four wind profiling radars in operation. These radars and the Platteville radar (originally developed by the Aeronomy Laboratory (AL) and jointly operated by AL and WPL for several years) form the Colorado Wind Profiler Network. These radars are described by STRAUCH et al. (1984a) and experiences with operation are summarized in another paper (STRAUCH et al., 1984b) in this workshop. Plans and improvements for the Colorado Wind Profilers are summarized below.

(a) VHF Radar at Platteville

Funds permitting, our plans to make the following improvements:

1. The 100 m x 100 m antenna arrays that are used to observe horizontal wind components are not nearly as efficient as the newer zenith-pointing antenna. The dipole elements of the older antennas have more loss, and the phasing of the array is not as accurate. We want to replace these antennas with new 100 m x 100 m collinear-coaxial dipole antennas. The ground must also be leveled; there is presently a 0.6-degree slope across the array.

2. The computer and data system will be replaced with the data systems used with the newer VHF radars. This will enable the radar to operate with the height resolution that is allowed by the bandwidth allocation (0.4 MHz), and it will improve sensitivity because the pulse repetition rate can be increased. The new data system also provides remote control of the radar and calculates hourly-averaged winds at the site.

With these two improvements, we expect the Platteville radar to be more sensitive than the other 6-m wavelength radars in the network because of the 6-dB greater antenna aperture. Comparison of winds measured by Platteville with those measured by the other VHF radars will allow an intelligent judgement as to the cost effectiveness of the additional expense of the larger antennas. In particular, we need to determine if the increased sensitivity radars suffer signal dropout.

3. Separate (Yagi) receiving antennas will be added to the zenith antenna to allow us to test the spaced antenna drift method of wind measurement.

(b) VHF Radars Near Sterling, Craig and Cortez

These radars have been operated for more than one year. There are a number of changes we would like to make on the basis of our experience.

1. These radars are operated with high pulse repetition rates so that echoes from the mesosphere will be range-aliased into the heights where we measure tropospheric winds. These echoes can be effectively eliminated by changing the phase of each transmitted pulse with a psuedo-random binary phase code; time-domain integration then will randomly sum the aliased signals. All the necessary hardware has been built into the radars, but software modifications are needed to implement the coding (STRAUCH, 1984).

2. We want to develop a simple method for using an aircraft to check the antenna pointing angles and the antenna sidelobes. We believe that most of the "unusual" data points we obtain can be explained by our antenna patterns and specular echoes observed through antenna sidelobes.

3. We want to decrease the minimum height that can be measured when we use a 3-μs pulse duration. The present minimum height is about 1.7 km AGL and is limited by the transmit/receive switch and associated transients; a new switch may be required.

4. Limited data recording on-site will be implemented to aid in investigations of the causes of invalid data points. The data recorder will be controlled remotely to record Doppler spectra during particular events.

5. The format of the data are transmitted hourly from the remote sites will be expanded to include estimates of spectral width. We will also transmit wind component data instead of speed and direction.

(c) UHF Radar at Stapleton Airport

The only component failures that have occurred on this 33-cm wavelength radar in more than one year of operation have been associated with the mechanical switches that select the antenna pointing direction. These switches are being replaced with switches rated for 10^6 operations.

The data processing used with this radar is identical to that used with the VHF radars. With VHF radars the dwell time required to obtain the time series input for spectral analysis is 5 to 6 s, so the 1 to 2 s needed to calculate power spectra in software is relatively unimportant. However, with the 33-cm radar the dwell time is only about 0.5 s so the calculation time significantly reduces the available averaging time. We are planning to add a hardware spectral processor to our data system to reduce this overhead time. The processor will be added to the hardware preprocessor that performs the time-domain integration.

(d) UHF Radar at Boulder

We are completing construction of a 74-cm wavelength radar at Boulder, CO. It will use the same generic receiver and data processing that are used on all the Colorado Network Radars. The antenna is a phased array of 100 Yagi elements (60 m^2) with two sequential pointing directions. The transmitter has 30-kW peak power, 1.2-kW average power. The radar will use 1-, 3-, and 9-μs pulse durations (the same as the UHF radar at Stapleton Airport). Testing is expected to start in the spring of 1984.

REFERENCES

Strauch, R. G. (1984), Elimination of range-aliased echoes in VHF radars, paper 7.1B, this volume.

Strauch, R. G., D. A. Merritt, K. P. Moran, K. B. Earnshaw and D. Van de Kamp (1984a), The Colorado wind-profiling network, J. Oceanic Atmos. Tech., in press.

Strauch, R. G., K. B. Earnshaw, D. A. Merritt, K. A. Moran and D. Van de Kamp (1984b), Performance of the Colorado Wind Profiler Network, paper 1.5A, this volume.

9.10A THE MU RADAR NOW PARTLY IN OPERATION

S. Kato*, T. Ogawa*, T. Tsuda*, T. Sato*, I. Kimura** and S. Fukao**

*Radio Atmospheric Science Center
Kyoto University

**Dept. Electrical Engineering, Kyoto University
Kyoto, Japan

ABSTRACT

The MU radar (middle- and upper-atmosphere radar) of RASC (Radio Atmospheric Science Center, Kyoto University) is now partly in operation, although the facility will be completed in 1985. The active array system of the radar makes it possible to steer the radar beam as fast as in each interpulse period. We expect various sophisticated experiments by the system. A preliminary observation was successful to elucidate atmospheric motions during Typhoon No. 5 which approached the radar site in August, 1983.

INTRODUCTION

The MU radar (middle- and upper-atmosphere radar) has been under construction since 1981 at Shigaraki (35°N, 136°E) northeast of Kyoto. Whilst the total system will be completed in 1985, the system is now, on a reduced scale, in operation for observations of the troposphere and lower stratosphere. In the present paper we shall first outline the MU radar system, which was improved from that originally designed in 1980 (FUKAO et al., 1980), and, later, present some results so far obtained.

SYSTEM OUTLINE

The MU radar under construction is a pulse-modulated monostatic Doppler radar with active antenna array working on the frequency of 46.5 MHz. The basic idea of the system design was discussed by FUKAO et al. (1980) and has remained very similar even after some later improvements; the bandwidth is now given as 1.65 MHz which allows us to have the 1 μs-wide pulse equivalent with 150 m height resolution. The basic parameters are listed in Table 1 where some parameters are changed from those on the original design in 1980. The block diagram of the system under construction is illustrated in Figure 1, where the number of the subgroup of antennas is now 25, increased from 15 in the original 1980 design. Figure 2 shows a recent photo of the MU radar system. The radar site is in hilly national forests and fairly well protected against radio noise interference.

The radar antenna system consists of 475 antennas of 3-subelement crossed Yagi arrayed in a circular area with diameter of, approximately, 100 m (Figure 2). The array is divided into 25 subgroups. Each subgroup consists of 19 elements which are on equilateral triangular grids in each hexagon. Exception is for the 6 subgroups, distributed along the circular periphery, for precise correction or the desirable antenna pattern. This basic triangular distribution with an antenna at each apex of the regular triangle of its side 0.7 λ long, where λ is the radar wavelength, is found to prevent grating lobes from appearing in the antenna beam steering not exceeding 40° from the zenith. Thus, under such beam steering, the side lobe level for elevation angle less than 20° is suppressed smaller than $\frac{1}{2}$40 dB to the main lobe. The circular array has an effective area of 8330 m^2 producing the main beam of 3.6° in width. When the radar beam is directed vertically, the sidelobe is symmetric about the main lobe, the first sidelobe being as low as -18 dB to the main lobe. The crossed Yagi can produce two linear (mutually orthogonal) polarizations and also

TABLE 1. Basic Parameters of the MU Radar

Location:	Shigaraki, Shiga, Japan (34.85°N, 135.10°E)
Frequency:	46.5 MHz
Antenna configuration:	circular array of 475 crossed Yagi antennas
Aperture:	8330 m^2 (103 m in diameter)
Beam width:	3.6°
Polarizations:	linear or circular
Beam directions:	0-30° zenith angle
Transmitter:	
Power amplifier:	475 solid-state amplifiers
Peak power:	1 MW
Average power:	50 kW (duty ratio 5%)
Bandwidth:	1.65 MHz max (pulse length: 1-512 μs variable)
Receiver:	
Bandwidth:	1.65 MHz Maximum
Dynamic range:	70 dB
IF:	5 MHz
A/D converter:	12 bit x 4 channels

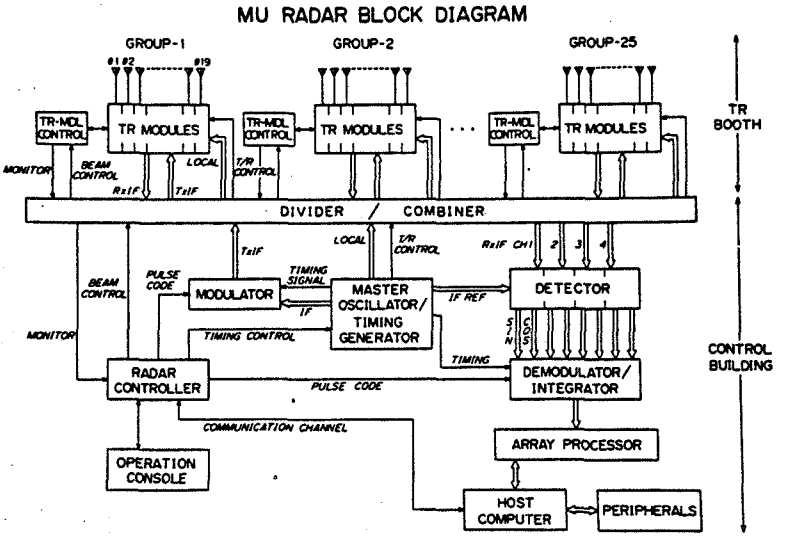

Figure 1. Block diagram of the MU radar system. The radar controller (HP 9835) basically controls all parts of the system, both in the observation rooms and the booths. Computer (Vax 11/750) is used for data analysis (as calculating various spectral moments) and data taking, and for controlling an array processor (MAP 300) which works for calculation of FFT and ACF, and incoherent integration: TR module control is done by 25 microprocessors; the received signal can be processed in four channels, each for sine and cosine detection; the basic signal generator uses a rubidium vapor frequency standard.

Figure 2. Bird's-eye view of the MU radar system. The antenna circular area is marked by white paint line, along and just outside of which the six booths are distributed; each subgroup of the antenna corresponds to each hexagon or each peripheral region as marked by white paint, solid or broken lines, the solid line showing the territorial boundary of each booth; the booth and the antenna element being connected by coaxial cables extended along the surface; the antenna level is lower by 15 m than the surrounding bank on which the iron net fence of 10 m high is built, mainly for avoiding the ground clutter due to the sidelobe radiation in low elevation angle; the two-storied building on the left on the bank is the control building, next door is the guest house; the white circle just beyond the fence on the right is a heliport.

left-handed and right-handed polarizations.

A remarkable feature of the MU radar system is that each antenna element is activated by its own solid-state power amplifier, its peak output power being 2.4 kW. Since the total number of the antenna is 475, the total peak output power becomes approximately 1 MW allowing for antenna loss. Each antenna has also its own receiver preamplifier. Both of the power amplifiers and preamplifiers are mounted on transmitter-receiver (TR) modules. Each of the six booths near the antenna accommodates the modules of four subgroups i.e. (19 x 4) modules except for one booth which accommodates the modules of five subgroups i.e. (19 x 5) modules. Conversion of the 5-MHz IF frequency to and from 46.5 MHz for transmission and reception, respectively, takes place in the modules, thereby simplifying the signal transfer between the booth and the control building which is on the bank overlooking the antenna.

The main advantage of this active array system is that the phase of signal transmitted from each antenna required for beam steering is electronically controlled at low power level. The beam can be tilted to as many locations as 1657 within 30° from the zenith for each interpulse period i.e., as short as

400 ms. Thus, it would contribute to observing the fast varying dynamic behavior of the atmosphere, e.g., gravity waves with fairly short periods.

Each independently operative antenna subgroup is expected to realize various sophisticated observations as that of the close-spaced antenna method (e.g. BRIGGS, 1980) which detects propagation of the interference pattern among the signals received at each antenna. Further technical details of the MU radar are shown elsewhere (SATO, 1980). They remain the same in many respects to the 1980 original design.

The system, now in operation, is on a reduced scale as having 3 subgroups (57 antennas) which are transmitting, approximately, the 120 kW pulse in the 10°-wide beam. This system is, however, complete in other parts as in controlling, modulation, demodulation and signal-processing, all of which are installed in the control building (Figure 1). We have already confirmed various operations of the present system to be in good shape. Figure 3 illustrates an observation in which the beam was steered azimuthally, keeping it in a constant zenith angle of 30° (VAD method (velocity azimuth display); BALSLEY and FARLEY, 1976). The beam was steered in every interpulse period. The result shows the well-behaved system (Figure 3(b)).

OBSERVATION OF THE TROPOSPHERE AND THE LOWER STRATOSPHERE DURING TYPHOON NO. 5 IN 1983

Since April, 1983, we have attempted to measure the wind velocity between 4 and 15 km in height on many occasions using the three subgroups which are now complete. Observation is limited only for periods with no construction work for additional parts of the antenna system.

Figure 4 gives observations in August, 1983 when typhoon No. 5 approached Japan as shown in Figure 5. The observation was done using the complementary code of 16 bits of the 1 μs subpulse, the pulse repetition frequency of 2.5 kHz; after 128-times coherent integration of the orthogonally detected signal, 128-point FFT was carried out and averaging was done on every ten of the result. Since the sampled levels were 64 in number between 4 km and 15 km from the ground, this implies an observation at each level approximately in every one minute. Note that in Figure 4 further averaging is done for approximately 30 minutes. The antenna beam was tilted by 30° from the zenith towards the east, so one can get zonal velocity by doubling the line-of-sight velocity, positive for the leaving and negative for the approaching given in Figure 4. Note that since the averaged vertical velocity is much smaller than the horizontal the positive and negative values correspond to eastward wind (westerly) and westward wind (easterly), respectively. It is clear that the wind observed by the MU radar is consistent with that observed by the conventional radiosonde at Wajima and Shionomisaki considering the location of the typhoon; the distance between Shionomisaki and Shigaraki is about 150 km and that between Shigaraki and Wajima 250 km. The wind velocity distribution with height was obtained from the spectral peak at each altitude and the distribution changed with the typhoon location relative to Shigaraki, as is expected. Figure 4(a), (b) and (c) give such features where one can readily find the wind field to have returned normal i.e., a westerly when the typhoon left. The overall wind distribution varying with time is shown in Figure 6.

Further analysis of the data for typhoon No. 5 has revealed existence of temporal fluctuation of the wind as shown in Figure 7 where the contour map (top) distinguishes between positive and negative velocity regions; the data used are those obtained approximately in every one min and filtered to pick up only shorter period components than 10 min. The period of fluctuation is around several min which corresponds to the Brunt-Vaisala frequency. Figure 7 (b) shows height profiles of wind averaged over 23 min.

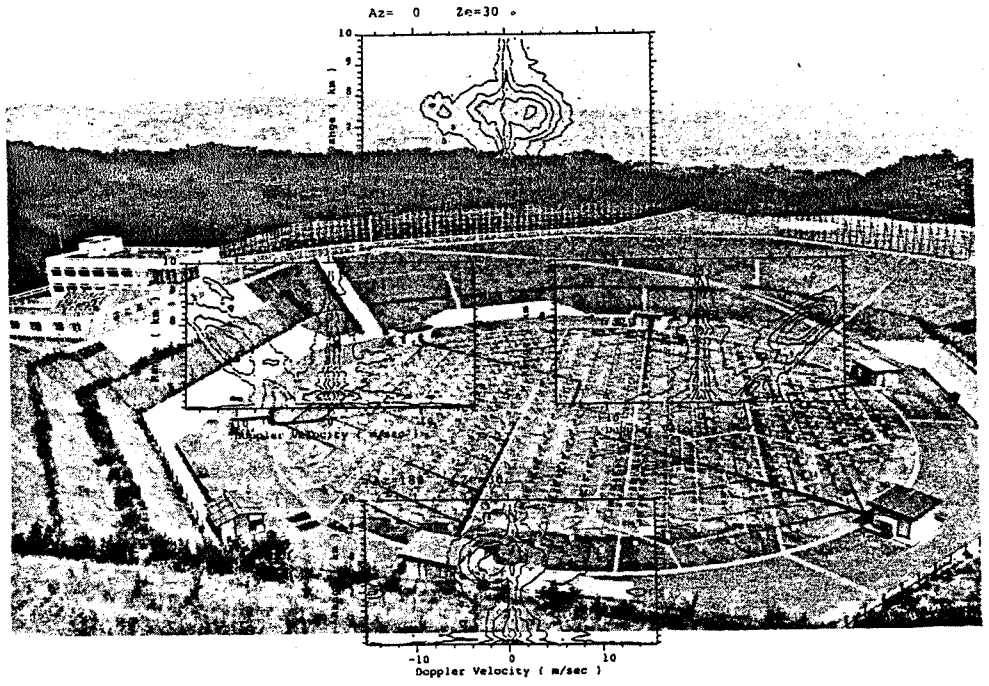

a)

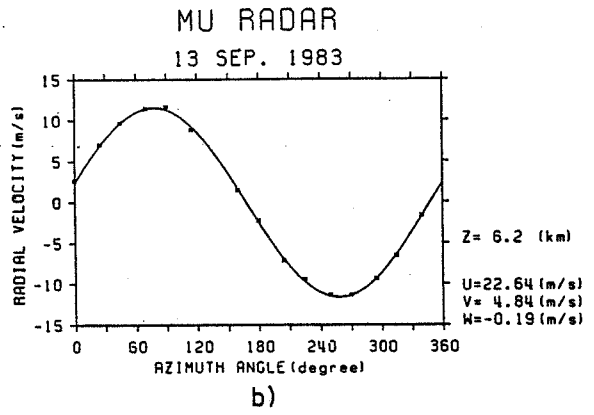

b)

Figure 3. VAD observation. (a) Height distribution of Doppler spectrum of line-of-sight velocity is shown as contour map; positive for leaving and negative for approaching. Each beam steering was completed during an interpulse period, i.e., 400 μs for the 16-bit complementary code with the 1 μs-wide subpulse; the antenna zenith angle was kept at 30° and the azimuth angle changed, from the north, by 25° or 20° in every other swinging, completing 16 observations in one round; two consecutive rounds are required to finish one observation set for a pair of complementary codes. After coherent integration of 16 sweeps, FFT was done by 128 points. The wind along the radar line-of-sight varies with the azimuth as is expected. The wind remained almost unchanged during the observation period as short as 0.1 s. (b) The line-of-sight (radial) velocity at 6.2 km varying with azimuth; the observed value (small cross) follows well the expected sinusoidal curve (solid curve) giving the wind velocity U (eastward) V (northward) W (upward) as shown.

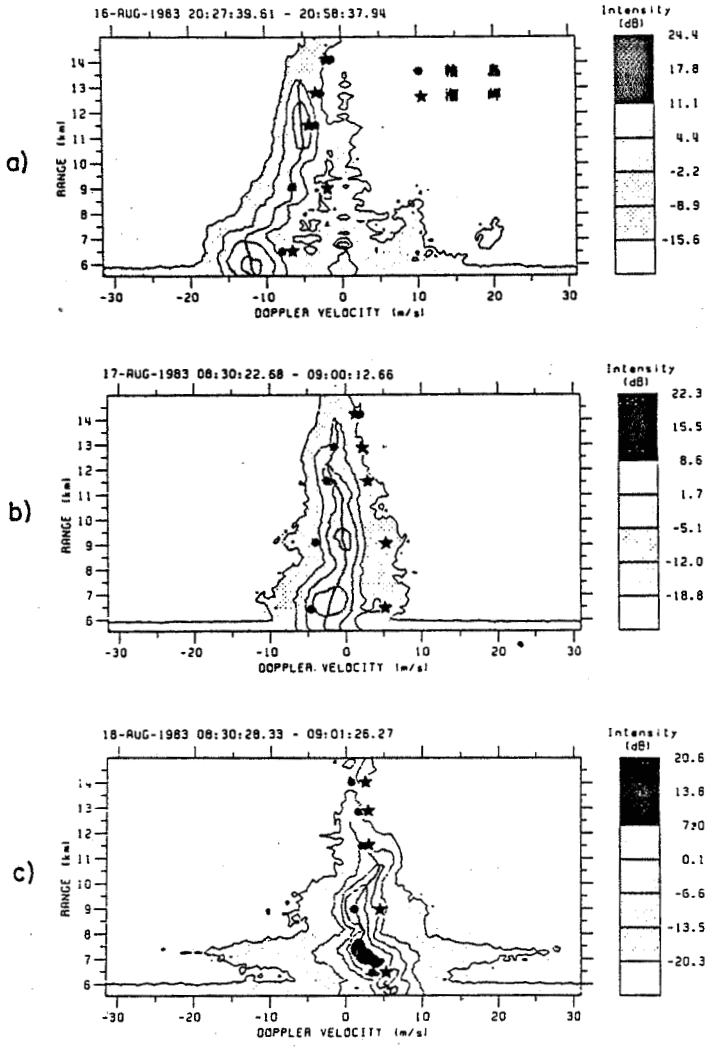

Figure 4. Doppler spectrum of the line-of-sight wind velocity for the 30° tilting from the zenith towards the east. Contour is subject to the dB scale as shown beside the main diagram. The dark asterisk denotes observation at Shionomisaki and the circle at Wajima. Average on 20h28m-20h59m, August 16 in (a), 08h30m-09h00m, August 17 (b), and 08h30m-09h01m, August 18 in (c).

DISCUSSION

The MU radar is now in operation only on a reduced scale. However, as is shown above, we have already been successful in the observation of a typhoon, detecting some of its temporal dynamical behavior varying with altitudes.

Figure 4(a) shows that typhoon No. 5 produced strong westward winds on the left-hand side to the direction of the typhoon course, its intensity attaining as strong as 20 m/s near Shigaraki, distance about 250 km, then decreasing with distance, yet still detectable at Wajima, distance about 520 km; the ob-

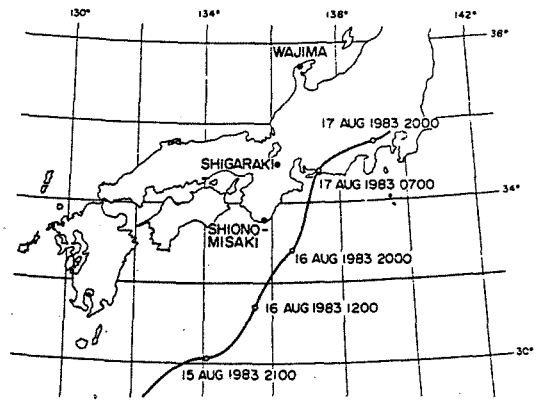

Figure 5. Path of typhoon No. 5. The thick solid line shows the typhoon path. The three dark small circles on the path are the location of the typhoon center on August 15 (21h), 16 (20h) and 17 (20h), respectively. The movement was as slow as 18 km/h.

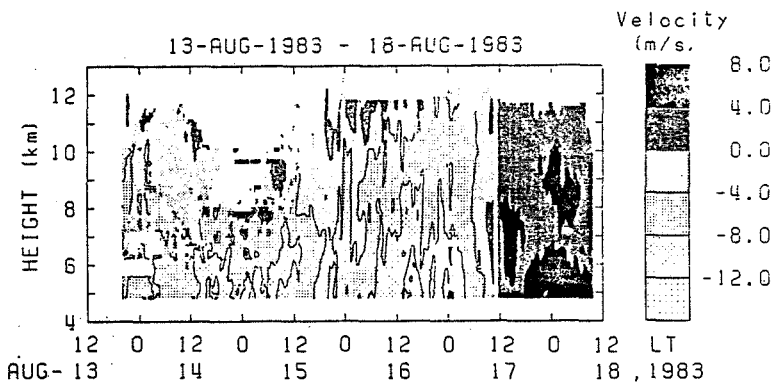

Figure 6. Line-of-sight (tilted towards the east by 30° from the zenith) wind distribution varying with time during typhoon passage. Contour is subject to the m/s shown in the column beside the diagram.

served wind, at this time, at Shionomisaki, was weaker partly because of its location which is more deflected to the west than that of Shigaraki relative to the typhoon. Such effects of the typhoon as reversing the weak westerly usually present, i.e., the eastward wind, were very remarkable at the lowest level observed though the effects became less with altitude. When typhoon No. 5 moved further northeastwards and reached the east side of Shigaraki (Figure 4(b)), the typhoon effect became very weak on the zonal wind as is expected; considering the anticlockwise spiral wind into the typhoon center, the typhoon then should produce mainly southward winds. This is much more remarkable at Shionomisaki (Figure 4(b)) where the typhoon effect had almost disappeared as understood from comparison of the observation there between Figure 4(b) and Figure 4(c). At this time Wajima is most disturbed by the typhoon. However, the general situation is unclear because of no data for meridional winds at all. Nevertheless, a dynamic behavior of typhoon No. 5 seems to be fairly clearly

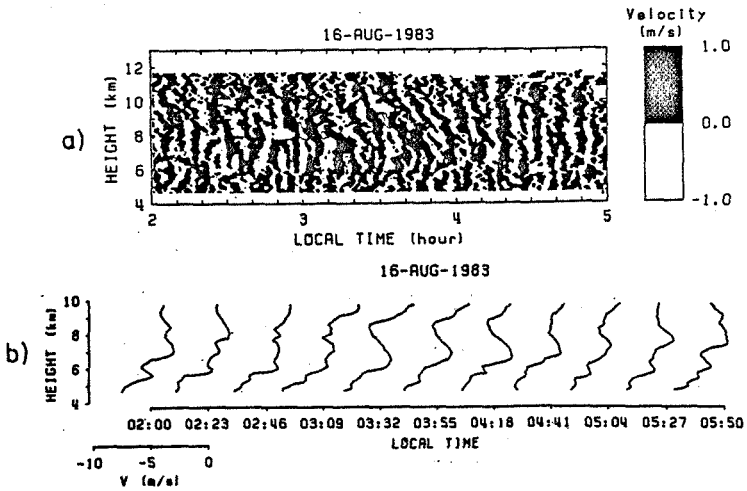

Figure 7. Fluctuating winds in typhoon No. 5. (a) Contour distinguishes between positive and negative velocity regions; averaged values for 1 min are used, removing longer period components than 10 min. (b) Height profiles at various times; averaged values for 23 min are used.

demonstrated by the MU radar as in Figure 4(a-c). The facility would play a role in typhoon monitoring for practical purposes.

Severe weather activity such as typhoons and intense tornadoes has been suspected to be a generator of gravity waves which propagate upwards to the ionosphere, producing small TIDs (traviling ionosphere disturbances) (e.g., TSUTSUI and OGAWA, 1973; HUANG et al., 1978). Some meteorological observations have also been carried out to detect gravity waves with periods long as a few hours in association with severe convective storms (UCCELLINI, 1975). The present observation as in Figure 7 would be novel in that it is a direct wind observation with good time resolution as one minute. The contour pattern in Figure 7(a) recurs with a period of 7 min. The updraft of the typhoon vortex is likely to stimulate the Brunt-Vaisala oscillation overshooting the equilibrium height for the heated air of the updraft (PIERCE and CORONITI, 1966). Looking at Figure 7(b), one can imagine phase progression both upward and downward from a height of 6 km at which the stimulation occurs. Figure 8 illustrates the

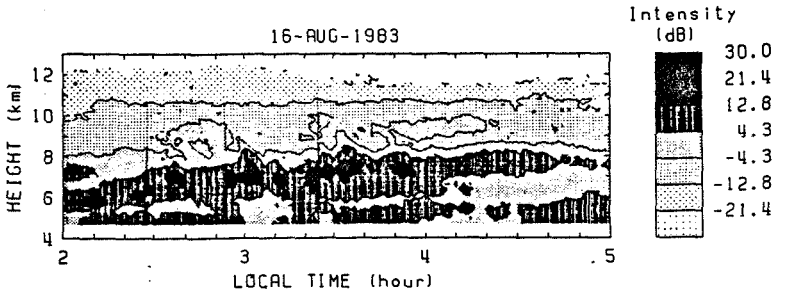

Figure 8. Echo power during typhoon No. 5. The contour corresponds to relative intensity in dB as given by the scale beside the diagram. Intense echo occurs around 7 km height first, descending with time.

signal power during the same period. The power is found intense corresponding to this height suggesting existence of a strongly disturbed situation. Since no data were available for meridional winds, the horizontal wind vector remained unknown. Note that the horizontal wind vector is an important quantity, because it is along the horizontal direction of the gravity-wave propagation. Another drawback of the present observation is the fact that, while the pulse width used in the observation is as short as 1 μs, the beam width of the present small system is as wide as 10°, yielding the height resolution as only 1 km, a resolution which is not enough to decide the phase variation very precisely in Figure 7(b). In atmosphere dynamics it seem important to study three-dimensional wind fluctuation during typhoons under better height-resolution.

ACKNOWLEDGMENT

The MU radar was designed under financial support by Science Grant for Unified Research B 1976 and 1977 and that A 1978 Ministry of Education, Science and Culture Japan. The present observation is also supported partially by Science Grant for Unified Research A 1983 and 1984 and that for General Research B 1982, 1983 and 1984. Partial support is further given to the present work by the Nissan Science Foundation 1981—1983. The present authors are indebted much to many graduate students, Department of Electrical Engineering and Electronics, Kyoto University. They have assisted the present authors in designing the radar system, developing the operation software and participating in the present observations. Cooperation of Dr. K. Wakasugi, Kyoto Institute of Technology, in solving all of these problems, is also much appreciated.

REFERENCES

Balsley, B. B. and D. T. Farley (1976), Auroral zone winds detected near the tropopause with Chatanika UHF Doppler radar, Geophys. Res. Lett., 3, 525-528.

Briggs, B. H. (1980), Radar observation of atmospheric winds and turbulence: a comparison of techniques, J. Atmos. Terr. Phys., 42, 823-833.

Fukao, S., S. Kato, T. Aso, M. Sasada and T. Makihira (1980), Middle of upper atmosphere radar (MUR) under design in Japan, Radio Sci., 15, 225-231.

Huang, R., J., T. Phan and R. E. Smith (1978), Observation of gravity waves during the extreme tornado outbreak of 3 April 1974, J. Atmos. Terr. Phys., 40, 831-843.

Pierce, A. D. and S. C. Coroniti (1966), A mechanism for the generation of acoustic-gravity wave during thunderstorm formation, Nature, 210, No. 5042, 1209-1210.

Sato, T. (1980), Coherent radar measurement of the middle atmosphere and design concepts of MU radar, Ph.D. Thesis, Inst. Electrical Engineering, Faculty of Engineering, Kyoto University.

Tsutsui, M. and T. Ogawa (1973), HF doppler observation of ionospheric effects due to typhoons, Rep. Ionos. Space Res. Japan, 27, 121-123.

Ucellini, L. W. (1975), A case study of apparent gravity wave imitation of severe connective storms, Mon. Wea. Rev., 103, 497-513.

D78

9.11A NETWORK ST RADAR AND RELATED MEASUREMENTS AT PENN STATE UNIVERSITY: A PROGRESS REPORT

D. W. Thomson, C. W. Fairall and R. M. Peters

Department of Meteorology
Pennsylvania State University
University Park, PA 16802

Mesoscale meteorological measurements, analysis and prediction are some of the principal areas of research in the Department of Meteorology at Penn State. For more than a decade those members of the faculty concerned with mesoscale analysis, numerical modeling and forecasting have been frustrated by the spatial and temporal inadequacy of conventional network observations for both research and operational applications. For more than five years the Department had sought the substantial financial resources required to deploy a network of VHF Doppler (ST) radars and millimeter wave radiometers for "operational" test and evaluation for wind and thermodynamic profiling, respectively. Construction of the ST radar network began in Fall of 1983 using funding provided by the Air Force Office of Scientific Research (through the DOD University Research Instrumentation Program) and the University.

For the foreseeable future the Penn State ST radar program will be focused entirely on applications rather than systems development research. Deployment of the systems now under construction would not have been possible without the outstanding cooperation provided by C. G. Little and R. Strauch and their colleagues at the Wave Propagation Laboratory, and also J. Brosnahan of Tycho Technology from whom we are buying all of the receivers, transmitters and antennas. With regard to other major systems components, we are assembling in-house from WPL documentation the Time-Domain-Integrators and Computer Interfaces and have purchased WPL software-compatible Data General Eclipse computers for each system.

The Penn State Network will consist first of two 6-m radars; one sited south of State College on Shantytown Road near McAlevys Fort and the second NW of Dubois, PA. The third radar, a "portable" 70-cm system, is to be initially sited SW of Johnstown, PA. The three radars thus form a mesoscale triangle with about 160-km legs (Figure 1). Specifications for the three systems are summarized in Table 1.

In anticipation of a staged turn-on of the three systems during the Summer and Fall of 1984, the nonconstruction-related efforts in the Department have focused on the software development necessary to allow essentially immediate use of network data. A 16-bit microcomputer has been programed to serve as the network controller, communications interface and, at least for real-time purposes, the operational display system. Insofar as possible we have in this task built upon our substantial accumulated experience in working with the processing and display of Doppler sodar system signals. Once the radar-derived wind and turbulence profiles are communicated to the various interconnected Departmental computers they become just one component of a comprehensive data base (Figure 2) which can be applied to a diverse set of ongoing basic and operational research programs.

The scientific applications for which specific program planning is in progress include:

(1) Intercomparison of wind and turbulence statistics derived from spatial (aircraft and radar network) and temporal (radar) sampling
(2) Meso-synoptic scale analysis and forecasting studies

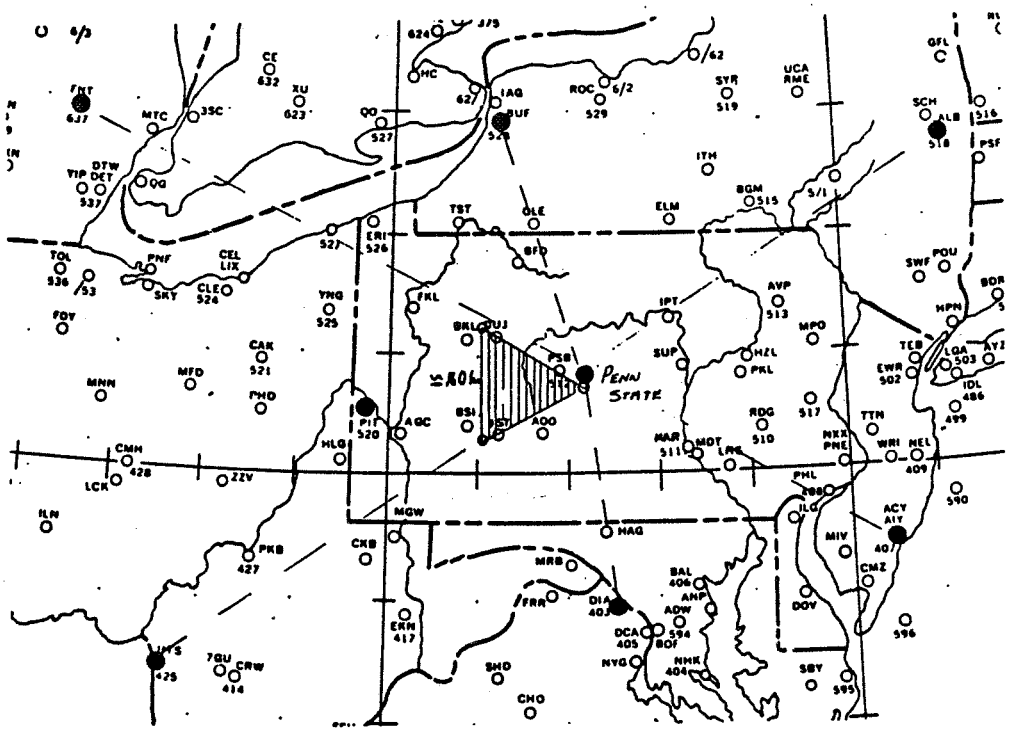

Figure 1. Mesospheric triangle of Penn State VHF (east and northwest) and UHF (southwest) radars. Station separations are approximately 160 km.

Table 1. Specifications for Penn State ST Radars

Item	Units 1 and 2	Unit 3
Type	Pulsed Doppler	Pulsed Doppler
Location	1: S of State College 2: NW of Dubois	SW of Johnstown
Frequency	1: 49.92 MHz 2: 49.80 MHz	405 MHz
Bandwidth	0.4 MHz	2%
Peak Power	30 kW	30 kW
Pulse Width	3.67, 9.67 μs	1, 4, 16 μs
Antenna:		
Type	Phased Array CoCo	64 7-element Yagis
Dimensions	50 m x 50 m	8 m x 8 m
Angle(s)	75° and 90°	75°
On Site Computer	Data General Eclipse	Data General Eclipse
On Site Processing at PW =	3.67 μs or 9.67 μs	1, 4, 16 μs
Time Domain Aver.	≈400 or ≈125	112, 70, 35
Spectral Aver.	8 or 16	16, 32, 64
Max. Radial Vel.	±15.7 m/s or ±19.6 m/s	18.25 m/s
Spectral Vel. Resol.	0.49 m/s or 31 m/s	0.29 m/s
Altitude Resolution	290 m or 870 m	100, 300, 800

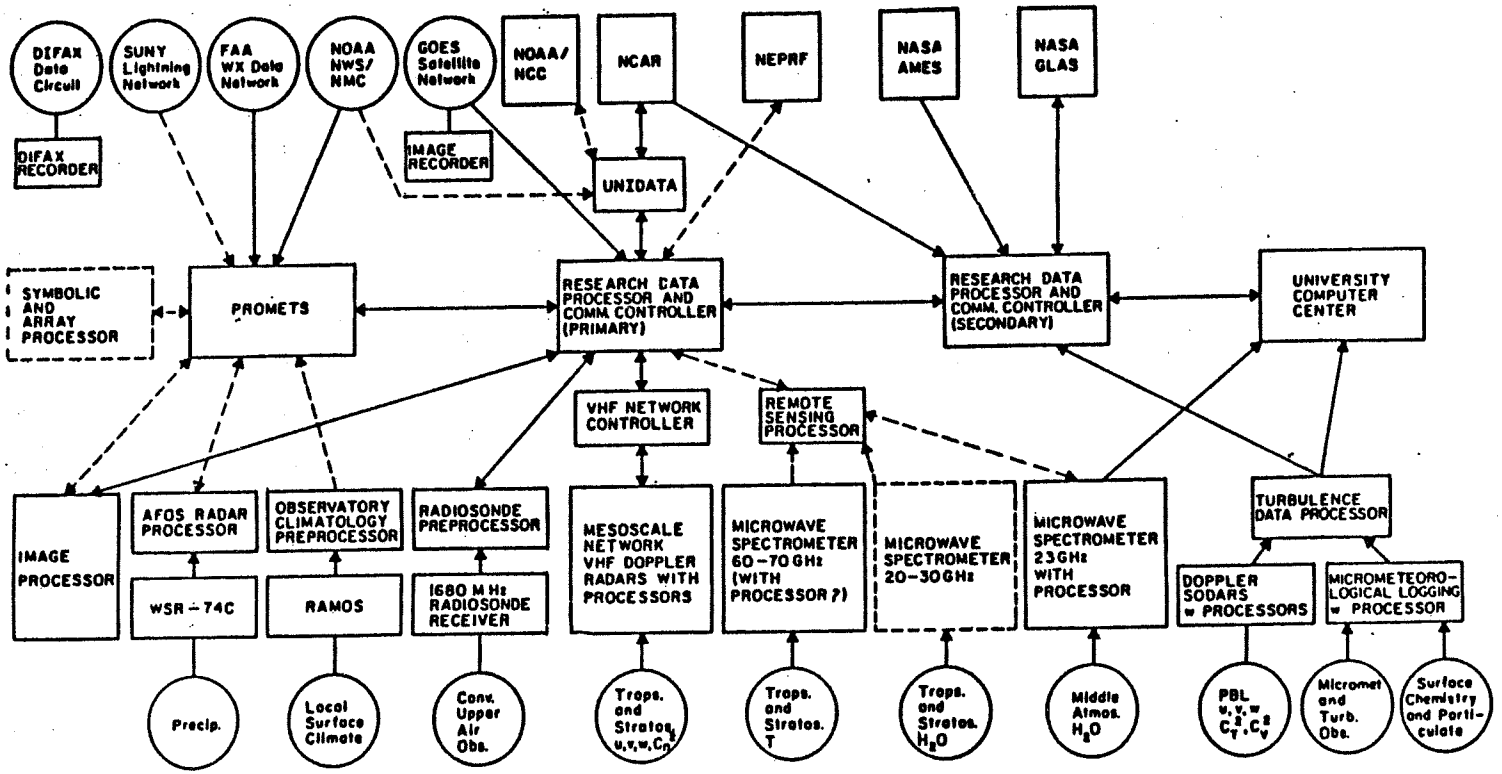

Figure 2. Schematic block diagram illustrating integration of measurement, data processing and modeling systems in the Department of Meteorology.

(3) Variability in mesoscale winds and turbulence
(4) Structure parameter statistics for NE U.S.
(5) Applications for assessment of acid deposition-related trajectories
(6) Assessment of forecast improvements for significant weather events in NE U.S.
(7) Deployment of a shipborne 400-MHz system (in conjunction with the network) for studies of coastal cyclogenesis.

Figures 3, 4, 5 and 6 are samples of the types of processed data available on a real-time basis in the University Weather Observatory with which the ST radar data will be combined and used. Figure 1 is a typical rawinsonde sounding from Pittsburgh as observed on 1 May 1984. For synoptic analysis purposes a cross section was evaluated along the computer-generated corridor illustrated in Figure 4. The vertical lines on the cross section (Figure 5) shown between stations 520 and 403 depict the scale between radars in the new ST network. Until thermodynamic profiler measurements are available we will use the existing PROMETS software to generate interpolated thermodynamic soundings from the analyzed cross sections. Such an interpolated sounding is shown in Figure 6.

Notification of funding for the 50-60 GHz millimeter wave radiometer for temperature sounding was recently received. The temperature profiler will be operated in conjunction with one of the VHF Doppler radars and a sodar. We hope it will be possible to use the radar and sodar measurements to infer probable inflection points (e.g. tropopause and PBL capping inversion) in the temperature profile and, thereby, improve the quality and resolution of the derived sounding. Development of software for this purpose is already in progress.

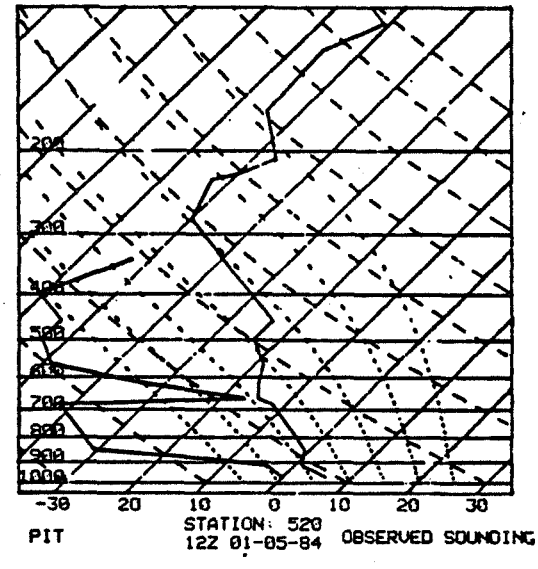

Figure 3. Example of plotted National Weather Service radiosonde sounding as plotted on PROMETS system from data received on the FAA network. Abscissa is temperature in °C and ordinate pressure is mb. The plotted data depict the temperature (R.H.) and dewpoint (L.H.) profiles.

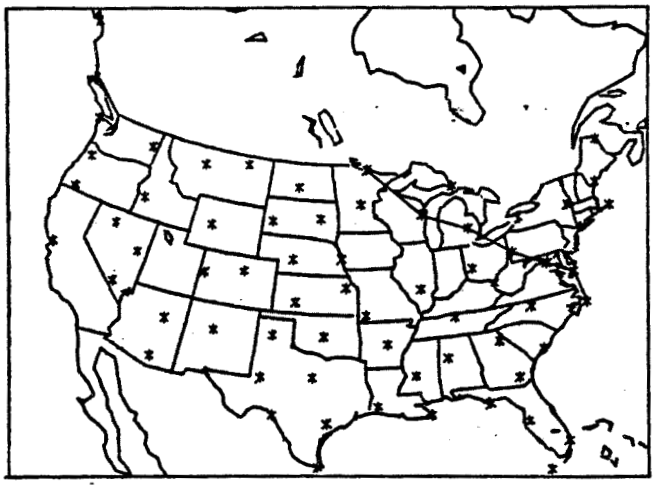

Figure 4. Corridor of upper air sounding stations chosen by the PROMETS software on the basis of specified end points. Station data subsequently processed by PROMETS to generate the isentropic cross section shown in Figure 5.

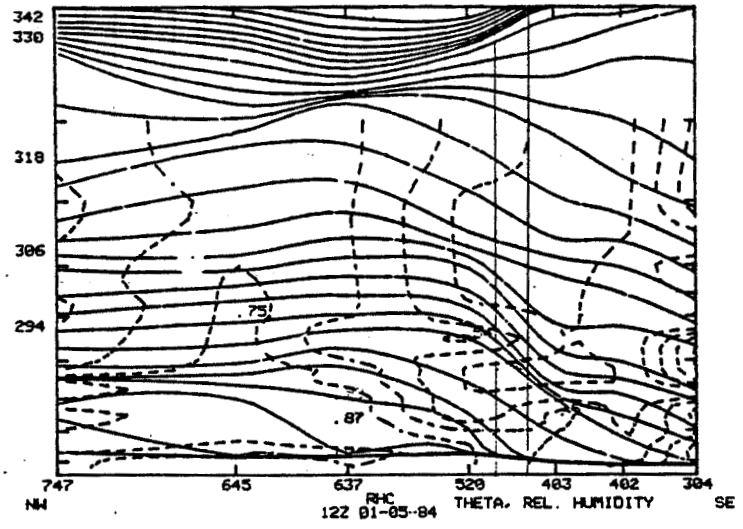

Figure 5. Isentropic cross section (solid sloping lines) including depiction of the smoothed relative humidity field (broken lines of varying orientation) along corridor shown in Figure 4. The two thin vertical solid lines depict the scale of the radar network in comparison to the spacing of the weather service radiosonde network.

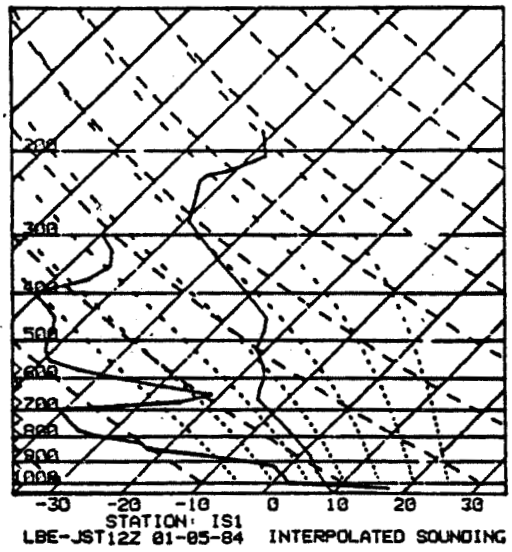

Figure 6. Example of vertical air and dewpoint temperature profiles generated from the preceeding isentropic cross section for a position corresponding to the placement of the new 400-MHz radar near Johnstown, Pennsylvania.

D-7

9.12A A NOTE ON THE PROPOSED UK VHF RADAR

A. J. Hall

Rutherform Appleton Laboratory
Chilton, Didcot, Oxon, UK

The proposal for the establishment of a VHF radar in the UK reported in MAP Handbook No. 9, 1983 pp 387-397 is still under active consideration, although for financial reasons no start has yet been made on an installation.

Several changes have been made to the scheme as described and these are listed below.

(1) The initial installation will be suitable for ST operation only using 64 antennas and 2 power modules.

(2) An existing site is being examined on the west coast of Wales, which because it is a former Loran ground station is provided with the buildings, power and communications facilities to enable a radar to be assembled much more quickly than a green field site would allow. Because the site is not within a mountain valley as originally intended, careful early attention will have to be given to the possible problems of local interference and sea-surface returns.

(3) Preliminary discussions with the UK licensing authorities suggest that a frequency of 47 MHz is more likely than 50 MHz.

(4) Minor changes are planned in the antenna array connection scheme of the 400-element MST array to allow more precise sidelobe suppression to be achieved in the receive mode.

It is hoped that an ST radar will be in operation before the end of 1985.

9.13A THE ADELAIDE VHF RADAR - CAPABILITIES AND FUTURE PLANS

B. H. Briggs, B. Candy, W. G. Elford, W. K. Hocking,
P. T. May and R. A. Vincent

Department of Physics
University of Adelaide
Adelaide 5000, Australia

The VHF radar at Buckland Park, South Australia (35°S, 138°E) commenced operation in January, 1984. The radar is located adjacent to the 2-MHz ionospheric radar. The routine method for measuring horizontal wind velocity is the spaced antenna technique (SA) while the Doppler technique is used to measure vertical velocities. It is possible to swing the transmitting beam in the east-west plane, allowing Doppler measurements of the EW wind component.

The basic system parameters (SA mode) are given in Table 1. The Yagi arrays are arranged in an equilateral triangle 40 m on a side with the spacing determined by theoretical calculations of the scale of the received pattern. The transmitting and receiving equipment is microprocessor controlled. The data are analyzed in real time on a minicomputer; the results are stored on magnetic tape for further off-line analysis.

Winds are measured in the lower stratosphere and regularly up to 9 km in the troposphere. Comparisons between the radar measurements and radiosonde measurements taken at Adelaide Airport (35 km to the south) show excellent agreement (e.g. Figure 1).

FUTURE DEVELOPMENTS

The transmitter power is to be increased to a mean of about 10 kW. Three approaches have been considered: a single high power transmitter to drive the whole array; individual solid-state modules driving each element; individual valve modules driving each element. The relative attributes of these approaches is given in Table 2. It is clear from this table that the solid-state approach is the most advantageous.

One module has been designed, built and tested. It appears that 500 watts peak output can be obtained from each output transistor without failure even when "operated into an infinite VSWR". With an optimum load connected, failure becomes significant above 700 watts peak. We have decided to operate the devices at the conservative output power of 500 watts per device. The gain at this level is about 12 dB and the efficiency is better than 50%. Table 3 summarizes the characteristics of each module.

Varicap diodes will be used to set the relative phase of the modules when swinging the beam. The phase of each module will be stabilised by phase feedback.

The receiver for the main array will consist of a low noise preamplifier connected to each antenna element followed by a phase shifter and combining network. Sixteen modules capable of delivering 5 kW mean power to the antenna are now under construction and will be in operation by late 1984. Construction of another sixteen modules is planned for 1985.

With the construction of a TR switch it is now possible to make Doppler wind studies using the large array for both transmission and reception. Beam pointing studies in the EW plane are now being started to find the optimum pointing and to study the effect of aspect sensitivity on the effective beam

Table 1. Buckland Park VHF radar, operating frequency 54.1 MHz

TRANSMITTING ARRAY	RECEIVING ARRAYS
32 coaxial colinear antennas Area: 8000 m^2 Half power beamwidth: 3.2° Ground plane spacing: 0.1λ	3 x square arrays of 16 five-element Yagis Area: ~250 m^2 Half power beamwidth: 18°
Transmitter	**Receiver**
Peak power: 40 kW Pulse length: 7 μsec PRF: 512 Hz Mean power: 200 W	3 separate dual-channel receivers with own digitizer and coherent averagers. Integration time: 0.25 or 0.50 s.

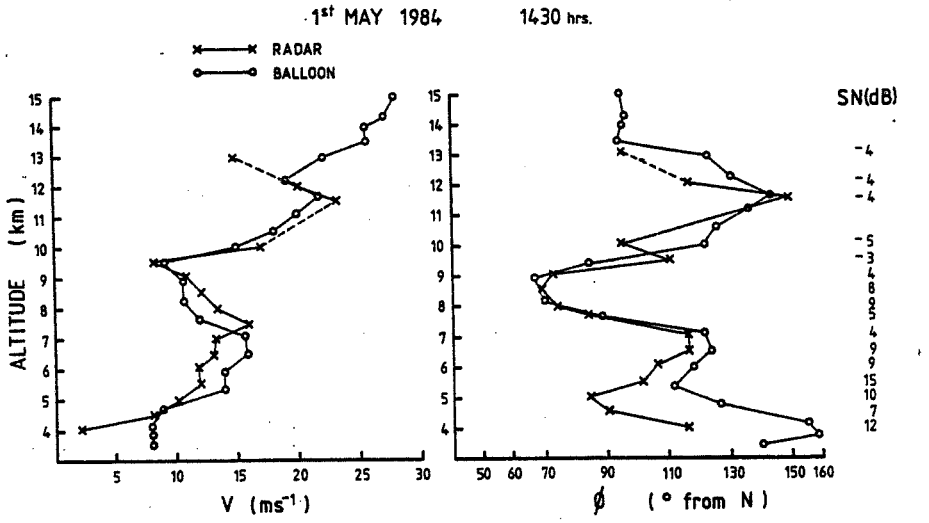

Figure 1

Table 2

		MULTIPLE MODULES	
	SINGLE UNIT	SOLID-STATE	VALUE
Flexibility in steering array	3 or at most 5 positions	continuous	continuous
Cost excluding labor	?*	$46,000* (32 units)	>$70,000*
Cooling	forced air	active water chiller	forced air
Availability of components	difficult	readily available	moderately difficult
Danger in terms of voltage	high	very low	high
Maintenance		lowest	highest

*Only the transistor version has been carefully priced.

Table 3

Peak power	3.5 kW
Maximum duty cycle	20%
Efficiency	50%
Supply voltage	50 V
Bandwidth	7 MHz
Physical dimensions	20 x 15 x 7 cm
Cost	<$1,000 (excl. labor and cooling)

point angle. Four angles are being used for the tests: 4, 7, 11 and 15°. Once the optimum angle has been chosen then a relay controlled system will be used to point the transmitter beam at complementary angles in the EW plane and thus measure the upward flux of zonal momentum, u'w', carried by gravity waves using the technique of VINCENT and REID (1983).

With the higher transmitter powers available at the end of 1984, simultaneous studies of scattering from the mesosphere at 3 frequencies, (54, 6 and 2 MHz) will be made in order to investigate the structure of the scattering irregularities.

Studies of irregularities in the lower atmosphere are also being undertaken using interferometric techniques. To improve the angular resolution a long baseline interferometer will be constructed by placing a small array composed of yagis at a distance of 500-1000 m from the center of the present system.

Finally, a lidar will be installed adjacent to the VHF radar in 1985. This will be used to measure neutral densities and temperatures throughout the middle atmosphere. The lidar system is now under construction and has been designed by Dr. F. Jacka of the Mawson Institute, University of Adelaide.

D21

9.14A THE PROUST RADAR

M. Petitdidier

C.R.P.E.
4 Avenue de Neptune
94107 Saint-Maur Cedex
France

RADAR CHARACTERISTICS

Location: Saint-Santin, France (incoherent facility)
Operating frequency: 935 MHz
Bistatic
Transmitting facility: incoherent scatter transmitter 150 kW
and antenna 2000 m2
Pulse width: 4 µs
PRF: 7.5 kHz
- Receiving facility: Parabolic antenna: 95 m2
Receiver noise: 300 K
- Coherent integration 64
- Digital recording
- FFT: 512 complex points - off line
- Profile - height resolution: 600 m
number of gates: 32

Results of the March 1984 campaign are shown in Figures 1 and 2

FUTURE

- pseudo complementary coding with 20 sub-codes; height resolution/30 m
December 1984: 32 gates of 30 m height resolution contiguous or not
- FFT in real time - TMS 320 - (1985)

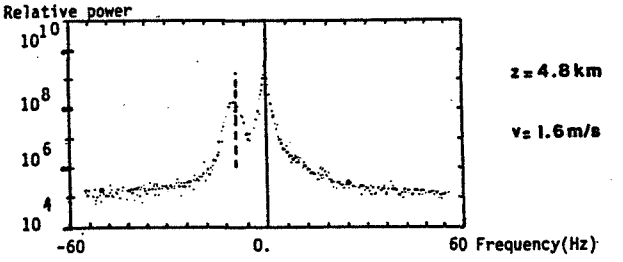

Figure 1. Example of a spectrum.

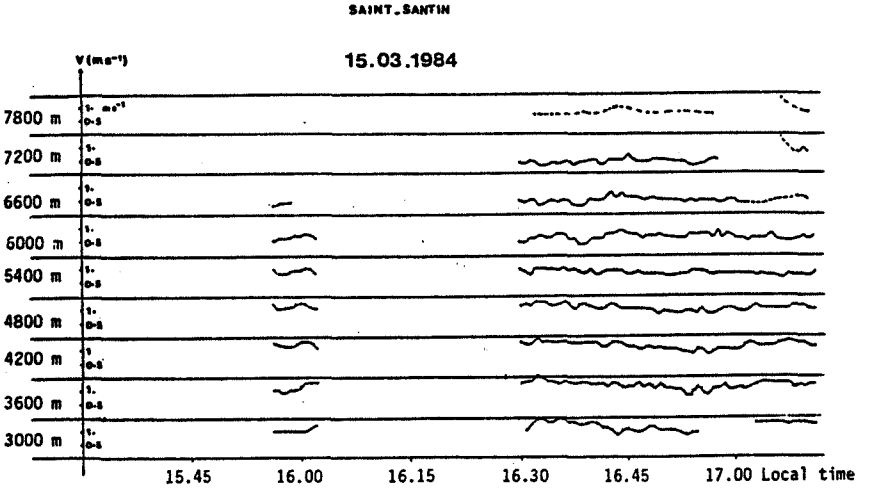

Figure 2. Wind as a function of time and altitude.

D82

9.15A MILLSTONE HILL RADAR: CAPABILITIES FOR S/T OBSERVATIONS

G. B. Loriot
Haystack Observatory
Westford, MA

During the past several years, the 440-MHz radar at Millstone Hill has been modified to detect coherent echoes from clear-air turbulence in the stratosphere/troposphere (S/T) over the altitude range 4-25 km. Two distinct modes of data acquisition have been developed, and data reduction programs have been completed for one of these modes. This mode (I-mode) transmits a 10 microsec (1.5 km) pulse on the fully steerable antenna. Typically, the antenna is set at a low elevation angle (e.g., 15 deg.) to reduce the altitude resolution to ~1 km., and power spectra are collected at some 40 range gates. The antenna may be scanned in azimuth to obtain the total wind vector, held fixed to monitor wave motion, or scanned in elevation to monitor the horizontal extent or the turbulent activity. This steerability gives Millstone a flexible system to focus on localized events, such as lee waves or convective storms. An additional advantage at low elevations is the relatively large Doppler shift of the signal, since the LOS velocity contains a large component of the horizontal velocity. This shift separates the turbulence signal sufficiently far from the ground clutter to allow the spectral moments to be readily inferred. Some 500 hours of S/T I-mode data have been reduced to geophysical parameters, and reside on a data base at Millstone Hill.

The second mode of operation (M-mode) is designed for a fine range resolution (less than 500 m) with adequate signal-to-noise ratio to probe into the stratosphere (up to 25 km altitude). A coded pulse waveform was developed, using complementary codes, and a range resolution of 300 m was achieved. In order to obtain a comparable altitude resolution with no degradation from beam width, the antenna was operated at high elevation angles (75-80 deg). Echoes were obtained up to 23-25 km altitude, but the Doppler shifts were very small, often overlapping the fading ground clutter. Programs to reduce these data will probably require parameterized fitting routines, but such routines have not yet been developed for M-mode data.

The S/T program at Millstone Hill has been dormant since December 1983. All processing programs have been retained, including an option in I-mode to operate with a 2 microsec pulse (with a large reduction in maximum range). The Millstone S/T radar is best suited for focused experiments using the steerable antenna at low elevation, with a 1.5 or 0.3 km range resolution. For example, the radar could monitor the dynamics of storms, or measure turbulence in lee waves above nearby mountains. Plans are being considered for such experiments in the future.

Some operating characteristics of Millstone Hill I-mode operations are given below. Values in parentheses will be valid as of 12/84, due to scheduled transmitter upgrades.

Transmitter frequency	440 MHz
RF pulse width	10 μs or 2 μs
Pulse repetition frequency	500 Hz (1000 Hz 12/84)
Peak power	1.4 MW (2.5 MW 12/84)
System temperature	150 K
Antenna	150 ft., fully steerable
Minimum range	10 km (3 km 12/84)
Maximum altitude (10 μs pulse)	21 km (25 km 12/84)

9.16A THE PONAPE ST RADAR

D. A. Carter, W. L. Ecklund and B. B. Balsley

Aeronomy Laboratory
National Oceanic and Atmospheric Administration
Boulder, Colorado 80303

In May, 1984, a 50-MHz ST radar was installed on the island of Ponape in the western equatorial Pacific (7°N, 158°E) by the Aeronomy Laboratory of NOAA. The radar consists of a 100 m x 100 m array with a single, vertically directed, beam and is initially transmitting 15 μsec (2.25 km) pulses. The radar is operating continuously, with Doppler spectra being recorded at approximately 1 1/2 minute intervals and sent to Boulder for later analysis. One of the principal goals of the radar is to measure vertical motions in the troposphere and lower stratosphere at a location which is within the intertropical convergence zone during part of the year. First results, during generally fair weather conditions, show detectable echoes up to about 21 km with the tropopause at 17-18 km. Once daily balloon soundings are available locally from a NOAA Weather Service Office on the island. It is planned that this radar will be joined in the coming year by two others with oblique as well as vertical beams on two yet-to-be-selected equatorial islands as part of the TOGA (Tropical Oceans Global Atmosphere) program.

9.17A MEASUREMENTS OF VERTICAL VELOCITY OVER FLAT TERRAIN BY ST RADAR AND OTHER RELATED USES OF THE RADAR DATA SET

J. L. Green and G. D. Nastrom*

Aeronomy Laboratory, NOAA, Boulder, CO 80303
*Control Data Corp., Minneapolis, MN 55440

INTRODUCTION

The first part of this communication points out the need to study vertical velocity measurements from an ST radar located on the plains, far from the mountains. As all presently available clear-air radars are located in or near mountains, the second part discusses the construction and operation of a VHF Doppler (ST) radar in the midwestern part of the United States to make meteorological measurements. While our primary interest is in measuring the synoptic-scale vertical velocities in the troposphere and lower stratosphere, it should be stressed, however, that the radar data set generated during the radar experiment would have many other valuable uses of interest to us and others some of whom are listed below. The required radar parameters, approximate costs, and recommended mode of operation are also detailed.

SCIENTIFIC ISSUE

The vertical velocity is the atmospheric variable most closely linked with weather, except perhaps moisture, yet it has been almost impossible to measure directly. Clear-air, or ST radars offer an opportunity to measure the vertical velocity directly and continuously. In a recent study we found that the time-average vertical motion over the Platteville, Colorado ST radar compared favorably with the computed synoptic-scale vertical velocity under certain synoptic conditions: when the prevailing winds were light or from the east and the synoptic-scale vertical velocity was over one or two centimeters per secone. When the prevailing winds were from the west, across the Rocky Mountains, the meteorological noise was too large to permit computing a mean vertical velocity with sufficiently small statistical uncertainty, or else standing lee waves made the radar site unrepresentative of the large geographical area of the synoptic-scale system. In either case, it is a meteorological signal-to-noise problem induced by the mountains. We have found a similar situation in the ALPEX data from Southern France, i.e., when the winds were off the sea the measured and computed vertical velocities agreed favorably but when the winds were across the mountains the agreement was poor or uncertain. Thus, we can conclude that at ST radar stations near mountains the synoptic-scale vertical velocity can be measured only under restricted conditions. These statistics strongly suggest that it may be possible to measure the large-scale vertical velocity under general conditions at a radar site located in the plains. This question should be addressed by using radar data from a site on the plains. The only MST radar located in the central plains at this time is at the University of Illinois; it does not measure the vertical velocity and according to Prof. S. A. Bowhill, it could not easily be adapted for that purpose.

Thus we propose installing an ST radar at a site in the central plains, and operating continuously for at least a year, taking measurements of the vertical velocity in the troposphere and lower stratosphere, and comparing the radar w's with computed values and with proxy indicators of the large-scale vertical motion such as weather-radar echoes and satellite pictures. We expect these "Flatlands" data would be of interest for other purposes as well, both meteorological and radar engineering, and we would, of course, make it available to other scientists. If the ability to measure the synoptic-scale vertical velocity can be demonstrated, this technique should impact a wide meteorological community. For example, research programs such as the upcoming

STORM project may be enhanced by adding vertical velocity measurements to their data base.

This radar could be constructed to point just vertically or be made to point its antenna beam sequentially to the vertical and four oblique directions. A practical data rate is one complete sequence of antenna directions in 500 s. This technique has already been tested at the Sunset radar; it offers the advantage of horizontal wind measurement to aid interpretation and provides, by the continuity equation, a kinematic check on the vertically pointed beam's measurements. This capability would permit us to resolve any lingering questions regarding the interpretation of the vertical velocity measurements from a vertically directed radar beam. For example, a primary reflecting mechanism for the vertical beam is specular reflections from specular layers. If the stable layers are moving vertically at a rate different from the air velocity, say at some phase velocity, the radar could give misleading results. By using the steering capability we can address this and any other issues of interpretation. Additionally, the slant antenna beam reflectivity would provide a measure of the intensity of turbulence versus altitude (the variable C_n^2). Studies of the specular reflection phenomenon and tropopause detection would be enhanced by the comparison of the vertical beam with the off-vertical beams. Spectra from the time series of the slant as well as the vertical velocity measurements are of interest. The use of the u' w' from the various beams would allow the computation of the vertical momentum flux due to gravity waves.

The antenna configuration and design required for accurate vertical velocities will give this radar a useful mesospheric capability and will frequently obtain echoes in the 65-85 km altitude region. Recording this additional data will add only about 2 K/yr to the cost of the operation.

THE EXPERIMENT

(a) Site Selection

Since we already have data in or near mountains, the site should be at the other orographic extreme -- smooth terrain. Midwestern states, especially Indiana and Illinois, are flat and relatively far from mountains. We have already contacted the Base Commanders at Grissom Air Force Base, IN, Whiteman Air Force Base, MO, and Chanute Air Force Base, IL, and find that they have space available and technicians (who would change tapes and check dials) on duty even during holiday periods. Purdue University, Lafayette, IN, has space available and has expressed interest in a cooperative experiment. We have arranged to personally inspect these and perhaps other prospective sites in late May of this year.

(b) Frequency

Although a frequency allocation must be obtained when the site is selected, a frequency near 49 MHz is likely (wavelength = 5 m). We have had experience with the proposed measurement in this frequency band.

(c) Equipment

A phased dipole antenna would be purchased or built at the Aeronomy Laboratory. A 100-kW transmitter and the necessary data-processing equipment would be purchased. The individual components would be checked out at the Sunset Radar in combination with an existing radar before shipment and assembly at the new radar site. It should be noted that the checkout of the new radar at Sunset would provide a unique comparison of operation at 7.4 m and 6 m wavelengths.

The multiposition antenna configuration would require a second antenna colocated with the first but at a right angle to it. Steering would be by remote controlled phase shifters developed for use at the Sunset Radar.

(d) Operation

The proposed "Flatland" radar would operate continuously at a range resolution of 1 km with a minimum of interruption. If the steerable option is implemented with its wide range of experimental possibilities, the mode of operation would be optimized for the vertical velocity measurement. It is proposed that this mode of operation be changed infrequently, if at all, during the first year of operation. As it turns out, this is also the optimum measurement technique for most of the additional scientific uses of data listed above, since they require a consistent data set of long duration.

(e) On-Line Procesing and Data Collection

A variety of methods are available: One mode is to hire a technician to change the tapes at the radar site (estimated at $30 K per year) or asking an Air Force Base to assign someone to do it. The mode of collection that we favor is to bring the radar output back to Boulder, CO, by a leased telephone line. As shown this would cost about $15,000 per year and would allow experienced people at the Aeronomy Laboratory to monitor the quality of the data. The cost of changing tapes would of course be eliminated. In principle, telephone access could be provided for those experimenters requiring real-time data.

CHARACTERISTICS OF "FLATLAND" RADAR

Location	Somewhere in Missouri, Illinois or Indiana
Wavelength	probably 6 m
Antenna	
Type	Two colocated arrays of coaxial-colinear dipoles
Feed	Tapered to reduce sidelobes
Size	50 - 100 m square
Steerability	Five preset positions
Transmitter	Vert, 15° (E, W, N, S)
Peak power	100 kW
Average power	3 - 5 kW
Range resolution	1 km (will have capabilities for 150 m - 2.4 km)
Operation	Fixed mode (continuously sequenced through 5 antenna positions)

AUTHOR INDEX

G. W. Adams, Utah State University, Logan, UT
S. K. Avery, CIRES, Boulder, CO
S. A. Bowhill, University of Illinois, Urbana, IL
J. Brosnahan, TYCHO Technology Inc., Boulder, CO
D. A. Carter, NOAA, Boulder, CO
H-C. Chang, Stanford University, Stanford, CA
J. K. Chao, National Central University, Taiwan, ROC
W. L. Clark, NOAA, Boulder, CO
C. R. Cornish, Cornell University, Ithaca, NY
T. S. Cress, Bolling AFB, DC
R. Davis, University of Illinois, Urbana, IL
E. M. Dewan, Air Force Geophysics Lab, Hanscom AFB, MA
C. W. Fairall, Pennsylvania State University, University Park, PA
D. T. Farley, Cornell University, Ithaca, NY
D. C. Fritts, University of Alaska, Fairbanks, AK
K. S. Gage, NOAA, Boulder, CO
M. A. Geller, Goddard Space Flight Center, Greenbelt, MD
S. Gnanalingam, University of Illinois, Urbana, IL
J. L. Green, NOAA, Boulder, CO
A. J. Hall, Rutherford Appleton Lab, Chilton, UK
S. W. Henson, University of Illinois, Urbana, IL
H. M. Ierkic, Arecibo Observatory, Arecibo, PR
P. Karhunen, Vaisala Oy, Helsinki, Finland
M. F. Larsen, Cornell University, Ithaca, NY
C. H. Liu, University of Illinois, Urbana, IL
G. B. Loriot, Haystack Observatory, Westford, MA
P. E. Mayes, University of Illinois, Urbana, IL
C. E. Meek, University of Saskatchewan, Saskatoon, Canada
K. Merewether, University of Illinois, Urbana, IL
E. A. Mueller, State Water Survey, Urbana, IL
G. D. Nastrom, Control Data Corporation, Minneapolis, MN
J. J. Olivero, Pennsylvania State University, University Park, PA
J. Parker, University of Illinois, Urbana, IL
R. M. Peters, Pennsylvania State University, University Park, PA
M. Petitdidier, CNET/CRPE, Saint Maur des Fosses Cedex, France
P. K. Rastogi, Case Western Reserve University, Cleveland, OH
I. M. Reid, University of Saskatchewan, Saskatoon, Canada
A. Rennier, University of Illinois, Urbana, IL
A. D. Richmond, NOAA, Boulder, CO
A. C. Riddle, CIRES/NOAA, Boulder, CO
R. G. Roper, Georgia Institute of Technology, Atlanta, GA
J. Rottger, EISCAT Scientific Association, Kiruna, Sweden
O. Royrvik, University of Illinois, Urbana
J. E. Salah, Haystack Observatory, Westford, MA
D. Sarwate, University of Illinois, Urbana, IL
T. Sasamori, University of Illinois, Urbana, IL
A. O. Scheffler, University of Illinois, Urbana,IL
M. R. Schoeberl, Goddard Space Flight Center, Greenbelt, MD
C. F. Sechrist, University of Illinois, Urbana, IL
L. G. Smith, University of Illinois, Urbana, IL
G. R. Stitt, University of Illinois, Urbana, IL
R. G. Strauch, NOAA, Boulder, CO
R. B. Stoltzfus, University of Illinois, Urbana, IL
R. A. Vincent, University of Adelaide, Adelaide, South Australia
D. Voelz, University of Illinois, Urbana, IL
J. M. Warnock, NOAA, Boulder, CO
A. T. Waterman, Stanford University, Stanford, CA
B. J. Watkins, University of Alaska, Fairbanks, AK
S. R. Williams, Pennsylvania State University, University Park, PA
K. C. Yeh, University of Illinois, Urbana, IL
B. Yu, University of Illinois, Urbana, IL

CUMULATIVE LISTING FOR THE MAP HANDBOOK

Volume	Contents	Date of Publication
1	National Plans, PMP-1 Report; PMP-2 Report, PMP-3 Report, MSG-4 Report, Approved MAP Projects	June 1981
2	Symposium on Middle Atmosphere Dynamics and Transport, (extended abstracts)	June 1981
3	PMP-5 Report, MSG-1 Report, MSG-2 Report, MSG-3 Report, Antarctic Middle Atmosphere Project (AMA), EXOS-C Scientific Observations, WMO Report No. 5, Updated Chapter 2 of MAP Planning Document, Condensed Minutes of MAPSC Meetings	November 1981
4	Proceedings of MAP Assembly held in Edinburgh, 14-15 August 1981, Condensed Minutes of MAP Steering Committee Meetings held in Edinburgh, Proceedings of MAP Open Meeting held in Hamburg, 19 August 1981	April 1982
5	A Catalogue of Dynamic Parameters Describing the Variability of the Middle Stratosphere during the Northern Winters	May 1982
6	MAP Directory	November 1982
7	Acronyms, Condensed Minutes of MAP Steering Committee Meetings, Ottawa, May 1982, MAP Project Reports, National Reports, Committee Reports, PMP and MSG Reports, Workshop Reports, Announcements and Corrigendum	December 1982
8	MAP Project Reports: DYNAMICS, GLOBUS, and SSIM, MSG-7 Report, National Reports: Czechoslovakia, USA	July 1983
9	Papers presented at the URSI/SCOSTEP Workshop on Aspects of MST Radar, May 23-27, 1983, Urbana	December 1983
10	Papers presented at the International Symposium on Ground-Based Studies of the Middle Atmosphere, May 9-13, 1983, Schwerin, German Democratic Republic	May 1984
11	Condensed Minutes of the MAP Steering Committee Meetings held in Hamburg 13-14 August 1983, Research Recommendations for Increased US Participation in the Middle Atmosphere Program, GRATMAP Project Report, MAP Study Group MSG-7 Report	June 1984
12	Coordinated Study of the Behavior of the Middle Atmosphere in Winter (PMP-1) Workshops	July 1984
13	Ground-Based Techniques	November 1984
14	Papers presented at the URSI/SCOSTEP Workshop on Technical Apsects of MST Radar, May 22-25, 1984	December 1984